Food Structure

Volume 4 | Number 2 Article 1

1985

Food Microstructure

Follow this and additional works at: https://digitalcommons.usu.edu/foodmicrostructure

Recommended Citation
(1985) "Food Microstructure," *Food Structure*: Vol. 4 : No. 2 , Article 1.
Available at: https://digitalcommons.usu.edu/foodmicrostructure/vol4/iss2/1

This Article is brought to you for free and open access by the Western Dairy Center at DigitalCommons@USU. It has been accepted for inclusion in Food Structure by an authorized administrator of DigitalCommons@USU. For more information, please contact digitalcommons@usu.edu.

ISSN 0730-5419
CODEN – FMICDK
Vol. 4, No. 2, 1985

FOOD MICROSTRUCTURE

An International Journal on the Microstructure and Microanalysis of Foods, Feeds and their Ingredients

Published semiannually by

Scanning Electron Microscopy, Inc.
AMF O'Hare (Chicago), IL 60666
U.S.A.

FOOD MICROSTRUCTURE

An International Journal on the Microstructure and Microanalysis of Foods, Feeds and their Ingredients

EDITORS

M. Kalab, Food Research Institute, Agriculture Canada, Ottawa, Ontario, Canada K1A 0C6 (613-995-3700 x 272)

S.H. Cohen, Science and Advanced Technol. Lab., U.S. Army Natick R&D Ctr., Natick, MA, 01760 USA (617-651-4578)

E.A. Davis, Dept. of Food Science & Nutrition, Univ. of Minnesota, St. Paul, MN 55108 USA (612-373-1158)

D.N. Holcomb, Kraft Inc., R&D, 801 Waukegan Rd., Glenview, IL 60025 USA (312-998-3724)

W.J. Wolf, USDA Northern Regional Res. Ctr., Peoria, IL 61604 USA (309-685-4011 x350)

MANAGING EDITORS

Om Johari, SEM Inc. (312-529-6677)

Sudha A. Bhatt, SEM Inc.

EDITORIAL BOARD

D.B. Bechtel, U.S. Grain Marketing Res. Ctr., Manhattan, KS

W. Buchheim, Bundesanst. Milchforschung, Kiel, W. Germany

R.J. Carroll, Eastern Reg. Res. Ctr., USDA, Philadelphia, PA

R.G. Cassens, Univ. Wisconsin, Madison

J.M. deMan, Univ. Guelph, Ontario, Canada

P.S. Dimick, Penn. State Univ., University Park, PA

R.G. Fulcher, Agriculture Canada, Ottawa, Canada

D.J. Gallant, Ministry Agriculture, Nantes, France

N.C. Ganguli, Indian Coun. Agri. Res., New Delhi

A.M. Hermansson, Swedish Food Inst., Goteborg, Sweden

N. Krog, Grindsted Products, Brabrand, Denmark

K. Larsson, Univ. Lund, Sweden

R. Moss, Bread Res. Inst., North Ryde, Australia

Y. Pomeranz, U.S. Grain Marketing Res. Ctr., Manhattan, KS

P. Resmini, Inst. Industrie Agrarie, Milano, Italy

M.W. Ruegg, Fed. Dairy Res. Inst., Liebefeld-Berne, Switzerland

K. Saio, National Food Res. Inst., Tsukuba, Japan

Z. Saito, Hokkaido Univ., Japan

G.R. Schmidt, Colorado State Univ., Fort Collins, CO

M.V. Taranto, Frito-Lay Inc., Irving, TX

M.A. Tung, Univ. British Columbia, Vancouver, Canada

E. Varriano-Marston, Hercules Res. Ctr., Wilmington, DE

J.G. Vaughan, Queen Elizabeth College, London, U.K.

C.A. Voyle, AFRC Food Res. Inst., Bristol, U.K.

Annual Subscription Rates:
(including postage and handling)

U.S. $50.00 (U.S. delivery)
U.S. $55.00 (elsewhere)

Business Communications:
Address all communications regarding subscriptions, change of address, etc. to Dr. Om Johari at SEM, Inc.

Editorial Correspondence and Inquiries:
Submit papers (see instructions to authors), news items, books for review, etc. to one of the editors or to **SEM Inc., AMF O'Hare, IL 60666-0507, USA.**

Copyright © 1985 Scanning Electron Microscopy, Inc., except for contributions in the public domain. All rights reserved. See inside back cover.

Where necessary, permission is granted by the copyright owner for libraries and others registered with Copyright Clearance Center (CCC) to photocopy, provided that the base fee of $1.00 per copy of the article, plus .05 per page is paid directly to CCC, 21 Congress Street, Salem, MA 01907. Copying done for other than personal or internal reference use, without the expressed permission of the SEM, Inc. is prohibited. Those articles without a fee-code are not included in the CCC service. Serial fee code: 0730-5419/85$1.00 +.05.

FOOD MICROSTRUCTURE, Vol. 4 (1985), pp. 183–189
SEM Inc., AMF O'Hare (Chicago), IL 60666-0507 U.S.A.

0730-5419/85$1.00+.05

MICROSTRUCTURAL CHANGES IN MATURING SEEDS OF THE COMMON BEAN (*Phaseolus vulgaris* L.)

Joe S. Hughes and Barry G. Swanson

Department of Food Science and Human Nutrition
Washington State University
375 Clark Hall
Pullman, WA 99164–6330

Abstract

Seeds of *Phaseolus vulgaris* L. beans were collected at weekly intervals throughout maturation and examined by scanning electron microscopy (SEM). No major structural changes were observed on the surface of the seed coat during the seven week study period. A cross-sectional examination of the seed coat revealed a substantial increase in thickness of the parenchyma cell layer in young seeds followed by a dramatic decrease in thickness as the seed approached maturity. In the cotyledons, the diameter of the storage cells and starch granules increased over time, with distinct protein bodies becoming visible only in the later stages of maturity. An extensive vascular system responsible for rapid delivery of water and nutrients to the cotyledons was observed in both immature and mature beans.

Initial paper received March 27 1985
Manuscript received August 16 1985
Direct inquiries to B.G. Swanson
Telephone number: 509-335-4015/1702

Key Words: Seed microstructure, seed coat, cotyledons, scanning electron microscopy, common bean, *Phaseolus vulgaris* L., hard seeds, starch granules, protein bodies, vascular system, parenchyma cells.

Introduction

In recent years, both scanning electron microscopy (SEM) and transmission electron microscopy (TEM) have been used to study the microstructure of legume seeds. The susceptibility of legume seeds to hardening is one reason for research interest in legume microstructure. Two different types of hardness have been observed in legumes – hardseed or hardshell and hard-to-cook. Hardseed or hardshell legumes are seeds that do not imbibe water in a reasonable length of time (18–24 h). Hard-to-cook legumes, on the other hand, imbibe water but do not soften even after cooking. An increased understanding of seed microstructure will provide a better understanding of the causes of seed hardness. Most recent research on legume microstructure has focused on the cotyledons of mature seeds (McEwen et al., 1974; Saio, 1976; Sefa-Dedeh and Stanley, 1979a; Silva and Luh, 1978; Wolf and Baker, 1972). Microstructural changes occurring in seeds during storage (Jackson and Varriano-Marston, 1981; Sefa-Dedeh et al., 1979; Varriano-Marston and Jackson, 1981), water imbibition (Sefa-Dedeh and Stanley, 1979c) and cooking (Rockland and Jones, 1974; Sefa-Dedeh and Stanley, 1979b; Sefa-Dedeh et al., 1978) have also been observed and reported.

Little research on the microstructural changes occurring during development and maturation of bean seeds has been reported (Opik, 1968; Yeung, 1983). Most previous research on maturing bean seeds has used TEM to study intracellular metabolic changes occurring in the cotyledons. The objective of this research was to use SEM to examine the microstructural changes occurring in maturing common bean seeds (*Phaseolus vulgaris* L.). Attention was directed at changes occurring in both seed coats and cotyledons.

Materials and Methods

The beans studied (*Phaseolus vulgaris* L., cv. Black Turtle Soup) have black seed coats. The beans were grown at the Washington State University Irrigated Agriculture Research and Extension Center, Prosser, Washington, during the 1984 growing season. Plots were planted on June 6, 1984 and pods were collected on five separate dates in August and September. Seeds were removed from the pods immediately after harvesting and fixed in an aqueous solution of 4% formaldehyde and 1% glutaraldehyde in phosphate buffer (pH 7.0). Prior to viewing with SEM, seeds were postfixed in 4% osmium tetroxide for 18 h and

Table 1. Microstructural changes in cell dimensions in the seed coat of maturing bean seeds (*Phaseolus vulgaris* L.)

Maturity, days after flowering	Pl[1]	E[1]	Pr[1] (μm)	SC[1]	Figure number
13	28.4 ± 2.8	14.3 ± 1.2	95.7 ± 6.1	138.4	2A
19	34.4 ± 1.0	17.1 ± 1.5	191.9 ± 4.7	243.4	2B
28	34.6 ± 3.6	18.9 ± 3.0	91.9 ± 5.4	145.4	2C
35	40.3 ± 1.1	25.1 ± 1.0	77.0 ± 3.5	142.4	2D
49	38.1 ± 1.0	24.6 ± 3.0	29.8 ± 4.6	92.5	2E

[1]Pl = Palisade, E = Subepidermal, Pr = Parenchyma and SC = Seed Coat. Measurements were made using a Bioquant II image analysis system.

dehydrated in a graded ethanol series (30–100%). As a control for swelling and other possible effects of aqueous fixation, one group of mature seeds was not fixed. After harvest, seeds not fixed were stored over a desiccant and later dehydrated in 100% ethanol. All seeds were freeze-fractured in liquid nitrogen with a razor blade, critical point dried in carbon dioxide (Bomar SPC-1500), and sputter-coated with 300 A gold (Hummer-Technics). Fractured seeds were observed and photographed with an ETEC U-1 scanning electron microscope (Hayward, CA) at 20 kV.

Results and Discussion

Seed coat surface

Seed coats serve as a protective barrier between the embryo (cotyledons) and the external environment. The seed coat protects the nutrient-rich cotyledons from microorganisms and other pests, as well as fungal contamination. Often the exterior surface of the seed coat contains a distinctive pattern or "fingerprint" (Wolf et al., 1981). The fingerprint is formed during seed development by pressure between the seed coat and the endocarp, the innermost layer of the pod wall. Seeds of many plant species have distinctive species-specific seed coat patterns. Seeds of various cultivars of the same species have few distinctive differences, but often can be identified by seed coat pattern. SEM has been used extensively to study seed coat pattern for purposes of seed identification. Using SEM, Banerjee and Chauhan (1981) were able to demonstrate how the pattern on the surface of the grain (caryopsis) of wheat (*Triticum spelta*) genetically evolved from its progenitors.

Observations of the seed coat surface of maturing *Phaseolus vulgaris* L. seeds revealed the characteristic pattern which developed as the seeds matured (Figs. 1A-E). The seed coat surface of the youngest seeds appears to be covered with small, pebble-like bumps (Fig. 1A), but does not exhibit the distinctive pattern that characterizes mature seeds. The absence of a distinctive seed coat pattern in young seeds probably results from the seeds being so small that no pressure had yet developed between the seed coat and the endocarp. However, as the seeds mature, a seed coat pattern increasing in distinctiveness and complexity becomes visible (Figs. 1B-E). Increased pressure between the seed coat and endocarp appears to be responsible for the characteristic fingerprint development on the seed coat surface as the seed matures.

Wolf et al. (1981) studied the seed coat surface of thirty-three cultivars of soybeans (*Glycine max*), and noted a wide variety of characteristics including pits, cracks and surface deposits. No pits or cracks were observed in the seed coats of maturing *Phaseolus vulgaris* L. seeds, though some scattered surface deposits were noted (Fig. 1C). The composition of the surface deposits was not ascertained.

Seed coat cross-section

SEM has been used to evaluate cowpea (Sefa-Dedeh and Stanley, 1979a), soybean (Wolf and Baker, 1972), adzuki bean and common bean (Sefa-Dedeh and Stanley, 1979b; Swanson et al., 1985) seed coats in cross-section. Several cell layers have been observed in the different legumes and a different nomenclature is reported for each. Three distinctive cell layers are visible in the seed coat of the common bean – the palisade, subepidermal and parenchyma cell layers.

Palisade cells are long, columnar cells which make up the outermost cell layer of the seed coat. Subepidermal cells are somewhat shorter columnar cells that lie immediately beneath the palisade layer (Fig. 2A). Subepidermal cells are also commonly referred to as pillar or hourglass cells if they exhibit a characteristic pillar or hourglass shape (Esau, 1977). Approximately 10–15 layers of parenchyma cells make up the innermost portion of the seed coat that lies closest to the embryo (Fig. 2A). Both the palisade and subepidermal layers consist of a single layer of tightly packed cells. Both cell layers increase slightly in length as the seed matures (Table 1), but do not undergo any major structural changes (Figs. 1A and E).

The parenchyma layer, in contrast, consists of 10–15 layers of irregularly shaped, randomly organized cells with frequent intercellular spaces (Fig. 2A). During the early stages of seed development (13–19 d after flowering), the parenchyma layer is 2–5 times thicker than the palisade and subepidermal layers (Figs. 2A and B). As maturation progresses (28–35 d after

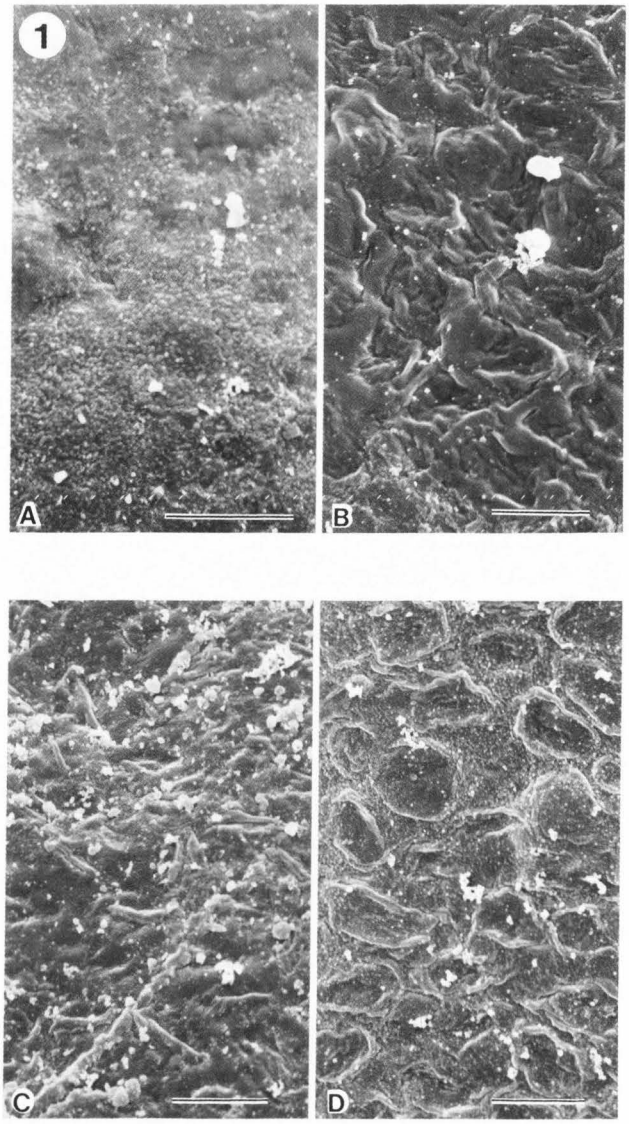

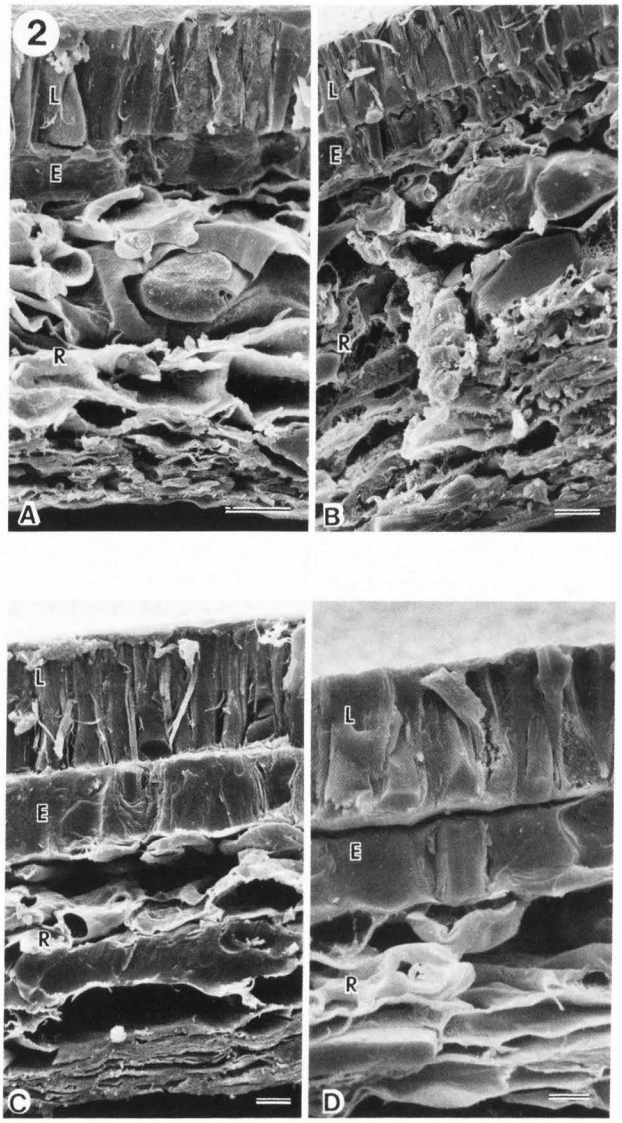

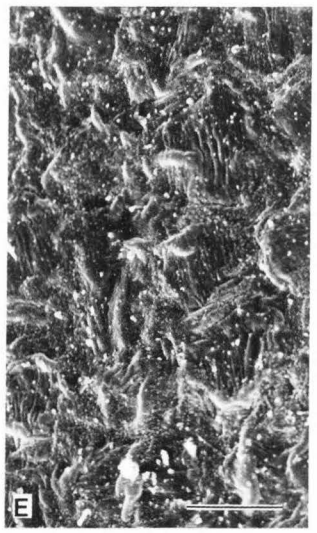

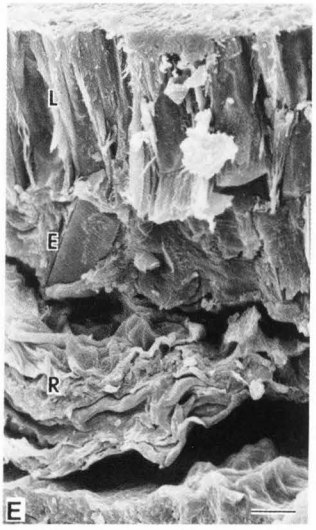

Fig. 1. (above & left) Exterior of seed coat of developing *Phaseolus vulgaris* L. bean seeds. Micrographs were taken of seeds harvested at: A = 13 d, B = 19 d, C = 28 d, D = 35 d, and E = 49 d after flowering. Bar = 10 μm.

Fig.2. (above & right) Cross-sectional view of seed coat of developing *Phaseolus vulgaris* L. bean seeds. Micrographs were taken of seeds harvested: A = 13 d, B = 19 d, C = 28 d, D = 35 d and E = 49 d after flowering. The palisade (L) subepidermal (E), and parenchyma (R) layers are visible. Bar = 10 μm.

Table 2. Microstructural changes in the cotyledons of maturing bean seeds (*Phaseolus vulgaris* L.)

Maturity, days after flowering	Mean cell diameter[1] (μm)	Mean starch granule diameter[1] (μm)	Figure number
13	51.7 ± 10.9	12.6 ± 6.1	3A
19	53.3 ± 19.7	13.3 ± 1.4	3B
28	54.7 ± 11.3	15.7 ± 2.9	3C
35	58.2 ± 9.3	20.7 ± 3.7	3D
49	62.1 ± 12.5	19.8 ± 4.9	3E, 3F

[1]Measurements were made using a Bioquant II image analysis system.

flowering), the size of the entire seed increases, and the thickness of the parenchyma layer decreases (Figs. 2C, D, and E; Table 1). The parenchyma layer is thickest (100–190 μm) during the period of greatest seed growth, but the cells disintegrate and the layer is compressed as the seed approaches full size and seed growth slows. It is generally believed that the seed coat functions solely as a protective covering for the embryo. However, in using TEM to study the branched parenchyma cells of maturing *Phaseolus vulgaris* L. seeds, Yeung (1983) observed a great deal of metabolic activity including dilation of endoplasmic reticulum cisternae and an increase in abundance of other cytoplasmic organelles. As a result, Yeung (1983) theorized that the seed coat may supply nutrients to the embryo. Increased thickness in the parenchyma layers of young seeds, as observed with SEM, appears to support the theory that in addition to serving as a protective barrier, the seed coat may play a nutritive role and may be important in controlling development of the embryo (Yeung, 1983).

In mature beans, the parenchyma layer has been compressed to approximately the same thickness (30 μm) as each of the two outermost layers (Fig. 2E; Table 1). Because of the compression of the parenchyma layer, the total thickness of seed coat decreases as the seed approaches maturity and seed growth slows (Table 1).

Microstructure of cotyledons

More research has been reported on the microstructure of legume cotyledons than on legume seed coats. Cotyledons have been of particular interest for researchers investigating the causes of "hardness" in legumes (Saio, 1976; Sefa-Dedeh et al., 1979; Varriano-Marston and Jackson, 1981).

Bean cotyledons contain large (10–50 μm) spherical starch granules and small (5–10 μm) round protein bodies embedded in a protein matrix. Starch granules are present throughout maturation, distinct protein bodies only became evident during the later stages (35–49 d after flowering; Figs. 3D and F). Studying maturing *Phaseolus vulgaris* L. seeds, Opik (1968) also observed that protein bodies become visible later than starch granules.

In young seeds (13 d), both starch granules and plastids are present. The starch granules resist fracturing and retain a characteristic spherical shape, while plastids are fractured (Fig. 3A). Starch granule synthesis is initiated in the plastids, with the starch granules expanding and rupturing the plastid membrane when the granules become larger than the plastid. Some of the thin fragments present on the surface of the starch granules may be remnants of ruptured plastid membranes (Fig. 3F, arrow). As the embryos mature, both the size and number of starch granules increase (Fig. 3; Table 2).

The overall size of bean cotyledon cells also increases as maturation progresses (Table 2). In developing seeds (13–19 d after flowering), several intercellular spaces (I) surrounded each cell (Figs. 3A and 3B), but the intercellular spaces disappear as the seed matures (28–35 d) due to pressure from expanding cells (Figs. 3C and D).

In seeds fixed in the aqueous glutaraldehyde-formaldehyde solution, cotyledon cells are increasingly resistant to freeze fracturing as the seeds mature. In young seeds (13–19 d; Figs. 3A and B), fracturing occurred through the cells, revealing internal starch granules, plastids and protein bodies. However, as the seeds matured, cotyledon cells were increasingly resistant to fracturing; some cells fractured while others remained intact leaving visible the exterior of the cytoplasm separated from the cell wall (Figs. 3C and D). Finally, in mature beans (49 d) fixed in aqueous solution, many cotyledon cells were resistant to fracturing, limiting observation to the exterior of the cytoplasm, cell walls and a few isolated starch granules (Fig. 3E). Though interesting artifacts may have been created, the resistance of mature cells to fracturing appears to be a result of aqueous fixation. In the control group of unfixed mature beans, fracturing occurred through the cells, and starch granules and protein bodies were readily visible (Fig. 3F).

Another interesting structural feature in aqueous fixed cotyledons is the finger-like projections or pegs extending from the exterior of the cotyledon cells (Fig. 4A). The finger-like projections appear too large to be individual plasmadesma, protoplasmic bridges that pass through the cell wall and connect contiguous cells. However, the projections may be pit fields where groups of plasmadesmata pass through the cell wall together.

The presumed pit fields were visible only in aqueous-fixed seeds in which cell walls were removed by freeze-fracturing, leaving the exterior of the cytoplasm visible. In some instances, the cell wall was only partially removed or separated from the

Fig. 3. Microstructure of the cotyledons of developing *Phaseolus vulgaris* L. bean seeds, harvested at: A = 13 d, B = 19 d, C = 28 d, D =35 d, and E and F = 49 d after flowering. Starch granules (S), protein bodies (P), plastids (T), intercellular spaces (I) and cell walls (C) have been identified. The arrows in C point to separations between cell wall and exterior of the cytoplasm. Arrow in F points to a possible remnant of a ruptured plastid membrane. Figs. A, B, D, E and F, bar = 10 μm; Fig. C, bar = 20 μm.

Fig. 4. Cotyledon cells of *Phaseolus vulgaris* L. bean seeds. Fig. 4A illustrates separation between cell wall and exterior of the cytoplasm. Fig. 4B illustrates the interior of a cell wall after the cytoplasm has been removed. The cell wall (C), presumed pit fields (D) and middle lamella (M) have been identified. Arrows point to holes where pit fields passed through the cell wall; the asterisk (*) shows the channel left by removal of the middle lamella. Bar = 10 μm.

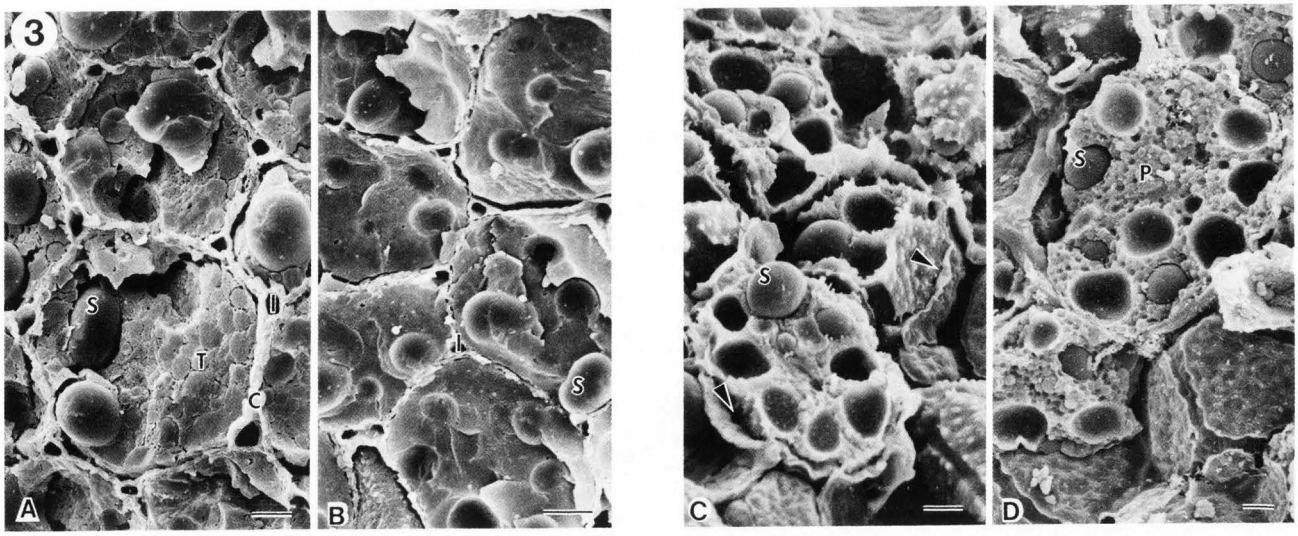
3
S
U
T
C
A
L
S
B
S
C
S
P
D

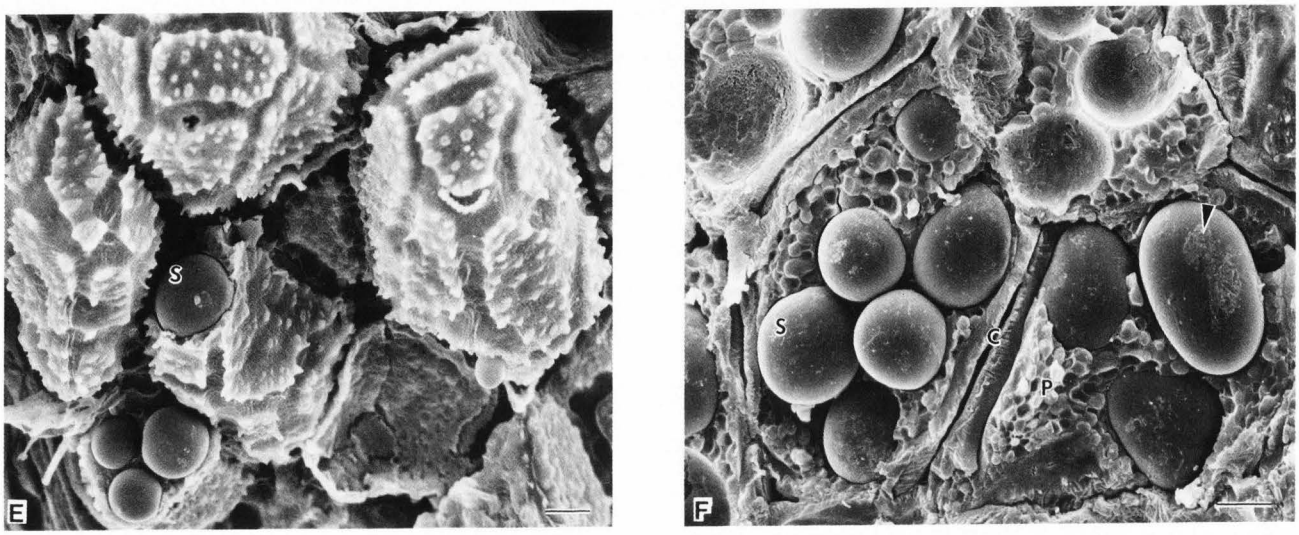
S
E
S
C
P
F

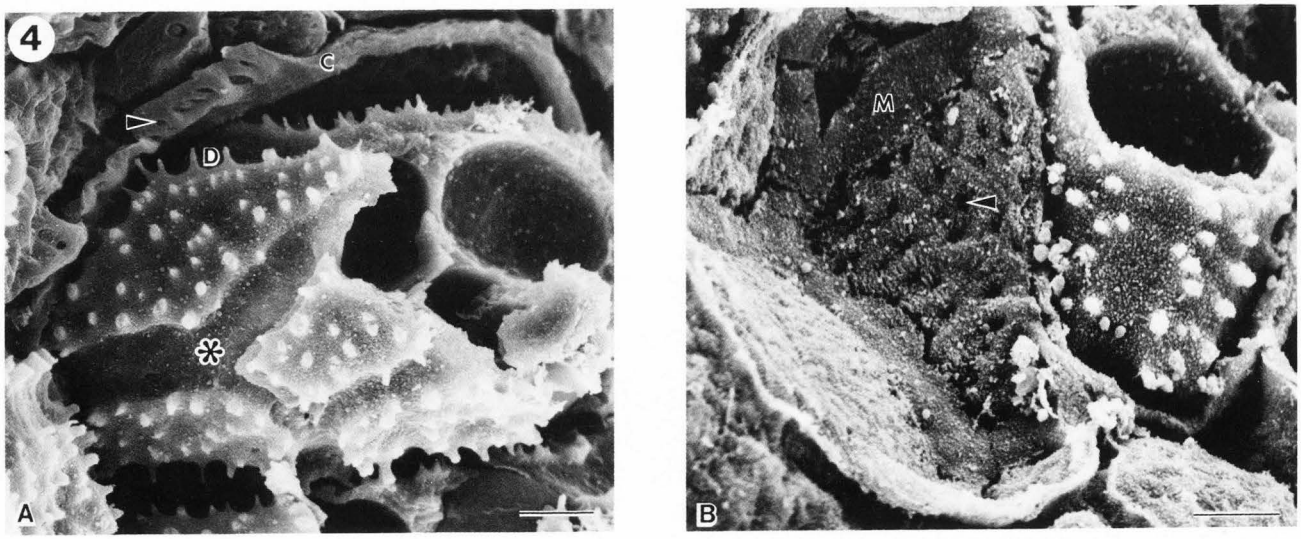
4
C
D
A
M
B

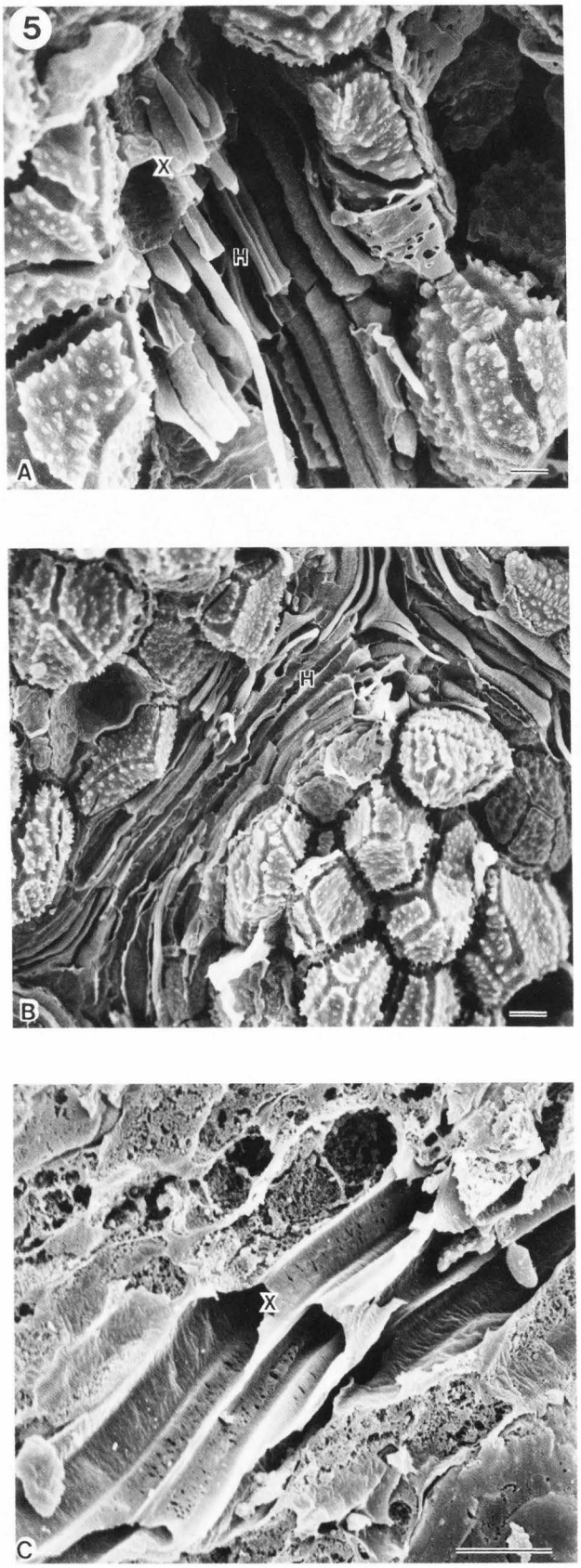

cytoplasm (Fig. 3C, arrows). In a cotyledon cell where the cell wall has been separated from the cytoplasm, small openings or holes can often be observed where pit fields are presumed to have passed through the cell wall (Fig. 4A, arrow). Examining the interior of a cotyledon cell after the cytoplasm has been removed also reveals small holes where pit fields from the extracted cytoplasm appear to have passed through the cell wall (Fig. 4B, arrow). Long strips of what appears to be middle lamella are also present (Fig. 4B). The middle lamella is a pectinaceous intercellular layer responsible for cementing contiguous cells together (Esau, 1977). Strips of presumed middle lamella appear to be responsible for the channels (Fig. 4A, asterisk) in the exterior of the cytoplasm where pit fields are not present.

Vascular system

The vascular system, which provides rapid transport of nutrients and water from the plant to cotyledon storage cells, is also visible in the cotyledon (Fig. 5). The vascular system is made up of xylem, which transports water and ions, and phloem, which transports organic materials including nutrients. Although certain aspects of the role of the vascular system in legume seeds have been studied, a comprehensive investigation is lacking. Corner (1951) reported great variation in the vascular supply systems of different legume seeds, and diagrammed a few of the more common systems. Thorne (1981) used TEM and SEM to study the vascular system in soybeans in an attempt to determine the probable pathways of photosynthate transport.

Portions of the vascular system in the embryo of *Phaseolus vulgaris* L. seeds are readily visible 28 d after flowering. The vascular system appears to develop and become more elaborate as the seed matures, with a complex, highly developed vascular system being evident in fully mature seeds 49 d after flowering (Figs. 5A and B).

Conclusion

Significant structural changes occur in the seed coat and cotyledons of developing common bean seeds. In the seed coat, increased thickness of the parenchyma layer during the period of greatest seed growth is of particular interest, indicating that parenchyma cells may be involved in nutrient storage and/or supplying nutrients to growing cotyledons. In cotyledons, the overall size of storage cells and starch granules increased as development progressed, with protein bodies becoming evident later than starch granules. Relatively little is known about the microstructure of the vascular system that supplies water and nutrients to bean cotyledons. However, the vascular system does appear to become more elaborate as the seed matures.

Fig. 5. Vascular system of the cotyledon of *Phaseolus vulgaris* L. bean seeds. A, B and C are of fully mature seeds (49 d after flowering). Both phloem (H) and xylem (X) are visible. Figs. A and C, bar = 10 μm; Fig. B, bar = 20 μm.

Acknowledgements

The authors acknowledge the use of the facilities of the Electron Microscopy Center, Washington State University. Partial financial support for this research was provided by USAID Title XII Dry Bean/Cowpea CRSP. Scientific Paper No. 7224. Agricultural Research Center, College of Agriculture & Home Economics, Washington State University, Pullman, WA 99164-6240.

References

Banerjee SK, Chauhan KPS. (1981). Studies on the evolution of seed coat pattern in wheat by scanning electron microscopy. Seed Sci. & Technol. **9**, 819-822.

Corner EJH. (1951). The leguminous seed. Phytomorph. **1**, 117-150.

Esau K. (1977). *Anatomy of Seed Plants*, Second Edition. John Wiley & Sons, NY pp. 465-466.

Jackson GM, Varriano-Marston E. (1981). Hard-to-cook phenomenon in beans: Effects of accelerated storage on water absorption and cooking time. J. Food Sci. **46**, 799-803.

McEwen TJ, Dronzek BJ, Bushuk W. (1974). A scanning electron microscope study of faba bean seed. Cereal Chem. **51**, 750-757.

Opik H. (1968). Development of cotyledon cell structure in ripening *Phaseolus vulgaris* seeds. J. Exp. Bot. **19**, 64-76.

Rockland LB, Jones FT. (1974). Scanning electron microscope studies on dry beans. Effects of cooking on cellular structure of cotyledons in rehydrated large lima beans. J. Food Sci. **39**, 342-346.

Saio K. (1976). Soybeans resistant to water absorption. Cereal Foods World **21**, 168-173.

Sefa-Dedeh S, Stanley DW. (1979a). Microstructure of cowpea variety Adua Ayera. Cereal Chem. **56**, 379-386.

Sefa-Dedeh S, Stanley DW. (1979b). Textural implications of the microstructure of legumes. Food Technol. **33**(10), 77-83.

Sefa-Dedeh S, Stanley DW. (1979c). The relationship of microstructure of cowpeas to water absorption and dehulling properties. Cereal Chem. **56**, 379-386.

Sefa-Dedeh S, Stanley DW, Voisey PW. (1978). Effects of soaking time and cooking conditions on texture and microstructure of cowpea (*Vigna unguiculata*). J. Food Sci. **43**, 1832-1838.

Sefa-Dedeh S, Stanley DW, Voisey PW. (1979). Effect of storage time and conditions on the hard-to-cook defect in cowpeas (*Vigna unguiculata*). J. Food Sci. **44**, 780-796.

Silva HC, Luh BS. (1978). Scanning electron microscopy studies on starch granules of red kidney beans and bean products. J. Food Sci. **43**, 1405-1408.

Swanson BG, Hughes JS, Rasmussen HP. (1985). Seed microstructure: Review of water imbibition in legumes. Food Microstructure **4**, 115-124.

Thorne JH. (1981). Morphology and ultrastructure of maternal seed tissues of soybean in relation to the import of photosynthate. Plant Physiol. **67**, 1016-1025.

Varriano-Marston E, Jackson GM. (1981). Hard-to-cook phenomenon in beans: Structural changes during storage and imbibition. J. Food Sci. **46**, 1379-1385.

Wolf WJ, Baker FL. (1972). Scanning electron microscope study of soybeans. Cereal Sci. Today **17**, 125-130.

Wolf WJ, Baker FL, Bernard RL. (1981). Soybean seed-coat structural features: Pits, deposits and cracks. Scanning Electron Microsc. 1981; III: 531-534.

Yeung EC. (1983). Development changes in the branched parenchyma cells of bean seed coat. Protoplasma **118**, 225-229.

Discussion with Reviewers

E. Varriano-Marston: What was the moisture content of the seeds after removal from the pod? If they were 14% or less, then one need not dehydrate with ETOH. Just fracture and observe with SEM.
Authors: The moisture content of the seeds was about 5%, yet dehydration and preparation without dehydration, either or both are appropriate.

E. Varriano-Marston: In regard to the finger-like projections extending from the exterior of cotyledons fixed in aqueous solution (Fig. 4A), we have also observed these projections in aged beans that were not subjected to any aqueous treatment.
Authors: Thank you.

K. Saio: There are area-to-area differences on the surface of the seed coat even in one seed. What area of the seed coat was observed in this experiment? Are differences between Figures 1C-E due to maturation or to area examined?
Authors: An attempt was made to orient fractured bean seeds so that seed coat adjacent to the hilum was observed. We believe the observed differences are a result of maturity differences and not a result of observing different areas of the seed coat.

FOOD MICROSTRUCTURE, Vol. 4 (1985), pp. 191-198
SEM Inc., AMF O'Hare (Chicago), IL 60666-0507 U.S.A.

0730-5419/85$1.00+.05

CHANGES IN TYPICAL ORGANELLES IN DEVELOPING COTYLEDONS OF SOYBEAN

K. Saio, K. Kondo* and T. Sugimoto

National Food Research Institute, 2-1-2 Kannondai, Yatabe, Tsukuba, Ibaraki, Japan 305

*Nagano State Laboratory of Food Technology, 205 Nishibanba, Kurita, Nagano-shi, Japan 380

Abstract

Soybean cotyledonary cells harvested every 5-10 days at 15 to 60 days after flowering (DAF), were investigated by means of light and transmission electron microscopy. In the early developing stages (15-20 DAF) most of the cells were occupied by large, centrally located vacuoles while the cytoplasm was restricted to a thin layer against the cell wall and contained numerous ribosomes, mitochondria, plastids, small amounts of endoplasmic reticulum (ER) and minute lipid bodies. At about 25 DAF, spherical organelles which contained protein, lipid and sugar (PLS bodies), appeared and then increased in number and in size. Vacuoles had protein deposits lining the inner surfaces of the tonoplasts. At 30-35 DAF, the PLS bodies lost their characteristic circular shape because of invaginations containing cytoplasmic materials and small vacuoles. Such transformed PLS bodies, fragmented vacuoles and protein bodies became difficult to distinguish from each other. At this stage, the cytoplasm contained abundant rough ER with cisternae, dictyosomes, lipid bodies and plastids. At 35-40 DAF, protein bodies which varied in size and shape were observed in cells along with lipid bodies and rough ER. At about 40 DAF the plastids reached maximum size and number and then most disappeared. In the final stage (55-60 DAF), protein bodies became homogeneous in electron density with completion of protein accumulation.

Initial paper received April 16 1984
Manuscript received June 22 1985
Direct inquiries to K. Saio
Telephone number: 81-2975-6-8051

Key words: Soybean, protein body, PLS body, lipid body, plastid, starch granule, endoplasmic reticulum, ripening, light microscope, transmission electron microscope

Introduction

Protein body ontology during seed development has been investigated by many researchers. There are excellent reviews dealing with this problem (Millerd, 1975, Dieckert and Dieckert, 1976, Pernollet, 1978). A theory that protein is biosynthesized by polysomes attached to the exterior surface of protein body membranes (Burr and Burr, 1976) seems to lack sufficient experimental evidence. According to Adler and Müntz (1983) two different mechanisms of protein body generation have been proposed: 1) Protein bodies derive from the large vacuoles in which proteins are deposited (Dieckert and Dieckert, 1976, Bergfeld et al., 1980). These vacuoles seem to be transformed into protein bodies by fragmentation (Craig et al., 1980). 2) Protein bodies originate from the endoplasmic reticulum (ER), where the storage protein polypeptides are discharged from membrane-bound polysomes into the lumen of the rough ER (Higgins and Spencer, 1981, Weber et al., 1980). Most previous work on protein body formation was done using maize, wheat, mustard, castor bean, common bean, broad bean and cowpea. There is surprisingly little research on generation of protein bodies in soybeans (Bils and Howell, 1963, Yoo and Chrispeels, 1980, Norby et al., 1984), compared with the importance of soybeans as a protein resource. However, Kaizuma and coworkers (Kaizuma and Kasai, 1981, Sato et al., 1982) recently found organelles which contained nucleic acids (RNA and DNA), lipid and protein in the middle stage of development of soybean cotyledonary cells and have designated them RNA bodies or nucleo-globules. They also presented evidence that the isolated nucleo-globules could synthesize storage protein based on studies of incorporation of radioactive leucine (Kaizuma and Sato, 1983). In order to more clearly understand the process of formation of protein bodies in soybean cotyledons, we have conducted a detailed microscopic study, concentrating on special stages of development. Observations are also presented on other organelles that accompany protein body formation such as plastids, lipid bodies and rough ER.

Materials and Methods

Plant material

Soybeans used were from the 1983 crop, var. Enrei which were sown on June 8 and cultivated in the experimental field of the Agriculture Research Center, Tsukuba, Japan. During the first one-third of the flowering period, colored wires (about 0.2 mm in diameter) were placed through the floral axes of the opened flowers as tags (Brown series inserted on August 4 and Red series inserted on August 10 on the sample plants). Pods were harvested every 5 to 10 days after flowering. Stages of sampling are shown in Figure 1. Fresh seed weights were measured on 5 seeds and the average weight per seed is reported. Dried weights were calculated by correcting for moisture content which was determined by freeze drying (Kyowa RL-20-NA) for about 30 hrs.

Preparation of microscopic specimens

Cotyledonary tissues of developing soybeans were cut into small pieces with a razor blade, fixed with 5% glutaraldehyde and then with 1% osmium tetroxide (both in phosphate buffer containing 5% sucrose, pH 6.7), dehydrated with a graded alcohol series (40 to 100%), transferred to polypropylene oxide-Epon resin series (50 to 100%) and finally embedded in Epon resin (Epok 812). In the early stages of development whole seeds were fixed as described for the cut pieces.

For light microscopy (LM) the Epon block was sliced to 5-10 μm in thickness. The slices were affixed on a glass slide and stained with the Periodic Acid-Schiff reagent (PAS) for polysaccharides and with Commassie Brilliant Blue (CBB) for protein as described previously (Saio et al.,1983). The Epon block used for LM was also ultrathin sliced and the sections were observed under a transmission electron microscope (TEM, JEOL EX-1200) with or without staining with saturated uranyl acetate and lead acetate solutions.

Results and Discussion

Our experimental schedule is shown in Figure 1. Although we tried to minimize variability by tagging the flowers, the maturity of seeds differed slightly depending upon the weather, the location of the pods on the plants and the positions of the seeds within the pods; seeds harvested on a given day showed differences in size and in microstructure. As shown in

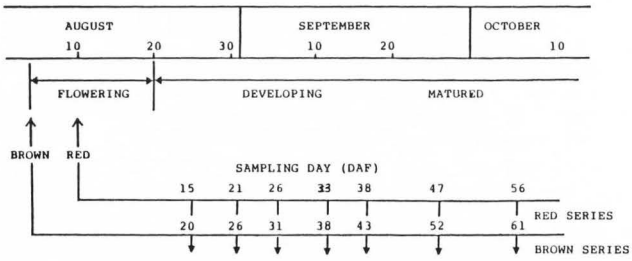

Figure 1 Sampling schedule as shown in seeds of 15-26 DAF. Seeds were classified as small, medium and large by their fresh weights and submitted for preparation of specimens for microscopy.

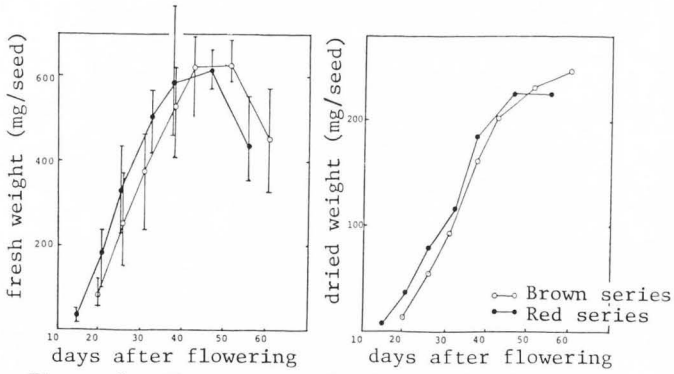

Figure 2. Changes in fresh and dried weights during seed development.

Figure 2, seeds of the Red (R) series showed a more rapid approach to maturity than those of the Brown (B) series probably because the flowers of the R series were located in upper positions in the plants and also because the temperature increased from August 10th when the flowers of Red series opened. Figure 3 shows LM micrographs of developing cotyledonary cells of soybeans which were stained by the PAS reaction (Figs. 3A-C) and by CBB (Figs. 3D-F). The size of cells increased markedly up to about 40 DAF. In Figure 3A (about 15 DAF), cell walls, nuclei (nucleolocentresomes were clearly stained) and small starch grains located in plastids were stained by PAS. By 20 DAF plastids increased in number, especially in the outer portions of the seeds (Fig. 3B). The starch grains in plastids continued to increase in size and in number up to about 40 DAF (Fig. 3E) and then disappeared rapidly as seeds reached maturity (Fig. 3F). The formation of vacuoles smaller than the large centrally located vacuole, was observed from about 25 DAF and sometimes the organelles found by Kaizuma et al.(1981) were also recognized (Figs. 3C, 3D). These organelles were distinctly stained by PAS, CBB and osmium and could also be distinguished from other structures by their spherical shape. Their number and size increased around 30 DAF. Until they are better understood, we are calling these organelles protein-lipid-sugar (PLS) bodies because they are stained by reagents which are positive for protein, lipid and sugar. As shown in Fig. 3E, at about 40 DAF the cytoplasm was rapidly occupied by protein bodies and plastids containing developed starch grains. The size and staining intensity of protein bodies varied within cells and also differed on a cell-to-cell comparison. As maturation progressed, this trend decreased, but at 55 DAF the size of protein bodies was still not uniform. After 55 DAF, the staining intensity of protein bodies was markedly reduced.

Figure 4 shows overall changes in developing soybean cotyledonary cells as a function of DAF as observed with TEM. The dates of harvesting the seeds are given in the caption but the microstructural changes did not always follow sequentially because of seed-to-seed and cell-to-cell variations.

In the early developing stages (Figs. 4A) most of cells were occupied by large centrally placed vacuoles with or without small electron

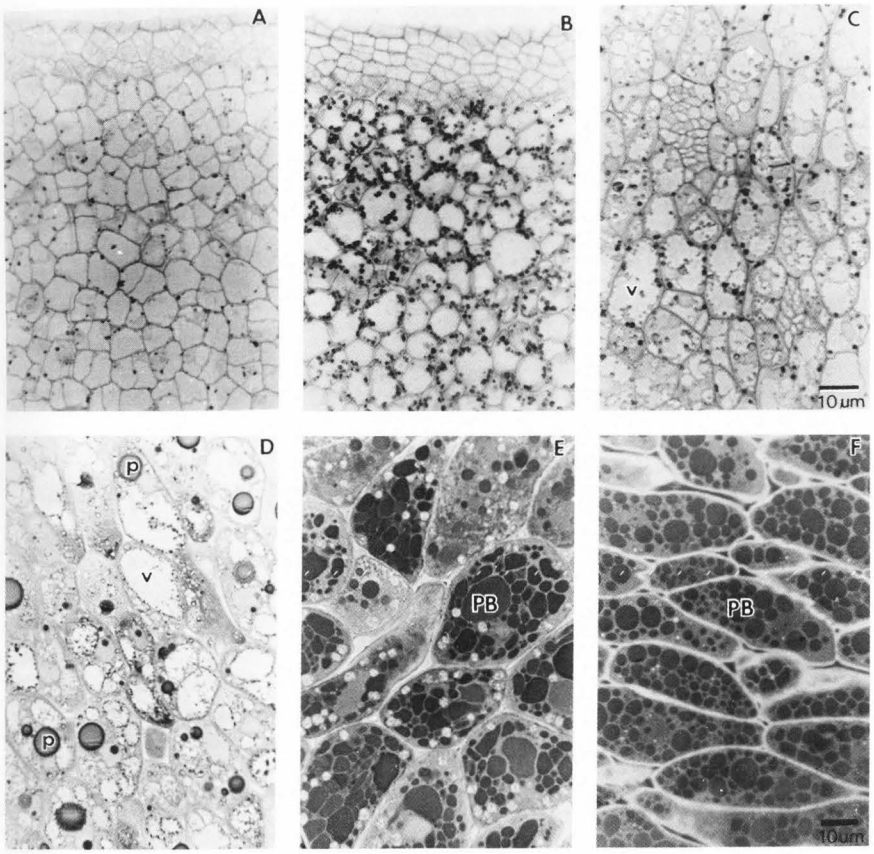

Figure 3. LM micrographs of developing soybean cotyledonary cells.

A) About 15 DAF. Top to bottom is from surface to center of a seed.
Dark dots correspond to small starch granules (plastids). Nuclei including nucleo-centresomes are shown.
B) About 20 DAF. Top to bottom is from surface to center. Dark dots are small plastids.
C) About 25 DAF. Large vacuoles (V) centrally placed in cells contain protein deposits attached on inner surface of tonoplast.
D) About 30 DAF. PLS bodies(P) have increased in number and in size.
E) About 40 DAF. Note protein bodies (PB) of various sizes, shapes and staining intensity, and starch granules (white dots) of increased size. Cell to cell difference is observed.
F) About 55 DAF. Note protein bodies (PB).
Figs A-C were stained with PAS while Figs D-F were stained with CBB. Magnification for all figures as shown in C.

dense bodies. The cytoplasm was restricted to a thin layer against the cell wall. Cell walls were thin with many plasmodesmata. The cytoplasm contained numerous free ribosomes and mitochondria, also numerous plastids which have developing grana structures and small starch grains, and small amounts of rough ER were observed. Minute electron dense bodies (probably lipid bodies) were also observed in the ground-plasm and increased in number as development progressed. Detailed changes in plastids are discussed later. In the succeeding stages of development (Figs. 4B, 4C), large vacuoles continued to occupy central portions of cells. Small vacuoles containing electron dense deposits and vacuoles having protein lumps lining the inner surfaces of tonoplasts were often observed (Fig. 4C). The cytoplasm contained ribosomes, dictyosomes, PLS bodies and plastids with enlarged starch grains and thylakoids. The PLS bodies appeared about 25 DAF (Fig 4C), and rapidly increased in number and size. The cytoplasm also contained a few more lipid bodies. In the next stage after 25 DAF (Figs 4D-F), extensive cell-to-cell microstructural variations were recognized. The cytoplasm contained lipid bodies in greatly increased numbers and sizes, abundant rough ER with enlarged cisternae, dictyosomes, protein bodies at various stages, plastids with larger starch grains and a few mitochondria. In the final stage of development after 50 DAF, protein bodies decreased in osmiophilicity and sometimes contained electron translucent inclusions (Fig. 4G) that may be globoids.

TEM micrographs shown in Figure 5 were selected from electron micrographs of soybean cotyledon samples collected on August 25 and 31 (see Figure 1). This stage corresponded to the formation of PLS bodies (25 to 30 DAF). The PLS bodies were in cytoplasm mainly occupied by vacuoles having protein deposits scattered or attached to tonoplasts in osmiophilic lumps (Figs. 3D, 4C). Normally, they were circular in cross section with a limiting membrane. However, occasionally one finds some with phagocytosing, irregular membranes (Fig. 5A), some without membranes (Fig. 5B; compare the two PLS bodies) and some that are coalescing (Fig. 5C). Finally, some of PLS bodies approached 10 to 20 µm in diameter, being comparable to the size of protein bodies. The PLS bodies seemed to be derived from vacuoles, but more evidence is needed for this conclusion.

TEM micrographs in Figure 6 were selected from electron micrographs of soybean cotyledons harvested September 9 and 12 (30 to 35 DAF). In this stage, the PLS bodies seemed to be transformed into provacuole-type bodies as observed by Bergfeld et al (1980) and Adler and Müntz (1983). Namely, they lost their specific circular shape as a result of invaginations containing cytoplasmic materials and small vacuoles (Figs. 6A-C). In the initial stage of such transformations, these bodies were observed in cytoplasm along with small and large vacuoles which contained protein deposits. However, in the next stage, large vacuoles changed into

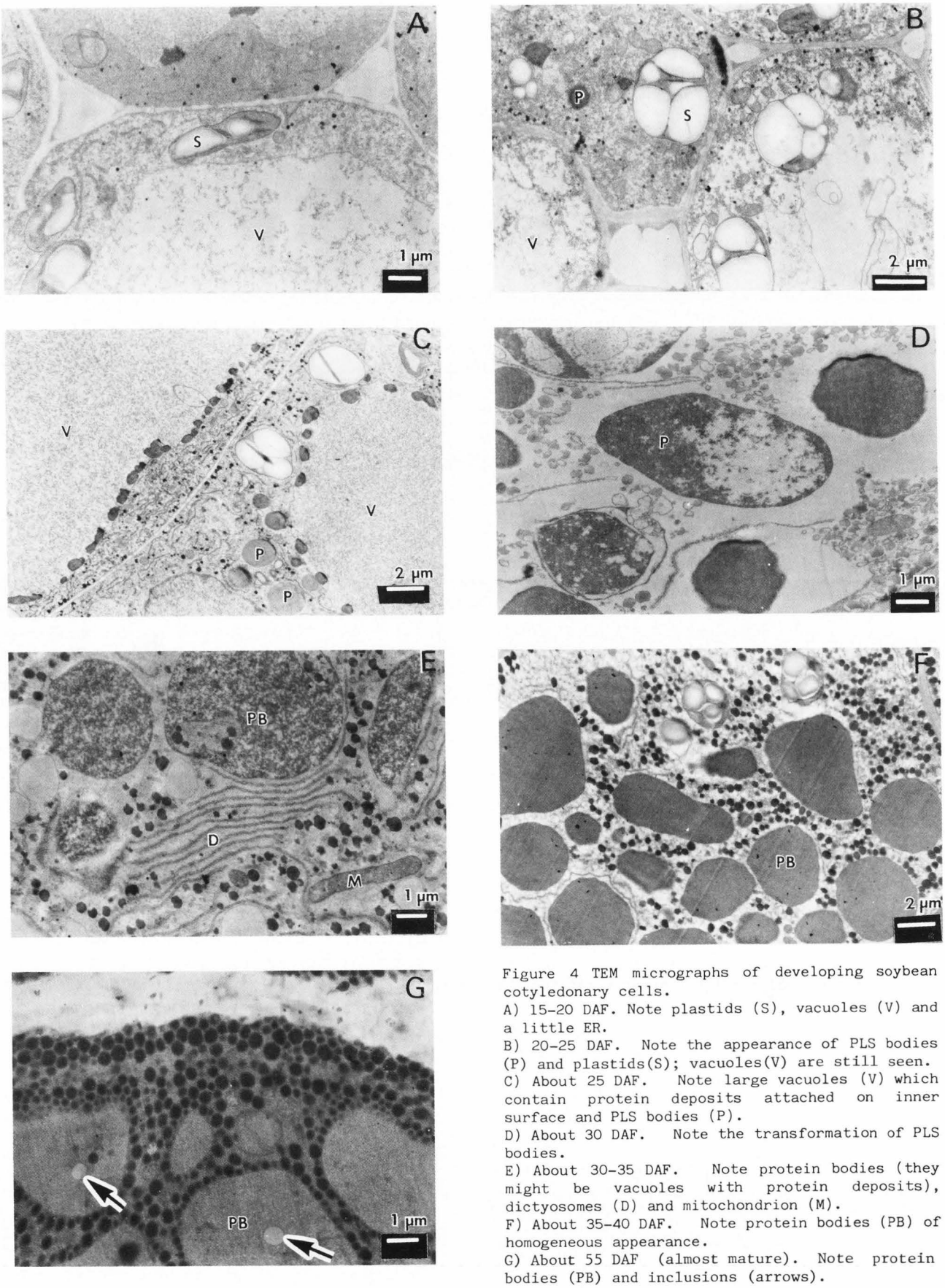

Figure 4 TEM micrographs of developing soybean cotyledonary cells.
A) 15-20 DAF. Note plastids (S), vacuoles (V) and a little ER.
B) 20-25 DAF. Note the appearance of PLS bodies (P) and plastids(S); vacuoles(V) are still seen.
C) About 25 DAF. Note large vacuoles (V) which contain protein deposits attached on inner surface and PLS bodies (P).
D) About 30 DAF. Note the transformation of PLS bodies.
E) About 30-35 DAF. Note protein bodies (they might be vacuoles with protein deposits), dictyosomes (D) and mitochondrion (M).
F) About 35-40 DAF. Note protein bodies (PB) of homogeneous appearance.
G) About 55 DAF (almost mature). Note protein bodies (PB) and inclusions (arrows).

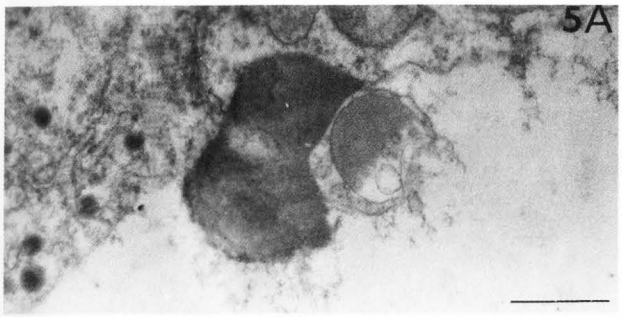

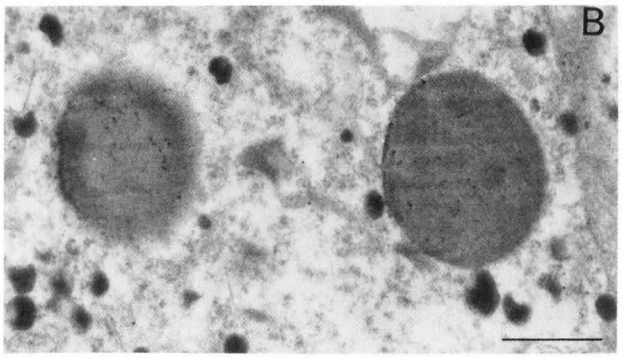

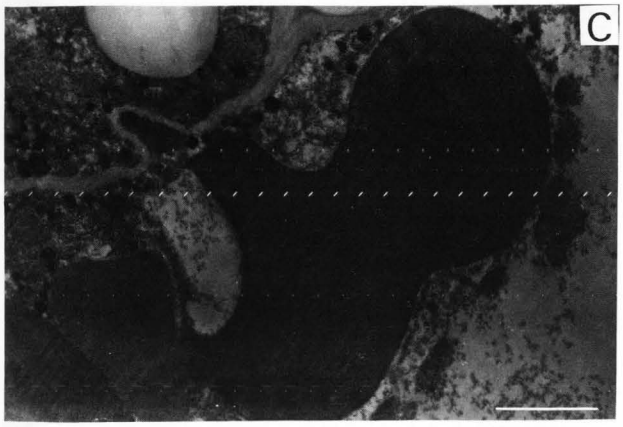

Figure 5 TEM micrographs of PLS body formation
A) PLS body with phagosytosing irregular membrane. B) Right PLS body has limiting membrane but left one does not. C) Coalescence of PLS bodies and protein deposits.
Bar of each micrograph equals 500 nm.
Figure 6. TEM micrographs of PLS body transformation. (below)
A) Note PLS bodies which lose their circular shape and become heterogenous.
B) PLS body invaginates cytoplasmic materials. Note rough ER with enlarged cisternae.
C) PLS body invaginates.
D) Bodies cannot be distinguished from vacuoles with protein deposits and developing protein bodies.
Magnification for all figures as in Fig. 6D.

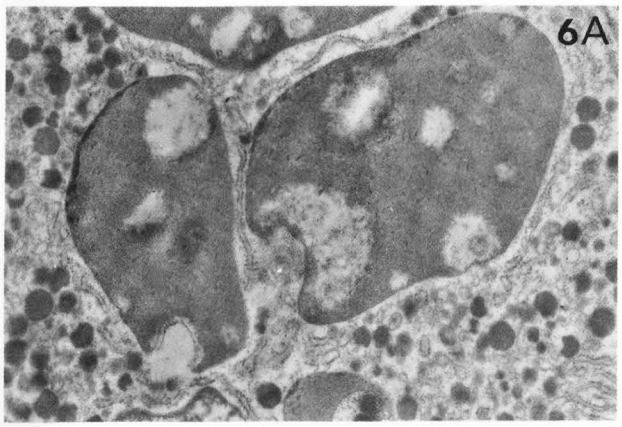

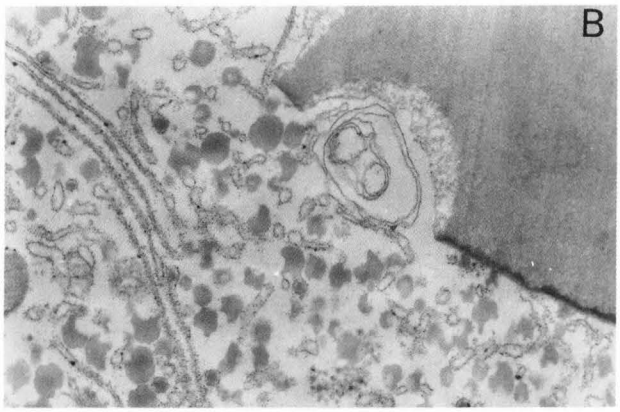

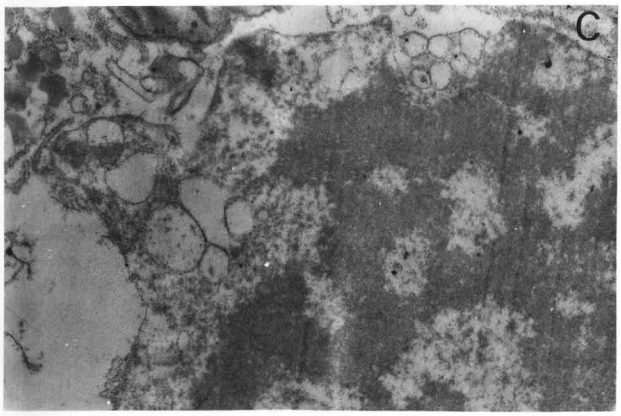

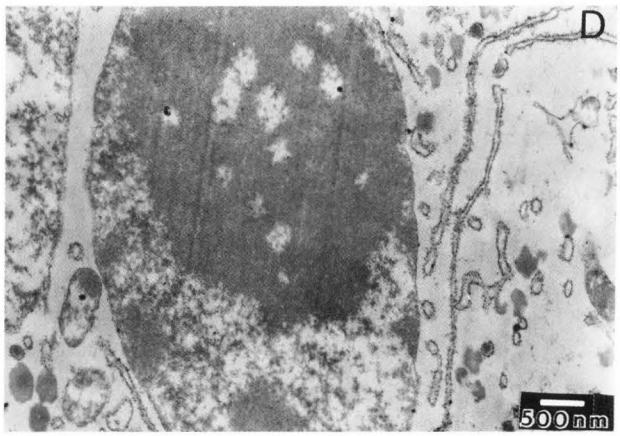

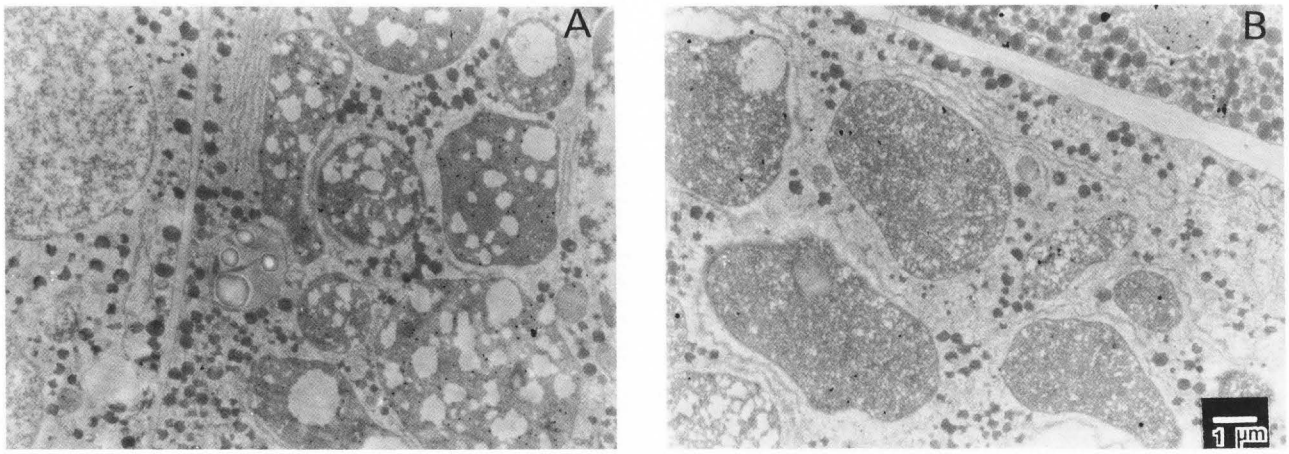

Figure 7. TEM micrographs of immature protein bodies.
A) Note the difference in protein bodies between right and left cells. The ones in right cell have many electron translucent parts while the ones in left have scattered protein deposits.
B) Protein bodies are not also homogeneous. Note long rough ER near protein bodies.
Magnification for both figures as in Fig. 7B.

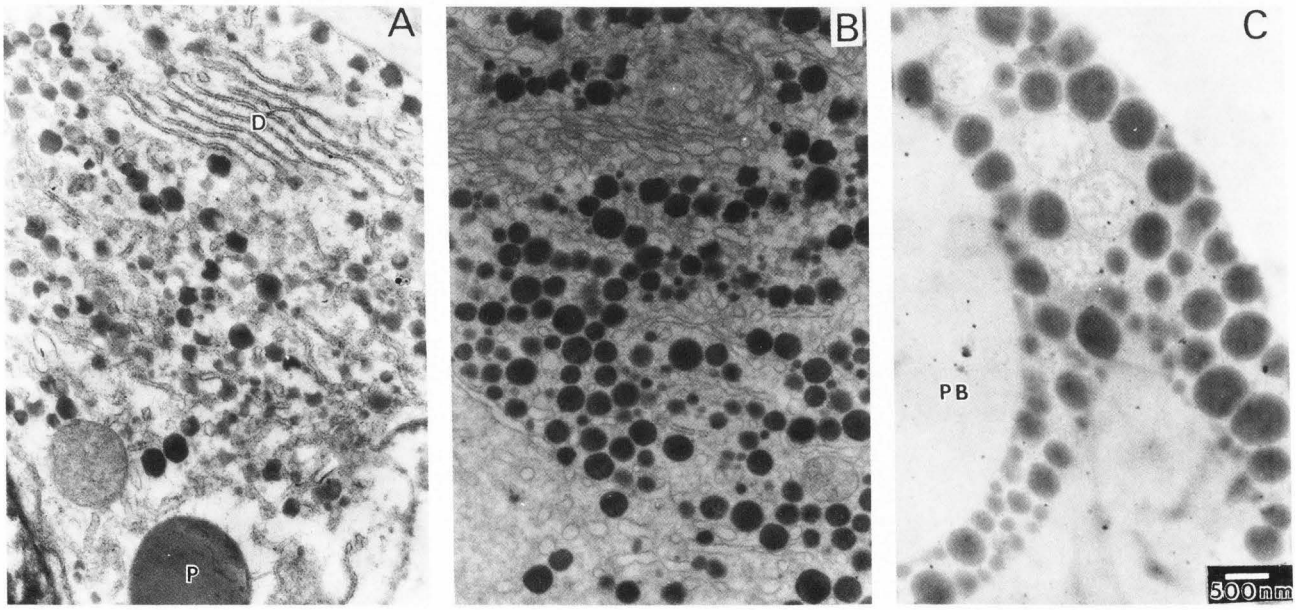

Figure 8. TEM micrographs of lipid bodies and ER in developing cotyledonary cells.
A) About 30 DAF. Note rough ER, dictyosome (D), number of lipid bodies and PLS body (P).
B) About 40 DAF. Note rough ER with enlarged cisternae and lumen, and lipid bodies increased in size.
C) About 55 DAF. Note protein body (PB) which has lost osmiophilic intensity.
Magnification is same on figures 8A, B, and C.

smaller vacuoles and it was difficult to distinguish between transformed PLS bodies, divided vacuoles and protein bodies. At this stage, abundant dictyosomes and rough ER were observed in the cytoplasm. Rough ER was markedly extended with cisternae (Figs. 6A, 6C, 6D) and often surrounded or located near vacuoles and PLS bodies (Figs. 6A, 6D).

TEM micrographs in Figure 7 were selected from electron micrographs of soybean cotyledons harvested on September 12 to 17 (35-40 DAF). Most cells contained various protein bodies of varying shapes and sizes. Lipid bodies increased in size and in osmiophilic intensity. Plastids were decreased rapidly in number and in size. Abundant rough ER and a small number of minute vacuoles were in the cytoplasm. After this stage of development, protein bodies became homogeneous in appearance with the completion of protein accumulation. In the 55 DAF and 60 DAF specimens, numerous lipid bodies were aligned along cell walls (Fig. 4G).

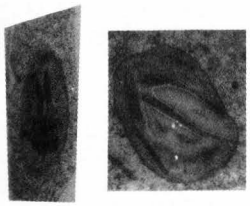

A. 15-20 DAF
Note small grana.

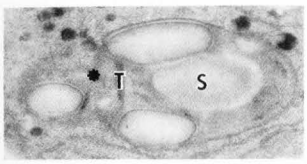

B. About 20 DAF
starch grain (S)
and thylakoid (T).
Plastid is dividing(*).

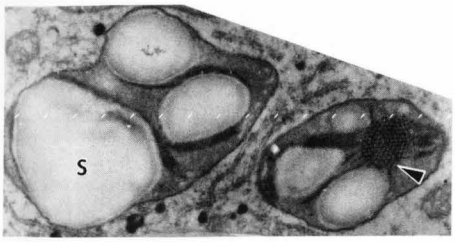

C. About
25 DAF
Note
proplastid
(arrow)
and starch
grains (S)

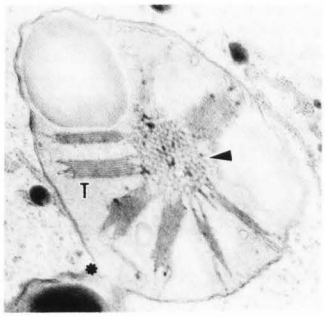

D. About
25-30 DAF
Note well-
developed
proplastid
(arrow) and
extended
radical
thylakoids(T)
divided into
two plastids
(*)

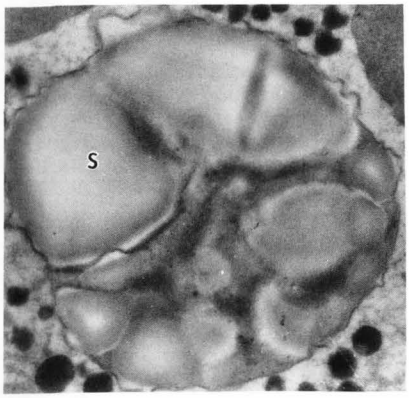

E. About
35-45 DAF
Note well-
developed
starch
grains (S)

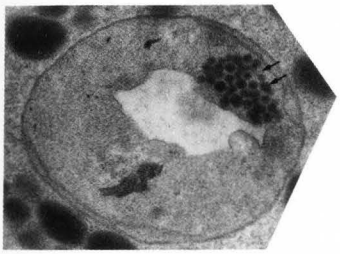

F. About
50-55 DAF
Note oil drop-
lets (small
arrows) near
vacuole-like
structure

Figure 9.
TEM micrographs of plastids in developing soybean cotyledonary cells.

Figure 8 shows changes of lipid bodies and ER in developing soybean cotyledons. After 25 DAF, the lipid bodies increased in size and numbers in accordance with more developed rough ER with abundant attached ribosomes and dictyosomes (Fig. 8A). At 40 DAF the lipid bodies assumed a more circular shape (Fig. 8B) than was noted earlier and numerous rough ER had developed cisternae. In the final stage of development some lipid bodies had continued to increase in size and also tended to attach to protein bodies as well as cell walls (Fig. 8C). The lipid bodies retained their osmiophilic intensity up to the final development stage. In this respect soybean lipid bodies differ from those of mustard (Rest and Vaughan, 1972, Bergfeld et al. 1980) and winged bean (Saio et al, 1983) which become less osmiophilic as the seed matures. Soybean lipid bodies are also smaller in size than those of mustard and those of sunflowers.

Changes in the plastids during development of soybean cotyledons are summarized in Figure 9. In early development, small plastids with only grana structure (Fig. 9A), were located in cytoplasm attached to cell walls. They increased in size and in number as time progressed, and some were undergoing division (Fig. 9B, mark *). Thylakoids were clearly recognized inside the plastids. The plastids became more numerous and increased in size and number. Centrally located proplastids were also observed (Figs. 9C-D). The plastids then reached almost maximum numbers and the starch grains enlarged in accordance with the reduction of the grana structure (Fig. 9E). At about 40 DAF the size of plastids was maximum at 5 μm. After 45 to 50 DAF, the plastids rapidly decreased in number accompanied by disappearance of the starch grains and appearance of small oil droplets (electron dense spheres, Fig. 9F) near the vacuole-like structure. Bilayered membranes bounding plastids were observed throughout the developing period and they were often surrounded by rough ER.

Examination of our electron micrographs reveals phenomena quite similar to those described by others for mustard, broad bean, and cowpea except for the formation of the PLS bodies. Our data offer some support for the hypothesis that protein bodies are derived from vacuoles, even if the biosynthesis of storage protein takes place in rough ER and dictyosomes. However, additional work will be necessary to establish this hypothesis more clearly.

Parallel to this microscopic study, we have also investigated changes in protein components by means of ultracentrifugation, SDS-electrophoresis, and incorporation of radioactive leucine and acetylglucosamine. A noteworthy observation that we made is that the stage of PLS body transformation coincided with the change from the formation of only α- and α'-subunits of 7S protein to the appearance of 11S protein and the β-subunit of 7S protein. These studies will be reported in detail elsewhere.

Acknowledgement

The authors thank Dr. I. Watanabe, Agriculture Forestry and Fisheries Research Council Secretariat, for his cultivation of the soybeans and also for his advice on crop production.

References

1) Adler,K. and Müntz,K. (1983) Origin and development of protein bodies in cotyledons of Vicia faba Planta **157**, 401-410.
2) Bergfeld,R., Kühnl,T. and Schpfer,P. (1980) Formation of protein storage bodies during embryogenesis in cotyledons of Sinapis alba L. Planta **148**, 146-156.
3) Bils,R.F. and Howell,R.W. (1963). Biochemical and cytological changes in developing soybean cotyledons, Crop Sci. **3**, 304-308.
4) Burr,B. and Burr,F.A. (1976) Zein synthesis in maize endosperm by polyribosomes attached to protein bodies. Proc. Nat. Acad. Sci. USA **73**, 515-519.
5) Craig,S., Goodchild,D.J. and Miller,C. (1980). Structural aspects of protein accumulation in developing pea cotyledons II. Three-dimensional reconstructions of vacuoles and protein bodies from serial sections. Aust. J. Plant Physiol. **7**, 329-337.
6) Dieckert J.W. and Dieckert M.Y.C. (1976) The chemistry and cell biology of the vacuolar proteins of seeds. J. Food Sci. **41**, 475-482.
7) Higgins,T.J.V. and Spencer,D. (1981) Precursor forms of pea vicilin subunits. Modification by microsomal membranes during cell-free translation. Plant Physiol. **67**, 205-211.
8) Kaizuma,N. and Kasai,A. (1981). On the morphology of protein body and spherosome in soybean cotyledon cell. Japan J. Breed. **31**, (Suppl. 1) 222-223.
9) Kaizuma,N. and Sato,Y. (1983) Genetical studies on protein body development in soybean cotyledon cells. 3. Protein molecule species contained in nucleo-globules and incorporation of ^{3}H-leucine into them. Japan J. Breed. **33**, (Suppl. 1) 320-321.
10) Millerd,A. (1975) Biochemistry of legume seed proteins. Ann. Rev. Plant Physiol. **26**, 53-72.
11) Norby,S.W., Adams, C.A. and Rinne,R.W. (1984) An ultrastructural study of soybean seed development. University of Illinois at Urbana-Champaign,Department of Agronomy,Urbana,IL.p.36.
12) Pernollet, J.-C. (1978) Protein bodies of seeds: Ultrastructure, biochemistry, biosynthesis and degradation. Phytochemistry **17**, 1473-1480.
13) Rest,J.A. and Vaughan,J.G. (1972). The development of protein and oil bodies in the seed of Sinapis alba L. Planta **105**, 245-262.
14) Saio,K., Nakano,Y. and Uemoto,S., (1983) Microstructure of winged beans. Food Microstructure **2**, 175-181.
15) Sato,Y., Kaizuma,N and Kitamura K. (1982). Genetical studies on protein body development in soybean cotyledon cells. 2. Isolation and characterization of RNA-body. Japan J. Breed. **32** (Suppl. 1) 94-95.
16) Weber,E. and Neumann,D.(1980) Protein bodies, storage organelles in plant seeds. Biochem, Physiol. Pflanz. **175**, 279-306.
17) Yoo,B.Y. and Chrispeels,M.J. (1980). The origin of protein bodies in developing soybean cotyledons. Protoplasma **103**, 201-204.

Discussion with Reviewers

W.J. Wolf: Several of the micrographs in Figure 6 suggest degradation of the PLS bodies rather than mere invagination of the membrane.In Fig.6B, for example, part of the membrane is clearly missing and the PLS body has a ragged gouge in this area. Has digestion caused this partial degradation?
Authors: It is very difficult to explain total degradation and transformation processes of PLS bodies, since we cannot observe the changes of a PLS body under TEM with passing time. We do not think that the transformation is merely invagination of the membrane. Actually, PLS bodies which show partial degradation cannot easily be distinguished from protein bodies which do not complete protein accumulation.

D.J. Gallant: Figure 9 shows the evolution from the proplastid and young amyloplast to the chloroamyloplast and/or to the chromoplast, that is the normal evolution of the chloroplast or the amyloplast in many colored plant organs. In the case of your samples, are such structures related to the brown or the red series of the seeds? Did you find such organelles in the cotyledon cells of non pigmented soybean varieties?
Authors: Brown or red series refers to the color of the tags which were placed through the floral axes. The variety used, Enrei, is an ordinary soybean variety which is greenish in developing but changes to yellowish after maturation. These structures were already found in previous papers (ref. 11, for example). We used the word plastid, which encompasses organologically parallel organs such as chloroplasts, amyloplasts etc.

L.H. Bragg: What is the significance of the alignment of protein bodies and lipid bodies along the surface of other organelles and along the inner surface of the cell wall in the development process?
Authors: In a paper by Wolf and Baker (Scanning electron microscopy of soybeans and soybean protein products. Scanning Electron Microsc. 1980; III: 621-634.), SEM micrographs of protein bodies in mature soybeans show many depressions on the surface of the membrane which look like imprints caused by the alignment of lipid bodies. The alignment may not relate to development mechanisms but may result from dehydration during maturation.

FOOD MICROSTRUCTURE, Vol. 4 (1985), pp. 199-211
SEM Inc., AMF O'Hare (Chicago), IL 60666-0507 U.S.A.

0730-5419/85$1.00+.05

RHEOLOGICAL AND ULTRASTRUCTURAL STUDIES OF WHEAT KERNEL BEHAVIOUR UNDER COMPRESSION AS A FUNCTION OF WATER CONTENT

A. Al Saleh and D.J. Gallant

INSTITUT NATIONAL DE LA RECHERCHE AGRONOMIQUE
Laboratoire de Technologie des Aliments des Animaux
Unité Microscopie
rue de la Géraudière - 44072 Nantes cedex, France

Abstract

The rheological behaviour of two wheat varieties (Triticum durum), cultivated at different sites, was studied by INSTRON* as a function of water content. Patterns of crushed grains were investigated by scanning electron microscopy. The apparent modulus of elasticity of the wheat grains was apparently related to their vitreosity. The mealy grain generally had an apparent modulus of elasticity lower than that of the vitreous one and the modulus appeared to be related to the air spaces in mealy endosperm. Humidification favoured the conversion of vitreous endosperm to the mealy state. Grain morphology and particularly the kernel crease played an important role during grain crushing.

Initial paper received March 31 1985
Manuscript received October 04 1985
Direct inquiries to D.J. Gallant
Telephone number: 33 40 76 23 64

Key Words : Apparent modulus of elasticity, crushing, image analysis, scanning electron microscopy, vitreosity, water content, wheat grain.

*Instron Universal Testing Instrument, Model 1122.

Introduction

The final products of the milling process (flour, semolina, etc.) and baking are related to a number of factors including the grinding quality of wheat grains. The aim of milling is to remove the endosperm from bran. The endosperm is transformed into semolina and the bran should be kept in large flakes to aid its separation from the semolina particles.

In flourmilling, wheat grains pass a number of times between different fluted rolls in the break system and then through the smooth reduction rolls. Then, it becomes impossible to separate any endosperm particle without crushing the bran into fine particles which would contaminate the flour and modify the color and texture of bread (Lockwood, 1950). Best grinding is the process which produces mainly coarse semolina and large bran flakes. Wheat variety, water content, hardness and vitreosity of grain are all factors affecting milling quality.

In milling the following mechanical actions take place :

- shear : in breakmilling, this phenomenon occurs because of the difference in peripheral speeds of the rolls. The wheat grain is held by the grooves of the slow roll whilst the grooves of the fast roll exercise a cutting action (shear) on the grain;
- compression : compression is used to reduce the semolina to flour. This mechanism of fragmentation occurs mainly in the reduction system.

In recent years, many workers have investigated wheat grain hardness. Barlow et al. (1973) have used a micropenetrometer (Leitz Miniload hardness tester) to measure the hardness of starch and protein separately. Simmonds et al. (1973) suggested that adhesion between starch and storage protein was a more important factor in determining wheat grain hardness than the protein matrix composition. Stenvert and Kingswood (1977) found that the wheat hardness was determined by the physical structure of the endosperm protein matrix. Moss et al. (1980) concluded that the manner in which the wheat grain fractured was determined by hardness and water content of the grain. Yamazaki and Donelson (1983) used the particle size index (PSI) to express wheat hardness as a function of protein content.

Table 1. Site of culture and initial water content of selecteo varieties.

Variety	Agathe 3002	Agathe 1023	Agathe 1093	Mondur 1021	Mondur 1091
Site of culture	Montpellier	Montbartier	Fourques	Montbartier	Fourques
Initial water content % DM	11.0	11.0	12.5	11.5	13.7

Until now, grain vitreosity has not been investigated sufficiently. The aim of this study was to investigate the role of grain vitreosity and water content on rheological behaviour of wheat under uniaxial compression. Crushed grain particles were studied microscopically to determine the changes in physical structure during grinding.

Materials and Methods

Two wheat varieties (Triticum durum L.), Agathe and Mondur harvested in 1982 were studied. Agathe was cultivated in three different regions of France, whereas Mondur was cultivated only in two regions (table 1). Ecological factors influenced the physical characteristics of harvested grains.

The study of wheat grain fragmentation was carried out over a range of conditioning moisture levels between 10.0 and 17.5%. The water content of the grain was determined by the French standard method NF-V/03-701. After harvesting, the water content of the varieties varied between 11.0 and 13.7% (table 1). The samples were desorbed to about 9% water content with phosphorus pentoxide under vacuum (Al Saleh et al., 1984). To obtain a uniform water content for all grains within every sample, the samples held for 5 days prior to the determination of water content. Each sample was divided into 4 portions. Portions were equilibrated to 10.0, 13.8, 16.7 and 17.5 % water content using saturated saline solution (Multon et al., 1980). Wheat grain vitreosity was determined at 10.0% water content, by the Pohl grain cutter (Al Saleh et al., 1984).

Measurement of wheat grain apparent modulus of elasticity

The Instron Universal Testing Instrument, Model 1122, was used to carry out the apparent modulus of elasticity determination. Forty six grains of each sample were taken at random, then positioned individually between the plates of the Instron instrument so that the crease was down (fig. 1). To minimize the effect of the crease on the behaviour of the grain during the compression, a piece of silicon carbide adhesive paper (Transfol-N° 400 - STRUERS Cie) was used to avoid lateral displacement of the grain (thin arrows, fig. 1). The apparent modulus of elasticity was measured under the following conditions: the wheat grains were submitted to five successive identical compressions, the loading rate was 0.05 mm/min and the maximum load reached 500g. Preliminary loading-unloading tests showed

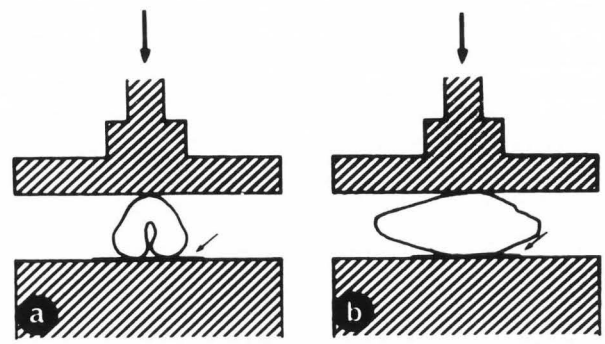

Fig. 1. Transversal and longitudinal views of a wheat grain loaded between two plates of the INSTRON.

that wheat grain deformation was approximately linear. Therefore, the behaviour of the wheat grains was considered to be Hookean. These observations are in agreement with those of Shelef and Mohsenin (1967) and Multon et al. (1981).

Calculation of apparent modulus of elasticity

We adopted Hertz's solution for the contact stresses between two elastic bodies submitted to uniaxial compression to calculate the apparent modulus of elasticity. According to Kozma and Cunningham (1962), who reviewed Hertz's solution, the material must be homogeneous, the contacting bodies must be large, and the radii of curvature, illustrated in fig. 2, must be very large when compared with the dimensions of the contact area. The study of Morrow and Mohsenin (1966) showed that the previous assumptions were applicable in the case of wheat grains. To determine the apparent modulus of elasticity, Arnold and Roberts (1969) showed that the utilization of uniaxial compression on the whole grain gave the best results.

Using the simplified Hertz equation that takes into consideration the geometrical characteristics of the wheat kernel (length, width and thickness), the apparent modulus of elasticity was calculated :

$$E = \frac{0.5\ P\ (1 - U)^2}{D_T^{\ 3/2}} \cdot \left[\frac{1}{R_1} + \frac{1}{R_1'} \right]^{\frac{1}{2}}$$

E : apparent modulus of elasticity
P : applied compressive load
U : Poisson's ratio

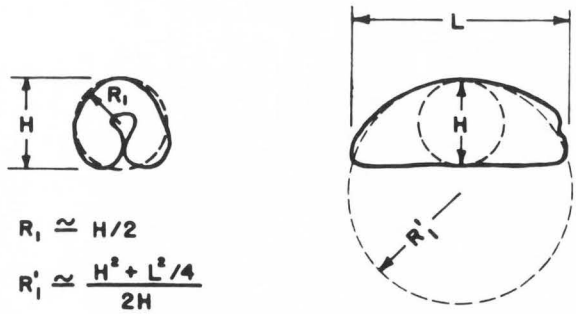

Fig. 2. Approximation of R_1 and R'_1 for wheat grain (after Mohsenin, 1978).

D_T : total grain deformation
R_1, R'_1 : principal radii of the grain at the contact surface.

Shelef and Mohsenin (1967) showed that the total deformation D_T within the linear range of the loading-unloading curve consisted of residual deformation D_r and elastic deformation D_e. Our preliminary tests showed that the residual deformation became practically constant after the fourth loading-unloading cycle (fig. 3). For that reason, in the apparent modulus of elasticity calculation we used the average of the fourth and the fifth loading-unloading cycles.

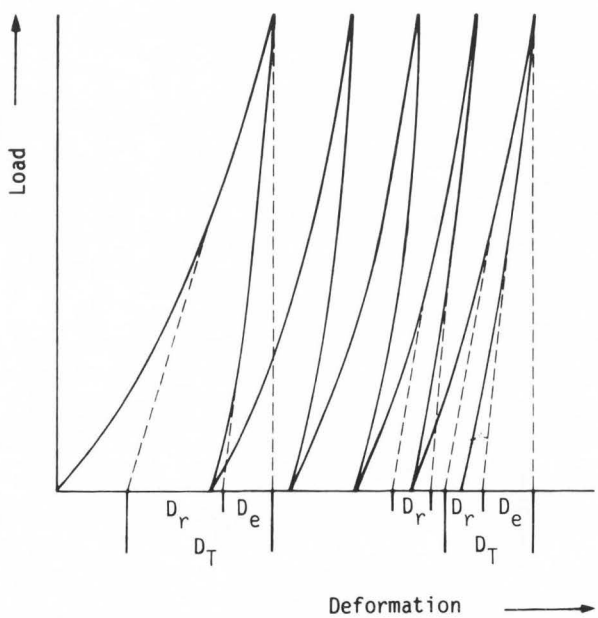

Fig. 3. Load-deformation curves : stability in the two last cycles utilized for the modulus of elasticity calculation.

Wheat grain crushing

Wheat grain crushing was performed immediately after the measurement of elasticity, each grain staying in the same position. The crushing conditions were: load rate 1 mm/min, maximum load 50 kg. The general shape of the load-deformation curve is represented in figure 4.

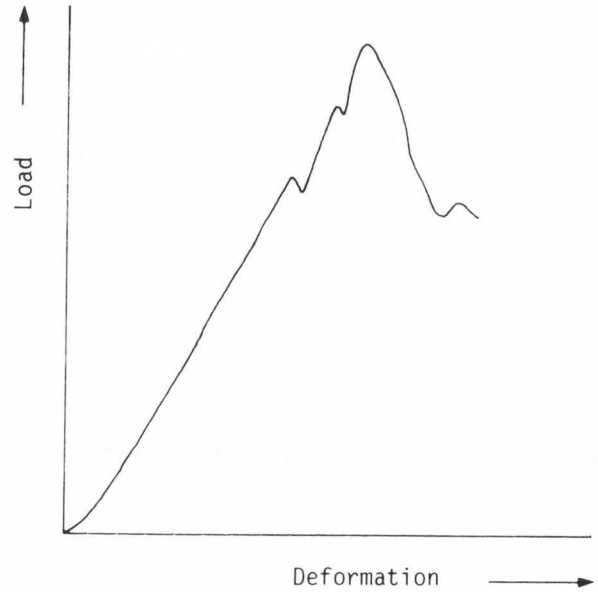

Fig. 4. General aspect of crushing load-deformation curve.

Scanning electron microscopy

After crushing, surfaces produced by INSTRON fracturing were coated with a thin layer of gold (40 nm) and observed with the scanning electron microscope (JEOL 50A). Many fragments were investigated from all samples. The general appearance of the crushed grain was observed with an accelerating voltage of 10 keV, whereas grain ultrastructure was observed under 20 keV.

Statistical analysis of images

A semi-automatic image analyser composed of a Kontron digiplan (Reichert Jung) MOP 1 interfaced with a microcomputer (Commodore CBM 3032) was used on enlarged (7.75X) photographs.

Results and Discussion

Vitreosity

The mean vitreosity values of the different varieties indicated (table 2): (i) there is a significant difference between the vitreosity values of the same variety cultivated in different geographical regions; and (ii) at most sites, the variety Agathe is more vitreous than the variety Mondur.

Table 2. Vitreosity of selected wheat grain varieties.

Variety	Agathe 3002	Agathe 1023	Agathe 1093	Mondur 1021	Mondur 1091
Vitreosity %	98.8	97.9	77.7	95.2	46.8

Apparent modulus of elasticity of wheat grain

Agathe 3002. The apparent modulus of elasticity of Agathe 3002 (10% water content) shows a normal distribution (fig. 5 a). At 13.8% water

Table 3. Mean apparent modulus of elasticity ($E.10^{10}$ dynes/cm^2).

Water Content %DM \ Variety	Agathe 3002	Agathe 1023	Mondur 1021	Agathe 1093	Mondur 1091
10.0	2.16±0.06	1.60±0.05	1.72±0.04	1.95±0.09	1.57±0.07
13.8	2.06±0.05	1.59±0.05	1.69±0.04	1.89±0.07	1.53±0.06
16.7	1.96±0.06	1.47±0.04	1.55±0.05	1.77±0.06	1.34±0.05
17.5	1.79±0.05	1.37±0.04	1.49±0.05	1.75±0.05	1.27±0.03

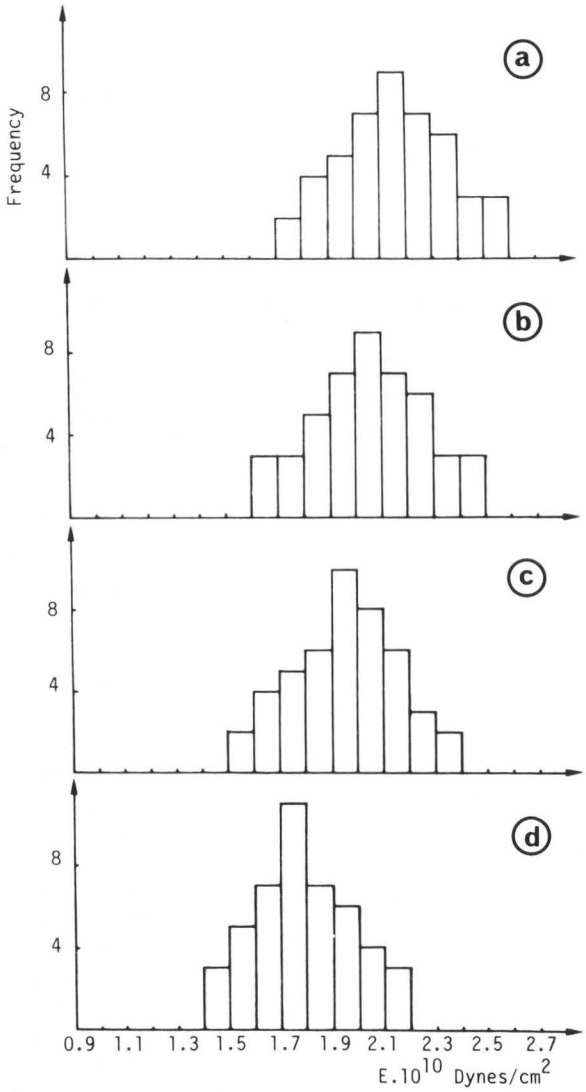

Fig. 5. Histograms of the apparent modulus of elasticity of Agathe 3002 at: a) 10.0%; b) 13.8%; c) 16.7% and d) 17.5% water contents.

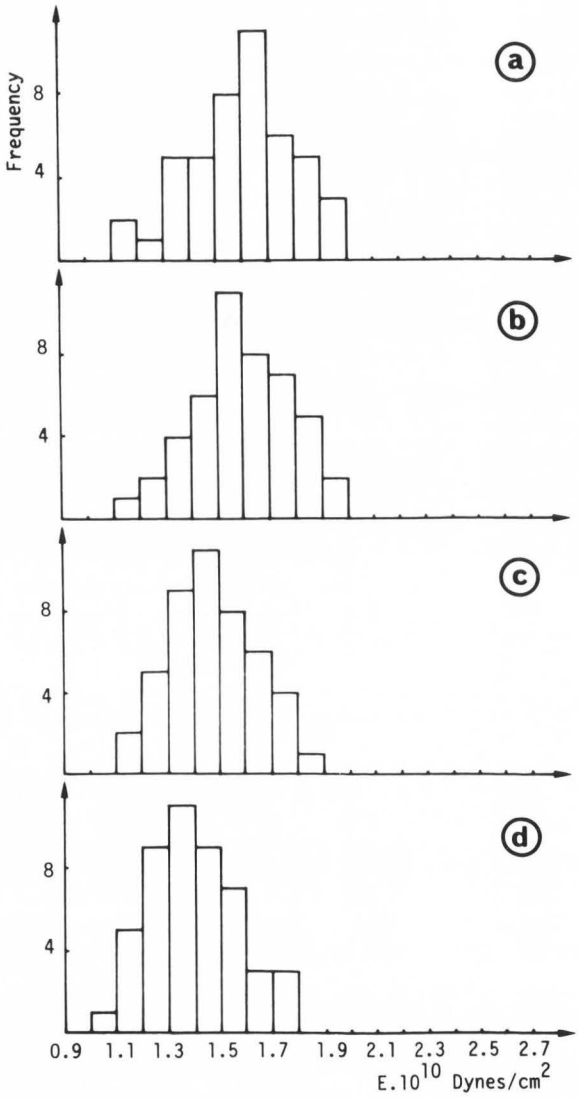

Fig. 6. Histograms of the apparent modulus of elasticity of Agathe 1023 at: a) 10.0%; b) 13.8%; c) 16.7% and d) 17.5% water contents.

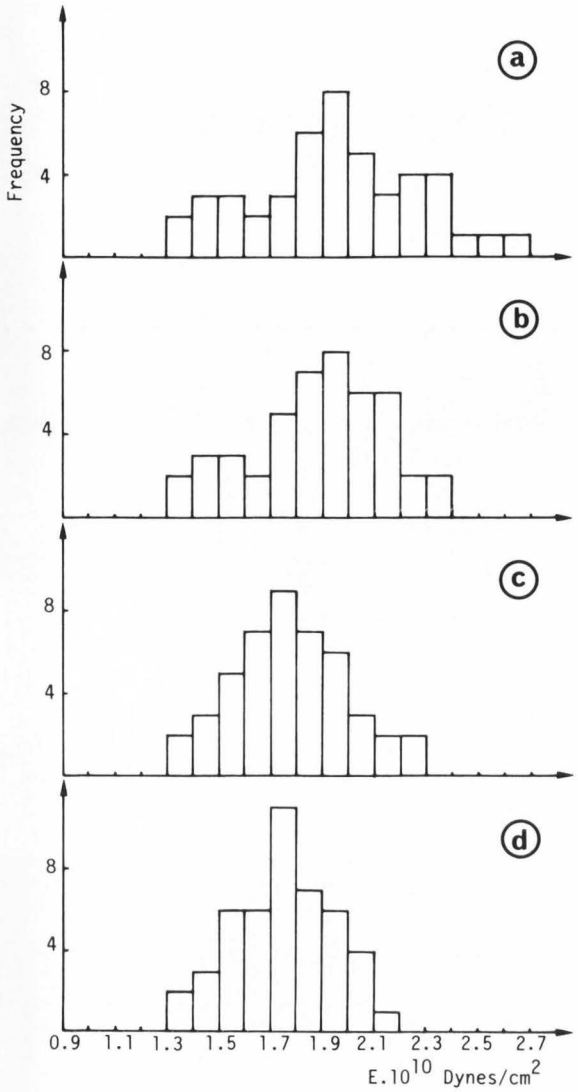

Fig. 7. Histograms of the apparent modulus of elasticity of Agathe 1093 at: a) 10.0%; b) 13.8%; c)16.7% and d) 17.5% water contents.

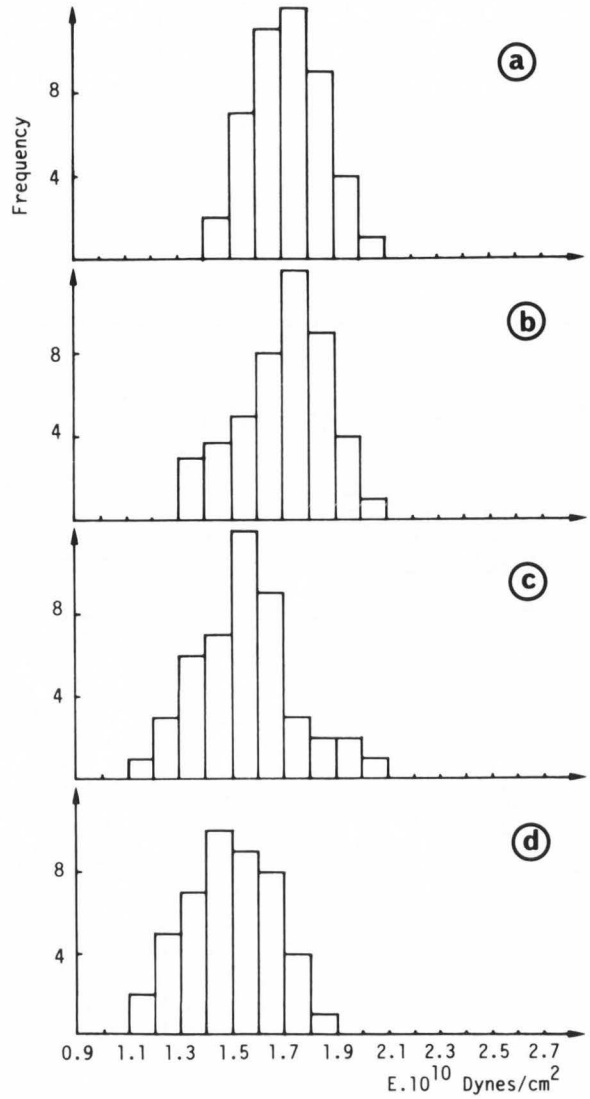

Fig. 8. Histograms of the apparent modulus of elasticity of Mondur 1021 at: a) 10.0%; b) 13.8%; c)16.7% and d) 17.5% water contents.

content the histogram (fig. 5 b) has an appearance similar to that of the preceding histogram, but it undergoes a slight shift towards the low end on the elasticity scale. This trend is repeated at high moisture levels and is a function of the water content (fig. 5 c). The mean value of the modulus of elasticity decreased by 3.7×10^9 dynes/cm^2 as the water content increased from 10.0 to 17.5% (table 3).

Statistical calculations showed that the difference between the mean values of the different moduli of elasticity was significant.

Agathe 1023. This is a vitreous variety (table 2) for which the values of the apparent modulus of elasticity at 10.0% water content (fig. 6 a), were distributed between 1.1×10^{10} and 2.0×10^{10} dynes/cm^2. This distribution stayed practically the same with 13.8% water content (fig. 6 b). With increasing water content there was a reduction in the mean value of the apparent modulus of elasticity (figs. 6 c, d). At 17.5% water content the reduction in mean value was 16% (table 3).

Agathe 1093. The wheat grains of Agathe 1093 can be divided into three categories: mealy, intermediate and vitreous. Each one of these categories corresponds to a part of the histogram figure 7a. The mealy wheat grains are represented by the values of the apparent modulus of elasticity lower than 1.6×10^{10} dynes/cm^2. The vitreous wheat grains are represented by the values greater than 2.1×10^{10} dynes/cm^2, whereas the values between 1.6×10^{10} dynes/cm^2 and 2.1×10^{10} dynes/cm^2 represent the intermediate wheat grains. The increase in the water content from 10.0 to 13.8% produces a diminution of the values of the apparent modulus of elasticity,

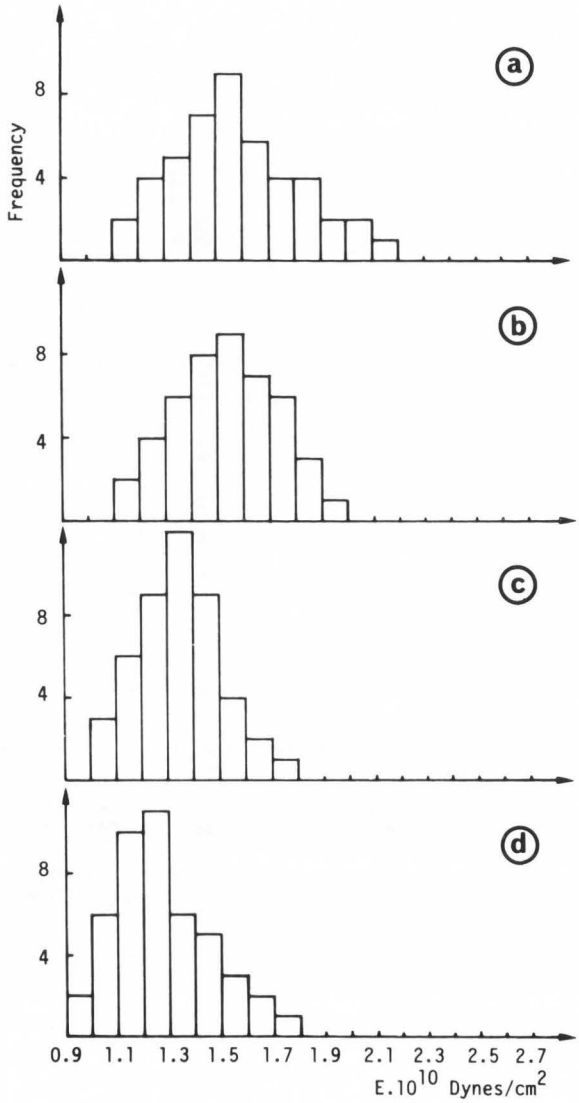

Fig. 9. Histograms of the apparent modulus of elasticity of Mondur 1091 at: a) 10.0%; b) 13.8%; c)16.7% and d) 17.5% water contents.

particularly, that part representing the vitreous grains (fig. 7 b). The largest decrease of the apparent modulus of elasticity corresponded to vitreous wheat grains indicating that they are more sensitive to variations in water content. Grain humidification initiated the amalgamation of the original three categories of wheat types (fig. 7 b). At 16.7% water content there was only one grain population. This trend was mainly due to the reduction of the apparent modulus of elasticity of the vitreous and intermediate wheat grains. At 17.5% water content, the distribution of the values of the apparent modulus of elasticity was approximately Gaussian (fig. 7 d). The increase in water content from 10.0 to 17.5% produced a decrease in the mean value of the apparent modulus of approximately 2 x 10^9 dynes/cm^2 (table 3).

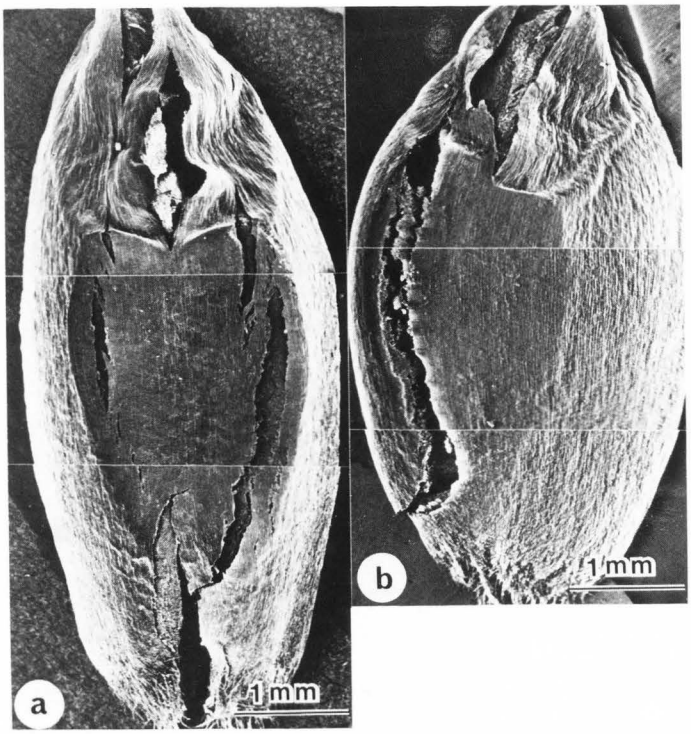

Fig. 10. Vitreous wheat grain crushed (Agathe 1093) at 10.0 % (a) and 16.7 % water content (b), showing grain crushing mode.

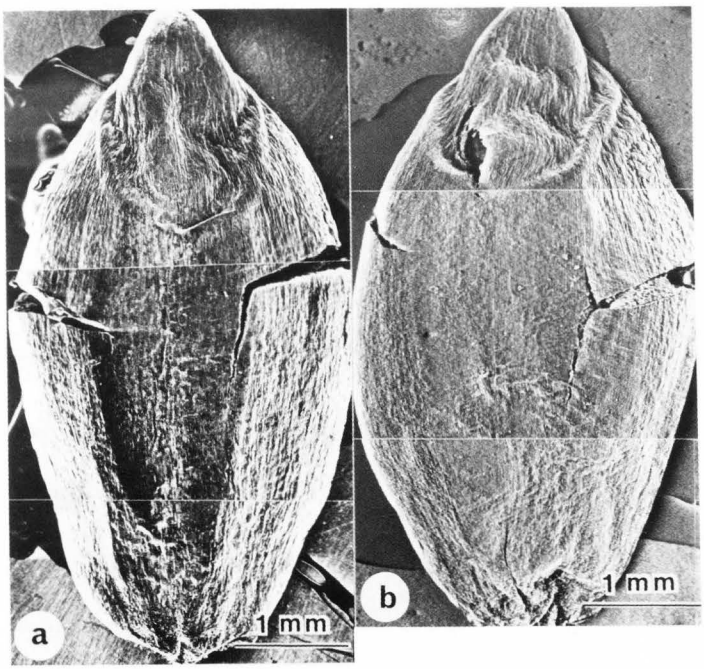

Fig. 11. Mealy wheat grain crushed (Mondur 1091) at 10.0% (a) and 16.7% water content (b), showing the fashion with which the grain crushed by INSTRON.

Table 4. Changes in endosperm texture in function of water content.

Variety	Agathe 3002		Agathe 1023		Mondur 1021		Agathe 1093		Mondur 1091	
Water content % DM	% surface area of mealy endosperm	% inter-mediate grains	% surface area of mealy endosperm	% inter-mediate grains	% surface area of mealy endosperm	% inter-mediate grains	% surface area of mealy endosperm	% inter-mediate grains	% surface area of mealy endosperm	% inter-mediate grains
10.0	1.9	6	3.9	26	4.4	19	20.2	42	63.5	92 2*
13.8	2.0	6	6.7	29	9.6	27	30.2	71	73.3	77 22*
16.7	2.8	9	12.2	57	19.8	64	37.6	82 4*	70.4	76 24*
17.5	6.5	26	15.7	63	18.8	80 2*	40.7	87 1*	72.3	70 30*
Vitreosity at 10% H_2O DM	98.8		97.9		95.2		77.7		46.8	

* % mealy whole grains.

Mondur 1021. In this vitreous variety, the values of the apparent modulus of elasticity were not altered to any appreciable content as the water content was increased from 10.0% to 13.8% (fig. 8 a, b). A significant decrease of the values of the apparent modulus of elasticity was only observed at 16.7% water content (fig. 8 c). This decrease was more marked at 17.5% water content (fig. 8 d). The difference between the mean value of the apparent modulus of elasticity at 10.0 and 17.5% water content was 0.23 x 10^{10} dynes/cm^2 (table 3).

Mondur 1091. This variety was the most mealy of those studied, and at 10.0% water content, it had the lowest mean value of the apparent modulus of elasticity (table 3). This mean value progressively decreased as the water content increased (fig. 9). A displacement of the whole histogram was observed (figs. 9 b, c). At 17.5% water content, the mean value of the apparent modulus of elasticity decreased at about 20% compared to that at 10.0% water content (table 3).

Statistical analysis of images

Agathe 3002. Humidification to 17.5% water content of Agathe 3002 grains increased the percentage of mealy endosperm area from 1.9 to 6.5% (table 4). This was at the expense of the vitreous area. The conversion of vitreous endosperm to mealy state also associated with an increase in the number of intermediate wheat grains from 6 to 26% when the water content increased from 10.0 to 17.5% (table 4). The change of endosperm texture from vitreous to mealy is a function of the water content and is responsible for the decrease in the apparent modulus of elasticity. This change appears to be due to the expansion of the protein matrix and starch of vitreous endosperm. But Agathe 3002 showed a high resistance to texture change because of the important compactness of its endosperm.

Agathe 1023. In this very vitreous variety, the percentage of mealy endosperm increased from 3.9 to 15.7% as the water content increased from 10.0 to 17.5% (table 4). At the same time, the percentage of intermediate grains increased by 37%.

Mondur 1021. This variety is also vitreous and the percentage of mealy endosperm increased by 14.4% as the water content increased from 10.0% to 17.5% (table 4). At the same time there was a four-fold increase in the number of intermediate grains. A comparison of the data for Agathe 3002 and Mondur 1021, showed that Mondur 1021 was more susceptible to the textural changes as a function of increased water content. This difference between the two varieties is related to vitreosity and is important in the technological processing of wheat grains.

Agathe 1093. The percentage of the vitreous endosperm in Agathe 1093 is dominant but its mean value decreased as a function of water content. The increase in water content enlarges the mealy endosperm areas. Above 16.7% water content, one observes the appearance of some completely mealy grains (table 4). At 17.5% water content, the intermediate grains reached the very high percentage of 87% (table 4).

Mondur 1091. Mealy endosperm predominated in Mondur 1091. The amount of mealy endosperm increased by 10% when the water content increased from 10.0 to 13.8%. However, a further increase in water content did not significantly increase the amount of mealy endosperm (maximum level

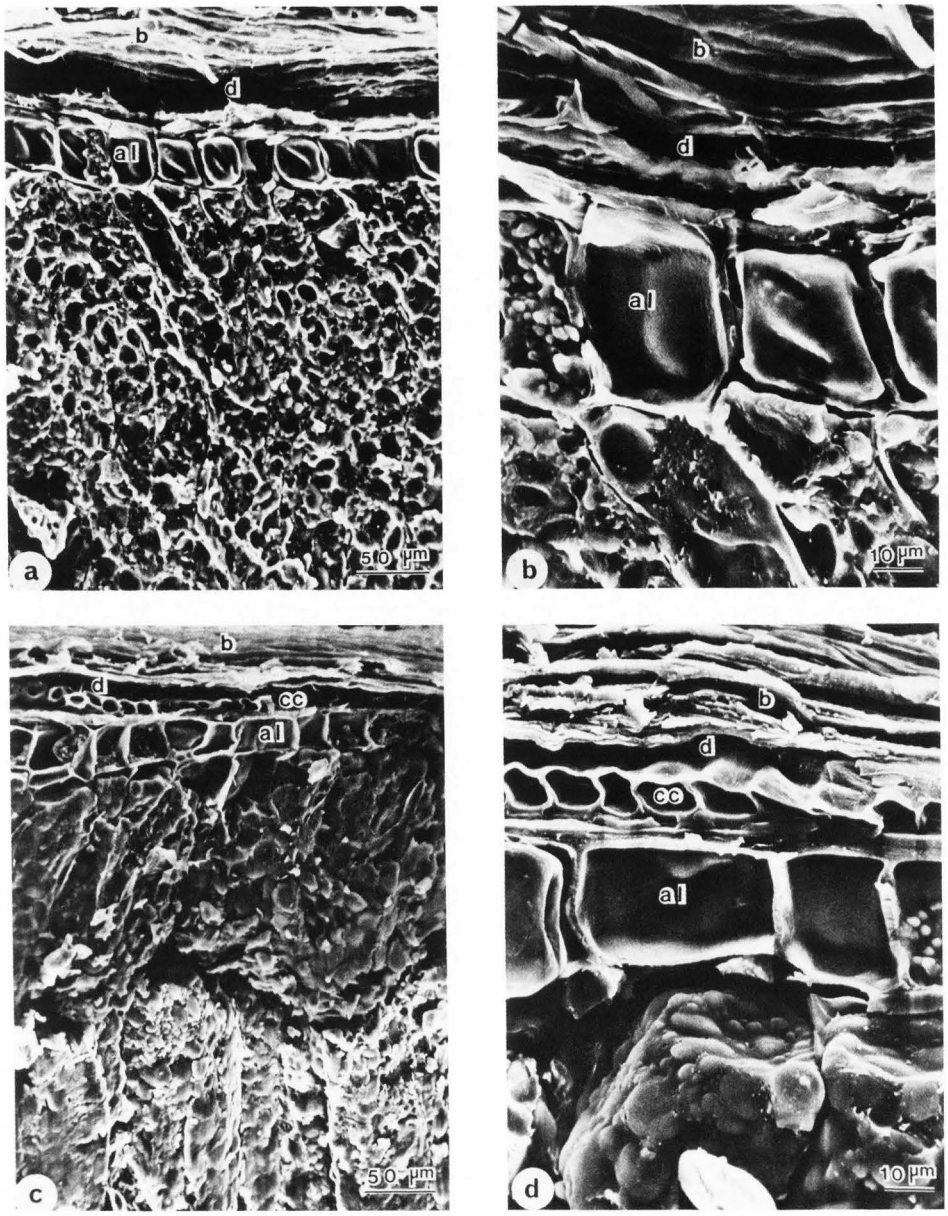

Fig. 12. Vitreous grains (Agathe 1023) at 13.8% water content (a and b), showing the bran grain detachment. Mealy grains (Mondur 1091) at 13.8% water content (c and d) showing the bran grain detachment. al : aleurone layer; as : air space; b : bran; c: cell; cc : cross cell; d : bran detachment; f : fracture; I : intact zone; P : proteic matrix; S : starch; Su : sub-aleurone layer; W : wall; Z : crushing zone.

approximately 72%). The decrease of the percentage of intermediate grains was due to the amalgamation of adjacent mealy spots. This conclusion was confirmed by the increase of the whole mealy grains from 2 to 30%.

SEM of crushed wheat grain

Whole crushed wheat grains. The most vitreous wheat grains crushed by the INSTRON, showed a longitudinal fragmentation along the major axis. This fragmentation pattern is shown in fig. 10a. Humidification did not change the fracture pattern of the vitreous grains during crushing. One observed a similarity between the aspect of the crushed wheat grain in the same variety at 10.0 and 16.7% water contents (figs. 10 a, b). The longitudinal fragmentation of vitreous wheat grain was principally caused by the morphology of vitreous grain. The deeper crease of the vitreous grains created a zone of low resistance to crushing.

In contrast, the mealy grains, represented by Mondur 1091, crushed transversally to the major axis (fig. 11 a). This difference between vitreous and mealy grain crushing relates also to the grain morphology, mealy grains being wider and the crease depth less than those of the

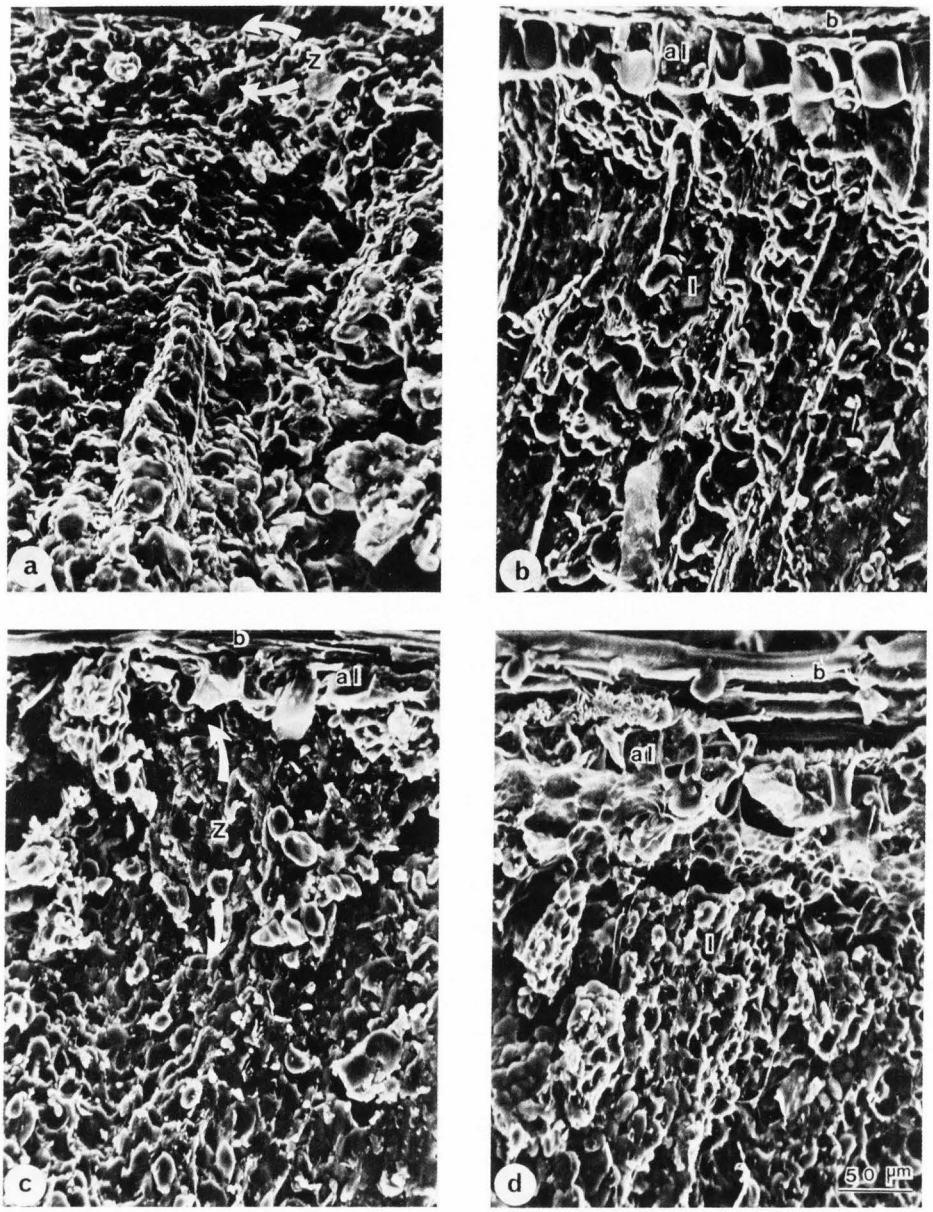

Fig. 13. Mealy endosperm (Mondur 1091) at 10.0% water content (a) showing the crushing zone when compared to non crushed zone at same water content (b). With higher water content (17.5%) the crushing zone is important (c); uncrushed zone at 17.5% water content (d). Same abbreviations as figure 12.

vitreous grains that favoured the lateral crushing (fig. 11 a). The increase in water content from 10.0 to 16.7% did not change the fracture pattern of the mealy grain, the grain only becoming flat (fig. 11 b).

Behaviour of wheat grain bran under compression. Compression applied to wheat grains at 13.8% water content caused detachment between the bran and the rest of the grain. This detachment was observed both in the vitreous variety, Agathe 1023 (figs. 12 a, b), and in the mealy one, Mondur 1091, particularly at the level of cross cells (figs. 12 c, d). This detachment is limited to the crushing zone. At high water content (17.5%), bran detachment was not observed.

Compression influence on wheat grain as a function of water content. Crushing the mealy grain Mondur 1091, produced disruptions in the endosperm. The appearance of the endosperm after crushing differed depending on grain water content. At low water content (10.0%), the structure of the crushed zone was totally disrupted (fig. 13 a). Compared to the undamaged zone (fig. 13 b) the crushed zone was not very deep. At higher water content (17.5%) the crushing zone was more extensive (figs. 13 c, d). Under compression, at the same water content, the vitreous grains such as Agathe 1023 behaved differently than the mealy grains such as Mondur 1091. Comparing the two

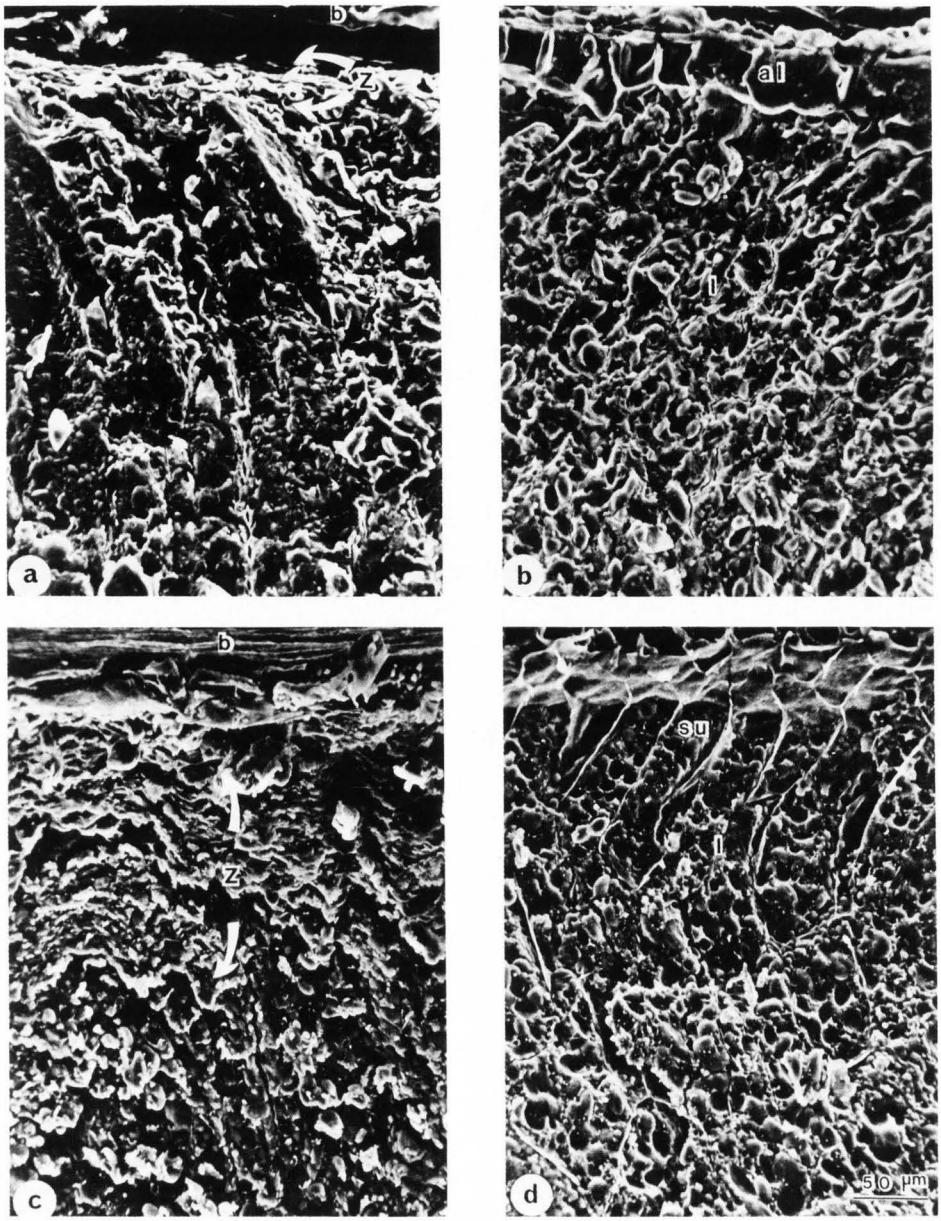

Fig. 14. Vitreous endosperm (Agathe 1023) at 10.0% water content (a), showing the very limited crushing zone compared with the intact zone (b). At 17.5% water content the crushed zone increased considerably (c); uncrushed endosperm grain (d).
Same abbreviations as figure 12.

photomicrographs a and b (fig. 14) representing Agathe 1023 at 10.0% water content, one observed that the crushed zone was limited to the aleurone layer, this limitation being caused by the low water content. However, at higher water content (17.5%) the crushed zone was larger (figs. 14 c, d).

Relation between endosperm crushing and vitreosity

Investigations of Agathe 3002, vitreous endosperm, outside the crushed zone showed that the first fissures occurred at the intercellular boundary (fig. 15 a). Similar data were observed in the other vitreous varieties such as Agathe 1023 (fig. 15 b). Therefore, cell walls play an essential role during wheat grain crushing. This is in accordance with the report of Moss et al. (1980) that the cell constituents (starch and protein) of vitreous wheats are very compact and the zones of weakness in the grain are the intercellular boundary. With increasing compression inter-cellular fissures spread within the cells.

The mealy endosperm showed a totally different fracture aspect than that observed in the

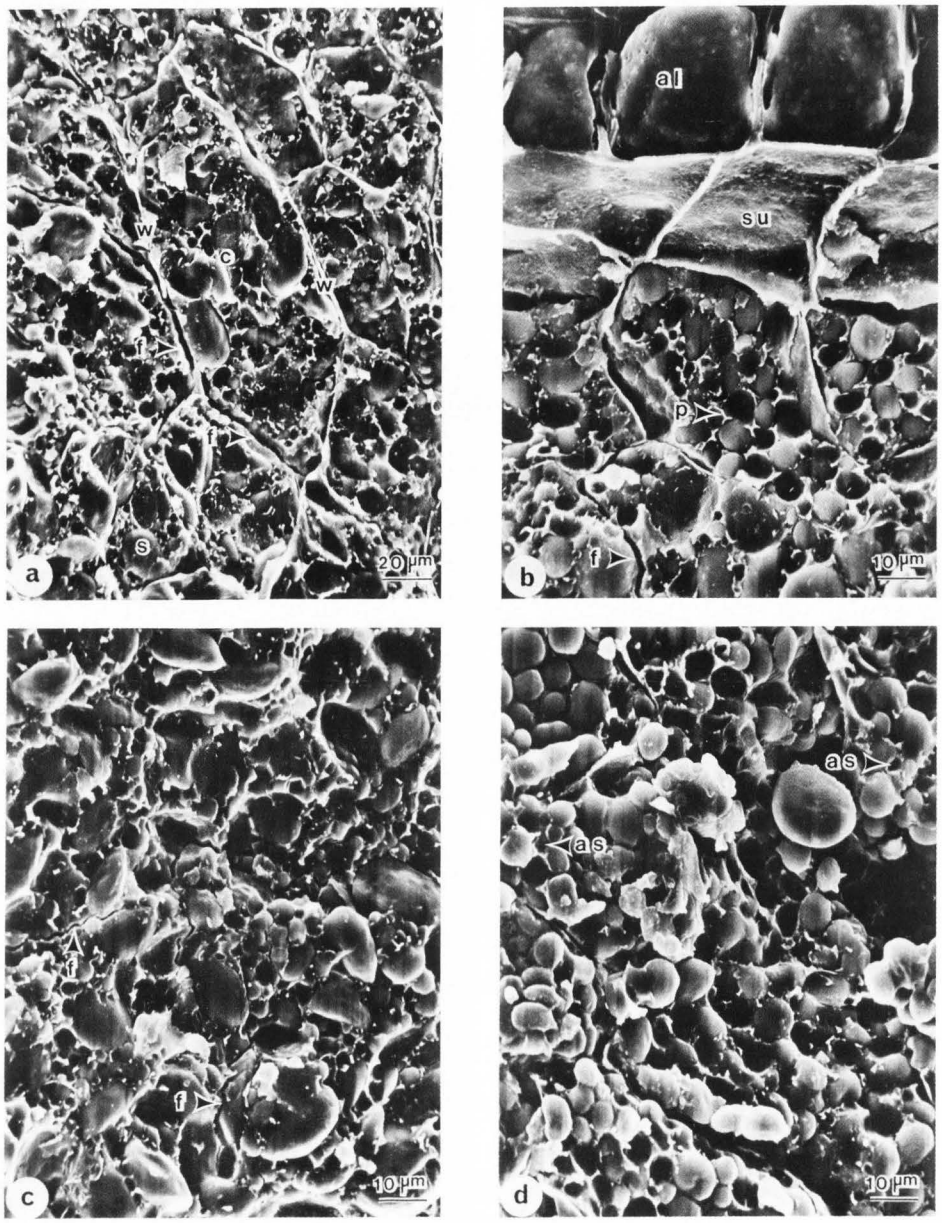

Fig. 15. Vitreous endosperm (Agathe 3002) at 17.5% water content, showing fractures at cell walls level; b) vitreous sub-aleurone (Agathe 1023) at 17.5% water content, showing inter cellular fractures; c) mealy endosperm (Agathe 1093) at 17.5% water content, showing fractures at the level of the proteic matrix; d) mealy endosperm (Mondur 1091) at 17.5% water content, showing air spaces and non compact structure.
Same abbreviations as figure 12.

vitreous endosperm. In the majority of mealy grains observed (Agathe 1093 at 17.5% water content), the fissuring took place within the endosperm protein matrix (fig. 15 c). Fissuring did not take place at the inter-cellular boundary (fig. 15 d).

Conclusion

At the same water content, the apparent modulus of elasticity of vitreous grains is greater than that of mealy grains. This appears to be related to the difference in the texture of mealy and vitreous endosperms. The air spaces in the endosperm of mealy grains result in a more open structure, and make the grain behaviour less elastic. The load initially expells the air from the grain structure, therefore, slopes and aspect of load-deformation curves have shown that more time is necessary for compression of mealy grains than is the case for vitreous grains where the physical structure is more compact. Humidification favours the transformation of vitreous endosperm to mealy endosperm due to the expansion of the protein matrix and starch which increases the number of air spaces. Grain humidification makes the endosperm destruction easier.

References

Al Saleh A, Bouchet B, Gallant DJ. (1984). Mineral migration in the wheat kernel during mill conditioning. Food Microstruct. 3, 149-158.

Arnold PC, Roberts AW. (1969). Fundamental aspects of load-deformation behavior of wheat grains. Trans. ASAE 12, 104-108.

Barlow KK, Buttrose MS, Simmonds DH, Vesk M. (1973). The nature of starch-protein interface in wheat endosperm. Cereal Chem. 50, 443-454.

Kozma A, Cunningham H. (1962). Tables for calculating the compressure surface stresses and deflections in the contact of two solid elastic bodies whose principal planes of curvature do not coincide. J. Ind. Math. 12, 31-39.

Lockwood JF. (1950). La meunerie (Milling). Ed. Louis David, Paris, France, 24-27.

Mauzé C, Richard M, Scotti G. (1972). Contrôle de la qualité des blés; Guide pratique (Wheat quality control; Practical guide-book). Institut Technologique des Céréales et des Fourrages, Paris, France, 59-65.

Mohsenin NN. (1978). Physical properties of plant and animal materials. Gordon and Breach Science Publishers, New York, 284-285.

Morrow CT, Mohsenin NN. (1966). Consideration of selected agricultural products as viscoelastic materials. J. Food Sci. 31, 686-696.

Moss R, Stenvert NL, Kingswood K, Pointing G. (1980). The relationship between wheat microstructure and flourmilling. Scanning Electron Microsc. 1980; III: 613-620.

Multon JL, Bizot H, Martin G. (1980). Eau-humidités relatives (Water-relative humidities), in:Techniques d'analyse et contrôle en industries agro-alimentaires, Lavoisier-Technique et Documentation (APRIA) 4, 1-60.

Multon JL, Bizot H, Doublier JL, Lefebvre J, Abbott DC. (1981). Effect of water activity and sorption hysteresis on rheological behaviour of wheat kernels, in:Water activity, influences on food quality, Academic Press, New York, 179-198.

Resmini P, Pagani MA. (1983). Ultrastructure studies of pasta. A review. Food Microstruct. 2, 1-12.

Shelef L, Mohsenin NN. (1967). Evaluation of the modulus of elasticity of wheat grain. Cereal Chem. 44, 392-402.

Simmonds DH, Barlow KK, Wrigley CW. (1973). The biochemical basis of grain hardness in wheat. Cereal Chem. 50, 553-562.

Stenvert NL, Kingswood K. (1977). The influence of the physical structure of the protein matrix on wheat hardness. J. Sci. Food Agric. 28, 11-19.

Yamazaki WT, Donelson JR. (1983). Kernel hardness of some US wheats. Cereal Chem. 60, 344-350.

Acknowledgments

The authors thank Drs J. Abecassis and P. Feillet (INRA, Montpellier) for sample availability and Drs J.L. Doublier and J.P. Melcion (INRA, Nantes) for helpful advice and assistance throughout the rheological study. Gratitude is expressed to Mrs. Martine Chapeau for typing this paper.

Discussion with Reviewers

P. Resmini: Can the authors give additional information about the vitreosity determination by the "Pohl grain cutter" ?

Authors: The "Pohl grain cutter", namely "Farinotome de Pohl" is a hand device used for the vitreosity determination. This device is described by Mauzé et al. (1972). It consists of a steel undermatrix supplied with 50 seed-holes where the seeds are placed vertically, and an overmatrix. Then the seeds are pressed between the two matrices, and a cutter is slid in a special slit in order to cut the seeds into two parts.

The 50 half-parts of the seeds remaining on the undermatrix are viewed and mealy, vitreous and intermediate grains are counted. This operation is done 6 times for each sample. Percentages are calculated from the cumulated data.

R. Moss: Fig. 12 c, the endosperm does not appear to be very vitreous when compared to other published photomicrographs. It would be helpful to readers comparing rheological data if the hardness of the grains tested was indicated using a standard method (e.g., particle size index or pearling resistance).

Authors: Our study was based on the vitreosity of wheat grain varieties and not on their hardness, which has not been measured.

The apparent modulus of elasticity gives an idea of the hardness of the seeds. But if we consider table 3 where the varieties are ranged decreasingly in function of the vitreosity, data of mean apparent modulus of elasticity do not follow the same pattern, probably because the rate of intermediate grains is more important in the case of Agathe 1093.

We agree that it should be interesting to compare hardness to vitreosity. To our knowledge such a comparison has not yet been published.

R. Moss: A comparison of the endosperm at 10.0-17.7% water content would be interesting (only 17.5% shown in fig. 15 a) and the air spaces are not very apparent.
P. Resmini: Fig. 15. The air spaces are very difficult to recognize.
Authors: Air space recognition needs some enlargement to see more details. That has been done under the microscope but was not possible to show in these pictures taken at lower magnification to show general features. Air spaces are similar to those already published elsewhere (Moss et al., 1980).

R. Moss: The crushed zone (fig. 15 a) in the endosperm is not clearly distinguishable from the remaining endosperm.
Authors: In comparison to non-crushed (fig. 13 b), peripheral part (aleurone layer) of crushed seeds is totally collapsed so that its apparent structure seems lost. In fact, it is condensed into a very thin layer by crushing.

P. Resmini: The authors should give information about the methods used for their statistical calculations. Is the tested difference significant from a statistical stand point ?
Authors: The statistical method was the two way analysis of variance (Snedecor GW, Cochran WG. (1967). Statistical methods (6th ed.) The Iowa State University Press (ed), Ames, Iowa, chapter 11) and was performed using the Hewlett Packard 9825 A Calculator. The tested difference is significant P(0.5%) varying from 1.6 to 1.8.

P. Resmini: Can the authors give some explanation for the phenomenon by which the number of air spaces increases ? Is it perhaps due to protein shrinkage ?
Authors: During hydration, same physical competition between proteins and starch occurs as described by Resmini and Pagani (1983) in pasta cooking. In our case, differences are the very low moisture and low temperature : starch cannot swell nor protein coagulate.

At room temperature and in saturated water, affinity for water by starch is about 40% (diameter increase of starch granule is 15%) and affinity by protein is about 150%.

In our case, at room temperature and low moisture, although the starch percentage is volumetrically higher (80%) than proteins (12%), competition for water must be overcome by the proteins of the seed. Thus, we think that, under low hydration proteins must swell and not shrink.

FOOD MICROSTRUCTURE, Vol. 4 (1985), pp. 213-219
SEM Inc., AMF O'Hare (Chicago), IL 60666-0507 U.S.A.

STRUCTURE OF COARSE AND FINE FRACTIONS OF CORN SAMPLES GROUND ON THE STENVERT HARDNESS TESTER

Y. Pomeranz[1] and Z. Czuchajowska[2]

[1]U.S. Grain Marketing Research Laboratory, USDA, Agricultural Research Service
1515 College Avenue, Manhattan, Kansas 66502
[2]Dept. of Chemical Engineering, Kansas State University, Manhattan, Kansas 66506

Abstract

Kernels from a pair of isogenic lines (with regard to hardness) and two commercial hybrids of dent corn (that varied in hardness) were ground on the Stenvert Hardness Tester and separated by sieving into coarse (>0.710 mm) and fine (<0.500 mm) fractions. The corn samples differed little in oil contents. The coarse particles from the hard corn samples were angular and sharp-edged; those from the soft corn samples were rounded. The yield of coarse particles was higher and they contained less oil in hard than in soft corn. Fine particles from all four corn samples had higher oil content than the coarse particles. Visual examination, observation at low magnification under a light microscope, and use of a scanning electron microscope revealed consistent differences in the extent and mode of corn kernel breakdown during grinding. Particles in the coarse fraction from hard kernels were to a large extent intact with little exposure of their contents. In the soft kernels, particles in the coarse fraction were broken extensively and their contents exposed. It is postulated that differences in the extent of mechanical breakdown and oil content are related to differences in shelf life of corn grits.

Initial paper received August 07 1985
Manuscript received September 19 1985
Direct inquiries to Y. Pomeranz
Telephone number: 913 776 2701

KEY WORDS: Corn Structure, Corn Hardness, Breakage Susceptibility, Dent and Flint Corn, Stenvert Hardness Tester.

Introduction

The production of corn grits of good shelf life is of great interest to the dry milling industry (Hopkins et al., 1903; Earle et al., 1946; Brekke, 1970; Brockington, 1970). Several methods of corn hardness determination were evaluated by Pomeranz et al. (1984) on corn varying widely in structure and composition as well as on pairs of isogenic lines with respect to hardness. We have reported on the use of the Stenvert tester to determine hardness of corn (Pomeranz et al. 1985a) and hardness of eight commercially dried corn hybrids equilibrated at two moisture levels (Pomeranz et al., 1985b). In a more recent study (Pomeranz et al., 1985c), kernels from seven classes separated according to size and shape from three hybrids were ground on the Stenvert Hardness Tester. The ground corn was sieved to obtain two main fractions: coarse (>0.710 mm in diameter) and fine (<0.500 mm in diameter). The oil contents of the coarse and fine fractions differed widely for the three hybrids. The effects of corn hardness on particle size and oil content of the coarse fraction were confirmed for corn hybrids dried under various commercial conditions. It was concluded that the Stenvert Hardness Tester has potential for predictive determination of corn properties in dry milling, both in terms of yields of products and of their particle size and composition. This report describes the effects of grinding corn with the Stenvert Hardness Tester on structure of the fine and coarse fractions. The structure was evaluated at low magnification by light-microscopy, and by scanning electron microscopy.

Materials and Methods

The two yellow dent corn hybrids (Stauffer 8500, relatively hard, and Bo Jac, relatively soft) were described previously (Pomeranz et al., 1985a). In addition, a pair of isogenic lines (dent and flint), from the breeding program of Cargill, Inc., Minneapolis, MN, was studied. The pair is considered to differ primarily, or only, in kernel hardness. The flint kernels were smaller and had higher density, larger particle size (when ground), and higher NIR (near

infrared) reflectance values at 1680 nm than their dent corn isogenic counterparts (Pomeranz et al., 1984). The NIR reflectance value at 1680 nm is an index of particle size; the higher the value, the larger the average particle size. The corn kernels were ground with the Stenvert Hardness Tester and separated into coarse (>0.710 mm in diameter) and fine fractions (<0.500 mm in diameter). The gross composition of the kernels was described by Pomeranz et al. (1985a).

Light microscopic examinations of ground samples were made on the Tessovar photomicrographic zoom system (Carl Zeiss Co., Oberkochen, W. Germany). The ground and sieved samples were viewed before and after staining with a green dye (Fast Green FCF, Color Index No. 42053) according to Chowdury and Buchele (1976). For examination by scanning electron microscopy (SEM), the samples were placed on double-stick Scotch® tape mounted on 9-mm diameter aluminum specimen holders. The samples were coated with a 10-nm layer of graphite and a 15-nm layer of gold, and viewed and photographed in the ETEC autoscan electron microscope at an acceleration voltage of 5 kV.

Results and Discussion

Characteristics of corn samples ground into coarse and fine fractions on the Stenvert tester are compared in Table 1. The hard kernels were higher than the softer counterparts in density and yield and lower in oil content of the coarse fraction. The fine fractions contained substantially more oil than the coarse fractions, and the fine fraction from soft corn was lower in oil than the fine fraction from hard corn.

Light micrographs of the coarse fractions (>0.710 mm) are shown in Figures 1-2 before staining and in Figures 3-4 after staining with Fast Green FCF. The hard, flinty and angular particles are more numerous in Figures 1 and 3 (from Stauffer 8500) than in Figures 2 and 4 (from Bo Jac).

Coarse particles from flint and dent isogenic pairs, examined by SEM, are shown in Figures 5a-h. The top line (Figures 5a-d) shows relatively little breakdown of the structure and relatively little exposure of starch granules in the flint corn. This is accompanied by little germ oil in the coarse particles and may explain the relatively good shelf life of coarse grits from flint corn during storage. In addition, differences in the amounts of germ and aleurone particles in the coarse fractions from soft and hard corn can affect shelf life. The particles from the dent corn (Figures 5e-h) are broken open and the starch granules are exposed. Whereas the cleavage in the flint particles is along wall lines in a manner that retains to a large extent cell integrity, the cleavage in the dent particles is across cell walls (Fig. 5g and h). The starch granules in the flinty corn, to the extent that they are exposed, are mainly polygonal with a few spherical. The starch granules in the dent corn are mainly spherical with a substantial amount polygonal.

Fine particles (<0.500 mm) from flint and dent isogenic lines, examined by SEM, are shown in Figs. 6a-f. In each figure, particles identified by an arrow indicate the site of subsequent examination at higher magnification. The fine particles, sieved after grinding on the Stenvert mill, varied widely in size. The fine particles from flint corn (Figures 6a-c) show breakdown of cell contents and cell wall and a somewhat porous and mechanically damaged structure. The exposed starch granules are of various sizes and shapes. The fine particles from dent corn (Figures 6d-f) seem less disintegrated, which may explain (in part) their relatively lower retention of oil from the germ. The highly variable distribution (in particle size and extent of mechanical breakdown) of the fraction <0.500 mm in flint corn is illustrated in Figures 7a and b. The starch granules varied widely in size and shape and the cell wall and protein matrix are extensively disintegrated and exposed.

Visual observation indicated small variations in hardness and vitreosity within coarse particles from isogenic corn lines ground on the Stenvert tester. In the particles from the commercial hybrids, however, there were visible differences in texture. Thus for instance, in Stauffer 8500 both hard and relatively soft areas were identified both visually and after examination under the SEM. They are demonstrated for coarse particles in the relatively hard Stauffer 8500 in Figs. 8a-e. A relatively soft piece is identified in Fig. 8a (bottom left) and shown at intermediate and

Table 1
Yields and Some Characteristics of Coarse (>0.710 mm) and Fine (<0.500 mm) Fractions of Stenvert Ground Corn Samples

Yields and Characteristics	Isogenic Lines		Commercial Hybrids	
	Flint	Dent	Stauffer 8500	Bo Jac
1000 kernel weight (g)	256.5	313.6	251.0	247.6
Density (g/cc)	1.324	1.280	1.339	1.283
Yield				
Coarse (%)	53.5	45.6	49.2	42.3
Fine (%)	30.0	38.4	35.4	40.2
Oil*				
Whole kernel (%)	3.88	3.93	3.95	3.66
Coarse fraction (%)	1.17	1.73	1.51	2.39
Fine fraction (%)	9.76	6.79	7.62	4.87

*14% moisture basis.

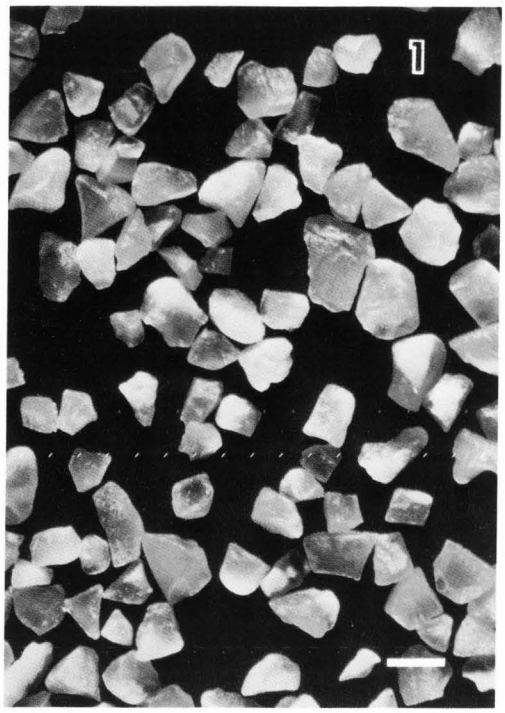

Fig. 1. Light micrograph of the coarse fraction (>0.710 mm) from Stenvert ground Stauffer 8500 corn; bar = 650 μm.

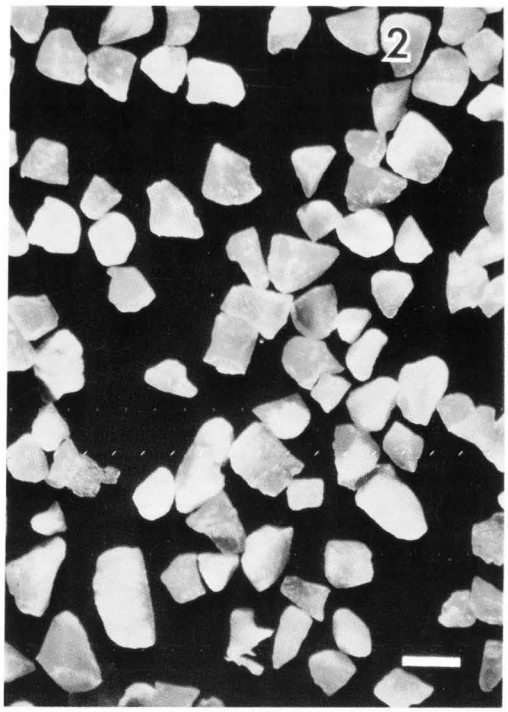

Fig. 2. Light micrograph of the coarse fraction (>0.710 mm) from Stenvert ground Bo Jac corn; bar = 650 μm.

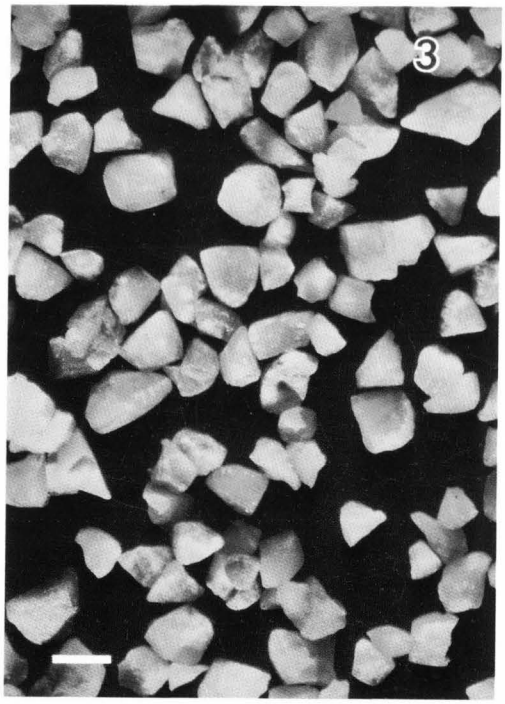

Fig. 3. Light micrograph of the coarse fraction (>0.710 mm) from Stenvert ground Stauffer 8500 corn after staining with Fast Green FCF; bar = 650 μm.

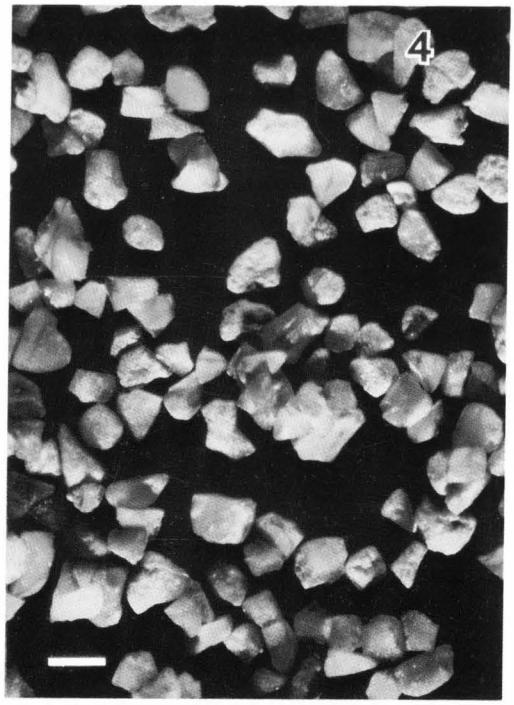

Fig. 4. Light micrograph of the coarse fraction (>0.710 mm) from Stenvert ground Bo Jac corn after staining with Fast Green FCF; bar = 650 μm.

Fig. 5a-h. SEM of the coarse fraction from flint (a-d) and dent (e-h) Stenvert ground corn (isogenic lines). a) Low magnifications of particles from flint corn. Arrow identifies the particle examined in Fig. b; bar = 700 μm. b) Intermediate magnification of particle from flint corn. Arrows identify particles examined at high magnification in Figs. c (low arrow) and d (top arrow); bar = 125 μm. c) High magnification of flint corn particle identified in Fig. b; bar = 10 μm. d) High magnification of flint corn particle identified in Fig. b; bar = 10 μm. e) Low magnification of particles from dent corn. Arrow identifies the particle examined in Fig. f; bar = 700 μm. f) Intermediate magnification of particle from dent corn. Arrow identifies particles examined at high magnification in Figs. g and h; bar = 125 μm. g) High magnification of dent corn particle identified in Fig. f. Note polygonal shape of starch granules and cleavage through cell wall; bar = 10 μm. h) High magnification of dent corn particle identified in Fig. f. Note spherical shape of starch granules and cleavage through cell wall; bar = 10 μm.

high magnification in Figs. 8b and 8c. A harder, more vitreous particle in Fig. 8a (bottom right) is shown at intermediate and high magnification in Figs. 8d and 8e. Again, whereas in the soft area there is much exposure of starch granules, in the hard area there is little exposure. Similar areas were selected for coarse particles of the relatively soft Bo Jac (Figs. 9a-c). The very soft piece (Fig. 9a, bottom right) is shown at high magnification in Fig. 9b and the somewhat harder piece (Fig. 9a, top middle) in Fig. 9c. Relative hardness is expressed by differences in appearance under low magnification (or even visually) and in the appearance under the SEM at high magnification.

Of particular interest is the fact that, whereas there was little difference in the oil contents between the pair of isogenic lines and the pair of hybrid corn samples (Table 1), the oil contents of the Stenvert ground coarse and fine fractions in the two pairs differed widely. The fine fractions were high in oil in all four samples; higher in the flint than in the dent isogenic line and higher in the relatively hard Stauffer than in the relatively soft Bo Jac. The high oil contents of the four fine fractions would reduce their shelf life by causing a rapid rise in rancidity. The coarse fractions, of value in food processing (breakfast cereals, hominy grits, brewers' grits, etc.), are relatively low in oil. Different relative amounts of germ oil were present in the coarse and fine particles from hard and soft corn.

In summary, the oil contents of the coarse and fine fractions from corn ground on the Stenvert mill were affected by corn hardness. Hardness governed the mode and extent of corn breakage, the texture of the broken particles, and their contents of germ oil. The distribution of oil in the coarse fractions of hard and soft corn is known to be related to shelf life of milled corn in food production.

It should be emphasized that the results of this study were obtained on corn equilibrated to a moisture content of about 12.3% as ground under the empirical conditions of the Stenvert Hardness Tester, a hammer/cutter mill that operates at 3600 rpm. The coarse fraction (>0.710 mm) in all samples contained some particles from outside the starchy endosperm (germ, pericarp, and aleurone). In addition, in the two commercial hybrids the coarse particles contained both flint and dent particles (and their mixtures). The flint particles in Stauffer 8500, however, were more numerous than in Bo Jac. The flint particles in the coarse fraction of all samples were consistently less broken open and showed less exposure of cell contents, and less oil than the coarse soft particles from the Stenvert ground corn.

References

Brekke OL. (1970). Corn dry milling industry, in: Corn: Culture, Processing, Products, G. E. Inglett (ed), AVI Publ. Co., Westport, CT, 262-291.

Brockington SF. (1970). Corn dry milled products, in: Corn: Culture, Processing, Products, G. E. Inglett (ed), AVI Publ. Co., Westport, CT, 292-306.

Chowdury MH, Buchele WF. (1976). Development of a numerical damage index for critical evaluation of mechanical damage of corn. Trans. ASAE 19, 428-431.

Earle FR, Curtis JJ, Hubbard JE. (1946). Composition of the component parts of the corn kernel. Cereal Chem. 23, 504-511.

Hopkins CG, Smith LH, East, ET. (1903). The structure of the corn kernel and the composition of its different parts. Illinois Agric. Exp. Stat. Bull. 87, 77-112.

Pomeranz Y, Czuchajowska Z, Lai FS. (1985b). Hardness and breakage susceptibility of commercially dried corn equilibrated at about 12.3% and 16.3% moisture. Cereal Chem. (In press).

Pomeranz Y, Czuchajowska Z, Lai FS. (1985c). Gross composition of coarse and fine fractions of small corn samples ground on the Stenvert Hardness Tester. Cereal Chem. (In press).

Pomeranz Y, Czuchajowska Z, Martin CR, Lai FS. (1985a). Determination of corn hardness by the Stenvert Hardness Tester. Cereal Chem. 62, 108-112.

Pomeranz Y, Martin CR, Traylor DD, Lai FS. (1984). Corn hardness determination. Cereal Chem. 61, 147-150.

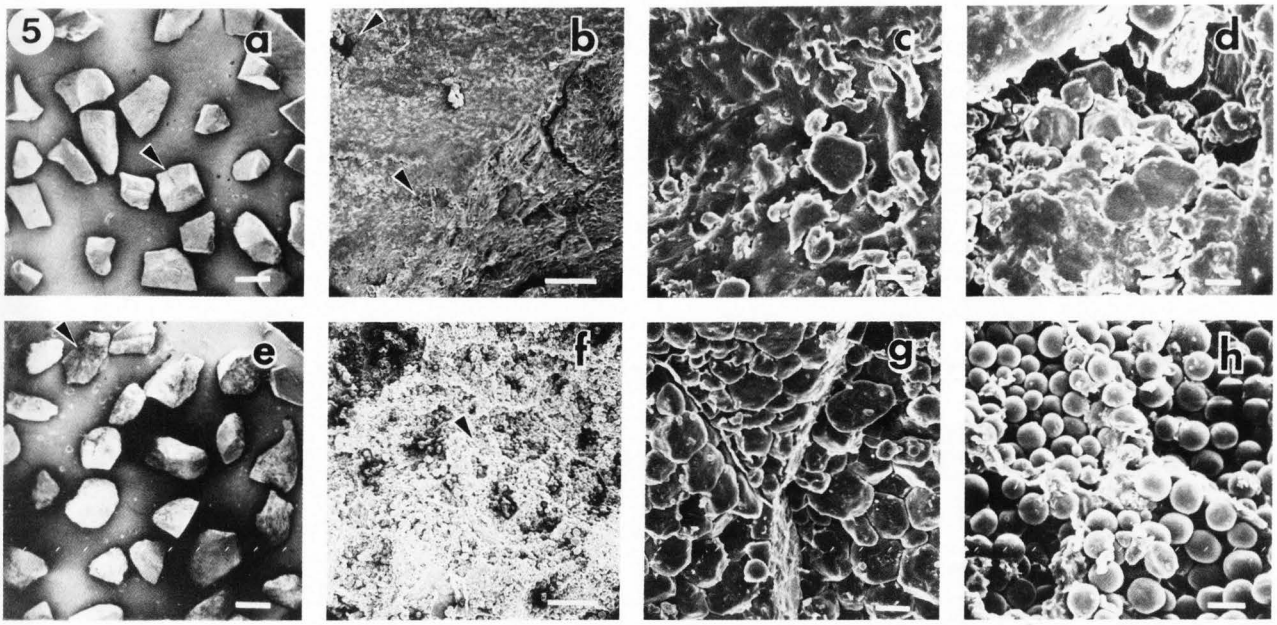

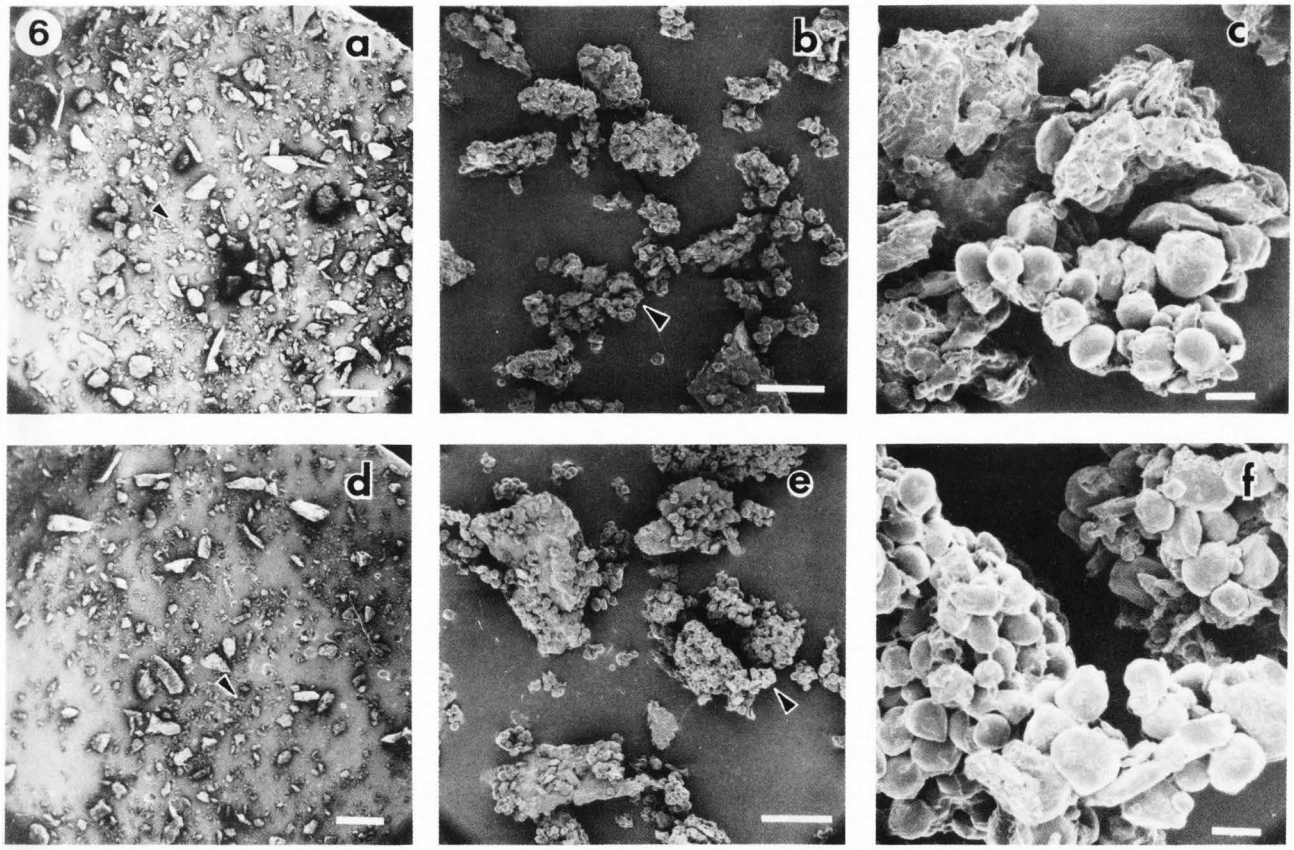

Fig. 6a-f. SEM of the fine fraction from flint (top line, a-c) and dent (bottom line, d-f) Stenvert ground corn (isogenic lines). Arrows identify particles examined at higher magnification in subsequent figures. Low (a), intermediate (b), and high magnification (c) of particles from flint corn. Low (d), intermediate (e), and high magnification (f) of particles from dent corn. The bar equals 800 μm in a and d; 100 μm in b and e; and 10 μm in c and f.

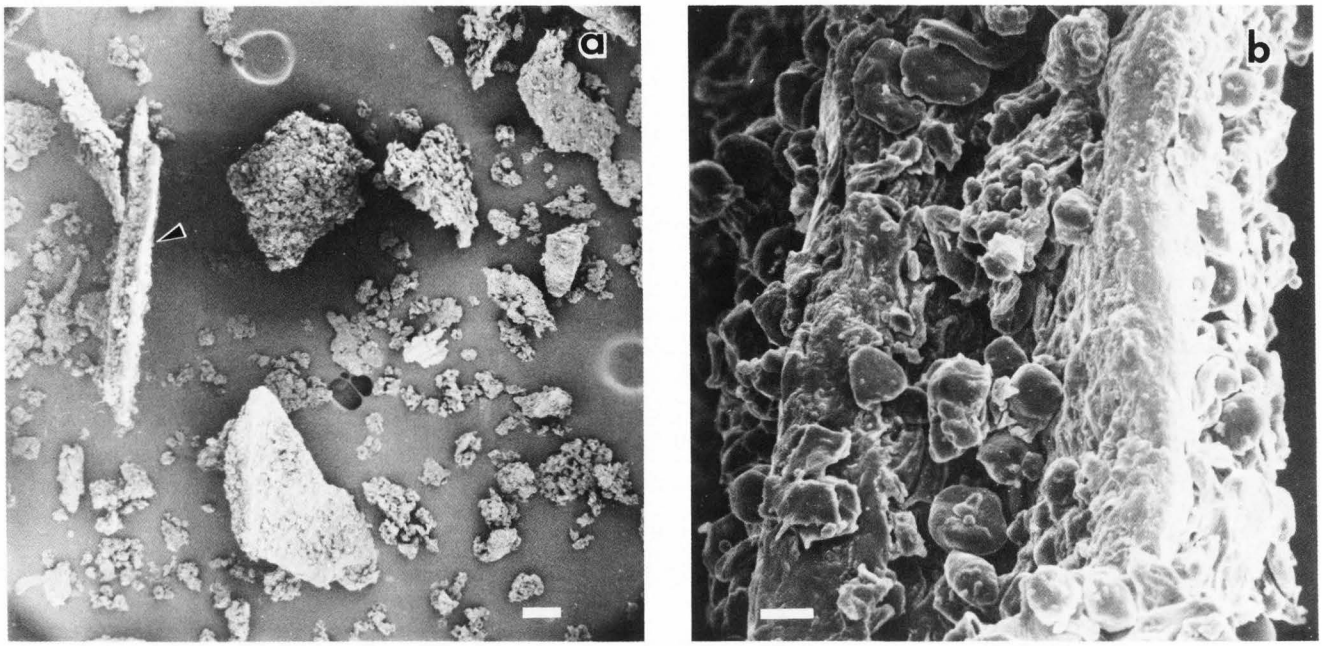

Fig. 7a-b. SEM of particles varying widely in size in the fine fraction (<0.500 mm) of Stenvert ground flint corn (isogenic line). Parts of the long particle identified by an arrow in a is shown at high magnification in b. The bar equals 100 μm in a and 10 μm in b.

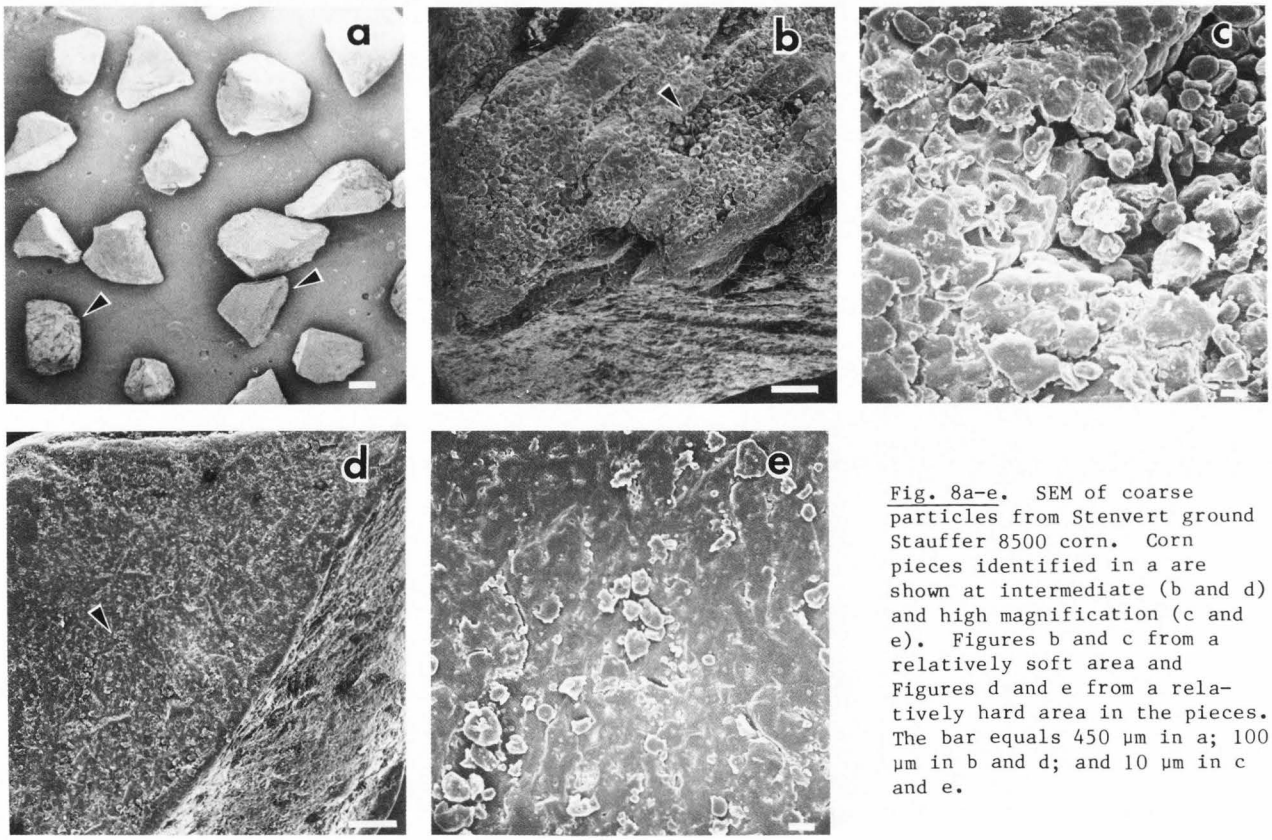

Fig. 8a-e. SEM of coarse particles from Stenvert ground Stauffer 8500 corn. Corn pieces identified in a are shown at intermediate (b and d) and high magnification (c and e). Figures b and c from a relatively soft area and Figures d and e from a relatively hard area in the pieces. The bar equals 450 μm in a; 100 μm in b and d; and 10 μm in c and e.

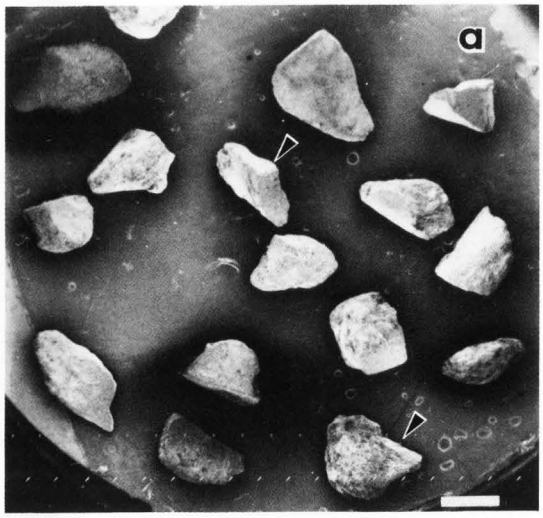

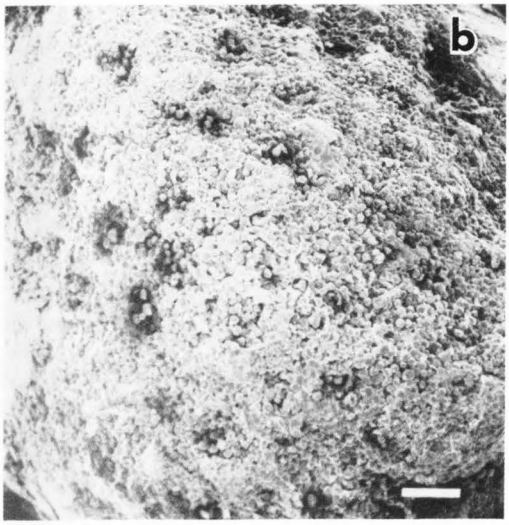

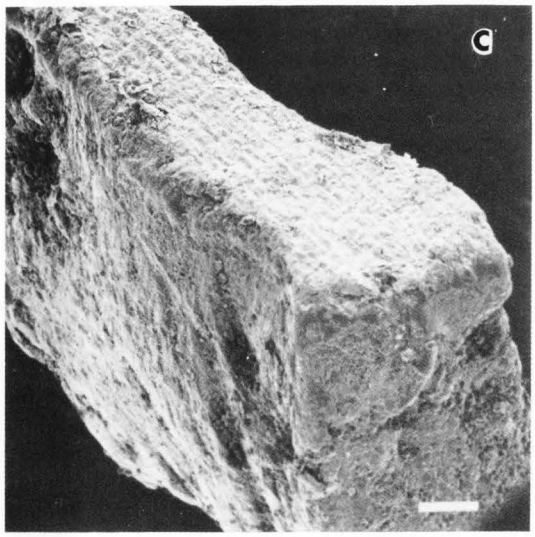

Fig. 9a-c. SEM of coarse particles from Stenvert ground Bo Jac corn. Corn pieces identified in Fig. a are shown at higher magnification in Fig. b (bottom right in a) and in Fig. c (middle top in Fig. a). The bar equals 700 μm in a and 100 μm in b and c.

FOOD MICROSTRUCTURE, Vol. 4 (1985), pp. 221–232
SEM Inc., AMF O'Hare (Chicago), IL 60666-0507 U.S.A.

0730-5419/85$1.00+.05

RELATION BETWEEN MICROSTRUCTURE, DESTABILIZATION PHENOMENA AND RHEOLOGICAL PROPERTIES OF WHIPPABLE EMULSIONS

W. Buchheim, N.M. Barfod,* and N. Krog*

Bundesanstalt für Milchforschung, D-2300 Kiel, West Germany
*Grindsted Products, DK-8220 Brabrand, Denmark

Abstract

The structure of spray-dried whippable emulsions (toppings) containing different types of lipid surfactants, was investigated by electron microscopy using the freeze-fracture technique. The size distribution of the lipid particles within the powders varied with the type of the surfactant used. After reconstitution of the topping powders in water, a strong destabilization phenomenon took place to an extent depending on the type of the surfactant. Simultaneously a crystallization of coalesced lipid particles occurred along with an increase in viscosity of the emulsions. The degree of crystallization was measured by p-NMR. It has been concluded that these phenomena are closely related to whippability and foam firmness.

The structure of whipped topping emulsions (foam) is characterized by the presence of large lipid crystals at the surface of air bubbles. This structure is different from the structure of whipped liquid (imitation) cream or dairy cream, where the air bubbles are predominantly stabilized by agglomerated fat globules from which the surface membrane has been partly removed during the whipping process.

Initial paper received February 13 1985
Manuscript received August 04 1985
Direct inquiries to N. Krog
Telephone number: 45-6-25 33 66

Key Words: Transmission electron microscopy, freeze-fracture technique, pulsed-nuclear magnetic resonance, X-ray diffraction, viscosity, destabilization of emulsions, imitation cream, topping emulsions, whippable emulsions, surfactants.

Introduction

The structure of whipped dairy cream has been investigated by Buchheim (2) who demonstrated by electron microscopy that the air bubbles in the foam are surrounded by a layer of fat globules which partially protrude into the air bubbles. Furthermore it was observed that the adsorbed fat globules had lost their protective membrane layers and that liquid fat was present in open spaces between solid fat globules.

Schmidt and van Hooydonk (5) used scanning electron microscopy to investigate the effect of homogenization on dairy cream and confirmed the structure described by Buchheim (2).

Whereas Transmission Electron Microscopy (TEM) and Scanning Electron Microscopy (SEM) studies on whipped dairy cream demonstrate the microstructure of dairy cream, no such investigations have yet been carried out on imitation cream or powdered toppings. It is well known that reconstituted topping emulsions show an increase in viscosity related to desired whippability, and that only certain types of surfactants give good foam properties (1). It has so far been anticipated that the whipping properties of topping emulsions are partially due to an agglomeration of the lipid droplets in the emulsions.

Since spray-dried, vegetable-fat based, whippable emulsions are being widely accepted in resemblance to dairy cream and offer advantages in cost, transportation and long term storage, it has been decided to study the structural characteristics of these systems in detail.

Materials and Methods

Preparations of topping powders and liquid imitation creams

The topping powders were made by spray-drying an emulsion containing 24–26% hydrogenated coconut oil with a final melting point (m.p.) of 31°C, 4–6% surfactant, 16% maltodextrin, 4% sodium caseinate, and 50% water. The emulsions were prepared by melting coconut fat and surfactant together at 80°C and separately dissolving the caseinate and maltodextrin in the water phase at 90°C. The two phases were then mixed together and homogenized on a one-stage high-pressure piston homogenizer with a Rannie liquid whirling type valve at a pressure of 100 kg/cm^2 at 80°C. The emulsion was then spray-dried, using a rotating atomizer (16,000 rpm), with an air inlet temperature of 150°C and an outlet temperature of 90°C. The spray-dried topping powder was cooled to 5°C for one hour and then stored at 20°C or at a lower temperature.

The following surfactants were used: Distilled propylene glycol monostearate (PGMS), distilled monoglycerides based on partially hydrogenated soy bean oil (GMO), and distilled monoglycerides based on fully hydrogenated soy bean oil (GMS). The surfactants contained a minimum of 90% monoesters and are commercial products manufactured by Grindsted Products A/S, Denmark having the following trade names: Promodan SP (PGMS), Dimodan O (GMO), and Dimodan PV (GMS). A topping powder based on coconut fat, sodium caseinate, and maltodextrin and containing no surfactant was used as a reference.

For comparison an ultra-high temperature (UHT) treated liquid, vegetable-fat based cream (imitation cream), was included in the experiments. It contained 29.4% hydrogenated palm kernel oil (m.p. 36°C), 0.6% lactylated monoglycerides (Lactodan P 22, manufactured by Grindsted Products A/S, Denmark), 0.05% sodium alginate, 1% sucrose and 68.95% skim milk. The fat and surfactant were melted together at 75°C, and added to the skim milk in which sodium alginate and sucrose had been dissolved with agitating during heating to 75°C. The mixture was first homogenized at a low pressure (15 kg/cm^2) to make a fairly stable emulsion, then UHT-treated (144°C, 4 s) followed by a second homogenization at 150 kg/cm^2, and finally cooled to 5°C.

Viscosity measurements

The topping powders were reconstituted in water at 15°C by mixing 1 part of powder with 3 parts of water. The emulsion was then transferred to the cup of a Haake Rotovisco Viscometer with sensor system MVII. The temperature in the sensor cup was thermostatically controlled at 15°, 18° or 20°C. The viscosity of the emulsion was measured continuously at a shear rate of 1.76 s^{-1} as a function of time up to two hours.

Whipping test and foam texture measurements

One part of the topping powders was reconstituted in three parts of water at 10°C and 15°C and whipped with a Kenwood Chief Mixer at maximum speed for 2 or 3 min depending on the type of emulsifier used. The whipped cream was then tested with a Voland Stevens Texture Analyzer using a cylindrical probe (TA 5) 12.7 mm in diameter, adjusted to a penetration depth of 10 mm at a speed of 2 mm s^{-1} and using a load range position 100 g.

Crystallization measurements

The extent of crystallization of the fat phase was analyzed by measuring the solid fat content (SFC) by a pulsed-wide-line proton NMR technique (6) in reconstituted emulsions using deuterated water (D_2O) instead of normal water.

Fat crystal modifications were determined at 22°C by X-ray diffraction analysis using an Enraf-Nonius Guinier-De Wolff Camera and a Philips X-ray generator with a Cu-anode as X-ray source. (Wavelength = 0.154 nm).

Transmission electron microscopy

The topping powders, the reconstituted systems, the liquid imitation cream, and the whipped systems were prepared for electron microscopy by the freeze-fracture technique using a BALZERS BA 360 M unit. Prior to cryofixation the various types of samples were treated as follows: 1) The topping powders were suspended in anhydrous glycerol as described earlier (3). 2) The powders were reconstituted in water (1:3) at 15°C. These emulsions as well as the liquid imitation cream were cryoprotected by mixing with glycerol to a final concentration of 30% (v/v). 3) The whipped systems were not cryoprotected, but the freeze-fracture specimen holders were covered with a small droplet of glycerol in order to achieve a better adhesion of the foam.

Small volumes (1–2 mm^3) of the various samples were transferred onto normal freeze-fracture specimen holders (Balzers), cryofixed by immersion into melting Freon 22 (−160°C) and stored under liquid nitrogen. Freeze-fracturing was carried out at −120°C, followed immediately by replication (ca 1.7 nm platinum/carbon under an angle of 45 degrees followed by ca 20 nm of pure carbon) using an electron gun.

The replicas were cleaned for 1 h with a 5% sodium hypochlorite solution followed by acetone. Distilled water baths were used as intermediate steps. Electron micrographs were taken with a Philips EM 301 electron microscope at 80 kV.

Results

Electron microscopy

Topping powders—By freeze-fracturing suspensions of spray-dried powders in non-aqueous media detailed information can be obtained about the surface as well as about the internal structure of powder particles (3). In the following text, results are reported exclusively on the internal structure, i.e., the size and appearance of the lipid droplets because these aspects are of relevance for the physical phenomena described in this paper. Characteristic views of the fine structure of the powder matrices are given for the 4 types of topping powders studied.

Fig. 1a shows a powder which contained PGMS (Promodan SP) as the surfactant. The lipid droplets are more or less globular, and their diameters vary between ca 0.1 and 1.5 μm. They appear to be very densely packed in the powder matrix, the remaining space between them is represented by maltodextrin and sodium caseinate. The lipid droplets are sometimes cleaved near their periphery showing irregularly shaped crystalline platelets, but more often they are cleaved internally (Fig. 1b). The very smooth appearance of the fracture planes can be described as cleaved crystalline platelets running like discs through the entire droplets.

The topping powder containing GMS (Dimodan PV) is shown in Fig. 2a. The lipid droplets are again of mostly globular shape but of distinctly more uniform size of approximately 0.5 μm.

Fig. 1. Topping powder with PGMS (Promodan SP). (a) Internal structure of a cleaved powder particle showing the dense packaging of lipid droplets (L). Bar = 1 μm. (b) Detailed view demonstrating the occurrence of peripheral (A) and internal (B) cleavages of individual lipid droplets. C: caseinate/maltodextrin matrix. Bar = 0.25 μm.

Fig. 2. Topping powder with GMS (Dimodan PV). (a) Internal structure of a cleaved powder particle. The lipid droplets are smaller and of distinctly more uniform size as compared to the topping powder with PGMS (Fig. 1). Bar = 1 μm. (b) Detailed view. Bar = 0.25 μm.

Fig. 3. Topping powder with GMO (Dimodan O). (a) Internal structure of a cleaved powder particle. The sizes and shapes of the lipid droplets resemble those in the topping powder with GMS (Fig. 2). Bar = 1 μm. (b) Detailed view. Internally cleaved lipid droplets (A) exhibit very often a smooth structure originating from a disc-like crystallization of the lipid phase. Bar = 0.25 μm.

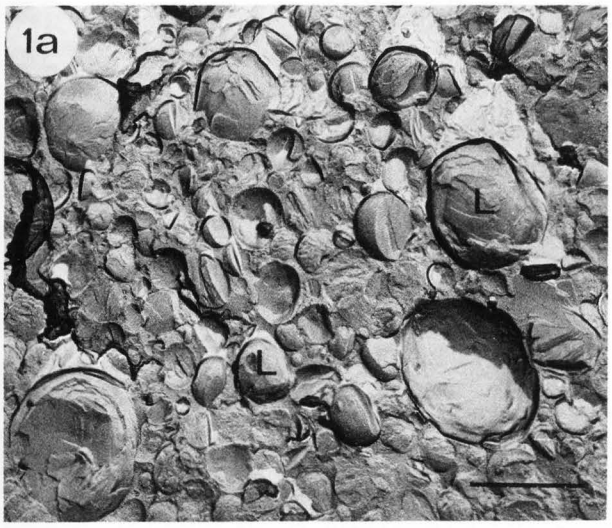
1a
L
L

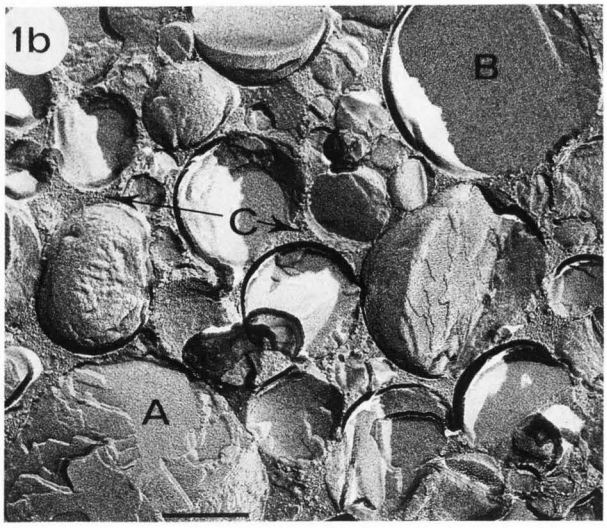
1b
B
C
A

2a

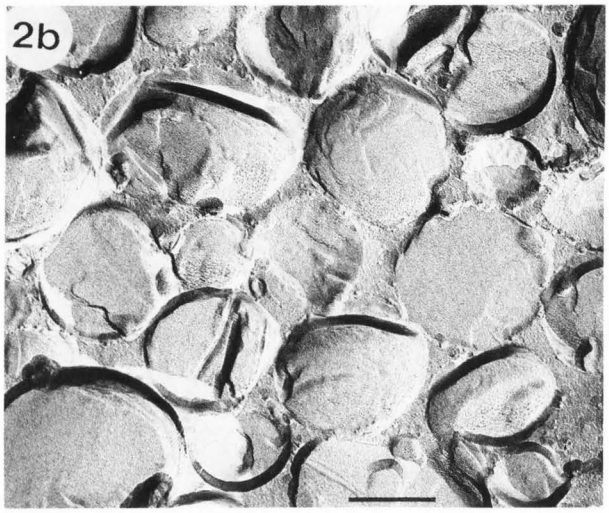
2b

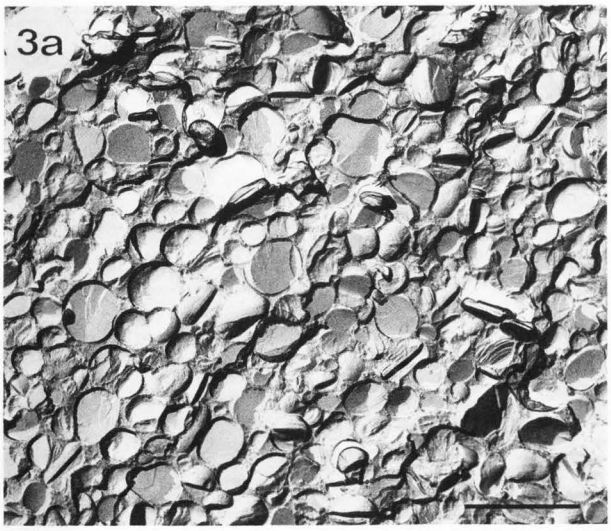
3a

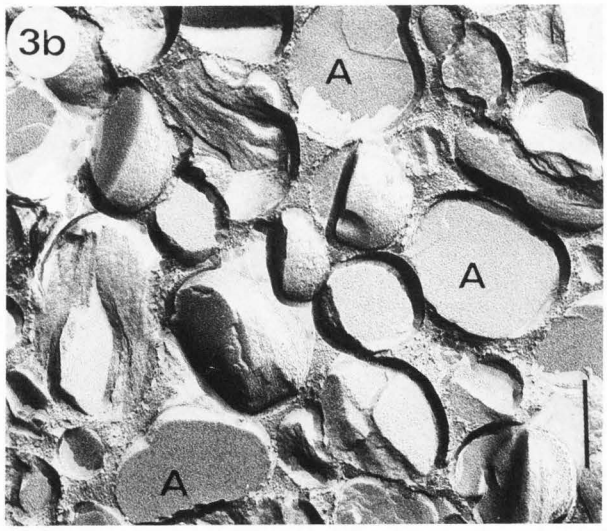
3b
A
A
A

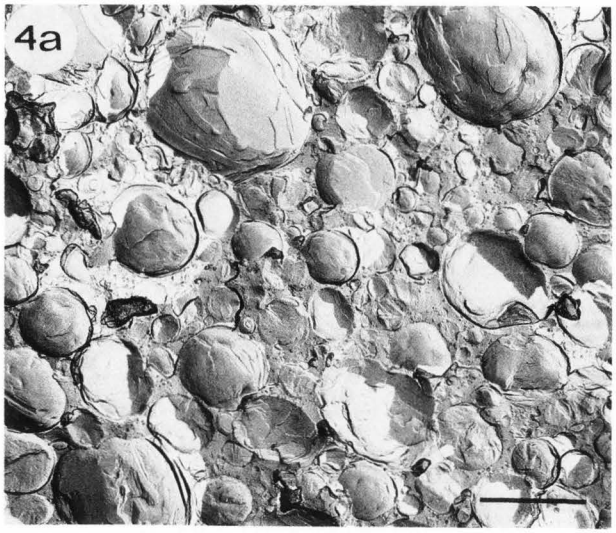
4a

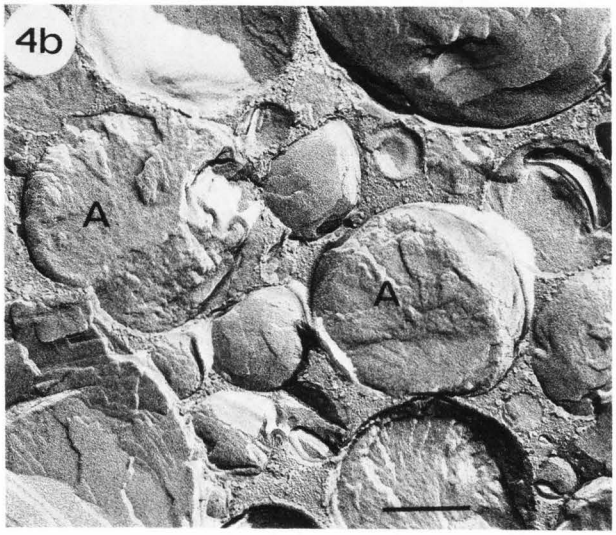
4b
A
A

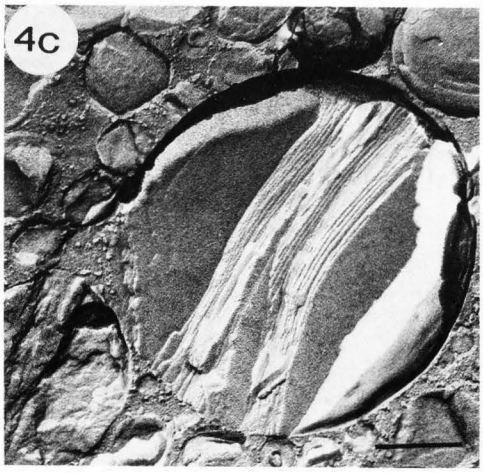
4c

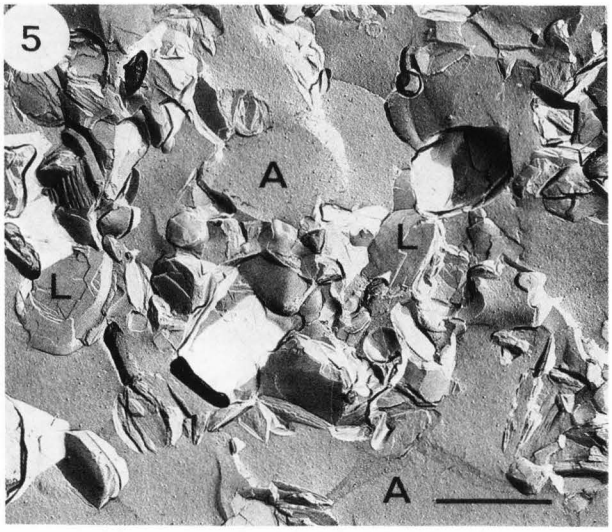
5
A
L
L
A

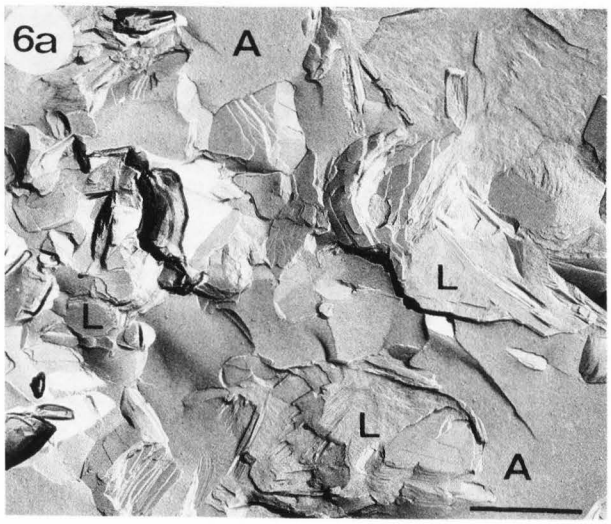
6a
A
L
L
L
A

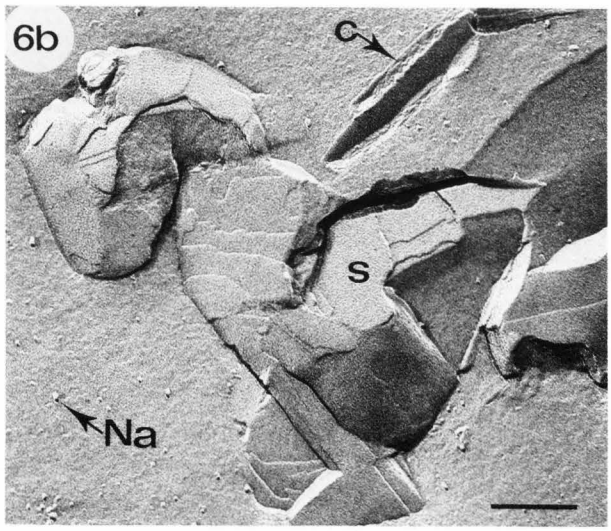
6b
C
S
Na

The individual droplets are either cleaved near their periphery or internally, showing again – similar to the PGMS sample – the smooth disc-like platelets (Fig. 2b).

When using GMO (Dimodan O) as the surfactant the sizes and the shapes of lipid droplets are similar to the GMS sample as demonstrated in Fig. 3a. The peculiar, disc-like crystallization within individual droplets appears, however, distinctly more pronounced as compared to the samples described above (Fig. 3b).

The spray-dried emulsion without surfactant shows lipid droplets on an average of larger sizes, which have been cleaved preferentially along crystal layers near their periphery (Fig. 4a). Internally fractured droplets sometimes show a fine structure of the oil which has to be interpreted as being amorphously solidified, i.e., having been liquid before cryofixation (Fig. 4b). Other droplets, although considerably less in numbers as compared to the other samples, also show regularly arranged crystal layers running like discs through them (Fig. 4c).

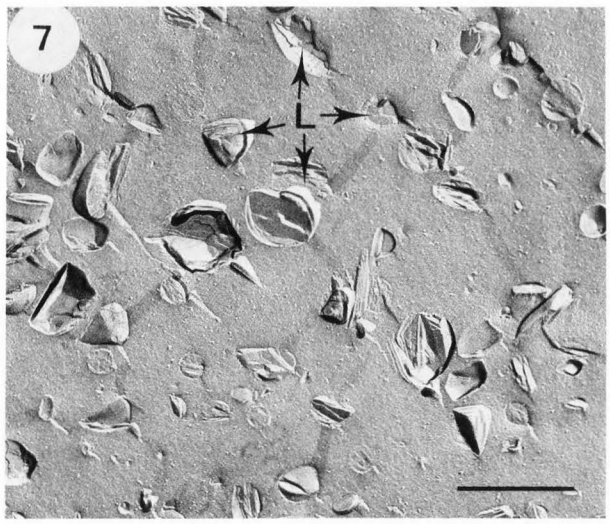

Fig. 4. Topping powder without surfactant.
(a) Internal structure of a cleaved powder particle. The sizes of the lipid droplets are on an average larger and less uniform as compared to the topping powders with GMS (Fig. 2) and GMO (Fig. 3). Note that comparatively more lipid droplets have been cleaved near their periphery. Bar = 1 μm. (b) Detailed view. Internally cleaved lipid droplets (A) exhibit sometimes a fine structure which has to be interpreted as being amorphously solidified, i.e., having been liquid before cryofixation. Bar = 0.25 μm. (c) Detailed view of a cleaved lipid droplet with regularly arranged, planar crystal layers. Bar = 0.25 μm.

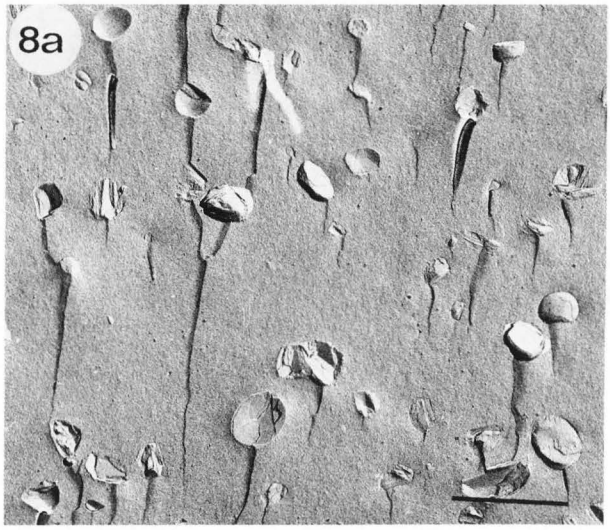

Fig. 5. Reconstituted topping emulsion with PGMS (after 5 min). The lipid phase (L) forms large, irregularly shaped aggregates of agglomerated, but strongly deformed lipid particles. The aqueous phase (A) is penetrating into the agglomerated lipid phase. Bar = 1 μm.

Fig. 6. Reconstituted topping emulsion with PGMS (after 24 h). (a) As compared to a period of 5 min (Fig. 5) the structural transformation process of the lipid phase (L) has considerably proceeded. It appears to represent a three-dimensional network which is penetrated by the aqueous phase (A). Bar = 1 μm. (b) Detailed view of the characteristic crystalline platelets which have formed from the lipid droplets within the powder particle (compare to Fig. 1). s: surface views of cleaved crystalline lipid aggregates; c: cross-fractured platelets; Na: sodium caseinate particles in the aqueous phase. Bar = 0.25 μm.

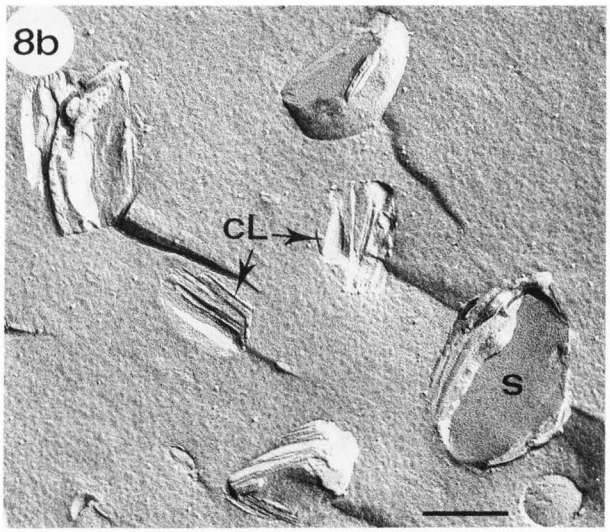

Fig. 7. Reconstituted topping emulsion with GMS (after 5 min). The lipid droplets (L) are slightly deformed but on an average of the same size as in the powder (compare to Fig. 2) and mostly not agglomerated. Bar = 1 μm.

Fig. 8. Reconstituted topping emulsion with GMS (after 24 h). The sizes and shapes of the lipid droplets as well as their distribution in the aqueous phase are similar to those after 5 min (Fig. 7). (a) General view. Bar = 1 μm. (b) Detailed view. Internally cleaved lipid droplets (cL) often show planar crystals; s: side view on such a crystal platelet. Bar = 0.25 μm.

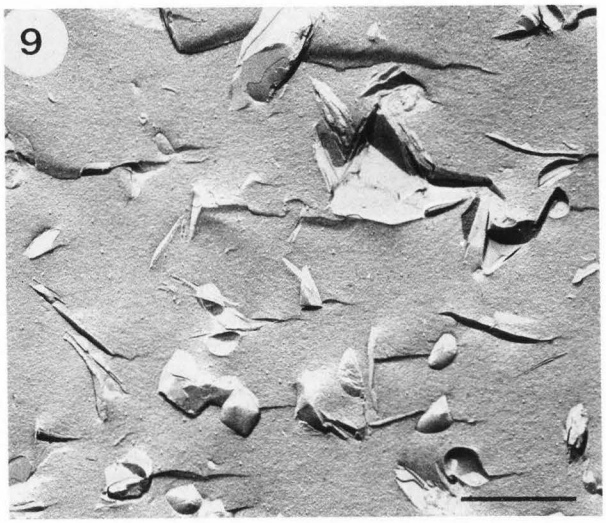

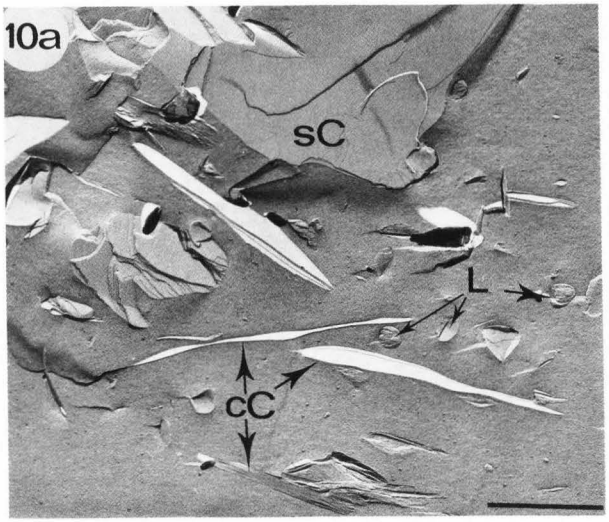

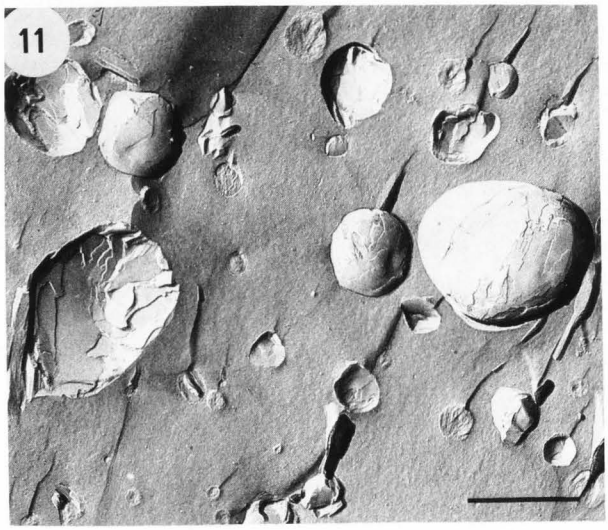

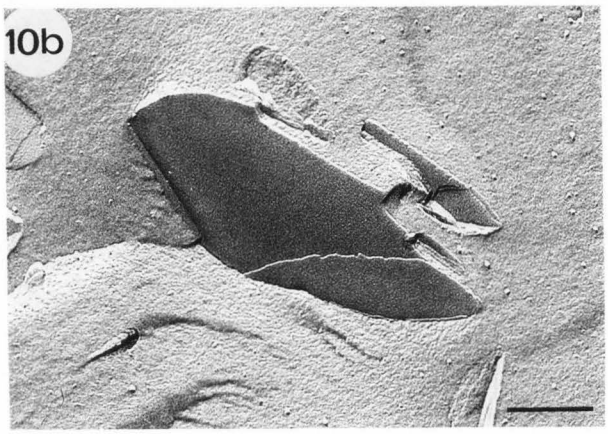

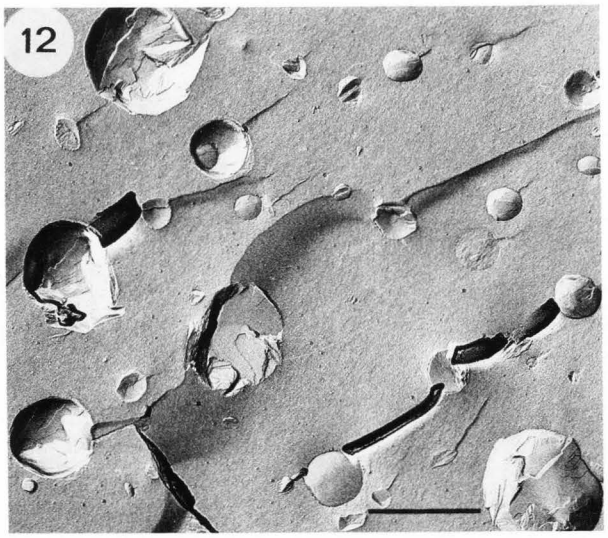

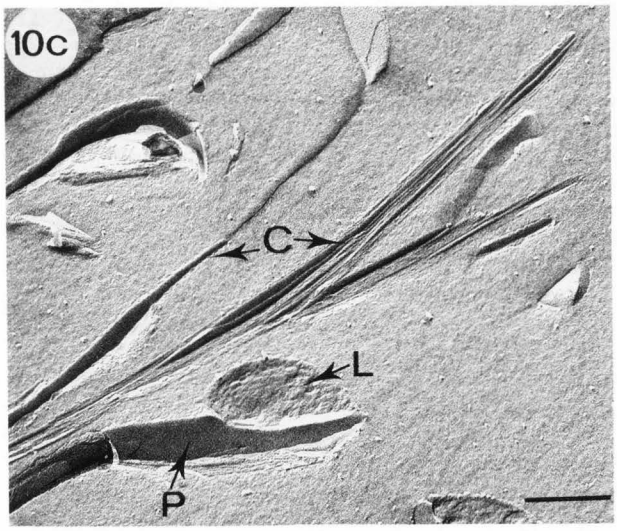

Fig. 12. Reconstituted topping emulsion without emulsifier (after 24 h). There are no structural changes detectable as compared to a period of 5 min (Fig. 11). Bar = 1 μm.

Fig. 9. Reconstituted topping emulsion with GMO (after 5 min). A strong structural transformation of the original lipid droplets (see Fig. 3) into elongated, plate-like particles has taken place. These platelets appear to be more or less separated from each other. Bar = 1 μm.

Fig. 10. Reconstituted topping emulsion with GMO (after 24 h). (a) The structural transformation of the lipid particles into large thin platelets has proceeded. These crystal platelets appear either cross-fractured (cC) or surface-fractured (sC) according to their orientation in the specimen. Only rarely globular lipid particles can be detected (L). Bar = 1 μm. (b) Detailed view of a platelet exposing the smooth surface of individual crystal layers. Bar = 0.25 μm. (c) Detailed view of cross-fractured platelets (c) which consist of stacks of crystalline monolayers. L: lipid droplet (Note the amorphous fine structure of previously liquid fat!) from which a crystal platelet (P) has grown. Bar = 0.25 μm.

Fig. 11. Reconstituted topping emulsion without emulsifier (after 5 min). The lipid droplets are on an average of the same size and shape as in the powder (compare to Fig. 4). Bar = 1 μm.

Reconstituted powders—The 4 different topping powders were reconstituted with water at 15°C (3 parts water added to 1 part of powder) and subsequently stored at 4°C for up to 24 h before further treatment. The structural changes occurring within the various emulsions can be demonstrated by comparing the state immediately after reconstitution with that after a longer period (24 h).

The topping system containing PGMS as a surfactant shows a very uneven distribution of the lipid phase following only a very short period of a few minutes in the aqueous environment (Fig. 5). Although a few particles still appear to retain their original sizes and shapes, i.e., the sizes and shapes which are typical for the dried system, the vast majority forms compact aggregates within which the globular shapes of lipid droplets can hardly be detected. Crystallization phenomena which resulted in a partial destruction of the lipid droplets and a peculiar agglomeration of crystalline platelets appear to have taken place. The aqueous phase in which the caseinate particles (10–20 nm in diameter) are clearly detectable, is penetrating into the agglomerated lipid phase.

The longer the influence of the aqueous environment on the lipid phase lasts the further the structural transformation process proceeds. Fig. 6a gives a typical view after 24 h of storage which is not too different from the view after the storage period of 1 h. The lipid phase shows pronounced crystalline structures (i.e., stacks of crystal monolayers) which are embedded in amorphous (i.e., previously liquid) fat. Lipid droplets are only rarely present, similar to the powder, and the lipid phase appears to be transformed into a three-dimensional network of interconnected, irregularly shaped aggregates, many of which are several μm in diameter. This final state of the lipid phase is also shown at a higher magnification (Fig. 6b).

After reconstituting the powder containing GMS, comparable structural changes do not occur (Figs. 7–8a). The state of the particles a few minutes after the dispersion of the powder in water is shown in Fig. 7. Most lipid droplets are floating separately in the aqueous phase, and agglomeration of the droplets is mostly absent. Most droplets are of the sizes found in the dried state; their shapes are not as globular as in the powder but the degree of deformation is moderate. The same situation occurs also after longer storage periods (Fig. 8a), i.e., the emulsion remains in a stable state. At a higher magnification, the extent and type of crystal formation within the lipid droplets can be well recognized (Fig. 8b).

When using GMO as surfactant, strong structural changes again occur in the reconstituted system but in quite a different manner as compared to the system containing PGMS. Fig. 9 demonstrates the state of an emulsion shortly after reconstitution. Globular lipid particles as in the powder are rare whereas elongated, plate-like particles are very frequent. It can be seen that they develop from more globular ones, are mostly up to 1 μm long and often 10–50 nm thick. These strongly deformed particles appear to be more or less separated from each other, i.e., they do not coalesce into larger aggregates as in the system with PGMS (compare Fig. 9 with Fig. 5). After 24 h the lipid particles in the reconstituted GMO system show a still more pronounced structural transformation into large thin platelets or lamellae which increase distinctly in size (Fig. 10a). It can be seen at higher magnification that these particles consist mainly of stacks of crystalline monolayers (Figs. 10b, c).

In the reconstituted topping made from the powder which contains no surfactant only lipid particles of globular shapes are found. The sizes of the lipid droplets are identical to those seen in the dry powder particles. Similar images were obtained irrespective of the time elapsed after reconstitution (Figs. 11, 12). Neither agglomeration nor stronger deformation of particles can be seen.

UHT imitation cream—The UHT-treated imitation cream has a fine structure which is very different from the reconstituted topping systems. As Fig. 13a demonstrates, the lipid particles are of an almost perfectly globular shape, not agglomerated and up to ca 1 μm in diameter. The most characteristic feature, however, is the type of crystallization within the lipid droplets. Concentric crystal monolayers are present within nearly each droplet and therefore cause preferentially a peripheral cleavage (Fig. 13b). When the globules have been cross-fractured, a rather thick shell of these concentric crystal layers becomes visible (Fig. 13c).

Whipped toppings—From the four different topping powders only those containing PGMS (Promodan SP) and GMO (Dimodan O) as surfactants formed stable foams when the reconstituted systems were whipped. The topping powder with GMS (Dimodan PV) gave a very soft, unstable foam.

For comparison, only one typical small area of the foam of each type of sample is shown; this area includes the air-water interface of a cross-fractured air bubble.

Fig. 14 shows the appearance of the air-water interface in the topping system with PGMS. The inner surface of the air bubbles is completely covered with crystalline lipid material, which appears to be adsorbed to the interface in the form of a continuous layer ca. 0.1 μm thick. In the foam lamella, i.e., in the serum phase between the air bubbles there are mostly irregularly shaped lipid aggregates, but sometimes also some more globular particles are present. This is to some extent similar to the situation in the reconstituted systems (compare to Fig. 5 or 6a).

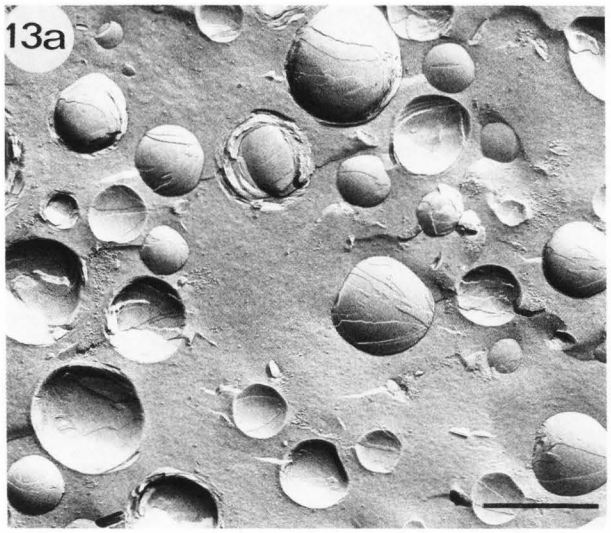

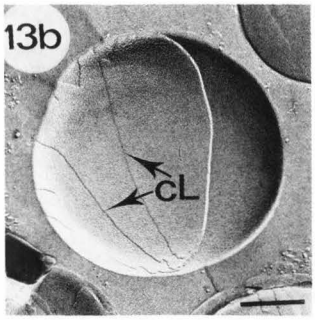

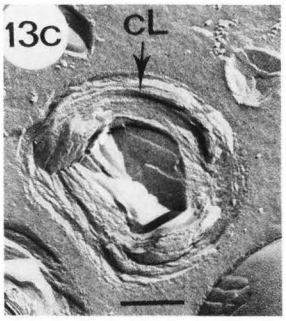

Fig. 13. UHT-treated imitation cream.
(a) General view of the emulsion. The lipid droplets are of an almost perfectly globular shape and not agglomerated. Most droplets have been peripherally cleaved due to the presence of concentric crystal monolayers. Bar = 1 μm. (b) Detailed view of a peripherally cleaved lipid droplet showing individual concentric monolayers (cL). Bar = 0.25 μm. (c) Detailed view of a cross-fractured lipid droplet showing these concentric monolayers (cL) from a direction perpendicular to that of Fig. 13b. Bar = 0.25 μm.

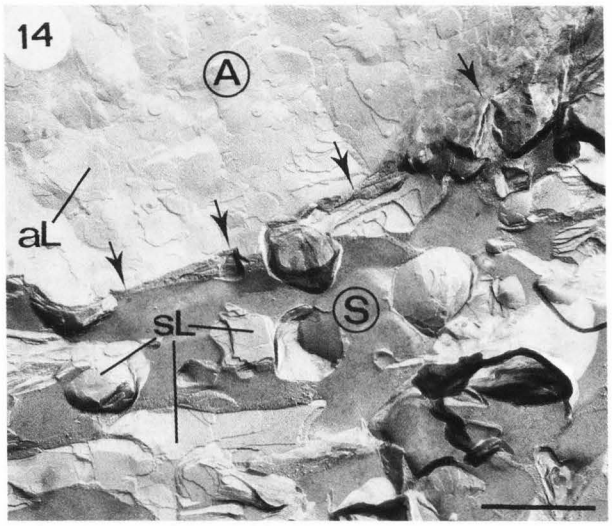

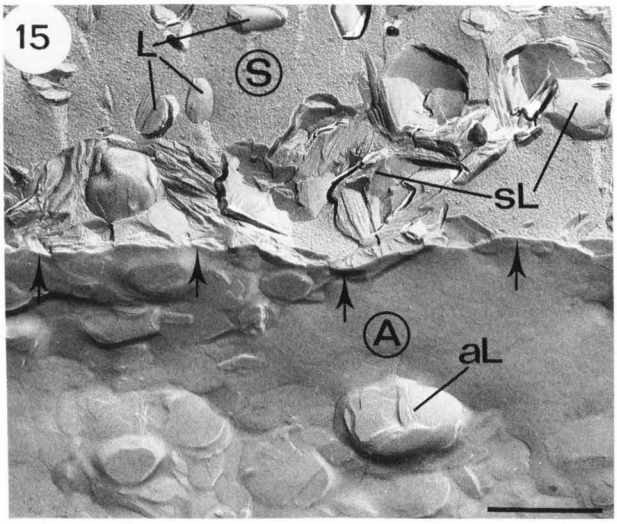

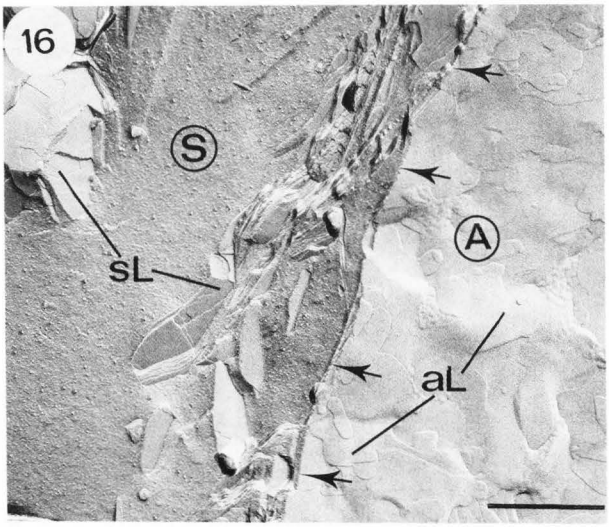

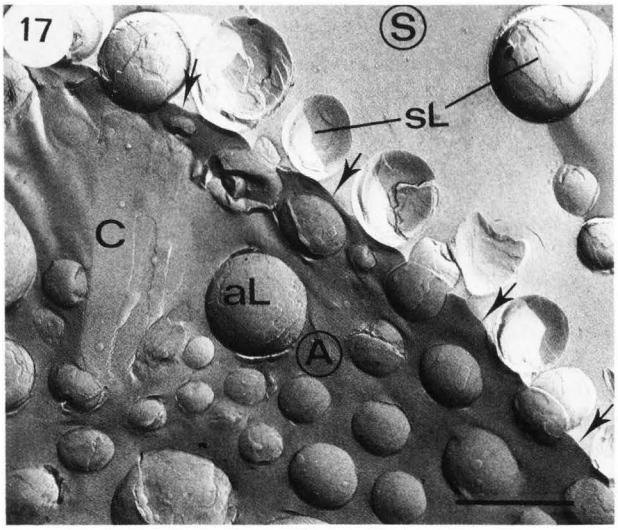

Table 1. Whipping tests and foam firmness of toppings at 10°C and 15°C.

Surfactant used	Overrun (%)		Foam firmness (g)		General remarks on the whipped toppings
	10°C	15°C	10°C	15°C	
Promodan SP (PGMS)	290	192	16	9	Soft, stable
Dimodan O (GMO)	50	65	26	24	Stiff, very stable
Dimodan PV (GMS)	270	50	5	<1	Very soft and unstable, syneresis
No surfactant	80	12	<1	<1	Extremely soft and unstable, syneresis

The whipped topping containing GMS as surfactant is shown in Fig. 15. The inner surface of the air bubble is not as completely covered with crystalline material as in the PGMS system (Fig. 14); frequently there are globular lipid particles protruding into the air. Within the serum phase of the foam, the lipid particles resemble those within the reconstituted system (compare Fig. 15 to Fig. 7 or 8a) but directly at the air-water interface they appear to be in a more agglomerated state.

When GMO is used as a surfactant, the inner surface of the air bubbles is nearly completely covered with flat crystal layers (Fig. 16), more similar to the PGMS system than to the GMS system. The dimensions of the crystal platelets are larger than in the PGMS system. Within the foam lamella, i.e., in the serum phase, the characteristic lamellae of platelet-like structures prevail; they have already been typical for the reconstituted system.

The structure of the whipped, liquid (UHT treated) imitation cream is completely different from the other whipped systems studied. Fig. 17 shows that the air bubbles appear to be covered with a monolayer of lipid globules which are rarely deformed and which protude with a substantial part of their volume into the bubble. Only rarely plate-like crystal layers are present at the interface.

Fig. 14. Whipped topping emulsion with PGMS. This micrograph (and also Figs. 15–17) represents a small but characteristic area of the boundary between an air bubble (A) and the serum phase (s) of the foam. aL: crystalline lipid material on the inner surface of the air bubble; sL: lipid aggregates in the serum phase. Arrows point to the air-water interface. Bar = 1 μm.

Fig. 15. Whipped topping emulsion with GMS. A: air bubble; S: serum phase; aL: globular lipid particle protruding into the air; sL: agglomerated lipid particles adhering to the air-water interface (arrows). In the serum phase also many lipid particles (L) are present in a non-agglomerated state similar to the reconstituted topping emulsion (compare to Figs. 7 and 8). Bar = 1 μm.

Fig. 16. Whipped topping emulsion with GMO. The inner surface of air bubbles (A) is nearly completely covered with flat crystalline lipid layers (aL). In the serum phase (S) lipid platelets (sL) in an aggregated or non-aggregated state prevail. Arrows point to the air-water interface. Bar = 1 μm.

Fig. 17. Whipped UHT-treated imitation cream. The air bubbles (A) appear to be covered with a monolayer of nearly undeformed lipid globules (sL) which protrude with a part of their volume into the bubble (aL). Occasionally crystal platelets (c) are present on the inner surface of the air bubble. S: serum phase. Arrows point to the air-water interface. Bar = 1 μm.

Emulsion viscosity, whippability and foam texture

Viscosity—When a topping powder is reconstituted into a cream by mixing 1 part of powder with 3 parts of water and the emulsion is kept below room temperature, an increase in viscosity will occur. The viscosity is dependent on temperature as shown in Fig. 18 for a topping emulsion with PGMS. At a temperature higher than 20°C, the increase in viscosity is negligible.

The rate of the viscosity increase is also dependent on the type of surfactant used as shown in Fig. 19. The emulsion viscosity is higher with GMO than with PGMS at 15°C; the topping emulsions with GMS or free of surfactants at all show no increase in viscosity on aging.

Whippability and foam firmness—The results of the whipping tests and the foam firmness measurements are shown in Table 1. The whipping test was done at two temperatures, 10° and 15°C. In general, a lower whipping temperature gave a higher overrun and firmness of the foam. Toppings with PGMS gave a fairly soft decoration foam, while the foam made from the GMO topping was firmer with good foam stability which was ideal for cake decoration.

However the GMO topping powder is not stable for extended storage periods. It loses its whipping property, probably due to a change in the crystalline properties of the fat phase.

Toppings with GMS or free of surfactants gave very light foams with large air bubbles. These foams were very unstable and separated quickly into a water phase with a collapsed cream layer at the top.

Crystallization measurements—The TEM studies described above indicate that crystallization of the lipid phase in the topping powders took place after they had been reconstituted in water. This crystallization process was evaluated using a pulsed-NMR technique with deuterated water as solvent in order to eliminate the proton signal from water. The topping emulsions were reconstituted, stored, and analyzed under isothermal conditions.

Fig. 20 shows the results of pulsed-NMR measurements of a topping emulsion with 8% of PGMS as surfactant. Since both the maltodextrin and the sodium caseinate are dissolved in D_2O, the signal from protons in the solid state can only arrive from the crystallized fraction of the lipid phase. From Fig. 20 it appears that at 20°C and 35°C there is no change in the solid fat

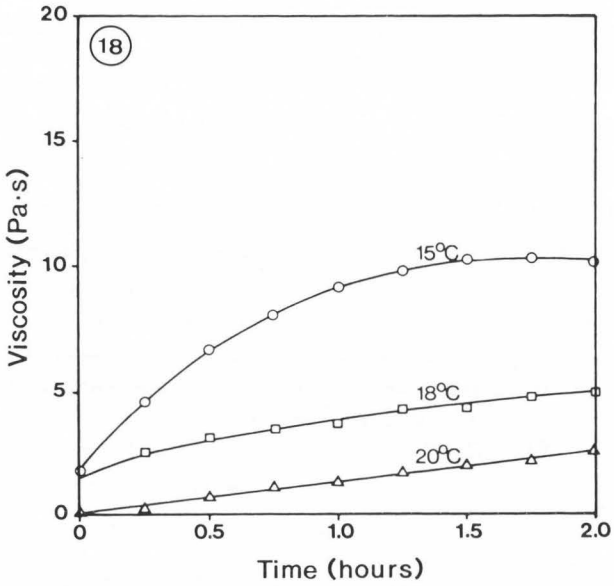

Fig. 18. Viscosity of the reconstituted topping emulsion (1:3) with PGMS (Promodan SP) at different temperatures as a function of time. Shear rate 1.76 sec^{-1}.

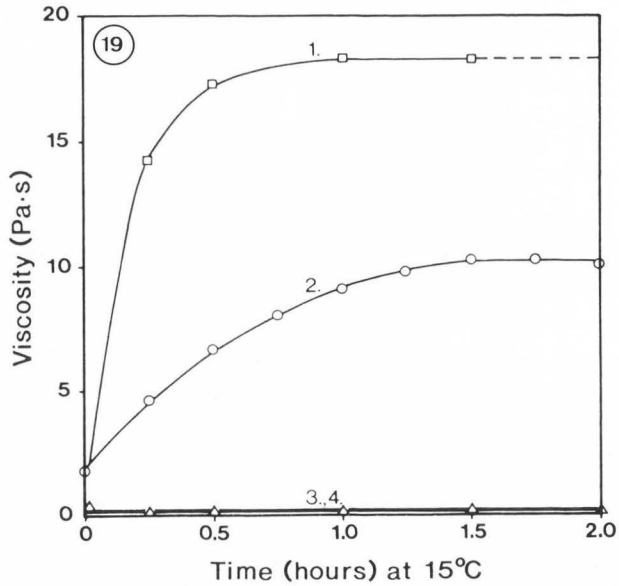

Fig. 19. Viscosity of reconstituted topping emulsions (1:3) with different surfactants as a function of time at 15°C. Shear rate 1.76 sec^{-1}. 1: GMO (Dimodan O), 2: PGMS (Promodan SP), 3: GMS (Dimodan PV), 4: no surfactant added.

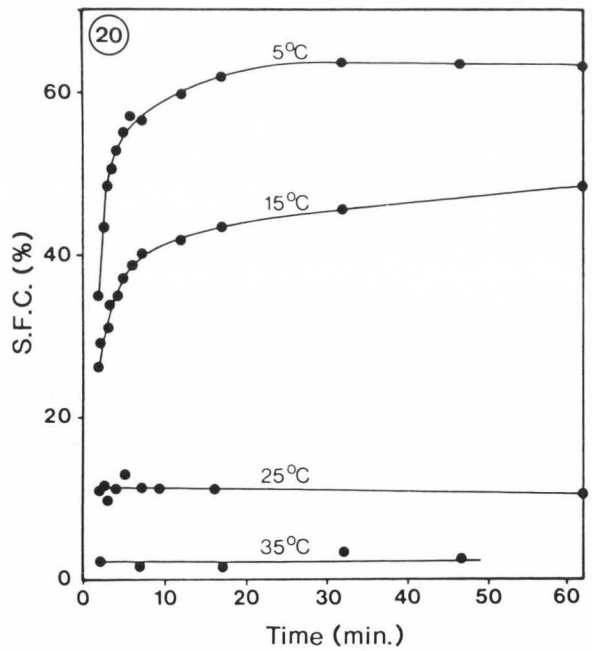

Fig. 20. Crystallization of supercooled lipid fractions in the topping emulsion with PGMS, reconstituted (1:3) in deuterated water (D_2O), measured by pulsed-NMR at different temperatures. SFC: solid fat content.

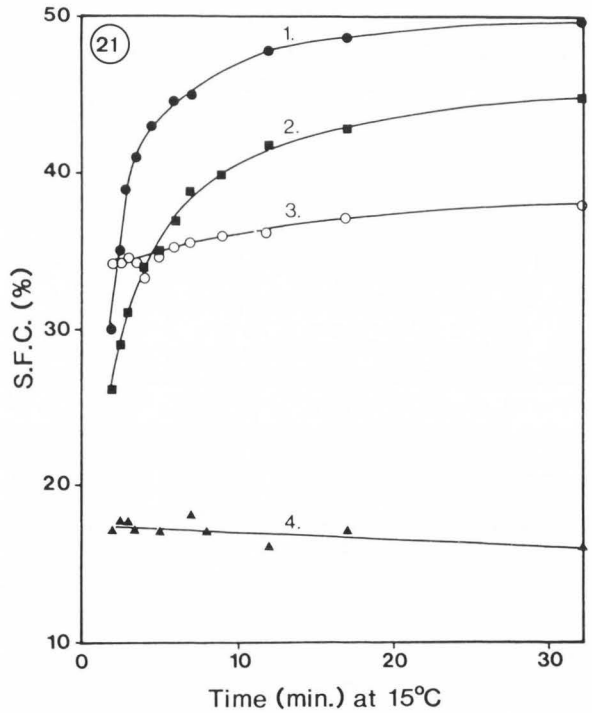

Fig. 21. Crystallization of supercooled lipid fractions in topping emulsions with different surfactants, reconstituted (1:3) in deuterated water (D_2O), measured by pulsed-NMR at 15°C. SFC: solid fat content. 1: GMO (Dimodan O), 2: PGMS (Promodan SP), 3: GMS (Dimodan PV), 4: no surfactant added.

content (SFC) with time, while at 15°C and even more so at 5°C there is an increase in the SFC indicating that a crystallization process is taking place in the emulsion immediately after reconstitution.

The SFC at 5°C and at 15°C increase rapidly in the first few minutes after reconstitution and reach a maximum after 10–20 min. The influence of various surfactants on the destabilization and crystallization after reconstitution in D_2O is shown in Fig. 21. The unsaturated monoglyceride (GMO) gives a higher rate of crystallization at 15°C than PGMS. The saturated monoglyceride (GMS) shows only a slight increase in the SFC after reconstitution in D_2O indicating minimal destabilization. Similarly the topping free of surfactants shows no increase in the SFC after reconstitution in D_2O. The higher level of the SFC curve for the GMS emulsion is due to the increased solid content in the lipid phase from the addition of saturated monoglycerides.

The spray-dried topping powders were examined by X-ray diffraction to establish the type of crystal modification of the fat.

Topping powders with PGMS were always found to be in the β'-form (short spacings of 0.38 nm–0.42 nm) even after a long term storage at 15°C. Toppings containing GMS or GMO were also in the β'-form in fresh powder, but after about 1 month storage, a mixture of β' and β-crystals (main short spacing 0.455 nm) was found. When the topping powders were reconstituted in water (1:1 by weight) at 15°C and then examined by X-ray diffraction crystal-forms similar to those in the dry state were found. However, in spite of the dilution with water, an increase in line intensity was observed indicating an increase in crystallinity after mixing with water at 15°C.

Discussion

The particle size distribution of the fat globules in the spray-dried topping powders varies considerably, dependent on the type of surfactant used. When using either saturated monoglycerides (GMS, Dimodan PV) or unsaturated monoglycerides (GMO, Dimodan O), a more uniform particle diameter is found than in powders made with PGMS or without surfactants. Furthermore, the internal structure of the lipid droplets is affected by the surfactants as observed by the different cleavage pattern, whether they contain GMS or GMO (Figs. 2a, b and Figs. 3a, b) or no surfactant (Figs. 4a, b). With PGMS, the particle size diameter is less homogeneous than with GMO and GMS which may be related to the hydrophilic/lipophilic properties of these surfactants, since PGMS is less hydrophilic than GMO or GMS.

After reconstitution of topping powders in cold water the emulsion is quickly destabilized and the structure of the fat phase is drastically changed from a dispersion of lipid droplets into a network of crystals formed from coalesced lipid particles. The degree of destabilization and subsequent lipid crystallization is dependent on the type of surfactant used in the topping powder. PGMS and GMO have a strong destabilization effect and increase the viscosity of the emulsions reconstituted in water, whereas the reconstituted emulsion with GMS remains stable and has a low viscosity.

The formation of a network of plate-like crystals as seen by electron microscopy is presumably the major cause for the increase in viscosity. The increase in viscosity is also closely related to the crystallization process as measured in emulsions by pulsed-NMR. Furthermore, the viscosity and the degree of crystallization in the emulsions are related to whippability and firmness of the whipped cream.

Because of the spontaneous fat crystallization as measured by pulsed-NMR after reconstitution of the powders in D_2O under isothermal conditions, it is believed that most of the lipid droplets in the spray-dried topping powders are in a supercooled state. This supercooling might be the driving force behind the crystallization taking place in the reconstituted emulsions. The destabilization process might be initiated by desorption of the protective protein layer (sodium caseinate) around the lipid droplets, followed by coalescence of the unprotected droplets leading to the crystallization of the supercooled lipid fraction. The degree of supercooling is being further investigated by the pulsed-NMR technique.

The electron microscopy observations on whipped toppings (Figs. 14, 15, 16) show that the air bubbles are stabilized by adsorbed plate-like lipid crystals of the destabilized emulsion. This shows a different foam structure as compared to that of liquid UHT imitation cream (Fig. 17) or as described for dairy cream (2, 4, 5). The air bubbles in whipped imitation cream as well as dairy cream are stabilized by agglomerated, yet genuine fat globules. In whipped dairy cream the flocculation of the fat globules is promoted by the presence of fat crystals on the surface of fat globules from which the milk fat globule membrane has been partially removed (2).

The microstructure of a whipped topping is thus significantly different from that of whipped imitation cream or whipped dairy cream. Further studies are necessary to understand the mechanism leading to the destabilization of the emulsions of the reconstituted systems, especially the role of the surfactants and the proteins.

Acknowledgement

The excellent technical assistance by Mrs. G. Falk is gratefully acknowledged. We are thankful to Dr. M. Kalab for his help in preparing this manuscript.

References

1. Andreasen J. (1981). Geeignete Emulgatoren und deren Wirkungsmechanismus in Milchdesserts. Deutsche Molkerei-Zeitung **36**, 1161–1166.

2. Buchheim W. (1978). Mikrostruktur von geschlagenem Rahm, Gordian **6**, 184–188.

3. Buchheim W. (1981). A comparison of the microstructure of dried milk products by freeze-fracturing powder suspensions in non-aqueous media, Scanning Electron Microsc. 1981; III: 493–502.

4. Darling DF. (1982). Recent advances in the destabilization of dairy cream. J. Dairy Res. **49**, 695–712.

5. Schmidt DG, Van Hooydonk ACM. (1980). A scanning electron microscopical investigation of the whipping of cream, Scanning Electron Microsc. 1980; III: 653–658, 644.

6. Van Putte K, Van den Enden J. (1974). Fully automated determination of solid fat content by pulsed NMR. J. Am. Oil Chemists Soc. **51**, 316–320.

Discussion with Reviewers

J.M. deMan: The cryofixation technique involves sample preparation at low temperature. How would the structural features of solidified fat relate to the actual conditions prevailing at the temperature of use of these products? What is meant by the expression "amorphously solidified" (e.g., in the legend to Fig. 4b)?
Authors: According to our experience the cooling rates during the cryofixation procedure used are generally high enough in order to avoid the formation of fat crystals. Liquid fat solidifies in a manner which results in a largely amorphous fine structure on freeze-fracture electron micrographs. For this reason visible fat crystals actually existed in the specimen before cryofixation. It appears, however, necessary to apply more advanced cryofixation procedures with much higher cooling rates (e.g., the propane-jet freezing method) in order to obtain further experience.

P. Walstra: In my view it is highly probable that in the emulsions with PGMS and GMO fat crystals stick partly out of the droplets, which makes the latter vulnerable to partial coalescence, particularly during shear (see e.g., M.A.J.S. van Boekel & P. Walstra, Colloids and Surfaces, **3** (1981), 109, and your reference 4). During dissolving, shear is inevitable and partial coalescence or clumping occurs. This may then trigger further crystal growth, as some droplets must have been devoid of crystals due to supercooling (see e.g., P. Walstra & E.C.H. van Beresteyn, Neth. Milk Dairy J. **29** (1975), 35). The size and shape of the crystals and particularly their contact angle with oil and water may depend on the surfactant, and these factors strongly affect the partial coalescence, which, in turn, causes the increase in viscosity and affects whipping properties.
Authors: In general, our TEM observations of reconstituted emulsions, containing GMO or PGMS, show that the lipid phase is present in the form of a network of crystal-plates rather than globular lipid droplets. The mechanism suggested by you may well be the initial step in the structural change from gloublar lipid droplets to a crystal matrix.

We think, however, that the crystallization taking place in toppings goes far beyond of what takes place at the surface of the globules, but rather involves the whole lipid phase. Here we also must consider the difference in composition of our topping emulsions compared to dairy emulsions referred to in the references given by you. The concentration of surfactants (i.e., PGMS) in toppings is as high as 12–20% based on the total lipid phase, while it is much lower in dairy emulsions. Furthermore the TEM observations of whipped toppings with GMO or PGMS show that the foam is stabilized by adsorbed lipid crystals oriented at the air-water interface, and not by globular lipid droplets as found with dairy cream according to ref. 2, 4 and 5, and as found here with imitation cream (see Fig. 17).

P. Walstra: Due to the presence of surfactant, the contact angle as measured in water may even become small enough for the crystals to become easily dislodged from the oil droplets (or their remnants). Perhaps they flocculate as such (although on the other hand the aggregates may just be due to partial coalescence). The crystals can easily become adsorbed into the air-water interface, thereby stabilizing the air bubbles aginst disproportionation and coalescence.
Authors: We think your comment is very relevant to our findings, especially in the light of the high surfactant concentration needed in topping system in order to obtain the necessary destabilization and to obtain satisfactory whipping properties.

FOOD MICROSTRUCTURE, Vol. 4 (1985), pp. 233-239
SEM Inc., AMF O'Hare (Chicago), IL 60666-0507 U.S.A.

0730-5419/85$1.00+.05

THERMAL ANALYSIS MICROSCOPY FOR THE STUDY OF PHASE CHANGES IN FATS

J.M. deMan, A.N. Mostafa and A.K. Smith

Department of Food Science, University of Guelph,
Guelph, Ontario, Canada N1G 2W1

Abstract

An investigation was carried out using the Mettler FP800 Thermosystem to study polymorphic transitions of several monoacid triglycerides and hydrogenated Canola oil. The system includes a central processing unit connected with a thermal microscopy hot stage that allows the measurement of heat flow to the sample. Scanning electron microscopy was also used to examine the same samples after osmium tetroxide fixation. The results obtained relate phase transitions occurring during heating and cooling with the morphology of the various crystal structures.

Initial paper received February 22 1985
Manuscript received July 17 1985
Direct inquiries to J.M. deMan
Telephone number: 519-824-4120 x2515

KEY WORDS: Fat crystallization, polymorphism, thermal analysis microscopy, polarized light microscopy, scanning electron microscopy, differential scanning calorimetry, triglycerides, crystal structure, crystal morphology, Canola oil.

Introduction

Polymorphism is the ability of a substance to exist in more than one crystalline form. Fats can crystallize in three major polymorphic forms, namely alpha (α), beta-prime (β') and beta (β), which have different melting points and crystal packing in the crystal lattice. The function and performance of fats in different foods are influenced by their crystal structure and by polymorphic transitions occurring during the manufacture and storage of these products. Several techniques have been applied to study polymorphism of lipids. In the forefront are X-ray diffraction, light and electron microscopy, infrared spectroscopy and thermal analysis. X-ray diffraction analysis is used for determining the different polymorphic forms by their characteristic short spacings and long spacings (7). This technique also allows the recording of diffraction patterns as a function of temperature on a moving film (11). Infrared spectroscopy was introduced by Chapman (2) for the study of polymorphic transitions in the field of lipids. He has shown that polymorphic changes occurring in triglycerides and fats are reflected in changes occurring in the CH_2-CH_2 rocking vibration region of the infrared spectrum. In recent years, differential scanning calorimetry (DSC) has been applied by several researchers to study changes occurring during cooling and heating of fats and triglycerides. This technique had wide application in the study of palm oil and its fractions (5); and in the study of the effect of crystal structure modifiers added to triglycerides (6). Light and electron microscopy have been successfully used to study the appearance of the different crystal forms and the arrangements of fats in food systems like milk, cream and butter. Several excellent reviews on this subject are available (1,3).

Recently, a new method has become available which enables the simultaneous microscopic observation of samples on a hot stage during heating and cooling and the recording of differential scanning calorimetry data (thermal analysis microscopy, TAM). This paper deals with the application of TAM to the phase transformations of triglycerides and hydrogenated Canola oil.

Materials and Methods

Tristearin (m.p. 68-70°C), tripalmitin (m.p. 60-62°C) and trimyristin (m.p. 57-59°C) were purchased from J.T. Baker Chemical Co., New Jersey; and recrystallized from acetone. Their purity was checked by GLC of the methyl esters on a 12% DEGS column. Canola oil was commercially refined and bleached (CSP Foods Ltd., Altona, Manitoba). It was hydrogenated under selective conditions (200°C; 48 kPa hydrogen pressure) to an iodine value of 60 in a Parr pressure hydrogenator. The hydrogenated product was treated with dioctylsulfosuccinate according to the method reported by Poot et al. (9) to remove the oil phase. Thermal analysis microscopy was carried out with a Mettler FP800 thermal analysis system consisting of a central processing unit (FP80) and a DSC hot stage (FP84). Transparent sapphire crucibles and covers were used to enable the observation of the samples under the microscope while the DSC curve was recorded. A polarizing light microscope (Olympus, model BH) was used with a PM-6 camera attachment.

For the first part of this study, the samples were heated (5°C/min) in the hot stage DSC cell, to a temperature 20°C above their beta form melting points and held there for 20 min to destroy any "memory" of earlier crystals (4). Cooling was then started (10°C/min) using liquid nitrogen as a coolant to 10°C below the respective alpha form melting points. The samples were then heated (5°C/min) and the scans were recorded and photographs taken at the same time to identify the polymorphic forms. Melting and recrystallization temperatures were determined using the method and formulas given in the Mettler FP800 instruction manual where the displayed event temperature corresponds to the cell temperature and the sample temperature can be calculated using the value determined for τ_{lag} (lag time constant of the furnace).

For the second part of this study, the samples were mounted on aluminum stubs and fixed using osmium tetroxide vapour (8). Osmium tetroxide was 99.95% pure, purchased in 0.5 g ampoules (Can-em Chemical Distr., Guelph, Ont., Canada). Crystals in the beta form were obtained by crystallization from acetone. This was done by dissolving the samples in acetone by heating in a water bath at 70°C. The solutions were then filtered while still warm and cooled to 10°C. The crystals thus produced were filtered, dried and stored in a desiccator at 10°C. The beta-prime form was obtained by isothermal crystallization from the melt in a DSC cell (DuPont 900). The samples were placed in aluminum pans and heated to 90°C at a rate of 10°C/min to ensure that all crystal nuclei were destroyed. This was followed by cooling the samples at a rate of 5°C/min to a temperature 6-8°C below the melting point of their respective beta-prime form where the samples were held isothermally to allow crystallization in the beta-prime form. A mixture of beta-prime and beta form was obtained only for tristearin by crystallization from ethyl acetate. Cooling (10°C/min) of the melted samples in the DSC cell, using liquid nitrogen, produced the alpha form of tristearin and tripalmitin, a mixture of alpha and beta-prime form of trimyristin and the beta-prime form of hydrogenated Canola oil. The polymorphic forms of all of the samples were confirmed by X-ray diffraction analysis at 10°C, using a Guinier camera model FR552 of Enraf-Nonius, Delft, The Netherlands. After fixation, the samples were coated with gold/palladium 30-40 um in a Hummer V Sputter coater prior to viewing under the electron microscope. An ETEC autoscan scanning electron microscope was used at an accelerating voltage of 5 kV.

Results and Discussion

The purified triglycerides differed slightly in their polymorphic transitions. Tristearin (SSS) and tripalmitin (PPP) were similar as is evident from the DSC scans shown in Figures 1 and 2. Both crystallized in the alpha form upon cooling and event 1 in both figures represents the onset of melting of this form. Further transition to the beta-prime form was evident from the exotherm (event 2), followed by an endotherm showing the melting of this form (event 3). Recrystallization in the beta form was slow and occurred only when the temperature was held above the beta-prime melting point for

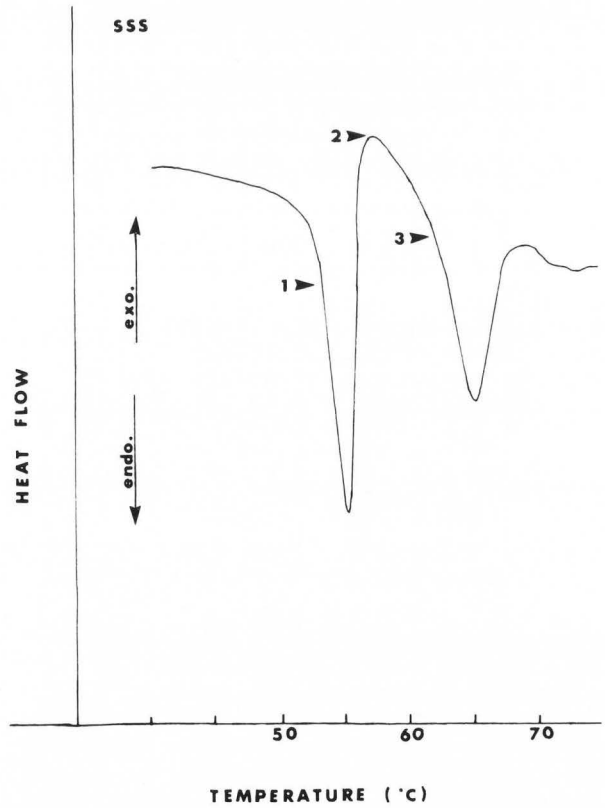

Fig. 1. DSC scan of tristearin recorded using the FP800 thermosystem.

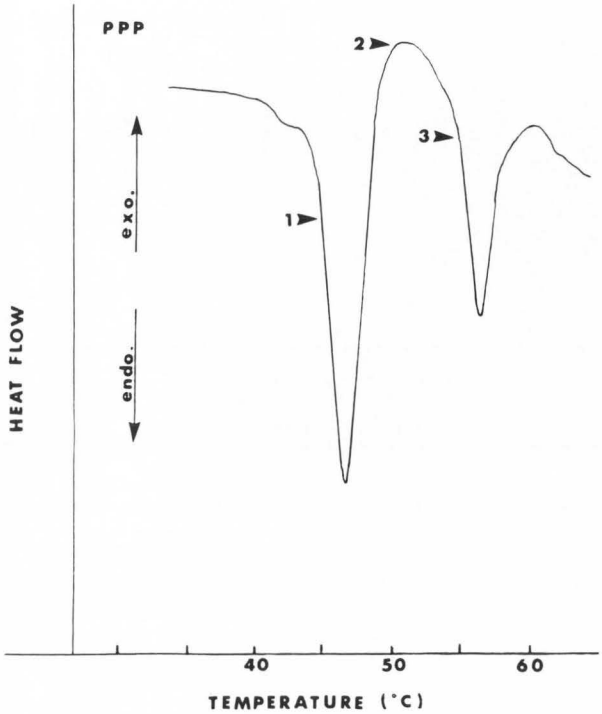

Fig. 2. DSC scan of tripalmitin recorded using the FP800 thermosystem.

at least one hour. Figure 3 represents the alpha form of tristearin and Figure 4 that of tripalmitin as viewed under the light microscope during recording of the DSC curve. Both micrographs show the spherulitic pattern that was also observed by other researchers (10). The beta-prime form of tristearin is shown in Figure 5 and that of tripalmitin in Figure 6. The

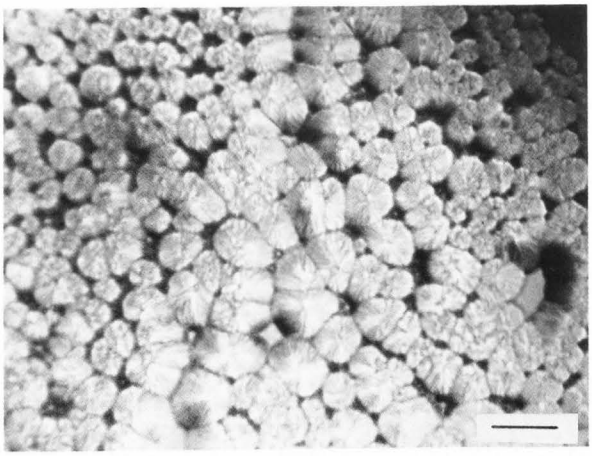

Fig. 3. Micrograph showing the alpha form of tristearin as viewed by polarized light microscopy (bar = 25 µm).

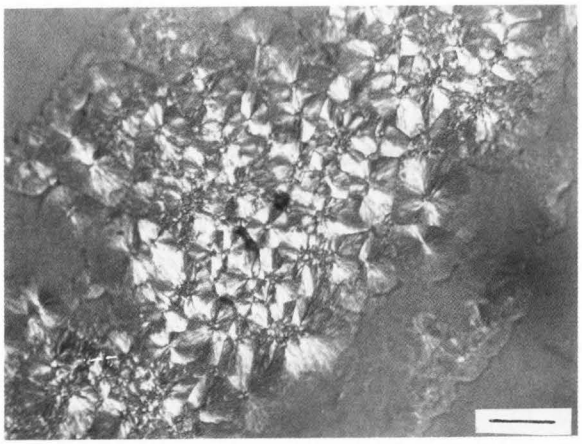

Fig. 4. Micrograph showing the alpha form of tripalmitin as viewed by polarized light microscopy (bar = 25 µm).

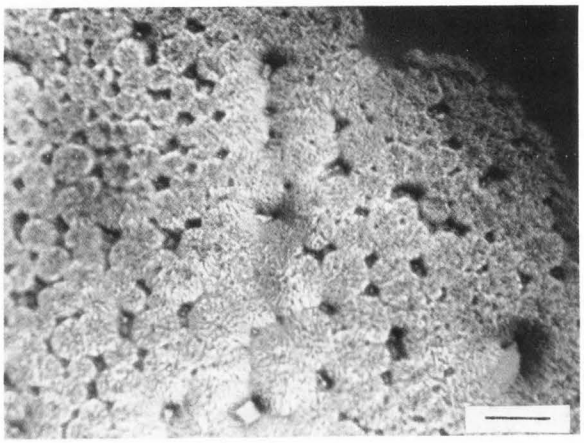

Fig. 5. Micrograph showing the beta-prime form of tristearin as viewed by polarized light microscopy (bar = 25 µm).

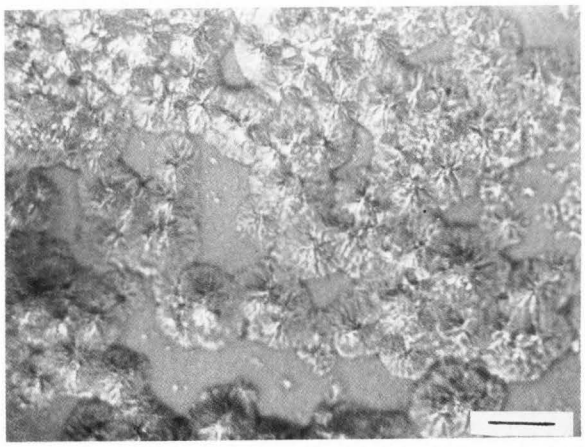

Fig. 6. Micrograph showing the beta-prime form of tripalmitin as viewed by polarized light microscopy (bar = 25 µm).

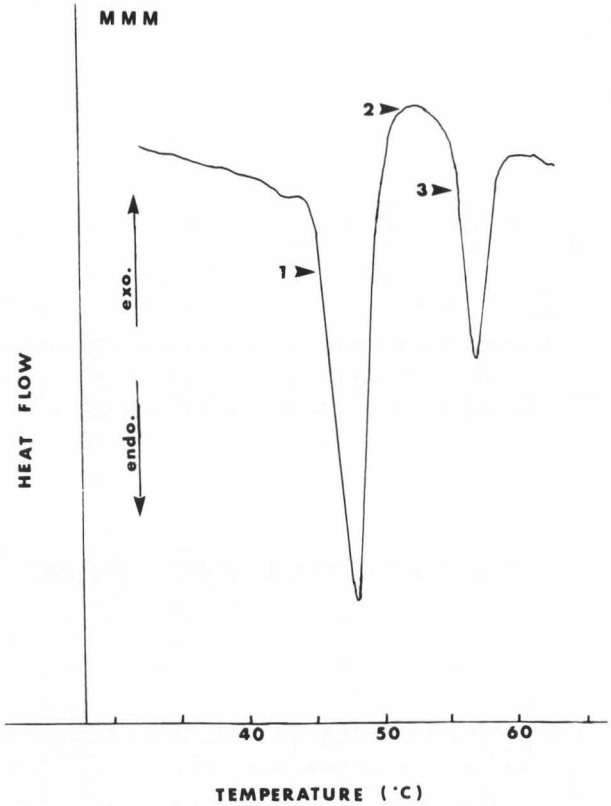

Fig. 7. DSC scan of trimyristin recorded using the FP800 thermosystem.

micrographs show loosely packed spherulites. When trimyristin was examined, a different pattern was observed. Quenching the melt resulted in a mixture of alpha and beta-prime forms (Figure 7) and this was confirmed by X-ray diffraction analysis. Event 1 in Figure 7 represents the onset of melting of the mixed crystals and event 2 represents recrystallization

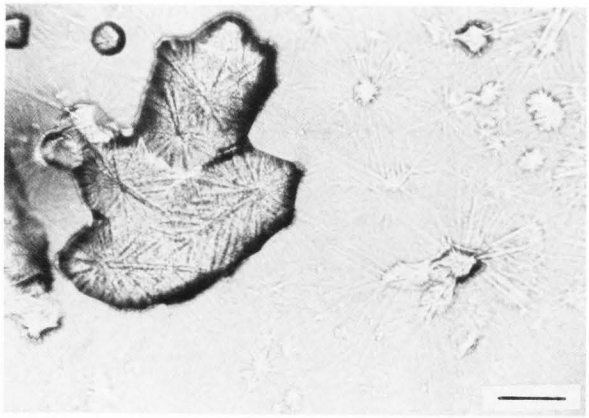

Fig. 8. Micrograph showing a mixture of alpha and beta-prime forms of trimyristin as viewed by polarized light microscopy (bar = 25 μm).

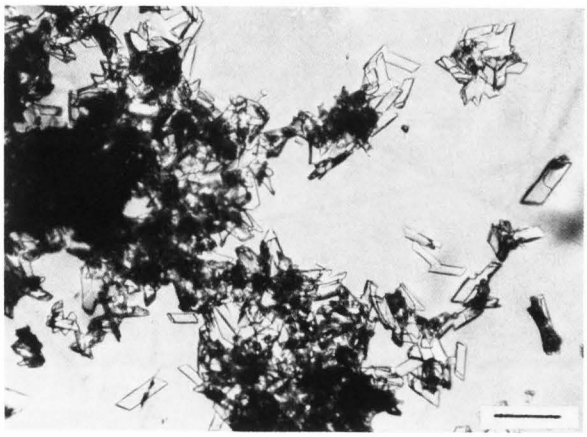

Fig. 9. Micrograph showing the beta form of trimyristin as viewed by polarized light microscopy (bar = 25 μm).

in the beta form followed by its melting (event 3). The mixed crystal form is represented in Figure 8 showing feather-like clusters. Figure 9 shows the beta form of the same sample with the chisel-like single crystals scattered around opaque clusters. Hydrogenated Canola oil (Figure 10) exhibited a broader and simpler DSC scan. There was only one endotherm (event 1) representing melting of the beta-prime form. The

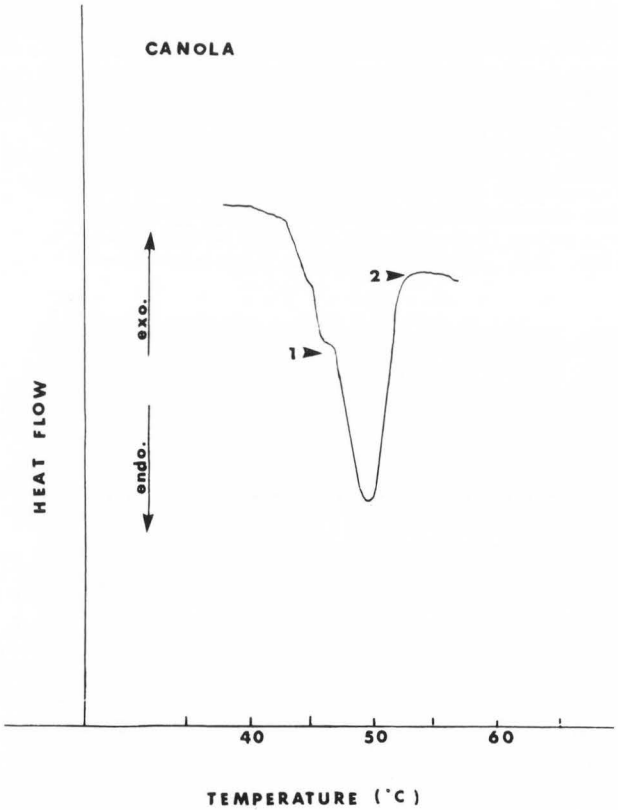

Fig. 10. DSC scan of hydrogenated Canola oil recorded using the FP800 thermosystem.

micrograph of this sample (Figure 11) shows the feather-like clusters of this form. Recrystallization in the beta form from the melt was very slow and the crystals of this form are represented in Figure 12. Table 1 summarizes the melting and transition points of all of the events noted on the DSC scans for the previously discussed samples.

In the second part of this study, recrystallization from acetone produced pure beta crystals. SEM micrographs of the samples studied are as follows: Figure 13 shows a round spherulite of tristearin surrounded by groups of stacked crystals. The same pattern of round spherulites was also observed for trimyristin (Figure 14) and hydrogenated Canola oil (Figure 15). Tripalmitin showed a pattern of stacked plates (Figure 16). Crystallization from ethyl acetate provided a mixture of beta-prime and beta crystals. This is represented in Figure 17 for tristearin showing a round spherulite surrounded by a loosely packed network of beta-prime crystals. Quenching the samples from the melt in the DuPont DSC cell resulted in alpha crystals for tristearin and tripalmitin respectively (Figures 18 and 19). Trimyristin yielded a mixture of alpha and beta-prime forms (Figures 20 and 21). X-ray diffraction analysis was used to confirm the polymorphic forms of all of the samples before fixation with OsO_4.

In this study, combining thermal analysis (DSC) with hot stage microscopy has been of great value in the simultaneous determination of the melting and transition points and their microscopic appearance. The appearance of various crystal forms or their morphology determines the texture of the final products. SEM used in the second part of this study made it possible to observe the crystals in their different forms without excessive handling which might result in artifacts.

The phase behaviour of fats and their mixtures has recently been reviewed by Timms (12). The availability of TAM microscopy has added another tool in the study of phase transformations of fats and this can significantly increase our knowledge of the morphology of the various crystal forms.

Acknowledgement

Financial support was received from the Natural Sciences and Engineering Research Council of Canada and the Ontario Ministry of Agriculture and Food.

References

1. Buchheim W, Aspects of sample preparation of freeze-fracture/freeze-etch studies of proteins and lipids in food systems. A review, Food Microstructure 1, 1982, 189-208.

2. Chapman D, Infrared spectroscopy of lipids, J. Am. Oil Chemists' Soc. 42, 1965, 353-371.

Table 1. Temperatures of the main events occurring during heating of tristearin, tripalmitin, trimyristin and hydrogenated Canola oil.

Sample	Corrected melting and transition points °C		
	Event 1	Event 2	Event 3
Tristearin	51.8	55.8	62.5
Tripalmitin	43.8	49.8	55.0
Trimyristin	42.8	50.0	55.8
Hydrogenated Canola oil	44.8	50.8	-

3. deMan J M, Microscopy in the study of fats and emulsions, Food Microstructure 1, 1982, 209-222.

4. Hernqvist L, On the structure of triglycerides in the liquid state and fat crystallization, Fette Seifen Anstrichmittel 86,1984, 297-300.

5. Kawamura K, The DSC thermal analysis of crystallization behaviour in palm oil, J. Am. Oil Chemists' Soc. 56, 1979, 753-757.

6. Lee S, deMan J M, Effect of surfactants on the polymorphic behaviour of hydrogenated Canola oil, Fette Seifen Anstrichmittel 86, 1984, 460-465.

7. Lutton E S, Review of the polymorphism of saturated even glycerides, J. Am. Oil Chemists' Soc. 27, 1950, 276-281.

8. Naguib Mostafa A, Smith A K, deMan J M, Crystal structure of hydrogenated Canola oil, J. Am. Oil Chemists' Soc. 62, 1985, 760-762.

9. Poot C, Dijkshoorn W, Haighton A J, Verburg C C, Laboratory separation of crystals from plastic fats using detergent solution, J. Am. Oil Chemists' Soc. 52, 1975, 69-72.

10. Quimby O T, Microscopic appearance of polymorphic forms of one acid triglycerides, J. Am. Chem. Soc. 72, 1950, 5064-5068.

11. Riiner Ü, Investigation of the polymorphism of fats and oils by temperature programmed X-ray diffraction, Lebensm. Wiss. Technol. 3, 1970, 101-106.

12. Timms R E, Phase behaviour of fats and their mixtures, Progr. Lipid Res. 23, 1984, 1-38.

Discussion with Reviewers

F.J. Sasevich: In fixation of triglycerides, osmium tetroxide is thought to react with the

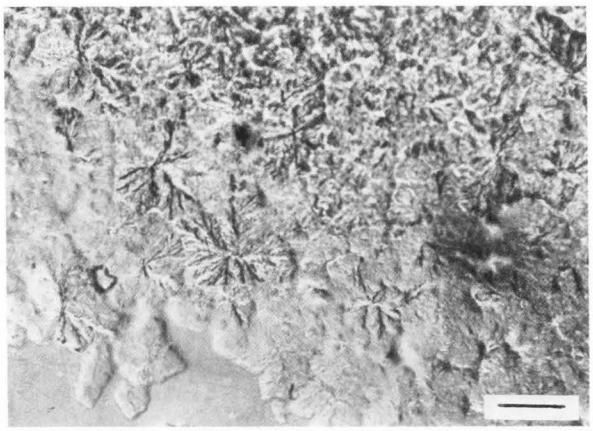

Fig. 11. Micrograph showing the beta-prime form of hydrogenated Canola oil as viewed by polarized light microscopy (bar = 25 µm).

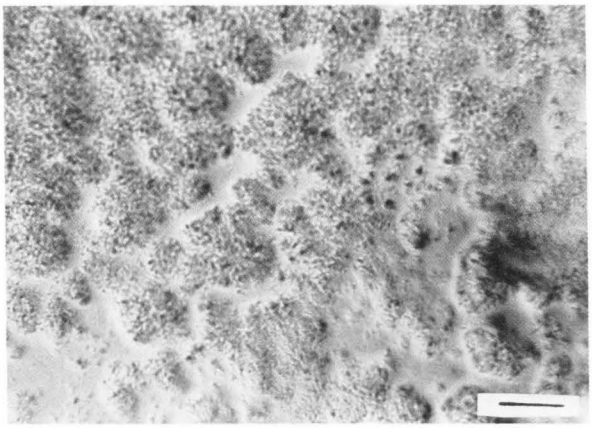

Fig. 12. Micrograph showing the beta form of hydrogenated Canola oil as viewed by polarized light microscopy (bar = 25 µm).

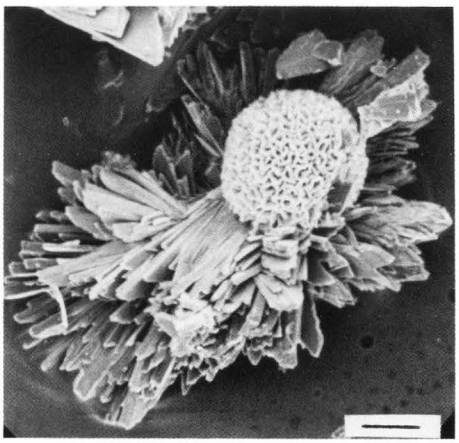

Fig. 13. Micrograph showing beta form of tristearin viewed by SEM (bar = 10 µm).

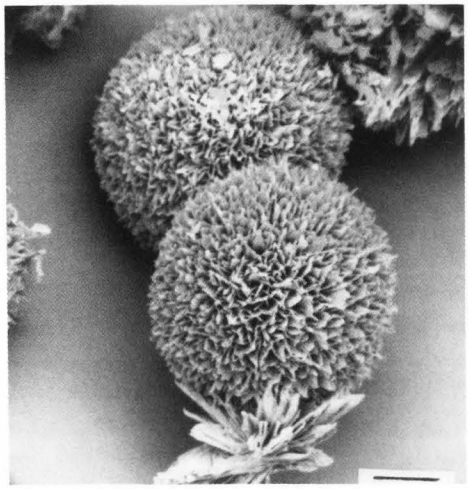

Fig. 14. Micrograph showing beta form of trimyristin viewed by SEM (bar = 10 µm).

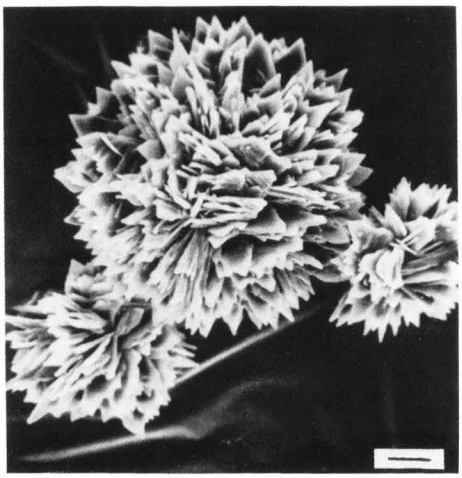

Fig. 15. Micrograph showing the beta form of hydrogenated Canola oil viewed by SEM (bar = 10 µm).

double bonds, forming crosslinks. Some saturated lipids such as phospholipids may also react with osmium tetroxide at elevated temperatures (60°C). How is osmium tetroxide reacting with your pure, saturated crystals in SEM preparation?

Authors: Spectroscopic data, including infrared and C^{13} nuclear magnetic resonance, indicate the following: The spectra of the saturated triglycerides, e.g. tristearin before and after fixation were identical. The infrared spectrum of hydrogenated Canola oil exhibited an additional band at 780 cm^{-1} after fixation. This indicated the possible interaction between the double bonds present in the unsaturated fat and OsO_4. The mechanism of this interaction has been discussed in reference 10. It appears that no chemical reaction is involved in the fixation of saturated lipids with OsO_4.

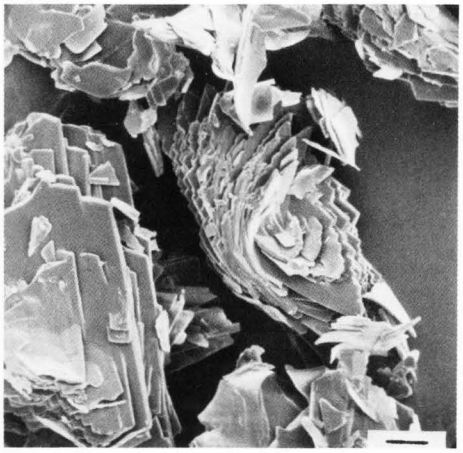

Fig. 16. Micrograph showing the beta form of tripalmitin viewed by SEM (bar = 10 µm).

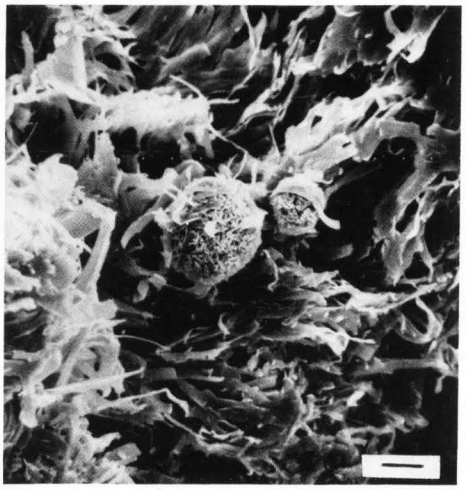

Fig. 17. Micrograph of a mixture of beta-prime and beta forms of tristearin viewed by SEM (bar = 10 µm).

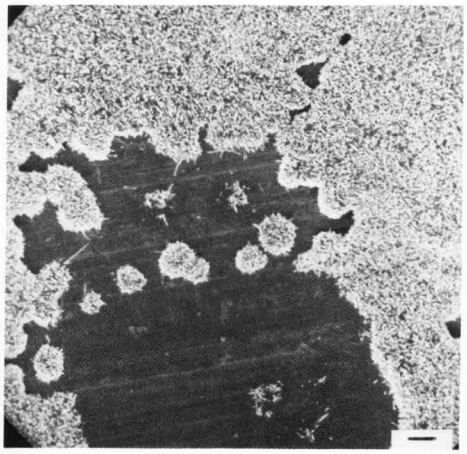

Fig. 18. Micrograph showing alpha form of tristearin viewed by SEM (bar = 10 µm).

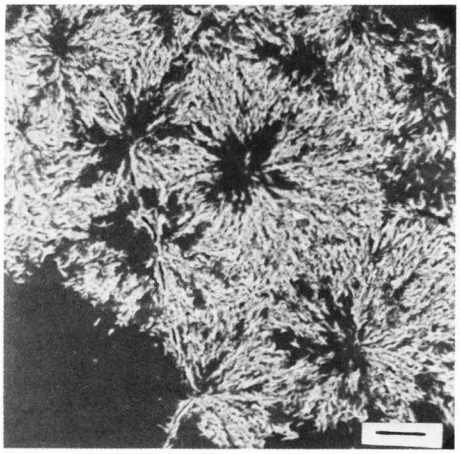

Fig. 19. Micrograph showing alpha form of tripalmitin viewed by SEM (bar = 10 µm).

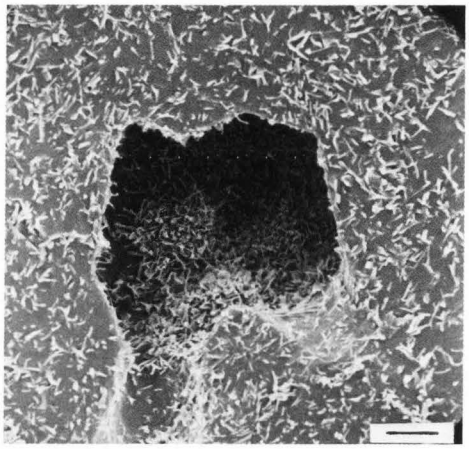

Fig. 20. Micrograph showing a mixture of alpha and beta-prime forms of trimyristin as viewed by SEM (bar = 10 µm).

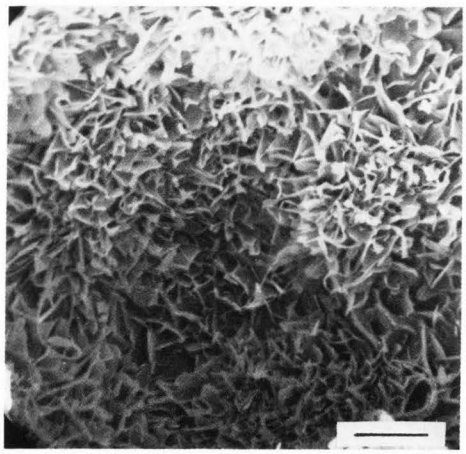

Fig. 21. Micrograph of the sample shown in Fig. 20 at a higher magnification (bar = 5 µm).

FOOD MICROSTRUCTURE, Vol. 4 (1985), pp. 241-248
SEM Inc., AMF O'Hare (Chicago), IL 60666-0507 U.S.A.

0730-5419/85$1.00+.05

COMBINING MICROSCOPY AND PHYSICAL TECHNIQUES IN THE STUDY OF COCOA BUTTER POLYMORPHS AND VEGETABLE FAT BLENDS

J. D. Hicklin, G. G. Jewell and J. F. Heathcock

Cadbury Schweppes plc
The Lord Zuckerman Research Centre, The University,
Whiteknights, PO Box 234, Reading, RG6 2LA, U.K.

Abstract

Transmission electron microscopy, differential scanning calorimetry and X-ray diffraction have been used to study the cocoa butter polymorphs and blends of cocoa butter with a hydrogenated vegetable fat. The results indicate the presence of six polymorphs and confirm observations made by other workers. Vegetable fat addition affects both the molecular structure and the morphology of the crystals observed. After temperature cycling, a blend containing 50% vegetable fat developed two crystal types and differences in the X-ray pattern were apparent. Correlations could be made between the known molecular structure and the morphology observed in most of the polymorphs. In selected cases, and particularly the blends containing vegetable fat, knowledge of the polymorphic form did not always enable an accurate prediction of morphology.

Initial paper received February 07 1985
Manuscript received August 16 1985
Direct inquiries to J.D. Hicklin
Telephone number: 44 734 868541

Key Words: cocoa butter polymorphs, hydrogenated vegetable fat, fat blends, Transmission Electron Microscopy, X-ray diffraction, Differential Scanning Calorimetry, freeze-fracture, chocolate.

Introduction

The study of cocoa butter continues to be of interest to the food industry due to its commercial importance in the manufacture of chocolate.

Although cocoa butter is a mixture of triglycerides it can exist in a number of distinct polymorphs (Wille & Lutton, 1966). A number of methods have been used to investigate them. Chapman et al. (1971) undertook a study comprising X-ray diffraction and Differential Scanning Calorimetry (DSC) on the polymorphism of cocoa butter. The carbon replica technique for Transmission Electron Microscopy (TEM) has been shown to be the most suitable E.M. technique (Berger et al. 1979) to study the morphological characteristics of cocoa butter. It was apparent from all these studies that no single method can successfully provide the required data to allow characterisation. The work described, therefore, used X-ray diffraction, Differential Scanning Calorimetry and Transmission Electron Microscopy as complementary techniques on the same set of samples, in order to study cocoa butter polymorphs and the effect of vegetable fat addition.

The legislation in certain countries permits incorporation of vegetable fats up to 5% of the chocolate (15% of the fat phase). They are known commercially as Cocoa Butter Equivalents (CBE), and Cocoa Butter Substitutes (CBS). They have been described recently by Haumann (1984). CBE have triglycerides closely resembling those found in cocoa butter. CBS have some triglycerides not found in the cocoa butter system, but still have a limited compatibility with cocoa butter. The study involved the effect of a hydrogenated vegetable fat (CBS) on the properties of the cocoa butter.

Nomenclature

Two systems of nomenclature have been derived from earlier studies on cocoa butter polymorphism. One is attributable to Wille & Lutton (1966) and based on melting point, the other on crystallographic structure and developed by Larsson (1966) Table 1.

For simplicity, this paper used the I-VI classification but reference will also be made to

the Larsson nomenclature in discussing crystal structure.

TABLE 1

POLYMORPH		MELTING POINT*
WILLE & LUTTON	LARSSON	
I	β'_2 (γ)	17.3°C
II	α	23.3°C
III	$\alpha + \beta'$	25.5°C
IV	β'	27.5°C
V	β_2	33.8°C
VI	β	36.3°C

* (from Wille & Lutton, 1966)

Materials and Methods

Preparations

Polymorphs: The cocoa butter polymorphs were prepared by a similar approach to that given by Wille & Lutton (1966). In all the preparations, the cocoa butter had been heated to 50°C with agitation until molten, and then kept at this temperature for at least 2 hours.

Form I: Approximately 5 cm³ of the cocoa butter melt was flash frozen in liquid nitrogen (-196°C).

Form II: Approximately 5 cm³ of the cocoa butter melt was flash frozen in liquid nitrogen (-196°C) and stored in aluminium foil at 0°C for 2 hours prior to analysis.

Form III: Approximately 10 cm³ of the cocoa butter was flash frozen in liquid nitrogen and stored at 6°C overnight.

Form IV: Approximately 10 cm³ of the cocoa butter was pre-cooled to 6°C for 15-30 minutes and then crystallised at 16°C for 4 hours.

Form V: Approximately 30 cm³ of the melt was hand tempered by stirring at 15°C until crystal seed formed and then at 24°C until a thick slurry was produced, poured into a mould and placed in a fridge at 6°C. It was demoulded and stored for 24 hours at 20°C.

Form VI: A tablet of Form V cocoa butter was stored in an incubator for one week, the temperature was cycled between 20°C and 30°C with the sample spending 4 hours at each temperature.

Vegetable fat: Blends containing 10%, 20%, 30%, 40% and 50% (w/w) commercially available hydrogenated vegetable fat with cocoa butter were prepared. The blends were melted at 50°C and kept at this temperature for at least 2 hours. The liquid fat blend was tempered using the same regime employed to prepare Form V. Once demoulded it was stored for at least 24 hours before examination. The 50% blend was also temperature cycled, as described in Form VI preparation.

Techniques

X-ray diffraction: The sample was mounted in an aluminium holder for examination. The more unstable polymorphs were sandwiched between aluminium foil frozen in liquid nitrogen (-196°C) and secured into a cold block (-20°C). The experiments were performed on a Philips 1011/00 X-ray generator operating at 40 kV and 20 mA to give Cu radiation of X-ray wavelength λ= 1.54180 (Å). A D.P.T camera was used to record the patterns on Kodak X-ray film. A 15 minutes exposure was given. The long spacing data was determined to within ± 1 Å, the short spacings to ± 0.02 Å. No obvious transformations occurred during the experiment, although it is possible that some might occur in the more unstable systems.

Differential Scanning Calorimetry: A 15 mg sample was put in an aluminium pan and placed in the temperature controlled chamber. DSC measurements were taken on a Dupont 1090 Thermal Analyser operating at 2°C/min, between 15°C and 45°C, recording at 2 points/second. The protocol used Indium as the standard, the melting point being defined as the peak maximum.

Transmission Electron Microscopy: The TEM was performed using a pre-shadowed carbon replica technique. A freshly prepared sample (≅ 1 cm³) was flash frozen in liquid nitrogen (-196°C) and placed on a pre-cooled block. Fracture faces and surfaces were prepared. The block was then transferred into a Polaron coating unit, and a vacuum of better than 6 x 10^{-6} Torr drawn. A second pre-cooled (-196°C) block acted as an anti-contaminator within the chamber. Platinum was evaporated at an angle of 40° to a thickness of 30 Å, carbon was evaporated from directly over the sample producing a 350 Å layer. After removal from the unit, the replica was cleaned using ether and 2:1 chloroform/methanol. The replicas were examined using the JEOL 1200EX TEM operating at 80 kV.

Results

The X-ray data are listed in Table 2 and examples of the X-ray patterns are given in Fig. 1a-c. The DSC data are in Table 3. Although mixed triglycerides have a melting range (Timms, 1984), rather than a distinct melting point, the results presented are termed "melting points" in common with other workers, as they are observed as single distinct peaks. The TEM micrographs are in Figs. 2-10 and 12. They are negative prints, making the shadows appear dark.

Form I

Few distinct features existed in the morphology of this polymorph. Some lamellae were observed, although with only limited ordering into layers (Fig. 2). The X-ray data corresponded with those observed in the literature (Wille & Lutton, 1966), with short spacings of 3.70 and 4.19 Å characteristic of the sub α-structure of the polymorph. The DSC gave a melting point of 17.9°C.

Form II

The sample had a morphology consisting of lamellae with layering of the sheets as shown in Fig. 3. The individual sheets or lamellae

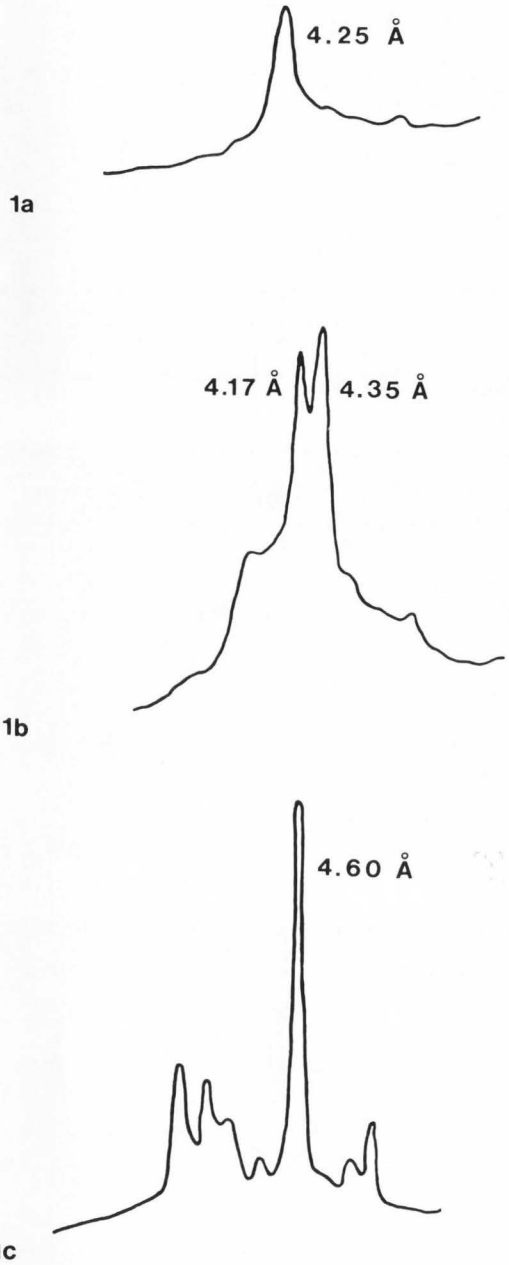

Figure 1. X-ray short spacings for Forms II, IV and VI. a. Short spacings of Form II. b. Short spacings of Form IV. c. Short spacings of Form VI.

appeared to be quite extensive spreading through the bulk of the sample. The individual lamella had a number of sheets stacked on one another. The X-ray pattern showed the disappearance of the 3.70 Å peak seen in Form I, and the development of a long spacing at 49 Å. The pattern typified the α-structure, Fig. 1a. The melting point was 24.4°C.

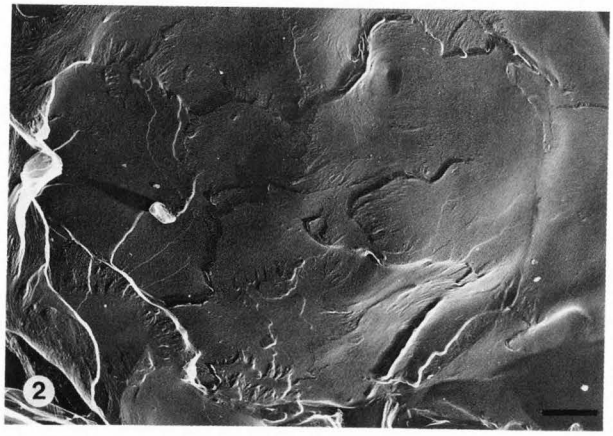

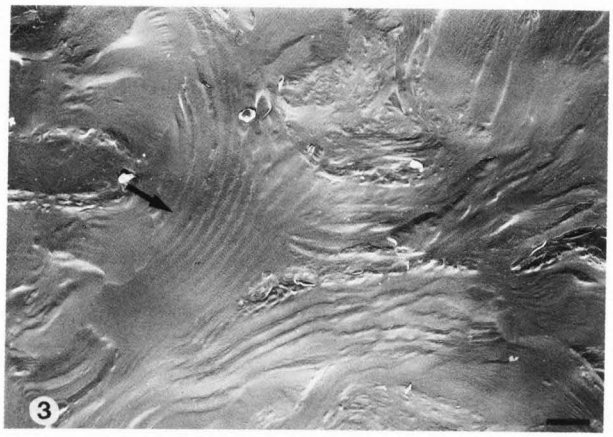

Figure 2. Form I Cocoa Butter, illustrating the lack of a distinct morphology. (Bar = 1 μm).

Figure 3. Form II Cocoa Butter, showing ordered lamellae (arrow). (Bar = 1 μm).

Figure 4. Form III Cocoa Butter, with protruding tubular crystals (arrow). (Bar = 1 μm).

Form III

The tubular crystals that protruded from the surface of the sample were very distinctive (Fig. 4). These crystals were distributed over all the surface, appearing as individual crystals (typically 2-3 μm long) though predominantly in clusters. The clusters appeared to involve 6 or more crystals within an area of about 4 μm. The background showed limited localised ordering. The X-ray pattern corresponded with that described by Wille & Lutton (1966). The development of two peaks at 15.24 and 16.6 Å, and a short spacing at 3.87 Å was characteristic. The melting point was 27.7°C.

Form IV

Form IV was characterised by needle-like crystals varying in length from 0.5 μm to 2 μm. They were distributed throughout the structure both on the surface and within the bulk (Fig. 5). The X-ray data had a doublet at 4.17 and 4.35 Å, and a long spacing of 46 Å, characteristic of the β' structure (Fig. 1b). The melting point was 28.4°C.

Form V

The crystals associated with Form V were up to 1 μm in length, well defined and regular in shape. They were frequently stacked on top of one another into multilayers of crystals (Fig. 6). The characteristic X-ray pattern had a strong 4.6 Å peak in the short spacing, and 66 Å in the long spacing - typical of the β structure. The melting point was 33.0°C.

Form VI

Significant differences in the morphology were observed in Form V following transformation to Form VI. Firstly, there was a general increase in the fat crystal size from 1 μm in Form V to 2-3 μm in Form VI. Secondly, a feature which was apparent on the surface was the protrusion of crystals (Fig. 7) often 3-4 μm or longer. Despite these significant differences in morphology the X-ray pattern only showed a small difference in relative intensities of some short spacing peaks from Form V. A single peak at 3.71 Å was observed, with lesser intensity peaks at 3.88 Å and 4.04 Å (Fig. 1c). The melting point increased to 34.6°C.

Addition of Vegetable Fat

The hydrogenated vegetable fat had a different morphology from that normally seen in cocoa butter, with large well defined crystals with an average size of 2-3 μm as seen in Fig. 8. The X-ray pattern was characteristic of a β' structure. The melting point at 38.1°C was significantly higher than for any of the polymorphs of cocoa butter.

Addition of the vegetable fat to cocoa butter at a level of 10% and 20% had little effect on the characteristic Form V morphology (Fig. 9). The X-ray pattern did show some differences. The peaks normally present in Form V were produced, but in addition a low intensity peak at 4.25 Å was present, and a 49 Å peak had developed. The DSC showed a single melting point at 32.1°C, close to the melting point of Form V. It was apparent, therefore, that some structural changes had occurred which did not have a marked effect on the morphology.

As the vegetable fat content was increased to 30% and above, significant changes occurred in morphology. Crystal size decreased from 1 μm to 0.25 μm, and the crystal outlines became less distinct (Fig. 10). The X-ray pattern showed a suppression of the characteristic β structure of the Form V, with finally, at the 50% addition, domination of the β' structure of the vegetable fat (Table 2). The DSC trace broadened with the increase of the vegetable fat content as shown in

TABLE 2

X-RAY DIFFRACTION DATA

	Short Spacing (Å)	Long Spacing (Å)
POLYMORPH I	3.70 (S) 4.19 (VS)	34 (W)
POLYMORPH II	4.25 (S)	16.6 (M) 49 (VS)
POLYMORPH III	3.87 (M) 4.25 (S) 4.63 (M)	15.24 (M) 16.6 (S) 49 (VS)
POLYMORPH IV	4.17 (VS) 4.35 (VS)	14.9 (S) 46 (VS)
POLYMORPH V	3.68 (W) 4.6 (VS) 3.76 (M) 5.43 (M) 3.88 (W) 3.99 (M)	8.08 (W) 13.15 (W) 16.20 (W) 34 (S) 66 (S)
POLYMORPH VI	3.71 (S) 4.6 (VS) 3.88 (S) 5.16 (W) 4.04 (M) 5.47 (M) 4.28 (W)	8.18 (W) 13.2 (W) 35 (S) 66 (S)
HYDROGENATED VEG. FAT	3.87 (S) 4.08 (M) 4.24 (S) 4.39 (M)	15.3 (S) 49 (VS)
10% VEG FAT, 90% COCOA BUTTER	3.68 (W) 4.6 (VS) 3.75 (M) 5.45 (M) 3.89 (W) 4.00 (M) 4.25 (W)	8.18 (W) 13.26 (VW) 35 (S) 49 (M)
50% VEG FAT, 50% COCOA BUTTER UNCYCLED	3.87 (S) 4.08 (M) 4.24 (S) 4.39 (M)	15.3 (S) 49 (VS)
CYCLED	3.89 (M) 4.25 (S) 4.6 (S)	15.3 (W) 49 (VS)

Key: S = Strong
M = Medium
W = Weak

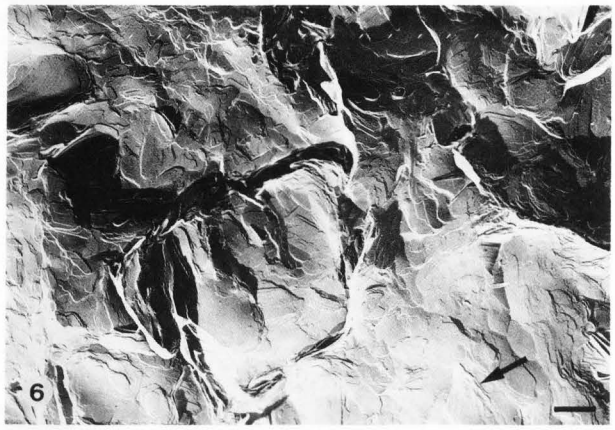

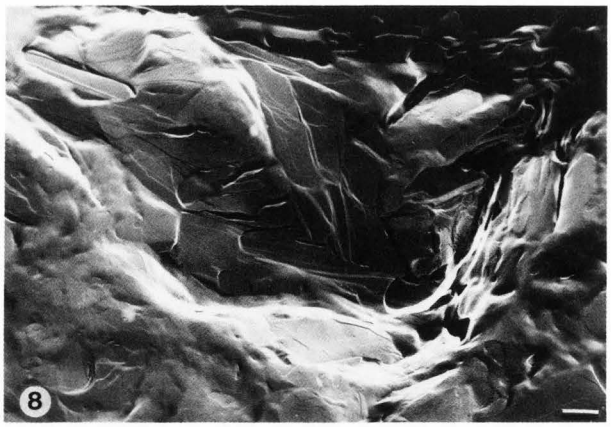

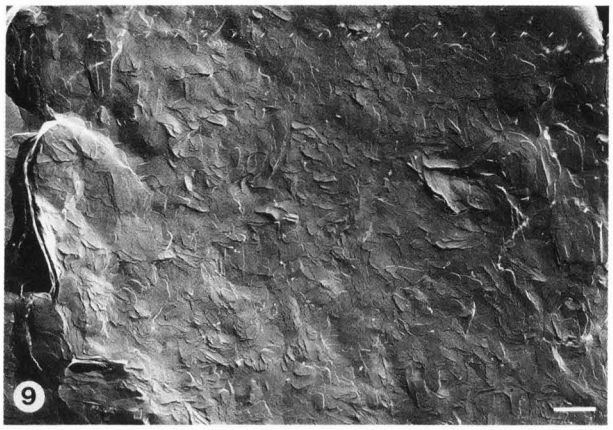

Figure 5. Form IV Cocoa Butter, made up of densely packed needle-like crystals. (Bar = 1 μm).

Figure 6. Form V Cocoa Butter, multilayered crystals (arrow), regular in shape. (Bar = 1 μm).

Figure 7. Form VI Cocoa Butter, crystals protruding (arrow) from a matrix of more regularly shaped crystals. (Bar = 1 μm).

Figure 8. Hydrogenated vegetable fat with long crystals arranged into layers. (Bar = 1 μm).

Figure 9. 10% vegetable fat, 90% cocoa butter blend, with a crystal shape similar to Form V morphology. (Bar = 1 μm).

Figure 10. 50% vegetable fat, 50% cocoa butter blend with small ill defined crystals. (Bar = 1 μm).

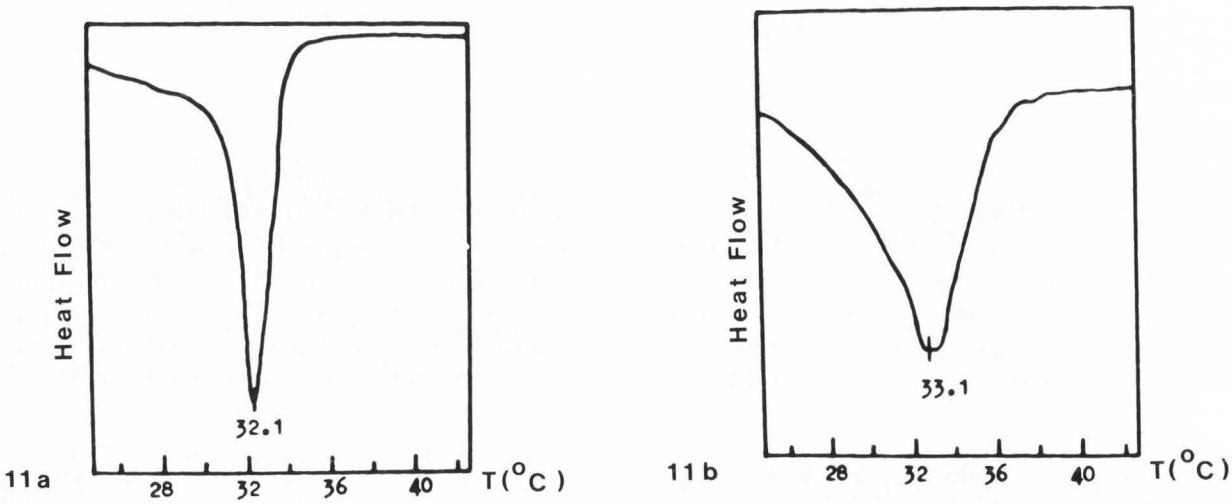

Figure 11. DSC traces for two of the vegetable fat blends. a. DSC trace - 10% vegetable fat addition. b. DSC trace - 50% vegetable fat addition.

Fig. 11a and b and a small increase to 33.1°C occurred in melting point. After temperature cycling two distinct crystals could be observed. One appeared to be rounded crystals 1-2 μm in length stacked on one another into multilayers (Fig. 12a). The other long elongated crystals up to 3-4 μm long, and stacked (Fig. 12b). The X-ray showed the development of a peak at 4.6 Å, and the loss of the 4.08 Å and 4.39 Å peaks from β' pattern (Table 2). The DSC gave a main peak at 35.8°C and a shoulder at about 38°C.

TABLE 3

MELTING POINT DATA

POLYMORPH I	17.9°C
POLYMORPH II	24.4°C
POLYMORPH III	27.7°C
POLYMORPH IV	28.4°C
POLYMORPH V	33.0°C
POLYMORPH VI	34.6°C
HYDROGENATED VEG. FAT	38.1°C
10% VEG. FAT 90% COCOA BUTTER	32.1°C
50% VEG. FAT 50% COCOA BUTTER	
UNCYCLED	33.1°C
CYCLED	35.8°C

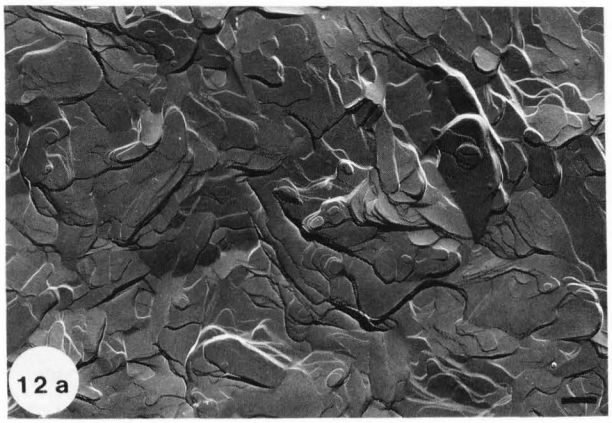

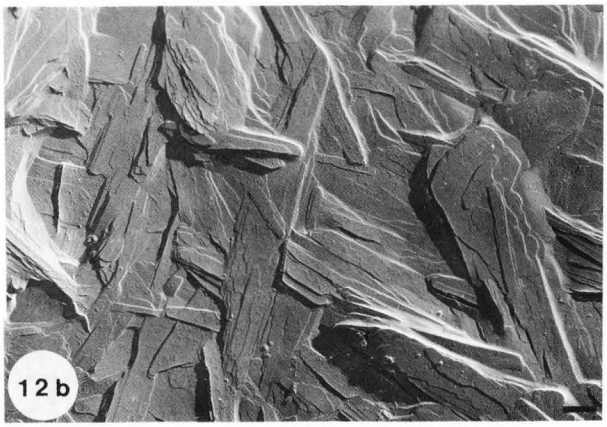

Figure 12. 50% vegetable fat, 50% cocoa butter blend after temperature cycling. Showing two types of crystalline form (a and b).
a. Rounded crystals stacked together. (Bar = 1 μm). b. Elongated crystals arranged into layers. (Bar = 1 μm).

Discussion

The crystal structure of solid triglycerides in the α, β', β described by Larsson (1982) for triundecanoin, can be used to understand some of the morphologies observed in the cocoa butter polymorphs. The α structure is thought to consist of inefficiently packed bimolecular layers. These allow penetration of triglyceride chains between layers inhibiting interlayer packing. Growth will therefore occur laterally to form the lamellae structures as observed in Form II. The β' structure, though reducing interplane chain penetration by the tilt of the bimolecular units in the structure also places limitations on growth of the crystals. In one axis lateral growth is facilitated by the structure, but in the other it involves more complicated packing and so growth is slow. This causes more needle-like crystals as seen in Form IV. deMan (1982) described a similar effect in margarine fats examined by light microscopy. The β structure significantly reduces chain penetration, producing thicker and more equidimensional crystals, being less affected by the constraints on lateral growth found in the β' structure. This close correlation between structure and morphology is not always observed. Form III is not easily classified into an α or β' structure, morphologically. Its characteristic crystals protruding from a poorly structured background suggest two crystal types might be present. Form VI shows small differences in the X-ray pattern, but significant differences in morphology and melting point when compared with Form V.

This complex relationship between structure and morphology is shown in the study of the cocoa butter/vegetable fat blends. Differences in structure are observed at lower percent additions than differences observed in morphology. The structural differences observed may relate to the molecular packing of the triglycerides. Analysis of the hydrogenated vegetable fat shows it to contain a high proportion of triglycerides containing trans acids in comparison to cocoa butter in which the triglycerides have a predominant cis configuration in the oleo chain (Jewell, 1981). Precht (1977) postulated from work using X-ray diffraction on binary triglyceride systems that incorporation of triglycerides containing trans acids would preferentially stabilise the β' rather than β structure. The β' structure being more able to accommodate the lattice defects produced by these triglycerides.

The complexity of the cocoa butter and vegetable fat blends makes detailed interpretation of the X-ray data difficult. It is apparent, however, that the blends containing higher levels of the vegetable fat had a strong 49 Å peak and short spacings indicative of β' structure. This suggested that a change from the β structure in Form V cocoa butter to a β' structure had occurred. It is possible that some incorporation of triglycerides containing trans acids may have taken place causing preferential stabilisation of the β' structure in accordance with the model suggested by Precht. This difference in X-ray data might have been expected to cause the morphology to revert to that of the vegetable fat. It was observed, however, that crystal size diminished markedly. The DSC peak broadened at the higher levels of vegetable fat addition suggesting that the solid was not a purely crystalline phase. Overall this indicates that a β' structure was present in much of the solid phase, but a high level of disorder exists, inhibiting crystal growth and the development of a distinct crystal morphology. The effect of temperature cycling on such blends allows re-ordering of the triglycerides to form two distinct crystalline phases, with corresponding changes in X-ray and DSC data.

The TEM replica technique is a very effective method for examination of fat systems but some consideration of artefacts in the preparation is necessary. Freezing rate is not as critical in fats as in aqueous systems, liquid nitrogen being an adequate cryogen, and unlikely to cause distortions of the crystals during cooling. Melting during preparation can be a problem, the sample requiring to be kept at a low temperature (≅ -100°C). Despite these potential problems, the method has been shown to be relatively straightforward, and to provide useful data to complement DSC and X-ray results.

Acknowledgements

The authors wish to thank fellow members of Structural Studies and Physical Chemistry for their help and advice during the course of this work. David Spybey for his photographic assistance, and Shelley Challenger and Janet Wendy for their secretarial skills and patience.

References

BERGER KG, JEWELL GG and POLLITT RJ. (1979). Oils and Fats, in: Food Microscopy, J.G. Vaughan (ed), Academic Press, London, 445-495.

CHAPMAN GM, AKEHURST EE and WRIGHT WB. (1971). Cocoa butter and confectionery fats. Studies using programmed temperature X-ray diffraction and Differential Scanning Calorimetry, Journal of American Oil Chemists Society 48, 824-830.

deMAN JM. (1982). Microscopy in the study of fats and emulsions, Food Microstruc. 1 (2), 209-222.

HAUMANN BF. (1984). Confectionery fats - for special uses, Journal of American Oil Chemists Society 61, 468-472.

JEWELL GG. (1981). Factors influencing the crystallisation of chocolate, in: Proceedings of the Thirty-Fifth Annual Production Conference, Pennsylvania Manufacturing Confectioners' Association, 1981, 63-66.

LARSSON K. (1966). Classification of crystal forms, Acta. Chem. Scand. 20, 2255-2260.

LARSSON K. (1982). Some effects of lipids on the structure of foods, Food Microstruc. 1 (1), 55-62.

PRECHT D and FREDE E. (1977). The crystal structure of fats. I. Molecular arrangements of saturated triglycerides and triglyceride mixtures, Kieler Milchw. Forschungsber. 29, 265-285.

TIMMS RE. (1984). Phase behaviour of fats and their mixtures, Prog. Lipid Res. 23, 1-38.

WILLE RL and LUTTON ES. (1966). Polymorphism of Cocoa Butter, Journal of American Oil Chemists Society 43, 491-498.

Discussion with Reviewers

Reviewer II: Is it correct to consider a mixed triglyceride system such as cocoa butter to have distinct polymorphic forms? To what extent does compound crystallisation occur?
Authors: Natural fats are often a complex mixture of triglycerides with intrinsic variations in composition and physical properties. The studies undertaken by Wille and Lutton (1966) and others, however, indicate that cocoa butter has a polymorphism which can be defined by a series of distinct X-ray patterns. The exact composition of the solid phase is liable to change between polymorphs, all of which have some level of liquid content, allowing interchange between the liquid and solid states. The development of possibly two or more solid solutions (Timms, 1984) and compound crystallisation are likely to occur particularly in the less stable polymorphs. Despite this potential complexity, the behaviour of the system appears adequately defined by six states with specific X-ray patterns and crystal morphologies and provides useful data for chocolate technology.

D. Manning: Is it possible to have crystalline melting points ranging between those stated for Form I through Form VI? For example, after solidification is it possible to have a crystalline melting point of 30.7°C which lies between polymorphs IV and V? How would such a crystal be classified?
Authors: Yes, this is possible, and has been observed in thermal data (Jewell, 1981). Their characterisation is difficult as X-ray diffraction does not often show a corresponding difference. In the example given, the crystalline material probably consists of metastable mixtures of β and β' structures.

D. Manning: In reference to Form I polymorphs, is it possible to have a crystalline material without continuously repeating lamellae? How would the crystalline data of Form I polymorphs compare to the same sample of cocoa butter in the liquid state?
Authors: It is unlikely that a crystalline state would exist without continuously repeating lamellae. It is, however, possible to have limited repeating lamellae present which, although not crystalline material, would contrast with the liquid state which is highly disordered.

J. deMan: The electron micrographs of the crystals convey the impression of an almost continuous sheet of crystal. Is this the way we have to envisage the structure of cocoa butter?
Authors: Although the impression is of continuous crystalline material, in Form V, SFI data indicates that at 20°C it is ≅ 80% solid. It is likely that the fracture of the fat occurs preferentially through the crystalline material.

D. Manning: In what manner does interpretation of the X-ray data differ when investigating pure single triglycerides as compared to a triglyceride mixture like cocoa butter?
Authors: In a single triglyceride the exact composition of the solid phase is known. This is not always the case in a mixed triglyceride system. Full interpretation of the X-ray data is more complex therefore and information on the packing of individual triglycerides cannot be ascertained directly.

D. Manning: Was there any evidence of annealing or crystal transition with Form I or II polymorphs at the 2°C/min heating rate? Was there any experimentation conducted with faster heating rates?
P. Dimick: Would the 15 mg sample weight induce upward shifts in melting point?
Authors: Heating rates of 2 and 5°C/min have been used routinely in our laboratory without any apparent problems of annealing. The sample weight has been standardised for the protocol used.

P. Dimick: What were the SFI for Forms V and VI samples? Similarly what was the SFI for the blends?
Authors: SFI data are shown in Table 4. Form VI data were not obtained.

TABLE 4

	20°C	25°C	27.5°C	30°C	35°C
	% solids				
Form V	80	75	66	43	-
Vegetable Fat	67.8	60.2	56.0	49.6	31.4
10%	73.2	65.5	54.9	31.7	1.3
20%	69.4	60.5	51.3	30.2	1.7
30%	69.8	59.7	44.4	21.7	2.2
40%	66.7	55.8	40.9	18.5	3.0
50%	62.2	48.3	36.3	19.1	5.2

P. Dimick: Does β' crystal formation occur satisfactorily at 16°C, and is β' formation likely to occur during the protocol used for production of Form VI?
Authors: The methods as described produce the required polymorphs satisfactorily, without any evidence for mixed products or unwanted transformations.

FOOD MICROSTRUCTURE, Vol. 4 (1985), pp. 249-265
SEM Inc., AMF O'Hare (Chicago), IL 60666-0507 U.S.A.

0730-5419/85$1.00+.05

CRYSTAL MORPHOLOGY OF COCOA BUTTER

D. M. Manning* and P. S. Dimick

Food Science Department, The Pennsylvania State University,
116 Borland Laboratory, University Park, PA 16802

*Current Address: M & M Mars, Brown St., Elizabethtown, PA 17022

Abstract

The multiple melting points of triglycerides have been known and studied for more than a century by numerous workers. The ability of fat to undergo polymorphic changes is important mainly due to its effect on product texture and appearance. Polymorphic resolidification during storage of cocoa butter into higher melting forms can destroy the smooth glossy appearance of a confectionery product. This manuscript will review the polymorphic characteristics and composition of cocoa butter from Theobroma cacao. A discussion of common fat behavior relative to tempering and bloom formation will be included. Scanning electron microscopy and polarized light microscopy aided in visually defining the crystalline forms of cocoa butter during crystallization. Thermal and compositional properties of cocoa butter during crystallization indicates that a high-melting crystal seed forms which promotes the solidification of additional quantities of less stable triglycerides.

Initial paper received January 27 1985
Manuscript received June 09 1985
Direct inquiries to P.S. Dimick
Telephone number: 814 863 2962

KEY WORDS: cocoa butter, scanning electron microscopy, polarized light microscopy, differential scanning calorimetry, tempering, fat bloom, crystal seed.

Introduction

Theobroma cacao is the source of the cocoa bean. Cacao beans are cultivated from the tropical regions of Western Africa, Brazil, and many other locations within 20° latitude of the equator. The fermented dried cocoa beans entering the US and Europe are processed into various products. To assure cleanliness and quality, the beans are placed through air lifts, screens, and magnetic separators to remove fiber, stones, and immature small beans. Once the beans are cleaned, roasting is carried out to develop flavor and aroma. Roasting facilitates the removal of the shell during winnowing and also reduces the moisture content of the bean. The beans are then passed through breakers and winnowing machines which operate by cracking the shell and bean into large pieces. The fractured shell and bean fragments are separated by sieving and air elutriation. This separation process is dependent on a difference in density between the bean cotyledon fragments and the shell. The cotyledon fragments, called nibs, are converted into a fluid paste known as chocolate liquor. In the production of chocolate, the addition of sugar, milk solids (in the case of milk chocolate), and additional cocoa butter are added to the liquor prior to refining. After a small particle size (<25μm) has been established in the refiners, the chocolate blend is conched. Along with producing the desired flavor, conching promotes a continuous fat phase that evenly coats the sugar and cocoa solids thus producing a flowable liquid.

The final processing steps are tempering and solidification of the confectionery product. Immediately after tempering, the chocolate is molded and cooled to approximately 16°C for proper contraction. If the chocolate is shock cooled or if the cooling time is too short, product quality may be affected. A problem associated with poor tempering is the formation of fat bloom which visually appears as gray swirls or as large white circular fat crystals on the surface. Thus the snap, gloss, proper melting point, contraction, and other attributes are dictated by the fat crystalline forms present (Musser, 1973). Taste, smell, mouthfeel, hearing, and especially sight are involved in the total perception of a

food product. If the cocoa butter crystals present in a chocolate product are not in a stable form, mouthfeel, hearing, and sight are adversely affected.

Clearly defining the mechanisms involved in cocoa butter crystallization remains an interesting but controversial area of confection science. The following includes research efforts aimed at defining the compositional and thermal characteristics of cocoa butter crystals formed during crystallization. A discussion based on thermal and compositional data will shed new insight on the mechanisms of cocoa butter crystallization. There still may be art involved in cocoa butter crystallization and tempering but scientific studies are increasingly providing new answers.

Polymorphism and Molecular Packing

In order to understand the mechanism of fat crystallization it is first necessary to understand how triglycerides crystallize at the molecular level. The phenomenon of triglyceride polymorphism has been known for over 100 years (Duffy, 1852). Throughout recent history numerous scientists have conducted research to demonstrate that the basis for multiple melting points of triglycerides was polymorphism (Clarkson and Malkin, 1934; Lutton, 1945). Nearly all fats exhibit polymorphism in a monotropic manner, in that transformations take place from less stable, lower melting forms to more stable, higher melting forms.

Fatty acids and glycerides have been observed to exist in at least two crystalline forms and some have as many as three or four (Bailey, 1950). When a transition occurs the molecular packing of the triglycerides shift to confer greater stability to the crystal. Clarkson and Malkin (1934) were the first to clearly demonstrate triglyceride polymorphism with X-ray diffraction analysis. It is known that if tristearin is melted and suddenly cooled, it first melts at 55°C, then solidifies again and melts at 71°C. The hypothesis to explain the different crystal stabilities was polymorphism.

The crystallization mechanism of monoacid saturated triglycerides is related to the packing of the hydrocarbon chains. Triglycerides in the liquid state present an X-ray diffraction pattern similar to liquid monoglycerides. Due to similar diffraction patterns, Larsson (1972) believed that liquid triglycerides exist in tuning fork conformations at temperatures above the melting point. It was believed that the triglycerides laterally interlock and possibly form a lamellar-like structure. Particular long spacing diffraction lines exhibited the same intensity distribution whether the triglycerides were liquid or crystalline. It was accepted that tristearin and other monoacid saturated triglycerides existed in three different polymorphic crystalline forms called alpha (α), beta prime (β'), and beta (β), the latter being the most stable. The data obtained from X-ray diffraction analyses of triglycerides can be separated into two groups: long and short spacings. The long spacings are related to the distance between the planes formed by the terminal methyl groups of the fatty acids. The interpretation of the short spacings are related to the cross-sectional arrangement of the fatty acids on the triglyceride molecules (Chapman, 1962). For tristearin, as the melting point increases, the long spacings decrease as shown in Table 1. Thus the long spacing recorded for tristearin and most other saturated monoacid triglycerides is dictated primarily by the geometry of the triglycerides upon crystallization. For most saturated monoacid triglycerides the structure formed will be the double chain length structure. Larsson, (1964) altered the conventional tuning fork structure to a modified tuning fork configuration. This is believed to be the more correct arrangement, where the central and one of the alkyl groups are aligned along the same axis.

Table 1

Comparison of the melting points and long spacings for the three crystalline states of tristearin (Chapman, 1962).

Crystalline state	Melting point (°C)	Long spacing (Å)
α	54.0	50.6
β'	64.0	47.2
β	73.1	45.0

The unstable α form of tristearin is a vertically oriented (zero tilt) structure (Fig. 1α) and the molecules are loosely packed in an inefficient manner. The uneven alignment of the terminal methyl plane complicates the packing of one bilayer in relation to adjacent layers. If the crystal of tristearin undergoes resolidification into the β' or β form, the long spacing decreases from 50.6 Å to 47.2 Å and 45.0 Å, respectively. The triglycerides in the β' and β forms are thought to tilt with respect to the methyl plane (Fig. 1β',β). As the angle between the triglyceride and methyl plane decreases, a closer chain packing is adopted and the plane between adjacent bilayers is more even. Close chain packing produces a more dense structure with a higher melting point. It is believed that the terminal methyl groups in a β crystal are located in one plane. The packing of the bimolecular layers is complicated if the chains from one bilayer penetrate neighboring bilayers (Larsson, 1982).

As the triglyceride becomes more complex in its fatty acid composition, a change from the double chain length structure occurs. If fatty acid chain lengths on a triglyceride differ by four or more carbons, triple chain length structures may form (Lutton, 1948). In this case, the alignment of glyceride fatty acids is dictated by sorting of short chain from long chain acids.

The last case to be discussed is the unsaturated glycerides which more closely resemble the composition of cocoa butter. The majority of the triglycerides present in cocoa butter are the 2-monounsaturated type such as POP, POS, and SOS where S = stearic acid, P = palmitic acid, and O = oleic acid. Mixed oleic-saturated glycerides

tend to form triple chain length structures. X-ray analyses reveal the long spacings for the β form of SOS to be ≅64 Å which corresponds to a triple chain length structure. Lutton (1972) has illustrated the conventional tuning fork packing for a 2-monounsaturated triglyceride, while Larsson (1972) has illustrated the triple chain length structure in the modified tuning fork (Fig. 2A,B).

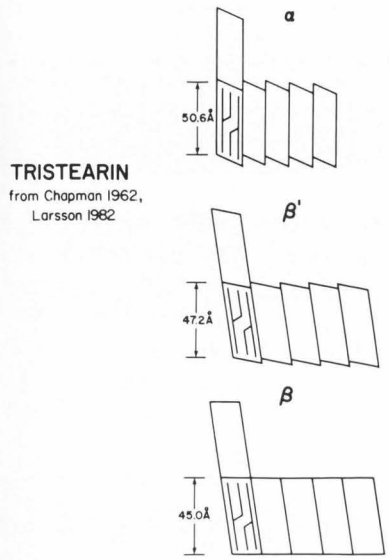

Fig. 1. Diagrams of saturated triglyceride dimers in a crystalline lattice: proposed triglyceride structure for the α form; proposed triglyceride structure for the β' form; proposed triglyceride structure for the β form (Larsson, 1982). Long spacings illustrate the α, β', and β crystals for tristearin (Chapman, 1962).

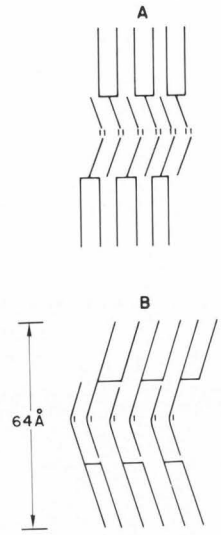

Fig. 2. Illustration of the arrangements of 2-monounsaturated triglycerides: conventional tuning fork packing (A) (Lutton, 1972); modified tuning fork packing (B) (Larsson, 1972).

Polymorph Classification

Since the discovery of polymorphism, numerous scientists have reported different numbers of polymorphs and conflicting melting points for the various crystalline forms found in cocoa butter. In general, the various nomenclatures assigned to each classification has compounded the problem due to a lack of consistency (Table 2). In 1951, four crystalline forms with different melting points were observed and labelled gamma (γ), alpha (α), beta double prime (β"), and (β) (Vaeck, 1951). Nine years later, Vaeck (1960) again examined cocoa butter and concluded four polymorphic forms, but melting points were slightly different, than previously reported. In 1964, a fifth polymorphic form was observed and recorded as β' (Duck, 1964). Two years later, six polymorphic forms were observed; however, the nomenclature denoting the various crystalline forms was changed to Roman numerals (Wille and Lutton, 1966). The most recent work of Lovegren et al. (1976) revealed six polymorphic forms, but in this case the nomenclature was exactly opposite that proposed by Wille and Lutton.

A technique commonly used to thermally analyze the polymorphic crystalline forms of cocoa butter is differential scanning calorimetry (DSC). Huyghebaert and Hendrickx (1971) recorded six polymorphic crystalline forms of cocoa butter using the DSC. A heating rate of 4°C/min with a 2 mcal/sec range produced six endotherms that varied in melting point from 14.9° to 34.9°C. More recent experimentation with the DSC resulted in the reconfirmation of only four polymorphic

Table 2. Classification and temperature (°C) of cocoa butter crystalline forms.

Vaeck (1951)		Vaeck (1960)		Duck (1964)		Wille & Lutton (1966)		Chapman et al. (1971)		Lovegren et al. (1976)	
γ	18.0	γ	17	γ	18.0	I	17.3	I		VI	13.0
α	23.5	α	21-24	α	23.5	II	23.3	II		V	20.0
						III	25.5	III		IV	23.0
β"	28.0	β'	28	β"	28.0	IV	27.5	IV	25.6	III	25.0
β	34.5	β	34-35	β'	33.0	V	33.8	V	30.8	II	30.0
				β	34.4	VI	36.3	VI	32.2	I	33.5

forms of cocoa butter (Merken and Vaeck, 1980). Therefore Forms V and VI may be phases differing in composition rather than existing as a distinct polymorphic form.

The problem existing by the presents of numerous polymorphic forms is identifying exactly which form or crystallite is desired at the completion of tempering in chocolate production. The ability to clearly define the origin of the desired stable crystal has not yet been resolved. However, the data obtained with X-ray analysis, DSC, dilatometry, and microscopy have increased our understanding of the mechanisms involved in cocoa butter crystallization.

Tempering

Formulated chocolate is essentially composed of cocoa, sugar, milk solids (milk chocolate), vanillin, and lecithin, all of which are suspended in a crystalline matrix of cocoa butter. Chocolate with crystals in the less stable form has a tendency to be soft and also undergoes crystal transitions which could adversely affect product appearance. In order to ensure that the final chocolate product is in the proper crystalline form a process termed "tempering" is undertaken. Tempering is the controlled formation of a sufficient number of stable seed crystals. The conventional process of tempering involves cooling chocolate from 50°C to 32°C with constant agitation. Once 32°C is reached the temperature is then decreased to 28°C to produce stable cocoa butter seed crystals. After seed formation, the temperature is increased to between 30° and 32°C depending on the chocolate formulation (Kleinert, 1970). The chocolate is poured into molds, vibrated to remove air, and cooled to approximately 16°C. Cooling removes the latent heat of crystallization to ensure the formation of the largest number of small stable crystals. During cooling, contraction occurs which is an indication of proper temper. Exactly which crystal form is desired at the completion of tempering is still speculative. Vaeck (1960) believes that β' or β crystals are present in the final tempered product, while Wille and Lutton (1966) believe Form V is the crystal desired in the final product.

Fat crystals should be small for visual appearances, but also for texture and mouthfeel reasons (Musser, 1973). Problems may occur during tempering for numerous reasons. The presence of unstable crystals after tempering may cause production problems due to the absence of contraction upon cooling. The amount of stable seed formed and the manner in which the product is cooled has a large effect on product quality. Insufficient cooling may lead to large crystal formations and fat bloom (see below). The addition of foreign fat in confectionery products may affect the tempering procedure and product appearance. For example, addition of milkfat to a milk chocolate requires the reduction of the tempering temperature by approximately 1°C (Koch, 1956). During tempering there should be adequate agitation to assure proper heat transfer between the chocolate product and the cooling medium. Mechanical agitation usually involves a narrow working area which constantly fractures fat crystals which in turn become optimum seed. It is possible to temper cocoa butter through a mechanical process that influences polymorphic transition (Feuge et al., 1962). The procedure consisted of mechanically working triglycerides by extrusion under pressure to physically manipulate the crystals.

Bloom Formation

The crystalline problem associated with the storage of chocolate is called bloom. Bloom can be of two distinct types, one being sugar bloom and the other fat bloom. Sugar bloom is characterized by a sandy, gritty texture and consists of sugar crystals that have accumulated on the surface of the bar. Fat bloom is a problem that causes the glossy surface of chocolate to become dull and covered with a grey film. This discoloration resembles the bloom on grapes thus it is termed bloom (Cerbulis et al., 1957). It is known that bloom on the surface of chocolate is definitely crystalline in structure (Neville et al., 1950). Whymper (1933) originally proposed that cooling produced an unstable solution in which the individual fat components separate. The higher melting fractions aggregate and separate away from the lower melting fractions thus producing fat bloom. Becker (1958) proposed a theory involving phase diagrams of various cocoa butter components and stated that the fractionation of triglycerides ultimately leads to bloom formation. Vaeck (1960) proposed a theory in which bloom is caused by a transition from an unstable crystal form into the stable form. During this change the crystal volume decreases allowing air to penetrate into the mass producing an opaque reflection. At elevated temperatures the cocoa butter melts and resolidifies into large high melting crystal formations. An example of bloomed and unbloomed chocolate is illustrated in Figure 3.

The crystalline triglycerides present in fat bloom have lower iodine values and higher melting points than those triglycerides dispersed throughout the chocolate mass. The composition of bloomed fat is rich in the triglycerides POS and SOS (Steiner and Bonar, 1961). The polymorphic crystalline form of bloomed fat is thought to be β. In most cases the crystals present after tempering are believed to be β' (Giddey and Clerc, 1961). Jewell (1972) indicated that bloom formation is not solely a surface phenomena, but can be found permeating throughout the chocolate mass.

Most investigations aimed at preventing fat bloom employed food additives. The addition of butterfat or a mixture of sorbitan monostearate 60 and polysorbate 60 has been used extensively in the past to control fat bloom (Musser, 1980). Milkfat was thought to be a good selection because it is already used in the manufacture of milk chocolate. Campbell et al. (1969) reported bloom inhibition two to four times longer with the addition of 2.5% hydrogenated milkfat as compared to an equal addition of unhydrogenated milkfat.

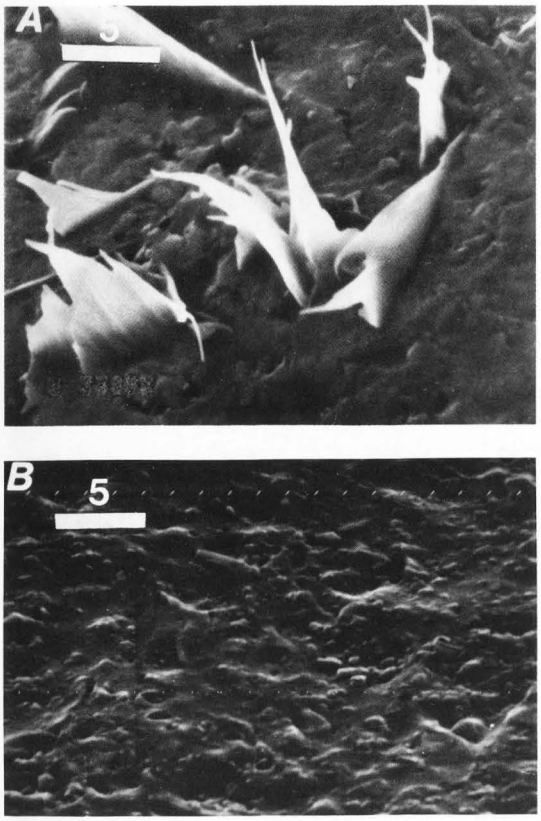

Fig. 3. SEM surface view of bloomed (A) and properly tempered (B) semi-sweet dark chocolate. **Scale bars in μm for all figures.**

The bloom problem is very complex and the cause may be a combination of factors instead of one single factor. Above all, the formation of bloom is affected by the way in which the chocolate is handled in the factory and in the marketplace.

Polarized Light and Scanning Electron Microscopy Studies

The primary objectives of this section are to discuss the use of polarized light microscopy (PLM) and scanning electron microscopy (SEM) to characterize the crystalline structures of cocoa butter. Ivory Coast cocoa butter was utilized for these studies and had been isolated using the following processing conditions: 218°C air temperature of roaster; 36°C temperature of beans out of roaster; 82°C liquor temperature; 96°C liquor temperature filling presser; 71°C #1 press; 67°C #2 express cocoa butter temperature.

Microscopic techniques employed included the use of the Bristoline Bristolscope that utilizes polarized light. In conjunction with the polarized light microscope, a Leitz temperature variation stage was used to control the sample temperature. Along with polarized light microscopy (PLM), the International Scientific Instruments (ISI) Model-60 scanning electron microscope (SEM) was used in the comparative study.

For polarized light and scanning electron microscopy, cocoa butter was heated to 60°C for at least 6 hr. The aliquots for PLM were removed from the liquid butter and placed on glass slides equilibrated to the preset incubation temperature. A cover slip was placed on the sample and the slides were incubated at prescribed temperatures in a Precision Scientific Model 808, a Shel-Lab Model 35960-054, and a Precision Scientific Freas 815. For SEM, the stubs were

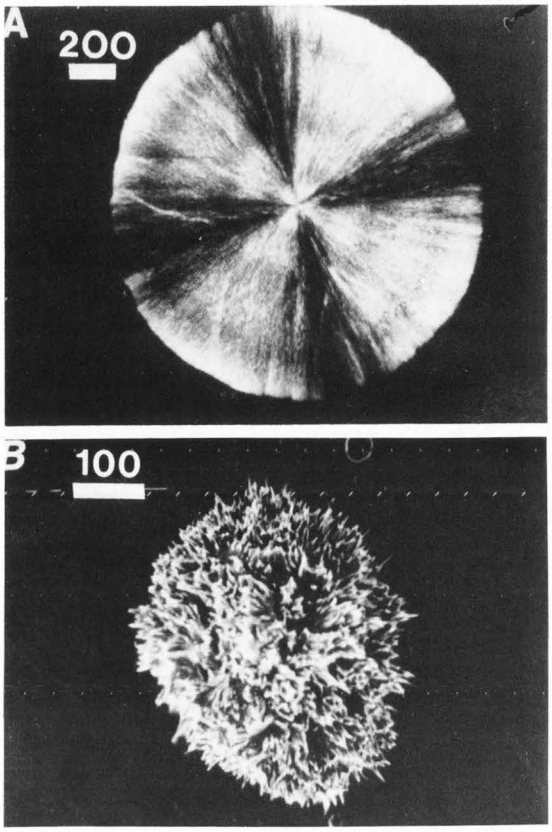

Fig. 4. Cross-sectional view of a 30°C cocoa butter crystal utilizing polarized light microscopy (A); and a micrograph of a similar 30°C crystal visualized by scanning electron microscopy (B).

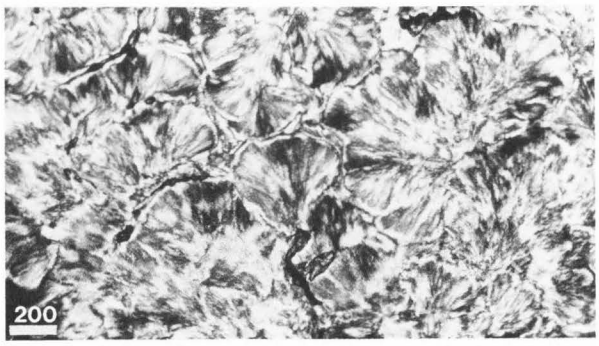

Fig. 5. Polarized light pattern produced after compressing numerous free growing cocoa butter crystals.

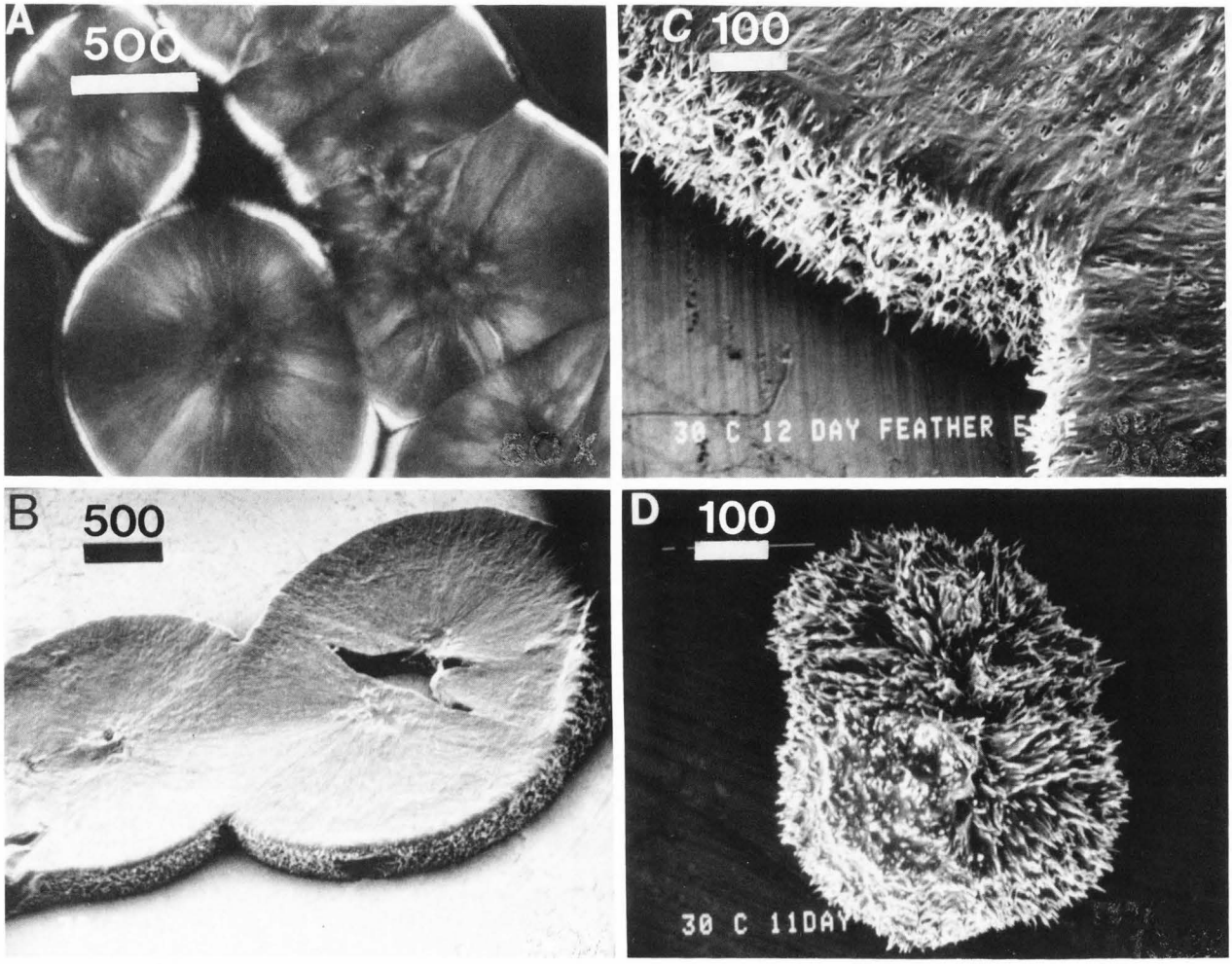

Fig. 6. Cross-sectional view of thick cocoa butter crystals utilizing polarized light (A); identical crystals from (A) viewed by SEM (B); SEM enlargement of peripheral edge of crystal (C) and SEM of free growing crystal (D).

tempered to the desired incubation temperature and approximately 50μl cocoa butter were placed on the stub surface. A blank stub was placed against the sample stub, rotated, and then removed. This action produced a thin film of cocoa butter on each stub, thus, upon crystallization small groups of crystals or even individual crystals could be visualized with the SEM. After incubation, the stubs were placed in the ISI PS-2 coating unit, cooled for 5 min at approximately 0-5°C and then gold coated (280Å) at 1.4 kV, and 10 mA for 4 min. Cooling conditions in the present studies did not alter the original crystals formed during incubation. The stubs were then placed in the SEM and viewed at an accelerating voltage of 10 kV and working distance of 8 mm.

The procedure to determine crystalline melting points utilized the Brabender Pressure Circulator, Leitz stage, and the Bristoline Bristolscope. The pressure circulator pumped temperature-controlled water through a network in the Leitz stage, thus maintaining a specific constant stage temperature. Prior to determining melting points the Leitz stage was allowed to equilibrate at the predetermined temperature for 15 min. After stage equilibration a sample was removed from the incubator after approximately 2 wk and placed directly upon the stage. The melt was then viewed with the PLM. This method was used rather than an increasing temperature-time gradient due to the fact that crystalline transition could occur making melting point data less precise.

The photographs obtained from each of the two microscopic methods demonstrate a dramatic difference in visual appearance of cocoa butter crystals. The PLM photographs represent a cross-sectional or internal structure view (Fig. 4A) while in SEM a surface reflection view resulted (Fig. 4B). When cocoa butter was placed on a slide with a cover slip and incubated, crystal growth was physically restricted, but without a cover slip crystals grew multidirectionally. To substantiate this physical phenomenon a free growing crystal was compressed to reveal the smooth feather-like internal structure (Fig. 5) which correlated well with Fig. 4A. When viewing thick crystals with polarized light the centers

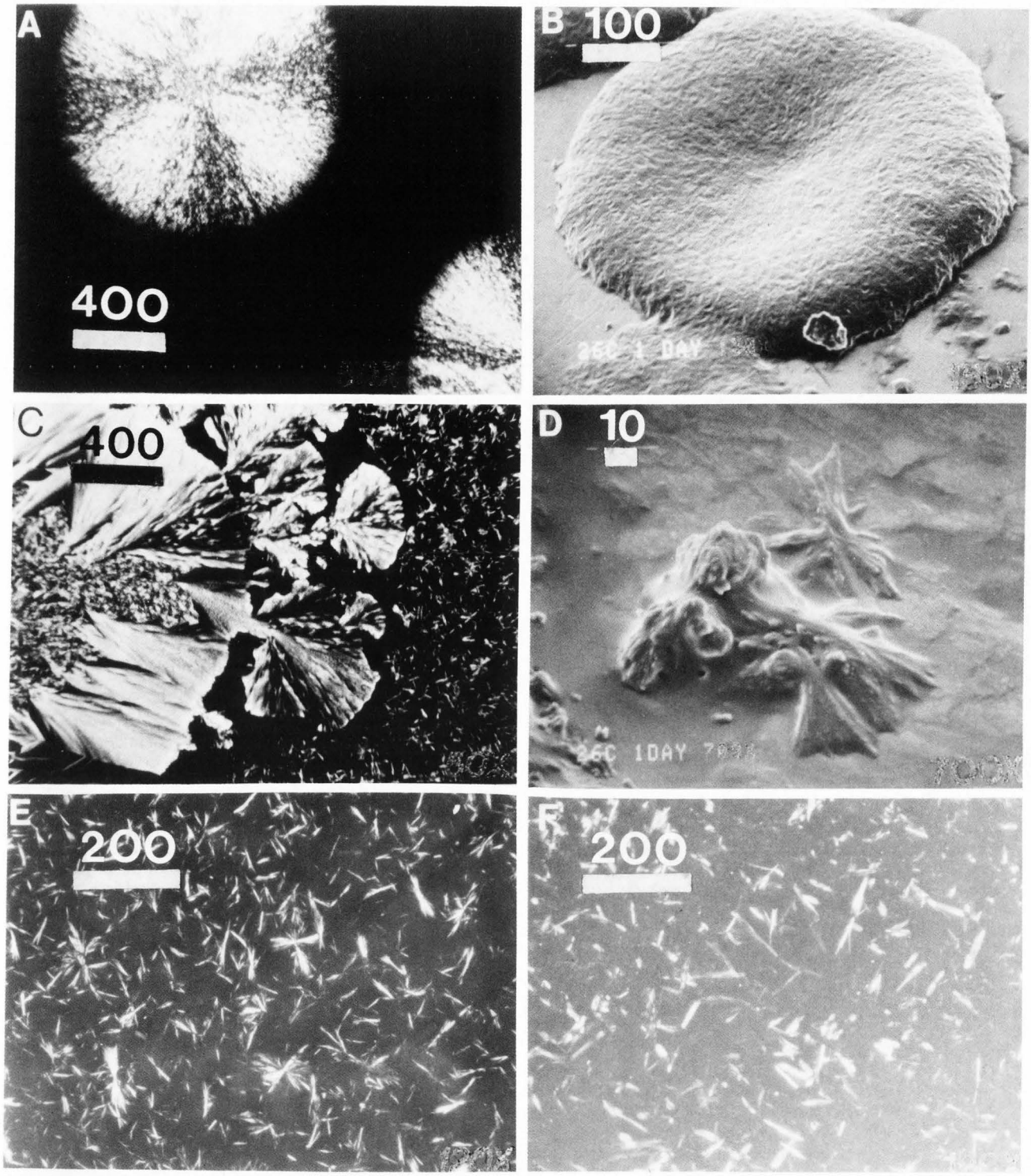

Fig. 7. At 26°C the tempered (mesh) crystal is observed utilizing PLM (A); a similar tempered crystal viewed with SEM (B); PLM of 'feather' crystals with 'individual' crystals on right (C); individual crystals viewed by SEM (D); individual crystals viewed by PLM (E) and 'opaque blade'crystals by PLM (F).

Scale bars in μm for all figures.

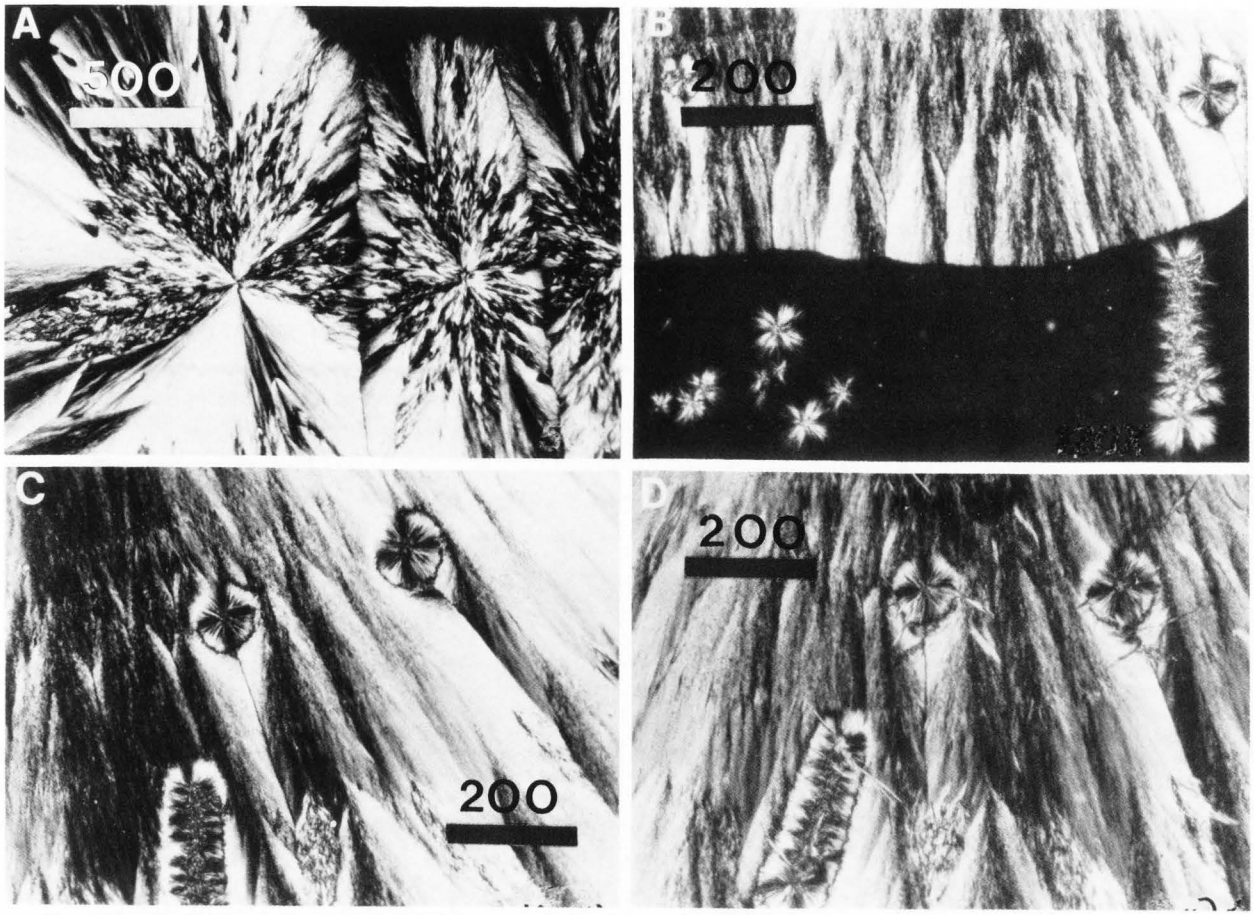

Fig. 8. Cross-sectional view of the 'ordered' (tempered) central area of a 28°C crystal with the predominant feather occurring on the periphery (A); 'feather' crystal growth engulfing the smaller 'spiney' crystals (B,C) and 'needle' type crystals forming in 'spiney' crystal matrix (D).

appeared dark due to less light transmittance while the periphery appeared lighter (Fig. 6A). The same crystals were then removed from the slide and placed on a SEM stub, gold coated, and viewed (Fig. 6B). Upon close examination an irregular peripheral edge (Fig. 6C) was visible which closely resembles the surface seen with the SEM surface reflection view of an unrestricted crystal (Fig. 6D). This was evidence that the two visualizations observed by different techniques were truly the same crystal structure. It was evident that the PLM technique visualized a cross-sectioned view of the crystal while the SEM micrographs visualize the actual unrestricted free growing crystal.

Crystal formation temperatures were pre-established and ranged from 26° to 34°C. In order to follow the natural order of transition from the less stable to the more stable form, the 26°C crystals will be discussed first. The first sign of crystal growth during incubation at 26°C occurred after approximately 2 hr. At 3 hr a non-distinct crystalline mesh was observed in areas throughout the liquid sample. At first this mesh lacks any obvious crystalline form, but as time elapsed a few circular forms begin to show a rosette pattern (Fig. 7A) and a uniform round shape as illustrated by SEM (Fig. 7B). After this center crystalline mesh has formed there appears on the periphery distinct 'feather' crystal growth (Fig. 7C). Also, during the same time interval, other smaller yet distinct crystals were observed (PLM) throughout the sample (Fig. 7C) and also by SEM in Figure 7D. As the 26°C crystals mature after 2 to 3 days there were two major distinct crystalline changes. The most dominant was the extension of 'feather' crystalline form (Fig. 7C) and, with time, these crystals predominated throughout the sample.

The less common crystallization change at 26°C involved the small 'individual' crystals in proximity with the feather type. In this case, if there was no visible growth in 'feather' crystals at 26°C, the smaller 'individual' crystals did not melt and thus did not contribute to the larger 'feather' structure. As time evolves these 'individual' crystals visualized with SEM (Fig. 7D) and PLM (Fig. 7E) slowly melted within approximately 30 days and another less distinct crystal type developed which was blade-like in appearance (Fig. 7F). In most

Fig. 9. PLM micrographs of the stepwise crystal growth from the 'bow-tie' seed to the 'feather' crystals (A,C,E,G,); the stepwise crystal growth visualized by SEM (B,D,F,H).

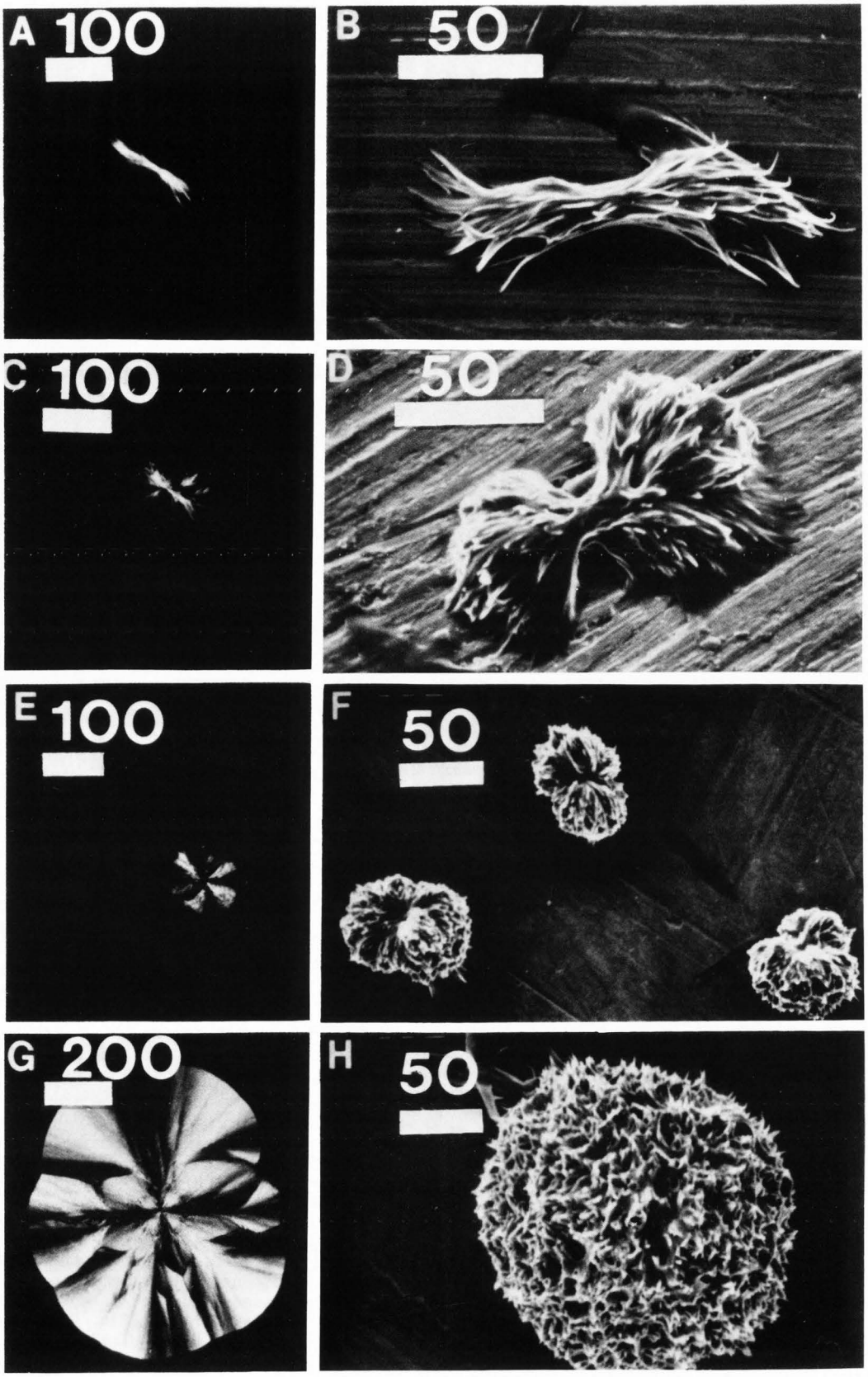
A 100
B 50
C 100
D 50
E 100
F 50
G 200
H 50

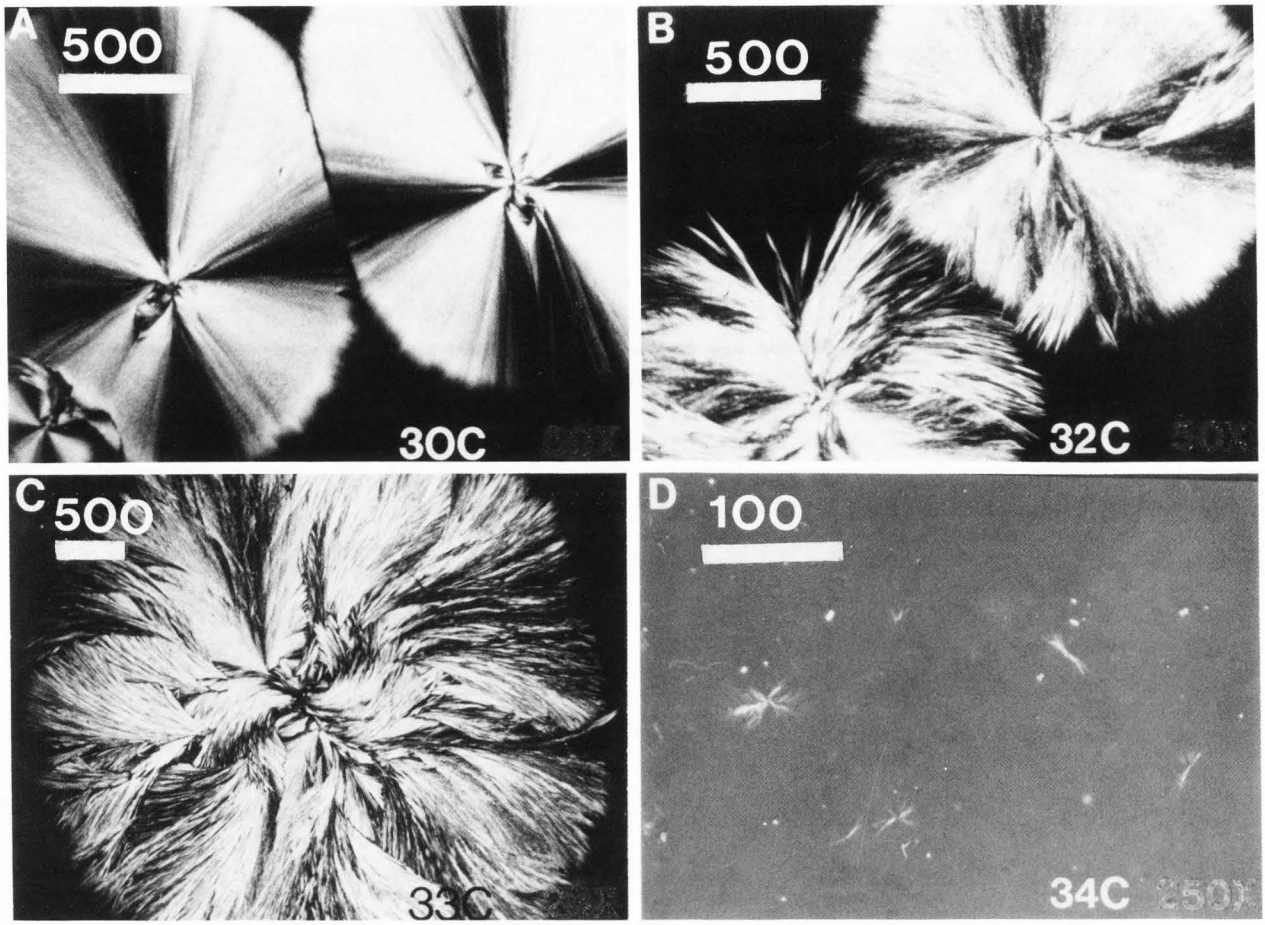

Fig. 10. PLM micrographs of cocoa butter crystals formed at 30°C (A); 32°C (B); 33°C (C) and 34°C (D).

cases these 'blade' crystals had a life of at least 60 days when the temperature was held constant at 26°C. Usually with extended time these crystals were engulfed by and blend with the 'feather' crystals thus losing their identity. However, there were instances when the opaque blades were not obscured by the 'feather' crystals. At this time a possible transition occurred from the 'opaque blade' to the slender 'needle' crystal (Fig. 7F).

At 28°C the crystalline 'mesh' was first observed, however, this area was more ordered in its appearance than that observed at 26°C. The difference between the mesh area of the two crystals was that at the higher temperature (28°C) the crystalline form appeared more feather-like in structure. After approximately 2-3 days the 'feather' crystal predominated and continued growing in this form (Fig. 8A). Concurrent with 'feather' crystal growth, smaller crystalline forms were developing. These crystalline forms were stable in that they were not melted during the growth of the large 'feather' crystal (Fig. 8B). Eventually these smaller crystals were entrapped by the 'feather' crystal networks (Fig. 8C). It is speculated that at 28°C the heat of crystallization was insufficient to melt these smaller 'spiney' crystals, thus it is thought that they have greater stability than the 'individual' crystal observed at 26°C. As time elapsed at 28°C the 'feather' crystals enlarged and spread as long as there was liquid cocoa butter available to supply the growing crystals. The small entrapped crystals remained intact within the 'feather' crystal structure but after approximately 3-4 wk these small crystals underwent a transition to a form characterized by slender 'needle' projections that occurred singly or in orderly bunches (Fig. 8D). It appeared this transition occurred more rapidly when the small 'spiney' rosettes are engulfed within the 'feather' crystals.

At the 30°C incubation a dramatic change was visualized in the initial crystal form. Crystallization first occurred (3-4 hr) in the form of a 'bow-tie' shape (Fig. 9A,B). The term 'bow-tie' is descriptive in that it depicts the crystal form that has a constriction in the center from which crystal growth fans out in opposite directions. As time passes (5-6 hr) the 'bow-tie' form enlarged primarily in the distal areas while the medial or central area of the crystal remained in a constricted form (Fig. 9C,D). As time progressed the crystals spread and began to show a circular pattern (Fig. 9E,F) and eventually became smooth and had a distinct rigid pattern which is characteristic of 30°C crystals (Fig. 9G,H).

As the temperature was increased above 30°C, PLM was utilized more extensively due to a decrease in the amount of actual crystal formation and growth (Fig. 10A). At the temperature of 32°C the crystals viewed were similar to those found at 30°C except they tended to be more irregular from the onset of crystallization (Fig. 10B). When the temperature was increased to 33°C the crystal was predominately the 'irregular' form. As pointed out previously, these higher melting point crystals originally formed from a 'bow-tie' like seed crystal. In the center of the 33°C crystal a 'bow-tie' configuration was readily visible (Fig. 10C). At a temperature of 34°C the only crystals produced were very similar to the 'bow-tie' form. This trend indicated that the 'bow-tie' may act as a seed for 'feather crystal' formation. The fact that the 'bow-tie' crystals were formed in a short incubation time (4 hr) and were also present at extremely high temperatures indicated that they may be composed of more saturated triglycerides. Fatty acid and glyceride composition data were needed to fully characterize crystal structure and behavior.

Crystal melting points are related to their formation temperature in that basically the higher the temperature of formation the higher the melting point range. The results obtained by past investigators state only two or maybe three polymorphic forms with melting points above 28°C. The results presented here show numerous crystals with melting points at 28°C and above (Table 3). The lowest melting point crystals observed were the 'individual' crystals formed at 26°C. A low melting point (29°C) gives the crystals poor stability compared to the other crystals. The life of this crystal was approximately 30 days. All other crystals formed in this study melted between 32-39°C. The 'tempered' crystals which form first at 26°C possessed a melting point at 33°C. The 'feather' crystals commonly form on the edges of the 'tempered' crystals and these crystals have been implicated in bloom formation. These crystals being the most common high melting point crystals can produce a white circular pattern common in untempered or heavily bloomed chocolate. The last high melting point crystals formed at 26°C are the 'opaque blade' crystals which formed after approximately 20 days of incubation. The 'opaque blades' were not as common as the 'feather' crystals but also may be a cause of bloom formation due to its 'blade' appearance. The 'opaque blade' has a melting point of approximately 34-36°C.

During crystal formation at 28°C the inner 'ordered' area which corresponds to the 'tempered' crystal area observed at 26°C temperature has a melting point between 33-36°C. Again the 'feather' crystals formed at the edges of the inner 'ordered' area and predominate during further crystallization. Also the 'feather' crystals produced at 28°C have slightly higher melting points than those formed at 26°C. This was thought to be due to the increased energy input (heat) which allows the triglycerides to align themselves in a more stable manner. The third crystal observed at 28°C was the 'spiney' crystal which has a high melting point of 37-38°C. At 30°C, the 'feather' crystals have a melting point of 33-36.5°C while the 'spiney' crystals melt at 37-39°C. The 32°C crystals melted at 35.0-37.5°C whereas the small 'spiney' crystals melted at a temperature greater than 40°C.

Table 3
Melting points of cocoa butter crystal forms.

Formation temperature (°C)	Crystal description[a]	Melting point range (°C)
26	Individual	28-29
	Mesh (tempered)	32-34
	Feather	32-34.5
	Blade	34-36
28	Ordered (tempered)	33-36
	Feather	33-36
	Spiney	37-38
	Needle	36-37
30	Feather	33-36.5
	Spiney	37-39
32	Irregular	35-37.5
	Spiney	> 40

[a]Descriptive term established by authors to denote the various crystals (See text).

Based on these data, the melting points of the numerous crystals found would fall in the β and β' form classification. One must realize then that the polymorphic forms are very diverse in visual structure and crystal appearance.

An investigation of crystallization in cocoa butter compared with that of semi-sweet dark chocolate was undertaken. The chocolate was incubated under the same conditions as the pure cocoa butter and examined by SEM. The crystals appeared very similar to those found in pure cocoa butter (Fig. 11).

The changes during cocoa butter crystallization are subtle and variable. A one-degree change in incubation temperature can permanently alter crystal formation. Also the consistency of crystallization with time is variable in that one sample may solidify in 3 days while an identically handled sample may take 3 wk. The procedures and methods undertaken in this investigation have shown trends in overall crystalline change. In the past most literature dealing with cocoa butter crystallization was based solely on melting point characteristics. Melting points of particular crystals are important but just as significant are the formation temperatures these crystals require. By controlling the temperatures which crystals form we can indirectly control their melting points along with other important characteristics.

Thermal and Compositional Properties During Dynamic Crystallization

Ivory Coast cocoa butter and a semi-sweet chocolate were utilized in these crystallization studies. A Brabender viscometer and pressure circulator were used to induce and control crystallization. All samples were heated to 60°C for 6 h prior to experimentation to assure that all crystal structures were liquified. After

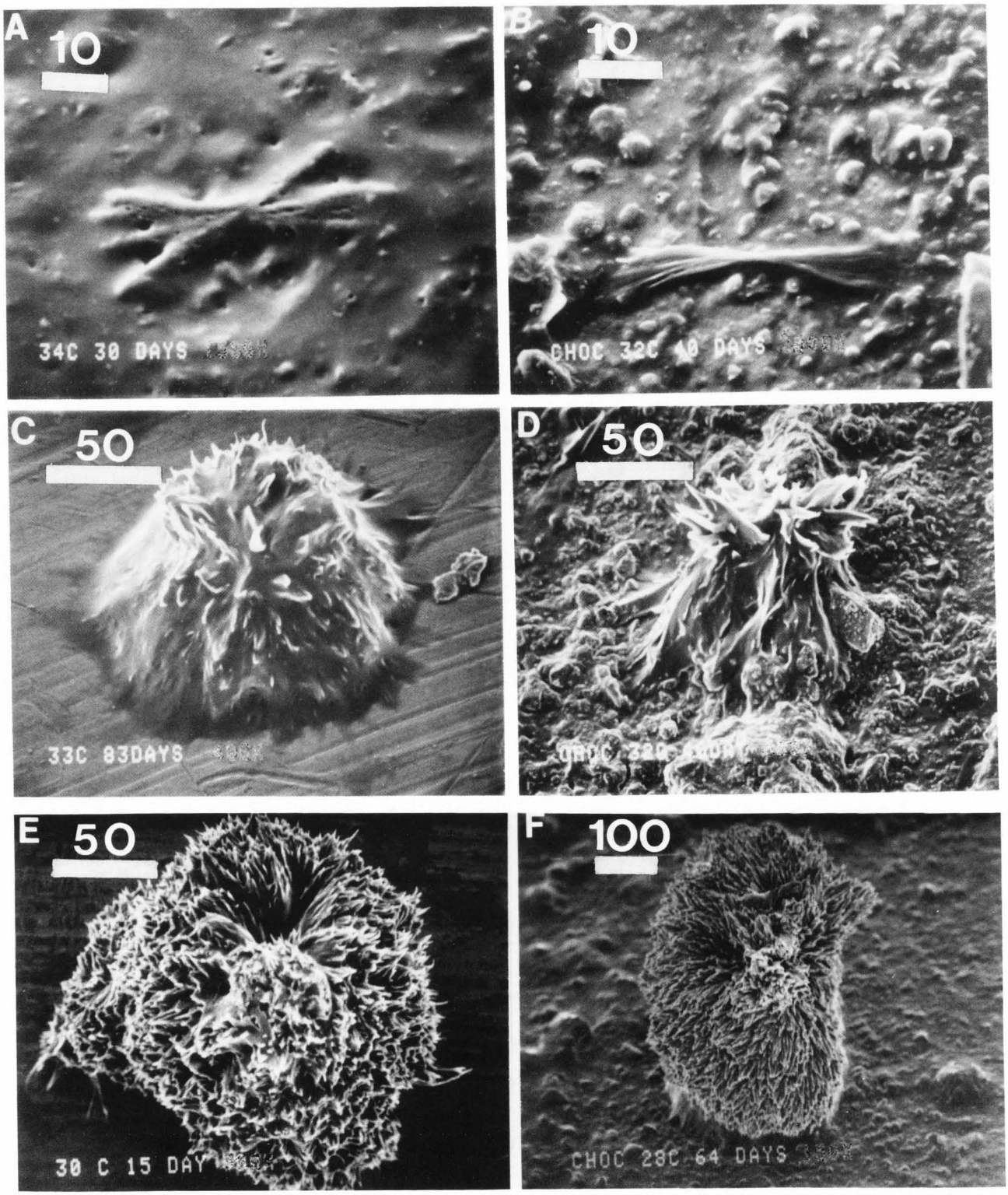

Fig. 11. SEM micrographs of Ivory Coast cocoa butter (A,C,E,) and semi-sweet dark chocolate (B,D,F).

Scale bars in μm for all figures.

heating, 50 g Celite was slowly added to the Brabender cup (45 rpm) which contained 165 g cocoa butter. The Celite addition to the butter produced a crystallization in a shorter period of time when compared to pure cocoa butter. The temperature cycles evaluated were 32.5° - 28.0° - 32.5°C and 32.5° - 30.0° - 32.5°C for both the cocoa butter and chocolate tempering studies. Samples were removed for analysis based on Brabender viscosity readings. Discussion of all the data would be rather lengthy, therefore only two trials will be discussed. A complete treatment of these data can be found elsewhere (Manning, 1984).

A Perkin Elmer DSC-2 was used to monitor crystalline melting points. A small spatula was used to obtain and transfer samples from the revolving Brabender cup to the DSC sample pan. Once the sample was in the pan, a lid was immediately placed on the sample to gently spread it over the bottom of the pan. The pan was immediately placed in the calorimeter for sample assay at 20°C/min over a temperature range of 15° to 45°C. Parameters used to characterize the thermal analysis of cocoa butter using DSC have been reported (Manning and Dimick, 1983).

It was found that the small cocoa butter crystals forming during tempering in the cup could not be isolated and analyzed, thus a method was developed to separate the liquid butter from the solid crystalline butter. At various viscosity levels, a 5 ml sample was removed from the Brabender cup and immediately placed into a filtering centrifuge tube (Fig. 12) which was in a temperature controlled Sorval GLC-1 centrifuge.

Fig. 12. Diagram of the centrifuge tube used to separate the liquid from the crystalline cocoa butter.

The cocoa butter-Celite samples were centrifuged at 800 rpm (107 x g) for 55s to separate a small amount of liquid cocoa butter from the crystalline slurry. The temperature of the centrifuge was held at the same temperature as the sample. The semi-sweet chocolate was handled in a similar manner except centrifugation was at 1000 rpm (168 x g) for 75s. The liquid filtrates from the cocoa butter-Celite and semi-sweet chocolate trials were solubilized in chloroform and filtered with a 0.45 Millipore type HA filter.

Triglyceride determinations were conducted using a Waters Associates HPLC pump and a Waters differential refractometer (Model 401). An acetonitrile-chloroform 6:4 (v/v) mobile phase was pumped at 0.7 ml/min through an Alltech Associates C-18, 5μm reversed phase column. The column was 25 cm in length with an internal diameter of 4.6 mm. Commercial triglycerides (Supelco, Inc.) POO, SOO, POP, POS and SOS were used as qualitative and quantitative standards. Triglycerides for which standards were not available (PLiP, SLiS, and SOA, where Li = linoleic acid and A = arachidic acid) were identified by retention volume data and also by interpreting chromatographic data from Shuklu et al. (1983). In order to determine the weight percent of PLiP, PLiS, SLiS, and SOA in each sample, the standard with the closest retention time was used.

Figure 13 illustrates a pure cocoa butter Brabender viscosity curve and the times when samples were removed and placed on a 16°C sample head for thermal assay. At 26°C, 2 h elapsed before crystals could be observed in the sample cup. After initial seed formation, a high rate of crystallization was observed as evident by a sharp increase in viscosity. Following this initial crystallization at 26°C, the resulting crystals exhibited a 30.8°C melting point. When the viscosity began to increase rapidly, the temperature of the butter was increased to 32.5°C to prevent solidification of the entire mass. After this temperature increase, a shift in the melting point of the crystals was observed. The melting point gradually increased after 7 min at 32°C and two endotherms were recorded on the thermogram. The melting point continued to increase to approximately 34°C and endotherms representing two crystal types were clearly evident in the last three samplings (Fig. 13C,D,E).

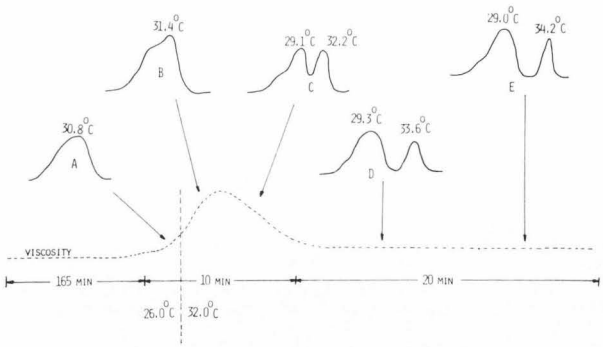

Fig. 13. An illustration of dynamic crystallization of cocoa butter occurring over time with changes in temperature.

Interestingly, the lower melting point endotherm (≅29°C) was not originally present in the Brabender cup and was an artifact as a result of the procedure. It must be remembered that the sample removed from the Brabender cup was a mixture of liquid and crystalline cocoa butter and the 29°C crystals originated from the liquid portion. To demonstrate this, and to prove that liquid cocoa butter was solidifying on the DSC head, a sample was rapidly cooled to 5°C to solidify the liquid fraction into low melting, unstable polymorphs. When the sample reached the temperature range at which the 29°C melting point crystal could form, an exotherm was observed indicating that the heat of crystallization was being released. An exotherm prior to the formation of the 29.3°C endotherm signaled that crystallization was occurring on the DSC sample head and was not representative of the original solid butter crystals in the Brabender cup (Manning and Dimick, 1983).

Semi-sweet chocolate also was studied with the Brabender viscometer and DSC to study cocoa butter seed formation in a formulated product. The viscosity of chocolate was much greater than pure cocoa butter due to the solids present. Small changes in crystallinity of the cocoa butter in chocolate produced large fluctuations in viscosity which were easily monitored. Seed formation in semi-sweet chocolate during a 32.5°C - 28.0°C - 32.5°C tempering cycle was a slow gradual process. After approximately 100 min at 28.0°C, seed formation commenced resulting in a small amount of 33.8°C melting point crystal (Fig. 14A). After approximately 135 min at 28.0°C, the stable seed concentration increased slightly which helped to form low melting point crystals when the liquid and solid sample was momentarily cooled to 15°C on the DSC head prior to analysis (Fig. 14B). After 165 min at 28.0°C, the viscosity began to increase rapidly due to increased amounts of crystals being formed from the stable seed. Figure 14C illustrates an increase in the amount of crystals present in the Brabender cup and also a decrease in overall melting point at 32.4°C. The dashed endotherm in Figure 14C illustrates the stable seed superimposed under the newly formed less stable 32.4°C crystal.

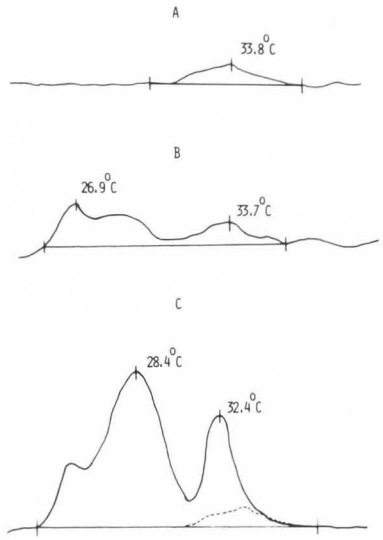

Fig. 14. DSC endotherm of the initial high melting point seed semi-sweet chocolate formed at 28.0°C (A); melting curve of the unstable crystals forming during cooling on the DSC sample head and the 33.7°C melting point seed (B); illustration of the less stable 32.4°C crystal that crystallized from the high melting point seed which is present -- but hidden under the large endotherm (C).

Throughout these dynamic studies, crystals of differing stability formed in varying amounts depending on the tempering cycle used. To determine the influence the different triglyceride types exert throughout the dynamic crystallization process, triglyceride analyses were performed during two different temperature cycles. Figures 15 and 16 represent typical cocoa butter-Celite viscosity curves for 32.5° - 28.0° - 32.5°C and 32.5° - 30.0° - 32.5°C tempering cycles. Samples were removed from the cup at three different times during agitation. Sample 1 was removed after a 40 BU viscosity increase to determine the triglyceride composition of the initial seed formed during both the 28° and 30°C tempering cycles. In the 32.5° - 28.0° - 32.5°C cycle, samples 2 and 3 were collected in duplicate from the Brabender cup.

Each sample drawn during the two temperature cycle experiments demonstrated a decrease in the concentration of SOS triglycerides in liquid cocoa butter filtrate. For example, the weight percent of SOS in the liquid cocoa butter filtrate of a 32.5° - 28.0° - 32.5°C tempering cycle decreased from 28.8% to 21.5% (Fig. 15). This decrease in SOS in the liquid butter signaled that these triglycerides were crystallizing and not passing through the filtering centrifuge in the liquid filtrate. The decrease in SOS glycerides in the liquid resulted in the concurrent increase in the solid crystals at all sampling times. Thus, since the viscosity increased after each cycle it appeared that the SOS-rich fraction was instrumental in the crystallization process. The triglyceride POS did not exhibit a consistent trend with regard to concentration during any of the temperature cycles. It is believed that since POS remained at approximately 46% of the total glycerides and did not consistently increase in percent composition in the liquid filtrate, it must have contributed to the solid fraction to some extent. For both tempering cycles large decreases in SOS in the liquid butter resulted in proportional increases in POO, PLiS, SOO, and POP indicated they were not crystallizing. For example, SOO increased from 3.4% to 4.7% in the liquid filtrate after two 32.5° - 28.9° - 32.5°C tempering cycles. The triglycerides SLiS and PLiP (not included in figures) were excluded from the crystalline structure because their percentage in the liquid increased after each sample was removed from the cup. Similar triglyceride trends were observed in the 32.5° - 30.0° - 32.5°C tempering cycle (Fig. 16).

Cocoa Butter-Celite, Temperature Cycle 32.5° - 28.0° - 32.5°C, 2.3°C/min

Fraction Collected	Triglyceride Types					
	POO	PLiS	SOO	POP	POS	SOS
Pure butter	1.7A	2.5A	3.4A	14.8A	45.5A	28.8A
Sample 1	2.3B	2.9B	3.7A	15.2A	45.4A	26.6B
Sample 2	2.3B	3.0B	4.4B	16.7B	45.8A	23.3C
Sample 3	2.8C	3.6C	4.7B	17.2B	45.5A	21.5D

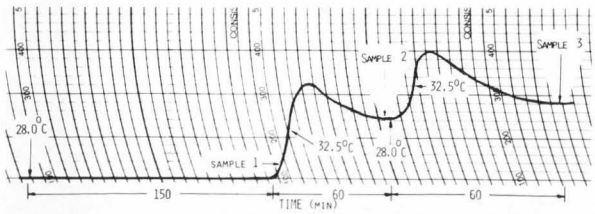

Fig. 15. Illustration of a 32.5° - 28.0° - 32.5°C tempering cycle for cocoa butter with the triglyceride analysis of samples 1, 2, and 3. (Means in a column with the same capital letter are not significantly different at the 0.05 alpha level).

Cocoa Butter-Celite, Temperature Cycle 32.5° - 30.0° - 32.5°C, 2.3°C/min

Fraction Collected	Triglyceride Types					
	POO	PLiS	SOO	POP	POS	SOS
Pure butter	1.7A	2.5A	3.4A	14.8A	45.5A	28.8A
Sample 1	2.2B	3.3B	4.1B	15.7B	44.0A	26.1B
Sample 2	2.8C	3.8C	4.3B	17.2C	45.6A	21.9C
Sample 3	2.9C	3.7BC	4.9C	17.7C	45.9A	20.7D

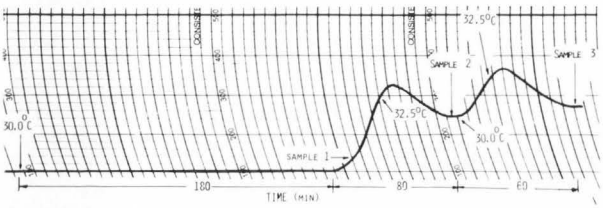

Fig. 16. Illustration of a 32.5° - 30.0° - 32.5°C tempering cycle for cocoa butter with the triglyceride analysis of samples 1, 2, and 3. (Means in a column with the same capital letter are not significantly different at the 0.05 alpha level).

Summary

Techniques were developed using SEM, PLM, DSC, and HPLC to study the crystalline, thermal and compositional properties of cocoa butter crystals. The initial crystal formed during tempering exhibited the properties of a high-melting-point seed. The stability of the seed increased as the formation temperature in the cycle increased from 26.0° to 30.0°C. The composition of the seed was not positively identified, however it is believed to be an SOS-rich fraction. The stable seed acted as a surface for further crystallization to continue. After a rapid viscosity increase, the temperature was increased and the viscosity decreased as the crystals partially melt and anneal. Throughout the temperature increase and afterwards, the crystals annealed and exhibited higher melting points. During the tempering cycle, the triglyceride POS is partially excluded from the crystalline structure, whereas POP and other liquid triglycerides are excluded to a greater degree. The resulting crystal formed after the temperature cycle is composed of a high percentage of SOS and lesser amounts of POS.

This dynamic study is applicable in understanding the thermal and compositional trends occurring during tempering. These studies could be continued using different formation and final temperatures. Furthermore, a study defining the properties of crystals formed upon cooling after tempering would be beneficial in understanding the total solidification process.

Acknowledgements

The authors wish to thank Dr. Ian R. Harrison for the use of the DSC facilities of the Polymer Science Program. This work was supported in part by the Pennsylvania Manufacturing Confectioners' Association. Authorized for publication as Paper No. 7090 in the Journal Series of the Pennsylvania Agricultural Experiment Station.

References

Bailey, AE. (1950). "Melting and Solidification of Fats." Interscience Publishers, Inc., New York, NY, 22-24.

Becker, K. (1958). The causes of fat bloom in coated and solid chocolates. Rev. Int. Choc. 13:254-256.

Campbell, LB, Anderson DA, Keeney PG. (1969). Hydrogenated milk fat as an inhibitor of the fat bloom defect in chocolate. J. Dairy Sci. 52:976-979.

Cerbulis J, Clay C, Mack CH. (1957). The composition of bloom fat in chocolate. J. Amer. Oil Chem. Soc. 43:533-537.

Chapman D. (1962). The polymorphism of glycerides. Chem. Rev. 62:433-455.

Chapman GM, Akehurst EE, Wright WB. (1971). Cocoa butter and confectionery fats. Studies using programmed temperature X-ray diffraction and differential scanning calorimetry. J. Amer. Oil Chem. Soc. 48:824-830.

Clarkson CE, Malkin T. (1934). Alternation in long-chain compounds. Part III. An X-ray and thermal investigation of triglycerides. J. Chem. Soc. London, Part I: 666-671.

Duck WN. (1964). Determination of solid fat in melted fat, their role in formation and polymorphic form by viscometry. A Masters Thesis, Franklin and Marshall College, Lancaster, PA, 72 p.

Duffy P. (1852). IVIII - On certain isometric transformations of fats. J. Chem. Soc. 5:197.

Feuge RO, Landmann W, Lovegren NW. (1962). Tempering triglycerides by mechanical working. J. Amer. Oil Chem. Soc. 39:310-313.

Giddey C, Clerc ET. (1961). Polymorphism of cocoa butter and its importance in the chocolate industry. Rev. Int. Choc. 16:548-554.

Huyghebaert A, Hendrickx H. (1971). Polymorphism of cocoa butter shown by differential scanning calorimetry. Lebensm - Wiss u technol. 4:59-63.

Jewell GG. (1972). Some observations on bloom on chocolate. Rev. Int. Choc. 27:161-162.

Kleinert J. (1970). Cocoa butter and chocolate. The correlation between tempering and structure. Rev. Int. Cho. 25:386-399.

Koch J. (1956). Chocolate tempering in theory and practice. Rev. Int. Choc. 11:344.

Larsson K. (1964). The structure of the β-form of trilaurin. Arkiv Kemi. 23:1.

Larsson K. (1972). Molecular arrangement in glycerides. Fette Seifen Anstrichmittel. 74:136-142.

Larsson K. (1982). Some effects of lipids on the structure of foods. Food Microstructure. 1:55-62.

Lovegren NV, Gray MS, Feuge RO. (1976). Effect of liquid fat on melting point and polymorphic behavior of cocoa butter and a cocoa butter fraction. J. Amer. Oil Chem. Soc. 53:108-112.

Lutton ES. (1945). The polymorphism of tristearin and some of its homologs. J. Amer. Oil Chem. Soc. 67:524-527.

Lutton ES. (1948). Triple chain-length structures of saturated triglycerides. J. Amer. Oil Chem. Soc. 70:248-254.

Lutton ES. (1972). Lipid structures. J. Amer. Oil Chem. Soc. 49:1-9.

Manning DM. (1984). Thermal and compositional properties of cocoa butter during static and dynamic crystallization. Ph.D. Thesis. The Pennsylvania State University, University Park, PA, 197 p.

Manning DM, Dimick PS. (1983). Interpreting the thermal characteristics of cocoa butter using the differential scanning calorimeter. Manufacturing Confectioner. 63:28-32.

Merken GV, Vaeck SV. (1980). Etude du polymorphisme du beurre de cacao per calorimetrie DSC. Lebensm - Wiss u Technol. 13:314-317.

Musser JC. (1973). Gloss on chocolate and confectionery coatings. Proc. from the 27th Annual PMCA Production Conference, 3404 Verner St., Drexel Hill, PA, 46-50.

Musser JC. (1980). The use of monoglycerides in chocolate and confectionery coatings. Proc. of the 34th Annual PMCA Production Conference, 3404 Verner St., Drexel Hill, PA. 51-59.

Neville HA, Easton NR, Bartron LR. (1950). The problem of chocolate bloom. Food Technol. 4:439-441.

Shuklu VK, Nielsen WS, Batsberg W. (1983). A simple and direct procedure for the evaluation of triglyceride composition of cocoa butters by high performance liquid chromatography - a comparison with the existing TLC-GC method. Fette Seifen Anstrichmittel. 85:274-278.

Steiner EH, Bonar AR. (1961). Separation of some glycerides of cocoa butter by paper chromatography. J. Sci. Food Agric. 12:247-250.

Vaeck SC. (1951). The polymorphism of certain natural fats: cocoa butter. Rev. Int. Choc. 6:100.

Vaeck SC. (1960). Cacao butter and fat bloom. Manufacturing Confectioners. 40:35, 50, 74.

Whymper R. (1933). "The Problem of Chocolate Fat Bloom." The Manufacturing Confectioner Publishing Company, Chicago, IL, 18-20

Wille RL, Lutton ES. (1966). Polymorphism of cocoa butter. J. Amer. Oil Chem. Soc. 43:491-496.

Discussion with Reviewers

G.G. Jewell: Do you consider that the morphologies observed in a static system occur during dynamic crystallization?
Authors: No, we would not venture to say that. However, one could speculate that the 'feather' crystal seed ('bow-tie') or the 'feather' crystal itself is closely related to the seed formed during tempering. The morphological characteristics would not carry over, however, the compositional and thermal characteristics may be similar. The crystals formed during dynamic crystallization are extremely small while those formed during static crystallization are very large. The 'feather' crystals and those crystals formed during dynamic crystallization have compositions containing largely SOS and POS triglycerides.

G.G. Jewell: Did the centrifugation process produce a consistent separation of seed from the liquid? What percentage of liquid, if any, remained with the solid?
Authors: Centrifugation was carried out very rapidly. Approximately 3 seconds elapsed from the point of sampling to centrifuge start up. The temperature controlled centrifuge system was energized for a minimal preset time for each run. The cocoa butter - celite system was centrifuged 55 seconds while the dark chocolate filtrate samples were collected after 75 seconds. The amount of liquid butter collected was low to minimize the effect of crystallization after sampling. Thus, liquid still remained with the solid. It was not quantified. The data presented in the thesis "Thermal and Compositional Properties of Cocoa Butter during Static and Dynamic Crystallization" (1984) D.M. Manning, The Pennsylvania State University, exhibit compositional and viscosity differences based on formation temperature.

G.G. Jewell: Mention is made of changes in the liquid phase on sampling for DSC. Is it not possible that changes in the solid phase also occur, not only in the DSC, but during centrifugation?

Authors: The only changes to occur in the solid fat during DSC analysis would be annealing at slow scan rates. Solid material should not change if the temperature is lowered.

J.S. Patton: What is the lipid class composition of cocoa butter? I realize it is mostly TG, but what about minor components?
Authors: Approximately 97% of the fat is triglyceride, and about 1% may be diglyceride with less than 1% being free fatty acids. Minor components commonly found in natural cocoa butter would include tocopherols, phospholipids, organic acids and numerous lipid soluble compounds formed during cocoa fermentation and processing. The extraction method (solvent versus pressing) as well as the parameters of extraction will influence the composition. All samples used in these studies were extracted by pressing.

J.S. Patton: Is it possible that the 'individual' crystals and the 'blade' crystals (at 26°C) both originated from the same nucleation centers?
Authors: It is possible that the 'blade' crystals were formed through a transition of the 'individual' crystals. The 'blade' crystals were an exception to the commonly observed crystals formed at 26.0°C. As time progressed at 26.0°C, the 'individual' crystals slowly underwent a change and the 'blade' crystal gradually appeared. This transition was repeatedly seen.

K. Larsson: It is indicated in the paper that a main factor in the crystallization involves molecular segregation, so that high-melting crystallization nuclei separate, and even in crystal growth there should be an enrichment of high-melting triglycerides. Were experiments done at different cooling rates in order to evaluate the expected time dependence of such segregation?
Authors: Unfortunately, we did not pursue the effect of cooling on the seeded cocoa butter and chocolate. We are interested in determining what was occurring during moulding and cooling. The subject of cooling, seed formation, and crystal propagation is very important and worthy of future experimentation. We are currently initiating studies on characterization of the nucleation process.

K. Larsson: Although it was stated that there are only four crystal forms ("forms V and VI maybe forms differing in composition") I think that this is still an open question. With regard to your results and your interpretations in this respect, do you consider blooming as mainly a segregation phenomenon, not a phase transition towards a more stable form?
Authors: We feel that fat bloom is a combination of migrating triglycerides to form larger, more stable crystals, thus leaving a less homogeneous fat dispersion throughout the confection product. When chocolate is subject to higher temperatures the more stable crystals composed of higher proportions of SOS will anneal and become more stable. There are numerous other crystals formed after tempering and cooling which are not as stable as the initial seed. When the ambient temperature is increased these triglycerides partially melt and anneal. The newly formed liquid triglycerides may migrate and form larger crystals upon cooling or the liquid material may crystallize from the initial stable seed resulting in larger crystals.

Process variables like degree of temper, cooling temperature, and cooling time along with cocoa butter triglyceride composition probably exert a significant effect on chocolate fat stability and bloom formation. Simply stated, bloom is a combination of triglyceride segregation to larger crystals and also an increase in crystal stability.

J.M. deMan: What in your opinion would be required to resolve the uncertainties and lack of uniformity in the classification of the polymorphic forms as listed in Table 2?
Authors: To undertake a long term static study with numerous sources of cocoa butter. Techniques used in this paper would be useful along with traditionally used tempering cycles and procedures commonly used with DSC. Temperatures of formation should vary from approximately 5°C to 33°C. Thermal, morphological, and compositional data would be useful. Further development of new procedures using transmission electron microscopy or X-ray diffraction analysis would be very advantageous. It is a challenge.

J.M. deMan: With increasing use of SEM more of the spherical crystal structures are observed. In this paper they are described as 'feather' crystals. Are these the same type of crystals usually given the name spherulites?
Authors: Yes, 'feather' crystal is a term used to describe the internal structure of the spherulite as viewed by polarized light microscopy.

FOOD MICROSTRUCTURE, Vol. 4 (1985), pp. 267-277
SEM Inc., AMF O'Hare (Chicago), IL 60666-0507 U.S.A.

0730-5419/85$1.00+.05

STRUCTURE FORMATION IN ACID MILK GELS

I. Heertje, J. Visser, P. Smits

Unilever Research Laboratorium Vlaardingen
P.O. Box 114, 3130 AC Vlaardingen, The Netherlands

Abstract

The structure formation in acid milk gels is influenced by many factors such as heat, salt system, pH, culture and thickening agents. Understanding of the mechanism of structure formation is important in order to be able to influence the final texture of these products.

In the present study the network formation in acid milk gels during acidification is monitored by freeze-fracture electron microscopy. Network formation appears to be a much more complex process than just an aggregation of the original milk casein micelles; it is accompanied by subtle dissociation and association phenomena of the milk caseins. The observed sequence of events can be explained from the course of the zeta potential, the association of the beta casein, the release of colloidal calcium phosphate from the micelle, the influence of heat treatment and from some observations on the internal structure of the casein micelle.

Initial paper received January 18 1985
Manuscript received July 19 1985
Direct inquiries to I. Heertje
Telephone number: 31 10 605513

Keywords: Acid milk gels, structure formation, protein aggregation/disaggregation, salt system, casein micelle, calcium phosphate, freeze fracture electron microscopy, zeta potential, beta casein, pre-heating of milk.

Introduction

Cultured dairy products, e.g. yoghurt and fresh cheese, are produced using very subtle microbiological and physicochemical processes. Without careful process control and due to seasonal variations in milk composition they are therefore subject to large variations in properties such as gel strength and texture, whey separation, smoothness or granularity, ropiness, etc. Factors responsible for these variations are heat, salt system, milk composition, pH, type of culture, added thickening agents, etc.

A well known example of an acid milk gel is yoghurt, resulting from the acidification of skim milk by a symbiotic culture of *Lactobacillus bulgaricus* and *Streptococcus thermopilus*. It appears as a three dimensional network of caseins and culture bacteria (10, 15-17) (Fig. 1).

The casein micelle which is considered to be the building element in this network is a macromolecular assembly of α_s-, β- and κ-caseins held together by an amorphous calcium phosphate citrate complex and occurs as a separate entity in milk.

Acidification and network formation is induced by the formation of lactic acid from lactose in the milk by the bacterial culture. The current view is that upon acidification the casein micelles become aggregated by charge neutralization under the formation of a network of chains and clusters (10, 15-17). In this view inorganic constituents present have no separate role.

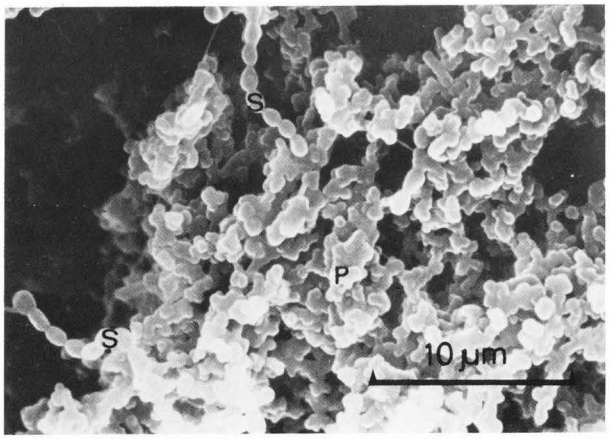

Fig. 1. Structure of yoghurt. p: protein network; s: *Streptococcus thermophilus*.

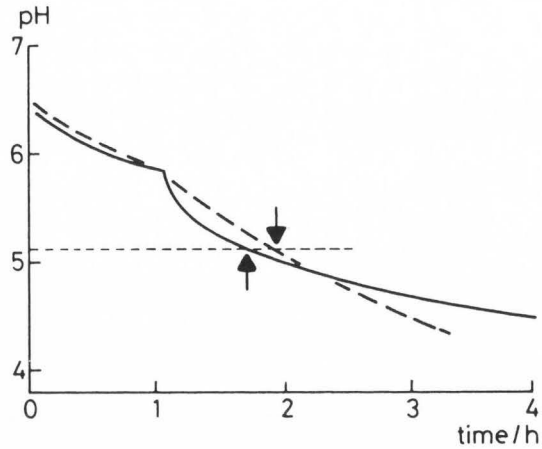

Fig. 2. pH-time profile of the acidification of skim milk. Comparison between glucono-δ-lactone (GDL) and a yoghurt culture. --- yoghurt culture; ——— GDL. Arrows indicate onset of gelation (pH 5.1).

However, the inorganic constituents, in particular calcium phosphate, perform an important function in that they maintain the integrity of the casein micelle (26, 34). Removal of calcium by calcium sequestering agents results in the disintegration of the micelles into separate protein subunits (18, 19, 28).

It is known that upon acidification of milk, micelle bound calcium phosphate is solubilized. At a pH of 5.1, calcium is almost completely removed from the micelle (11) and there are reasons to believe that at this pH the casein micelle also is disrupted. Since this pH is very close to the pH where gelation starts, one might wonder whether indeed the acid induced gelation of milk should be described as an aggregation process of the original individual micelles, or whether first a (partial) disintegration in casein subunits is taking place before an aggregation sets in.

For this reason, an in-depth study into the aggregation process during the acidification of milk has been carried out. Insight into the mechanism of aggregation is important for understanding the factors that influence the final texture of acid milk gels. In the present study, freeze-fracture electron microscopy was used to investigate the processes taking place during acidification and gel formation. The acidification process, as it occurs in the preparation of yoghurt, was imitated by the use of glucono-δ-lactone (GDL), which on hydrolysis gradually produces H_3O^+ ions. In order to better understand the mechanism of gelation, in this study also the internal structure of casein micelles was examined.

To support a proposed sequence of events, physico-chemical data, including zeta potential, the voluminosity of the casein micelles and changes in the milk salt system will be included.

Materials and Methods

Three kinds of milk samples were used. Sample I consisted of commercial pasteurized skim milk (9% dry matter) to which spray-dried medium heat skim milk powder was added to a final concentration of 12% solids and which was heated for 15 min at 90°C as is normal practice in yoghurt making. This sample was used to obtain a complete set of measurements on the microstructure during the acidification of milk. The other two samples were used to show the influence of pre-heating the milk on the microstructure, in particular in the region where gelation starts.

Samples II and III were made by dissolving freeze-dried milk powder, obtained from pasteurized skim milk in water to a final concentration of 12% solids. To study the influence of heating, sample II was pre-heated for 15 min at 90°C before use. Sample III was used directly.

Upon addition of 1% GDL (purum, ex Fluka A.G. Switzerland) at 20°C to sample I the pH dropped from 6.6 to 5.8; hereafter the mixture was heated to 30°C and an additional amount of 1% GDL was added. This procedure was chosen to obtain an acidification regime which conforms as close as possible to a normal yoghurt culture acidification. A comparison between GDL and a yoghurt culture is given in Fig. 2. To samples II and III, 1.2% GDL was added at 43°C. pH-time curves similar to those given in Fig. 2 were obtained.

All the samples, I–III, were observed by freeze-fracture electron microscopy at properly selected intervals during the acidification process. Special attention was paid to samples with a pH close to the onset of gelation. Freezing is considered to be the most suitable fixation technique in studies of the aggregation and disaggregation processes of caseins, because in such a sensitive system chemical fixation techniques may induce artefacts. To avoid ice crystal artefacts and phase separation during freezing, either rapid freezing or the addition of a cryoprotectant such as glycerol is essential. In our acidification experiments, rapid freezing has been applied, since addition of a cryoprotectant may influence the aggregation and disaggregation behavior. To attain complete vitrification in systems containing much water, like the present one, very high freezing velocities are required (10,000°C/s or higher). These conditions were obtained by propane jet freezing in a Balzers propane jet freezing system. The samples were placed between two copper plates and fixed between two nozzles through which liquid propane (−180°C) was blown from opposite directions onto the sample. The samples were subsequently fractured in a Balzers freeze-fracture unit (BAF 400D) at a low temperature (−100°C), etched for 15 s to expose the structure, and shadowed with platinum and carbon at an angle of 45°. The resulting replicas were viewed in a JEOL 100C transmission electron microscope operated at 80 kV.

Sample I was observed at pH 6.6, 5.9, 5.5, 5.2, 4.8 and 4.5, sample II was observed at pH 5.5, 5.4, 5.2 and 5.1 and sample III was observed at pH 5.4, 5.2, 5.1 and 5.0.

The structure of casein micelles was studied by the freeze-fracture methodology described by Schmidt and Buchheim (28, 29). Milk samples were mixed with glycerol to a final concentration of 30% and rapidly frozen in melting nitrogen (nitrogen slush). These experiments were performed at the normal pH of milk (about 6.7). The addition of a glycerol was considered to be permitted as there is no question of subtle aggregation and disaggregation phenomena as expected during acidification. Freeze fracturing was again carried out in a Balzers (BAF 400D) freeze-fracture unit. Apart from unidirectional shadowing, also rotary shadowing was applied. The latter procedure is particularly suitable for recognition of elongated structures.

Sodium citrate (0.02 M) was used to study the influence of calcium removal on the internal structure of the casein micelle.

Negative staining was applied in the study of the heat induced association of whey proteins and casein micelles as a function of pH. The heated samples were fixed in a 1% solution of glutaraldehyde in milk salt buffer during 1 h at room temperature.

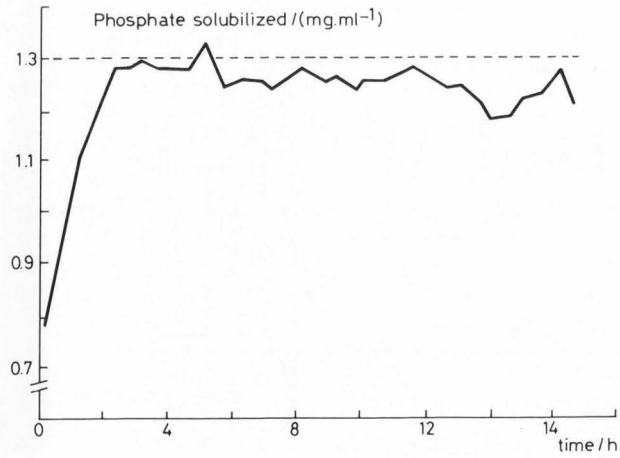

Fig. 3. Solubilization of phosphate upon acidification of skim milk at 30°C by GDL (2%) as determined by ^{31}P NMR. (---) level of soluble phosphate in milk.

After fixation the solution was dialysed to remove glutaraldehyde and any interfering inorganic ions. A drop of the protein solution was brought onto a freshly prepared parlodion carbon-coated grid. For good adhesion of the protein particles to the carbon film it is essential to use the carbon film within a few hours after preparation. Then, a drop of a 1% solution of uranyl acetate at pH 4.0 was applied to the grid and dried with filter paper.

^{31}P-NMR spectra were measured on a Bruker EP-200 WB NMR spectrometer operating at 81.0 MHz. Total soluble phosphate was estimated by comparing the resonance intensity of total soluble phosphate with the resonance intensity of an external standard consisting of a saturated solution of pyrophosphate in D_2O. The skim milk was brought into an NMR tube with an outer diameter of 20 mm and the saturated pyrophosphate solution into a tube with an outer diameter of 5 mm which was placed in the center of the first tube. The saturated pyrophosphate solution was calibrated against a known concentration of inorganic phosphate.

The viscosities of the acidified milk up to the point of gelation were measured with a Deer Rheometer. The milk was sheared between a thermostatic plate and a perspex cone of 1.5°. The shear rate was monitored during acidification while a constant shear stress of 0.24 Pa was applied. The pH at which the shear rate was reduced to zero was taken as the pH of onset of gelation.

Results and Discussion

Acidification/gelation

The pH region where gelation starts depends on the temperature of gelation (30°C and 43°C in this study) and on the heat pretreatment of the milk. Table 1 presents pH values at the onset of gelation. It appears that both pre-heating of milk and a higher temperature during acidification increase the pH of onset of gelation.

Another aspect of the structure formation is the milk salt system, especially the behavior of colloidal calcium phosphate. The solubilization of phosphate upon acidification of skim milk is shown in Fig. 3. By using 2% GDL as the acidification agent at 30°C all inorganic (colloidal) phosphate present in milk is solubilized after approximately 2 h at a pH of about 5.0. These observations substantiate earlier findings (11) that at pH 5.0 calcium is completely removed from the casein micelle.

The results of the microstructural observations during acidification are given in Figs. 4–16. In interpreting these figures it should be realized that they represent arbitrary cross-sections through a three-dimensional structure, which may cause chains of particles to appear as single particles, depending on the angle of cross-section.

The micrographs in Figs. 4, 5 and 6, taken from sample I show that the casein micelles keep their integrity, shape and dimensions during the initial drop in pH from 6.6 till 5.5. Some small particles are noticeable, however, at pH 5.5.

At pH 5.2 (Figs. 7, 8) the individual casein micelles appear to lose their integrity. The freeze-etch replica (in particular Fig. 8) shows separate particles. However, this structure should be carefully interpreted; it may be indicative of an aggregated network structure as has been observed before (1, 35). An observation supporting this view is the inhomogeneity of the apparent particulate distribution. Under the electron microscope, fields of these particles are observed, separated by empty spaces. This also points to an aggregated structure.

At pH 4.8 various structures can be distinguished. Fig. 9 shows a continuous field of particles, Fig. 10 shows more empty spaces, which are even more apparent in Fig. 11. These observations suggest that after a stage of aggregation, a stage of contraction and rearrangement occurs under formation of a particulate network. This view is supported by a micrograph of the final gel structure at pH 4.5 (Fig. 12).

These results show that at a certain pH different stages of protein aggregation and disaggregation can be distinguished.

An analogous behavior is observed for mixtures II and III, which differ in their detailed gelation pattern, in particular with respect to the pH of the onset of gelation (see Table 1). This is reflected in the microstructure. The unheated milk still shows a homogeneous distribution of micelles at pH 5.2 (Fig. 13) whereas at pH 5.1 an inhomogeneous distribution, apparently of aggregated caseins is observed (Fig. 14). On the other hand the heated milk already shows this inhomogeneous aggregated structure at pH 5.5 (Fig. 15). The same type of structure is observed at pH 5.2 (Fig. 16).

Role of the casein micelle

The current view is that the formation of yoghurt is achieved by the aggregation of the individual casein micelles into a 3-dimensional network of chains and clusters (10, 14, 16).

Table 1. pH at onset of gelation determined by viscosity measurements (Deer Rheometer)

	Sample		
	I heated milk 30°C	II heated milk 43°C	III unheated milk 43°C
pH	5.1	5.5	5.1

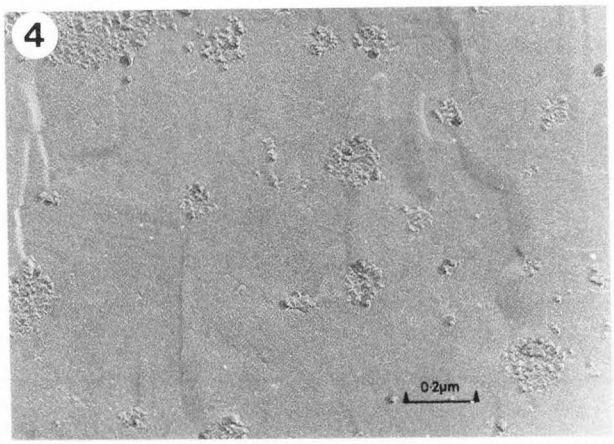

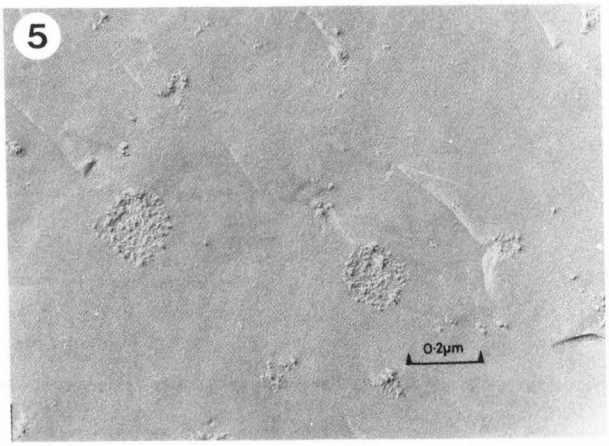

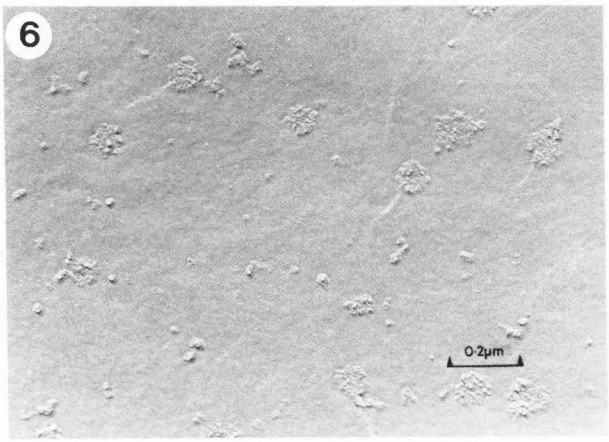

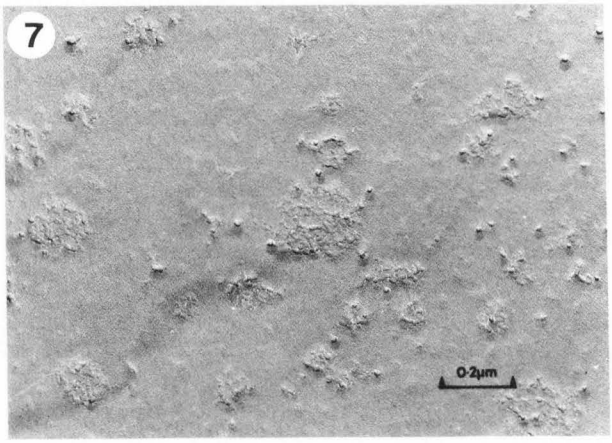

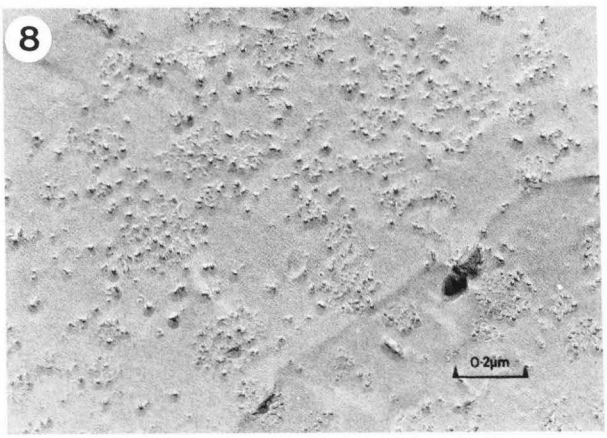

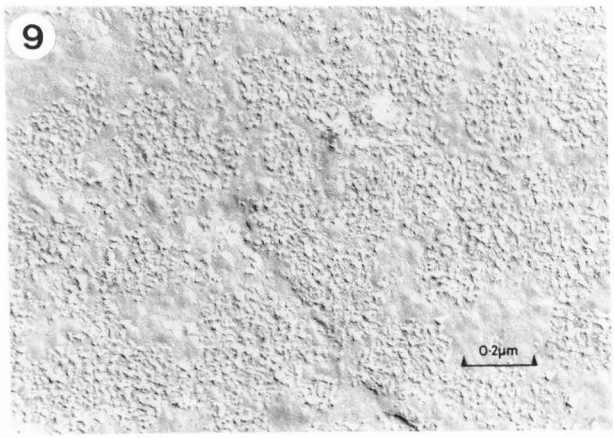

Fig. 4. Intact micelles at pH 6.6 (sample I).

Fig. 5. Intact micelles at pH 5.9 (sample I).

Fig. 6. Intact micelles and some small particles at pH 5.5 (sample I).

Fig. 7. Small particles and intact micelles at pH 5.2 (sample I).

Fig. 8. Fields of aggregated particles at pH 5.2 (sample I). Aggregation stage.

Fig. 9. Fields of aggregated particles at pH 4.8 (sample I).

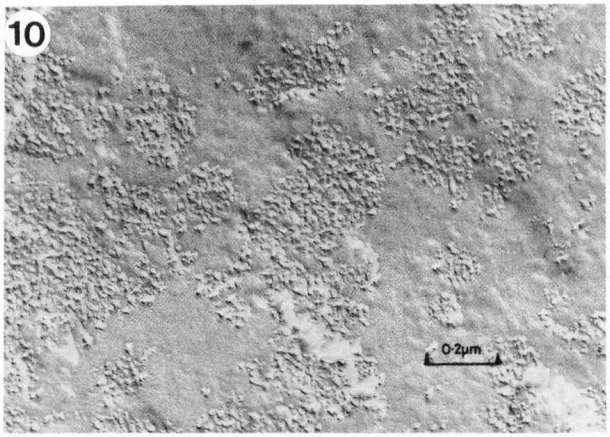

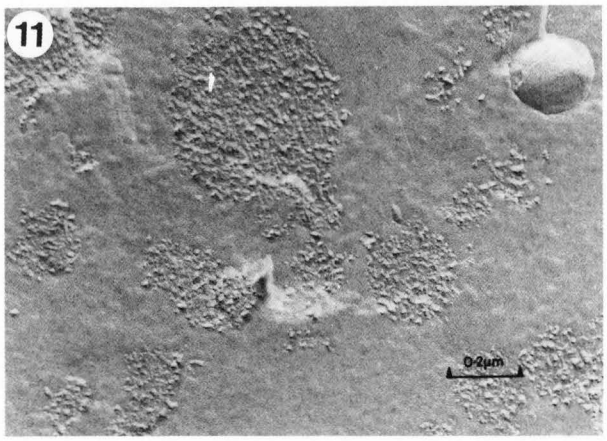

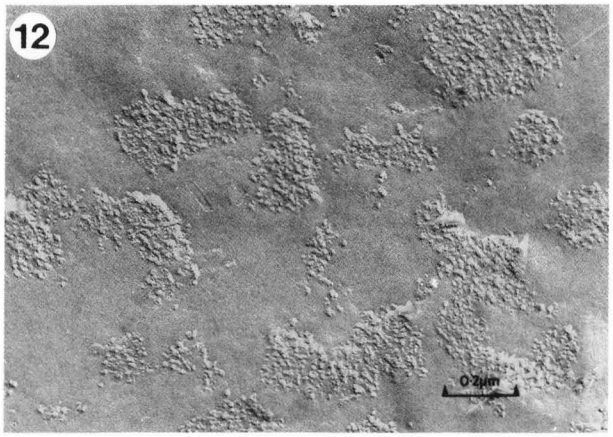

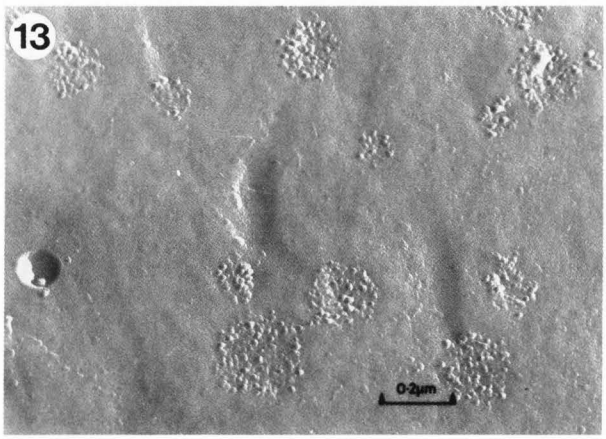

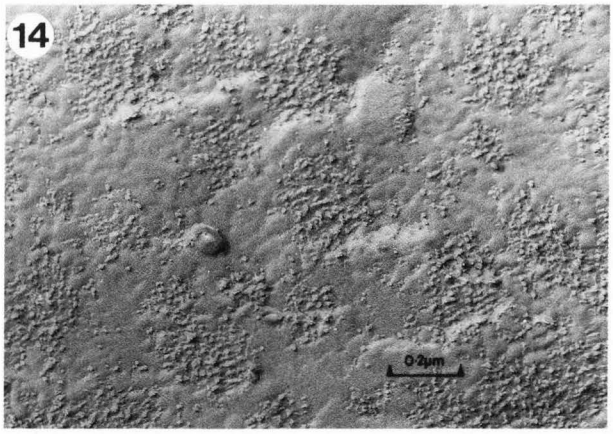

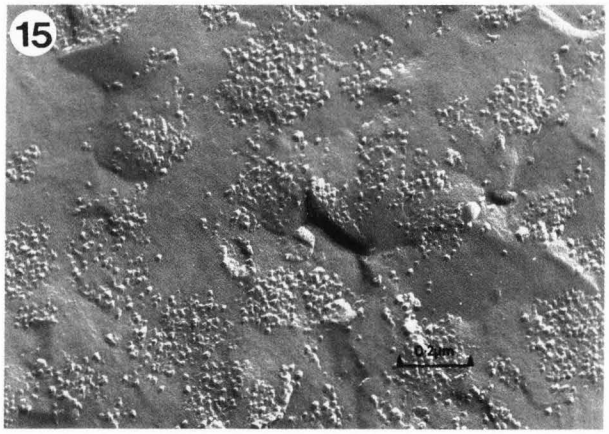

Fig. 10. Aggregates of particles at pH 4.8 (sample I). Start of contraction stage.

Fig. 11. Aggregates of particles at pH 4.8 (sample I). Contraction stage.

Fig. 12. Aggregates of particles at pH 4.5 (sample I). Final network.

Fig. 13. Intact micelles at pH 5.2 (sample III).

Fig. 14. Aggregates of particles at pH 5.1 (sample III).

Fig. 15. Aggregates of particles at pH 5.5 (sample II).

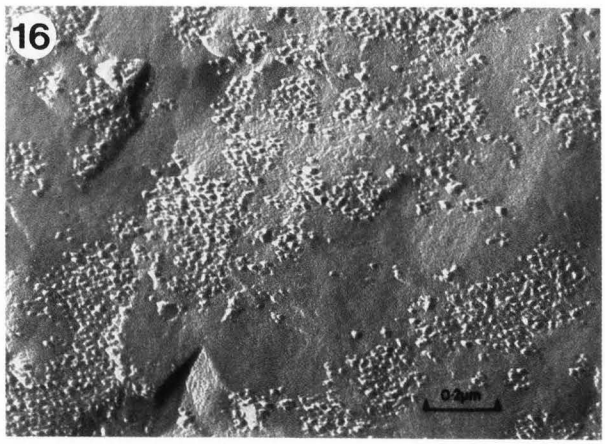

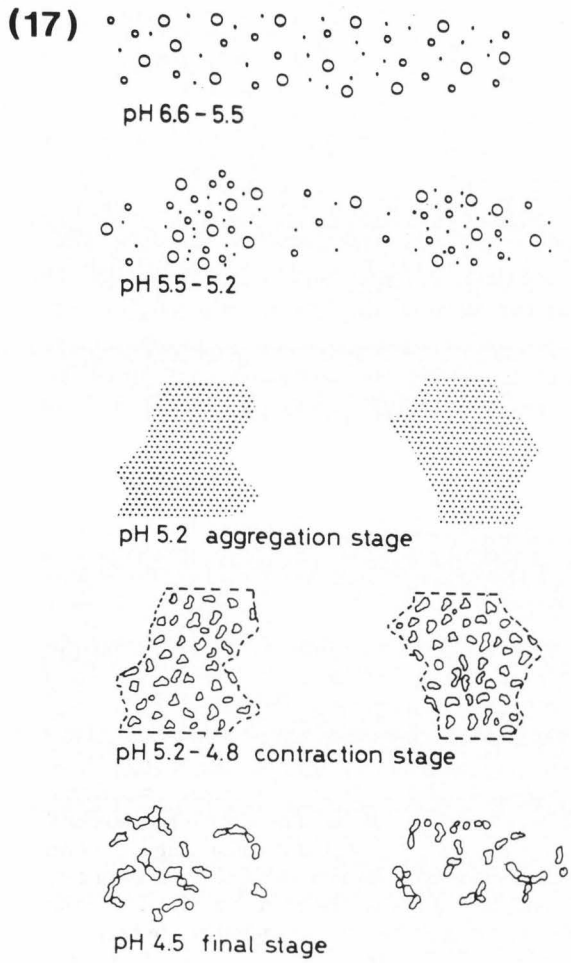

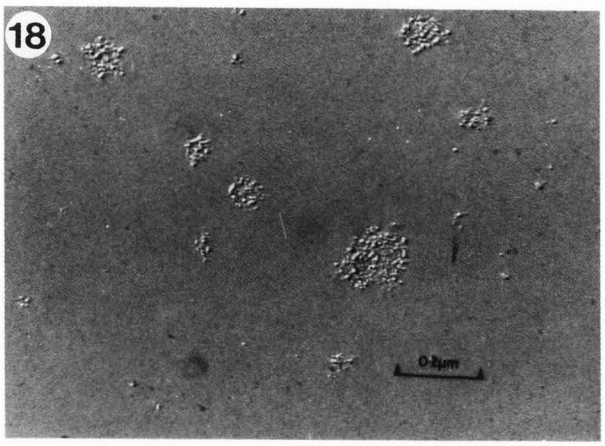

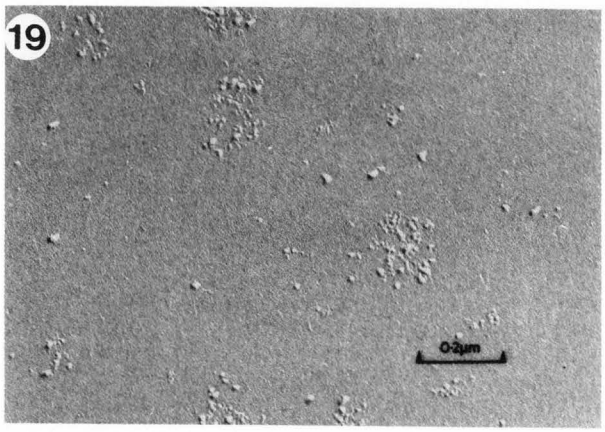

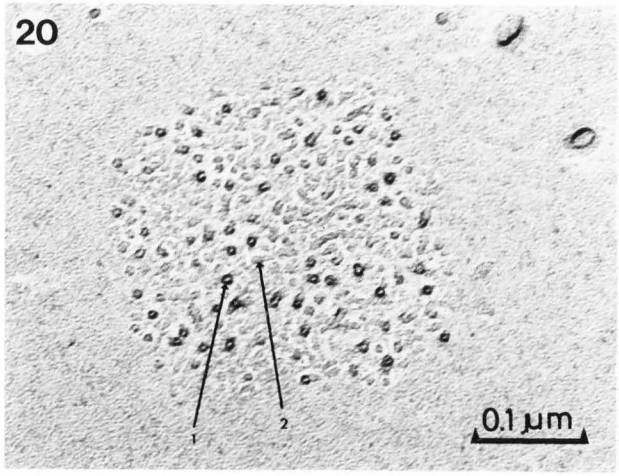

Fig. 16. Aggregates of particles at pH 5.2 (sample II).

Fig. 17. Schematic drawing of the structure formation in acid milk gel.

Fig. 18. Casein micelles in milk, showing a closely packed structure.

Fig. 19. Casein micelles treated with 0.02 M sodium citrate, showing an open coherent structure.

Fig. 20. Structure of casein micelles in milk. Rotary shadowed. 1: corpuscular structure; 2: thread-like elements.

Scanning electron microscopy in particular showed (14), however, that the observed casein particles must have undergone considerable changes in their dimensions and shapes, considering that casein micelles in milk are spherical and approximately 0.1 μm in diameter.

Based on the information obtained in the present study, we have come to the conclusion that the aggregation of milk proteins into a network is more complex than has been considered so far. A summarizing schematic drawing of the findings on mixture I is given in Fig. 17. At pH 6.6 and 5.9 casein micelles of an approximate size of 0.1 μm are present, homogeneously distributed in space. Micellar disintegration takes place at lower pH. Apparently the release of calcium phosphate upon acidification has progressed so far (Fig. 3) that its cementing role in keeping the individual casein molecules together in the form of a micelle has been reduced and part of the casein is released from the micelle. It has been shown (18) that calcium removal from native micelles initially dissociates the weakly bound β- and κ-caseins from the micelle, while the size-determining micellar framework of α_s-caseins remains intact.

The existence of such a size-determining frame work on which β- and κ-casein become reversibly attached is more in accordance with a model considering the micelle as a continuum of linear and branched polymers of molecular casein subunits (12, 13) than with a submicellar model (2, 3, 22, 26–28, 30, 31). This view is also in accordance with a number of microstructural observations on the internal structure of the casein micelle.

The internal structure of the casein micelle

The findings on the structure formation were supported by a study of the structure of casein micelles containing calcium and casein micelles depleted of calcium. To avoid any additional pH effect, use was made of the effect of sodium citrate, known as a calcium complexing agent at neutral pH, on the structure of the casein micelle. Micrographs of casein micelles in milk and in milk treated with 0.02 M sodium citrate are presented in Figs. 18 and 19. The addition of sodium citrate results in the partial disintegration of the micelle while forming smaller particles, which is in agreement with the observations of Lin et al. (18) on the removal of calcium from casein micelles. In addition to the large number of small particles formed, large particles are still present which show a more open structure than the original micelles. The most likely explanation is that the small particles (most likely β- and κ-casein) have been released from the micelles, leaving behind a micellar framework of α_s-caseins, without affecting the structural integrity of the original particle.

Fig. 20 shows a micrograph of the casein micelle structure obtained by rotary shadowing. Apart from a corpuscular structure apparently identical with the particulate structure shown in Figs. 18 and 19, also thread-like structures are observed. The corpuscular structure appears to be connected to the thread-like structure and is most likely formed by stretching linear protein aggregates out of the plane of fracture by plastic deformation.

These observations suggest that the casein micelle is a continuous network structure of protein molecules rather than a structure based on separate spherical sub-micelles. One may expect that such a network structure indeed can release particles without affecting the overall structure. Moreover, such a model representing a continuity in protein aggregation accounts better for the aggregation behavior of proteins in general (4) and caseins in particular, because of the known readily formed polymers of α_s- and β-caseins and their mixtures (8, 20, 21, 23, 24), whereby κ-casein known as a protective colloid has a limiting effect on the aggregation of these proteins (37).

On the basis of these observations, we consider the casein micelle to be a continuous structure of thread-like protein strands. In our view, a discontinuity in the aggregation of the constituting proteinaceous material, which would have to be assumed if the casein micelles were composed of spherical submicelles, does not occur. In this particular respect we strongly support the model as proposed by Garnier (12, 13), in so far as the casein micelle is considered as a continuum of protein strands. The length of the polymeric filaments and consequently the size of the micelles is limited by their interaction with the κ-casein.

This model of the casein micelle structure is indeed much better able to explain the events occurring during the acidification of milk. After the stage of partial micellar disintegration between pH 5.5 and 5.2, leaving a micellar framework of α_s-caseins, extensive fields of aggregated structures, apparently indicating interaction of caseins, with a size of a few μm are formed (at pH 5.2) with empty space in between. This aggregation stage is followed by a contraction stage, in which again identifiable particles appear to be formed, although these particles are considerably larger than the original micelles. In this stage and in particular in the final stage, rearrangement and aggregation of particles take place under formation of the ultimate milk protein network.

The zeta potential and the role of β-casein

The complex behavior of disintegration and integration phenomena may well be connected with the change in the zeta potential of the caseins as a function of pH. Micelles at normal pH (6.6) owe their stability to surface hydration and an overall negative potential of about 15mV. Hydration, steric repulsion and a negative surface charge together provide a barrier towards close approach and aggregation of the micelles (7, 22, 25, 36). Normally on lowering the pH the zeta potential of colloidal protein particles drops continuously till it becomes zero at the isoelectric point (IEP).

In the case of caseins (36) the pH dependence of the zeta potential shows an anomalous behavior (Fig. 21) (36). The exact course of the curve depends on temperature (9) and milk pretreatment. The minimum in zeta potential shown at pH 5.2, coincides with the start of the aggregation phase (for mixture I). On further lowering the pH the potential starts to increase again accompanied by contraction and separation of particles. The newly formed particles start to aggregate, forming a network as soon as their potential is sufficiently reduced. An explanation for the observed phenomena and the anomalous behavior of the zeta potential may be found in the behavior of β-casein. In the pH region between 5.5 and 5.2, β-casein is predominantly found in the serum phase (33) till it starts to precipitate at its IEP at pH 5.2, where the zeta potential has its minimum (Fig. 21) and the reaggregation process starts. As may be observed in Fig. 8, the structure differs from that of the original micelles as well as from the final structure, in the sense that a more loose type of aggregation is apparent. This may well be connected with the fact that after release of β-caseins at higher pH, leaving a relaxed frame work of α_s-caseins reabsorption of β-caseins on this framework starts to occur at its IEP.

In addition, it is found (unpublished results; 33) that at this pH (5.2) a relative maximum in the "micelle" voluminosity occurs, also indicating the presence of a reassociation mechanism without contraction. On further lowering the pH (5.2–4.8), the

β-casein acquires a positive charge and may then act as a center for aggregation with the α_s-casein framework which is still negatively charged. This leads to the formation of new particles and a corresponding lowering of "micelle" voluminosity. Due to the described disaggregation and aggregation phenomena, induced by the solubilization of calcium phosphate, these particles are completely different in structure from the original micelles. The total evidence for the proposed sequence of events has been included in Fig. 21.

Finally, the higher pH at the onset of gelation in pre-heated milk (sample II) in comparison to the same milk without heating (sample III) may be related to changes which occur during heating of the milk at 90°C as described below.

Heat induced association of whey proteins and casein micelles

Model studies have shown that upon heating skim milk the whey proteins present interact with κ-casein in two ways. At low pH (6.4), the whey proteins adhere to the casein micelle surface via reaction with κ-casein, whereas at high pH (7.0), whey proteins and the κ-casein form separate aggregates, which are present in the serum phase (5, 6, 32). This influence of pH is illustrated by electron micrographs, obtained by negative staining, showing the interaction between beta-lactoglobulin (the major whey protein) and casein micelles (Figs. 22–24). It is clear that the adherence of whey proteins to casein micelles as a consequence of heating critically depends on pH. In the present acidification model experiments, the milk has been preheated at pH 6.6. This means that a part of the whey proteins become associated with the casein micelles. It is assumed that such an association increases the hydrophobicity of the micellar surface. The hydration barrier preventing the aggregation of the casein micelles thus is lowered and gelation takes place already at pH 5.5. It may be speculated that if this is the case, disintegration of the micelles will proceed to a lesser extent and the network formation should rather be described as an aggregation of micelles that have maintained their integrity.

Another explanation for a higher pH value at the onset of gelation may be found in the effect of heating on the distribution of the caseins over micellar and serum phase. This effect is accompanied by a decrease in serum α_{s1}-casein and by an increase in serum β-casein (unpublished results). The resulting change in micellar composition (i.e., the increase in the α_{s1}-casein content) will lead to a higher calcium sensitivity and thus to a more rapid development of a framework of aggregated α_s-casein and consequently to an earlier start of gelation. In this case, micellar integrity is lost and the network formation with newly formed particles occurs along the lines described earlier (Fig. 17). The experimental evidence contained in the micrographs on structure formation of preheated milk supports this view.

In conclusion, the aggregation of caseins into a network during the acidification of milk is a much more complex process than just the aggregation of the casein micelles. It involves the disaggregation of the micelles and formation of a loosely aggregated α_{s1}-casein accompanied by release of β-casein and bound calcium phosphate; followed by reabsorption of β-casein on the α_s-casein framework under formation of new particles completely different in structure and composition from the original micelles. This hypothesis is supported by the dependence of the zeta potential and the micelle voluminosity on pH and by an internal structure of the casein micelle composed of continuous protein aggregates rather than a discontinuous structure of submicelles.

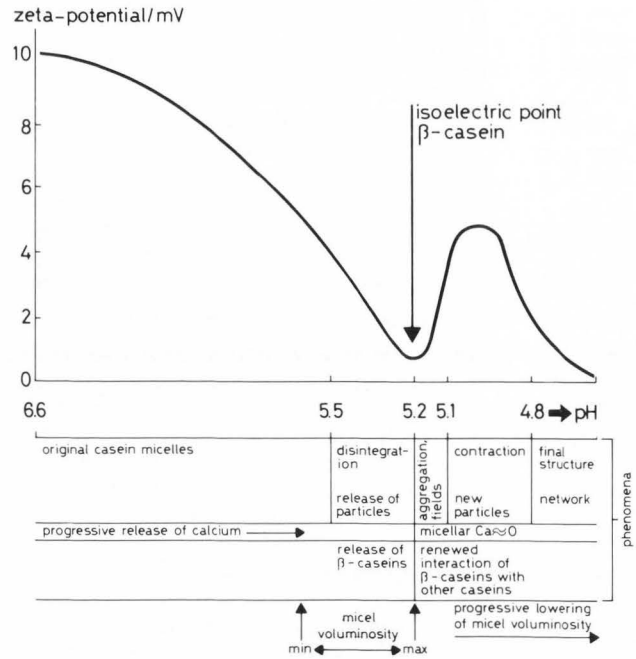

Fig. 21. Zeta potential as measured on the acidification of casein micelles in skim milk (schematic) and further evidence for the proposed structure formation.

References

1. Buchheim W. (1982). Aspects of sample preparation for freeze fracture/freeze-etch studies of proteins and lipids in food systems: A review. Food Microstructure **1**, 189–208 (see page 196).

2. Buchheim W, Welsch U. (1973). Evidence for the submicellar composition of casein micelles on the basis of electron microscopical studies. Neth. Milk Dairy J. **27**, 163–180.

3. Calapaj GC. (1968). An electron microscope study of the ultra structure of bovine and human casein micelles in fresh and acidified milk. J. Dairy Res. **35**, 1–6.

4. Clark AH, Judge FJ, Richards JB, Stubbs JM, Sugett A. (1981). Electron microscopy of network structures in thermally-induced globular protein gels, Int. J. Pept. Protein Res. **17**, 380–392.

5. Creamer JK, Matheson AR. (1980). Effect of heat treatment on the proteins of pasteurized skim milk. New Zealand J. Dairy Sci. Technol. **15**, 37–49.

6. Creamer JK, Berry GP, Matheson AR. (1978). The effect of pH on protein aggregation in heated skim milk. New Zealand J. Dairy Sci. Technol. **13**, 9–15.

7. Dalgleish DG. (1982). The enzymatic coagulation of milk, In: Developments in Dairy Chemistry, Vol. I, PF Fox (Ed.), Applied Science Publishers, London, 157–187.

8. Dalgleish DG, Parker TG. (1979). Quantitative α_s-casein aggregation by the use of polyfunctional models. J. Dairy Res. **46**, 259–263.

9. Darling DF, Dickson J. (1979). Electrophoretic mobility of casein micelles. J. Dairy Res. **46**, 441–451.

10. Davies FL, Shankar PA, Brooker BE, Hobbs DG. (1978). A heat-induced change in the ultrastructure of milk and its effect on gel formation in yoghurt. J. Dairy Res. **45**, 53–58.

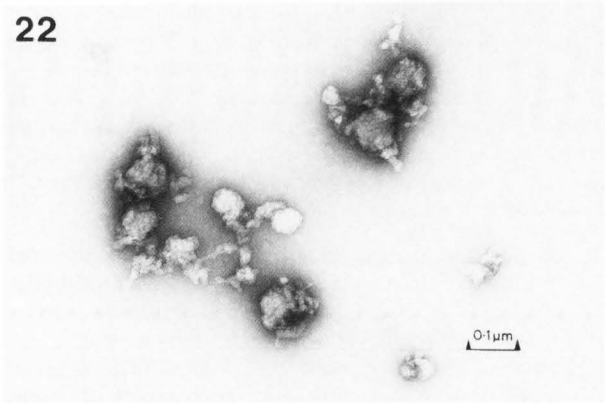

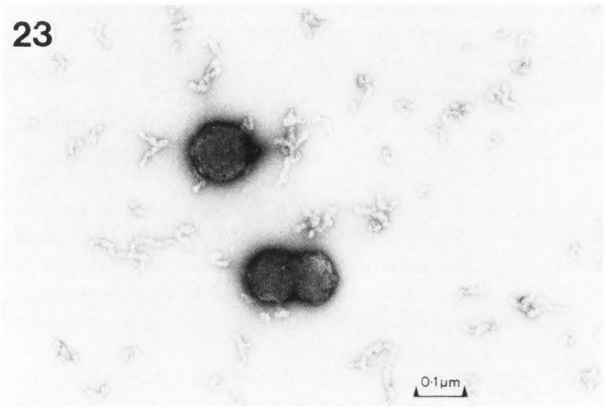

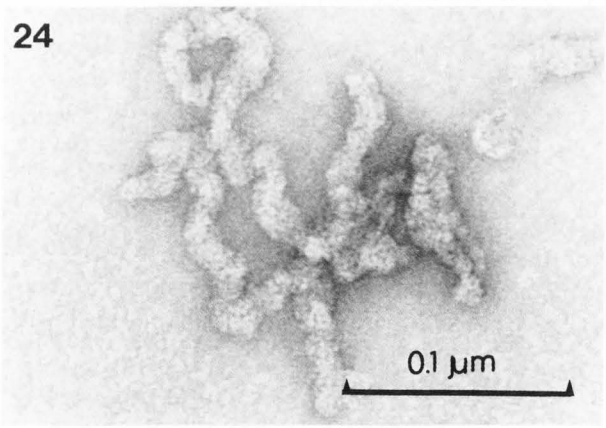

Fig. 22. Structure of a heated mixture of β-lactoglobulin and casein micelles at pH 6.5, showing the adherence of β-lactoglobulin to casein micelles.

Fig. 23. Structure of a heated mixture of β-lactoglobulin and casein micelles at pH 7.0, showing micellar structure and loose particles.

Fig. 24. Structure of the loose protein aggregates in a heated mixture of β-lactoglobulin and casein micelles at pH 7.0.

11. Evenhuis N, De Vries ThR. (1959). The condition of calcium phosphate in milk. Neth. Milk Dairy J. **13**, 10.

12. Garnier J. (1973). Models of casein micelle structure. Neth. Milk Dairy J. **27**, 240–248.

13. Garnier J, Ribadeau Dumas B. (1970). Structure of the casein micelle. A proposed model. J. Dairy Res. **37**, 493–504.

14. Harwalkar VR, Kalab M. (1980). Milk gel structure XI. Electron microscopy of glucono-δ-lactone induced skim milk gels. J. Text. Stud. **11**, 35–39.

15. Kalab M. (1978). Milk gel structure VIII. Effect of drying on the scanning electron microscopy of some dairy products. Milchwissenschaft **33**, 353–358.

16. Kalab M, Emmons DB, Sargent AG. (1976). Milk gel structure. V. Microstructure of yoghurt as related to the heating of milk. Milchwissenschaft **31**, 402–408.

17. Kalab M, Wotjas PA, Phipps-Todd BE. (1983). Development of microstructure in set-style nonfat yoghurt – a review. Food Microstructure, **2**, 51–66.

18. Lin SHC, Leong SL, Dewan RK, Bloomfield VA, Morr CV. (1972). Effect of calcium ion on the structure of native bovine casein micelles. Biochemistry, **11**, 1818–1821.

19. Morr CV. (1967). Effect of oxalate and urea upon ultracentrifugation properties of raw and heated skim milk casein micelles. J. Dairy Sci., **50**, 1744–1751.

20. Parker TG, Dalgleish DG. (1977). The potential application of the theory of branching processes to the association of milk protein. J. Dairy Res., **44**, 79–84.

21. Parker TG, Dalgleish DG. (1977). The use of light-scattering and turbidity measurements to study the kinetics of extensively aggregating proteins: α_s casein. Biopolymers, **16**, 2533–2547.

22. Payens TAJ. (1979). Casein micelles: the colloid-chemical approach. J. Dairy Res. **46**, 291–306.

23. Payens TAJ, Schmidt DG. (1966). Boundary spreading of rapidly polymerizing α_s-, β- and κ-casein during sedimentation. Arch. Biochem. Biophys., **115**, 136–145.

24. Payens TAJ, Van Markwijk BW. (1963). Some features of the association of β-casein. Biochem. Biophys. Acta, **71**, 517–530.

25. Schmidt DG. (1982). Association of caseins and casein micelle structure, In: Developments in Dairy Chemistry, Vol. I, PF Fox (Ed.), Applied Science Publishers, London, 61–86.

26. Schmidt DG. (1980). Colloidal aspects of casein. Neth. Milk Dairy J., **34**, 42–64.

27. Schmidt DG. (1974). On the formation of artificial casein micelles, Milchwissenschaft, **29**, 455–459.

28. Schmidt DG, Buchheim W. (1970). Elektronen microskopische Untersuchung der Feinstruktur von Caseinmicellen in Kuhmilch. Milchwissenschaft, **25**, 596–600.

29. Schmidt DG, Buchheim W. (1976). Particle size distribution in casein solutions. Neth. Milk Dairy J. **30**, 17–28.

30. Shimmin PD, Hill RD. (1964). An electron microscope study on the internal structure of casein micelles. J. Dairy Res. **31**, 121–123.

31. Slattery CW. (1973). A model for the formation and structure of casein micelles from subunits of variable composition. Biochem. Biophys. Acta **317**, 529–538.

32. Smits P, Brouwershaven JH. (1980). Heat-induced association of β-lactoglobulin and casein micelles. J. Dairy Res. **47**, 313–325.

33. Snoeren THM, Klok HJ, Van Hooydonk ACM, Damman AJ. (1984). The voluminosity of casein micelles. Milchwissenschaft **39**, 461–463.

34. Visser J, Schaier RW, Van Gorkom M. (1979). The role of calcium phosphate and citrate ions in the stabilization of casein micelles. J. Dairy Res. **46**, 333–335.

35. Waki S, Harvey JD, Bellamy AR. (1982). Study of agarose gels by electron microscopy of freeze-fractured surfaces. Biopolymers **21**, 1909–1926.

36. Walstra P, Jeness R. (1984). The electrical double layer, In: Dairy Chemistry and Physics, John Wiley & Sons, New York, 220–221.

37. Waugh DF. (1971). Formation and structure of casein micelles, In: Milk Proteins, Vol. II, HA McKenzie (Ed.), Academic Press, New York, 3–85.

Discussion with Reviewers

M. Kalab: Freeze-fracturing followed by freeze-etching reveals a corpuscular ultrastructure of the casein micelles in milk. Should not a continuum of protein strands be appearing as a uniform, i.e., non-granular, ultrastructure?

Authors: This is not the case, certainly under conditions of limited etching as has been applied in the present study. An important aspect of the observed freeze-fracture morphology is the non-complementarity of the replicas. This points to the phenomenon of plastic deformation. Networks, strands and even spheres will be stretched out of the plane of fracture and will show up as a corpuscular structure. Typical examples of network structures showing a corpuscular freeze fracture morphology can be found in references 35 and 1.

M. Kalab: It has been mentioned in the section on the internal structure of the casein micelles that a discontinuity in the aggregation would have to be assumed, were the casein micelles composed of spherical submicelles? How would this discontinuity be manifested?

Authors: One important aspect of micellar behavior is the influence of calcium complexing agents (EDTA, citrate) on micellar structure. A "pure" submicellar structure, i.e., a structure of spherical submicelles with colloidal calcium phosphate holding the submicelles together (text reference 26) would show a sudden and total decomposition of micelles into its subcomponents on addition of calcium complexing agents at a given concentration. This is not observed: literature data and the evidence presented in this paper suggest that, up to a certain level, calcium can be removed from the micellar structure, under release of casein-components, without the structural integrity of the casein micelle being affected.

M. Kalab: An interesting core-and-lining structure in casein particles was observed by Harwalkar and Kalab (Effects of acidulants and temperature on microstructure, firmness and susceptibility to syneresis of skim milk gels (Scanning Electron Microsc., 1981; III: 503–513) in milk precipitated at 70–90°C at pH 5.5. Can the development of that structure be explained on the basis of your results?

Authors: The formation of this interesting structure is probably connected with the release of β-casein upon acidification and the dependence of micelle voluminously on the pH of the system as described in this paper. At 20°C and pH 5.5 a considerable release of β-casein takes place and micelle voluminosity is high. At higher temperature these effects are less pronounced and it is very likely that under these circumstances redeposition of β-casein on the micellar periphery occurs.

It may be suggested that the observed "lining" is caused by differences in contraction of the various proteinaceous components of the reconstituted particles during the applied temperature increase.

D.G. Schmidt: The rejection of the submicellar model in favor of a model in which micelles consist of a three-dimensional network of protein filaments is based on the appearance of filamentous structures in Fig. 20. This does not convince me.

Moreover, if chains of polymeric casein do exist, such chains must also be observed when the calcium phosphate has been removed and that is not the case.

Authors: The rejection of the submicellar model is not only based on the filamentous structure observed in Fig. 20, but also on other evidence:

– the morphology of the casein micelles on the addition of 0.02 M sodium citrate (this paper).

– the agreement between this morphology and literature data showing that calcium and proteinaceous components (i.e., β- and κ-caseins) can be removed from the micelle without the structural integrity being affected. In addition it should be considered that the most convincing piece of evidence in favor of a sub-micellar model is the corpuscular structure shown in freeze-fracture replicas of casein micelles. As already has been said in our reply to M. Kalab such a structure is no proof for the existence of corpuscular particles.

Concerning the role of calcium phosphate, we certainly consider calcium and calcium phosphate to be important constituents of the polymeric chains. Without these inorganic components no polymeric structure would exist. In this context the aggregation behavior of α_s-casein under the infuence of calcium, described by a polyfunctional model, should be mentioned (Refs. 23, 20, 21).

D.G. Schmidt: Figs. 18 and 19 would demonstrate that addition of sodium citrate results in loosely structured micelles, consisting of a framework of α_s-casein. If this were the case why did the authors not apply some etching, because that would reveal such a three dimensional structure much better? Is it possible that glycerol causes detrimental effects in this respect?

Authors: In the present experiments etching could not be applied because of the presence of glycerol. An alternative would be to do these experiments by propane jet freezing without the addition of glycerol. First attempts in this direction indeed indicate the presence of a network structure after deep etching (−100°C, 60 s), whereas the familiar corpuscular structure is observed after mild etching (−100°C, 10 s).

D.E. Carpenter: Much of the recent evidence for micelle structure points to more κ-casein on the outside than on the inside of the micelle. Would you care to comment on this, with respect to the Garnier model and your microscopic observations?

Authors: We have clearly stated that we only support the Garnier model in so far as the casein micelle is considered as a continuum of protein strands. We certainly do not support the idea of the detailed location of the κ-casein in nodes of the polymer chains.

We suggest that the length of the polymeric threads and consequently the size of the micelles is limited by the interaction with κ-casein, known as a protective colloid. In this concept it is quite possible and even likely that the hydrophylic κ-casein is located on the outside of the micelle.

D.E. Carpenter: Kalab has seen shell and core and "ragged" micelles due to heat treatment. Do you have any direct microscopic evidence for interaction of β-lactoglobulin with the micelle by the freeze-fracture technique?
Authors: No, we have only looked for the heat induced interaction of β-lactoglobulin with casein micelles by the technique of negative staining. It would be interesting to do this by the freeze fracture technique, certainly when some etching can be applied and keeping in mind the effects of plastic deformation.

FOOD MICROSTRUCTURE, Vol. 4 (1985), pp. 279-287
SEM Inc., AMF O'Hare (Chicago), IL 60666-0507 U.S.A.

0730-5419/85$1.00+.05

RHEOLOGICAL AND SCANNING ELECTRON MICROSCOPIC EXAMINATION OF SKIM MILK GELS OBTAINED BY FERMENTING WITH ROPY AND NON-ROPY STRAINS OF LACTIC ACID BACTERIA

S. M. Schellhaass and H. A. Morris

Department of Food Science and Nutrition
University of Minnesota
1334 Eckles Avenue
St. Paul, Minnesota 55108

Abstract

Physical and rheological parameters of skim milk gels fermented with slime producing (ropy) cultures and non-ropy cultures were compared. The skim milk gels were made from steamed reconstituted nonfat dry milk inoculated with 2% of a single strain starter culture and incubated at 32, 37, and 45°C until pH 4.5 ± 0.05 was attained.

Skim milk gels fermented by slime-producing strains of Streptococcus thermophilus, Streptococcus cremoris, and Lactobacillus bulgaricus exhibited similar rheological and physical characteristics. Electron micrographs of the ropy skim milk cultures showed that slime produced by the organisms was associated with the cell surface as well as the protein matrix of the system.

Skim milk gels fermented by the slime-producing strains exhibited decreased susceptibility to syneresis as compared to skim milk which had been fermented with non-ropy strains at the same temperatures. Excessive slime production (when cultures were incubated for a longer time at a lower temperature) resulted in a coagulum with decreased relative firmness and apparent viscosity. However the skim milk gels fermented by the ropy strains at the higher incubation temperatures exhibited greater viscosity than skim milk fermented by non-ropy strains at the same temperatures.

Initial paper received February 18 1985
Manuscript received September 03 1985
Direct inquiries to H.A. Morris
Telephone number: 612 373 1076

KEYWORDS: Skim milk gel; slime producing lactic acid bacteria; yogurt; rheology; scanning electron microscopy; exopolymer.

Introduction

There have been many investigations involving optimization of yogurt texture. These studies have demonstrated that the total solids and fat levels in the milk, heat treatment of the milk prior to inoculation, homogenization, incubation conditions and handling of the ripened coagulum will all affect the body of the final product (Rasic and Kurmann, 1978). Another major way to affect the body of yogurt is through the addition of stabilizers such as gelatin, pectin, or starch. Stabilizers are added to the product to increase viscosity as well as to decrease susceptibility to syneresis.

An alternate way to improve yogurt viscosity is to utilize slime-producing (ropy) bacteria in the starter culture. The use of slime-producing strains to increase the viscosity of yogurt and decrease susceptibility to syneresis has been advocated by many dairy researchers (Davis, 1975; Galesloot and Hassing, 1973; Kosikowska et al., 1979; Rasic and Kurmann, 1978). Ropy cultures have been used extensively in France and The Netherlands because the addition of stabilizers is prohibited in unfruited yogurts (Humphreys and Plunkett, 1969). The manufacture of yogurt without the addition of stabilizers gained popularity in the United States. The increased desire of the consumer for "100% real yogurt" and for the "natural" product in general may have explained the trend (Steinberg, 1979). Also stirred yogurts, yogurt drinks and lowfat yogurt products gained popularity in the United States (Tramer, 1973). The use of viscous cultures in the manufacture of these products has been claimed to give a smooth thick body in unfortified skim milk and to enhance the smoothness of the mouthfeel (Andres, 1982; Vedamuthu, 1982). The use of a slow acid-producing slimy starter culture has been claimed to reduce the mechanical damage (from pumping, blending and filling machines) to the consistency of stirred type yogurt (Tramer, 1973). Also a slimy starter may render the coagulum more resistant to thermal and physical shocks (Robinson, 1981).

Dairy starter cultures that contain strains of Streptococcus cremoris, Streptococcus thermophilus and Lactobacillus bulgaricus capable of producing slime are commercially available in Europe and in the United States. However, little

Table 1. Bacterial Strains

Designation		Source	Description
S. thermophilus	yp	Commercial	Ropy
S. thermophilus	33	G.A. Somkuti, USDA	Non-ropy
L. bulgaricus	RR	NIZO Netherlands	Ropy
L. bulgaricus	LB	Dept. of Food Science and Nutr., U. of Minnesota	Non-ropy
S. cremoris	351	Commerical Direct Set-Frozen Culture Concentrate	Ropy
S. cremoris	351-U	Mutant from S. cremoris 351	Non-ropy

published information exists regarding the culture conditions which affect the ability of the organisms to produce slime and the resultant rheological properties of fermented milk systems.

The objective of this study was to investigate the physical and rheological properties of a model nonfat yogurt fermented with slime-producing lactic acid bacteria.

Materials and Methods

Lactic Acid Bacteria

The lactic acid bacterial strains were obtained from the collection of H.A. Morris. The source of each strain is listed in Table 1.

During the course of the investigation the cultures were routinely propagated in 11% reconstituted nonfat dry milk (NFM). The NFM was steamed for 1 hour and tempered to 37°C prior to inoculation. A 0.5% inoculum was added to the NFM and the culture was allowed to incubate at 37°C overnight (32°C for the Streptococcus cremoris strains).

Surface Structure of Ropy Strains

Appropriate dilutions of overnight ropy milk cultures were spread on 5% skim milk agar plates and incubated for 48-70 h at 32 (S. cremoris) or 37°C (S. thermophilus and L. bulgaricus). A 2-4 mm cube of the agar with a colony on it was cut from each plate. The samples were fixed at 4°C for 20 h in a 2.0% glutaraldehyde/500 ppm ruthenium red/0.33M sodium cacodylate (pH 7.0) solution; followed by three 10 minute rinses in 0.033 M cacodylate buffer.

Post fixation of the samples was done in a 2% osmium/500 ppm ruthenium red/0.33M sodium cacodylate buffer (pH 7.0). Primary dehydration was carried out at room temperature using an acetone dehydration series (10 min each in 25%, 50%, 75%, 99% and three changes in 100%). Final dehydration was performed in a Bomar SPC/EX critical point dryer using CO_2 as the transition medium.

The specimens were mounted on aluminum SEM stubs with carbon paint and coated with a layer of gold palladium by a Kinney vacuum evaporator model KSE-2AM. Specimens were viewed on a Philips 500 scanning electron microscope operated at 12 kV accelerating voltage.

Microstructure of Ropy Milk Cultures

A template was made by gluing 4x10mm glass rods to the inside surface of a petri dish cover. A 3% agar sol (60°C) was poured 13 mm deep into the petri dish. The template was then placed into the agar sol. The template was removed after the agar had solidified, which resulted in the formation of cylindrical pores in the agar. The coagulated ropy 11% NFM cultures were then pipeted into the pores. The surface was overlaid with 3% agar which had been tempered to 45°C. After the agar overlay had solidified, 6 mm cubes containing a single cylindrical pore of coagulated milk, were cut out of the agar.

The agar cubes were fixed in 2.0% glutaraldehyde in 0.33 M sodium cacodylate buffer (pH 6.0) solution followed by three 10 minute rinses in 0.033 M cacodylate buffer. Post fixation was done in 2% osmium tetroxide in 0.33 M sodium cacodylate buffer solutions. Primary dehydration was carried out at room temperature using an acetone dehydration series: 10 min each in 25%, 50%, 75%, 99% and three changes in 100%. Final dehydration was performed in a Bomar SPX/EX critical point dryer using CO_2 as the transition medium.

The specimens were mounted on aluminum scanning electron microscopy (SEM) stubs with carbon paint and coated with a layer of gold-palladium by a Kinney vacuum evaporator model KSE-2AM. Specimens were viewed on a Philips 500 scanning electron microscope operated at 12 kV accelerating voltage.

Susceptibility to Syneresis

The susceptibility of nonfat yogurt to syneresis was evaluated according to the method of Harwalkar and Kalab (1981). The method is based on measuring the amount of whey expelled from a milk gel when the gel is subjected to increasing amounts of g-force. A 2% inoculum of a ropy or a non-ropy strain was added to steamed (1 h) 11% NFM (NFM mixture was tempered to the appropriate incubation temperature prior to inoculation). Ten ml aliquots of the inoculated milks were placed in sterile centrifuge tubes, followed by incubation at 32, 37 and 45°C until pH 4.8 was achieved. The gels were then cooled to 4°C in ice water until pH 4.5 $\pm$ 0.05 was attained (1-5 h depending on the culture and prior incubation temperature). Triplicate tubes, corresponding to each strain and each incubation temperature, were centrifuged in a Beckman J-21C centrifuge with a JA-14 rotary head for 10 minutes each at 500, 1000, 1500, 2000, 2500, and 3000 rpm (i.e., 38-1375 x g). The clear supernate was decanted and measured by volume. The extent of susceptibility of the gels to syneresis was estimated from the slope of the regression line of % volume of whey separated on the application of g-force.

Water Activity

Steamed (1 h) 11% NFM was inoculated and incubated as described in the previous method. The water activity (a_w) of ropy and non-ropy milk cultures was determined by cryo-osmometry. The instrument used was an advanced Digimatic

Osmometer 3DII (Advanced Instruments, Inc., Needham Heights, MA). It was equipped with an internal microprocessor which automatically translated freezing point depression into an effective osmotic concentration (n_2'), given as milliosmoles per kg water (mOsm). The determination of a_w from mOsm values was obtained by a rearrangement of Raoult's law (equation 1) to equation 2, where n_2' is a function of γ and n_2:

$$a_w = \frac{\gamma\ n_1}{n_1 + n_2} \quad (1)$$

$$a_w = \frac{n_1}{n_1 + n_2'} \quad (2)$$

γ = activity coefficient

n_1 = mole fraction of water

n_2 = mole fraction of solute

n_2' = effective osmotic concentration; mOsm/1000 g of H_2O.

Viscosity

Steamed (1 h) 11% NFM was inoculated and incubated as described in the previous method. The samples were cooled in ice water for 2 h and then stored for approximately 24 h at 5°C. Viscosity analysis was performed using a Haake Rotovisco RV2 rotational viscometer with an MVII sensor system (Haake, Inc., Saddle Brook, NJ). The temperature of the sample was maintained at 8°C by continuously circulating water at 8°C through the jacket surrounding the sensor system by means of an Aquamatic K thermocirculator (Garman-Rupp Industries, Billville, OH). The rotor speeds in the experiment were programmed to reach 30 to 100 rpm in 6 min.

Values of rotor speed (rpm) and the resistance to shear (recorded as "scale units") were converted to shear rate and shear stress values, respectively, by multiplying by predetermined instrument constants. The constants (A, M, & G) are dependent upon the characteristic geometry of the sensor system, the electrical specifications of the RV2 and the torque caused by the cylinder end faces. The constants were determined by means of an absolute test of "weighing torques" as outlined by the Haake Manual 105.

Gel Strength

A 2% inoculum of a ropy or non-ropy strain was added to steamed (1 h) 11% NFM. Four hundred ml aliquots of each inoculated milk were then distributed into three 11 x 7.5 cm cylindrical containers followed by incubation as described in the previous method. The gels were then cooled in ice water for 2 h and stored for approximately 24 h at 5°C.

Gel strength was determined from the first peak of the force-distance curve obtained by the Instron Universal Testing Machine 1122 equipped with compression load cell CB. Crosshead speed and chart speed were 50 and 100 mm/min, respectively, and the chart full scale was 20 or 50 grams. A 13/16 inch (2 cm) diameter probe was placed into each sample to a constant depth (4.5 cm below the surface of the gel).

Results and Discussion

Microstructure of the Ropy Cultures

Scanning electron micrographs of the ropy strains (Figures 1A and 2A) demonstrate the existence of cell surface appendages not present on the cell surfaces of the non-ropy strains (Figures 1B and 2B). As can be seen in the micrograph of the ropy *S. thermophilus* strain (Figure 1A) the web-like slime material is associated with the cell surface as well as with the protein matrix of the skim milk gel. This confirms the finding of Kalab et. al. (1983) and Tamime et. al. (1984).

Susceptibility to Syneresis

Whey separation (syneresis) from the coagulum is undesirable in yogurt and many other fermented milk products. The major factors which contribute to syneresis in yogurt include:

a) a product with low acidity (pH > 4.6) or with high acidity (pH < 4.0).
b) high temperatures during incubation or storage.
c) agitation during manufacture or during transportation of the final product.
d) low level of milk solids in the milk
e) low heat treatment of the milk
f) milk is not homogenized prior to fermentation.

Several investigators (Rasic and Kurmann, 1978) have observed that the use of slime-producing strains in starter cultures reduces susceptibility to syneresis (Vedamuthu, 1982; Tramer, 1973; Rasic and Kurmann, 1978). The methods used by these workers and others to measure syneresis include measurement of the volume of whey on the surface of the coagulum after a certain length of time in quiescent storage, pouring the coagulum into a funnel lined with filter paper and collecting the exudate, or allowing the product to warm to room temperature for an arbitrary set time and then measuring the amount of whey on the surface of the coagulum.

Harwalker and Kalab (1981) evaluated the susceptibility of acidified gels to syneresis by subjecting the gels to increasing centrifugal force and then measuring the whey syneresed from the gels. The slope of the regression line of volume of whey syneresed on g-force was used as an index of the susceptibility to syneresis.

The Harwalker-Kalab method was chosen to compare syneresis of 11% NFM fermented with ropy versus non-ropy strains for several reasons. This method allows for a standardized subjective measurement as opposed to the visual assessment of some methods. Another advantage lies in the dynamic nature of the method, which is more representative of the forces to which fermented milk products are subjected during manufacture and distribution than to measurements made after quiescent storage.

Ropy and non-ropy strains of *S. thermophilus*, *S. cremoris* and *L. bulgaricus* were used to ferment 11% NFM at 3 different incubation temperatures. The plots of % volume of whey syneresed versus g-force are presented in Figures 3-5. The solid and dashed lines represent the calculated regression of the volume of whey syneresed on centrifugal force for ropy and non-ropy cultures respectively. The R^2 values

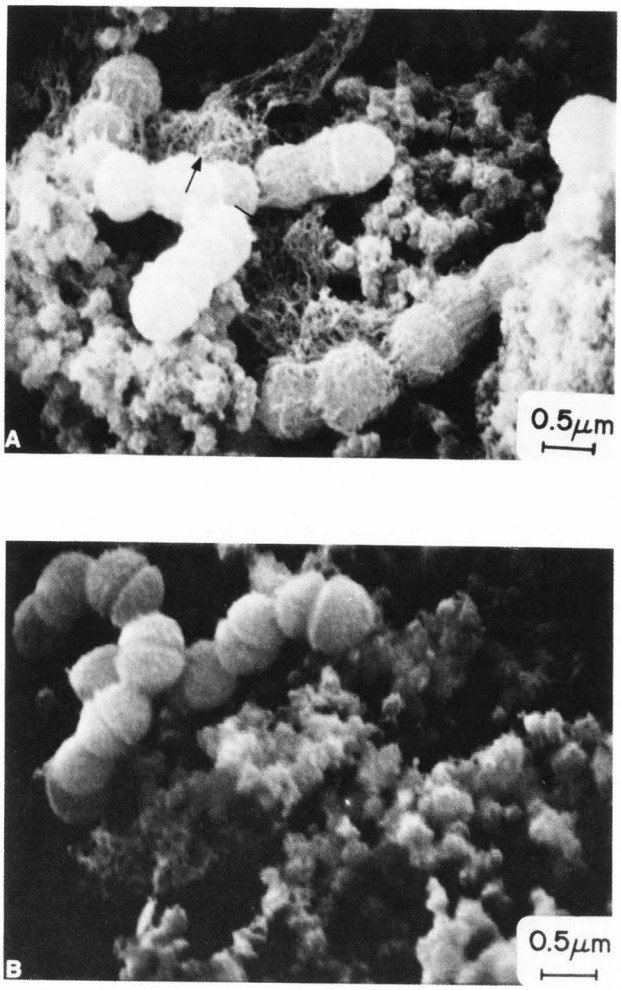

Figure 1. SEM micrograph of S. thermophilus grown in nonfat milk (11% solids).
A) ropy strain yp
B) non-ropy strain 33 the arrows on A) indicate exopolymer material

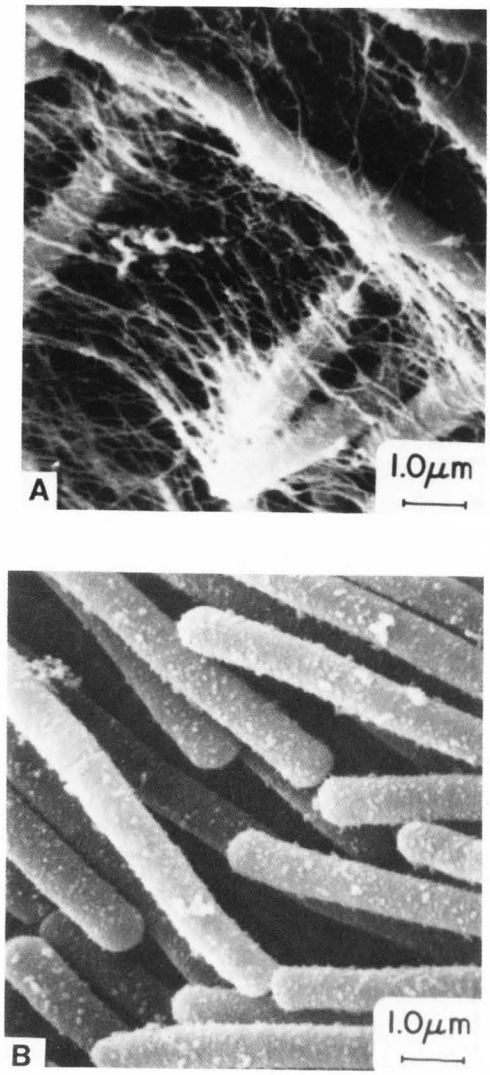

Figure 2. SEM micrographs of L. bulgaricus strains (Surface structure).
A) ropy strain RR
B) non-ropy strain LB

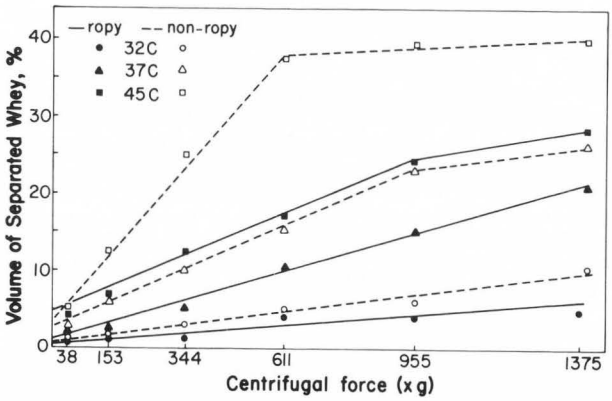

Figure 3. Susceptibility to syneresis of ropy S. thermophilus yp and non-ropy S. thermophilus 33 milk cultures incubated at 32C, 37C, and 45C.

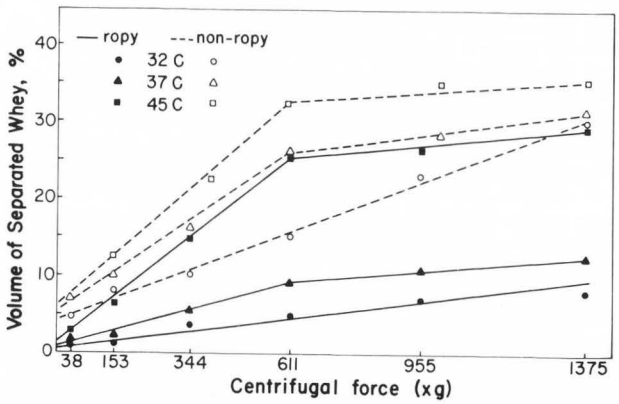

Figure 4. Susceptibility to syneresis of ropy L. bulgaricus RR and non-ropy L. bulgaricus LB milk cultures incubated at 32C, 37C, and 45C.

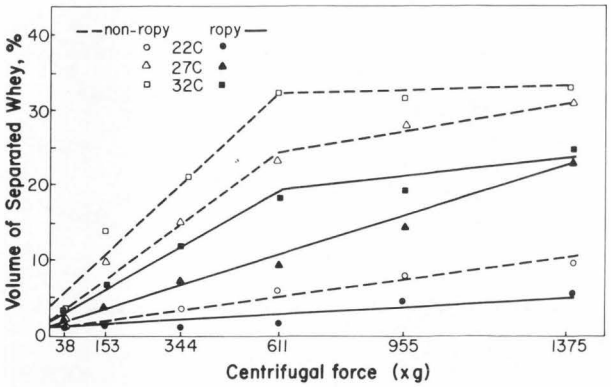

Figure 5. Susceptibility to syneresis of ropy S. cremoris 351 and non-ropy S. cremoris 351-U milk cultures incubated at 22C, 27C, and 32C.

(coefficient of determination) for each of the regression lines was calculated and ranged between 0.88 - 0.96 indicating a good linear relationship between % volume of whey syneresed versus g-force prior to the gel cracking. Some of the milk gels formed whey pockets and began to crack at the greater levels of g-force. Therefore, it was not possible to recover all the whey which syneresed into the pockets and capillaries. The force at which the gels cracked can be determined from the bend in the regression line. If the gel began to break down in this way then a second regression line was determined for the volume of whey separated at the higher centrifugal force levels.

It is clearly evident from the initial slopes in the regression lines of Figures 3-5 that skim milk gels fermented with ropy strains were less susceptible to syneresis than those fermented with non-ropy strains at all three incubation temperatures.

The data also exhibit the relationship between susceptibility to syneresis and incubation temperature; as the temperature of incubation increased so did syneresis. This has been noted by others (Lundstedt, 1974; Meiklejohn, 1977; Galesloot, 1958; Rasic and Kurmann, 1978) and probably is due to the increasing rigidity in the gel structure formed at the higher temperatures (Galesloot, 1958). Meiklejohn (1977) and Lundstedt (1974) advocated the use of low temperature incubation (30-33°C for 16 h) to increase gel stability. However, many yogurt processors prefer a higher incubation temperature (40-42°C for 4 h) because the shorter incubation time allows for greater production within the same facility. The results of this investigation suggest that the use of slime-producing bacteria in a yogurt starter culture could allow the processor to incubate at higher temperatures with less risk of syneresis in the final product.

Water Activity

Milk fermented with ropy strains was shown to synerese less than milk fermented with non-ropy strains. The increased water-holding capacity (WHC) of the milk gels might be due to increased water-binding by the slime produced from the ropy strains. True water-binding differs from WHC in that it reflects a physiochemical alteration in water structure which affects the colligative properties of water and results in a decrease in the a_w of the system (T. P. Labuza, personal communication).

According to a review by Labuza (1975) the common a_w measurements using instruments such as the vapor pressure manometer, electric hygrometer, and dew point device begin to lose accuracy in the very high a_w region. However, the cryoscopic osmometer was shown to be capable of measuring a_w of carrageenan gels in the range of 0.96-0.99 (Rey, 1981).

An attempt was made to determine if exocellular slime lowered the a_w of nonfat yogurt. The a_w of nonfat yogurt fermented by ropy and non-ropy strains was determined by cryo-osmometry to range from 0.994 to 0.996. No difference was found between the a_w of nonfat yogurt fermented by the ropy or the non-ropy strains based on cryo-osmotic measurement. These findings suggest that the slime produced by ropy strains does not significantly affect the water-binding of an acidified skim milk gel.

Viscosity

There have been several reports in the literature stating that the use of slime-producing strains in the starter culture will increase the viscosity of yogurt (Galesloot, 1958; DeHaast et al., 1979; Galesloot and Hassing, 1973; Bouillane and Desmazeaud, 1980). However, all of the viscosity measurements were made at a single shear rate.

A preliminary investigation was carried out to determine if the viscosity of 11% NFM cultures was shear dependent. Milk cultures fermented with the ropy and non-ropy strains exhibited shear thinning (pseudoplastic) behavior when subjected to increasing shear rates in a Haake Rotovisco viscometer.

This finding indicated that the viscosity of milk cultures could not be adequately characterized from measurements made at a single shear rate. Therefore, shear stress data were collected for the ropy and non-ropy 11% NFM gels at increasing shear rates.

The power law (3) is an empirical equation utilized by many investigators (Muller, 1973; Holdsworth, 1969; Rao, 1977) to characterize fluids that demonstrate pseudoplastic behavior.

$$\log \tau = \log k + n \log - \frac{dv}{dr} \qquad (3)$$

where τ = shear stress

$-\frac{dv}{dr}$ = shear rate

k = consistency coefficient

n = flow behavior index

Two parameters (k and n) can be obtained from this mathematical model. The consistency coefficient (k) has been shown to coincide with the "thickness" of the fluid and varies with temperature. The flow behavior index (n) is a

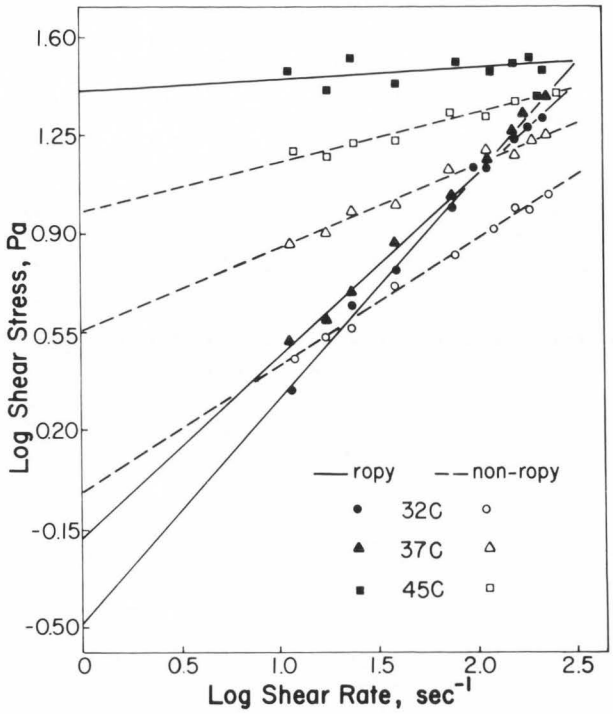

Figure 6. Rheological parameters of ropy S. thermophilus yp and non-ropy S. thermophilus 33 milk cultures incubated at 32C, 37C, and 45C.

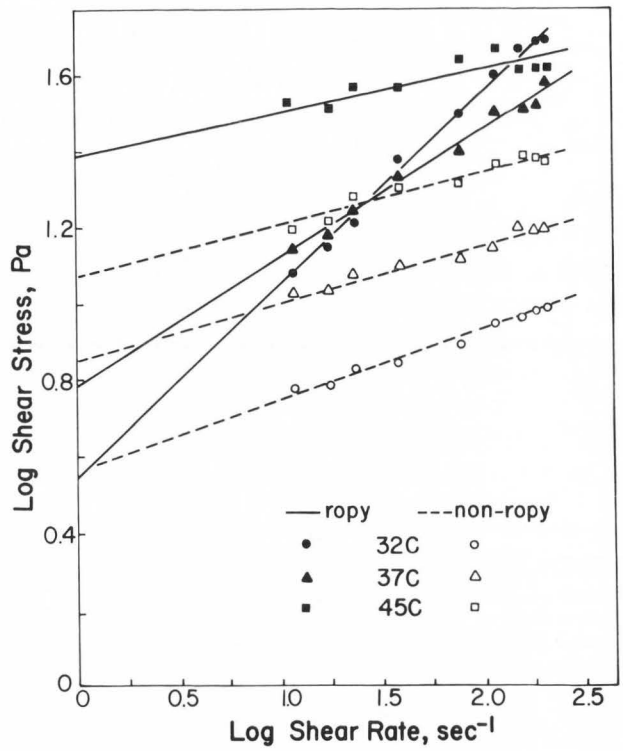

Figure 7. Rheological parameters of ropy L. bulgaricus RR and non-ropy L. bulgaricus LB milk cultures incubated at 32C, 37C, and 45C.

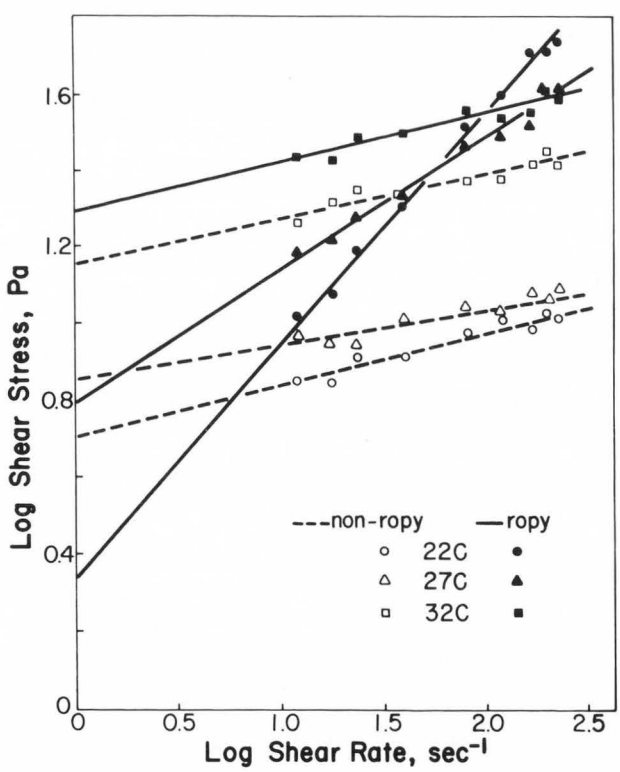

Figure 8. Rheological parameters of ropy S. cremoris 351 and non-ropy S. cremoris 351-U incubated at 22C, 27C, and 32C.

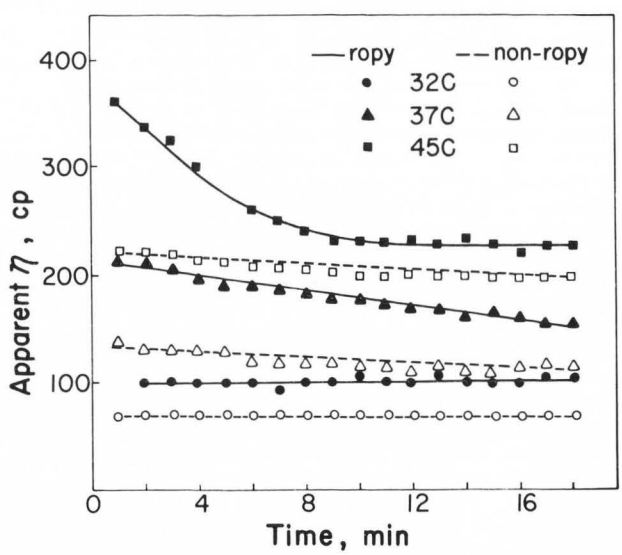

Figure 9. Effect of time of shearing on the apparent viscosity of ropy S. thermophilus yp and non-ropy S. thermophilus 33 milk cultures incubated at 32C, 37C, and 45C. Shear rate D : 70 sec^{-1}.

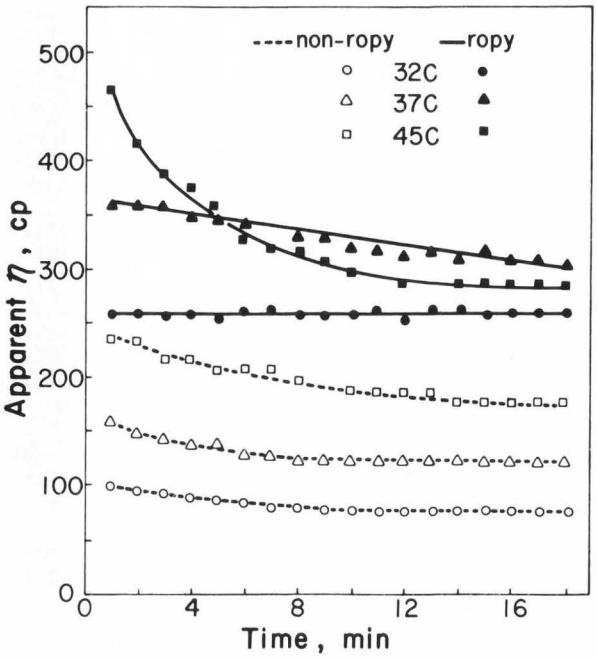

Figure 10. Effect of time of shearing on the apparent viscosity of ropy L. bulgaricus RR and non-ropy L. bulgaricus LB milk cultures incubated at 32C, 37C and 45C. Shear rate D: 70 sec^{-1}.

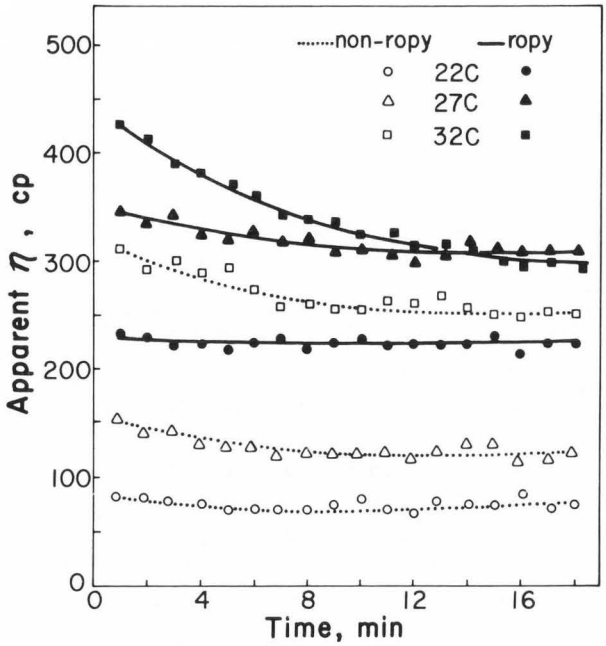

Figure 11. Effect of time of shearing on the apparent viscosity of ropy S. cremoris 351 and non-ropy S. cremoris 351-U milk cultures incubated at 22C, 27C, and 32C. Shear rate D: 70 sec^{-1}.

measure of the departure from Newtonian flow, and the temperature effect is usually small. These parameters have been used to predict flow rates in pipes of different diameter, to select pump sizes to give the required flow rate, and to determine mixing and agitation conditions in other food systems (Holdsworth, 1969).
Log-log plots of shear stress as a function of shear rate for ropy and non-ropy cultures are presented in Figures 6-8. The plots show that the consistency coefficient (y-intercept) increases as the temperature of incubation increases for both ropy and non-ropy cultures. The ropy cultures incubated at lower temperatures show slightly lower consistency coefficient values than non-ropy cultures incubated at the same temperature. However, the flow behavior index (slope of the line) is much greater for the ropy cultures incubated at the lower temperatures than for non-ropy cultures which were incubated at the same temperatures. The greater flow behavior index values indicate that the ropy cultures exhibit less pseudoplastic behavior than the non-ropy cultures, i.e., the cultures exhibit less of a decrease in viscosity at higher shear rates.

The ropy cultures which were fermented at the highest temperature of incubation had the largest consistency coefficient value. However, the flow behavior index for the ropy cultures fermented at the highest temperature were similar to those of the non-ropy cultures fermented at all three temperatures (i.e. L. bulgaricus RR culture incubated at 45°C had a similar flow behavior index as L. bulgaricus yp culture incubated at 32, 37 and 45°C).

The effect of time of shearing on the apparent viscosity of ropy and non-ropy milk cultures was determined at a constant shear rate of 70 sec^{-1} (Figures 9, 10 and 11). The viscosity of the nonfat yogurt fermented by the ropy cultures at the higher incubation temperatures decreased with time. This finding agrees with the observation made by Galesloot and Hassing (1973) that yogurt made with a slime-producing starter culture experienced a greater decrease in flow-through time when it was repeatedly passed through a funnel than yogurt made without slime-producing bacteria.

Excessive slime production (at lower incubation temperatures) thus results in a decrease in the consistency of the coagulum, which would be undesirable in the manufacture of most yogurt products. However, at higher incubation temperatures, less slime is produced and the protein structure of the coagulum is more rigid. The lower slime production coupled with the rigid protein structure appears to result in a coagulum with a greater consistency. However, it exhibits greater shear-thinning than a coagulum without slime. The time-dependent shear-thinning behavior would need to be considered when determining the agitation conditions in the manufacture of a stirred yogurt.

Gel Strength

The relative firmness of ropy and non-ropy cultures was estimated by a penetration measurement using an Instron Universal Testing Machine

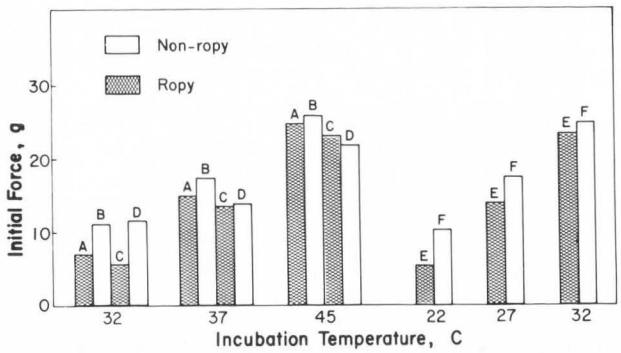

Figure 12. Relative firmness of milk cultures which were fermented with:
A) L. bulgaricus RR
B) L. bulgaricus LB
C) S. thermophilus yp
D) S. thermophilus 33
E) S. cremoris 351
F) S. cremoris 351-U

(Figure 12). The results of the analysis indicate that relative firmness of both ropy and non-ropy cultures increases with incubation temperature. As stated previously, the increased rigidity of milk coagulated at higher temperatures was believed to be due to the effect of acid on protein structure at higher temperatures (Galesloot, 1958). However, this alone will not explain why 11% NFM which had been coagulated at 22, 27 and 32°C by S. cremoris strains showed similar relative firmness values, respectively, as 11% NFM coagulated at 32, 37 and 45°C by S. thermophilus and L. bulgaricus strains. It appears that the rate of acid production also affects gel firmness.

The relative difference in gel firmness among ropy and non-ropy cultures is greater at the lowest incubation temperature. These results correlate with the results obtained in the viscosity investigations. The ropy cultures that were incubated at the lower and intermediate temperatures had lower consistency coefficient and gel firmness values than the non-ropy cultures.

However, the gel firmness results do not correlate with the consistency coefficient obtained for ropy and non-ropy S. thermophilus cultures incubated at 45°C. Galesloot and Hassing (1973) also found a lack of complete correlation between yogurt viscosity and firmness. Both viscosity and firmness must thus be determined to more completely evaluate the texture of yogurt fermented with slime-producing strains in the starter culture.

Acknowledgements

Published as Paper No. 14,338 of the scientific journal series of the Minnesota Agricultural Experiment Station on research conducted under Minnesota Agricultural Experiment Station Project No. 18-75 supported by Hatch Funds.

We wish to thank S. M. Halambeck for help on the SEM work.

References

Andres D. (1982). New fermentation cultures from genetic manipulation permits food formulations previously not attainable. Food Process. 43, 41.

Bouillane C, Desmazeaud MJ. (1980). Etude de quelques caracteres de souches de Streptococcus thermophilus utilisus en fabrization de yoghourt et proposition d'une methode de classment. Le Lait. 60, 458-473.

Davis JG. (1975). The microbiology of yoghurt. In: Lactic Acid Bacteria in Beverages and Food. Eds. Carr, JG., Cutting, CV., Whiting, GC., Academic Press, New York, New York. 245-263.

DeHaast J, Lategan AM, Novello JC. (1979). Some aspects of yoghurt quality - a review. S. Afric J. Dairy Technol. 11, 11-13.

Galesloot TE. (1958). Onderzoekingen over de consistentie van yoghurt. Ned Milk-en Zuivellijdschr. 12, 130-161.

Galesloot TE, Hassing F. (1973). Handhaven van de stymstofproduktic van yoghurt culturen. Nederlands Inst. voor Zuivelonderzoek. NlZO Mededalengia. 7, 57-62.

Harwalker VR, Kalab M. (1981). The effect of acidulants and temperature on microstructure, firmness, and susceptibility to syneresis of skim milk gels. Scanning Electron Microsc. 1981; III: 503-513.

Holdsworth SD. (1969). Processing of non-Newtonian foods. Proc. Biochem. 4, 15-21.

Humphreys CL, Plunkett M. (1969). Yoghurt: a review of its manufacture. Dairy Sci. Abstr. 31, 607-622.

Kalab M, Allan-Wojtas P, Phipps-Todd BE. (1983). Development of microstructure in set-style nonfat yoghurt - a review. Food Microstruc. 3, 51-66.

Kosikowska M, Lipenska E, Jakubczyk E, Bijok F, Luczynska M, Wajnert T, Kazimieczak W, Lipniewska D. (1979). Influence of Slime-Forming Bacterial Strains on the Rheological Properties of Yoghurt. Dairy Sci. Abstr. 41, 110.

Labuza TP. (1975). Sorption phenomena in foods: Theoretical and practical aspects. In: Theory Determination and Control of Physical Properties of Food Materials. Ed. Chokyun. D. Leidel Publishing, Dordrecht, Holland. 197-219.

Lundstedt E. (1974). Improved methods for manufacturing yogurt. American Dairy Rev. 36, 38A-38D.

Meiklejohn PB. (1977). How to achieve better yoghurt viscosity. Cultured Dairy Prod. J. 12, 6-7.

Muller HG. (1973). An Introduction to Food Rheology. Craine Russak and Co. New York. 59-71.

Rao MA. (1977). Measurement of flow properties of fluid foods - Developments, limitations and interpretation of phenomena. J. Text. Studies. 8, 257-282.

Rasic JL, Kurmann JA. (1978). Yoghurt. Technical Dairy Publishing House, Copenhagen, Denmark. 56-68, 192-199, 291, 299.

Rey D. (1981). Characterization of the effect of solutes on the water-binding and gel strength properties of carrageenan. M.S., Thesis Univ. of Minnesota.

Robinson DK. (1981). Yoghurt manufacture-some considerations of quality. Dairy Ind. Intern. 46, 31-35.

Steinberg AF. (1979). Yogurt, the Cinderella product, I. Am. Dairy Rev. 41, 17-18.

Tamime AY, Kalab M, Davies G. (1984). Microstructure of set-style yoghurt manufactured from cow's milk fortified by various methods. Food Microstruc. 3, 83-92.

Tramer J. (1973). Yogurt cultures. J. of the Soc. of Dairy Technol. 30, 15-22.

Vedamuthu ER. (1982). Stabilizer producing *Streptococcus thermophilus*. U.S. Patent. 4,339,464.

Discussion with Reviewers

A. Y. Tamime: Have the authors isolated and identified the "slimy" material?

Authors: The slimy material has been isolated and identified (Schellhaass, 1983). The slime isolated from *S. thermophilus* yp and *L. bulgaricus* RR were similar in composition as indicated by similar ^{13}C-NMR spectra. The slime isolated from each of the ropy strains had absorption patterns indicative of hexoses in the L-cypteine-sulfuric acid reaction. The monosaccharide composition of the exopolymers was determined by a gas chromatographic method and the hexoses were galactose and glucose in a 2:1 ratio.

E. R. Vedamuthu: The authors found that syneresis from ropy gels was less than from non-ropy gels at all three incubation temperatures studied. Is the lower level of syneresis from ropy gels entirely caused by "water-holding" (absorption of water by the slime) capacity of the slime or does mechanical entrapment of water between strands of material also play a part?

Authors: It is likely that the decreased syneresis in the ropy gels is due to: The water-holding capacity of the slime as well as interaction of the slime within the protein network. Perhaps the interaction of the slime with protein helps to prevent excessive protein - protein interactions and allows far better protein hydration.

Kalab et. al. (1983) hypothesized that void spaces surrounding yogurt starter bacteria introduced stress into the casein matrix. Perhaps the exocellular slime extending from the cell surface to the casein aids in reducing stress caused by the void spaces thereby reducing syneresis.

E. R. Vedamuthu: At higher temperatures there was greater syneresis with both ropy and non-ropy gels. The authors suggested that increasing rigidity in the gel structure at higher temperatures leads to increase in syneresis. Could they explain how rigidity affects syneresis? Is this a mechanical or physiochemical phenomenon?

Authors: The rate of acid production was greater at the higher incubation temperatures. Rapid acid formation during incubation favors the formation of a rigid gel. The increased rigidity is due to the formation of a dense aggregation of protein particles with a corresponding decrease in the hydration of the protein network (Rasic and Kurmann, 1978). It is most probably a physiochemical phenomenon (decrease in protein water-holding capacity) which accounts for the greater syneresis.

Additional Reference

Schellhaass SM. (1983). Characterization of Exocellular slime produced by Bacterial Starter Cultures Used in the Manufacture of Fermented Dairy Products. Ph.D. Thesis. University of Minnesota, St. Paul, Minnesota.

FOOD MICROSTRUCTURE, Vol. 4 (1985), pp. 289-296
SEM Inc., AMF O'Hare (Chicago), IL 60666-0507 U.S.A.

0730-5419/85$1.00+.05

OBSERVATIONS ON THE AIR-SERUM INTERFACE OF MILK FOAMS

B. E. Brooker

Food Research Institute, Shinfield, Reading
Berkshire RG2 9AT, U.K.

Abstract

A new rapid method for the preparation of milk foams for transmission electron microscopy is described. The air-serum interface of foams made from skimmed milk consists of a uniform electron dense layer (5 nm thick) to which casein micelles become secondarily attached. Changes in bubble volume lead to the formation of folds of excess interfacial material which project into the aqueous phase. Using collapsed bubble ghosts to study the attachment of micelles to the air-serum interface it was concluded that neither disulphide bridge formation nor hydrophobic interactions were of major importance. Similar preparations of interfacial material but without casein micelles attached were prepared from milk plasma and solutions of β- lactoglobulin. The former fragmented slowly into small particles at room temperature but very rapidly when heated to 55° C whereas material derived from β- lactoglobulin was quite stable. The destruction of bubble ghosts in skimmed milk by heating is attributed to interface breakdown rather than to micelle detachment. The air-serum interface, of which casein micelles do not form an integral part, probably consists of a mixture of globular whey proteins and some soluble caseins. Thus, using high pressure liquid chromatography, foamed milk plasma from which bubble ghosts had been removed was shown to be depleted in both α- lactalbumin and β- lactoglobulin.

Initial paper received December 27 1984
Manuscript received June 22 1985
Direct inquiries to B.E. Brooker
Telephone number: 44-734-883103 x283

KEY WORDS: Foam, milk, interface, casein micelle, bubble, heat stability, composition, milk plasma, β-lactoglobulin, high pressure liquid chromatography.

Introduction

It is well established that solutions of many different types of proteins readily foam when they are whipped or shaken. During the formation of a foam, protein molecules become adsorbed at the air-liquid interface of each bubble where they may suffer conformational changes, undergo intermolecular rearrangement and form a stabilising film (Alexander and Johnson, 1949). Foamability of a solution is related to the rapidity with which this protein film is formed at the surface of each air bubble whereas foam stability is determined very largely by the rheological properties of the interface (Graham and Phillips, 1976). Although individual milk proteins have been used to elucidate the mechanisms by which adsorbed protein layers at air-water interfaces are able to stabilize foams (Graham and Phillips, 1976; Halling, 1981), the very existence of such an interfacial layer in the case of milk foams has never been demonstrated directly using electron microscopy. The structure and properties of this interface are of importance in determining the foamability and stability not only of milk foams but also perhaps of fat-rich foams such as whipped cream and ice cream in the early stages of their formation. Thus, the observations of Schmidt and vanHooydonk (1980) on whipped cream suggest that for fat globules to stabilize air bubbles they must penetrate and partially replace a film-like air-serum interface which is probably formed by the adsorption of proteins early in the whipping process.

The virtues of using freeze fracturing methods with scanning and transmission electron microscopy in the study of foams, especially fat-rich foams such as ice cream and whipped cream, have been extolled by several authors (Berger et al., 1972; Buchheim, 1978; Schmidt and vanHooydonk, 1980; Kalab, 1983). Whilst it is true that such methods are very valuable in preventing the extraction of fat during processing, their advantage over conventional sectioning methods for the examination of protein foams is less convincing; the resolution of the scanning electron microscope can be too limiting and the featureless but distinct interfacial layers between air and aqueous phases can be difficult to detect in the

metal replicas produced by freeze fracturing methods for transmission electron microscopy. However, when using conventional sectioning methods the initial fixation of foams is a problem. With robust protein foams containing a relatively large concentration of protein e.g., egg albumen foam, fixation prior to embedding can be performed by direct addition to an aqueous fixative (Meyer and Potter, 1975); in the case of the more fragile milk foams, even fat-rich foams, more care is required. In the present study, the vapour fixation method of Graf and Muller (1965) for whipped cream was adapted for fat-free milk foams to give a relatively rapid procedure.

Materials and Methods

The skimmed milk used was: a) bulk tank milk from the Institute's herd of Friesian cows. The milk had been separated by centrifugation at 3,000xg for 10min in the laboratory without any heat treatment and b) separated bulk tank milk which had been pasteurized in the Institute's dairy. All milks were stored at 6°C prior to use.

Milk serum was obtained from pasteurized or unpasteurized skimmed milk by centrifugation at 100,000xg for 2h using a Beckman L8-80 ultracentrifuge fitted with an SW 25 rotor. The milk serum was removed by piercing the side of the centrifuge tube with a syringe.

Aqueous solutions of purified β- lactoglobulin (Sigma Chemical Co.) contained 3 mg/ml.

Foam production

Two different controlled methods were used to produce foams from pasteurized and unpasteurized skimmed milk. In one of these, 10 ml of milk were placed in a 50 ml conical flask held in a Stuart flask shaker and shaken horizontally for 1-2h with a frequency of 40Hz and an amplitude of 10mm.

In another method, 5ml of milk were placed in a filter funnel fitted with a sintered glass filter of diameter 30mm. Air was then passed through the filter at a rate of 0.5 ml/sec for 1-2h to produce the foam.

Foam collection and processing

Samples of foam for electron microscopy were collected 0.5, 1 and 2h after the initiation of foaming. The foam was supported on a wire loop (3.5 mm diameter) consisting of 2 coils of 0.2 mm diameter platinum wire which had been set into the cap of a 5 ml bottle. The wire loop was dipped into the foam, quickly removed and then fixed for 10 min at room temperature in glutaraldehyde vapour. This was achieved by sealing the loop into a 5 ml glass bottle containing 0.5 ml of 25% glutaraldehyde. The foam was transferred on the loop to osmium tetroxide vapour for 0.5-1h at room temperature and then placed in acetone vapour for a further 0.5h to harden the foam. It was then briefly dipped into molten 2% agar at 50°C, allowed to solidify and dipped a second time. From this stage the foams could withstand immersion in liquids. If additional electron density was required, the specimen could be further treated by immersion in buffered 1% osmium tetroxide and aqueous 1% uranyl acetate for 0.5h before being dehydrated in a series of acetone-water mixtures and 100% acetone. The wire loop was removed from the bottle top and the foam was embedded in Araldite. In the final embedding moulds, the foam was carefully dislodged from the wire loop and the resin allowed to polymerize. In order to obtain the maximum number of bubble profiles in any one section, the disc of foam was flat embedded so that sections could be cut parallel to the plane of the original loop.

Thin sections were cut on a Reichert OmU3 ultramicrotome, stained in lead citrate and examined at an accelerating voltage of 100kV in a Hitachi 600 transmission electron microscope.

Preparation of bubble ghosts

The association of casein micelles with the air-water interface of air bubbles was most easily studied using the ghosts resulting from foam collapse. In these studies, foams were produced from pasteurized skimmed milk; a) at room temperature, b) at 6°C and c) at room temperature, but to which 0.2mM p-chloromercuribenzoate (PCMB) or 5mM N-ethylmaleimide (NEM) had been added to block free sulphydryl groups; in treatments b) and c) a control foam was made at room temperature without any additives. The milk containing bubble ghosts together with the collapsing foam was fixed for 1h by addition of sufficient 25% glutaraldehyde to give a final concentration of 3%; milk which had been foamed at 6°C was fixed in the cold using pre-cooled fixative. The milk was mixed in a ratio of 1:1 with 2% agar at 50°C, allowed to solidify and chopped into 0.5mm wide strips with a razor blade. After washing in 0.2M cacodylate-HCl buffer (pH 7.2) for 1h, specimens were postfixed in 0.1M cacodylate buffered 1% osmium tetroxide for a further hour. Specimens were washed in distilled water and stained *en bloc* for 0.5h in aqueous 1% uranyl acetate. They were then dehydrated, embedded and sectioned as described above.

In another study, the stability of the association of casein micelles with the air-serum interface was examined. Bubble ghosts obtained by foaming pasteurized skimmed milk at room temperature were kept at ambient temperature and fixed for electron microscopy at hourly intervals for 4h after foaming had ceased. The stability of the air-serum interface itself was investigated by electron microscopy using bubble ghosts prepared from milk plasma and from solutions of β- lactoglobulin. Collapsed foams were fixed and embedded as described above; a) immediately after preparation, b) after heating in a water bath at 55°C for 10min and c) after storage at room temperature for 24h in the presence of 0.05% sodium azide to stop bacterial growth. Changes in light absorption (at 490nm) of the milk sera were followed using a Cecil CE272 spectrophotometer.

Analysis

The involvement of globular whey proteins in the formation of the air-serum interface was determined indirectly in a depletion study. After the collapse of a milk serum foam, bubble ghosts were removed by centrifugation at 3,000xg for 10 min and the levels of the major whey proteins in the supernatant and in an untreated control serum were compared using high pressure liquid chromatography (HPLC). This was performed using a

TSKG 3000 SW column with a Pye PU 4020 UV detector (operating at 280nm wavelength) and an Altex 100A dual piston pump. 20 μl injection of the samples was used and the column was eluted with 0.1M phosphate buffer (pH 6.8) at a rate of 1 ml/min.

Results and Discussion

Foams

In all foams made from pasteurized and raw skimmed milk, the interface between the air and aqueous phases of each bubble was marked by a uniform layer of electron dense material 5 nm thick (Fig. 1). Casein micelles were attached to the milk serum side of this interface, usually as a discontinuous layer. Since the milk-filled space between two air bubbles (lamella) contained numerous casein micelles it was difficult at first sight to decide whether micelles in contact with the interface were firmly attached to it or whether the contact was transitory. However, during the preparation of some foams for electron microscopy, the milk occupying a proportion of the lamellae drained away and was lost. Because in such cases the micelles remained associated with the interface (Fig. 1 inset), it was concluded that they were truly attached. There was no evidence to suggest that attached micelles were in any way deformed or spread over the air-serum boundary and there was no suggestion that casein submicelles form an integral part of the interfacial layer. Because casein micelles were not in direct contact with air and do not form part of the interface sensu stricto, it is not surprising that their behaviour during foaming differed from that seen in situations where they are truly surface active e.g. , in homogenized milk (Henstra and Schmidt, 1970).

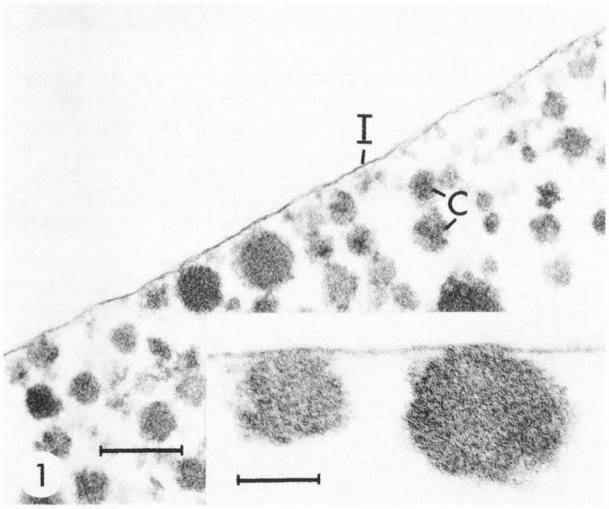

Fig. 1 Air-serum interface (I) of a bubble in pasteurized milk foam. C = casein micelle. Bar = 0.2 μm. **Inset:** Interfacial layer with two attached casein micelles. Free micelles have drained from the lamella. Bar = 0.1 μm.

The presence of a continuous interfacial boundary layer described here poses a difficult problem when considering the changes in bubble surface area that occur during coalescence and the loss of air by diffusion especially from small bubbles. Both of these events result in an excess of the interfacial layer relative to the new surface area of the bubble and it is usually considered necessary to postulate either loss of protein surfactant by desorption or an increase in its surface concentration i.e., the interface thickening. That an entirely different mechanism operates in milk foams is suggested by observations in the present study which showed that the air-serum interface possessed folds projecting beyond the curved surface of the bubble into the aqueous phase, sometimes for several micrometres (Figs 2, 3). Serial sections showed that the folds were sheet-like in form and that although the two interfacial layers were closely apposed over much of their area, there were also dilated zones which still contained some air. The large numbers of such appendages projecting from the surface of air bubbles in milk foams suggest that they accumulate as the foam ages and that they are therefore relatively stable structures. It seems highly likely that the presence of such appendages affects the properties of the foam by influencing both the rate of water drainage from the lamellae and the forces of cohesion between the interfaces of adjacent bubbles. There is every reason to suppose that the same phenomenon of interface folding occurs in other protein foams; thus, micrographs of protein foams obtained by Meyer (1974) show similar folds in the air-protein interface of whipped egg albumen.

Bubble Ghosts

When the air bubbles in milk foams burst, no matter how they were produced, the spherical interfacial layer together with its single layer of attached casein micelles collapsed and generally formed a concavo-convex structure that will be referred to here as a bubble ghost(Fig. 4). These bodies were first described in detail from whole milk by Hekma and Brouwer (1923) who realised that they resulted from the foaming of milk. Indeed, they concluded that separator slime was composed very largely of collapsed foam cells. Mulder and Walstra (1974) demonstrated by electron microscopy that micelles are associated with the surface of collapsed air bubbles and suggested that in skimmed milk foams micelles aggregate into a 2-dimensional network in the air-serum interface but they did not detect the true non-micellar interface. More recently, Hill et al.(1982) showed that ghosts could give rise to falsely high electronic cell counts in milk and concluded that the wall of each ghost consisted solely of several layers of casein micelles. Because the interfacial layer is difficult to detect unless it is sectioned perpendicular to its plane (Fig. 5) or unless the specimen is tilted, it is not surprising that Hill et al. (1982) did not observe it. However, Fig. 4 demonstrates how a single layer of casein micelles can appear to consist of several layers if the section is tangential to the ghost surface.

At least two mechanisms for the attachment

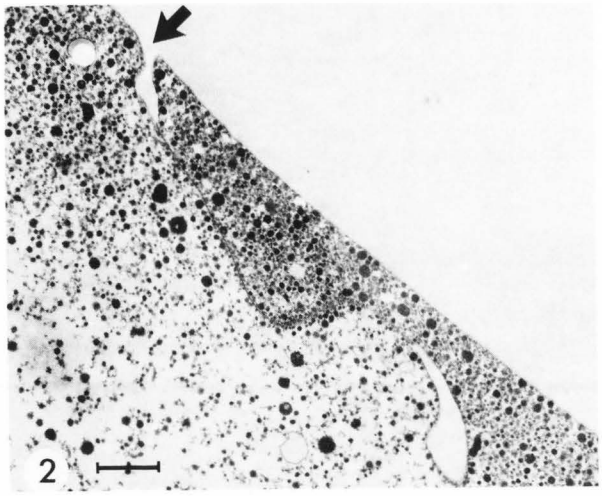

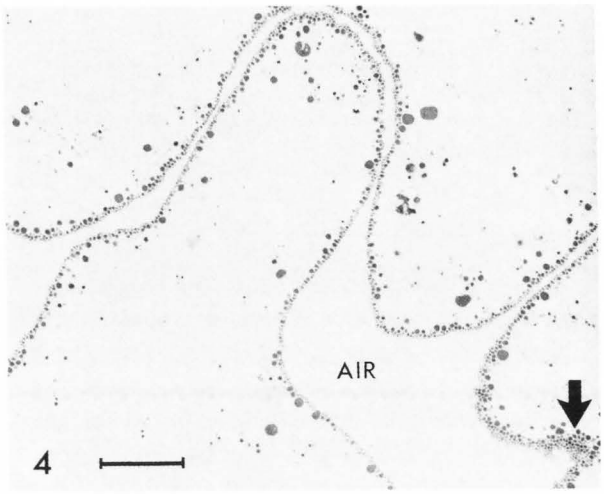

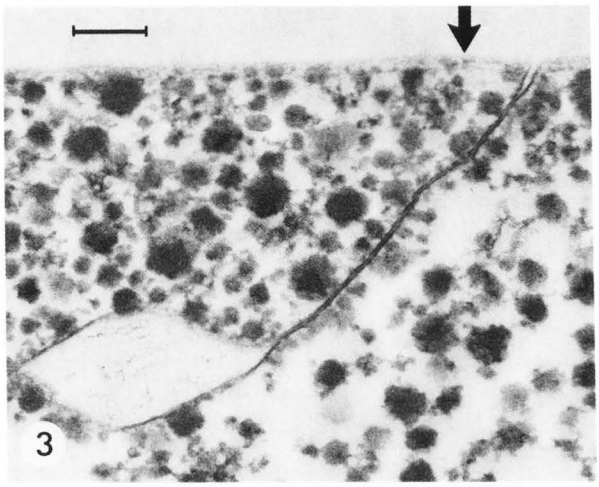

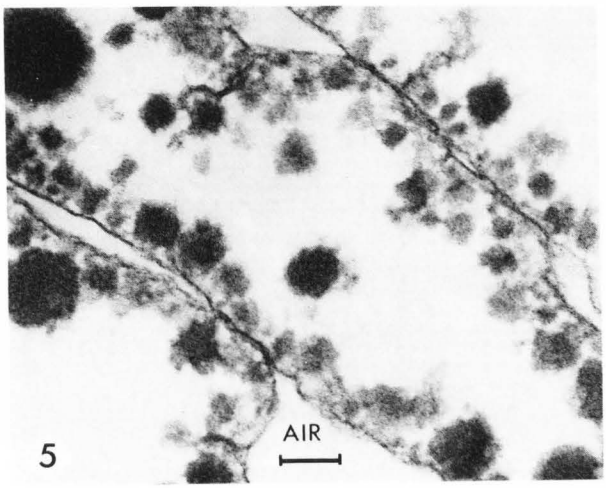

Fig. 2 A fold of the air-serum interface in skimmed milk foam. The origin of the fold is shown by an arrow; the interface of the bubble is sectioned tangentially and so does not appear as a clearly defined structure. Bar = 1 μm.
Fig. 3 Part of a fold in the air-serum interface showing the two closely apposed interfacial layers. The interface proper (arrow) is sectioned tangentially. Bar = 0.2 μm.

Fig. 4 Bubble ghost consisting of a single layer of casein micelles. Several layers of micelles appear to be present in areas where the ghost is cut tangentially (arrow). The interfacial layer cannot be seen at this magnification. Bar = 2 μm.
Fig. 5 Bubble ghosts showing the attachment of micelles to the interfacial layer. Bar = 0.1 μm.

of casein micelles to the air-serum interface can be postulated. In one of these, attachment is mediated through an intermolecular disulphide bridge arising from the interaction of sulphydryl groups on the κ- casein of the micelle and β- lactoglobulin (see below) in the interface. Although in undenatured β- lactoglobulin the sulphydryl groups are masked (Lyster, 1964), it is possible that they become exposed and therefore highly reactive as a result of the conformational changes that take place during adsorption at the interface (Phillips, 1977; 1981). In the present experiment, milk was foamed in the presence of PCMB or NEM to block sulphydryl groups (Sawyer, 1968; Sawyer et al., 1963) as and when they became exposed at the interface. However, bubble ghosts fixed immediately after foaming were studded with micelles in the normal way and were identical in appearance to those formed from control milk. It appears therefore, that intermolecular disulphide bridging is not of great importance in micelle attachment.

According to unsubstantiated reports by Mulder and Walstra (1974) and Walstra and Jenness (1984), 'ghost membranes' are not found in milk that is foamed at refrigerator temperature. Such a clear temperature dependence for the association of micelles with the interface might indicate an underlying hydrophobic interaction between the two. In the present study however, foams were produced at 6°C on several occasions without

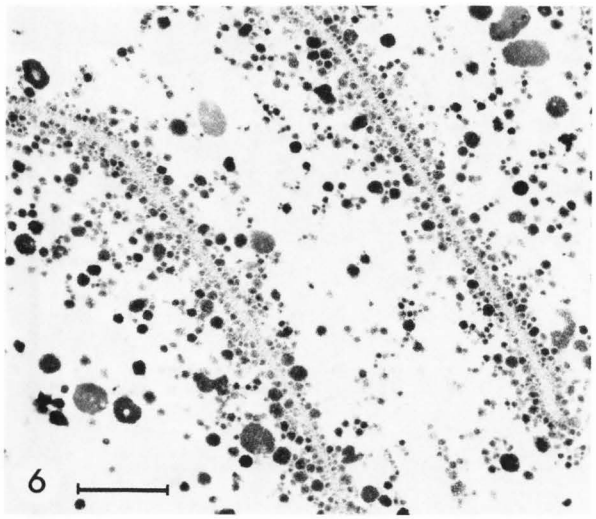

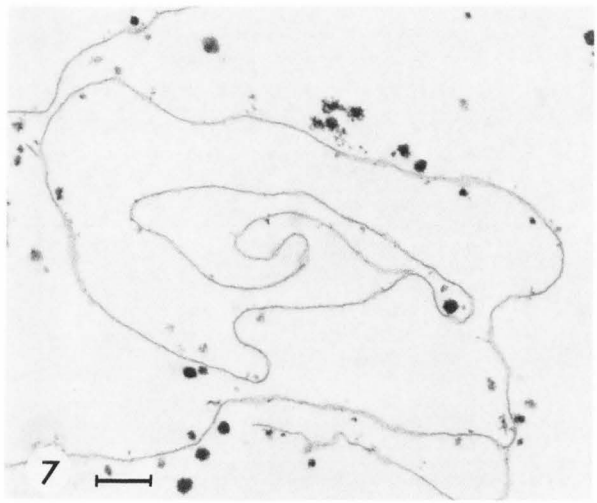

Fig. 6 Bubble ghosts from pasteurized milk foamed at 6°C. Bar = 1 μm.
Fig. 7 Bubble ghost in milk 1h after cessation of foaming showing almost complete dissociation of micelles from the interfacial layer. Bar = 0.5 μm.

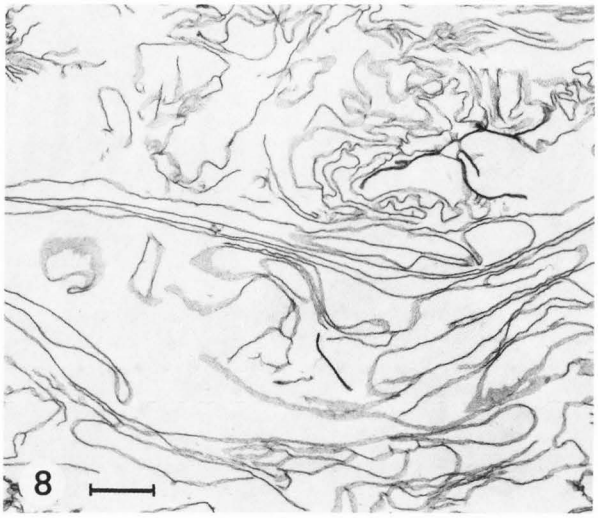

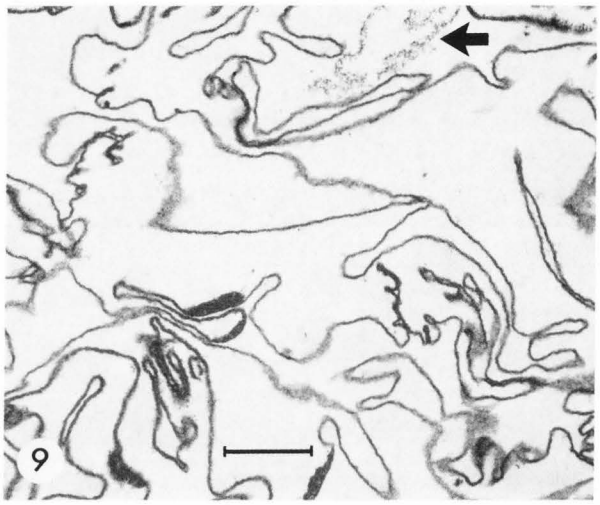

Fig. 8 Centrifugation (3,000xg, 10min) pellet of collapsed bubble ghosts from a foamed solution of β- lactoglobulin. Each dark line consists of two layers of closely apposed interfacial material. Bar = 1 μm.
Fig. 9 Centrifugation (3,000xg, 10min) pellet of bubble ghosts from foamed milk plasma. In some areas (arrow) there is evidence of interface fragmentation. Bar = 1 μm.

observing any decrease in the number of micelles associated with the collapsed interfacial material (Fig. 6). Similarly, in some of the so-called 'adsorptive bubble separation techniques ' where the attachment of non-protein colloids to air bubbles is used to commercial advantage, neither hydrophobic interactions nor electrostatic attraction to the bubble surface appears totally to explain the observed behaviour of the colloid (Melville and Matijevic, 1976). The possible involvement of London-van der Waals forces of attraction in such phenomena (Melville and Matijevic, 1976) remains to be investigated in the case of casein micelles and the air-serum interface. It is interesting to note, moreover, that foaming at low temperature had no effect on the formation or structure of bubble ghosts produced from milk plasma or solutions of β- lactoglobulin.

The association of casein micelles with the interfacial layer of bubble ghosts was reversible. Experiments in which bubble ghosts, from pasteurized and unpasteurized skimmed milk, were allowed to age for up to 4h before fixing for electron microscopy showed that the micelles gradually became detached when aged at room temperature (Fig. 7). The percentage of ghosts without micelles or with reduced numbers increased steadily after 1h from 1.4% to 21% at 4h; it is possible therefore that the collapsed interface would

became completely denuded of micelles if stored long enough. Although the loss of micelles can be explained in terms of a simple reversal of the attachment mechanism, the desorption of protein molecules in the interfacial layer to which micelles are irreversibly attached could lead to the same result.

Interfacial layer

Except for the complete absence of casein micelles, the air-serum interface in foams produced from milk plasma is identical to that seen in skimmed milk foams and the collapsing foam produces bubble ghosts. Similarly, when a solution of a single, purified plasma protein, β-lactoglobulin, was foamed by shaking, collapsed bubble ghosts were produced (Fig. 8) and in such profusion that the solution became turbid within a matter of minutes. Whilst it is widely accepted that soluble proteins can be quantitatively precipitated by bubbling air through their solutions (e.g., Alexander and Johnson, 1949), the form of the insoluble protein as collapsed bubbles, as demonstrated here, is less well known.

Since casein micelles in milk foams do not appear to form an integral part of the air-serum interface, milk plasma was used to produce purified preparations of interfacial material in the form of bubble ghosts for experimental purposes and for electron microscopy. The appearance of interfacial material from foamed milk plasma after centrifugation is shown in Fig. 9. Such preparations consisted of numerous compacted bubble ghosts and there were always clear signs that interfacial membranes break down naturally into loose chains of particles (20 - 30 nm diameter) (Fig. 10). Although evidence of interface instability was always found, fragmentation is evidently a slow process at room temperature for even after storage for 24h no more than 10% of the ghosts showed signs of disruption. At higher, but still moderate, temperatures (55°C) however, the interfacial material was very unstable and within minutes broke down into particulate aggregates of protein of very variable size (Fig. 11). It is interesting to note that ghost membranes obtained from β- lactoglobulin foams were stable at this temperature even after extended treatment (1.5h). Interface degradation could be followed by spectrophotometry, for the light scattering properties of the numerous small protein aggregates caused a rapid increase in light absorption measurements (fig. 12) and the suspensions turned visibly more turbid. These observations are relevant to the report by Hill et al. (1982) that bubble ghosts in whole milk are dispersed by heating to 55°C for 10min. The authors supposed that this was because the casein micelles undergo increased Brownian movement as the temperature rises but the present work suggests ,in addition, that the dispersion of casein micelles may be only secondary to the breakdown of the air-serum interface. The temperature instability of milk plasma bubble ghosts suggests that hydrophobic forces between molecules are not predominant in stabilizing the interface and that at least some of the intermolecular forces between proteins are weaker than in interfacial material composed entirely of β- lactoglobulin.

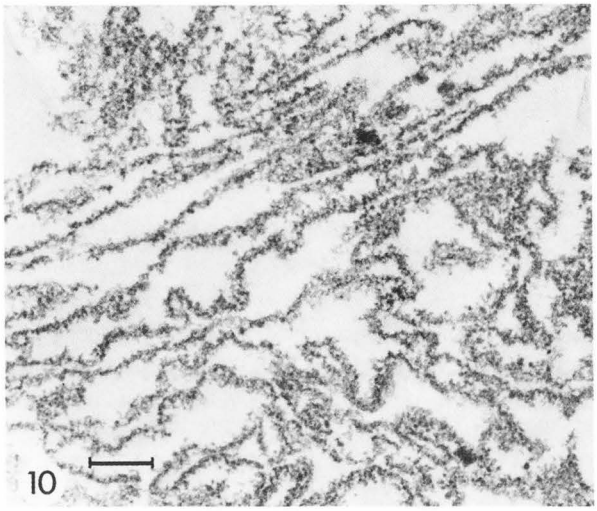

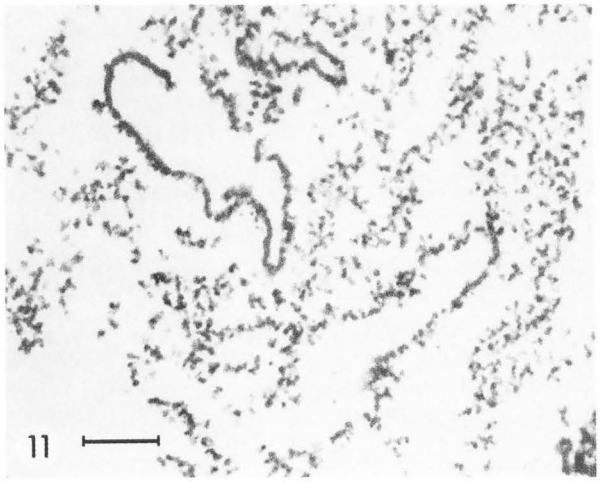

Fig. 10 Same pellet as in Fig. 9 showing a collection of interfacial membranes in the process of fragmentation. Bar = 0.5 μm.
Fig. 11 Same material shown in Fig. 10 which has been heated at 55°C for 3min before fixation. Most of the interfacial material is in the form of small fragments. Bar = 0.5 μm.

Interface Composition

Sharp et al., (1936) found that milk proteins accumulated in skimmed milk foams in approximately the same proportions as they occur in milk. Because of this, they supposed that at the instant of bubble formation, all milk proteins that happened to be at the bubble surface, including casein micelles, were fixed in position to form an interface. However, it is clear from the present study that micellar casein is only secondarily associated with the air-serum interface and that it cannot be regarded as a component of the interface proper. It follows from these observations that the interface may consist of a mixture either solely of the globular whey proteins or together with the soluble caseins. This is consistent with the

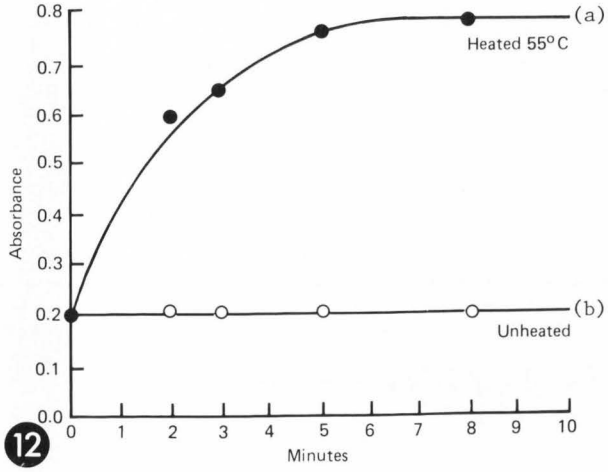

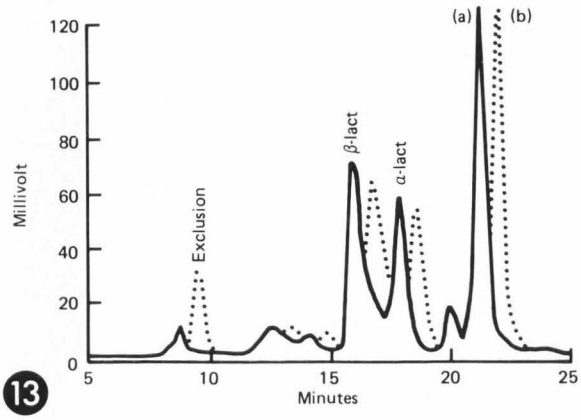

Fig. 12 Change in light absorption (490 nm) of a suspension of bubble ghosts a) heated to 55°C and b) held at room temperature.
Fig. 13 Part of elution profile (at 280 nm) of a) normal milk plasma and b) foamed milk plasma from which bubble ghosts have been removed. The two curves are slightly offset for the sake of clarity. Results obtained by HPLC.

results obtained from a depletion experiment in which levels of α- lactalbumin and β- lactoglobulin were compared in milk plasma and in foamed milk plasma from which interfacial material in the form of collapsed bubble ghosts had been removed by centrifugation. In foamed samples, the levels of both these proteins were consistently diminished by proportionately the same amount (Fig. 13). The increase in size of the exclusion peak (material of M.W. > 120,000) after foaming can be attributed to protein aggregates resulting from the spontaneous breakdown of interfacial material. However, a more complete and direct analysis of interfacial material is required to clarify the possible involvement of the caseins. It should be noted, for example, that since part of the casein, especially the β- casein, is lost from casein micelles at lower temperatures, its opportunity for involvement in interface formation and for influencing the properties of a foam produced in the cold, increases. Although other factors are undoubtedly involved, it is interesting to note that the foamability and stability of milk foams are considerably affected by temperature (Sanmann and Ruehe, 1930; Mohr and Brockmann, 1931).

Acknowledgement

The valuable technical assistance of Mr G. A. Payne is gratefully acknowledged.

References

Alexander AE, Johnson P. (1949) Foams. In: Colloid Science, vol.2, Clarendon, Oxford, 635-639.

Berger KG, Bullimore BK, White GW, Wright WB. (1972) The structure of ice cream. Dairy Industries, 37, 419-425.

Buchheim W. (1978) Mikrostruktur von geschlagenem Rahm. Gordian, 78, 184-188.

Graf E, Muller HR. (1965) Fine structure and whippability of sterilized cream. Milchwissenschaft, 20, 302-308.

Graham DE, Phillips MC. (1976) The conformation of proteins at the air-water interface and their role in stabilizing foams. In: Foams, ed. RJ Akers. Academic Press, London, 237-253.

Halling PJ. (1981) Protein stabilized foams and emulsions. CRC Critical Rev. Food Science & Nutrition, 15, 155-203.

Hekma E, Brouwer E. (1923) Over melkschuimvliesjes en de aan hunne vorming ten grondslag liggends substantie. Versl. Landbouk. Onderz., 28, 46-59.

Henstra S, Schmidt DG. (1970) On the structure of the fat-protein complex in homogenized cow's milk. Neth. Milk Dairy J., 24, 45-51.

Hill AW, Hibbitt KG, Davies J. (1982) Particles in bulk milk capable of causing falsely high electronic cell counts. J. Dairy Res., 49, 171-177.

Kalab M. (1983) Electron microscopy of foods. In: Physical properties of foods, ed. M Peleg, EB Bagley. AVI Publishing, Westport, CT, 43-104.

Lyster RL. (1964) The free and masked sulphydryl groups of heated milk and milk powder and a new method for their determination. J. Dairy Res.,31, 41-51.

Melville JB, Matijevic E. (1976) Microbubbles: generation and interaction with colloid particles. In: Foams, ed. RJ Akers. Academic Press, London, 217-234.

Meyer R. (1974) Ultrastructural changes in egg albumen subjected to heating, whipping, and freezing with and without functional additives. Ph.D. Thesis, Cornell University, Ithaca, N.Y.

Meyer RL, Potter NN. (1975) Ultrastructural

changes in unwhipped and whipped egg albumin containing sodium hexametaphosphate and triethyl citrate plus trisodium acetate. Poultry Science, 54, 101-108.

Mohr W, Brockmann C. (1931) Beitrage zum Schaumproblem. Milchwirt. Forsch., 11, 48-61.

Mulder H, Walstra P. (1974) The milk fat globule: emulsion science as applied to milk products and comparable foods. Wageningen: PUDOC, 213-215.

Phillips MC. (1977) The conformation and properties of proteins at liquid interfaces. Chemistry and Industry, March, 170-176.

Phillips MC. (1981) Protein conformation at liquid interfaces and its role in stabilizing emulsions and foams. Food Technol., 35, 50-57.

Sanmann FP, Ruehe HA. (1930) Some factors influencing the volume of foam on milk. J. Dairy Sci.,13, 48-63.

Sawyer WH. (1968) Heat denaturation of bovine β- lactoglobulin and relevance to disulphide aggregation. J. Dairy Sci., 51, 323-329.

Sawyer WH, Coulter ST, Jenness R. (1963) Role of sulphydryl groups in the interaction of κ- casein and β- lactoglobulin. J. Dairy Sci., 46, 564-565.

Schmidt DG, van Hooydonk ACM. (1980) A scanning electron microscopical investigation of the whipping of cream. Scanning Electron Microsc. 1980;III: 653-658.

Sharp PF, Myers RP, Guthrie ES. (1936) Accumulation of protein in the foam of skim milk. J. Dairy Sci., 19, 655-662.

Walstra P, Jenness R. (1984) Dairy Chemistry and Physics. John Wiley, New York, 279-287.

Discussion with Reviewers

W. Buchheim: Do you have experience with regard to the applicability of this preparation method to fat-rich foams such as dairy or non-dairy whipped creams?

Author: Yes. The method produces equally good results with fat-rich foams but because of the danger of lipid extraction by processing solvents, it is necessary to use osmium tetroxide buffered with imidazole (Allan-Wojtas P, Kalab M. 1984 Michwissenschaft, 39, 323-327) if the fat is to be preserved in situ.

W. Buchheim: On Fig. 6 short chains of associated casein micelles can be seen very frequently. Could this represent a special artifact?

Author: I think that these may represent the remains of disrupted bubble ghosts in which micelles are still held together by remnants of interfacial material.

D. G. Schmidt: Bubble ghosts from milk serum are subject to break down during storage, particularly at higher temperature, whereas ghost membranes from β- lactoglobulin are stable. Should this be ascribed to the incorporation of soluble casein, particularly of β - casein, into the membranes? This would result in "weak" sites in the membrane, possibly due to weaker binding between β - lactoglobulin and β - casein. Please comment.

Author: I very much agree with you. We have experiments in progress to test ideas such as these. Certainly, our preliminary results do suggest the presence of β- casein in the interface. In a single protein solution it is possible to imagine chemical interaction between sulphydryl groups of adjacent β- lactoglobulin molecules on a scale that would not be possible by the addition of β-casein to the system.

D. E. Carpenter: It would seem that direct compositional analyses of the bubble ghosts themselves (or even of the protein in the excluded volume of the chromatogram) would be preferred, rather than the less sensitive difference method which you used. It is interesting to speculate about the nature of the interfacial membranes, especially in terms of the nature of interaction with themselves and degree of denaturation. Would you care to comment?

Author: Direct analysis of interfacial material is now in progress using polyacrylamide gel electrophoresis. Initial results suggest that β- casein is a major component of the interface with smaller amounts of α- casein, β- lactoglobulin and α- lactalbumin. Furthermore, much of the protein is undenatured. The thermal lability of bubble ghosts from skimmed milk suggests that hydrophobic interactions between molecules are not predominant in stabilizing the interface. It is possible that because of changes in the conformation of molecules at the interface reactive groups become exposed and take part in chemical reactions in an entirely unknown way. Such events would be expected to produce stable structures that may be represented by the particulate material remaining at the end of heating to 55°C.

D. E. Carpenter: The similarity of these ghosts to nonnative milk fat globule membranes is interesting, especially in terms of integral and peripheral proteins (micelles).

Author: Although there is a strong morphological similarity between the two, I think it is worth emphasizing that in bubble ghosts produced from skimmed milk the casein micelles do not form an integral part of the interface. This is quite unlike fat/water emulsions where micelles are surface active and contribute to the structure of the interface.

Reviewer I: The author mentioned that the collapsing foam was fixed by addition of glutaraldehyde. Did the author have any idea how fast the foam collapsed? If so, at what decay stage should the foam be fixed in order to obtain the bubble ghosts with best representation?

Author: The rate of foam collapse after the addition of glutaraldehyde was not measured. The foam can of course be fixed and forced to collapse at any stage in its formation. One might, for instance,wish to compare the structure of the interface produced in the very earliest stage of foaming with that in later stages. The foam can be collected at both stages and collapsed by addition of the fixative. My experience has been that structure of the interface is identical no matter when it is collected. This is not to say of course that interface composition will be found to be identical.

FOOD MICROSTRUCTURE, Vol. 4 (1985), pp. 297-312
SEM Inc., AMF O'Hare (Chicago), IL 60666-0507 U.S.A.

0730-5419/85$1.00+.05

EFFECTS OF EMULSIFYING AGENTS ON THE MICROSTRUCTURE AND OTHER CHARACTERISTICS OF PROCESS CHEESE - A REVIEW

Marijana Carić, Miroslav Gantar, and Miloslav Kalab*

Faculty of Technology and Faculty of Science
V. Vlahovića 2, 21000 Novi Sad, Yugoslavia
*Food Research Institute, Agriculture Canada, Ottawa, Ontario, Canada

Abstract

Sodium phosphates, polyphosphates, and citrates are melting salts (emulsifying agents) most commonly used in the manufacture of process cheese either alone or in mixtures. Their role during processing is to sequester calcium in the natural cheese, to solubilize protein and increase its hydration and swelling, to facilitate emulsification of fat, and to adjust and stabilize pH.

Changes taking place in natural cheese during processing can be studied by microscopy. Micrographs demonstrating the emulsification of fat, presence of salt crystals, and partial solubilization of protein in laboratory-made and commercial process cheeses have been used to illustrate the various effects of the emulsifying agents. Optical, particularly polarizing and fluorescence microscopy provides rapid information. Electron microscopy reveals greater detail. In combination with energy dispersive spectrometry, electron microscopy can be used to analyze the chemical composition of salt crystals in the process cheese. However, detailed studies of the relationships existing among the microstructure of the process cheese, its composition, and physical properties such as consistency, spreadability, capability of remelting etc. have yet to be carried out.

Initial paper received July 26 1985
Manuscript received October 06 1985
Direct inquiries to M. Carić
Telephone number: 38 21 59549

KEY WORDS: Cheese; Citrates; Emulsifying agents; Light microscopy; Melting salts; Microstructure of cheese; Phosphates; Process cheese; Scanning electron microscopy; Transmission electron microscopy.

Introduction

Process cheese has a relatively short history with the first attempt to develop it dating back to 1895. The first patent was granted to a German cheese company in 1899 but at that time the cheese was processed only with heat and no additives were used. In 1912, citric acid was introduced in Switzerland as a melting salt. After this important discovery, industrial production of process cheese commenced in Europe in 1919 (9). A combination of citrates and phosphates was used to develop process cheese independently in the USA in 1917 (49). The introduction of phosphates as melting salts resulted in a marked increase in the production of process cheese.

The original idea of processing cheese was to increase its keeping quality (49) and also to utilize cheese which would otherwise be difficult to sell, e.g. remnants from cheese-cutting operations or cheese containing minor defects such as deformations, over-ripening, localized incidence of molds, etc. Later the producers found that a wide assortment of novel products could be made using various types of cheese (ripened to different degrees), by incorporating other dairy products such as skim milk powder, whey powder, whey protein concentrate, cream, butter, flavourings, and emulsifying agents, and by varying the processing conditions. In most countries, the production of process cheese has been steadily on the increase because of the many variations in flavour, consistency, size, and shape of the product. These properties make it simple and attractive to use process cheese in the preparation of meals both at home and in public dining establishments.

Melting salts are of great importance to cheese processing because they affect the chemical, physical, and microbiological properties of the finished product. Melting salts are not emulsifiers in the strict sense, i.e. they are not surface-active substances, yet they are commonly included in the group of ingredients called 'emulsifying agents' (49, 61). True emulsifiers such as mono- and diglycerides are used in combinations with the melting salts by some process cheese producers. It is generally recognized that there are inconsistencies in the nomenclature of the 'emulsifying agents'.

The objective of this review is to compile information on the effects of the most commonly used emulsifying agents such as citrates and phosphates on selected properties, including microstructure, of process cheese.

Principles of process cheese production

Process cheese is produced by blending shredded natural cheeses of various types and degrees of maturity with emulsifying agents (which consist of melting salts and may include other ingredients, such as pectin, modified starch and/or mono- and diglycerides), and by heating the blend under reduced pressure, with constant stirring, to produce a smooth and homogeneous mass. Kosikowski (40) suggests melting temperatures in the range from 71 to 80°C for process cheese and from 87 to 90.6°C for process cheese spreads. In contrast, the cheese blend is heated under pressure to 140°C for several seconds in continuous process cheese operations. This treatment destroys all clostridia but has no detrimental effect on cheese protein (49). Water is added to the cheese blend as a vehicle for the emulsifying agents and to adjust the dry matter content in the final product. The operations are carried out in the following order:

SELECTION OF CHEESE → COMPUTATION OF THE INGREDIENTS → BLENDING → TRIMMING → SHREDDING → ADDITION OF EMULSIFIERS AND OTHER INGREDIENTS → HEATING (PROCESSING) → PACKAGING → COOLING → STORAGE → RETAIL OF PROCESS CHEESE.

firm and have a low moisture content (45%) (70) and low acidity (pH = 5.6-5.8) (29); process cheese spreads are soft (spreadable), have a higher moisture content (55%) (70) and should have a higher acidity (pH = 5.2) than the two former products (29).

The emulsifying agents (melting salts) are used to provide a uniform structure during the melting process. Phosphates, polyphosphates, and citrates (22, 29, 41, 65, 70) are most common. Other salts may also be used, e.g., sodium potassium tartrate (41, 70) or complex sodium aluminum phosphates of the general formula:

$$X\ Na_2O\ .\ Y\ Al_2O_3\ .\ 8\ P_2O_5\ .\ Z\ H_2O,$$

where X = 6 to 15, Y = 1.5 to 4.5, and Z = 4 to 40 (70).

Other emulsifying agents such as sodium potassium tartrate, trihydroxyglutaric acid, or diglycolic acid are rarely used and are not discussed further in this review. A list of emulsifying agents most commonly used, their chemical formulae, molecular mass, P_2O_5 content, solubility in water at 20°C, and pH values of 1% aqueous solutions is presented in Table 3.

A thorough yet concise review of the process cheese principles was recently published by Shimp (61).

Table 1. INGREDIENTS USED IN THE MANUFACTURE OF PROCESS CHEESE

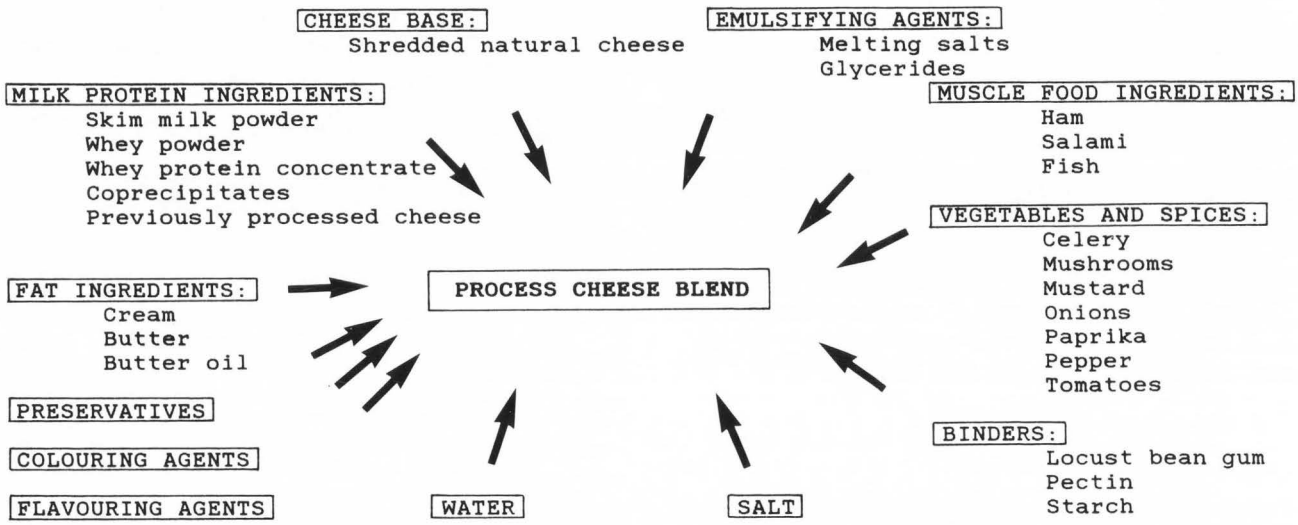

In addition to natural cheese, other ingredients are also used; some of them are mandatory such as emulsifying agents and water, and others may be optional as indicated in Table 1.

Binding agents such as tragacanth, locust bean gum, caraya, pectin, or starch are frequently used along with emulsifying salts in the production of process cheese. Their role is to act as water-binding agents which prevent the drying out of the cheese, and as thickening agents to provide a suitable texture. They are used, in particular, in the manufacture of process cheese spreads.

Depending on the ingredients used, three kinds of product are distinguished: block process cheese, process cheese food, and process cheese spread (49). Their characteristics are summarized in Table 2. Only block process cheese and process cheese spread are being dealt with in this review.

Block process cheese and process cheese food are

Effects of emulsifying agents on the production of process cheese

The essential role of the emulsifying agents in the manufacture of process cheese is to supplement the emulsifying capability of cheese proteins. This is accomplished by

1. removing calcium from the protein system,
2. peptizing, solubilizing, and dispersing proteins,
3. hydrating and swelling proteins,
4. emulsifying fat and stabilizing the emulsions,
5. controlling pH and stabilizing it, and
6. forming an appropriate structure after cooling.

The ability to sequester calcium is one of the most important functions of the emulsifying agents. For simplicity, casein in cheese may be viewed as molecules which have one end nonpolar and thus lipophilic, whereas the other end, which contains calcium phosphate, is

Table 2. SOME CHARACTERISTICS OF PROCESS CHEESE, PROCESS CHEESE FOOD, AND PROCESS CHEESE SPREADS (40, 70)

Type of product:	Ingredients:	Cooking temperature:	Composition:	pH:	Author:
Process cheese	Natural cheese, emulsifiers, NaCl, colouring	71-80°C	Moisture and fat* contents correspond to the legal limits for natural cheese	5.6-5.8	Kosikowski (40)
		74-85°C	45% moisture		Thomas (70)
Process cheese food	Same as above plus optional ingredients such as milk, skim milk, whey, cream, albumin, skim milk cheese; organic acids	79-85°C	No more than 44% moisture, no less than 23% fat	5.2-5.6	Kosikowski (40)
Process cheese spread	Same as process cheese food plus gums for water retention	88-91°C	No less than 44% and no more than 60% moisture	<5.2	Kosikowski (40)
		90-95°C	55% moisture		Thomas (70)

* 1% higher for Cheddar cheese.

hydrophilic (Fig. 1). This arrangement makes the casein molecule function as an emulsifier (14, 61). As the amount of calcium phosphate is decreased, the solubility of casein in water is increased and so is its emulsifying capability. When calcium in the Ca-paracaseinate complex in the natural cheese is removed by the ion exchange reaction initiated by the addition of melting salts, insoluble paracaseinate is converted into a soluble form. This soluble form is most frequently Na-caseinate; monovalent sodium is provided by the emulsifying agent.

Various emulsifiers have varying affinity, i.e. sequestering ability, for calcium. This affinity increases, for example, in the following order: NaH_2PO_4, Na_2HPO_4, $Na_2H_2P_2O_7$, $Na_3HP_2O_7$, $Na_4P_2O_7$, $Na_5P_3O_{10}$.

Polyvalent anions (phosphates, citrates) have a high water-adsorption ability. They become bound by calcium to protein molecules in the cheese and provide them with a negative charge. The addition of basic salts also increases the pH value of the cheese. The increases

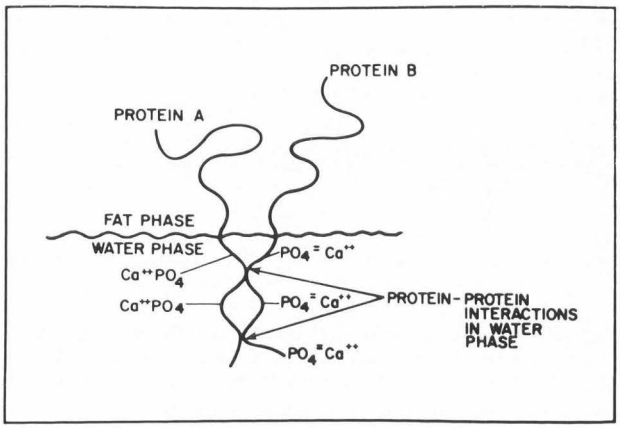

Fig. 1. Protein-protein interactions in process cheese as affected by calcium phosphate added as an 'emulsifying agent'. According to Shimp (61).

Table 3. EMULSIFYING SALTS USED IN THE PROCESSING OF CHEESE (40, 70)

Group:	Emulsifying salt:	Formula:	Mol. mass:	P_2O_5 content (%):	Solubility at 20°C (%):	pH value (1% soln.):
Citrates	Trisodium citrate	$2\ Na_3C_6H_5O_7 \cdot 11H_2O$	714.31	-----	High	6.23-6.26
Orthophosphates	Monosodium phosphate	$NaH_2PO_4 \cdot 2\ H_2O$	156.01	59.15	40	4.0-4.2
	Disodium phosphate	$Na_2HPO_4 \cdot 12H_2O$	358.14	19.80	18	8.9-9.1
Pyrophosphates	Disodium pyrophosphate	$Na_2H_2P_2O_7$	221.94	63.96	10.7	4.0-4.5
	Trisodium pyrophosphate	$Na_3HP_2O_7 \cdot 9\ H_2O$	406.06	34.95	32	6.7-7.5
	Tetrasodium pyrophosphate	$Na_4P_2O_7 \cdot 10\ H_2O$	446.05	31.82	10-12	10.2-10.4
Polyphosphates	Pentasodium tripolyphosphate	$Na_5P_3O_{10}$	-----	57.88	14-15	9.3-9.8
	Sodium tetrapolyphosphate	$Na_6P_4O_{13}$	-----	60.42	14-15	9.0-9.5
	Sodium hexametaphosphate (Graham's salt)	$(NaPO_3)_n$	-----	69.60	infinite	6.0-7.5

of both the negative charge and the pH value result in a higher water absorption by the proteins. Analytical determination of calcium and phosphorus in process cheese showed that the concentration of these elements was twice as high in the insoluble portion of the process cheese as in the initial natural cheese. The reactivity between the emulsifier and protein is defined by the ratio of insoluble to total proteins in the initial natural cheese and in the process cheese (22). Lee et al. (44) investigated protein disaggregation and structure of process cheese and found that the affinity of protein for the cations and anions of the melting salts was determined by the valency of such ions.

Ideal emulsifying characteristics are possessed by salts which consist of a monovalent cation and a polyvalent anion. Some salts have better emulsifying effects than other salts but may have inferior calcium-sequestering abilities, or may not sufficiently solubilize and hydrate protein. To achieve excellent emulsifying and melting characteristics simultaneously and to produce a homogeneous and stable process cheese, it is necessary to combine two or more salts into mixtures.

The pH value is important for several reasons. It affects the protein configuration and solubility as well as the extent to which emulsifying salts bind calcium (61). In process cheese, pH is maintained between 5.0 and 6.5. At the lower limit of pH 5.0, which is close to the isoelectric point of cheese proteins, the cheese texture may become crumbly. The crumbliness is probably caused by weakened protein-protein bonds and the onset of the fat emulsion breakage because the interactions of the protein molecules with other protein as well as fat molecules are reduced. At the upper limit of pH 6.5, the cheese becomes excessively soft. Microbiological problems, which affect the shelf life, may also be encountered. However, shelf life may be prolonged by sterilization or drying of the process cheese produced (8). The effect of pH on the texture of process cheese was demonstrated by Karahadian (31), who used monosodium, disodium, and trisodium phosphates. The respective pH values of their 1% solutions were 4.2, 9.5, and 13.0. Cheese made with monosodium phosphate (low pH) was dry and crumbly whereas cheese made with trisodium phosphate (high pH) was moist and elastic; texture of cheese made with disodium phosphate was in between. Similar pH effects apply to other emulsifiers (61).

Emulsifying agents vary in their bacteriological effects. Specific bacteriostatic action was observed with monophosphates and was even more pronounced in higher phosphates and polyphosphates (40, 70). Citrates lack such effects and may, in contrast, even themselves be the subject of bacterial spoilage. As the usual heat treatment of the cheese during processing is rather mild, process cheese is not sterile. Although the final product contains no viable bacteria, it contains viable spores, probably even including clostridia, which may originate from the natural cheese or from the spices added (9, 40, 70). Tanaka et al. (67) reported that orthophosphate suppressed the germination of *Clostridium botulinum* spores in process cheese whereas citrates were without effect. Differences in the processing conditions such as the kind of emulsifier used, pH, moisture level, etc. also affect spore germination.

Characteristics of individual melting salts and their mixtures have been studied to a great extent for the effects which they have on process cheese during manufacture and storage (1, 9, 10, 30, 32, 33, 62-64, 71). Effects of some selected emulsifying agents on process cheese are summarized in Table 4.

Phosphates

Phosphates used as emulsifying salts (Table 3) have been intensively studied (4, 9, 10, 12, 16, 17, 21, 37, 42, 43, 47, 48, 51, 52, 57, 60, 64, 70, 71, 76, 77). They belong to the following groups:

(a) monophosphates (orthophosphates), e. g. NaH_2PO_4; Na_2HPO_4; Na_3PO_4;

(b) condensed polyphosphates:

- polyphosphates - chains (oligophosphates and high molecular polyphosphates), e.g.:

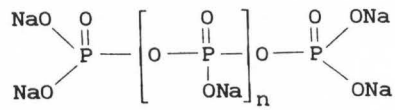

- metaphosphates - rings, e.g. $Na_3P_3O_9$; $Na_4P_4O_{12}$;
- condensed phosphates - rings with chains and branches.

Sequestering of calcium was found to be closely related to the solubilization of protein. These abilities differ from one salt to another. According to Heide (21), the solubilization of fat-free rennet casein was 30% with orthophosphate, 45% with pyrophosphate, and 85%

Table 4. CHARACTERISTICS OF EMULSIFIERS MOST COMMONLY USED IN THE MANUFACTURE OF PROCESS CHEESE AND RELATED PRODUCTS (40)

Emulsifier*:	Characteristics:
Sodium citrate	Versatile; produces cheese with good melting properties; inexpensive; best qualities.
Disodium phosphate	Good firming, buffering, and melting properties, poor creaming properties. Least expensive.
Trisodium phosphate	Highly alkaline; improves sliceability when used in combination with other emulsifiers; good buffering ability; used at low concentrations.
Sodium hexametaphosphate (Graham's salt)	Produces tartish flavour and a very firm body; product does not melt easily; least soluble of all; bacteriostatic.
Tetrasodium diphosphate	Good creaming properties; strong buffering capacity; high protein solubility; excellent ion exchange; tartish flavour.

* Other emulsifiers permitted by the U.S. Federal Standards of Identity are: sodium acid pyrophosphate, sodium potassium tartrate, tetrasodium pyrophosphate, dipotassium phosphate, potassium citrate, calcium citrate, and sodium aluminum phosphate.

with polyphosphate. Similar findings were made by Daclin (12). Sodium polyphosphates were found to be superior to ortho- and metaphosphates in the manufacture of process cheese from mixtures of 60-70% Swiss and 30-40% Gruyère cheeses. Lee and Alais (42) reported that the concentration of soluble nitrogen was increased with an increased concentration of the polyphosphate added in the range from 1 to 3%. Hydrolysis of polyphosphates into orthophosphates in the process cheese was clearly evident after cooling.

Ney and Garg (52, 53) compared cyclic polyphosphates having 3 and 4 phosphorus atoms with linear phosphates: calcium sequestering was markedly lower with sodium metaphosphate than with sodium tetrametaphosphate; a smooth homogeneous process cheese was obtained with the latter salt. Kirchmeier et al. (37) studied the flow properties of process cheese manufactured by various techniques (continuous kettle, blender, or the UHT process) using various phosphates. Differences in depolymerization of casein and changes in the flow properties were attributed to differences in calcium complexation in mono- and tetrapolyphosphates.

Nakajima et al. (51) varied the polyphosphate-to-pyrophosphate ratio in condensed phosphates used as melting salts. Melting rate, ultrafiltrable calcium concentration, and textural properties such as stress relaxation, hardness, gumminess, and elasticity in the finished product were affected more by varying the condensed phosphate than the polyphosphate concentrations.

Bonell (4) assumed that the theory about the ion-exchange effect of polyphosphates, whereby Ca-paracaseinate is converted into Na-paracaseinate, has been confirmed by the finding that ethylenediaminetetraacetic acid (EDTA), which has a high affinity for calcium, can be used successfully in the manufacture of process cheese. Scharpf (60) suggested that the emulsifying effect of chain phosphates is associated with their interaction with paracasein in such a way that phosphate anions form bridges between protein molecules.

In the USSR, Zakharova et al. (76) investigated the possibility of reducing the customary quantity of phosphates because phosphorus from the added emulsifiers increases the P:Ca ratio in the process cheese and this is considered to be nutritionally detrimental. Monoglycerides as true emulsifiers were used to partly replace phosphates. Process cheese of good quality was produced using 1% of a surface-active monoglyceride preparation in combination with only one half of the amount of phosphate usually used. The P:Ca ratio was reduced from 1.6, when Na-tripolyphosphate was used alone, to 1.1, when the same salt was used along with 1% of monoglyceride. Gavrilova (16) reported the preparation of process cheese with improved rheological properties and storage stability using an emulsifier consisting of tripolyphosphate and monoglycerides. Zakharova et al. (77) showed that the addition of monoglycerides increased the hydrophilic properties of the cheese immediately after processing as well as during storage.

A suggestion was made in Japan to enrich process cheese with calcium. Using colloidal calcium carbonate (48), the Ca:P ratio could be restored to 1-2:1 despite the presence of polyphosphates in the emulsifiers used.

All condensed polyphosphates hydrolyze in aqueous solutions. Hydrolysis also takes place during the melting procedure and after it. Glandorf (17) found that the degradation of polyphosphates was increased with the duration of processing irrespective of the rate of stirring and with an increase in the UHT temperature employed. According to Roesler (57), about one half of the amount of polyphosphates added as emulsifiers becomes hydrolyzed during the melting procedure and the other half becomes hydrolyzed by the end of a 7-week storage period in process cheese and after 10 weeks in process cheese spread. Roesler (57) also established that the hydrolysis of condensed phosphates leads to monophosphates and diphosphates in block cheese, which is related to the high dry matter content of the cheese, and to monophosphates in the process cheese spreads.

Citrates

Of a variety of citrates available, only trisodium citrate is used as an emulsifying agent in process cheese production. Citric acid as such can be used to correct the pH value of the cheese. Potassium citrate is not suitable because it renders the finished product bitter in taste.

Thomas (70) reported that monosodium citrate caused emulsion breakdown during cheese melting because of high acidity. Disodium citrate led to moderate to extensive water separation during solidification of the process cheese, also because of high acidity of the salt. For these reasons, trisodium citrate has been used either alone or in combinations with other salts.

Kapac-Parkačeva (29) compared the effects of sodium citrate, sodium citrophosphate, and sodium potassium tartrate, on chemical changes in process cheese. The highest and the lowest acidity was found with citrophosphate and tartrate, respectively. Soluble nitrogen was higher in all three variants of the process cheese than in the initial natural cheese and was highest with sodium citrate.

Swiatek (66) studied the effects of trisodium citrate, disodium phosphate, and tri-, tetra-, and hexapolyphosphates on the consistency of process cheese. He concluded that trisodium citrate and disodium phosphate exhibited similar effects and produced the softest cheese whereas polyphosphates produced considerably harder cheeses. Firmness of the cheese increased with the degree of phosphate condensation.

The effects of citrate, orthophosphate, pyrophosphate, tripolyphosphate, and Graham's salt $[(NaPO_3)_n.H_2O]$ on physico-chemical properties of process cheese were examined by Kairyukshtene et al. (22). pH values of 3% solutions of the salts used were 8.16, 8.89, 6.61, 9.31, and 5.49, respectively. Soluble protein contents were increased and the water-binding capacity and plasticity during processing were improved to a great extent in the presence of the alkaline salts. The finest fat dispersion and structure were obtained by using citrate, tripolyphosphate, or orthophosphate in the processing of fresh curds or green cheese, and by using citrate or Graham's salt in the processing of well-ripened cheese.

Effects of citrate, orthophosphate, pyrophosphate, and sodium potassium tartrate were also studied in the processing of curds obtained from concentrated milk (41). Addition of any of the above salts at a concentration of 3% led to products with poor sensory attributes. In contrast, the addition of 2% citrate resulted in the most rapid processing and yielded a product with good sensory attributes.

Salt combinations

It has already been mentioned that salt mixtures are used to combine the best effects of their individual components (1, 9, 10, 30, 33, 62-64, 71). Some results obtained earlier (33, 63) seem to favour citrate in the melting salt combinations but more recent studies emphasize the desirable effects of phosphates.

According to Shubin (63), a combination of sodium

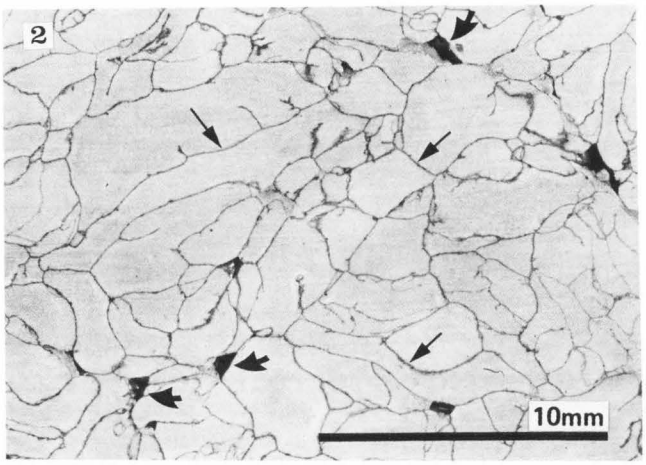

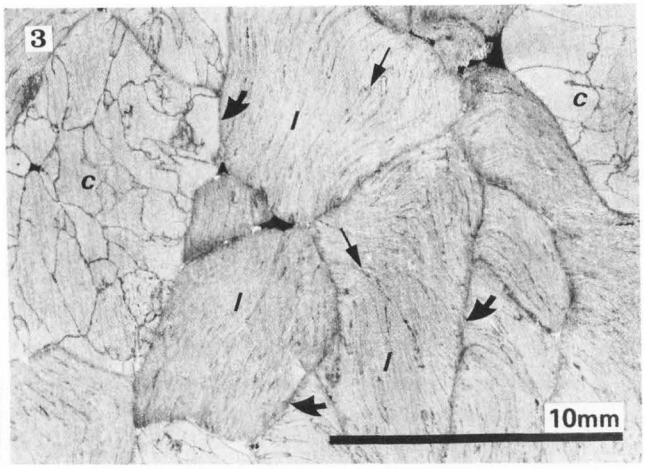

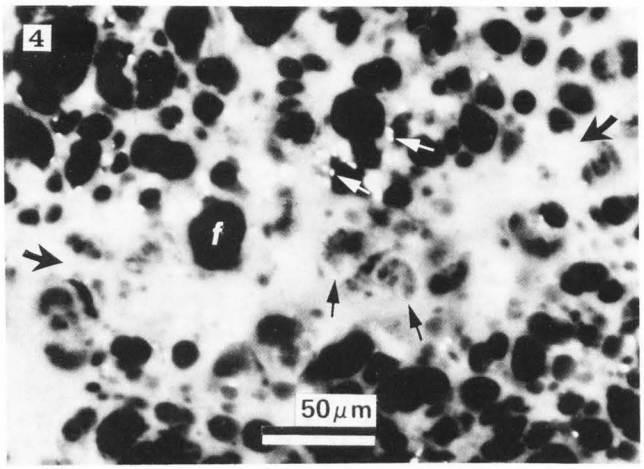

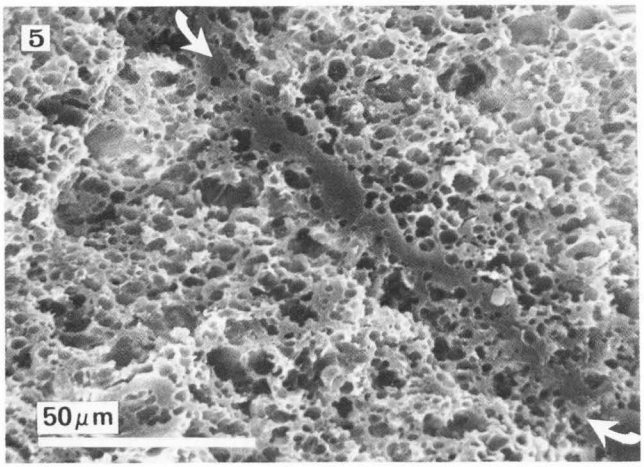

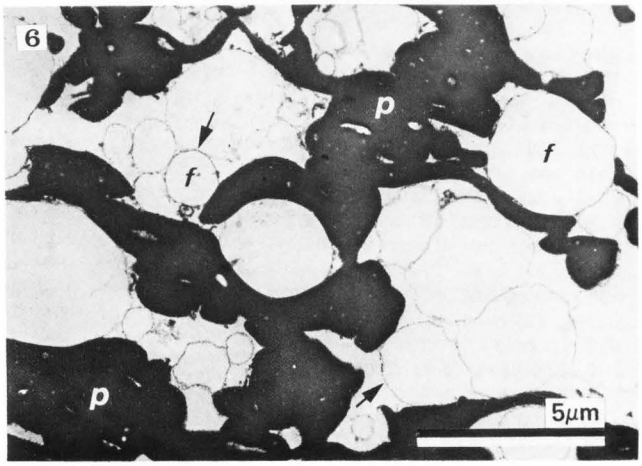

Fig. 6. Fat globules (f) in 1-day old Cheddar cheese are encased in fat globule membranes (arrows). p = Protein; (TEM of a thin section).

Fig. 2. Curd granule junctions (small arrows) in Brick cheese. Dark areas (large arrows) are void spaces (air pockets) in the cheese.

Fig. 3. Curd granule junctions (small arrows) and milled curd junctions (large arrows) in Cheddar cheese form characteristic patterns. Depending on the orientation of the milled curd particles, cheddared curd granules are displayed in cross sections (c) or longitudinal sections (l).

Fig. 4. Light (fluorescence) microscopy of a curd granule junction (light area between large arrows). Dark structures (f) are fat globules. Small dark arrows point to calcium phosphate crystals and light arrows point to lactic acid bacteria appearing as very light points. Courtesy of S. H. Yiu.

Fig. 5. SEM of a curd granule junction (dark area between light arrows) indicates that the junction is devoid of fat globules as evident from the low incidence of empty cavities which contained fat before it had been extracted with chloroform.

citrate and trihydroxyglutarate produced the best results as emulsifying agents in the manufacture of process cheese. A mixture of these salts (10-20%) with disodium phosphate (80-90%) yielded a high-quality process cheese, as far as the solubility of protein, emulsification of fat, and the pH value of the finished product were concerned.

Some earlier results of Kiermeier (33) had shown that orthophosphates and pyrophosphates were generally unsatisfactory whether employed alone or in a combination, but citrate was useful to a limited extent. Polyphosphates proved to be satisfactory in every respect.

Thomas et al. (71) produced process cheese with a 3% addition of disodium phosphate, tetrasodium

diphosphate, pentasodium triphosphate, or trisodium citrate or with the addition of a mixture of equal quantities of sodium polyphosphate and tetrasodium phosphate. General acceptability was about the same for all process cheeses. However, cheeses made with disodium phosphate, tetrasodium diphosphate, or pentasodium triphosphate had an elevated content of water-soluble nitrogen compared to cheeses made with trisodium citrate or the mixture of sodium polyphosphate and tetrasodium phosphate. By decreasing the amount of the melting salts to 2% or by increasing it to 4%, no differences were detected in the water-soluble nitrogen fraction in the process cheeses or in their stickiness, crumbliness, sliceability, or general acceptability.

Csók (11), working with a commercial emulsifying agent, reported that an increase in the melting time up to 1080 s resulted in an increase of the total bound water as well as osmotically bound water.

In general, polyphosphates had superior effects on the structure and keeping quality of process cheese (1) compared to other emulsifying agents. This has been attributed by the authors to the ability of polyphosphates to solubilize calcium paracaseinate because of their high calcium-sequestering capacity. Pyrophosphates and, in particular, orthophosphates have been found to introduce unfavourable sensory attributes to the process cheese. Citrates were as efficient emulsifiers as polyphosphates but lacked their bacteriostatic effect.

Sood and Kosikowski (64) investigated the possibility of replacing cheese solids with plain or enzyme-treated skim milk retentates in the manufacture of process Cheddar cheese. Casein in the retentates is mostly insoluble, for which reason the retentates cannot be used alone for processing. However, process cheese containing up to 60% of retentate solids (treated with food grade fungal protease and lipase preparations) had better sensory attributes than the reference process cheese. Of a variety of melting salts tested, a combination of sodium citrate (2.7%) and citric acid (0.3%) was best suited to produce the retentate-containing process cheese. Increasing the retentate content to 80% resulted in an unacceptable product having a hard, long-grained texture.

Microstructure of process cheese

Optical as well as electron microscopy have been used to select natural cheese for processing, to check the progress of processing, and to evaluate the finished product.

Boháč (3) examined the suitability of cheese for processing by using a polarizing microscope equipped with a hot stage. Cheese slices were heated to 85-95°C within 8-10 min and the interface between the cheese and the melting salt solution was observed. The following phenomena were noted: Some samples disintegrated along the curd granule junctions after a temperature of 70°C was reached. A diffuse zone containing protein and fat globules released from the cheese was formed around most samples or their fragments. The suitability of the cheese for processing was assessed from the dimensions of the fat globules and the amount of fat released and from the temperature at which it melted. Ripe and over-ripened cheeses sometimes rapidly diffused into the salt solution even before the melting temperature had been reached. At 60-70°C, some cheese samples rapidly contracted, remained unchanged until a temperature of 95-98°C was reached, and then melted.

The behaviour of melting salts in an aqueous medium or in the presence of cheese was studied using the same microscope: small glassy crystals dissolved relatively slowly or occasionally only after firstly aggregating. Instantized salts formed minute globules which dissolved more rapidly than regular salts. Fine bubbles of carbon dioxide sometimes developed and facilitated the dispersion of the salt crystals in the cheese mass. Time lapse photography using a movie camera showed the changes in succession.

The microstructure of process cheese resembles, to some extent, the microstructure of the natural cheese.

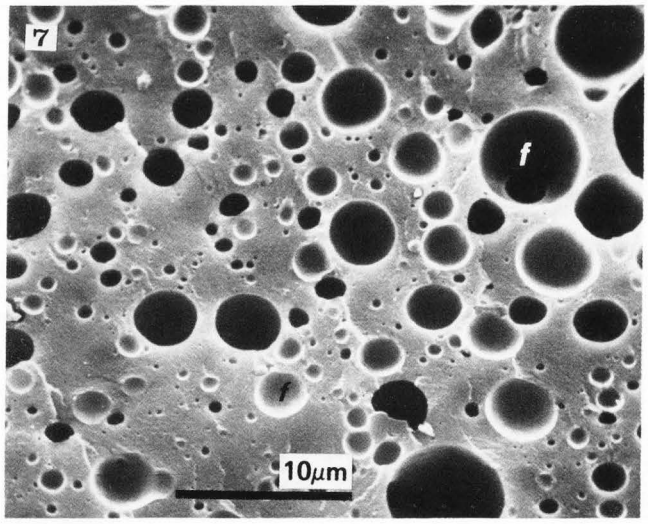

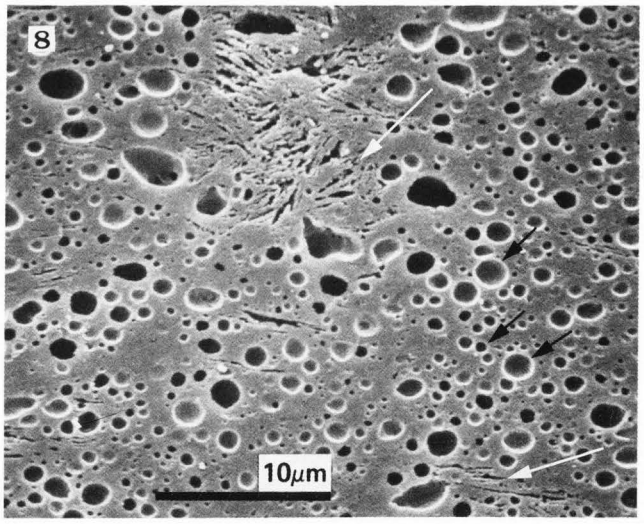

Fig. 7. Large fat particles (f) in process cheese at the beginning of melting.

Fig. 8. Fat particles (dark arrows) in process cheese 40 min after the melting temperature had been reached. Emulsification has reduced dimensions of the fat particles. Light arrows point to cavities initially occupied by sodium citrate crystals which were used as the melting salt.

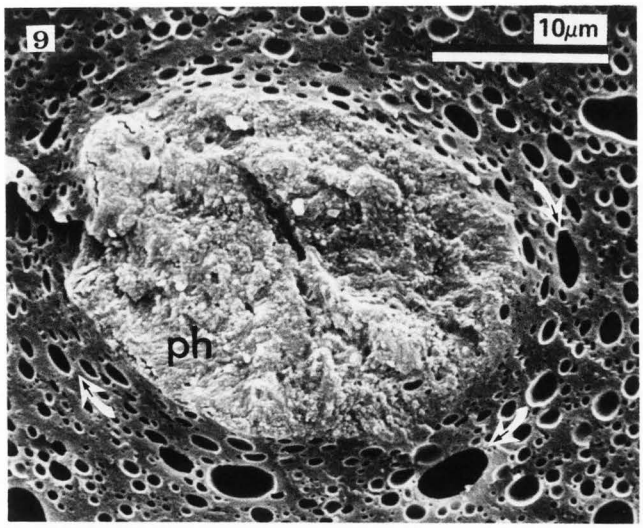

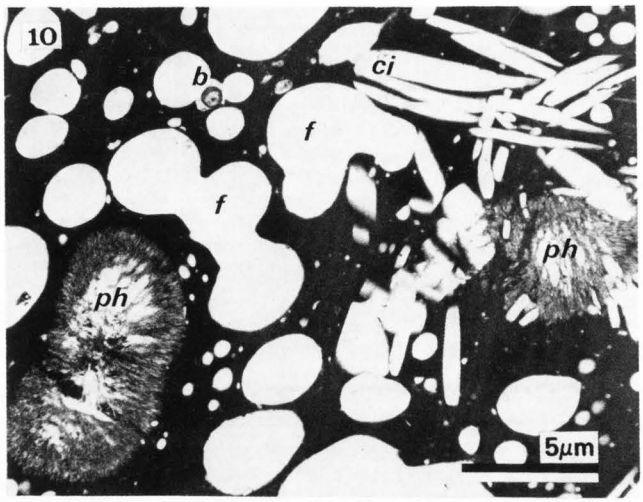

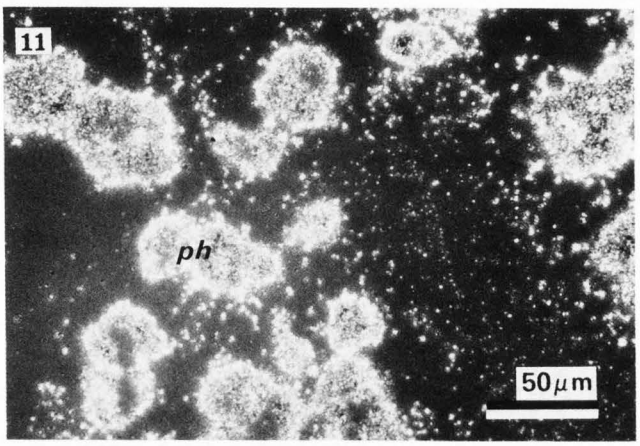

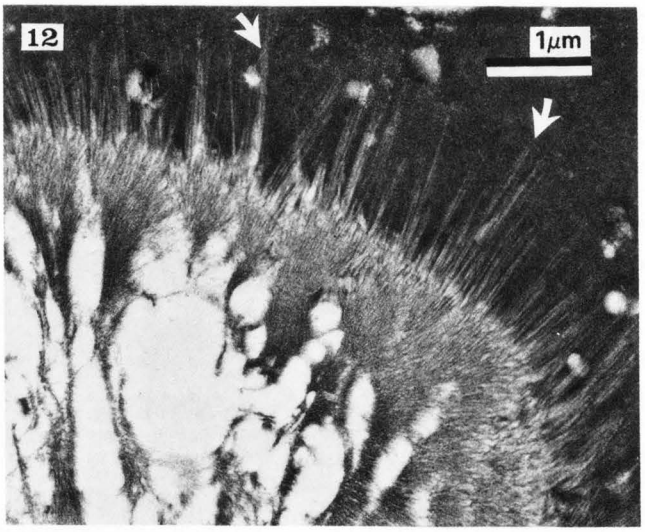

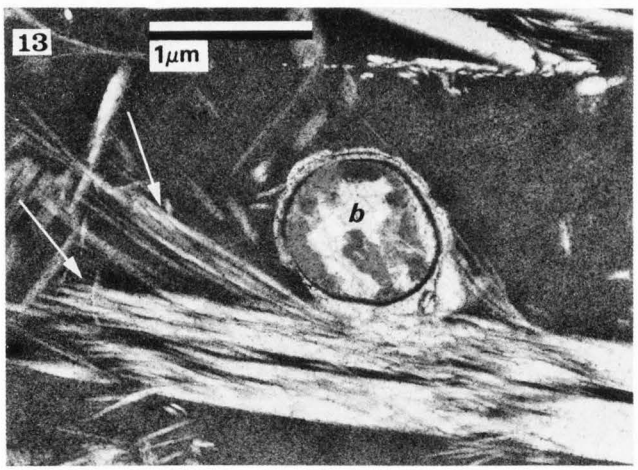

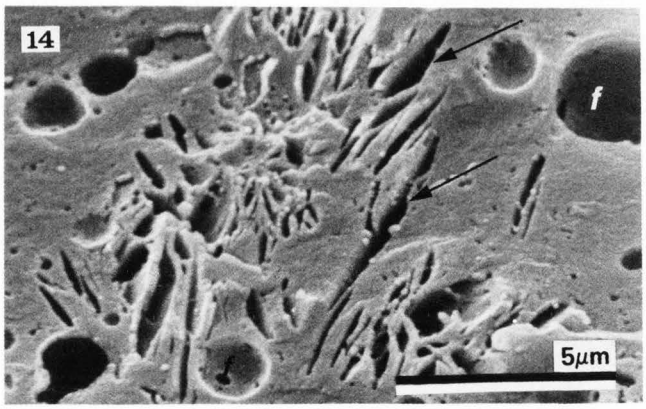

Fig. 9. *A large calcium phosphate crystal (ph) in process cheese (SEM). Fat globules around the crystal (arrows) show signs of distortion.*

Fig. 10. *Calcium phosphate (ph) crystals and void spaces (ci) in a process cheese blend cooked for 10 min. The void spaces are the imprints of sodium citrate crystals which had dissolved in aqueous glutaraldehyde during fixation for SEM. Fat (f) is in the process of emulsification. b = Bacterium. From Rayan et al. (56).*

Fig. 11. *Light microscopy of calcium phosphate crystals (ph) specifically stained for calcium with Alizarin Red. Courtesy of S. H. Yiu (75).*

Fig. 12. *Crystallization takes place with disodium phosphate used as the melting salt in the preparation of process cheese and is indicated by needle-shaped outgrowth (arrows). From Rayan et al. (56).*

Fig. 13. *Crystallization takes place also with tetrasodium pyrophosphate (arrows). b = Bacterium. From Rayan et al. (56).*

Fig. 14. *Detail of cavities (arrows) indicating that sodium citrate was used as the melting salt in the preparation of this process cheese. f = Cavities initially occupied by fat particles.*

However, there are several differences. Some can be studied by light microscopy and others may be studied by electron microscopy.

Natural cheese is made by pressing curd granules, consisting mostly of insoluble calcium caseinate and fat droplets, into a homogeneous mass. The sites, where the granules fuse with each other, are called curd granule junctions (23-28, 46, 54, 59, 69, 75). At a low magnification, they are seen to form characteristic patterns. Compared to simple patterns in stirred-curd cheeses such as Brick cheese (Fig. 2), the patterns are complex in Cheddar cheese (Fig. 3) because an additional type of milled curd granule junction develops as the result of milling cheddared curd and pressing milled curd. Curd granule junctions are areas depleted of fat globules, as is evident from optical (Fig. 4) as well as SEM micrographs (Fig. 5). Their development was described earlier (27, 28).

The distribution of fat in natural cheese was studied by optical (3, 13, 75) as well as electron microscopy (2, 18, 19, 23-27, 34, 39, 43, 45, 55, 56, 58, 69). Most fat globules have been found to have their fat globule membranes preserved; this can be best observed by transmission electron microscopy (TEM) of thin sections (Fig. 6) (23, 24, 27, 34).

During processing, both the curd granule junctions and the fat globule membranes vanish as the result of heating, melting, and stirring the cheese. The fat melts and forms particles several micrometers in diameter. The relatively insoluble protein in the natural cheese is partially solubilized by the action of the calcium-sequestering melting salts and is converted into a smooth and homogeneous mass. The salts increase the natural emulsifying properties of the cheese proteins, and the fat disperses in the form of minute globules.

Rayan (55) and Rayan et al. (56) used SEM and TEM to study the emulsification of fat during the processing of Cheddar cheese. The melting salts used were sodium citrate, disodium phosphate, tetrasodium pyrophosphate, and sodium aluminum phosphate. Depending on the processing conditions, the initially large fat particles were emulsified into smaller droplets (Figs. 7 and 8).

In addition to the dispersion of fat, electron microscopy also documents the presence of crystalline

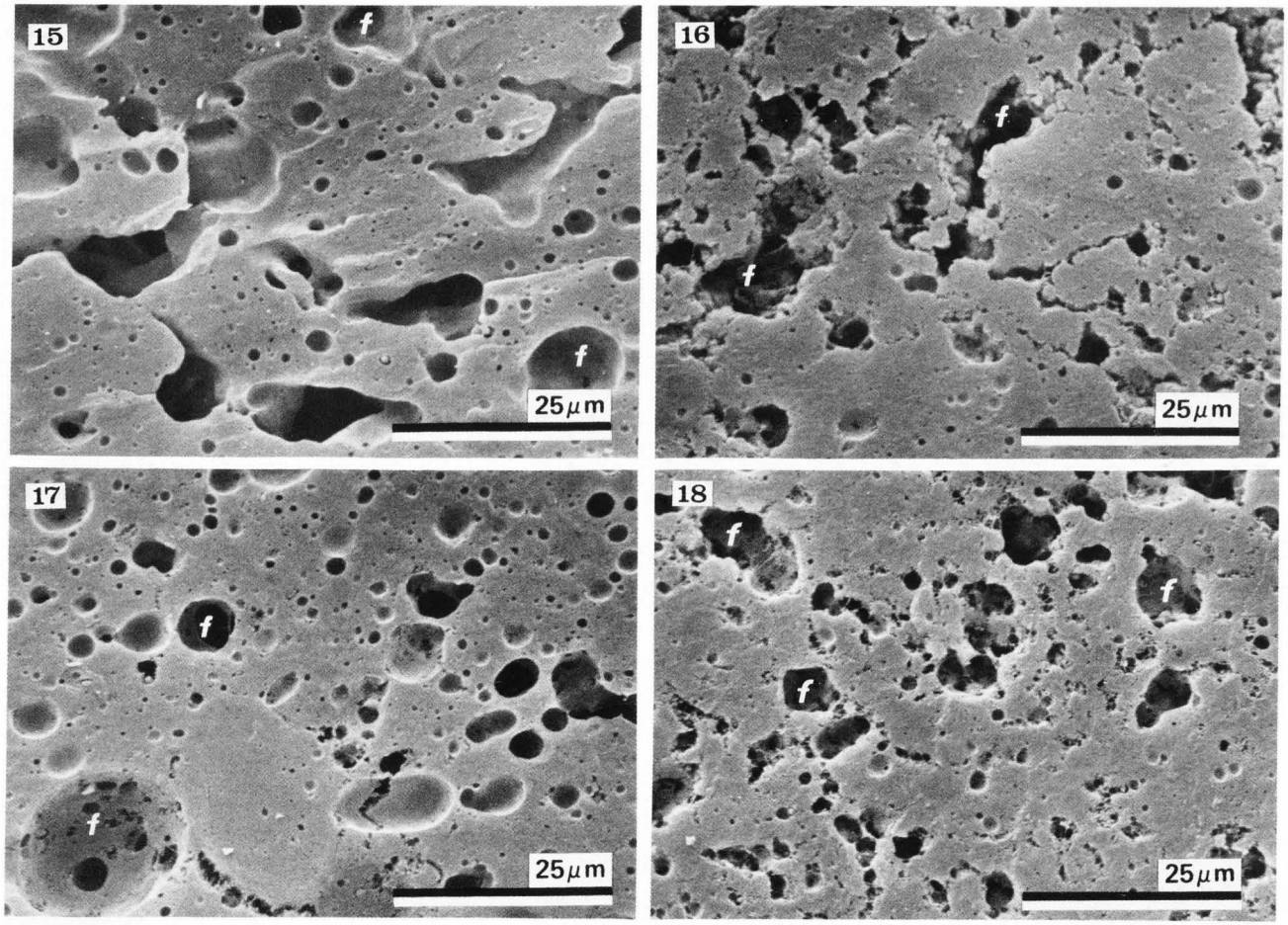

Figs. 15-18. Experimental process cheese made from a blend of Feta, Gouda, Kachkaval, and White cheeses using the following emulsifiers: Fig. 15. Commercial emulsifier consisting of 51% sodium phosphate (SP) and 49% sodium polyphosphate (SPP); Fig. 16. Laboratory-made mixture of 61% SP and 39% SPP; Fig. 17. A mixture of 15% SP, 70% SPP, and 15% modified starch; Fig. 18. A mixture of 10% SP, 65% SPP, 15% modified starch, and 10% mono- and diglycerides (1:1, w/w). The distribution of fat (f) differs from cheese to cheese (see the text).

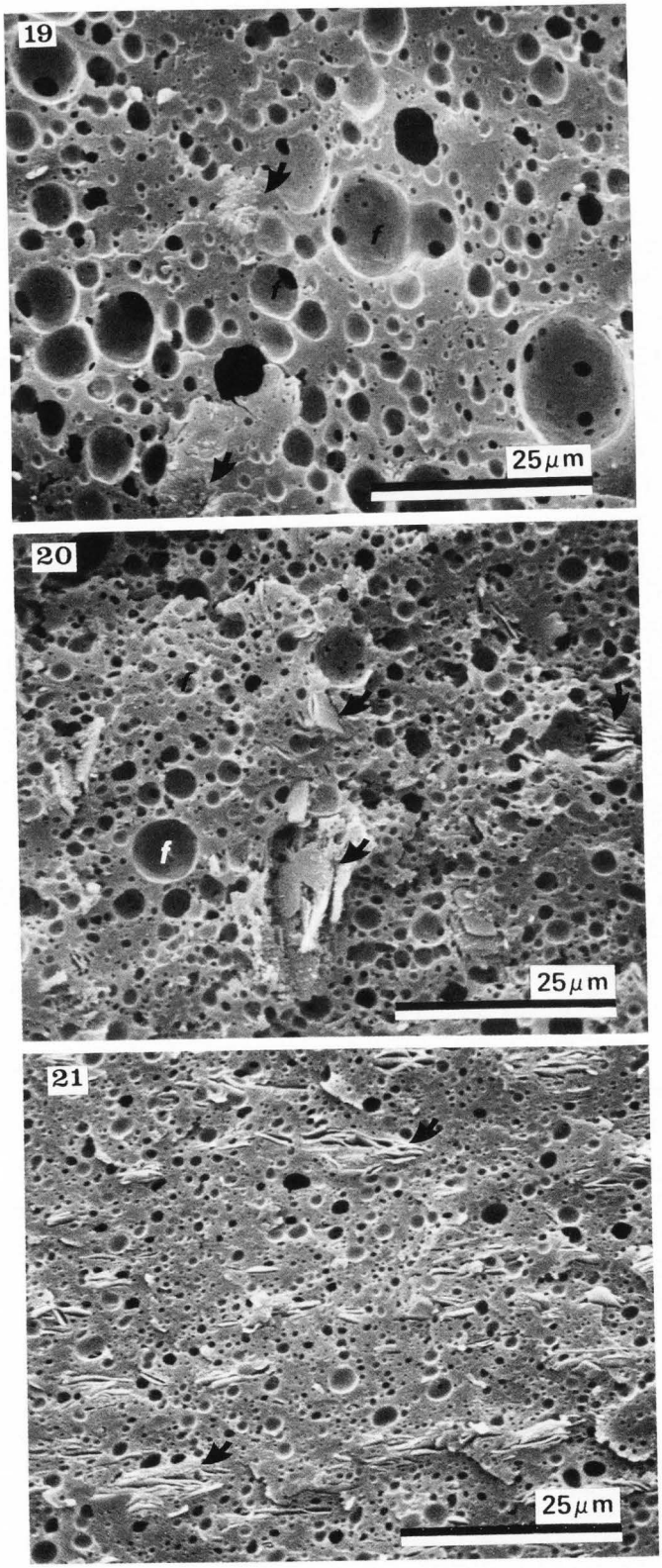

Figs. 19-21. Commercial process cheeses: Fig. 19. Processed Cheddar cheese with the declared use of sodium phosphate, sodium-aluminum phosphate, sodium triphosphate, and sodium citrate contains only a small number of calcium phosphate crystals (arrows). Fat particles (f) vary widely in dimensions. Fig. 20. Processed Gruyère cheese A made with sodium-calcium citrate. Fat particles (f) are considerably smaller than in processed Cheddar cheese. Large crystals and their clusters (arrows) are abundant. Fig. 21. Processed Gruyère cheese B made with sodium citrate. Fat is emulsified into minute globules. Crystals (arrows) are abundant.

inclusions in natural cheese (2, 5-7). One of the earliest reports on crystals of inorganic and organic origin is from Steinegger (65). The incidence of crystals in cheese was reviewed by Brooker (6). Calcium phosphate and lactate crystals are most common. Calcium phosphate crystals are abundant and are present in cheese in the form of aggregates up to 30 μm in diameter. Aggregates of Ca lactate crystals are irregular in shape, may measure up to 80 μm in diameter, and consist of randomly arranged bundles of slightly curved, needle-like crystals (5, 6). Flückiger and Schilt (15) found tyrosine crystals in Swiss cheese by light microscopy. Using chromatography, SEM, and energy dispersive spectrometry, Blanc et al. (2) identified calcium tyrosinate crystals in Swiss cheese with secondary fermentation.

Sodium phosphates react with calcium in the cheese and produce insoluble calcium phosphate (40). Because of their insolubility, calcium phosphate crystals withstand the processing of cheese and are found in the finished product (Figs. 9 and 10). Specific staining for calcium makes it possible to characterize the crystals by optical microscopy (Fig. 11). Anhydrous phosphates absorb water and form large aggregates (40).

Tinyakov and Barkan (73) established that the number of calcium salt aggregates formed in process cheese made with sodium citrate as the emulsifying salt was lower and their dimensions were smaller than in process cheese made with sodium phosphate.

Small white crystals occasionally develop on the surface of process cheese. Morris et al. (50) reported their development as early as a week after manufacture. The crystals were identified to be calcium citrate and their incidence was prevented by eliminating citrate from the emulsifying agent.

Another kind of crystal was found in process cheese slices by Klostermeyer et al. (38). The crystals were characterized by the Debye-Scherrer x-ray analysis and were chemically identified as a new tertiary sodium-calcium citrate, $NaCaC_6H_5O_7$. The authors suggested to reduce the incidence of this salt in some process cheeses by reducing the concentrations of Ca^{2+} and Na^+.

Melting salt crystals are present in process cheese as the result of using an excessive amount of the emulsifying agent or because of incomplete dissolution of the salt (74). The crystals are usually larger than calcium phosphate crystals initially present in the cheese and also differ in their appearance. When sodium diphosphate was used as a melting salt (56), additional growth of calcium phosphate crystals initially present in the cheese was observed in the form of fine spikes (Fig. 12). Recrystallization was also observed with tetrasodium pyrophosphate (Fig. 13). Sodium citrate is found in the form of needles (Figs. 10 and 14). Because this salt is soluble in water, its crystals are washed out from the protein matrix during preparative steps and are not seen by electron microscopy. The patterns observed (56) in both TEM (Fig. 10) and SEM micrographs (Fig. 14) are imprints of the soluble crystals in the

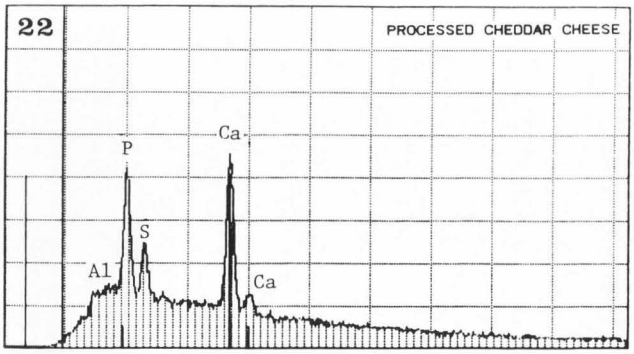

Fig. 22. Diagram of energy dispersive spectrometric analysis of a crystal in commercial processed Cheddar cheese. Peaks of aluminum (Al), phosphorus (P), sulphur (S), and calcium (Ca) are identified. Courtesy of S. H. Yiu.

Fig. 24. (Below) Diagram of energy dispersive spectrometric analysis of a crystal in commercial processed Gruyère cheese. Peaks of sodium (Na), phosphorus (P), sulphur (S), and calcium (Ca) are identified. Courtesy of S. H. Yiu.

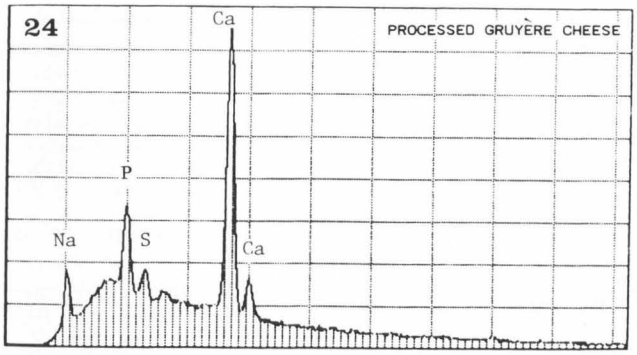

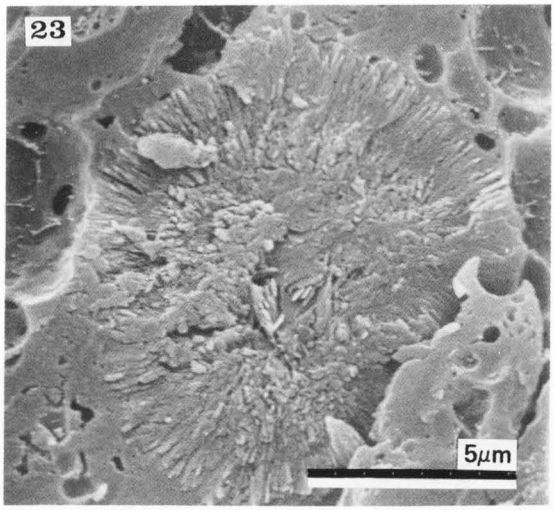

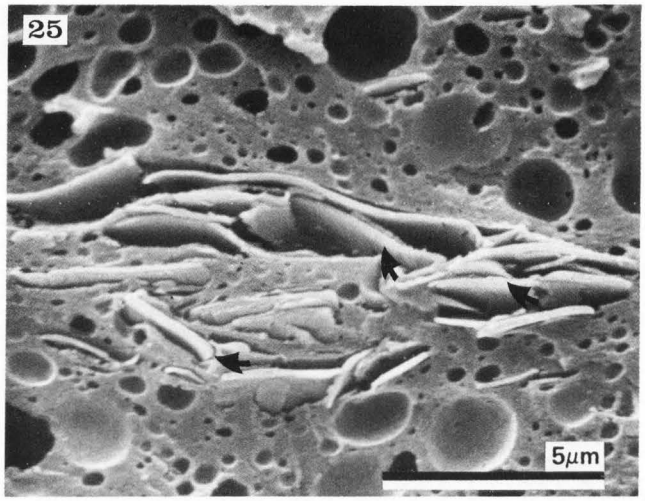

Fig. 23. Detail of a crystal in commercial processed Cheddar cheese similar to the crystal subjected to energy dispersive spectrometry in Fig. 22.

Fig. 25. Detail of crystals in commercial processed Gruyere cheese similar to crystals subjected to energy dispersive spectrometry in Fig. 24. Although sodium citrate crystals were usually washed out from process cheese samples destined for SEM, sheet-like crystals (arrows) are noticeable in this commercial sample.

fixed protein matrix (26).

Cheddar cheese forms the base for most process cheeses in the USA, Canada, and the United Kingdom, but Gruyère, Gouda, and Emmental cheeses are used the most in continental Europe. In our experiments, a mixture of Feta, Gouda, Kachkaval, and White cheeses (20% fat, 58% moisture, pH = 5.6) was processed to assess the effects of various emulsifying agents such as (a) a commercial emulsifier consisting of 51% sodium phosphate (SP) and 49% sodium polyphosphate (SPP) (Fig. 15), (b) a laboratory-made emulsifier consisting of 61% SP and 39% SPP (Fig. 16), (c) an emulsifier consisting of 15% SP, 70% SPP, and 15% modified starch (Fig. 17), and (d) an emulsifier consisting of 10% SP, 65% SPP, 15% modified starch, and 10% of a monoglycerides and diglycerides mixture (1:1, w/w) (Fig. 18). The emulsifiers were added to the shredded cheese at a concentration of 3%, and the cheese blend was heated by direct steam at 95°C for 600 s (including the warming of the blend to 95°C) with stirring at 90 rpm. The finished products were stored at <10°C and examined 24 h after production.

Compared to other process cheeses presented in this review, these experimental samples were almost completely free of salt crystals; their absence is probably due to a rapid dissolution of the melting salts because direct steam was used to heat the cheese blend. Samples (c) and (d), which contained modified starch, had more compact microstructures than samples (a) and (b). The appearance of the fat globules suggested that the emulsification process had been completed only in sample (c): the fat globules were spherical with few signs of their continuing separation. In contrast, the emulsification process was still in progress in the other samples when their processing had been terminated. This is evident from elongated fat particles or strings of fat particles not yet separated from each other.

Three commercial process cheeses purchased in retail stores were examined for comparison. Composition of the cheeses and the emulsifiers used were declared (in descending order) by the manufacturers as follows: processed Cheddar cheese (28% fat, 44% moisture, Na phosphate, Na-Al phosphate, Na triphosphate, Na citrate) (Fig. 19), processed Gruyère cheese A (25% fat, 43%

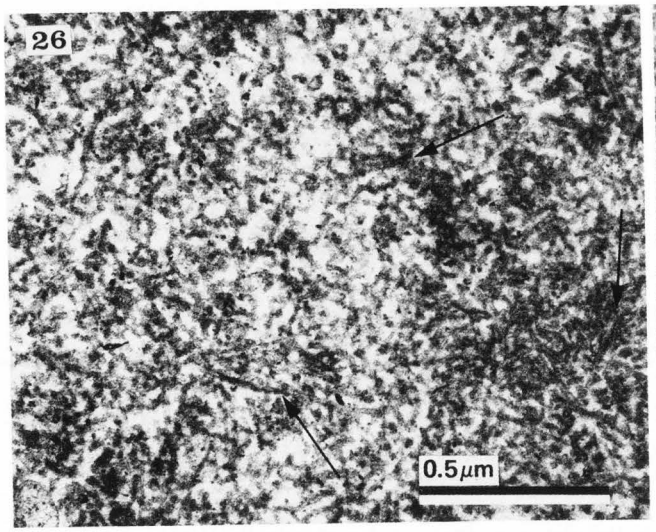

Fig. 26. Protein strands (arrows) are present in the protein matrix of a process cheese of the hard type (block process cheese) made with 2.2% sodium polyphosphate. Courtesy of T. Kimura.

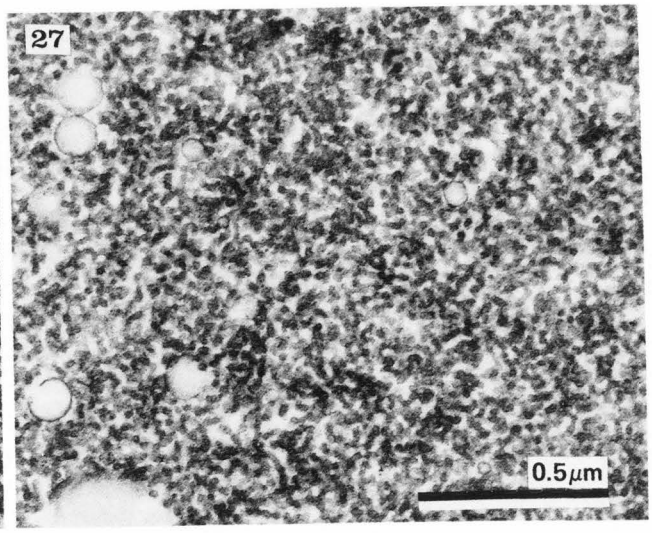

Fig. 27. Protein is in the form of single particles in the protein matrix of a process cheese of the soft type (process cheese spread) made with a mixture of 1% sodium citrate and 1.5% sodium polyphosphate. Courtesy of T. Kimura.

moisture, Na-Ca citrate) (Fig. 20), and processed Gruyère cheese B (23% fat, 46% moisture, Na citrate) (Fig. 21).

All the three commercial process cheeses examined differed in microstructure. The dimensions of fat globules in processed Cheddar cheese (Fig. 19) varied over a wide range (up to 20 μm in diameter). The incidence of salt crystals in freeze-fractured samples viewed by SEM was low. Calcium, phosphorus, sulphur, and aluminum were found by energy dispersive spectrometry (Fig. 22) to be present in the crystals (Fig. 23). In contrast, the processed Gruyère cheese samples (Figs. 21 and 22) had their fat emulsified to a considerably greater extent; in processed Gruyère cheese B, no fat globules were found to exceed the diameter of 5 μm. Also, in these cheeses there was a considerably higher incidence of melting salt crystals than in the processed Cheddar cheese. Calcium, phosphorus, sodium, and sulphur figured prominently in energy dispersive spectra (Fig. 24) of large crystals visible in sample B (Fig. 25), although this particular process cheese was made with sodium citrate. Evidently, there is discrepancy between the micrographs of this commercial cheese and process cheese made with sodium citrate on a laboratory scale. The commercial cheeses have been used to demonstrate the potential of electron microscopy and of energy dispersive spectrometry in studies of process cheese aimed at the elucidation of various relationships among its microstructure, composition, and physical properties.

Differences in the protein matrices of soft and hard process cheeses were studied by Kimura and Taneya (35), Kimura et al. (36), and Taneya et al. (68) using thin-sectioning and freeze-fracturing techniques for electron microscopy. The soft type process cheese had been made using a mixed emulsifying agent (1% sodium citrate and 1.5% polyphosphate). The cheese exhibited predominantly single particles in the protein matrix, whereas the hard process cheese (made with 2.2% polyphosphate) consisted of a network structure containing long protein strands (Figs. 26 and 27). The authors assumed that the protein strands contributed to the ability of hard process cheese to retain its shape on heating. The existence of the string-like protein structures was confirmed by Heertje et al. (20). Investigating the submicroscopic structure of process cheese, Tinyakov (72) reported microvacuoles with shape and size variations dependent upon the type of cheese. Cheeses produced with sodium citrate were found to have a fibrous structure.

Conclusions

Process cheese is a complex system composed of protein, fat, mineral salts, and other ingredients. Its properties are affected by many variables such as the composition and nature of the initial natural cheese, the nature and amount of the emulsifying agents, the manufacturing regimen, and additional factors. Emulsifying agents play one of the most important roles. Although a large number of such agents has been tested, citrates and phosphates have been used most frequently in process cheese manufacturing practice. To be used commercially, emulsifying agents must perform several functions at the same time and must not adversely affect the sensory attributes of the product. Because some emulsifying agents may perform better than others as far as individual functions are concerned, such emulsifying agents are combined in mixtures. In spite of their favourable technological properties, phosphates and polyphosphates have been raising the concern of nutritionists, because these salts introduce sodium and phosphorus into process cheese. In recent years, there has been a trend to reduce the concentration of sodium in foods. Effects of additives such as modified starch or mono- and diglycerides have been explored on an experimental scale.

Chemical composition and consumer acceptance are the ultimate criteria for process cheese. However, microscopy is very useful in examining the initial raw materials such as the natural cheese blend and, in particular, the effects of processing on the finished product. Optical as well as electron microscopy can reveal whether the amount of the emulsifying agents used is appropriate or excessive. The presence of large

amounts of emulsifying salt crystals indicates that such undissolved crystals do not participate in the emulsifying process and that the concentration of the emulsifying agent should be reduced. Fat globule dimensions are indicative of the extent of emulsification. The fat globule dimensions diminish as emulsification advances. Also the microstructure of the protein matrix is indicative of the extent of emulsification, during which casein first disaggregates and subsequently forms string-like structures.

It is assumed that future trends in process cheese research will be concerned with the development of new types of emulsifiers better acceptable from the nutritional viewpoint than the sodium phosphates used presently. Microscopy will play an increasingly important role in this research: conventional optical microscopy using specific staining techniques and fluorescence microscopy will be used to check the presence of salt crystals and the distribution of fat in the finished product. SEM in conjunction with energy dispersive spectrometry will make it possible to analyze the crystals. In conjunction with digital image analysis, SEM will be used to evaluate the distribution of fat globules in the product in greater detail. TEM is assumed to provide the solution to problems associated with the melting or the lack of it in cheese already processed. Defects in process cheese are a separate set of problems, to the solution of which all kinds of microscopy will contribute.

Acknowledgments

Skillful technical assistance provided by Mrs. Spasenija Milanović, MSc., and Mrs. Paula Allan-Wojtas, BSc., is acknowledged. The authors thank Dr. S. H. Yiu (Agriculture Canada, Ottawa) and Dr. T. Kimura (Snow Brand Milk Products Co., Ltd., Kawagoe, Japan) for permission to reproduce micrographs in Figs. 4, 11, 22, 24, 26, and 27, and Dr. H. W. Modler for useful suggestions. The SEM Photolaboratory, Faculty of Science at the University of Novi Sad, and the Electron Microscope Centre, Research Branch, Agriculture Canada in Ottawa provided facilities. This review is Contribution 652 from the Food Research Institute in Ottawa.

References

1. Becker E, Ney KH. (1965). Effect of different emulsifying salts on the quality and keeping quality of processed cheese. Z. Lebensmittelunters. Forsch. 127, 206-222 (In German).
2. Blanc B, Rüegg M, Baer A, Casey M, Lukesch A. (1979). Comparative tests on Emmental cheese with and without late fermentation. IV. Biochemical and physico-chemical comparison. Schweiz. Milchw. Forschung 8, 27-36 (In French).
3. Bohač V. (1984). Application of microscopy to cheese testing. In: The Collection of Papers from the Dairy Research Institute in Prague 1978-1983. L. Forman (ed.), Technical Information Centre for the Food Industry, Prague, Czechoslovakia, 203-212 (In Czech).
4. Bonell W. (1971). Chemico-physical process in the manufacture of processed cheese. Dte. Molkerei Ztg. 92, 1415 (In German).
5. Bottazzi V, Battistotti B, Bianchi F. (1982). The microscopic crystalline inclusions in Grana cheese and their X-ray microanalysis. Milchwissenschaft 37(10), 577-580.
6. Brooker BE. (1979). Milk and its products. In: Food Microscopy. J.G. Vaughan (ed.), Academic Press, New York, USA, 273-311.
7. Brooker BE, Hobbs DG, Turvey A. (1975). Observations on the microscopic crystalline inclusions in Cheddar cheese. J. Dairy Res. 42, 341-348.
8. Carić M. (1985). Dairy Technology I. Concentrated and Dried Dairy Products. 2nd ed. Naučna knjiga, Beograd, Yugoslavia, 294 pp. (In Serbian).
9. Carić M, Gavarić D, Milanović S, Kulić Lj, Kosovac Z. (1984). Investigations of the possibilities of imported additives substitution in process cheese production. Faculty of Technology, Novi Sad, Yugoslavia, 60 pp. (In Serbian).
10. Carić M, Gavarić D, Milanović S, Kulić Lj, Radovančev Ž. (1985). The effect of various emulsifying agents on process cheese quality. Mljekarstvo (in press) (In Serbian).
11. Csók J. (1982). The effect of holding time on free and bound water contents of processed cheese. XXI Int. Dairy Congress, Moscow, USSR, Mir Publishers, Moscow, Vol. I, Book 1, 475-476.
12. Daclin JP. (1968). Creamed Gruyère process cheese. Thesis No. 96. Ecole Nat. Vet. d'Alfort, France (In French).
13. Dean MR, Berridge NJ, Mabbitt LA. (1959). Microscopical observations on Cheddar cheese and curd. J. Dairy Res. 26(1), 77-82.
14. Ellinger RH. (1972). Phosphates as Food Ingredients. CRC Press, The Chemical Rubber Co., 18901 Cranwood Parkway, Cleveland, OH 44128, 69-76.
15. Flückiger E, Schilt P. (1963). Formation of salt crystals in Swiss cheese. Milchwissenschaft 18, 437-442 (In German).
16. Gavrilova NB. (1976). Improvement of structural and mechanical characteristics of sliced process cheese. Zernoper. Pishch. Prom. 1976(6), 131-136 (In Russian).
17. Glandorf K. (1973). Influence of processes, especially of UHT treatment, on various phosphates in the production of processed cheese. Dte. Molkerei Ztg. 94, 1020-1024, 1026 (In German).
18. Green ML, Turvey A, Hobbs DG. (1981). Development of structure and texture in Cheddar cheese. J. Dairy Res. 48, 343-355.
19. Hall DM, Creamer LK. (1972). A study of the submicroscopic structure of Cheddar, Cheshire and Gouda cheese by electron microscopy. New Zealand J. Dairy Sci. Tech. 7, 95-102.
20. Heertje I, Boskamp MJ, Kleef F van, Gortemaker FH. (1981). The microstructure of process cheese. Neth. Milk Dairy J. 35, 177-179.
21. Heide R von der. (1966). The binding capacity of phosphates. Dte. Molkerei Ztg. 87, 974-977 (In German).
22. Kairyukshtene I, Ramanauskas R, Antanavichyus A, Butkus K, Lashas V. (1973). Changes in cheese proteins and fat during the melting process with various emulsifying salts. Trudy, Litov. Filial Vsesoyuz. Nauchno-Isled. Inst. Maslodel. Syrodel. Prom. 1973(8), 85-96 (In Russian).
23. Kalab M. (1977). Milk gel structure VI. Cheese texture and microstructure. Milchwissenschaft 32, 449-458.
24. Kalab M. (1979). Microstructure of dairy foods. 1. Milk products based on protein. J. Dairy Sci. 62(8), 1352-1364.
25. Kalab M. (1979). Scanning electron microscopy of dairy products: An overview. Scanning Electron

Microsc. 1979;III:261-272.
26. Kalá̀b M. (1981). Electron microscopy of milk products: A review of techniques. Scanning Electron Microsc. 1981;III:453-472.
27. Kalá̀b M, Emmons DB. (1978). Milk gel structure. 9. Microstructure of cheddared curd. Milchwissenschaft 33(11), 670-673.
28. Kalá̀b M, Lowrie RJ, Nichols D. (1982). Detection of curd granule and milled curd junctions in Cheddar cheese. J. Dairy Sci. 65, 1117-1121.
29. Kapac-Parkačeva N. (1969). Effect of some emulsifying salts on chemical changes in processed cheese made from Kachkaval and Soft White cheeses. Sotsijal. Zemjodel. 21, 49-62 (In Macedonian).
30. Kapac-Parkačeva N. (1969). Effect of some emulsifying salts on the hardness of processed Kachkaval cheese and mixed Kachkaval and White cheese. Godisen. Zb. Zemjod.-Šum. Fak., Univ. Skopje-Zemjodel, Yugoslavia, 22, 49-62 (In Macedonian).
31. Karahadian C. (1984). Technological aspects of reduced-sodium process American cheeses. MSc. Thesis. University of Wisconsin, Madison, WI 53706.
32. Kicline TP, Stahlheber NE, Vetter JL. (1967). Basic alkali metal aluminum phosphate cheese emulsifier. US Patent 3337347.
33. Kiermeier F. (1962). The influence of inorganic phosphates on animal protein. IX. The use of polyphosphates in processed cheese manufacture. Z. Lebensm. Untersuch. 118, 128-140 (In German).
34. Kimber AM, Brooker BE, Hobbs DG, Prentice JH. (1974). Electron microscope studies of the development of structure in Cheddar cheese. J. Dairy Res. 41, 389-396.
35. Kimura T, Taneya S. (1975). Electron microscopic observation of casein particle in cheese. J. Electron Microsc. 24(2), 115-117.
36. Kimura T, Taneya S, Furuichi E. (1978). Electron microscopic observation of casein particles in processed cheese. XX Int. Dairy Congress, Paris, France, Congrilait,Paris, Vol. E, 239-240.
37. Kirchmeier O, Weiss G, Kiermeier F. (1978). Influence of different phosphates on the flow properties of processed cheese. Z. Lebensm. Untersuch. 166, 212-220 (In German).
38. Klostermeyer H, Uhlmann G, Merkenich K. (1984). Formation of crystals in processed cheese. II. Identification of a new citrate. Milchwissenschaft 39, 195-197 (In German).
39. Knoop A-M, Peters K-H. (1978). Is pasteurized Camembert cheese a process cheese? Dte. Molkerei Ztg. 34, 1186-1187 (In German).
40. Kosikowski FV. (1982). Cheese and Fermented Milk Foods. Edwards Brothers, Inc., Ann Arbor, Michigan, USA, 382-401.
41. Lapshina AD, Poplavets PI. (1976). Effects of some emulsifying salts on processing of semi-manufactured products. Nauch. Trudy, Omskii Sel'skokhoz. Inst. Im. S.M. Kirov 158, 46-50, 55-56 (In Russian).
42. Lee BO, Alais C. (1980). Biochemical study of the processing of cheese. II. Changes in phosphates and cations. Lait 60, 130-139 (In French).
43. Lee BO, Kilbertus G, Alais C. (1981). Ultrastructural study on processed cheese. Effect of different parameters. Milchwissenschaft 36, 343-348.
44. Lee BO, Paquet D, Alais C. (1982). Protein structure of processed cheese. XXI Int. Dairy Congress, Moscow, USSR, Mir Publishers, Moscow, Vol. I, Book 1, 504 (In French).
45. Lee Y, Marshall RT. (1981). Microstructure and texture of process cheese, milk curds and caseinate curds containing native or boiled soy proteins. J. Dairy Sci. 64, 2311-2317.
46. Lowrie RJ, Kalá̀b M, Nichols D. (1982). Curd granule and milled curd junction patterns in Cheddar cheese made by traditional and mechanized processes. J. Dairy Sci. 65, 1122-1129.
47. Mann EJ. (1981). Processed cheese. Dairy Ind. Int. 46, 13-14.
48. Meiji Milk Products K. (1981). Calcium-fortified processed cheese. Jap. Exam. Pat. 5619967.
49. Meyer A. (1973). Process Cheese Manufacture. Food Trade Press Ltd., London, UK, 1st ed., 330 pp.
50. Morris HA, Manning PB, Jenness R. (1969). Calcium citrate surface in process cheese. J. Dairy Sci. 52, 900.
51. Nakajima T, Tatsumi K, Furuichi E. (1972). Effect of melting salts on the texture of processed cheese. I. Effect of condensed phosphate on the texture of processed cheese. J. Agr. Chem. Soc. Japan 46, 447-457 (In Japanese).
52. Ney KH, Garg OP. (1970). Melting salt action of Na-trimetaphosphate. Jahresfachheft Molkereiwesen 72, 1 (In German).
53. Ney KH, Garg OP. (1970). Melting-salt action of Na-trimetaphosphate and Na-tetrametaphosphate. Fette Seifen Anstrichmittel 72(4), 279-285 (In German).
54. Rammell CG. (1960). The distribution of bacteria in New Zealand Cheddar cheese. J. Dairy Res. 27, 341-351.
55. Rayan AA. (1981). Microstructure and rheology of process cheese. Diss. Int. B, 41(8), 2954.
56. Rayan AA, Kalá̀b M, Ernstrom CA. (1980). Microstructure and rheology of process cheese. Scanning Electron Microsc. 1980;III:635-643.
57. Roesler H. (1966). Behaviour of polyphosphates in processed cheese. Milchwissenschaft 21, 104-107 (In German).
58. Rüegg M, Moor U, Blanc B. (1980). Changes in the fine structure of ripening Gruyère cheese. A scanning electron microscope study. Milchwissenschaft 35(6), 329-335.
59. Rüegg M, Moor U, Schneider J. (1985). On the size distribution and shape of the curd granules in Emmental cheese. Schweiz. Milchw. Forschung 14(1), 3-7 (In German).
60. Scharpf L. (1971). The use of phosphates in cheese processing. Symposium - Phosphates in Food Processing. The AVI Publishing Co., Inc., Westport, Connecticut, USA, 120-157.
61. Shimp LA. (1985). Process cheese principles. Food Technol. 39(5), 63-70.
62. Shubin EM, Kracheninin PF. (1960). Selection of salts for processed cheese manufacture. Trudy Tsentral. Nauchno-Issled. Inst. Maslodel. Syrodel. Prom. 1960(6), 75-85 (In Russian).
63. Shubin EM. (1961). Some structural and mechanical properties of processed cheese in relation to the emulsifying salts used. Izv. Vyss. Ucheb. Zaved., Pishch. Tekhnol. 1961(3), 70-74 (In Russian).
64. Sood VK, Kosikowski FV. (1979). Process Cheddar cheese from plain and treated retentates. J. Dairy Sci. 62, 1713-1718.
65. Steinegger R. (1901). Salt crystals, their chemical composition, development, and prevention. Landwirt. Jahrbuch Schweiz 15, 132-157 (In German).
66. Swiatek A. (1964). The effect of type and quantity of emulsifying salts on the consistency of pro-

cessed cheese. Milchwissenschaft 19, 409-413 (In German).
67. Tanaka N, Goepfert JM, Traisman E, Hoffbeck WM. (1979). A challenge of pasteurized process cheese spread with *Clostridium botulinum* spores. J. Food Prot. 42(10), 787-789.
68. Taneya S, Kimura T, Izutsu T, Buchheim W. (1980). The submicroscopic structure of processed cheese with different melting properties. Milchwissenschaft 35, 479-481.
69. Taranto MV, Wan PJ, Chen SL, Rhee KC. (1979). Morphological, ultrastructural and rheological characterization of Cheddar and Mozzarella cheese. Scanning Electron Microsc. 1979;III:273-278.
70. Thomas MA. (1977). The processed cheese industry. Dept. Agr. Bull. D44, New South Wales, Australia, 112 pp.
71. Thomas MA, Newell G, Abad GA, Turner AD. (1980). Effect of emulsifying salts on objective and subjective properties of processed cheese. J. Food Sci. 45, 458-459, 466.
72. Tinyakov VG. (1970). Study of the submicrostructure of cheese. Izv. Vyss. Ucheb. Zaved., Pishch. Tekhnol. 2, 165-167 (In Russian).
73. Tinyakov VG, Barkan SM. (1964). Effect of emulsifying salts on microstructural deposits of calcium in processed cheese. Izv. Vyss. Ucheb. Zaved., Pishch. Tekhnol. 1964(5), 62-63 (In Russian).
74. Uhlmann G, Klostermeyer H, Merkenich K. (1983). Formation of crystals in processed cheese. - I. The phenomenon and its sources. Milchwissenschaft 38(10), 582-585 (In German).
75. Yiu SH. (1985). A fluorescence microscopic study of cheese. Food Microstruc. 4(1), 99-108.
76. Zakharova NP, Gavrilova NB, Dolgoshchinova VG. (1979). The calcium-phosphorus ratio in processed cheese. Trudy, Uglich 27, 105-108, 121 (In Russian).
77. Zakharova NP, Gavrilova NB, Dolgoshchinova VG. (1979). Means of increasing the hydrophilic properties of the cheese mass. Trudy, Uglich 27, 108-111, 121 (In Russian).

Discussion with Reviewers

B. E. Brooker: How can the identity of crystals in cheese (Figs. 8-10) be so certain simply from the use of morphological features - especially in view of the results obtained by energy dispersive spectrometry (EDS) which seem to suggest that crystals with the same morphology as those purported to be sodium citrate do in fact contain Na, P, Ca, and S? More information should be given about the EDS analysis. How were the samples prepared and are Figs. 22 and 24 the results obtained from point or area analyses?

D. B. Emmons: EDS has indicated the presence of Ca and P in crystals assumed to be sodium citrate in the processed Gruyère cheese. Please comment.

Authors: Differences in the appearance of crystals in micrographs obtained with natural cheese and in micrographs of the same cheese to which a specific melting salt such as sodium citrate had been added have been attributed to the presence of the added salt. Preliminary results obtained by EDS have been shown only to demonstrate the potential of this technique. Fixed, dehydrated, defatted, and critical-point dried samples were mounted on carbon disks and coated with carbon. Area analyses were carried out at magnifications at which the crystals under study covered the SEM screen. EDS analysis of authentic salt crystals added to cheese is in progress in order to investigate the requirements of this technique.

D. B. Emmons: Could the absence of salt crystals in the process cheese made by the authors (Figs. 15-18) be due to using cheeses low in calcium and phosphate (acid cheeses such as White cheese?).

Authors: This is one possibility and the other is the use of direct steam to heat the cheese blend. Interestingly, the presence of White cheese in the process cheese was detected by preliminary TEM studies (unpublished) by the observation of the characteristic core-and-lining ultrastructure (80).

I. Heertje: It is mentioned that the suitability of the starting cheese for processing was assessed from the dimensions of the fat globules and the amount of fat released and from the melting temperature. Are these considered to be proper criteria in view of the fact that at that stage of observation no melting salts have been added?

Authors: The tests referred to were carried out by V. Boháč (Department of Cheese Technology, Dairy Research Institute, Tábor, Czechoslovakia), who has adapted a polarizing microscope specifically for the studies of cheese processing. Release of the fat globules and their dimensions were studied in relationship to the temperature of the cheese in the presence of melting salts.

D. P. Dylewski: What is "compact microstructure"? Can it be determined using morphometry or stereology?

Authors: Compact microstructure is characterized by the absence of void spaces resulting from the presence of air or whey pockets. We believe that morphometric analysis, particularly of cheese fixed with imidazole-buffered osmium tetroxide to retain fat will be useful in evaluating the compactness of the cheese protein matrix.

I. Heertje: Do all fat globules appear as cavities (Fig. 14)? Is this caused by the preparation procedure?

Authors: Fat globules were removed from the process cheese samples by extraction with chloroform prior to freeze-fracturing and, therefore, cavities are seen in the micrographs, where fat globules had been in the cheese. Not all cavities, however, originate from the removal of fat. Whey pockets and air bubbles also appear as void spaces. Fat globules may be retained in the sample by fixation with imidazole-buffered osmium tetroxide (78, 80).

D. P. Dylewski: How important are ultrastructural immunocytochemical studies of process and natural cheese? Would knowledge of protein distribution and interactions during cheese development be important?

Authors: Immunochemical studies of cheese and process cheese may be important to better understand allergies to these milk products. Then attempts can be made to locate individual proteins in the cheese matrix by immuno electron microscopy. Concerning the distribution of proteins and their interactions during cheese development and processing, very little is known about these phenomena. Proteolysis in Meshanger cheese was studied by fluorescence and interference light microscopy and by electron microscopy (79). By electron microscopy, protein in process cheese was found to form matrices having different ultrastructures depending on whether the product was soft or hard. String-like structures were

present in hard process cheese (35, 36, 68). Heertje et al. (20) assumed that such structures resulted from an association mechanism at the molecular level; they supported their assumption by reports that other proteins such as ovalbumin, insulin, and lysozyme produced similar structures on gelling under the effect of heat. The authors (20) consider string-like structures to be formed by unfolding of the protein molecules, followed by their non-random aggregation into continuous network structures.

I. Heertje: It is very striking that of the four investigated samples, only the modified starch product (Fig. 17) shows proper fat globules. Can you offer an explanation for this behaviour, considering that the starch will not act as an emulsifier?
Authors: Apart from mentioning that starch binds water and reduces the amount of free water in the cheese, we cannot comment until additional experiments are carried out using various cheese blends and melting salts in the presence or absence of modified starch.

I. Heertje: Is it likely that the distortion of the fat globule shapes in Fig. 9 is caused by some preparation artefact or by the image formation? The phosphate crystal appears to form the bottom of a crater and the 'distorted' globules are at the slopes of the crater.
Authors: A pair of stereo micrographs had not been taken to confirm your assumption that there is a slope between the crystal and the body of the cheese. It is probable that such a slope really exists although it should not. The fixed cheese sample under study had been dehydrated in ethanol, defatted in chloroform, impregnated with ethanol, and freeze-fractured. This procedure usually produces flat and smooth fracture planes. There is evidently an exception to this rule as shown in Fig. 9.

B. E. Brooker: The experimental process cheeses produced from Cheddar cheese and different combinations of emulsifying agents showed variation in the degree of fat dispersion. What effect does this have on the mechanical and textural properties of the cheese?
Authors: Processed Cheddar cheese was of commercial origin. Experimental cheeses were made from a mixture of Feta, Gouda, Kachkaval, and White cheeses. In general, fat emulsified into fine globules makes a firmer process cheese than fat present in the form of large globules. The total surface of very finely dispersed fat globules may be so high that there would not be enough protein to cover all the fat. The excess fat would separate as oil during processing and leave a hard nonmeltable cheese. This effect may be caused by tetrasodium pyrophosphate (with a high affinity for calcium), whereas sodium hexametaphosphate (with a lower affinity for calcium) produces a hard cheese without oil separation. Disodium phosphate (with a low affinity for calcium) produces a soft and meltable cheese which has large fat globules (81). In addition to the emulsifying salts used, the composition of the cheese blend and, in particular, heating of the blend with direct steam were other important factors which affected the physical properties of our experimental cheeses.

Additional References

78. Allan-Wojtas P, Kalab M. (1984). Milk gel structure. XIV. Fixation of fat globules in whole-milk yoghurt for electron microscopy. Milchwissenschaft 39(6), 323-327.
79. Jong L de.(1978). Protein breakdown in soft cheese and its relation to consistency. 3. The micellar structure of Meshanger cheese. Neth. Milk Dairy J. 32, 15-25.
80. Kalab M, Modler HW. (1985). Development of microstructure in a Cream cheese based on Queso Blanco cheese. Food Microstruc. 4(1), 89-98.
81. Shimp LA. (1983). Basic knowledge simplifies choice. Dairy Field 166(10), 116-117.

FOOD MICROSTRUCTURE, Vol. 4 (1985), pp. 313-321
SEM Inc., AMF O'Hare (Chicago), IL 60666-0507 U.S.A.

0730-5419/85$1.00+.05

PROPERTIES OF CALCIUM CASEINATES WITH DISPARATE PERFORMANCE IN IMITATION CHEESE

K. Fleming*, R. Jenness**, H. A. Morris*, R. Schmidt***

*Department of Food Science and Nutrition
**Department of Biochemistry
University of Minnesota
St. Paul, Minnesota 55108

***Department of Food Science and Human Nutrition
University of Florida
Gainesville, Florida 32611

Abstract

Two commercial lots of calcium caseinate preparations differing in performance in imitation cheese were analyzed for various characteristics. A imitation process cheese manufacturing classified the caseinates as good or poor based on appearances of the finished cheese, emulsification of fat, oiling-off during sheeting and melting properties. The sample which exhibited good functional properties in imitation cheese, had slightly higher calcium (16.4 mg/g protein), non-casein protein (2.87%) and γ-casein contents, a higher formol titre (8.95 mg free amino N/g protein), lower water absorption (138 mg/100 g protein), and lower stability to added calcium (8.0 min) than did the other sample (14.6 mg/g, 1.66%, 8.02 mg/g, 129 mg/100 g, and 15 min, respectively), which was described as having poor functionality according to the criteria of the imitation cheese producer.

Initial paper received February 11 1985
Manuscript received July 15 1985
Direct inquiries to H.A. Morris
Telephone number: 612 373 1076

KEYWORDS: Calcium caseinate; imitation cheese, γ-casein, scanning electron microscopy, water absorption.

Introduction

Calcium caseinates are being widely used in the manufacture of imitation cheeses and other food products. Functional properties of caseinates have been investigated in protein dispersions and in model systems (Hermansson, 1972, Hermansson and Akesson, 1975) and in imitation cheese systems (Hokes 1982, Hokes et al., 1982). Moreover, the relationship between casein structure and functionality has been reviewed (Morr 1979). Unfortunately, caseinates vary markedly in how they function in imitation cheese blends during manufacture and in their influence on the properties of the finished products. Development of a satisfactory formula and processing method does not always ensure a marketable product. Calcium caseinate exhibiting poor functionality may produce rough appearing imitation cheese that oils-off during sheeting, and does not melt satisfactorily. Further research data are needed to relate the properties of calcium caseinate to its performance in imitation cheese and to provide insight as to why variations occur. Therefore, the purpose of this investigation was to study selected physical and chemical properties of two commercial calcium caseinate samples that have been shown to have different functionalities in imitation cheese manufacture.

Materials and Methods

Caseinate Dispersions

Two calcium caseinates produced by two different manufacturers were chosen for this study. One caseinate exhibited good functionality in imitation cheese while the other was described as having poor functionality according to the criteria of an imitation cheese producer. Functionality evaluations were based on amount of oiling-off, melting properties, appearance of the product, mixing and emulsification problems. The good sample is of Dutch origin and is probably from Fresian (Holstein cows) and the poor sample is from New Zealand and probably from Jerseys. Caseinate solutions were prepared by dispersing caseinate powders in double distilled, deionized water at 35-40°C and by stirring for at least 30 min. with a magnetic stir bar.

Compositional Analyses

Moisture. One g samples were weighed into dried, preweighed, porcelain ashing dishes. Samples were dried in a vacuum oven at 70°C to a constant weight.

Ash and Mineral Determination. Following moisture determination, the casein samples were ashed overnight at 600°C cooled and weighed. Ash solutions were prepared by moistening the ash with water, dissolving in 5 ml of 1 N HCl, and adding distilled water to a final volume of 100 ml. Aliquots from these solutions were analyzed for phosphorus by the colorimetric method of Sumner (1944) and for calcium using the EDTA titration method of Jenness (1953).

Nitrogen Determination. The total, non-casein, and nonprotein nitrogen contents were determined using the semi-micro Kjeldahl method of Larson and Jenness (1950). Total nitrogen was determined directly on the casein sample. Noncasein and nonprotein nitrogen were determined on a 3% dispersion. A factor of 6.32 was used to calculate protein from the nitrogen content (Walstra and Jenness, 1984).

Soluble Calcium, Soluble Phosphorus, and Lactose Determinations. Fifteen ml of water was dialyzed against 1500 ml of 3% casein (or caseinate) dispersion (pH 7.0) at 4°C. After 24 h, the protein dispersion was changed and dialysis continued for an additional 24 h. The dialysate was then analyzed for lactose by the method of Marier and Boulet (1959), for phosphorus as previously described, and for calcium by the Nickerson et al. method (1964).

Formol Titration. Formol titration for free-amino nitrogen followed the procedure of Kuehler and Stine (1974). Three 5-ml aliquots of each 2.5% casein dispersion were titrated with 0.0183 N NaOH following the formaldehyde addition. Free-amino nitrogen was calculated as follows: mg free-amino N = (ml NaOH to pH 8.5) x (0.0183 N NaOH) x (14 mg N/meq. N).

Fat Determination. Fat content was determined by Soxhlet extractions using petroleum ether according to AOAC method 24.005 (1980).

Caseinate Properties

Buffering Capacity. Titration curves (buffering capacities) of 1, 2 and 3% caseinate dispersions were determined by titration with 1 N HCl from approximately pH 7.0 to pH 5.5. A Beckman 3550 digital pH meter was used to measure the pH one minute after each 20 l addition of HCl. Measurements were taken at 22°C with constant agitation.

Water Absorption. The absorptive capacity of the calcium caseinates was determined using the Brabender farinograph and the Baumann capillary device.

The farinograph was used according to the constant flour weight method (Locken et al., 1972). The method, using 300 g of flour on a 14% moisture basis, was modified by replacing 15 g of the flour with calcium caseinate. The required water was added within 30 sec and the absorption was determined at 30°C. Sample absorption was calculated as follows: Absorption (ml H_2O/100 g sample) = 100(x-y)/g protein in 15 g sample where x is the amount of water required in the caseinate determination, y is the amount of water absorbed by 300 g of flour (14% moisture basis), and (x-y) is the amount of water absorbed by 15 g of sample.

The dough stability time was measured and is defined as the difference in time between the point where the curve is first centered on the 500 Brabender units (B.U.) line and the point where the curve begins to leave the 500 B.U. line.

Water uptake using the Baumann capillary device was determined as described by Wallingford and Labuza (1983). Thirty to thirty-five mg of caseinate were used for each of four replicate determinations at 18°C. The absorption due to the filter paper (0.0204 ml) was substracted from the water uptake prior to plotting.

Stability in the Presence of Calcium and Phosphate. The stability of the caseinates in the presence of calcium and phosphate ions was determined using a method described by Thompson et al. (1969) with several modifications. Stock caseinate dispersions were treated with varying levels of $CaCl_2$ (0-20 mM) or K_2HPO_4 (0-100 mM), centrifuged, and the supernatant protein concentration determined as follows:

1) Four ml of stock calcium caseinate solution (5 mg/ml) were added to a 20 ml centrifuge tube containing 5 ml of 0.1 M imidazole-HCl buffer (pH 7.0) and 1 ml of $CaCl_2$ or K_2HPO_4 solution.
2) The tubes were inverted twice and incubated for 30 min at 30°C in a water bath.
3) The protein dispersions were centrifuged at 1500 x g for 15 min in an International Equipment Company (IEC) centrifuge.
4) Two ml of supernatant was mixed with 7 ml of water and 1 ml of 1 N sodium citrate.
5) Absorbance at 280 nm was converted to protein concentration using a standard curve based on total nitrogen as determined by semi-micro Kjeldahl. Supernatant protein was expressed as percent soluble protein.

Solvation. The solvation studies were performed in duplicate and at two centrifugal forces. The procedure, adapted from Thompson et al. (1969), was as follows:

1) Dry and weigh cellulose nitrate tubes (w_0).
2) Pipette 5 ml of 35 mg/ml caseinate dispersion into the preweighed tubes.
3) Centrifuge at 68,000/140,000 x g for 30 min at 20°C.
4) Remove the top 2 ml of supernatant and analyze for protein by the modified Lowry method (Hartree, 1972).
5) Drain tubes inverted for 5 min.
6) Weigh the tubes with pellets (w_1).
7) Freeze-dry the tubes and pellets for 20 hr and reweigh (w_2).
8) Calculate solvation by the following formula: Solvation g H_2O/g caseinate = w_1-w_2/w_2-w_0

Sedimentable Matter. To quantify the amount of unstable casein material, caseinate dispersions were treated in triplicate according to the method of Roeper (1977).

Ion Exchange Chromatography

Caseins were alkylated and chromatographed as described by Davies and Law (1977) except that

the flow-rate was maintained at 20 ml/hr with a peristaltic pump. The NaCl gradient was supplied from an eight-chambered gradient former with each chamber holding approximately 125 ml. Chambers 1-4 initially contained buffer with 0.03 M NaCl while chambers 5-8 contained buffer with 0.22 M NaCl. Column eluate was collected in 5.0 - 5.5 ml volumes using a Gilson microfractionator. Approximately 900 ml were collected and the absorbance of each fraction determined at 280 nm relative to buffer. Fractions were pooled according to the elution profile, dialyzed against distilled water, and freeze-dried. Peaks were characterized by disc gel electrophoresis according to Groves (1975) at pH 9.5 with 4 M urea. Duplicate samples were separated by chromatography. Protein recovery was calculated from the absorbance of a 1% solution at 280 nm in a 1 cm cell ($A^{1}_{1\%,}{}^{cm}$280 nm), the volume, and the absorptivity according to Rose et al. (1969).

Scanning Electron Microscopy (SEM) of Calcium Caseinates

A piece of double sticky tape was attached to an aluminum SEM stub and a small amount of dry calcium caseinate was applied to the tape. Fractured particles were prepared by slicing through the powder with a razor blade. Loose particles were removed from the tape by a stream of air. Silver paint was applied to the tape edge providing a conductive surface between the metal-coated particles and the metal stub. The stubs were coated with Au/Pd by vacuum evaporation and viewed under a Philips 500 scanning electron microscope at 12 kV.

Results and Discussion

Compositional Analyses

The results of the compositional analysis are given in Table 1. The caseinate exhibiting good functionality in imitation cheese had higher levels of ash, fat, lactose, noncasein protein, calcium (total and soluble), and phosphorus (total and soluble) than the poor caseinate. Formol titration data are given in Table 2. The poor caseinate had a titration value reasonably close to the theoretical calculation based on lysine content of bovine casein and noncasein protein. In contrast, the good caseinate had a considerably larger amount of free amino groups. This higher value may suggest a conformational difference, presence of more protein fragments of low molecular mass or a higher degree of protein hydrolysis. A study by Creamer and Matheson (1977) in New Zealand showed that when casein curd is dissolved in alkali at high pH and temperature, the protein is extensively damaged by hydrolysis of some peptide bonds and modification of some individual amino acids. Examination of 43 commercial samples showed amino acid modification to be absent from 27 New Zealand sodium and calcium caseinate samples. Six caseinates from other sources, including two calcium caseinates from The Netherlands, contained substantial amounts of lysinoalanine resulting from modified amino acids and indicating excessive alkali treatment during manufacture. Thompson and Farrell (1973) noted that exposure to high pH, as

Table 1. Composition of calcium caseinates

Sample	Moisture (%)	Ash (%)	Casein Protein (%)	Noncasein Protein (%)	Fat (%)
Good	7.27	3.64	81.2	2.87	2.62
Poor	6.82	3.42	85.3	1.66	1.22

Sample	Lactose (%)	Calcium Total (mg/g casein)	Calcium Soluble (mg/g casein)	Phosphorus Total (mg/g casein)	Phosphorus Soluble (mg/g casein)
Good	0.14	16.4	2.85	9.27	0.69
Poor	0.02	14.6	1.19	6.14	0.33

Table 2. Formol titration of caseinate dispersions

Sample	mg free-amino N / g protein
Good calcium caseinate	8.95
Poor calcium caseinate	8.02
Casein - theoretical value	7.84*

* Walstra and Jenness (1984)

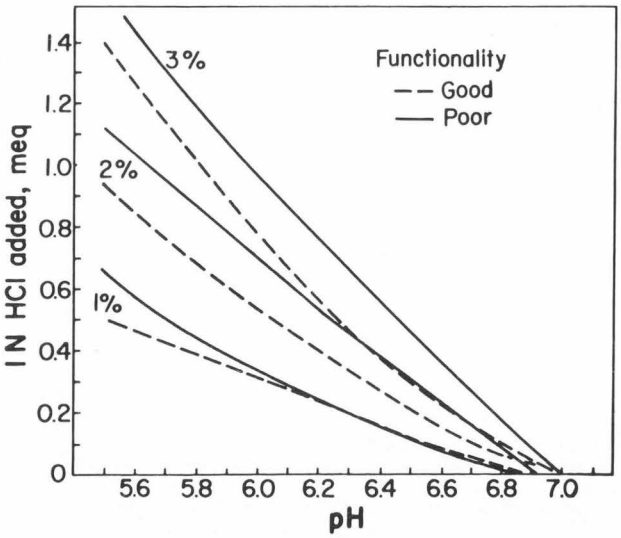

Figure 1. Titration curves (buffering capacities) of 1, 2, and 3% calcium caseinate dispersions. (100 ml of solution was titrated.)

in the production of caseinates, may result in protein degradation and lead to a product with altered characteristics.

Our formol titration data (Table 2) suggest that the good calcium caseinate may have been partly hydrolyzed during its manufacture. Such hydrolysis would liberate α-amino groups and might cleave off relatively lysine-poor fragments of low molecular mass that would be lost in whey or washings during manufacture. Hydrolysis by the enzyme plasmin resulting in the formation of γ-casein from β-casein actually lowers the lysine content of casein because the small peptides (proteose-peptone) lost in the whey are relatively richer in lysine than β-casein. An increase in formol titer signifies that increase in amino groups resulting from hydrolysis more than compensates for any loss of amino groups by interaction of lysine with sugar aldehydes or the formation of lysinoalanine.

Properties of Good and Poor Calcium Caseinates

Buffering Capacity

Titration curves for 1, 2, and 3% caseinate dispersions are shown in Fig 1. In the pH range 5.5 to 7.0, the good caseinate required less acid to achieve any given pH at the three protein levels titrated. The higher level of soluble calcium (2.85 mg/g casein) in the good sample may potentially result in the screening of ester phosphate groups and, therefore, in the suppression of the protonation of primarily phosphoserine residues. Comparison of titers of the two samples is complicated by differences in their contents of calcium and phosphate.

Water Absorption

The two methods used to determine water absorption - the farinograph and the Baumann capillary device - represent entirely different experimental conditions. The farinograph measures the viscosity of a dough containing approximately 5% caseinate. Water absorption in this system is due to several factors including the competitive absorption by flour. The Baumann capillary device, on the other hand, measures the water uptake due to the capillary suction pressure and swelling of the particles. Variations in particle porosity and swelling ability of the caseinates may be observed using this method.

Results from the Brabender farinograph experiment are shown in Table 3. The dough containing the good calcium caseinate absorbed more water than the poor sample and had a considerably shorter stability time, 8 min, compared to 15.0 min. Water-soluble constituents are known to have an effect upon the mixing characteristics of the dough. The higher level of soluble calcium in the good sample may have resulted in more protein calcium interaction thus causing water exclusion and a lower viscosity.

The mean absorption data of four replicate determinations for poor and good caseinates are plotted in Fig. 2. The poor sample, contrary to the farinograph data, absorbed more water throughout the 100 min test period. Microscopy data would have been helpful to observe the swelling and breakdown of the particles. It is tempting to speculate that the lower water uptake by the good sample may be due to a faster rate of particle breakdown. Our limited data suggest that the capillary device may be useful in distinguishing between caseinates with different swelling properties. Particle size and variations in particle porosity caused by different drying methods may influence swelling behavior.

Stability in the Presence of Calcium and Phosphate

Data presented in Fig. 3 show that the good sample was less soluble in the presence of increased levels of $CaCl_2$ than was the poor sample possibly reflecting a difference in protein aggregation. The phosphate ion stability experiment (Fig 4) shows that both caseinates were quite stable over a wide range of phosphate concentrations. The good caseinate, consistently exhibited lower (approximately 5% lower) stability than the poor sample.

Solvation

Results from the solvation experiments are tabulated in Table 4. At a centrifugal force of 68,000 x g good calcium caseinate had more protein in the pellet and a higher degree of solvation. However, unlike the poor sample, the good caseinate did not form an intact pellet which made complete draining difficult. At 140,000 x g both samples were compacted to the point of excluding water and were easily drained. In this case, the poor caseinate was slightly more solvated at 3.64 g H_2O/g solid compared to 3.39 g H_2O/g solid for the good one. The good sample again had more protein in the pellet suggesting a higher amount of unstable casein material or larger protein aggregates in the dispersion.

Sedimentable Matter

After centrifugation at 300 x g for 10 min the good caseinate dispersion had a mean sedimentation volume of 2.67 ml/10 ml of 5% dispersion. The poor caseinate had no visible sedimentation. After an additional 10 min at 300 x g, the poor sample had an average of 0.5 ml sediment/10 ml dispersion. The good caseinate showed an increase of 0.1 ml sediment after the additional 10 min centrifugation. According to Roeper (1977) volumes of 2.77 and 0.5 ml/10 ml represent approximately 83 and 15% respectively of the weight of the powder. The high amount of sedimentable matter in the good caseinate may partly explain the lower soluble protein values in the calcium and phosphate stability experiments. The amount of sedimentable matter has been used as a criterion for assessing the rate and completeness of conversion of casein into caseinate and the amount of unstable material in reconstituted spray dried calcium caseinate. Roeper (1977) discusses manufacturing variables that account for large sedimentation (> 1.0 ml/10 ml) volumes. Our data again suggest the possibility of manufacturing differences between the two caseinates.

Ion-Exchange Chromatography

Figure 5 shows the elution profiles for the alkylated calcium caseinates when subjected to ion-exchange chromatography. Protein recovery was greater than 92% for both samples. Elution began at approximately 30 ml and stopped at approximately 730 ml. Based on the profile and

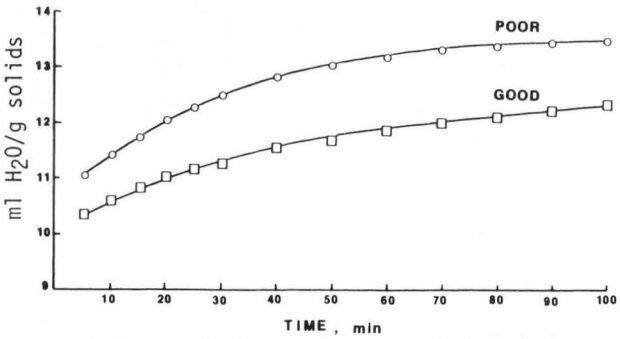

Figure 2. Water absorption or swelling behavior of calcium caseinates as determined by the Baumann capillary suction method.

Table 3. Effect of good and poor caseinates on water absorption of doughs determined using the Farinograph

Dough with	Water Absorption (%)	(mg/100g protein)	Stability (min)
no caseinate	62.7	498	7.0
good caseinate	118	138	8.0
poor caseinate	113	129	15.0

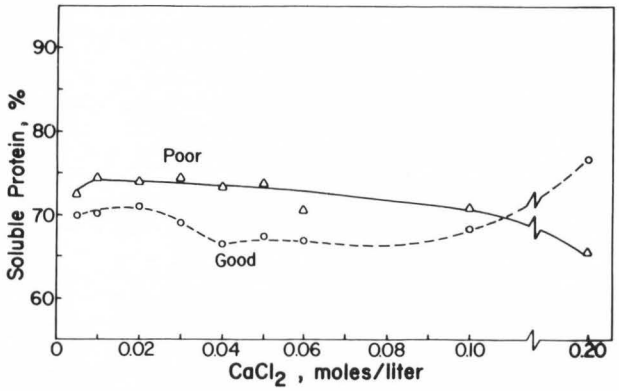

Figure 3. Stability of calcium caseinates in the presence of calcium ions. Plots are mean values from four experiments.

Table 4. Solvation of calcium caseinates

Force[1]	Calcium caseinate	Solvation H_2O g / solid g	Solvation H_2O g / protein g	Supernatant protein (%)
68,000	good	5.81	6.17	57.1
	poor	5.15	5.35	68.4
140,000	good	3.39	3.65	68.5
	poor	3.64	3.83	76.5

[1]Centrifugal force (x g)

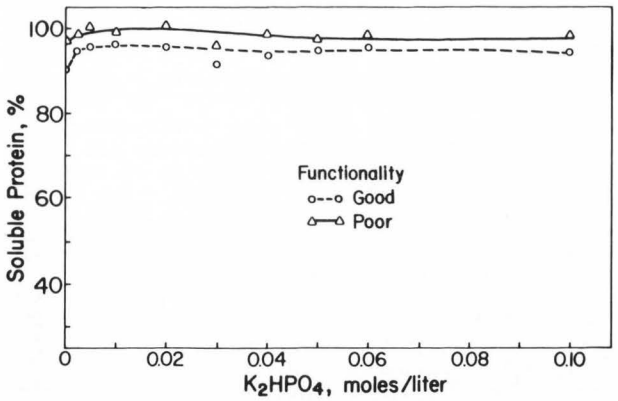

Figure 4. Stability of calcium caseinates in the presence of phosphate ions.

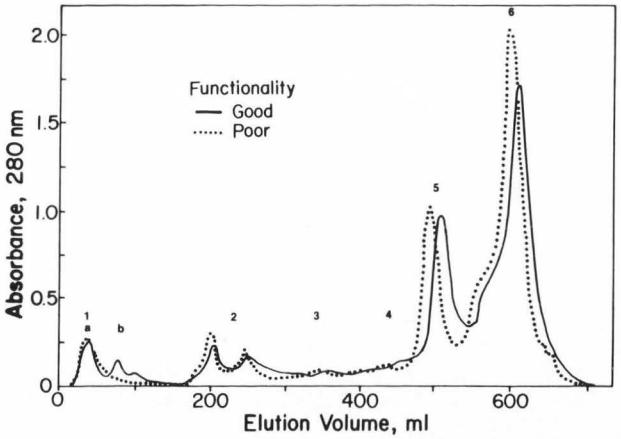

Figure 5. The fractionation of alkylated calcium caseinates by ion-exchange chromatography.

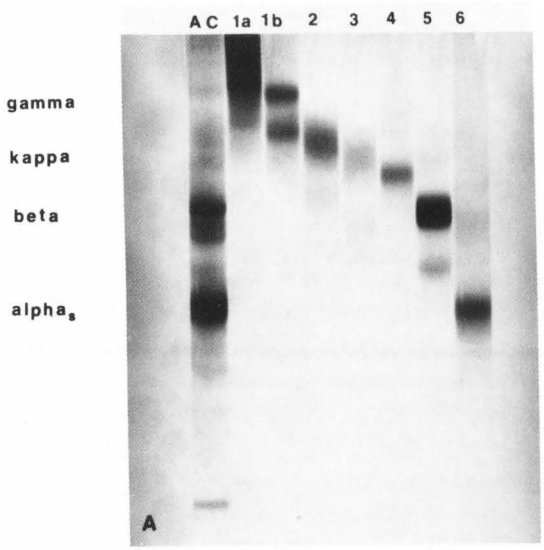

Figure 6. Disc ge lectrophoretic patterns for A) alk ed good calcium caseinate (AC) ar or peaks 1a, 1b, 2-6 as shown i igure 5; and B) alkylated poor ca um caseinate (AC) and for peaks 1 as shown in Fig. 5.

Figure 7. SEM micrographs of calcium caseinate powders: A) and B) are intact particles of the good caseinate; C) is a fractured particle from the good caseinate; D) and E) are particles of the poor caseinate and F) is a fracture particle from the poor caseinate.

data presented by Davies and Law (1977), the eluate was pooled into seven peaks for the good caseinate designated 1a, 1b, 2, 3, 4, 5, and 6, and into six peaks for the poor sample designated 1 through 6. The profiles show a number of main features common to both samples; however, the good caseinate had an initial elution of two peaks (1a and 1b) whereas the poor caseinate only had one initial peak. The numbers shown on the profiles correspond to the peaks subjected to disc gel electrophoresis (Fig 6). The gel pattern for peak 1a of the good sample shows the elution of some minor protein components. No distinct γ-casein bands were seen in 1a on this gel despite the application of a relatively large amount of protein. The eluate from peak 1b contained γ- and κ-caseins. In contrast, the poor caseinate eluate from peak 1 contained γ- and κ-caseins. The patterns for peaks 2-6 are identical for both samples. Peaks 2 and 3 consisted of κ-casein, peak 5 of β-casein, and peak 6 of α_s-caseins. Peak 4 is probably some type of modified β-casein, possibly dephosphorylated β-casein, as suggested by Davies and Law (1977).

Although the elution profiles for both samples are essentially the same, except for peak 1b, the absence of a distinct γ-casein band in peak 1a of good caseinate and the elution of two peaks initially suggest some differences in minor protein components or fragments. A study by Hokes et al. (1982) on the curd formation of calcium caseinates showed that following the formation of a protein aggregate, the remaining supernatant was "rich" in γ-casein and minor milk proteins. The authors suggested that further research was necessary to determine if the differences in the functional performance of different calcium caseinates are related to a variable amount of the proteins found in the supernatant. Our ion-exchange data support the need for further research in this area.

SEM

Figure 7 shows some obvious structural differences between good and poor calcium caseinates. The good caseinate had more spherical particles which were generally less indented. Approximately 60% of the particles were less than 10 μm in diameter. In contrast, the poor caseinate particles were imploded to a higher degree and had a more even particle size distribution with approximately 50% of the particles in the 11-30 μm range. Inside, the particles appeared to be similar. Whether or not these differences have an influence on functionality would need to be explored more fully.

Chemical and functional anaylsis of calcium caseinates with disparate functionalities in imitation cheese has shown differences in the following respects:

- amount of soluble minerals
- amount of free-amino nitrogen determined by formol titration
- elution profile when separated by ion-exchange chromatography
- water absorption determined with the Baumann capillary device
- amount of sedimentable matter in a 5% dispersion

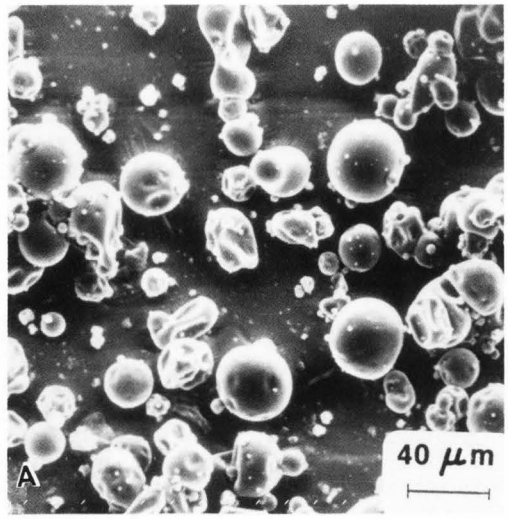
A
40 μm

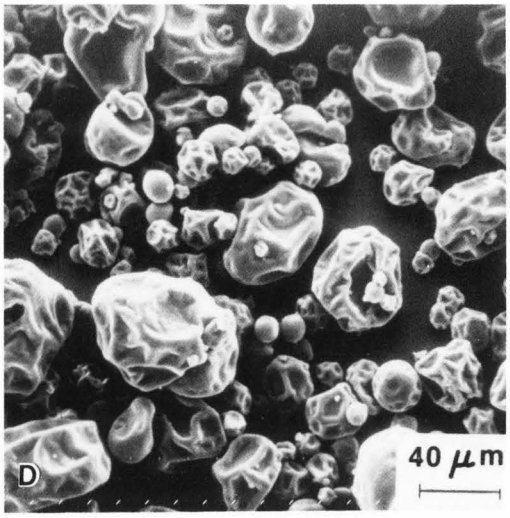
D
40 μm

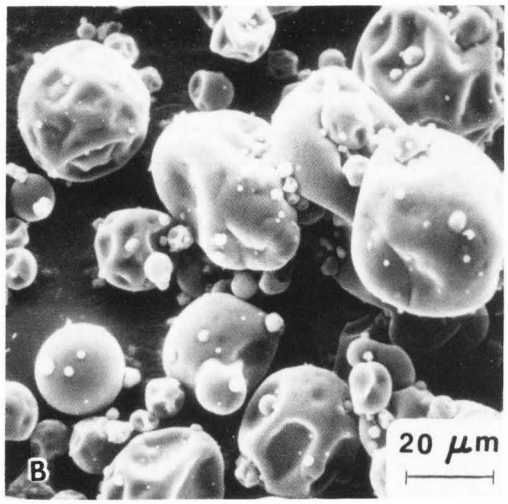
B
20 μm

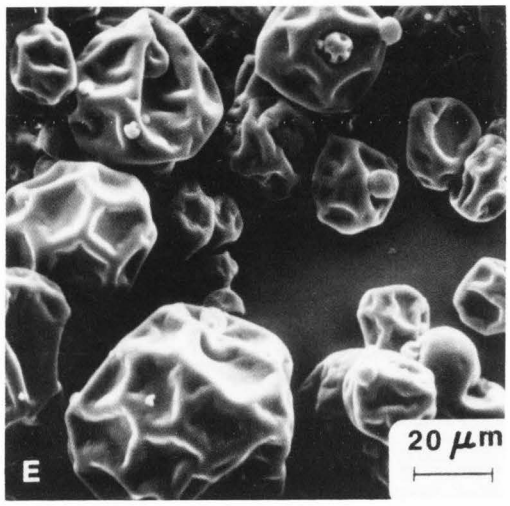
E
20 μm

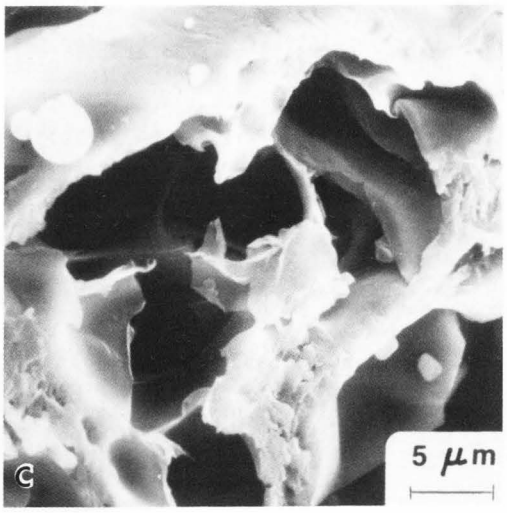
C
5 μm

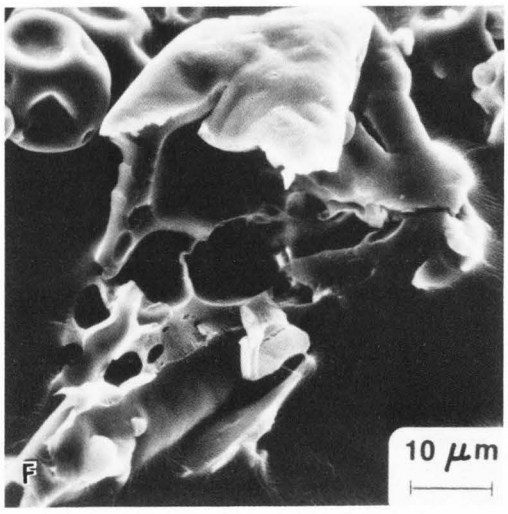
F
10 μm

Since a limited sample size was used, a larger number of samples would be necessary to determine the significance of the differences observed. Further study would also be necessary to determine whether the solvation or calcium ion stability data are useful in characterizing the caseinates.

The calcium caseinate described as having good functionality in imitation cheese appeared to have been prepared under conditions resulting in a higher degree of hydrolysis as indicated by formol titration and ion-exchange chromatography, and/or under conditions resulting in incomplete conversion as suggested by the amount of soluble minerals and sedimentable matter.

Acknowledgements

Published as Paper No. 14,336 of the scientific journal series of the Minnesota Agricultural Experiment Station on research conducted under Minnesota Agricultural Experiment Station Project No. 18-79 supported by Hatch Funds.

References

Association of Official Analytical Chemists (AOAC). (1980). Method of Analysis (13th ed.). Association of Official Analytical Chemists, Washington, D.C. Section 24.005.

Creamer LK, Matheson, AR. (1977). Action of alkali on casein. N.Z. J. Dairy Sci. Technol. 12, 253-259.

Davies DT, Law AJR. (1977). An improved method for the quantitative fractionation of casein mixtures using ion-exchange chromatography. J. Dairy Res. 44, 213-221.

Groves ML. (1975). Disc gel electrophoresis of minor milk proteins. Methods of Gel Electrophoresis of Milk Proteins, (H. Swaisgood, ed.), American Dairy Science Association Nomenclature and Methodology of Milk Proteins Committee, 26-29.

Hartee EF. (1972). Determination of protein: a modification of the Lowry method that gives a linear photometric response. Anal. Biochem. 48, 422-427.

Hermansson AM. (1972). Functional properties of proteins for food-swelling. Lebensm-Wiss. u. Technol. 5, 24-32.

Hermansson AM, Akesson C. (1975). Functional properties of added proteins correlated with properties of meat systems. Effect of concentration and temperature on water-binding properties of model meat systems. J. Food Sci. 40, 595-602.

Hokes JC. (1982). An analysis of the functional properties of calcium caseinate as related to imitation processed cheese. Ph.D. Thesis. Ohio State University, Columbus, Ohio.

Hokes JC, Mangino ME, Hansen PMT. (1982). A model system for curd formation and melting properties of calcium caseinates. J. Food Sci. 47, 1235-1240, 1249.

Jenness R. (1953). Titration of calcium and magnesium in milk and milk fractions with ethylene diamine tetraacetate. Anal. Chem. 25, 966-968.

Kuehler CA, Stine CM. (1974). Effect of enzymatic hydrolysis on some functional properties of whey protein. J. Food Sci. 39, 379-382.

Larson BL, Jenness R. (1950). The reducing capacity of milk as measured by an iodimetric titration. J. Dairy Sci. 33, 896-903.

Locken L, Loska S, Shuey WC. (1972). The Farinograph Handbook, American Association of Cereal Chemists, Inc., St. Paul, Minnesota. 1-71.

Marier JR, Boulet M. (1959). Direct analysis of lactose in milk and serum. J. Dairy Sci. 42,1390-1391.

Morr CV. (1979). Conformation and functionality of milk proteins. In Functionality and protein structure. Ed. A. Pour-El. Am. Chem. Soc. Symp. Ser. 92 Am. Chem. Soc., Washington, DC. 65-79.

Nickerson TA, Moore EE, Zimmer AA. (1964). Spectrophotometric determination of calcium in milk using 2, 2'-(ethanediylidene-dinitrilo) diphenol (glyoxal bis 2-hydroxyanil). Anal. Chem. 36, 1676-1677.

Roeper J. (1977). Preparation of calcium caseinate from casein curd. N.Z.J. Dairy Sci. Technol. 12, 182-189.

Rose D, Davies DT, Yaguchi M. (1969). Quantitative determination of the major components of casein mixtures by column chromatography on DEAE-cellulose. J. Dairy Sci. 52, 8-11.

Sumner JB. (1944). A method for the colorimetric determination of phosphorus. Science. 100, 413-414.

Thompson MP, Farrell Jr. HM. (1973). The casein micelle-forces contributing to its integrity. Neth. Milk Dairy J. 27, 220-239.

Thompson MP, Gordon WB, Boswell RT, Farrell Jr. HM. (1969). Solubility, solvation, and stabilization of αs1- and α-caseins. J. Dairy Sci. 52, 1166-1173.

Wallingford L, Labuza TP. (1983). Evaluation and the water binding properties of food hydrocolloids by physical/chemical methods and in a low fat meat system. J. Food Sci. 48, 1-5.

Walstra P, Jenness R. (1984). Dairy Chemistry and Physics. John Wiley and Sons, New York. 384-388.

Discussion with Reviewers

M. Kalab: The authors have suggested that differences in manufacturing may have been responsible for the differences in the chemical composition and physical properties of the two calcium caseinate preparations; it would be useful to describe, even briefly, the manufacturing of calcium caseinate and the possible technological differences. It would be also useful to briefly describe the manufacturing of imitation cheese using calcium caseinates, including the relative amounts of the caseinates used.

Authors: The conversion of casein curd to calcium caseinate is a slower, more sensitive process than the manufacture of sodium caseinate. Calcium caseinate dispersions are more sensitive to heat. Problems that may arise during processing (and reconstitution of the dried powder) include sedimentation, precipitation, and gelatin (Roeper, 1974; Hayes *et al.*, 1968).

Calcium caseinate is formed by neutralizing an acid casein dispersion with calcium hydroxide. The reaction product is a white, colloidal dispersion of relatively low viscosity which can be spray dried. The completeness of conversion is often measured by the level of sedimentable matter. Roeper (1977) studied some of the factors affecting the rate of conversion of acid casein curd into a dispersion with only 1-2% (by weight) sedimentable solids. He concluded that best results were obtained by reacting finely-milled, well-hydrated "soft" curd with alkali at or below 40°C. Heating above 40°C during the conversion adversely affected the solubility of the resulting caseinates.

Dispersions of calcium caseinate are unstable upon heating and may precipitate, especially as the pH is lowered or the soluble calcium content increases.

Roeper (1977) also noted reversible gelation upon heating calcium caseinate prior to spray drying. Reversible gelation appears to be peculiar to calcium caseinate.

Imitation process cheeses are made essentially the same as conventional process cheeses. The blends, of course,are different. Kosikowski (1977) provides compositions for some imitation process cheeses. The total protein he shows is 23.5% and the soluble protein is 1.7% for a Cheddar analog. The soluble protein is usually sodium caseinate and a large amount of the rest of the protein (21.8%) is calcium caseinate. Blend formulas are not readily available because they are proprietary.

H. E. Swaisgood: Comparison of the composition data and the calcium solubility data also deserves some comment because of the seeming inconsistency. Thus, the "good" sample contains less casein protein and more noncasein protein and yet it is less soluble in the presence of calcium. Perhaps the authors could expand their discussion to include their thinking as to the cause of this inconsistency.

Authors: If the proteins present in the "non-casein" fraction are, in fact, products from partial hydrolysis, it doesn't necessarily follow that they should be more soluble with respect to $CaCl_2$ addition. Depending upon which casein is partially hydrolyzed and depending upon where in the primary sequence the hydrolysis took place, it is conceivable that the calcium solubility profile could be extensively altered. For example, partial hydrolysis could result in two fractions: a low molecular weight fraction (1a and 1b) and a modified larger molecular weight fraction, which being largely hydrophobic in nature (if from β-casein or α-casein), would tend to aggregate more readily than prior to hydrolysis. Thus, the total "system" would be more susceptible and would exhibit lower solubility in the presence of $CaCl_2$. While the elution profiles and electrophoretic data show little differences in the larger casein components, it is possible that these techniques are not sensitive enough to show subtle alterations in structure.

Additional References

Hayes JF, Southby PM, Muller LL. (1968). Factors affecting the viscosity of caseinates in dispersions of high concentrations. J. Dairy Res. 35, 31-47.

Kosikowski F. (1977). Cheese and Fermented Milk Foods, Edwards Brothers. Ann Arbor, MI. 475-477.

Roeper J. (1974). The alkali Requirement of Acid Casein. N.Z.J. Dairy Sci. Technol. 9, 128-131.

FOOD MICROSTRUCTURE, Vol. 4 (1985), pp. 323-331
SEM Inc., AMF O'Hare (Chicago), IL 60666-0507 U.S.A.

ULTRASTRUCTURAL AND BIOCHEMICAL INVESTIGATIONS OF MATURE HUMAN MILK

Robert J. Carroll, Jay J. Basch, John G. Phillips
and Harold M. Farrell, Jr.

Eastern Regional Research Center
U.S. Department of Agriculture
600 E. Mermaid Lane
Philadelphia, PA 19118

Abstract

The casein complexes (casein micelles) of human skim milk were evaluated by electron microscopy. Fourteen samples of human milk were obtained from seven donors whose stage of lactation varied from 1 to 23 months. Compositional and biochemical parameters were measured to evaluate the nature of these samples. For mature human milks, 2-13 months of lactation, average percentage of solids-not-fat was found to be 8.32 ± 0.16. Protein compositions of the skim milks were studied by the Coomassie blue dye binding method and by SDS-gel electrophoresis; total protein and casein were found to be 0.62 ± 0.18 and 0.29 ± 0.02 percent, respectively. The lysozyme and lactoferrin contents were also determined. The total casein of the skim milks appeared to increase slightly as lactation progressed; an exception occurred in milks obtained from one donor at 22 and 23 months postpartum which exhibited decreased casein and elevated lysozyme and lactoferrin contents. The overall morphology of the casein micelles was evaluated by electron microscopy using platinum shadowing, negative staining, and thin sectioning methods. Platinum shadowing was largely unsuccessful, but negative staining showed a discrete substructure for human casein micelles. Average corrected diameters of 43.0 nm from the area and 47.5 nm from circumference measurements were obtained from analysis of fixed and pelleted human milk micelles.

Initial paper received February 13 1985
Manuscript received October 10 1985
Direct inquiries to R.J. Carroll
Telephone number: 215 233 6529/6528

KEY WORDS: Human Milk, Casein Micelles, Size Distribution, Ultrastructure, Lactation, Electron Microscopy, Fat Globule, Biochemistry

Introduction

In all species so far examined the major phosphoproteins of milk occur as colloidal aggregates referred to as casein micelles (Jenness, 1974). These complexes also contain the majority of the inorganic calcium and phosphate of milk (Farrell and Thompson 1974). The ultrastructure of the casein micelles of human milk has not been definitively characterized. The first report of electron microscopy of bovine casein micelles was in 1949 by Nitschmann, who fixed the micelles with formaldehyde and used gold shadowing for contrast. Later, Huth (1957) employed osmium staining of human casein micelles and reported an average diameter of 30 nm. D'Agostini and Calapaj (1958), using the same procedure as Nitschmann, found average diameters of 49 nm, while in a later study Calapaj (1962) found diameters of 75 ± 4 nm for human milk micelles. Ultrathin sections of methacrylate embedded human milk micelles were studied by Knoop and Wortmann (1960, 1967) who measured 2740 micelles and determined a mean diameter of 42 nm. Recently, Rüegg and Blanc (1982) examined human milk micelles from samples at partum and followed lactation for 6 months. By freeze fracture techniques, they found a trend toward increased micelle size with increased lactation and reported diameters between 11-55 nm for volume/surface mean diameter and 16-88 nm for volume moment mean diameter.

The intent of this paper is to evaluate the morphology and to determine size distributions of casein micelles with minimal disturbance of the protein fraction of human milk using the techniques of electron microscopy. Our observations on the casein micelles of human milk using a variety of sample preparation techniques and the problems encountered with the preparation of whole milk and air-dried casein micelles are reported. In the study of human milks, it is important to know that the composition of the samples used for electron microscopy represent normal mature milk and fall within certain limits. Analysis of biochemical parameters of the samples used to characterize the milks are also reported.

Materials and Methods

Freshly drawn milk samples were obtained from multiparous individuals whose stage of lactation ranged from 1 to 23 months. The donors were asked to take the samples during mid-nursing period; milks were maintained at 5°C and received at the laboratory within 24 h. However, four milks were frozen for 4 days and thawed upon receipt. The pH of each sample was determined, and the whole milk was separated by centrifuging in the cold at 1500 X g for 15 min. After samples for microscopy were taken, the skim milk fraction was weighed and lyophilized, and the solids-not-fat content was determined gravimetrically.

Biochemical Determinations

Discontinuous gel electrophoresis in the presence of sodium dodecyl sulfate, and gel densitometry were carried out as previously described by Basch et al. (1985), except that the human β-casein band was identified by co-electrophoresis with an authentic standard (Greenberg and Groves, 1984). Protein quantitation of the dried milks was by the Coomassie blue dye binding method as adapted to bovine milk by Douglas et al. (1981). Anti-human lactoferrin was purchased from Miles Scientific, Naperville, IL[1] and the purified standard human lactoferrin was the gift of Merton Groves of this laboratory. Lactoferrin content was determined by single radial immunodiffusion as previously described (Douglas et al., 1981). Lysozyme activity was determined spectrophotometrically as detailed by Shugar (1952).

Electron microscopy

Thin sectioning. The method of Salyaev (1968) involved microencapsulation of the whole human milk in 2 and 4% agar gels. The microcapsules containing the fat globules and casein micelles were fixed for 2 h in 2% glutaraldehyde in water adjusted to the pH of the samples, which ranged from pH 6.4 to 7.6. They were washed 3X with water, followed by postfixation overnight in 1% OsO_4 in water at the same pH. The samples were washed with water and were dehydrated through increasing acetone concentrations and embedded in Spurr resin (Spurr, 1969). Sections were stained with uranyl acetate and lead citrate. Sections (~60 nm) were prepared on a LKB Ultratome IV.

Human skim milk (0.8 ml) was added to 1 ml of 2% glutaraldehyde and fixed for 30 min. The sample was centrifuged at 96,000 X g for 45 min at 30°C to obtain a pellet. The pellet was cut into small pieces, washed 3X with water, and postfixed with 1% OsO_4. The samples were embedded and sectioned as above. Size distributions of the casein micelles were obtained on micrographs of sectioned micelles at 148,500X. In the pelleted fractions, few micelles with uncorrected diameters below 30 nm were observed. Only micelles with distinct peripheries were sized. The circumferences of individual micelles were traced using a Houston Instruments digitizing pad. Approximately 45 points per micelle were recorded. The error in measuring a circumference was ~1-2%. The outlines of 2150 micelles were traced. From these traces, diameters were calculated both from the measured circumferences and from the accumulated surface area by point to point triangulation with a chosen center. Frequency distribution of the diameters were then obtained using procedure frequency of the Statistical Analysis System (SAS) (1982).

Shadowing. Preparation of human casein micelles was carried out according to the method of Carroll et al. (1968). The skim milk (0.8 ml) was fixed for 15 min in 1 ml of 2% glutaraldehyde in water at the original pH of each sample. The sample was diluted in water, spread on freshly cleaved mica, air dried, shadowed with platinum, and backed with carbon. The film was scored lightly, floated onto a water surface, and picked up on copper grids.

Negative staining. Human skim milk was fixed in 2% glutaraldehyde for 15 min, diluted ~1:100 in water and negative stained with 1% phosphotungstic acid (PTA) at pH 7.0. All observations were carried out on a Zeiss 10-B electron microscope at either 60 or 100 kV.

Results

A series of 14 milk samples were obtained from seven donors, whose stage of lactation ranged from 1 month to 23 months (Table 1). The 1, 2, and 3 month samples are from donor P.W.; the 4, 5, 6, and 8 month samples are from a second donor (C.S.); the 22 and 23 month samples are from donor B.B.W. (Table 1). The pH of the samples varied from 6.4-7.6. One set of four samples which had been kept for 4 days in a home freezer gave severe flocculation upon thawing. Schöch and Matthaei (1983) have reported recently that flocculation of frozen human milks can be minimized by

Table 1 Milk samples

Donors	Months of lactation
C.S.	4[a],5,6,8
D.K.	7
B.W.	9,10[a]
B.B.W.	22,23[a]
P.W.	1[a],2,3
D.P.	13
R.W.	6[b]

[a]These samples were kept 4 days in a home freezer.
[b]This sample was frozen for 6 months.

[1]Reference to brand or firm name does not constitute endorsement by the U.S. Department of Agriculture over others of a similar nature not mentioned.

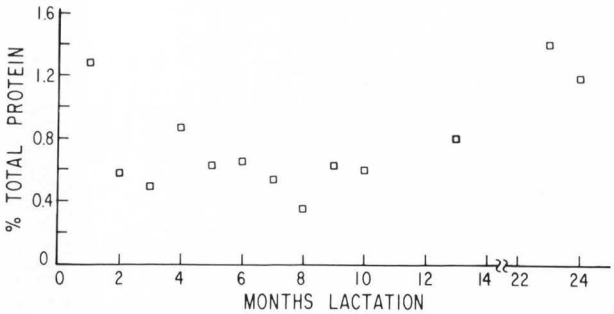

Fig. 1. Percent total protein (W/W) of human skim milks obtained at various stages of lactation.

gently shaking the milks while thawing under cold running water.

The total protein and solids-not-fat contents of the skim milks are plotted as a function of the time of lactation in Figs. 1 and 2. No direct correlation of solids-not-fat with time is observed. The total protein content as measured by the dye binding method was elevated in the first month of lactation in agreement with the data of Rüegg and Blanc (1982). Samples after prolonged lactation (22 and 23 months) also showed elevated protein contents. The frozen samples, after being skimmed, showed no unusual compositional trends.

Gel electrophoretic patterns of skim milk from donors at 3, 7, 9, and 22 months lactation are shown in Fig. 3. Standards for molecular weight calibration on these sodium dodecyl sulfate gels and a sample of bovine milk are included for comparison. Of special note in the 22 month samples was the high albumin, immunoglobulin, lactoferrin, and lysozyme contents. Both the lactoferrin and lysozyme concentrations of all the milks sampled were determined and are presented in Table 2. An increased lysozyme content does not necessarily mean an increase in the lactoferrin content, but the 8 month sample from the same donor as the 4, 5, and 6 month samples showed significant increases in both. Milks at 22 and 23 months showed a comparatively high lysozyme and lactoferrin content, indicating a probable infection. The four frozen samples showed no unusual protein distribution. No bands comparable to the major bovine α_{s1}-casein were observed, however, for purified caseins minor bands in this region can be visualized. The band in human milks comparable to bovine k-casein was not distinct. In similar gels, purified human k-casein migrates in the region above β-casein with a molecular weight of ∿ 37,000 (Brignon et al., 1985). The human k-casein bands were not visualized at the concentrations employed here. Acid precipitation of the caseins showed no clear cut separations of whey and casein as was achieved for bovine milks and demonstrated by electrophoresis (Basch et al., 1985). In samples such as those obtained at 8, 22, and 23 months, where the lysozyme

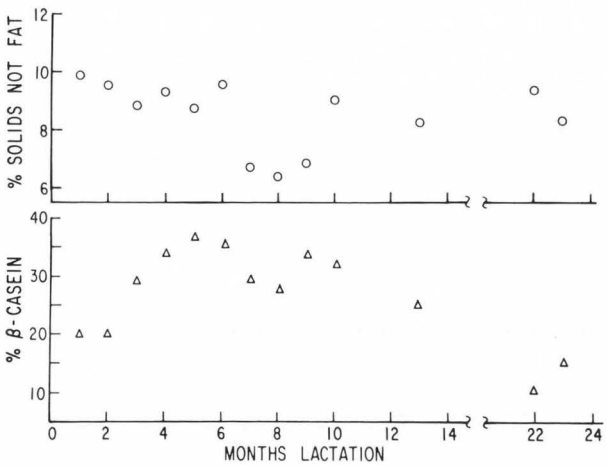

Fig. 2. Percent solids-not-fat (W/W) of human skim milks obtained at various stages of lactation; the β-casein content (% of total protein) was obtained by densitometry.

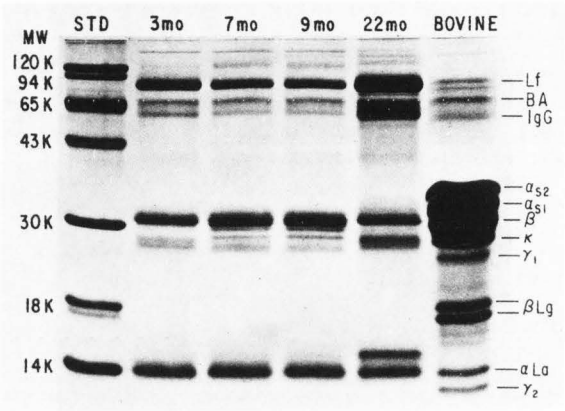

Fig. 3. Sodium dodecyl sulfate gel electrophoresis pattern of human skim milk from donors at 3, 7, 9, and 22 months. Bovine skim milk proteins on right for reference. Abbreviations are: lactoferrin LF, bovine serum albumin BA, heavy chain immunoglobulin IgG, β-lactoglobulin β-Lg, and α-lactalbumin α-La; the various caseins α_{s2}-, α_{s1}-, β-, k-, γ_1-, and γ_2. For the 22 month sample note the increased lactoferrin, albumin and immunoglobulin contents; the new band appearing just above α-La is lysozyme.

and lactoferrin contents were high, these proteins partially co-precipitated with the caseins. In the case of the whole human milks then, only the β-casein band could be clearly defined as a casein, and since it accounts for most of the stainable casein bands, all other bands were considered whey (noncasein) protein. The β-casein content was therefore calculated by densitometry and is shown in Fig. 2. The percent β-casein is lower initially, rises to a relatively constant level and decreases upon prolonged lactation. The 22 and 23 month samples showed decreased

Table 2 Lactoferrin and lysozyme contents of human skim milks

Months of lactation	Lysozyme units/mg protein	Lactoferrin mg/100 mg protein[a]
1	16	16.4
2	260	16.8
3	296	14.0
4	319	10.3
5	52	11.4
6	96	10.0
7	525	11.8
8	1 004	23.3
9	273	15.0
10	333	19.3
13	51	20.7
22	1 130	35.1
23	1 600	36.5
Average[b]	320 ± 281	15.2 ± 4.6

[a]Assay by radial immunodiffusion
[b]Average for mature milks (2-13 months).

casein with elevated total protein, lysozyme, and lactoferrin levels.

In Table 3, the average values obtained for the mature human skim milk composition are compared with similar averages reported by Blanc (1981). The results of this study compare favorably. The data for the 1, 22, and 23 month milks were not included in these averages.

Morphological evaluation of selected human milk samples was carried out by electron microscopy. Minimum manipulation of the milks was desirable in order to obtain reproducible electron micrographs to provide reliable size distribution data. The first method of choice in this case was the microencapsulation method of Salyaev (1968) in which whole milk is entrapped in an agar microcapsule and carried intact through fixation, dehydration, and embedding. No centrifugation steps are required and this method has been successfully used to prepare bovine milks for electron microscopy. Sectioned whole milk obtained by the microencapsulation procedure is shown in Fig. 4. Only fat globules and cell fragments associated with it are observed. Some of the membrane surrounding the fat globule appears to be missing, and few casein micelles are observed. Even at higher magnifications than that in Fig. 4, no casein micelles were observed, although some micelles were found entrapped in the agar wall of the microcapsule. Apparently, the casein micelles were not retained by the agar, only the much larger fat globules remained. The smaller casein micelles of human milk may have been lost through the pores of the agar microcapsule. Increasing the agar content of the microcapsule to 4% did not retain intact casein micelles. In

Table 3 Mature human milk composition (g/100 g milk)

	Blanc (1981)	This study[a]
Solids-not-fat	8.50	8.32 ± 1.16
Protein	0.90	0.62 ± 0.18[b]
Casein	0.25	0.29 ± 0.02[c]

[a]2-13 month data
[b]Protein by Coomassie blue dye binding
[c]Casein by densitometry considering only the β-casein fraction and reported as the fraction of total protein applied to the gel.

contrast to Fig. 4, frozen milk samples were highly disorganized. Little or no fat globule membrane remained intact and phase separation apparently occurred within the fat droplets.

Shadowing of the casein micelles was carried out according to the method of Carroll et al. (1968). The results obtained were disappointing; the micelles from human milk appeared collapsed as evidenced by lack of shadows. In an attempt to determine the reason for lack of shadows, bovine and human milk casein micelles were prepared and shadowed at the same time (Fig. 5). Relatively good results were obtained with the bovine micelles (Fig. 5a), while the human micelles appeared flattened with few shadows (Fig. 5b).

Negative staining with phosphotungstic acid was employed by Calapaj (1962) to determine size distribution of human milk micelles. Examples of negative stained human casein micelles are presented in Fig. 6. Nonuniform spread of the stain or excessive staining could lead to inaccurate size measurements. But the fine structure can be resolved, and a submicellar structure of the micelle as theorized for bovine casein (Farrell and Thompson, 1974) can be observed (Fig. 6, insert).

An example of a thin section of pelleted human milk micelles (8 months lactation) is shown in Fig. 7. The average diameters obtained as described in Materials and Methods are given in Table 4. Figure 8 shows a histogram of the observed values as derived from the area calculation. In this case the average diameter was found to be 42.4 nm (standard deviation = 8.9 nm), and the micelles ranged in size from 20 to 104 nm. Over 95% of the micelles were found to fall between 28 and 60 nm. A similar distribution was formed for the diameter calculated from the circumference except the mean was slightly larger, 47.3 nm (standard deviation = 11.7 nm). In addition, various moments of each distribution were calculated as described by Rüegg and Blanc (1982); the average diameters are

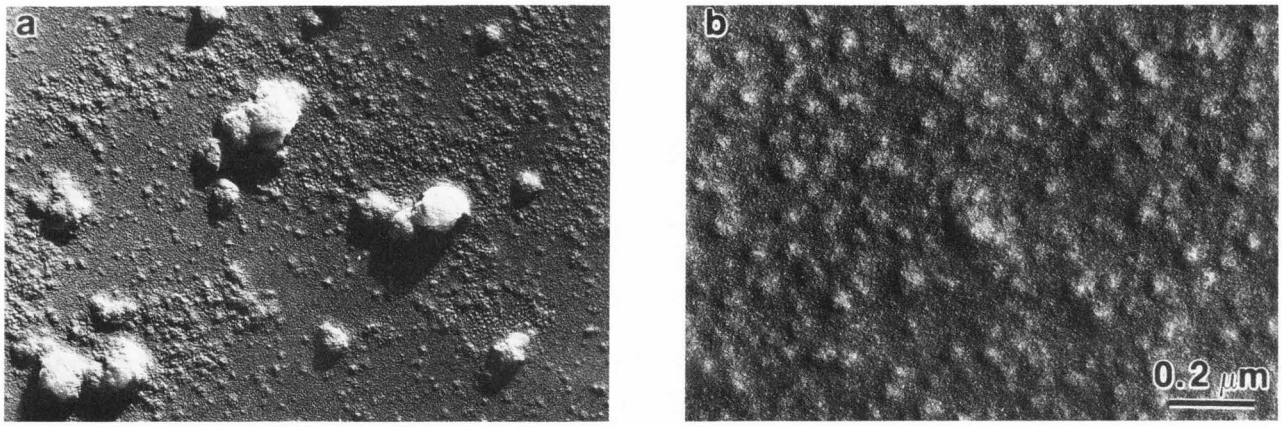

Fig. 5. Bovine (a) and human (b) casein micelles fixed in glutaraldehyde and then shadowed at the same time. The human casein micelles are much smaller, collapsed and flattened compared with the bovine micelles. (Sample shown (b): 12 months.)

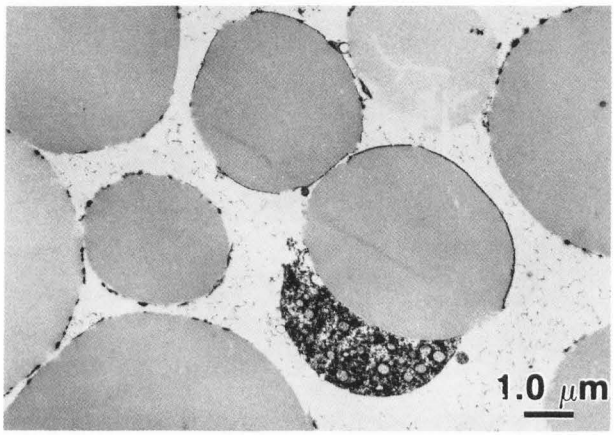

Fig. 4. Whole human milk prepared by micro-encapsulation method. Sections show fat globules without intact membrane and some cell fragments. No casein micelles are observed. (Sample shown: 13 months.)

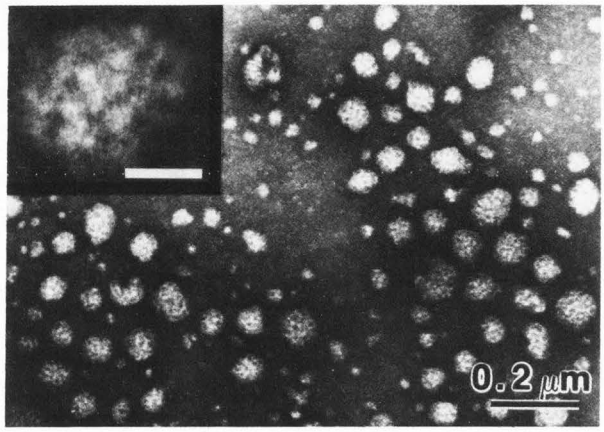

Fig. 6. Negative stained (1% PTA) human casein micelles showing a wide range of sizes and their spherical nature. Insert at higher magnification, the submicellar structure is clearly resolved. Bar = 30 nm. (Sample shown: 8 months.)

given in Table 4. The data from all of the size distribution measurements were also corrected using the method of Goldsmith (1967) which takes into account the relationship between micelle size and the section thickness. The correction changed the observed micelle diameters by less than 1 nm in each case (Table 4).

Discussion

Analysis of average compositional data of the human milk samples have indicated good agreement with literature values. However, milks obtained at 22 and 23 months showed high albumin, immunoglobulin, lysozyme and lactoferrin levels, while the 1 month sample with its elevated protein content seemed closer to colostrum than to mature milk. The 8 month sample, which yielded exceptional structural information, had an elevated lysozyme level, but its other compositional

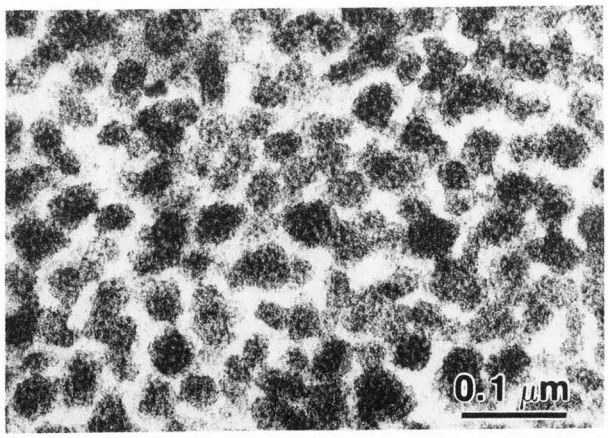

Fig. 7. Ultrathin section of human milk casein micelles. (Sample shown: 6 months.)

Table 4 Average diameters in nm for human milk casein micelles.

Distribution moments[a]	From Area[b]		From Circumference[c]	
	Observed	Corrected[d]	Observed	Corrected[d]
Number Average-d_n	42.4 s.d.8.9	43.0	47.3 s.d.11.7	47.5
Volume Average-d_v	44.4	44.9	50.5	50.4
Volume/Surface Average-d_{vs}	46.6	46.9	54.2	53.8
Volume moment Average-d_{vm}	49.8	49.9	59.8	59.1

[a]The various distribution moments calculated are defined by Rüegg and Blanc (1982)
[b]Diameters calculated from tabulated areas
[c]Diameters calculated from tabulated circumferences
[d]Each distribution was corrected for section thickness by the method of Goldsmith (1967)

data were well within 2 standard deviations of the means (compare Table 3 and Figs. 1 and 2). The milks were characterized to insure representative samples for observation with the electron microscope.

The average values for the solids-not-fat and the protein composition were comparable to the results calculated from the data of Rüegg and Blanc (1982) (Table 3). It was also observed that at prolonged lactation a lower casein content was correlated with higher lysozyme and lactoferrin contents (Table 2 and Fig. 2, 22 and 23 month samples). No evidence of bacteria was observed in these milks by electron microscopy, more samples would be needed to prove this conclusively, but few humans lactate for 22-23 months.

The determination of the ultrastructure of the human milks requires selection of the most appropriate method to adequately preserve both skim milk and fat globule fractions. The use of Salyaev's (1968) method was selected in order to preserve the lipid-protein relationships in human milk. This method was adapted by Henstra and Schmidt (1970) for bovine milks; unfortunately, the casein micelles of human milk were apparently lost during processing. The fat globules with their larger sizes were retained and are shown in Fig. 4.

The second method of choice was that of Carroll et al. (1968). This procedure conducted on skim milk does not require pelleting of the micelles and all sizes of micelles are uniformly dispersed. This method should give a reliable size distribution of the human casein micelles. As can be seen (Fig. 5a), the bovine casein micelles gave good shadows, while the human casein micelles (Fig. 5b) appear collapsed and flattened, as judged by the ratio of shadow length to measured diameters. In reviewing the literature, Rüegg and Blanc (1982) noted that β-casein is the major protein of the human casein micelle. This is

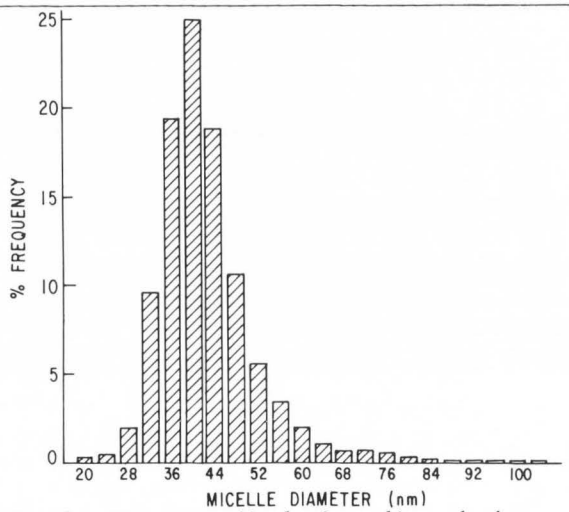

Fig. 8. Histogram displaying adjusted size measurements as obtained from sectioned human milk micelles. (Figure 7.)

confirmed by examination of the gel electrophoresis patterns; little or no α_s-caseins are found in the skim milks analyzed. Human milk also has a substantially lowered total inorganic calcium + phosphate level (Holt and Jenness, 1984), when compared to most species so far examined. The collapse of human milk casein micelles upon drying may be explained by their lack of the α_s-caseins with high calcium affinity, as well as their reduced colloidal calcium-phosphate content. Both of these factors could contribute to a three-dimensional structure which is less stable to drying than that of the bovine casein micelles. Even the introduction of glutaraldehyde crosslinking was not enough to prevent their collapse.

Examination of the fine structure observed (Fig. 6) for negative stained human casein micelles suggests that they, like their

bovine and rat counterparts, may be assembled through the aggregation of submicellar particles (Farrell and Thompson, 1974).

Measurements of human milk casein micelles were made on sections from milks at 8 months lactation (Fig. 7). The program used to measure the sizes of the thin sectioned micelles allows for the calculation of their diameters either from the length of the circumferences or from the accumulated surface areas. Diameters calculated from the circumferences were somewhat greater than those calculated from surface areas. If the surfaces of the micelles are somewhat rough (as would be anticipated based on Figure 6), then larger apparent diameters based on circumferences would be expected. However, it is difficult to predict which method is more accurate since both values are in reasonable agreement. The Goldsmith correction for section thickness has little effect on the average diameter, probably because the majority of the human milk micelles are contained within the 60 nm section thickness. The observed average diameters are also only slightly altered when volume, volume surface and volume moments are calculated (Table 4). This differs significantly from the responses of the freeze fracture data obtained by Rüegg and Blanc (1982), who reported micelle sizes ranging from 8-14 nm for d_n and 16-88 nm for d_{vm}. The insensitivity of our data to these calculations may be due to the fact that the centrifugal force used resulted in an uneven distribution of the micelles. In the pelleted fractions, few particles with uncorrected diameters below 30 nm were observed, because smaller micelles and submicelles would not have been sedimented.

This, however, raises an important question regarding the definition of a casein micelle. The casein micelles of most species are thought to be assembled from rather spherical submicelles (Farrell and Thompson 1974 and Schmidt 1982). For bovine casein these have been estimated to have an upper limiting size of 18 nm (Pepper and Farrell 1982); Rüegg and Blanc (1982) estimated them to range from 6 to 12 nm for human caseins. Thus casein micelles constructed from at least four submicelles of 10 nm each should have apparent diameters of at least 20 nm. Structures below this size might be considered to be non-micellar casein. Historically, one view of micellar casein has been considered to be that casein sedimented at 100,000 X g for half an hour or more. Thus the data given here could be considered valid for micellar casein based on method of isolation and particle diameters greater than those expected for a minimum spherical micelle composed of four submicelles. Admittedly the frequency distributions obtained are somewhat skewed.

In summary, compositional data were obtained on milks from donors at various stages of lactation up to 23 months. Several of the milks exhibited "high" lactoferrin and lysozyme as well as immunoglobulin levels. All the other milk samples fell within close limits. Attempts to observe whole milks were unsuccessful because of the loss of casein micelles. In addition, the use of shadowed micelles was unsuccessful due to collapse of the human milk micelles upon drying. Negatively stained human milk micelles show a distinct submicellar structure. Sectioned micelles were measured and a histogram developed which showed an uncorrected size distribution of human milk casein micelles ranging from 20-104 nm, with an average size of 42.4 nm for milk obtained at 8 months; this value was increased by only 0.6 nm by the correction of Goldsmith (1967). These results fall in the mid-range of previously published size distributions obtained by a variety of electron microscopic procedures.

Acknowledgments

The technical assistance of B. Maleeff and R. Walsh is gratefully acknowledged, as well as the assistance of T. Dobson and S. Graham. The authors extend their appreciation to S. Raimondo for securing the human milk samples.

References

Basch JJ, Douglas FW, Procino LG, Holsinger VH, Farrell HM Jr. (1985) Quantitation of caseins and whey proteins of processed milks and whey protein concentrates. J. Dairy Sci., 67, 23-31.

Blanc B. (1981) Biochemical aspects of human milk—comparison with bovine milk. World Rev. Nutr. Diet., 36, 1-89.

Brignon G, Chtourou A, Ribadeau-Dumas B. (1985) Preparation and amino acid sequence of human k-casein. FEBS Lett., 188, 48-54.

Calapaj GG. (1962) Ricerche al microscopio ellettronico sulla polidispersione della caseina de latte umano e bovine. (Electron microscope study of the polydispersed caseins of human and bovine milk.) Boll. Ist. Sier Oter Milan, 41, 276-291.

Carroll RJ, Thompson MP, Nutting GG. (1968) Glutaraldehyde fixation of casein micelles for electron microscopy. J. Dairy Sci., 51, 1903-1908.

D'Agostini BA, Calapaj GG. (1958) Ricerche al m.e. sulla caseina del latte di alcune specie animali. (Electron microscope study of the caseins of the milks of several animal species.) Acta Med. Vet., 4, 9-15.

Douglas FW Jr, Greenberg R, Farrell, HM Jr, Edmondson LF. (1981) Effects of ultra-high-temperature pasteurization on milk proteins. Ag. Food Chem. 29, 11-15.

Farrell HM Jr, Thompson MP. (1974) Physical equilibria proteins, in : Fundamentals of Dairy Chemistry, 2nd Ed, B.H. Webb, A.H. Johnson, J.A. Alford (eds.), The AVI Publishing Co., Westport, Connecticut, 442-473.

Goldsmith PL. (1967) The calculation of true particle size distributions from the sizes observed in a thin slice. Brit. J. Appl. Phys., 18, 813-830.

Greenberg R, Groves ML. (1984) Plasmin cleaves human β-casein. Biochem. Biophys. Res. Comm., 125, 463-468.

Henstra S, Schmidt DG. (1970) Ultradunnschnitte aus milch mit hilfe der mikrokapsel methode. (Ultra thin sections of milk by the means of the microencapsulation method.) Naturwissenschaften, 57 (5), 247.

Holt C, Jenness R. (1984) Interrelationships of constituents and partition of salts in milk samples from eight species. Comp. Biochem. Physiol., 77A, 275-282.

Huth E. (1957) Electronenoptische Untersuchungen zur Kolloidstruktur von Sauglingnahrungen. (Electron optical investigations of the colloidal structure of infant foods.) Kinderheilkunde, 105, 247-249.

Jenness R. (1974) The composition of milk, in : Lactation—A Comprehensive Treatise, B.L. Larson, V.R. Smith (eds.), Academic Press, New York, 3-37.

Knoop E, Wortmann A. (1960) Zur Grössenverteilung der Caseinteilchen in Kuhmilch, Ziegenmilch Und Frauenmilch. (The size distribution of casein particles in cow, goat, and human milk.) Milchwissenschaft, 15, 273-281.

Knoop E, Wortmann A. (1967) Das Auftreten von Kasein-Micellen im Kolostrum der Frau, der Kuh Und der Schweines. (The occurrence of casein micelles in human, bovine, and porcine colostrum.) Milchwissenschaft, 22, 198-205.

Nitschmann H. (1949) Elektronenmikroskopische Grössenbestimmung der Calcium-caseinatteilchen in Kuhmilch. (Electron microscopic size determination of calcium-casein particles in cow's milk.) Helv. Chim. Acta, 32, 1258-1264.

Pepper L, Farrell HM Jr. (1982) Interactions leading to formation of casein micelles. J. Dairy Sci. 65, 2259-2266.

Rüegg M, Blanc B. (1982) Structure and properties of the particulate constituents of human milk. A review. Food Microstruct., 1, 25-47.

Salyaev RK. (1968) A method of fixation and embedding of liquid and fragile materials in agar microcapsulae, in : Proc. 4th Europ. Regional Conf. Electron Microsc., Rome, D. S. Bocciarelli (ed.), Tipoerafia Polialotta Vaticana Rome, II, 37-38.

SAS Users Guide: Basics, (1982), SAS Institute, Inc., Box 8000, Cary, NC 27511 923 pp.

Schmidt DG. (1982) Association of caseins and casein micelle structure, In: Developments In Dairy Chemistry-1, P.F. Fox (ed.). Applied Science Pub., Essex, England, 61-86.

Schöch G, Matthaei S. (1983) Tiefgefrieren von Frauenmilch. (Deepfreezing of human milk.) DMW, 108, 49, 1894-1895.

Shugar D. (1952) Measurement of lysozyme activity. Biochim. Biophys. Acta 8, 302-308.

Spurr AR. (1969) A low-viscosity epoxy resin embedding medium for electron microscopy. J. Ultrastruct. Res., 26, 31-43.

Discussion with Reviewers

W. Buchheim: Which step of your preparatory treatment may have caused the loss of fat globular membrane material (Fig. 4)?

D. N. Holcomb: Does the agar encapsulation lead to any "extraneous" matter which might be visible in the micrograph?

W. Buchheim: On Fig. 4 there are numerous small particles visible between the fat globules which are of thread-like appearance. How do you interpret these structures?

Authors: These three questions are interrelated, and should be answered jointly. The "extraneous"-thread like material seen in Fig. 4 could have several origins. It could be from the encapsulating material as suggested by Dr. Holcomb. It could be artifactual; Dr. Schmidt at NIZO has some convincing evidence that some thread like structures as visualized by electron microscopy can be artifacts. The material could also represent shed fat globule membrane. Patton and coworkers (J. Dairy Sci. 63:697-700, 1980) have shown that for goat's milk, a significant amount of cholesterol and phospholipid are shed into the skim milk phase upon standing for 24 hr at 4°C; similar changes were not observed in cow's milk. They took this as evidence for fragility of the goat fat globule membrane. Our observations (Fig. 4) show little continuous membrane for human milk fat globules. A large portion of the bilayer may have been shed simply by standing overnight in the cold. Portions of the interfacial "fuzzy coat" (Freudenstein et al., Exptl. Cell Res. 118, 277-294, 1979) appear to be missing; it is possible that the thread like material may originate as part of this layer. The electron density of the

extraneous material appears to be more like that of the "fuzzy" coat than the agar capsule, the casein micelles or the lipid bilayer. However all the sources could contribute to the material observed in Fig. 4.

W. Buchheim: The number frequency distribution of casein particles (Fig. 8) exhibit a relative maximum at 42 nm. Do you believe that the decreasing number of smaller particles reflects the true situation in human milks?

C. Holt: Many studies by electron microscopy of the bovine casein micelle have revealed a large number fraction of particles in the smallest size class yet this work on human milk reveals few such micelles. Is there a real difference here?

Authors: As discussed in the manuscript, it would have been preferable to have conducted the micelle size distribution on whole or skim milks. However, our best results were obtained on micelles harvested by centrifugation. It is possible that some of the smaller micelles could have been excluded by this process, but where to draw the line between micellar and non-micellar caseins may be problematic for human milks.

Additional References

Freudenstein C, Keenan TW, Eigel WN, Sasaki M, Stadler J, Franke WW. (1979) Preparation and characterization of the inner coat membrane associated with fat globule membranes from bovine and human milk. Exptl. Cell Res. 118, 277-294.

Patton S, Long C, Sokka T. (1980) Effect of storing milk on cholesterol and phospholipid of skim milk. J. Dairy Sci. 63, 697-700.

FOOD MICROSTRUCTURE, Vol. 4 (1985), pp. 333-340
SEM Inc., AMF O'Hare (Chicago), IL 60666-0507 U.S.A.

0730-5419/85$1.00+.05

PARTICLE STRUCTURE IN SPRAY-DRIED WHOLE MILK AND IN INSTANT SKIM MILK POWDER AS RELATED TO LACTOSE CRYSTALLIZATION

Zenichi Saito

Faculty of Agriculture, Hokkaido University
Sapporo, Hokkaido, Japan 060

Abstract

The structure of instant skim milk and whole milk powders was studied by scanning electron microscopy with special respect to lactose crystallization during storage. X-ray diffraction analysis was used to confirm the crystallization. Some samples were ashed in a plasma asher and the residues were also examined by scanning electron microscopy. The structures of instant skim milk and whole milk powder particles were well-preserved after the ashing procedure.

The crystallization of α-lactose hydrate occurred in instant skim milk and whole milk powders according to moisture uptake. In instant skim milk powder, α-lactose hydrate crystals were observed on the particle surface. In whole milk powder, numerous droplets of free fat appeared on the surface of particles stored under conditions favoring the crystallization of α-lactose hydrate except few lactose crystals. Only β-lactose was in the state of crystal in whole milk powder stored at 37°C for 5 months at a relative humidity of less than 20%.

In fresh powders of skim milk and whole milk, prismatic crystals of lactose formed in Heinz fluid, whereas in stored powders, they did not.

Initial paper received February 02 1985
Manuscript received October 23 1985
Direct inquiries to Z. Saito
Telephone number: 81-11-7162111x2546

Key Words: Instant skim milk powder, whole milk powder, lactose, lactose hydrate, beta-lactose, X-ray diffraction, crystallization, scanning electron microscopy, plasma asher, Heinz fluid.

Introduction

The structure of milk powder has been studied by many researchers since the start of its industrial production. Lactose and its crystallization in the milk powders were extensively studied, because lactose forms a continuous medium in which proteins, fat globules and air cells are dispersed.

It has been generally accepted that in milk powder (spray-, roller-, or freeze-dried) lactose occurs in the amorphous state (Nickerson, 1974). When milk powder was placed in a humid atmosphere, amorphous lactose took up moisture and crystallized in the form of α-lactose hydrate. King (1965), in his review on the physical structure of milk powder, stated that the crystallization caused fine interstices and cracks along the sides and edges of crystals in the powder particles. Crystallization of lactose in milk powder was confirmed by X-ray diffraction technique (Tuckey and Ruehe, 1934; Knoop and Samhammer, 1962; Taneya, 1963) and/or infra-red spectroscopy (Goulden and White, 1958; Taneya, 1963; Bushill et al., 1965). The crystallization also accompanied changes in some physical properties, such as water absorption (Bushill et al., 1965), and porosity (Berlin et al., 1968a) and solubility (King, 1965) of the milk powder. Under the storage conditions which caused lactose crystallization, chemical deterioration such as browning (Saltmarch and Labuza, 1980a) and loss of lysine (Huss, 1970, 1974) occurred. Whey powder as well as skim milk and whole milk powders were used (Roetman, 1979; Saltmarch and Labuza, 1980a,b; Warburton and Pixton, 1978a,b) to study the transition of lactose from amorphous to crystalline form.

Miyawaki and Maeno (1938) observed particles of whole milk powder, which were fixed with osmium tetroxide, by means of a light microscope. They concluded that irregular crystals of lactose due to the absorption of moisture covered the surface of the particles and that only a part of total lactose crystallized regardless of the level of moisture uptake. Buma (1966) used a polarized light microscope to detect lactose crystallization in skim milk and whole milk powders kept in a humid atmosphere. He, however, did not present micrographs showing lactose crystals, but claimed that crystallization cracks were observed. He also demonstrated that paraffin oil, i.e. mounting medium, could penetrate into vacuoles in particles of whole milk powder, but not of skim milk powder, after lactose crystallization due to moisture absorption. Electron micrographs of lactose crystals on the surface of skim milk powder particles were presented

by Taneya (1963) who had applied a replica technique for electron microscopic observation.

Scanning electron microscopy succeeded in showing the detailed structure of particle surface on which lactose crystals have been located (Warburton and Pixton, 1978a,b; Roetman, 1979) and confirmed the previous findings obtained by X-ray diffraction and other physical methods. Roetman (1979) supported King's remarks by showing the rather porous structure of post-crystallized skim milk powder by means of the scanning electron microscope. To make sure that the substance which appeared after the uptake of moisture on the particle surface was crystallized lactose, other experimental techniques were necessary. For this purpose, Roetman (1979) compared the surface structure of spray-dried lactose solution with that of milk powder.

Most studies concerning lactose crystals in milk powder showed that it is the α-lactose hydrate form. As for crystals of β-lactose in milk powder, the following few papers have been published. Sharp (1938) detected the crystals of the β-form as well as α-hydrate in dried milk after moisture uptake at room temperature, though detailed experimental conditions were not given. Knoop and Samhammer (1962) found β-lactose crystals in a few samples of spray-dried whole milk powder and a mixture of α- and β-lactose crystals in some roller-dried milk powders. Recently, Würsch et al. (1984) reported crystallization of β-lactose in whole milk powder at high storage temperatures (55 and 60°C).

Ashing procedure using low temperature plasma have been generally used for plant tissue because it leaves inorganic residues in forms which show initial structures of the tissue. Saito (1980) applied the ashing procedure to skim milk powder particles to learn about the distribution of inorganic components in the particles.

The objective of this study is: (1) to find the advantage of ashing samples with a plasma asher as a pretreatment for scanning electron microscopy, (2) to examine the effect of lactose crystallization on the structure of milk powders, and (3) to demonstrate the presence of β-lactose crystals in stored whole milk powder.

Materials and Methods

Instant skim milk powder and ordinary whole milk powder, both of which were produced by a spray-dry process, were obtained through a local store and directly from the manufacturer, respectively. The materials (moisture: $\leqq 4\%$) packed in a commercial package (foil-laminated paper carton for 250 g or 300 g) or in a polyethylene bag were kept in a desiccator at room temperature until use.

In order to examine the inner structure, i.e. the cross sections, as well as the surface structure of the powder particles, the following pretreatment (Saito, 1980) for scanning electron microscopy was applied, whenever necessary: (a) chopping: about 0.2 g of the sample was chopped with a razor blade repeatedly for about 10 min, and (b) ashing: a small amount of the chopped sample was spread on a piece of quartz or on a stainless-steel plate (7 × 7 mm) and subjected to the ashing procedure in a plasma asher (Yanagimoto LTA 2SN) at 40 watts with an oxygen supply (40 ml/min, 2 kg/cm^2) for 5 h. The ashing temperature, which was estimated from the above operating conditions according to the operation manual for the plasma asher, was 200°C or less.

The samples were examined without any fixation procedure. The samples excepting the ashed ones were sprinkled on a piece of a double adhesive tape attached to a specimen holder. In the case of the ashed sample, the plate carrying the ashed particles was pasted on the specimen holder with a small amount of silver paint. The samples were coated with gold by an ion-sputtering method. Observations with a scanning electron microscope (JEOL JSM U3 and JEOL 25 S II) were made using an accelerating voltage of 15–20 kV.

A computerized X-ray diffractometer (Rigaku Geigerflex RAD-IIA, Cu target) was used to obtain X-ray diffraction patterns.

Heinz fluid (Warburton and Pixton, 1978a,b; Saito and Taguchi, 1980) was prepared according to the private communication of Warburton (polyvinyl alcohol 10 g, distilled water 60 ml, glycerol 10 ml, 1.5% phenol solution 25 ml, chloral hydrate 100 g, and lactic acid 35 ml). A small amount of the sample (< 50 mg) was mixed with a drop of the Heinz fluid. A part of the mixture was diluted with another drop of the Heinz fluid and observed under a light microscope at 500X magnification.

Results and Discussion

Instant skim milk powder

Samples taken from several packages produced by 3 manufacturers in Japan were examined. Conditions of the particle surfaces differed somewhat probably due to differences in the manufacturing systems. Even particles in the same package did not have similar surface structure, i.e. small particles had smooth surfaces and no dents but large ones showed wrinkled surfaces and dents. However, only a small difference was observed in the cross sections of particles within the same sample. The cross sections showed vacuoles and compact walls. An example of a cross section is shown in Fig. 1A which is similar to those demonstrated by others (Verhey, 1972; Buma, 1978; Roetman, 1979).

Since water was evaporated from the surface of the particle in the processing steps, a hard layer was produced at the surface of each particle. Therefore, water in the particle might not distribute evenly during the drying process. To learn about the difference in the compactness between outer and inner portions, ashing treatment by a plasma asher was applied. Since the treatment destroyed organic matter and left the inorganic residue, it was expected to illustrate differences in compactness.

The inner surface of a vacuole observed in an ashed sample was rough (Fig. 1D), although the particle surface was relatively smooth and dense (Fig. 1C). A kind of trench or dent was observed in the middle portion of the wall between the vacuoles and the particle surface (Fig. 1B, D). Thus unevenness in cross section, which was not observed in untreated samples, was detected after the ashing treatment.

According to the results of X-ray diffraction analysis, none of the instant skim milk powder samples included lactose crystals when they were examined at the beginning of the present experiment. It has been recognized that two-stage instantization, i.e. a rewet-redrying system which was the first invention to produce instant skim milk powder, caused the crystallization of lactose during the process (Bullock, 1962). No information about the manufacturing system for the instant skim milk powder used in the present study was available. However, recent developments in manufacturing, such as a single-stage instantizing

process, have made it possible to produce instant skim milk powder without lactose crystallization.

The instant skim milk powder was sealed again after samples had been taken and was stored at room temperature. After storage for 21 months, an X-ray diffraction analysis confirmed the formation of α-lactose hydrate. At the same time, a crystal-like substance was detected on the particle surface. The powder stored for 51 months after the opening of the package showed relatively large deposits of the crystal-like substance covering the surface of the particles (Fig. 2A). The structure of the cross section of stored powder particles was smooth, showing no change after the formation of the crystal-like substance (Fig. 2B, C). The cross section was not porous and showed no cracks, at least under the conditions used for observation. Needle-type crystals were detected on the inner surface of vacuoles (Fig. 2C). The inner surface of some small vacuoles, however, lacked the crystals. The cross section of an ashed sample (Fig. 2D) revealed a fine porous structure similar to that one presented in Fig. 1D. The stored sample, which contained 34% of insoluble materials according to solubility tests (Saito and Taguchi, 1980), was treated with a 2% glutaraldehyde solution or 20% ethanol, both of which dissolved water-soluble substances but did not dissolve dried proteins. After the treatment, globular shapes of the particles were well preserved (Fig. 2E, F), but the crystal-like substance was washed out by these solutions, which indicated high solubility of the substance in an aqueous solution. When the crystal-like substance was removed, X-ray diffraction patterns showed that no crystals were present in the particles. The crystal-like substance disappeared after ashing, which indicated that it was not of inorganic nature. Hence it was concluded that the crystal-like substance consisted of α-lactose hydrate. Lactose crystallization did not seem to affect the structure of the cross section of particles. The needle-type crystals on the inner surface of vacuoles differed in form from the crystal-like substance, and were probably another form of α-lactose hydrate crystal, i.e. long prismatic crystals, because crystals other than α-lactose hydrate were not detected by X-ray diffraction patterns.

The development of lactose crystals was accelerated when a portion of instant skim milk powder was kept in a closed container together with a saturated sodium chloride solution at various temperatures between 0 and 37°C. Relative humidity in the container was 75% (Rockland, 1960). Since the difference due to storage temperature was not great, the changes due to time of storage at 20°C are shown in Figure 3. A slight change in the surface, namely the formation of a plate-like structure, occurred after 1 day of storage. Tiny prismatic crystals appeared after 2 days of storage (Fig. 3B), but no subsequent increase in size and number of the tiny crystals was observed. With time the plate-like structures continued to develop and in 4 days crystals, which resembled those demonstrated by Roetman (1979), were found (Fig. 3D).

Whole milk powder

The structure of whole milk powder particles resembled the spray-dried buttermilk particles described by Kalab (1980, 1981), i.e. the main particles had a crater-like scar and a minute globule surrounded with a low rim at the junction (Fig. 4A). However, the interior of the crater in whole milk powder was not as smooth as that of buttermilk particles, but was porous in the same manner as the rest of the particles (Fig. 4B). It is likely that the minute globule left the crater after breaking away from the main particle. The particles of whole milk powder were also similar to those shown by Buma and Henstra (1971) and Buma (1978) with respect to the minute globule. However, cracks, but no craters, were observed in their micrographs. The cross section of whole milk powder (Fig. 4C) seemed to be porous owing to the presence of tiny vacuoles and fat globules, unlike the skim milk powder.

Plasma-ashing demonstrated that the interior of the whole milk powder particles (Fig. 4E) was of uniform porosity with no channels and thus differed from the instant skim milk powder. Ashing suggested that the solids-not-fat were evenly distributed in the dry particles. The rim of the crater was rather compact even after ashing (Fig. 4D, F).

Storage of the whole milk powder in a humid atmosphere caused the development of an adhered substance (Fig. 5A), which differed from the deposit on the surface of skim milk powder. The adhered substance was rather spherical in shape and had no sharp edges (Fig. 5B). The adhered substance was removed by washing with an organic solvent such as ethyl ether, and by ashing. Thus it was considered to be fat which emerged from the interior of the particles.

Portions of the whole milk powder were stored at 0 to 37°C for up to 1 month at 75% relative humidity in the same manner as the instant skim milk powder. Effects of the moisture uptake on the structure were evident after only 1 day of storage regardless of temperature. Powder structures after 1 month of storage are shown in Figure 6. The round shapes of an adhering substance were maintained at low temperature but not at 37°C. The development of α-lactose hydrate crystals was demonstrated by X-ray diffraction analysis in all samples that absorbed moisture. However, very few crystals of α-lactose hydrate were observed on the surface, although X-ray diffraction analysis revealed that a considerable amount of crystals existed in the particles. The particle surface was mostly covered with free fat (Buma, 1971; Buchheim, 1982) so that lactose at the surface portion probably could not crystallize or lactose crystals could not accumulate on the surface. Therefore, lactose crystals developed only inside of the particles and were rarely detected on the particle surfaces.

Another portion of the sample kept in an unsealed container, i.e. in a Petri dish with a slit between body and cover, in an incubator at 37°C (relative humidity $<20\%$) for 1 month showed no crystals, but the sample kept for 5 months under the same conditions demonstrated another type of X-ray diffraction pattern, which confirmed that all the lactose in the crystalline state was β-form. The pattern was typical for the crystals of β-lactose, i.e. there were peaks at 2Θ = 10.5, 21.0 and 24.7° (Knoop and Samhammer, 1962; Buma 1967) whereas peaks at 2Θ=12.4, 16.4, 19.5, 21.2 and 22.7°, which were typical for crystalline α-lactose hydrate, were missing. There were minor physical alterations in the whole milk powder exposed to a relative humidity as low as 20% (Berlin et al., 1968a). Lactose crystallization, i.e. the formation of α-lactose hydrate, did not occur at 20% relative humidity, because the moisture content of the milk powder was too low. According to Heldman et al. (1965), equilibrium moisture content of low-heat whole milk powder with 26% fat at 38°C at 20.4% relative humidity was 4.25%. The moisture content was lower than the critical level for lactose crystallization (Choi et al., 1951; Buma, 1966; Huss, 1970; Berlin et al., 1968b). Thus the lack of humidity prevented the formation of crystals as α-lactose hydrate, but not as β-lactose. Würsch et al. (1984) demonstrated that lactose crystallized completely in the β-form in a whole milk powder stored in a sealed metal can for 60 days at 60°C but did not crystallize at 37°C and 45°C. In

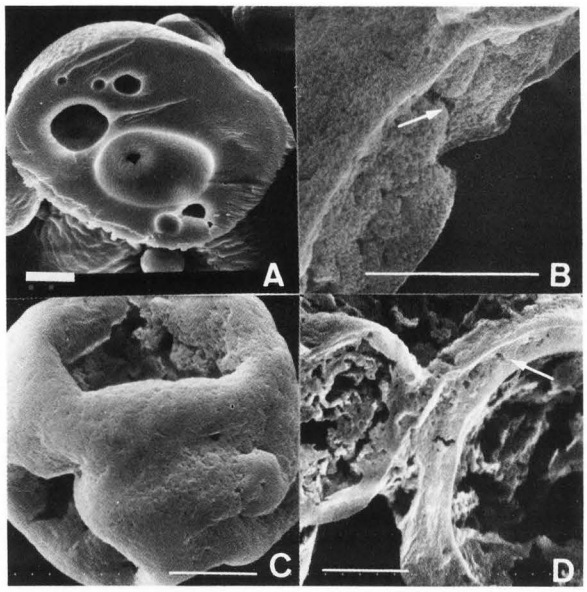

Fig. 1. Scanning electron micrographs of instant skim milk powder. A = cross section of chopped particle. B = ashed particle showing cross section. C = ashed particle. D = ashed particle showing cross section of particle wall. Arrows show trenches. Bars = 10 μm.

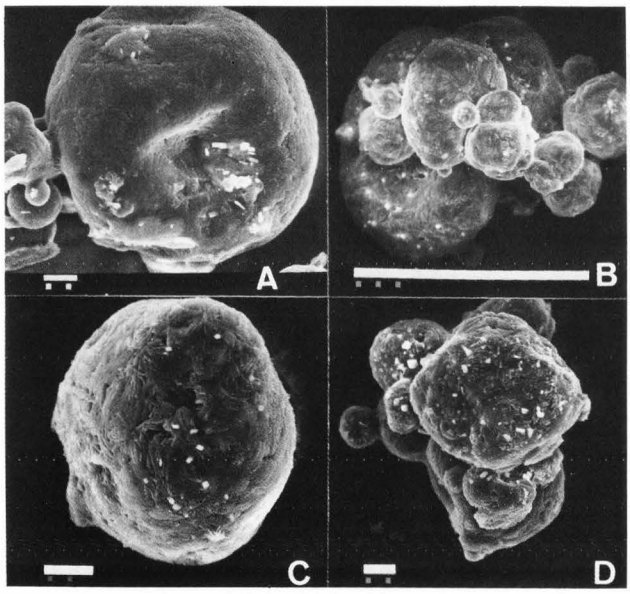

Fig. 3. Scanning electron micrographs of instant skim milk powder stored at 20°C at 75% relative humidity. A, B, C, D = stored for 1, 2, 3, 4 days, respectively. Bars in A, C, D = 10 μm. Bar in B = 100 μm.

this study, the lactose crystals of β-form developed during the storage at 37°C for 5 months. Mutarotation in amorphous lactose, namely the conversion of α-lactose to β-lactose, rapidly proceeded in milk powders at much higher temperatures than 37°C (Roetman and van Schaik, 1975; Olano and Martinez-Castro, 1983). However, mutarotation seems to occur at 37°C,

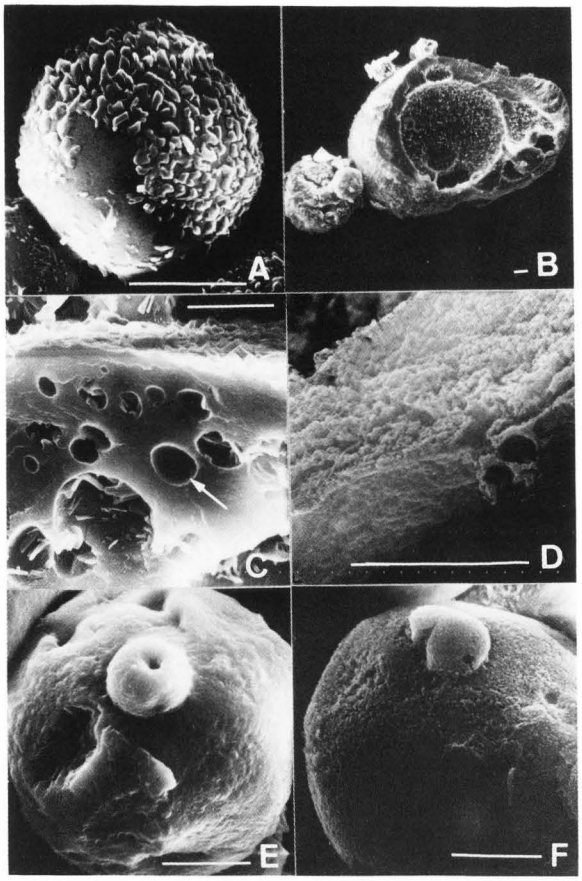

Fig. 2. Scanning electron micrographs of instant skim milk powder stored for 51 months at room temperature. A = particle covered with crystals. B = cross section of chopped particle. C = cross section showing vacuoles with and without (arrow) crystals. D = ashed particle, showing cross section of particle wall. E = particle washed with 2% glutaraldehyde. F = particle washed with 20% ethanol. Bars = 10 μm.

if sufficient time, such as several months, is allowed. Roetman and van Schaik (1975) also stated that mutarotation in amorphous lactose was possible even at 25°C, and postulated that mutarotation continues depending on the moisture content and temperature until an equilibrium β/α ratio of about 1.25 is attained.

Parrisch and Brown (1982) suggested that the conversion of α-lactose to β-lactose proceeds in the solid state and that the presence of a base favors the crystallization of β-lactose at 27°C. Würsch et al. (1984) mentioned that Amadori products, which are associated with browning by the Maillard reaction and are basic amines, might promote the crystallization of β-lactose. According to the results by Coulter et al. (1948) and Tarassuk and Jack (1948), the browning may not proceed to a detectable level under the conditions of the present study. However, it could be possible that at least the initial stage, which produces colorless condensation products and water and involves Amadori rearrangements (Hodge, 1953), of the Maillard reaction might proceed to some extent. Since milk powders were in a highly supersaturated state with respect to β-lactose as well as α-lactose,

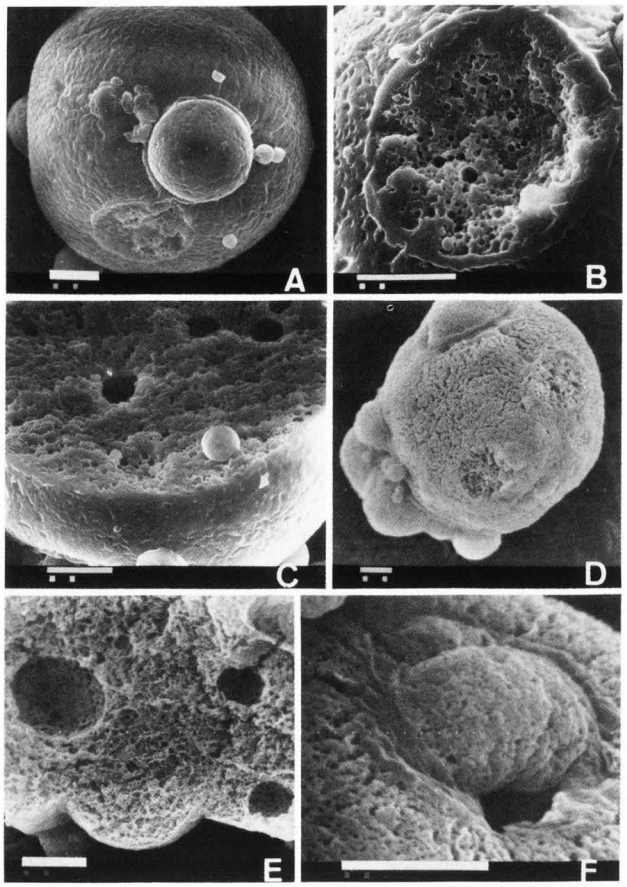

Fig. 4. Scanning electron micrographs of whole milk powder. A = typical particle. B = crater-like scar. C = cross section. D, E, F = ashed particles. E and F show cross section and surface, respectively. Bars = 10 μm.

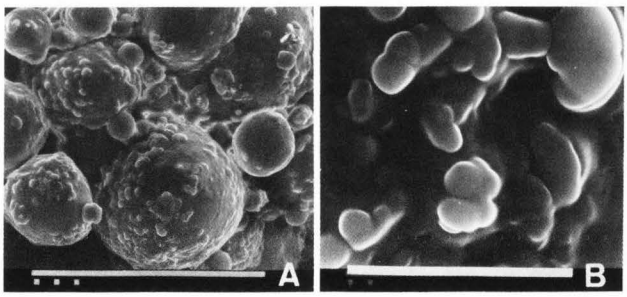

Fig. 5. Scanning electron micrographs of whole milk powder stored for 4 weeks at 75% relative humidity at room temperature. Entire view (A) and enlarged surface pattern (B) are shown. Bars in A and B = 100 and 10 μm, respectively.

β-lactose gradually crystallized at 37°C during the prolonged storage. The factors which initiated the crystallization of β-lactose are unknown at present.

The surface structure of powder particles containing β-lactose crystals is presented in Figure 7. The structure was quite different from that of the other stored powders (Figs. 5, 6) and from that demonstrated by Würsch et al. (1984). The substance which adhered to the powder particles and which was described by the latter authors as a molten material, presumably free fat, was

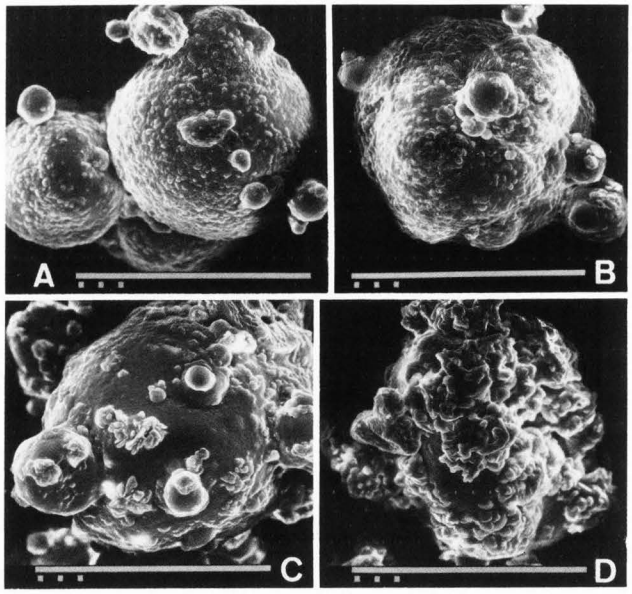

Fig. 6. Scanning electron micrographs of whole milk powder stored for 1 month at 75% relative humidity at various temperatures. A, B, C, D = stored at 0, 10, 20, 37°C, respectively. Bars = 100 μm.

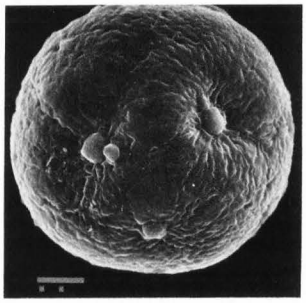

Fig. 7. Scanning electron micrographs of whole milk powder stored at 37°C (<20% relative humidity) for 5 months. Bar = 10 μm.

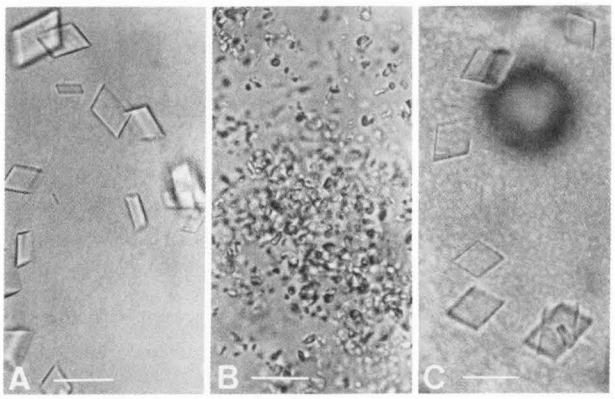

Fig. 8. Optical micrographs of fresh (A) and stored (B) instant skim milk powder and fresh whole milk powder (C) mounted in Heinz fluid. Lactose crystals were formed during the mounting procedure (A, C). Bars = 10 μm.

not observed in the powder examined in the present study. Since the whole milk powder was kept in unsealed container, accumulation of water (Würsch et al., 1984) produced via the Maillard reaction, if any, was avoided. Moisture seems to be required for the formation of the adhering substance or the molten material. Hydration of other constituents, particularly proteins (Berlin et al., 1968b) may expel free fat onto the surface of the particles.

Crystal formation by Heinz fluid

Heinz fluid, one of the mounting media for light microscopic observation, dissolved the dry milk particles but not the lactose crystals (Saito and Taguchi, 1980). The addition of the fluid to a saturated solution of lactose at twice the volume or more caused crystallization of lactose. The microscopic observation of instant skim milk powder mounted in the Heinz fluid detected many prismatic or diamond-shaped crystals (Fig. 8A). Since no crystals were detected by scanning electron microscopy and X-ray diffraction analysis in the fresh powder sample before mounting, a rapid crystallization of amorphous lactose must have occurred during the mounting procedure with the Heinz fluid, i.e. the Heinz fluid had caused lactose crystallization. The stored instant skim milk powder, however, was shown to contain only minute crystals and some insoluble material but no large prismatic crystals were present (Fig. 8B). Lactose in the stored instant skim milk powder did not develop into large crystals in the Heinz fluid, possibly because it was already in a fine crystalline form or because the Heinz fluid did not solubilize the stored instant skim milk powder completely. Similar results were obtained with the whole milk powder (Fig. 8C).

It seems possible that the Heinz fluid can be used to find the state of lactose in instant skim milk and whole milk powders.

Conclusions

Structures of instant skim milk and whole milk powder particles were well-preserved after ashing in a plasma asher. The ashing treatment did not detect the influence of lactose crystallization on the particle structure. It did, however, succeed to give some information about uniformity in distribution of constituents in the powders.

α-Lactose hydrate crystals developed rapidly in instant skim milk and whole milk powders according to moisture uptake. However, the changes in the surface structure caused by lactose crystallization were quite different in both powders. The moisture uptake proceeded through the surface of the skim milk powder particles, so that the lactose crystallization started at the surface and covered it. On the other hand, in whole milk powder, few lactose crystals but numerous droplets of free fat appeared on the surface of particles stored under conditions favoring the crystallization of α-lactose. It is highly probable that crystallizing lactose facilitated the movement of free fat onto the surface of particles due to the moisture uptake by other constituents, because the crystallization may have weakened the structure of the amorphous lactose phase in the particles. However, the relationship between lactose crystallization and the emergence of free fat is not fully understood.

Crystallization of β-lactose proceeded very slowly in whole milk powder at 37°C, when humidity was low enough to inhibit the crystallization of α-lactose hydrate. The X-ray diffraction analysis confirmed that β-lactose alone was in the crystalline state in whole milk powder stored at 37°C for 5 months at a relative humidity of less than 20%.

References

Berlin E, Anderson BA, Pallansch MJ. (1968a). Effect of water vapor sorption on porosity of dehydrated dairy products. J. Dairy Sci. **51**, 668–672.

Berlin E, Anderson BA, Pallansch MJ. (1968b). Comparison of water vapor sorption by milk powder components. J. Dairy Sci. **51**, 1912–1915.

Buchheim W. (1982). Electron microscopic localization of solvent-extractable fat in agglomerated spray-dried whole milk powder particles. Food Microstruc. **1**, 233–238.

Bullock DH. (1962). Recent developments in the drying of milk. Dairy Sci. Abstr. **24**, 60–66.

Buma TJ. (1966). The physical structure of spray-dried milk powder and the changes which take place during moisture absorption. Neth. Milk Dairy J. **20**, 91–112.

Buma TJ. (1967). X-ray powder patterns of lactose and unit cell dimensions of β-lactose. Neth. Milk Dairy J. **21**, 208–213.

Buma TJ. (1971). Free fat in spray-dried whole milk. X. A final report with a physical model for free fat in spray-dried milk. Neth. Milk Dairy J. **25**, 159–174.

Buma TJ. (1978). Particle porosity of spray-dried milk. Milchwissenschaft **33**, 538–540. (In German)

Buma TJ, Henstra S. (1971). Particle structure of spray-dried milk products as observed by a scanning electron microscope. Neth. Milk Dairy J. **25**, 75–80.

Bushill JH, Wright WB, Fuller CHF, Bell AB. (1965). The crystallization of lactose with particular reference to its occurrence in milk powder. J. Sci. Fd. Agric. **16**, 622–628.

Choi RP, Tatter CW, O'Malley CM. (1951). Lactose crystallization in dry products of milk. II. The effects of moisture and alcohol. J. Dairy Sci. **34**, 850–854.

Coulter ST, Jenness R, Crowe LK. (1948). Some changes in dry whole milk during storage. J. Dairy Sci. **31**, 986–1003.

Goulden JDS, White JW. (1958). Effects of crystallinity on the infra-red absorption spectra of lactose and dried milk. Nature **181**, 266–267.

Heldman DR, Hall CW, Hedrick TI. (1965). Vapor equilibrium relationships of dry milk. J. Dairy Sci. **48**, 845–852.

Hodge JE. (1953). Chemistry of browning reactions in model systems. Agr. Food Chem. **15**, 928–943.

Huss VW. (1970). Crystallization of lactose and availability of lysine after storage of dried skim milk at different relative humidities. Landwirtsch. Forsch. **23**, 275–288. (In German)

Huss VW. (1974). Temporal development of lysine damage during storage of skim milk powders under various conditions. Landwirtsch. Forsch. **27**, 199–210. (In German)

Kalab M. (1980). Possibilities of an electron-microscopic detection of buttermilk made from sweet cream in adulterated skim milk. Scanning Electron Microsc. 1980; III:645–652.

Kalab M. (1981). Electron microscopy of milk products: A review of techniques. Scanning Electron Microsc. 1981; III: 453–472.

King N. (1965). The physical structure of dried milk. Dairy Sci. Abstr. **27**, 91–104.

Knoop E, Samhammer E. (1962). Roentgenographic studies on the crystal structure of lactose in milk powder. Milchwissenschaft **17**, 128–131. (In German)

Miyawaki A, Maeno M. (1938). Physico-chemical properties of milk powder. Nihongakujutsukyokai Hokoku, **13**, 441–448. (In Japanese)

Nickerson TA. (1974). Lactose. In: Fundamentals of Dairy Chemistry, 2nd Ed. Webb BN, Johnson AH, Alford JA. (Eds.), AVI Publishing Co., Inc., Westport, CT, 273–324.

Olano N, Martinez-Castro I. (1983). Studies on β-lactose crystallization. Milchwissenschaft **38**, 471–474.

Parrisch FW, Brown MZ. (1982). Solid state transformation of α-lactose monohydrate in alcoholic media. J. Dairy Sci. **65**, 1668–1691.

Rockland LB. (1960). Saturated salt solutions for static control of relative humidity between 5° and 40°C. Anal. Chem. **32**, 1375–1376.

Roetman K. (1979). Crystalline lactose and the structure of spray-dried milk products as observed by scanning electron microscopy. Neth. Milk Dairy J. **33**, 1–11.

Roetman K, van Schaik M. (1975). The β/α ratio of lactose in the amorphous state. Neth. Milk Dairy J. **29**, 225–237.

Saito Z. (1980). The structure of skim milk particles as observed by scanning electron microscope. Jap. J. Dairy Food Sci. **29**, A101–A106. (In Japanese)

Saito Z, Taguchi A. (1980). Crystalline lactose in stored skim milk powder and whey powder. Jap. J. Dairy Food Sci. **29**, A133–A140. (In Japanese)

Saltmarch M, Labuza TP. (1980a). SEM investigation of the effect of lactose crystallization on the storage properties of spray-dried whey. Scanning Electron Microsc. 1980; III:659–665.

Saltmarch M, Labuza TP. (1980b). Influence of relative humidity on the physicochemical state of lactose in spray-dried sweet whey powders. J. Food Sci. **45**, 1231–1236, 1242.

Sharp PE. (1938). Seeding test for crystalline beta lactose. J. Dairy Sci. **21**, 445–449.

Taneya S. (1963). Surface structure of dried skim milk powder particle by electron microscopic observation. Jap. J. Appl. Physics **2** 637–640.

Tarassuk NP, Jack AL. (1948). A study of the browning reaction in whole milk powder and ice cream mix powder. J. Dairy Sci. **31**, 255–268.

Tuckey SL, Ruehe HA. (1934). The application of X-rays to research in dairy technology. J. Dairy Sci. **17**, 587–594.

Verhey JGP. (1972). Vacuole formation in spray powder particles 2. Location and prevention of air incorporation. Neth. Milk Dairy J. **26**, 203–224.

Warburton S, Pixton SW. (1978a). The significance of moisture in dried milk. Dairy Ind. Internatl. **43**, 23, 26–27.

Warburton S, Pixton SW. (1978b). The moisture relations of spray dried skimmed milk. J. Stored Prod. Res. **14**, 143–158.

Würsch P, Rosset J, Kollreutter B, Klein A. (1984). Crystallization of β-lactose under elevated storage temperature in spray-dried milk powder. Milchwissenschaft **39**, 579–582.

Discussion with Reviewers

E.A. Davis: Please provide examples of X-ray diffraction patterns of lactose crystals.

P. Allan-Wojtas: As X-ray diffraction technique was used to show differences between the α- and β- forms of lactose crystals and also between lactose and fat, please show one or two representative diagrams.

Author: X-ray diffraction patterns of the stored whole milk powder are presented in Figure 9. The peaks of α-lactose hydrate crystals (Fig. 9A) and β-lactose crystals (Fig. 9C) are demonstrated. The pattern showing no peaks (Fig. 9B) is the same as that of the fresh powder.

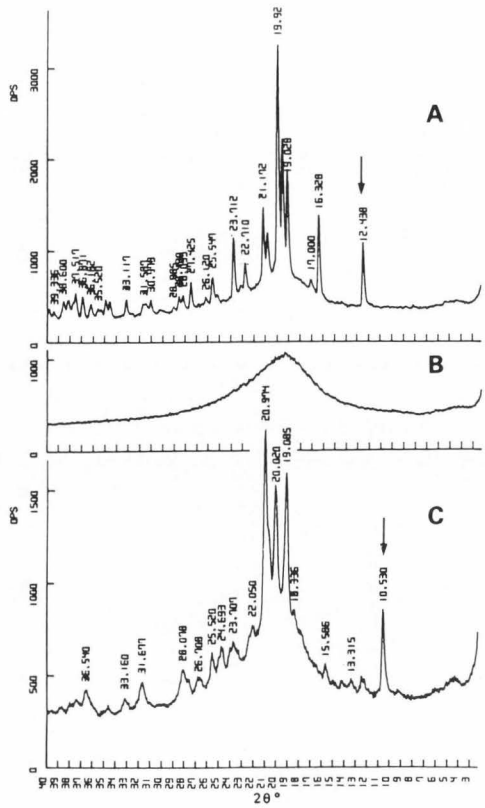

Fig. 9. X-ray diffraction patterns of whole milk powder stored at 37°C at 75% (A) or at <20% relative humidity (B, C) for 1 month (A, B) or for 5 months (C). Arrows in pattern A or C show one of the characteristic peaks of α- or β-lactose, respectively.

P. Allan-Wojtas: What converts the original skim milk powder into an instant skim milk powder while crystallization of lactose is prevented in the recent developments in the manufacturing process?

Author: I have not confirmed experimentally yet, but it must be amorphous lactose. There are two methods to produce instant skim milk powder, namely (1) to agglomerate fine particles, and (2) to produce large particles at the time of spray-drying. In the case of agglomeration process, lactose makes particles stick together. Recently, the agglomeration process, as well as the large-particle process, have been carried out by a single-stage process, which means that instant skim milk powder is produced from liquid milk in a single drying operation. Therefore, the rapidity of moisture evaporation during the process prevents crystallization of the lactose.

M. Kalab: You have found that there were differences between the surfaces of commercial skim milk and whole milk powder particles, whereby lactose crystals developed to a lesser extent on the whole milk particles because of the presence of fat. To eliminate the effects of differences in the manufacturing process and to confirm that the presence of fat in the whole milk powder was responsible for the surface features in that powder,

did you observe similar differences in experiments with original skim milk and whole milk powders exposed to a humid atmosphere?

Author: I did not examine the original (non-instant) skim milk powder. However, 3 samples of the instant skim milk powder produced by different manufacturers were examined after 1 month storage at 75% relative humidity. Similar results were obtained from these samples in respect to lactose crystallization on the particle surface.

D.P. Dylewski: In your paper you state that the hydration of proteins may expel free fat onto the surface of whole milk particles. Could you explain further what you mean by "free" fat and how it might differ from "bound" lipid?

Author: Free fat means the fat which is not in the form of fat globules. Initially all of the fat in milk exists as globular fat. Mechanical or physical force damages fat globules and produces free fat. In the whole milk powder, fat globules embedded in lactose matrix could be equivalent to "bound" lipid.

M. Saltmarch: What practical significance would you say the discovery of β-lactose crystals could have in instant skim milk powder?

Author: The finding about β-lactose crystals is a matter of interest in lactose crystallization rather than in the properties of instant skim milk powder. However, the effect of the crystallization of β-lactose on physical properties of milk powder particles may provide a new area for the use of milk powder in the food industry.

FOOD MICROSTRUCTURE, Vol. 4 (1985), pp. 341-348
SEM Inc., AMF O'Hare (Chicago), IL 60666-0507 U.S.A.

0730-5419/85$1.00+.05

MICROSTRUCTURE OF SPRAY-DRIED AND FREEZE-DRIED MICROALGAL POWDERS

L.P. Lin

Department of Agricultural Chemistry
National Taiwan University
Taipei, Taiwan, Republic of China

Abstract

Chlorella and *Spirulina* algae were spray-dried and freeze-dried under several different conditions, and the morphological changes induced were studied by scanning electron microscopy. The internal structure of the particles (granules) was revealed by cryofracturing. The cellular composition of the two algae, method of drying, cell concentration, feed conditions, temperature, and drying times all affected the external morphology of the resulting powders. In the case of spray-drying, at a temperature of 160°C for 6 sec, the particles shrunk or collapsed; if the drying time was over 10 sec at 160°C, similar results were observed. The cell concentration affected the thickness of the dried particle wall; a high concentration produced thicker and heavier particles, lower concentrations produced thinner and lighter particles. The rate and pressure at which the liquid was fed into the drying chamber affected the proper atomization of the liquid. When freeze-dried, the algal powder structure was different from particles formed by spray-drying. Spray-dried particles were individual spheres with a void space in the center. Each particle was composed of a few thousand cells in the case of *Chlorella* and several trichomes in the case of *Spirulina*. In contrast freeze-dried algae formed sheets of cells that were no longer spherical and which adhered together in a linear fashion.

The cryogenic process used in this study to fracture and study the structure of spray-dried microalgal powders should prove to be very helpful in selecting optimal conditions for the production of high quality health food products.

Initial paper received February 02 1985
Manuscript received June 03 1985
Direct inquiries to L.P. Lin
Telephone number: 886-2-3510231x2598

Keywords: *Chlorella, Spirulina,* Cryofracture, Spray-dried microalgal powder, Freeze-dried microalgal powder, Microstructure, Void space, Particle hardness, Health food.

Present Address (till July 31, 1986):
Department of Microbiology,
Michigan State University,
East Lansing, MI 48824

Introduction

Mass algal cultivation began in Germany during World War II when experiments were performed to grow certain algal strains as a source of lipids and proteins. During the late 1940's and 1950's, particularly in Japan, microalgae were produced as a potential source of food or animal feed (4). Subsequently, *Chlorella* species were produced on a commercial scale in Japan as a food or feed additive. In the U.S., algal products have also been used to treat waste and sewage in oxidation ponds in California (10), and they have also been used in conjunction with bioregenerative designs for long-duration space missions. *Chlorella* has been studied extensively under many different growth conditions (2,6,7).

The production of *Spirulina* began in the early 1960's with the work of the Institute Français du Petrole (IFP). Clement and her coworkers, as mentioned by Dubinsky's review (4), studied *Spirulina* after observing that tribes along the shores of Lake Chad used *S. maxima* as a substitute for meat source. Today, there are several commercial plants that produce *Spirulina* for the health food industry.

Spirulina is a cyanobacterium with relatively wide filaments normally coiled in large, lax helices. It can tolerate high intensities of sunlight, can grow rapidly in a warm, shallow, brackish lakes, and will reach high filament densities, making *Spirulina* relatively easy to harvest. It is one of the most abundant algae found in the many alkaline lakes of Africa and the Americas (4). The mass cultivation of *S. maxima* is now being practiced in alkaline waters at Lake Texcoco in Mexico, where production is 1 metric ton per day (10). *Spirulina platensis* is cultivated in Japan and Taiwan by using bicarbonate as a source of carbon and sunlight as a source of energy. Extensive research has also been performed in Israel (17). There have been several ultrastructural studies of *Spirulina* spp. (1,5,20).

Recently, *Chlorella* and *Spirulina* algae have been produced on a large commercial scale in Japan and Taiwan. Dried algal powders and tablets are used as health foods, and a concentrated water-soluble extract called "Chlorella Growth Factor" has also been produced by boiling the dry algal powder. The specific chemical composition of this extract has not yet been fully described, but it is already being used as a health food additive in a wide variety of foods.

A thorough understanding of the microstructure of dried *Chlorella* and *Spirulina* would be of great value for the improvement of processing techniques. In order to make a uniform,

dense, and pure dry form of these algae, the heating temperatures, duration times, feed conditions, cell concentrations, and cell densities during the drying process must be carefully regulated. When properly regulated, the quality and nutritional value of the algal powders will be greatly enhanced. In addition, when the health food industry uses these dried algae to make tablets, they cannot use cementing materials to make the particles adhere together as would a vitamin manufacturer or other non-health food industry. Instead, they must produce dry algae of sufficient density and appropriate structure or the tablet will disintegrate. Thus, an analysis of dried algal microstructure is essential for the health food industry.

The purpose of this paper is to examine the microstructure of spray-dried and freeze-dried microalgal powders in order to improve the manufacturing techniques available for use with these microalgae.

Materials and Methods

Algal cultures

Chlorella pyrenoidosa was used throughout this study. The inoculum was prepared in a modified Allen's medium containing mg/L: urea-600; $MgSO_4 \cdot 7H_2O$-300; KH_2PO_4-300; $FeSO_4 \cdot 7H_2O$-5; EDTA-7. Each liter contained 70 mL of glacial acetic acid (6); this medium was transferred into open culturing pools of 2 m in diameter, and then gradually scaled up to pools of 30 m in diameter. The cells were grown in autotrophic conditions; mineral nutrients and glacial acetic acid were periodically replenished to create favorable growth conditions (6,7).

Spirulina platensis was cultivated in a mineral medium (16) using two liter flat-flasks. The incident light intensity from cool white fluorescent lamps (40W) ranged from 0.3 to 21 KLux, and the culture temperature ranged from 25 to 30°C. Mass culturing was performed on the same scale as the *Chlorella* culturing; *Spirulina* was fed with bicarbonate as the source of carbon.

Drying

The cells were harvested and washed by continuous centrifugation at 5,000 g. Spray-dried powders were prepared in a Kochiwa spray dryer by means of centrifugal atomization (4,500 g) at an inlet temperature of 140–150°C and an outlet temperature of 80–85°C. The central portion of the chamber was maintained at 130–135°C. The powder was formed within 6–8 sec after being injected into the chamber. Two procedures were used for freeze-drying: slow-freezing and rapid-freezing. One mL samples of suspended *Chlorella* cells at a concentration of 10% (w/v) were placed in 15 mL screwcap bottles of methanol maintained at −60°C and were slowly frozen in 1 min Liquid nitrogen (−196°C) was used for rapid-freezing. In both cases, a VirTis freeze dryer (Model 10030) with a vacuum of 6×10^{-2} Torr was used for the 12 h drying period. The final moisture content was usually less than 3%.

Preparation of original algal cells for electron microscopy

Samples were periodically withdrawn from the bottles or pools. Cells were then harvested by centrifugation at 600 g for 15 min and washed wtih distilled water three times. The cells were fixed in 2.5% osmium tetroxide for observation by electron microscopy (11,12).

Transmission electron microscopy (TEM)

Fresh algal cells were fixed in cacodylate buffered glutaraldehyde-formaldehyde at 4°C for 1 h, washed in a cold 0.1 M cacodylate buffer, post-fixed in a cold buffered 2.5% osmium tetroxide solution for 2 h, then washed again in buffer. After fixation, all specimens were dehydrated by transferring them through a series of 10 min alcohol baths with concentrations ranging from 60, 70, 80, 90, 95, and 100% ethyl alcohol. They were then embedded in Epon 812 mixtures. Ultrathin sections were cut with a DuPont diamond knife on a Sorvall MT2-B "Porter Blum" ultramicrotome, and sections were picked up on uncoated grids. The sections were doubly-stained with uranyl acetate and lead citrate. Photomicrographs were taken with a Hitachi HU-12 electron microscope at an acceleration voltage of 75 kV; initial magnifications were from 4,000 to 20,000.

Scanning electron microscopy (SEM)

Fresh cells were fixed in 0.1 M phosphate buffered (pH 7.4) 1% glutaraldehyde for 2 h at 5°C. Specimens were dehydrated by transferring them through 10 min alcohol baths as described above; the alcohol was removed by a 10 to 15 min bath in isoamylacetate, and the specimens were dried with an HCP-1 critical point dryer (Hitachi Koki, Tokyo, Japan). The specimens were coated with a thin conductive layer of gold, and were then examined in a Hitachi S-550 scanning electron microscope using an acceleration voltage of 20 kV. Micrographs were taken on Fuji film (125 ASA), and the initial magnifications ranged from 500 to 5,000.

Examination of dried algal powders

In order to examine the external structure, dried *Chlorella* and *Spirulina* powders were attached to double-sided adhesive tape on SEM stubs, and were then sputter-coated with gold (20 to 40 nm) in an Eiko Ion Coater, Model IB-2. The specimens were kept in a dessicator (filled with silica gel) until placement in the SEM chamber. The specimens were examined in a Hitachi S-550.

The process used to examine the internal structure is outlined in Fig. 1. Spray dried powders were first encapsulated in an agar gel; this assured that the original particle structure would remain intact during the process of preparing the cells for electron microscopy. A slice was then cut from the coagulated gel, rinsed in distilled water, fixed in 1% osmium tetroxide for 2 h, and then dehydrated by immersion in the series of alcohol baths as mentioned above. The next stage was to freeze the dehydrated sample in liquid nitrogen; it was first wrapped in a cellophane film so that the small samples were more easily retrieved after fracturing. An alternate method would be to place the samples on small pieces of aluminum foil. The liquid nitrogen hardened the gel so that it could be gently cracked open with a razor blade while still in the liquid nitrogen after the boiling stopped. If done carefully, the original structure of the particle was not distorted. This fractured material was then stored in a bath of 100% ethyl alcohol until critical point drying. Critical point drying and ion coating procedures for SEM were the same as mentioned above.

Chemical and bacteriological analysis

Algal powders used in the health food industry must also be examined for purity and safety. We therefore performed preliminary chemical and bacteriological analysis on the dried powders in order to evaluate and compare the quality of various samples.

The water content was determined by drying the sample at 105°C for 12 h. The total chlorophyll content was determined by the methanol extraction method described by MacKinney (13). The relative activity of chlorophyllase was determined by the method described by Tamai, et al. (19); when spray-dried at 160°C for 6 sec, chlorophyllase was deactivated. The content

of toxic pheophorbide was estimated according to the method described by Wickliff and Arnoff (21).

The total bacterial count was estimated by using the conventional plate count method; coliform bacteria were counted by using deoxycholate media according to the Difco manual (3).

Results and Discussion

Chlorella pyrenoidosa grows autotrophically on CO_2, but as the rate of cellular growth is much too slow for industrial purposes, acetic acid may be added to the solution and the *Chlorella* will grow heterotrophically, thus rapidly increasing the rate of cell growth. As this alga grows both by means of autotrophy and heterotrophy, it may be called mixotrophic. Grown under these conditions, the cells (Fig. 2) were spherical, 2–8 μm in diameter with a relatively thin cell wall. The chromatophore was cup-shaped and a pyrenoid was occasionally present in the cell. The chloroplast was clearly differentiated and contained abundant photosynthetic storage material. Starch granules surrounded the pyrenoid and were also located in the interlamellar spaces of the chloroplasts. The SEM micrograph (Fig. 3) shows that the cells were spherical and measured 3 to 6 μm in diameter; there was no significant contamination of the cultures. In contaminated cultures, photosynthetic purple bacteria of the *Rhodopseudomonas* variety were usually stuck to the surface of the algal cells (11).

Spirulina was in the shape of a helix (Fig. 4), the pitch of which was proportional to the size of the cells. A transverse section through the trichome is shown in Fig. 5. The cell wall was divided into four layers and the septum into three layers. The photosynthetic lamellae were closed, irregularly shaped discs, and the membranes consisted of two parallel lines. Mesosomes were often located near the cross wall and were connected to the photosynthetic lamellae. These have been observed by Allen (1) and by van Eykelenburg (5). Polyhedral bodies (polyglucan-like granules) were observed in some preparations. These bodies were located near or enclosed within the photosynthetic lamellae. As mentioned by Titu, et al. (20), these granules are the most prevalent structural elements and are uniformly distributed in the region between the nucleoplasm and the cell wall. SEM micrographs revealed the steric configuration of the spiral structures. The structure of *Spirulina* resembles that of other Oscillatoriaceae and possesses all typical organelles found in procaryotic cells. The growth conditions affected the morphology and the dimensions of some organelles.

The morphological changes of *Chlorella* and *Spirulina* that occurred during spray-drying were investigated by SEM. Spray-dried algal powders consisted of globular particles (Figs. 6 & 7) with cavities in their centers (Figs. 8 & 9); this phenomenon was previously observed by Lee and Rha (8) in their study of spray-dried yeast powders. These void spaces had diameters of approximately one-half of the entire particle when viewed sectionally (Fig. 10). Considering that each granule has a diameter of approximately 50–80 μm (excluding the void space), it is estimated that each granule is composed of 3,000 to 7,000 *Chlorella* cells. The method used to determine this calculation was reported in a previous paper (9). Several entwined strips of cells comprised the granules of the *Spirulina* powder (Fig. 7); they were 40–100 μm in diameter, and ranged from a few to about a dozen trichomes, depending on the drying conditions. There was a striking difference between the two kinds of algal

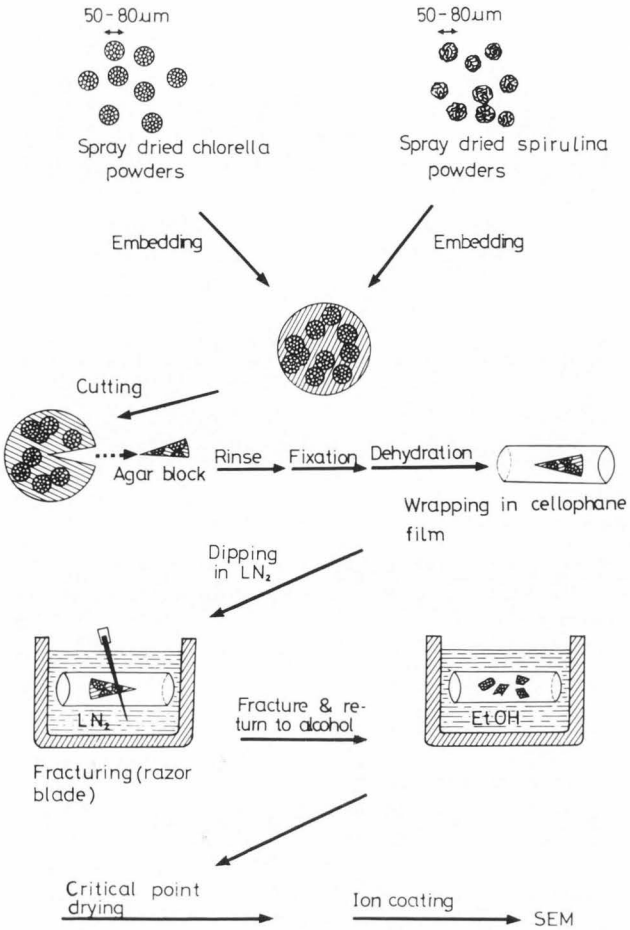

Fig. 1. Schematic diagram of a cryogenic process used to fracture spray-dried microalgal powders so that the internal structure could be studied in detail.

powders. The *Chlorella* powder granule appeared to be an aggregate of discrete cells adhered to one another (Fig. 6). The *Spirulina* powder particle, however, appeared to be a more amorphous structure of cells fused together; the boundaries between the original helical structures were no longer clearly defined (Fig. 7). This phenomenon may be related to the different chemical compositions of the cell walls of these algae. *Chlorella* is a eucaryotic cell and the surface layer is predominantly composed of cellulose (15). *Spirulina* is a procaryotic cell and the cell surface is mainly composed of mucopolysaccharide (5).

In most cases, the resulting spray-dried particle was spherical and hollow, with debris attached to the surface. Changing the feed conditions (inlet and outlet temperatures, time, and extent of atomization) led to changes in the appearance of the granules. For example, shrunken particles were observed when powders were dried at an elevated temperature (>160°C) for 6 sec or dried for a prolonged period of time (>10 sec) at 160°C. The *Spirulina* particles dried under these conditions were misshapen (Fig. 11), and the *Chlorella* particles also lost their spherical shape when improperly dried (Fig. 12); both showed an increase of smaller irregular fragments which vary considerably in size. The irregular formation of particles is attributed to the formation of a case-hardened outer surface on each particle which

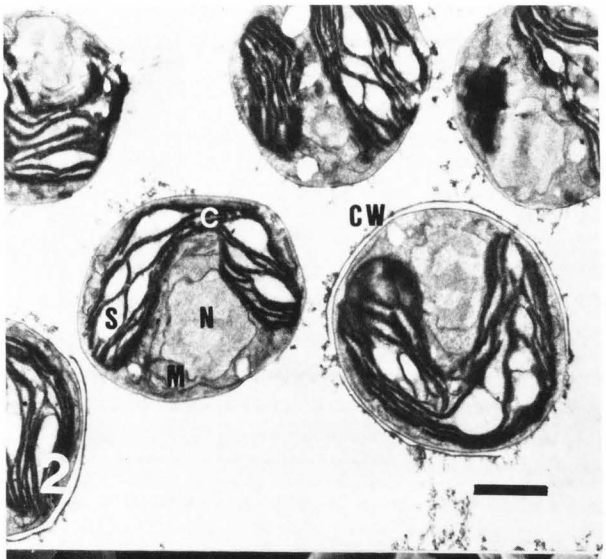

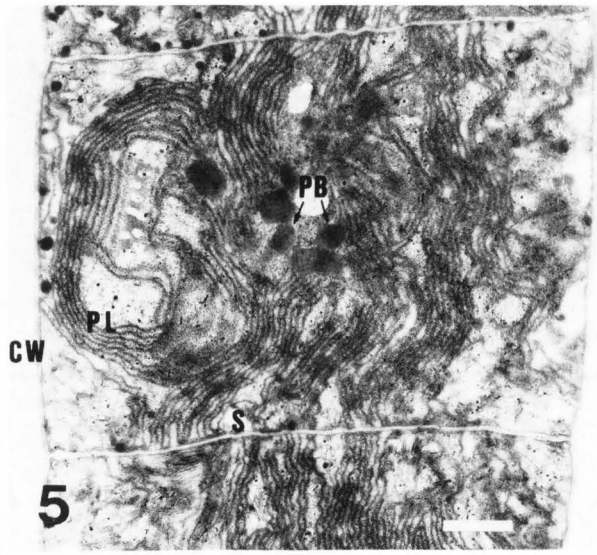

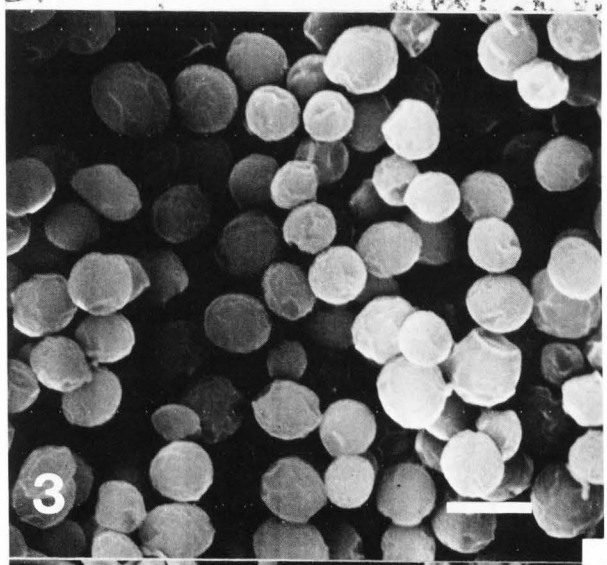

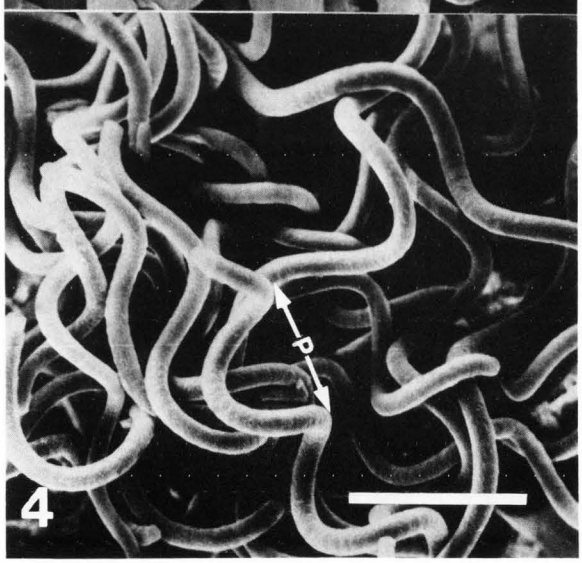

Fig. 2. Transmission electron micrograph of mixotrophically grown *Chlorella* cells, showing typical green algal characteristics. Note the cell wall (CW). The cell contains a cup-like chloroplast (C), a nucleus (N), mitochondrion (M), and starch grains (S). Bar = 1 μm.

Fig. 3. Scanning electron micrograph of *Chlorella* cells, showing spherical shape. Bar = 5 μm.

Fig. 4. Scanning electron micrograph of helical trichome of *Spirulina* showing the pitch (P) and the outer diameter of the helix. Bar = 50 μm.

Fig. 5. Transmission electron micrograph of a *Spirulina* cell, showing typical characteristics of blue-green algae. Note the cell wall (CW), and the septum (S), the photosynthetic lamellae (PL), and polyhedral bodies (PB). Bar = 1 μm.

prevented liquid from reaching the surface from the particle interior. Because of high heat transfer rates in the droplets, the liquid at the center of the droplet vaporized, causing the outer shell to expand and form a hollow sphere. Sometimes the rate of vapor generation within the droplet was sufficient to blow a hole through the wall of the spherical shell, as shown in Figs. 8 & 9; the entire structure then often collapsed (Fig. 12).

The ideal cell concentration was 10% (w/v), and the range from 5 to 15% was found to be acceptable. Higher concentrations produced dried particles with a thicker wall and a smaller void space. Lower concentrations produced dried particles with a thinner wall and a larger void space. If the cell concentration of the algal cells was over 20% it tended to stick in the atomizer disc of the spray drier. The rate at which the solution was fed into the drier also affected the size of the particles. The faster the atomizer disc of the spray drier spun, the smaller the particles became, but if it spun too fast, the particles stuck to the sides of the drier and burned. The shape of the holes in the atomizing disc also affected the shape of the dried particle.

Freeze-dried algal powders were non-spherical and instead resembled three-dimensional networks or sheet-like clusters (Figs. 13, 14, & 15). Slow freezing rates between −30 to −60°C and freeze-drying resulted in the development of large ice crystals in the intercellular spaces and the displacement of the constituent parts (Fig. 14). These ice crystals could exert pressure on the cells to the extent that dehydration of the cells would occur.

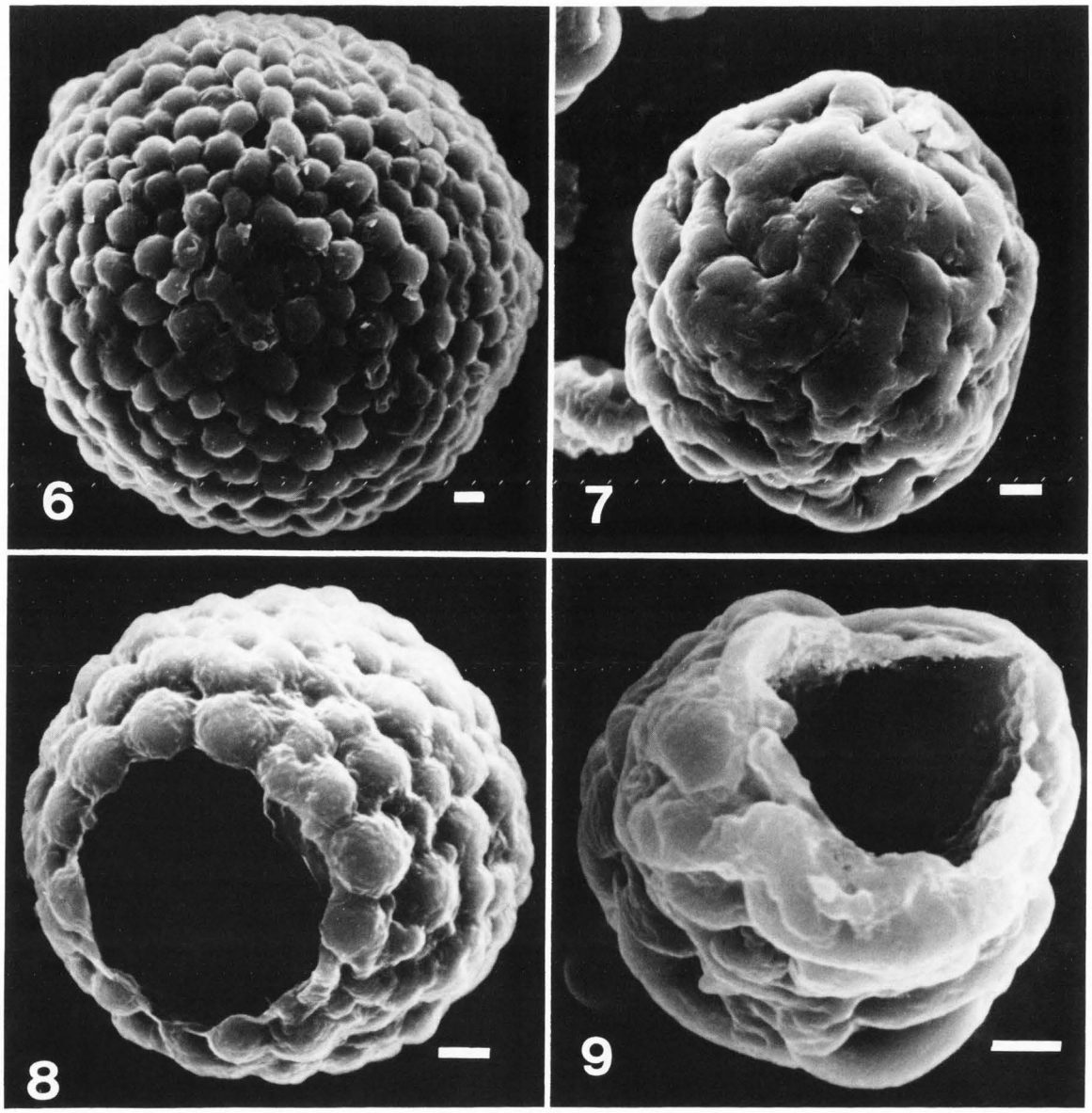

Fig. 6. Scanning electron micrograph of a spherical spray-dried *Chlorella* granule. Bar = 5 μm.
Fig. 7. Scanning electron micrograph of a spherical spray-dried *Spirulina* granule. Bar = 5 μm.
Fig. 8. A spray-dried *Chlorella* particle, showing the sectional view and hollow structure. Bar = 5 μm.
Fig. 9. A spray-dried *Spirulina* particle, showing the hollow structure. Bar = 5 μm.

If the cells were rapidly frozen in liquid nitrogen (LN_2) at −196°C, it was found that smaller intercellular ice crystals formed and the cell membranes were left intact. The degree of mechanical damage caused by ice crystal formation was thus reduced, and sheet-like clusters of the cells were observed. As a result, the original shape of the sample was preserved (Fig. 15).

Bacteriological and chemical analysis of the *Chlorella* powders (Table 1) showed that the total chlorophyll content was higher in the spray-dried than in the freeze-dried materials. In addition, no coliforms were found in the spray-dried powders. The total bacterial count ranged from 10^3 to 10^4 cells per gram, which reflected the non-sterile, mixed-culture conditions of the algal production (6,7). Sinsky and Silverman (18) reported that the average proportion of *Escherichia coli* cells which survived freeze-drying in 2% gelatin was 0.6% of the frozen cells; 28% of the cells which survived freeze-drying under these conditions incurred damage. A pronounced effect caused by freeze-drying and rehydration of *E. coli* was alterd permeability of the cell wall and cytoplasmic membrane. The toxic component pheophorbide, which is considered to be an undesirable component of *Chlorella*, was slightly higher in the freeze-dried samples.

Spray-dried algae formed individual spheres that were hollow and not aggregated. When freeze-dried, however, the algal particles adhered together in the form of a sheet; they were not spherical as were the spray dried particles, but were joined in

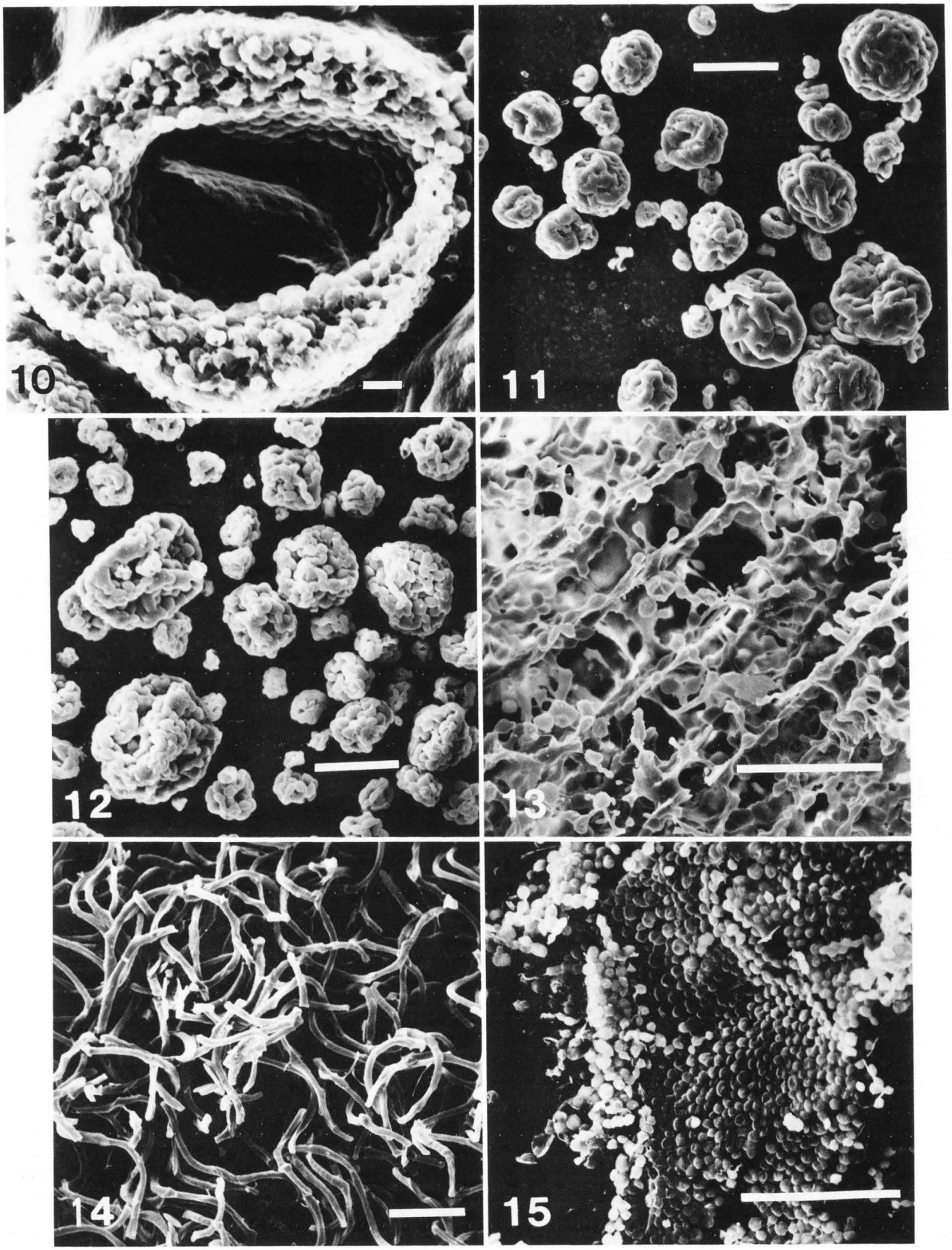
10
11
12
13
14
15

Fig. 10. A cross-sectional view of a spray-dried *Chlorella* particle, showing hollow structure. Bar = 5 μm.
Fig. 11. Scanning electron micrograph of spray-dried *Spirulina* powder which was formed after spray-drying at an elevated temperature, showing that most particles exhibited collapsed forms. Bar = 50 μm.
Fig. 12. Scanning electron micrograph of spray-dried *Chlorella* powder which was submitted to an elevated temperature, showing the shrunken and collapsed forms. Bar = 50 μm.
Fig. 13. Scanning electron micrograph of slowly frozen (−30°C) dried cells of *Chlorella*, showing fused appearances. Bar = 5 μm.
Fig. 14. Freeze-dried cells of *Spirulina*, showing cluster-like structure. Bar = 50 μm.
Fig. 15. Rapidly frozen (−196°C) cells of *Chlorella*, showing sheet-like arrangement. Bar = 5 μm.

a three dimensional network. In the case of *Chlorella,* slow freeze-drying and ice formation often fused cells together, thus making the distinction between separate cells difficult (Fig. 13). Fast freeze-drying, and the formation of smaller ice crystals, resulted in groups of discrete cells whose contents remained intact (Figs. 14 & 15). Freeze-drying appeared to be an effective method of preserving these algal strains (14).

Scanning electron microscopy is particularly well suited for a wide range of routine analyses of algal powdered foods. The process of dehydration is a major economic factor in the production of dried algal powders. It may constitute approximately 30% of the total production cost. By studying the structure of the particle, the most economical drying conditions may be determined and waste may be reduced. The method of dehydration also affects the food value, taste, color, texture, and digestibility of the final product. Spray-drying destroys toxic substances much more effectively than freeze-drying, and spray-drying produces a powder that is very hard (3.5–5.5 kg), while freeze-drying produces a powder almost half as hard (2.5 kg max). This is important for the production of hard tablets without using cementing materials.

The spray-drying of commercial quantities of algal powders is currently being practiced only in Taiwan. This study was the first to examine the microstructure of such algae in detail. A suitable cryogenic process was devised for that purpose. Both spray-drying and freeze-drying are expensive processes, but after an overall analysis of microstructure, bacterial and chemical content, they were found to be superior to conventional methods such as drum drying.

Table 1. Results of bacteriological and chemical analyses of dried *Chlorella* powders.[1]

	Spray-dried	Freeze-dried
Water content (%)	2–3	3–4
Ash (%)	5.1	5.4
Protein (%)	65.7	66.5
Total bacteria (#/g)[2]	1×10^3	3×10^4
Total coliforms (#/g)	negative	1×10^2 [3]
Chlorophyll (%)	2–3	4–5
Pheophorbide (mg%)[4]	25–50	50–60
Chlorophyllase (mg%)[4]	90–160	190–250
Hardness (kg)[5]	3.5–5.5	2.5 (max)
Color	deep green	light green

[1] The initial concentration of *Chlorella* suspension was 10–12% (w/v), as determined by dry weight.
[2] The total bacterial count in the *Chlorella* suspension was 10^6-10^7 colonies per mL. The majority were photosynthetic bacteria.
[3] Approximately 100 colonies appeared on deoxycholate media.
[4] The enzyme activity was converted to mg% for convenience, as described by Wickliff and Arnoff (21).
[5] Hardness was determined by testing 250 mg tablets with the Monsanto type hardness meter.

Acknowledgements

The author wishes to express his appreciation to the Taiwan Chlorella Industrial Company for providing culturing pools and spray-dried algal powders. The author also wishes to thank Mr. V.C. Liao, Miss S.W. Hsieh and Mr. C.S. Cheng for technical assistance.

References

1. Allen MM. (1972). Mesosomes in blue-green algae. Arch. Mikrobiol. **84**: 199–206.
2. Budd TW, Tjostem JL, Duysen ME. (1969). Ultrastructure of *Chlorella pyrenoidosa* as affected by environmental changes. Amer. J. Bot. **56**: 540–545.
3. Difco Laboratories. (1984). Difco manual—Dehydrated culture media and reagents for microbiology. 10th ed. p. 274–275. Difco Laboratories, Detroit, MI.
4. Dubinsky Z, Aaronson S. (1982). Review of the potential uses of microalgae. Biosaline Research: A look to the future. A. San Pietro (Ed.), Plenum Pub. Co., p. 181–206.
5. van Eykelenburg C. (1979). The ultrastructure of *Spirulina platensis* in relation to temperature and light intensity. Ant. Leeuw. **45**: 369–390.
6. Huang SA, Lin LP. (1981). Nutrient requirements on the growth of cultivated edible microalgae for mass production. J. Chinese Agr. Chem. Soc. (Taiwan) **19**: 208–217.
7. Huang SA, Lin LP. (1983). Effects of the culture conditions on conversion of *Chlorella pyrenoidosa* from autotrophic to mixotrophic culture. J. Chinese Agr. Chem. Soc. (Taiwan). **21**: 71–81.
8. Lee CH, Rha CK. (1979). Application of scanning electron microscopy for the development of materials for food. Scanning Electron Microsc. 1979; III: 465–471.
9. Liao VC, Lin LP. (1981). Electron microscopic studies on spray-dried and freeze-dried *Chlorella* powders. J. Chinese Agri. Chem. Soc. (Taiwan) **19**:125–135.
10. Litchfield JH. (1983). Single-cell proteins. Science **219**: 740–746.
11. Lin LP, Liao VC, Chen HC. (1980). Ultrastructural cytology of the cultivated green alga *Chlorella pyrenoidosa*. Mem. Coll. Agri., Natl. Taiwan Univ. (Taiwan) **20**:86–100.

12. Lin LP. (1980). Electron microscopy of fresh and dried cells of *Chlorella pyrenoidosa*. 38th Ann. Proc. Electron Microscopy Soc. Amer., San Francisco, CA, p. 490–491. Claitor's Publ. Div., Baton Rouge, LA.

13. MacKinney G. (1941). Absorption of light by chlorophyll solutions. J. Biol. Chem. **140**: 315–322.

14. McGrath MS, Daggett P-M, Dilworth S. (1978). Freeze-drying algae: Chlorophyta and Chrysophyta. J. Phycol. **14**: 521–525.

15. Northcote DH, Goulding KJ. (1958). The chemical composition and structure of the cell wall of *Chlorella pyrenoidosa*. Biochem. J. **70**: 391–397.

16. Ogawa T, Terui G. (1970). Studies on the growth of *Spirulina platensis*. (I) on the pure culture of *Spirulina platensis*. J. Ferment. Technol. **48**: 361–367.

17. Richmond A, Vonshak A. (1978). *Spirulina* culture in Israel. Arch. Hydrobiol. Beih. Frgebn. Limnol. **11**: 274–280.

18. Sinskey TJ, Silverman GJ. (1970). Characterization of injury incurred by *Escherichia coli* upon freeze-drying. J. Bacteriol. **101**: 429–439.

19. Tamai H, Shioi Y, Sasa T. (1979). Studies on chlorophyllase of *Chlorella protothecoides*. IV. Some properties of the purified enzyme. Plant Cell Physiol. **20**: 1141–1145.

20. Titu H, Popovigi G, Boldor O, Spiresgu I, Stanca D. (1980). The ultrastructure of homogonal cells in blue-green alga *Spirulina platensis* (Nordst.) Ceitl. Rev. Roum. Biol. **25**: 143–150.

21. Wickliff JL, Arnoff S. (1963). Degradation of chlorophyll a to pheophytin a, pheophorbide a and pyrroporphine XV for tracer studies. Anal. Biochem. **6**: 39–46.

Discussion with Reviewers

K. Saio: What shape is ideal when *Chlorella* or *Spirulina* are used for health foods? Do the shape and the hollowness of the particle affect its solubility in hot and cold water?

Author: A spherical spray-dried algal powder appears to be most suitable for the health food industry. It is much easier to produce than droplet-shaped or ellipsoid particles, and the thickness of the particle shell in relation to the void space is more easily regulated when the particle is spherical. If the void space is too large or too small, or the particle wall is too thin or too thick, the particle will be undesirable. If the wall is too thin, good tablets cannot be made; it will also dissolve too quickly in the human digestive system. If the wall is too thick, the particle is not as economical to produce. Of course, hot water will dissolve these particles much faster than cold water.

R.A. Holley: Do you agree with Pabst (1975) who felt that drum dried or boiled *Chlorella* were more digestible than powders produced by other methods? Why? (Pabst, W. (1975) Feeding trials for the determination of the nutritional value of microalgae. In Symposium Microbial Production of Protein 1975, F. Wagner (Ed.), Verlag Chemie, Weinheim, W. Germany (German)).

Author: The research done by Pabst mainly concerned *Scenedesmus*, while this study dealt with *Chlorella*. For human consumption, *Chlorella* is generally preferred because many feel that *Scenedesmus* does not contain a sufficient amount of "Growth Factor". Apart from this difference, the cellular structures of these algae are very different, and a spray-dried *Scenedesmus* particle may have a different microstructure than the spray-dried *Chlorella* particle.

In regard to digestibility, boiling or infusion will increase digestibility because it breaks down the cell wall of the algae, but this process may also cause soluble materials to leach out, causing the total nutritional value to change. Drum-drying and spray-drying are similar heating processes and thus the digestibility of both products is probably very similar as well.

M.V. Taranto: In order to study the internal structure of the dried algal cells, you encapsulated them in agar and then exposed the cells to water. This surely caused the cells to hydrate which more than likely altered the cell morphology. In addition, you fixed, froze, fractured and redried the cells. This surely caused morphological distortion. If your objective was to study the effect of the spray drying and freeze drying process, why did you not embed the dry cells in epoxy to immobilize the cells and then fracture the cured block? This procedure may have yielded fractured cells in the dry state which would more clearly demonstrate the effect of the drying process on cell morphology.

Author: The purpose of embedding the cells in the agar and cracking it open was to study the void space in the center of the sphere. Individual cells showed some distortion due to rehydration, but this was not critical to the overall morphology of the particle. When reexposed to water, the dried algal cells expanded about five percent. When they were redried, they again shrunk. Although this method was not ideal, I found that the morphological distortions were not critical for this study.

There are also complications if the cells are set in epoxy. It is difficult to mix dried algal powders with viscous epoxy resins. The dried powder also contains approximately 3% water, and this tends to hinder the proper adhesion of the epoxy. When frozen during the fracturing process, the water will freeze and affect the morphology. The benefits of using epoxy and avoiding the rehydration of the cells is an attractive possibility that will require further investigation.

FOOD MICROSTRUCTURE, Vol. 4 (1985), pp. 349-355
SEM Inc., AMF O'Hare (Chicago), IL 60666-0507 U.S.A.

0730-5419/85$1.00+.05

EFFECT OF IONIZING IRRADIATION AND STORAGE ON MUSHROOM ULTRASTRUCTURE. I. THE GILLS OF *AGARICUS BISPORUS* (LGE.) IMBACH and *PLEUROTUS OSTREATUS* (JACQ.EX FR.) KUMMER

Á.Keresztes[1], J. Kovács[2] and E. Kovács[3]

[1]Department of Plant Anatomy, Eötvös Loránd University, 1088 Budapest, Muzeum krt. 4/A

[2]Department of General Zoology, Eötvös Loránd University, 1088 Budapest, Puskin u. 3.

[3]Department of Microbiology, Central Food Research Institute, 1022, Budapest, Herman Ottó u. 15., Hungary

Abstract

We have investigated the gills of both the control and gamma-irradiated groups of A.bisporus and P.ostreatus (2.5 kGy or 2.5 and 5.0 kGy doses, respectively) by scanning (SEM) and transmission (TEM) electron microscopy. The primary aim of our study was to see, how gamma-irradiation used for shelf-life extension inhibits spore production. We have found in both species that inhibition of spore production in irradiated specimens is caused by the destroying of basidia rather than by retarding normal spore development. In P.ostreatus the hymenium appears to be more sensitive to irradiation than in A.bisporus. In both species the subhymenium and trama seem less sensitive than the hymenium.

Initial paper received January 08 1985
Manuscript received June 04 1985
Direct inquiries to E. Kovács
Telephone number: 36-1-152028/157341

KEY WORDS: Mushroom, Agaricus bisporus, Pleurotus ostreatus, scanning electron microscopy, transmission electron microscopy, ultrastructure, irradiation, growth retardation, shelf-life extension, ripening

Introduction

Staden (1964, 1965) was the first to report on a new method based on irradiation for the extension of storage life of mushrooms. Experiments have shown that irradiation inhibits the opening of the pileus and changes the sensory properties of the mushroom (Stoller 1968; Kovács et al., 1968, Kovács and Vas, 1970;1974a,b). An irradiation dose of 2.5 kGy strongly inhibited veil opening throughout the storage period (Wahid and Kovács, 1980). In the control samples the veil started to rupture on the first day, and on the second day all mushrooms were fully open. Spore formation was found to start while the caps were still closed. The beginning of opening coincided with the increase in spore count. After irradiation treatment not only does the pileus remain closed but the development of gills also stops, thereby inhibiting the formation and growth of spores as well (Kovács et al., 1981).

The question arises therefore whether the cessation of spore production is caused by lengthening of the juvenile stage of the cells, or due to the destructive processes, such as radiation damage.

In order to answer this question, we have performed scanning (SEM) and transmission (TEM) electron microscopic investigations on the gills.

Materials and Methods

Experimental materials and treatments

A.bisporus provided by Duna MgTSz (Budapest) and P.ostreatus provided by Borota MgTSz (Borota) were used for the experiments. From the freshly harvested young, closed A.bisporus carpophores, those of 3-5 cm diameter were selected for irradiation, while from P.ostreatus, 7-10 cm fresh fruit bodies were used.

Samples were irradiated at the Institute of Isotopes of the Hungarian

Academy of Sciences by ^{60}Co radiation source with a total activity of 3.7 pBq. A.bisporus was irradiated with 2.5 kGy, P.ostreatus with 2.5 and 5.0 kGy doses, the dose rate being 0.65 kGy x h^{-1}.

Carpophores were stored at 14-16°C with a relative humidity of 90-95 % for 6 days.

SEM

Samples taken from the middle of the gills were fixed in cold 2 % glutaraldehyde dissolved in 0.14 M cacodylate buffer (pH 7.0) for 24 hours. After washing with the buffer, they were postfixed in cacodylate buffered 1 % OsO_4 for 2 hours, dehydrated in a series of ethanol and amyl acetate and dried through liquid CO_2 in a Dupont-Sorvall critical point drying apparatus. The samples were then coated with gold in a Zeiss HBA vacuum-evaporator and examined in a JEOL JSM-50A type scanning electron microscope at a 20kV accelerating voltage.

TEM

Samples were cut out from the middle of the gills (about halfway between the stipe and the brim of the pileus) and parts close to the edge of the gill were fixed.

The fixation and embedding procedure was based on the method used by Dieleman-van Zaayen and Igesz (1969) and on our earlier experiences with plant cells. Fixation was carried out in 6 % /v/v/ glutaraldehyde (in 0.035 M K-Na phosphate buffer, pH 7.2) for 2 hours at 4°C. After thorough washing in the above buffer samples were postfixed in 1 % /w/v/ OsO_4 for 1.5 hours, dehydrated in an acetone series and embedded in Spurr's resin. Using flat molds, samples could be oriented so that the gill was always sectioned transversely. Sections were made with a Porter-Blum ultramicrotome equipped with an LKB glass knife, and after contrast-staining with uranyl acetate and lead citrate, were examined in a Tesla BS 500 electron microscope operated at 60kV.

Results

A.bisporus

SEM: In the fresh, closed control, developing basidia are seen, some of them with two protruding spores (Fig. 1 A). In the six day old control there are basidia with sterigmata which have lost their spores partly because of their maturity, or of preparation procedures (Fig. 1 B). In the six day old irradiated samples the basidia are deformed and the hymenium is discontinuous (Fig. 1 C).

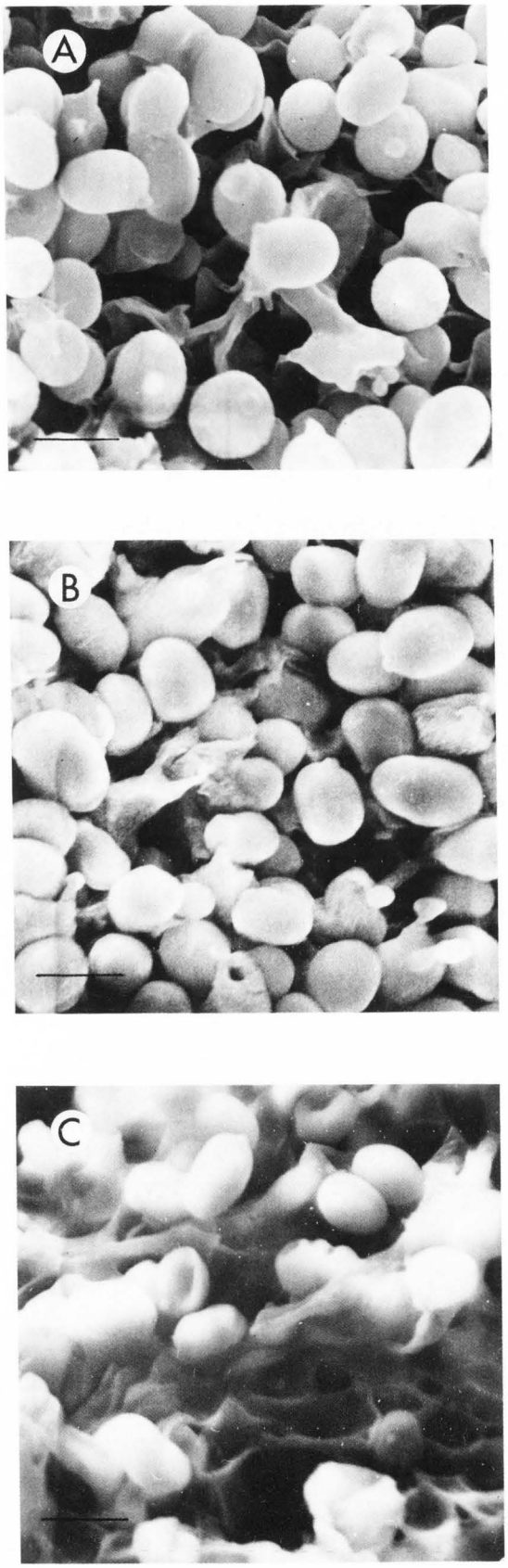

Fig. 1. SEM micrographs of the fresh control (A), stored control (B) and irradiated then stored (C) samples of A.bisporus. Bars equal 4 μm.

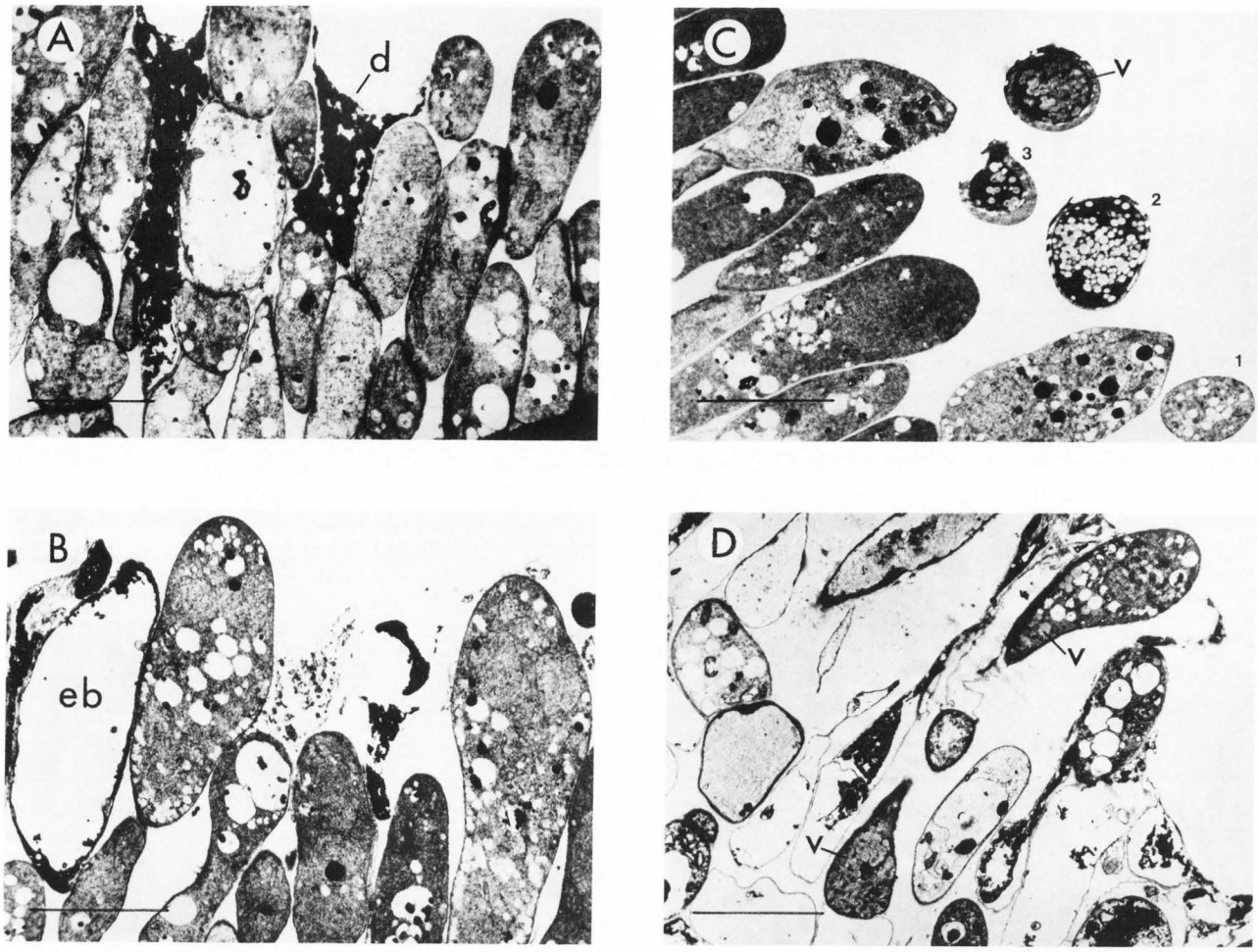

Fig. 2. TEM micrographs of the hymenium of A.bisporus. Bars equal 4 µm.
A: fresh, closed fruit body, d= dense cell
B: stored, open fruit body, eb=empty basidium
C: spore development on an open fruit body (from 1 to 3 the spores are in a developmental sequence), v=vesicle
D: irradiated then stored, closed fruit body, v=vesicle.

TEM: The hymenium of the fresh, closed carpophore consists of hypha cells elongated perpendicularly to the surface (Fig. 2 A). Basically two cell types build up this layer; convex cells with moderately electron dense plasm and the less frequent multiconcave cells with very dense plasm. We could not find forms intermediate between these two types. There occurred also cells with large vacuoles and rarely mature spores could be found on the surface. We identify the dominating cell type (i.e. the convex cells with moderately dense plasm) with developing basidia. They are connected with intermediate forms to the highly vacuolized cell type which is considered as the degenerative end stage of basidium development. The multiconcave dense cells may be cystidia (A. Keresztes, E. Kovács in preparation).

During six days of storage (and cap opening) the number of the vacuolized cells increased in the hymenium (Fig. 2 B). However, young developing basidia could be found even at this stage. The preparative procedures used permitted preservation of the inner structure of several spores (Fig. 2 C). Inside their thick walls vesicles dominate, probably containing storage lipids.

When storage was preceded by irradiation the number of vacuolized and necrotized cells increased dramatically (Fig. 2 D).

In some places the hymenium became discontinuous, or (mainly at the edge of the gill) separated from the hymenophoral part. Basidia (if not necrotized) attained an unusual structure characterized mainly by the accumulation of vesicles of medium density. Such masses of vesicles can be seen in spores (Fig. 2 C), which allows the supposition that certain cytoplasmic processes of spore formation may continue independently of the inhibition of nuclear processes in the basidium. Sometimes

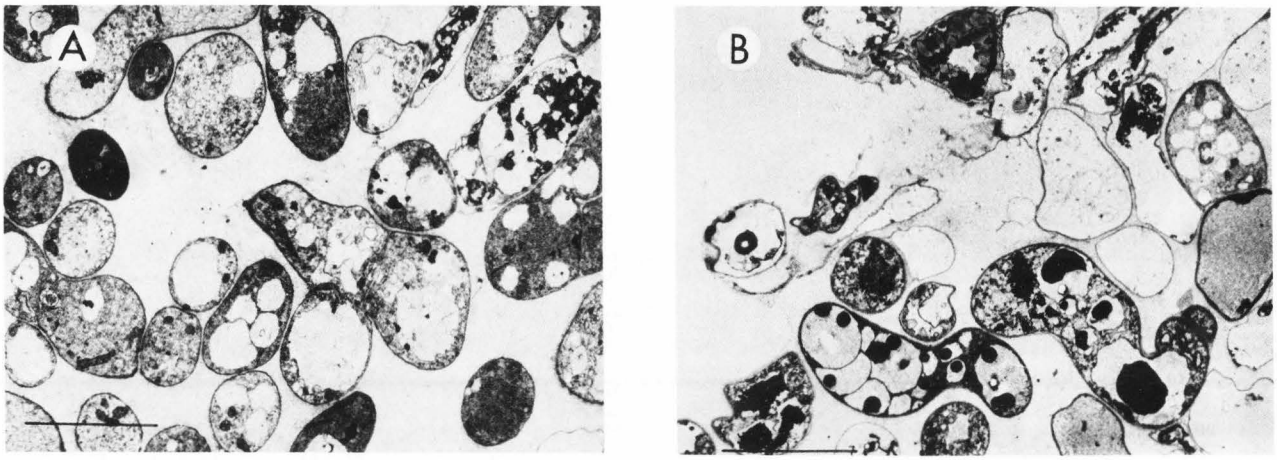

Fig. 3. TEM micrographs of the subhymenium and trama of the gill of A.bisporus. Hymenophoral cells in cross section, except the right upper corners of both micrographs, where parts of hymenial cells are in longitudinal section. Bars equal 4 µm. A: fresh, closed fruit body B: irradiated then stored fruit body.

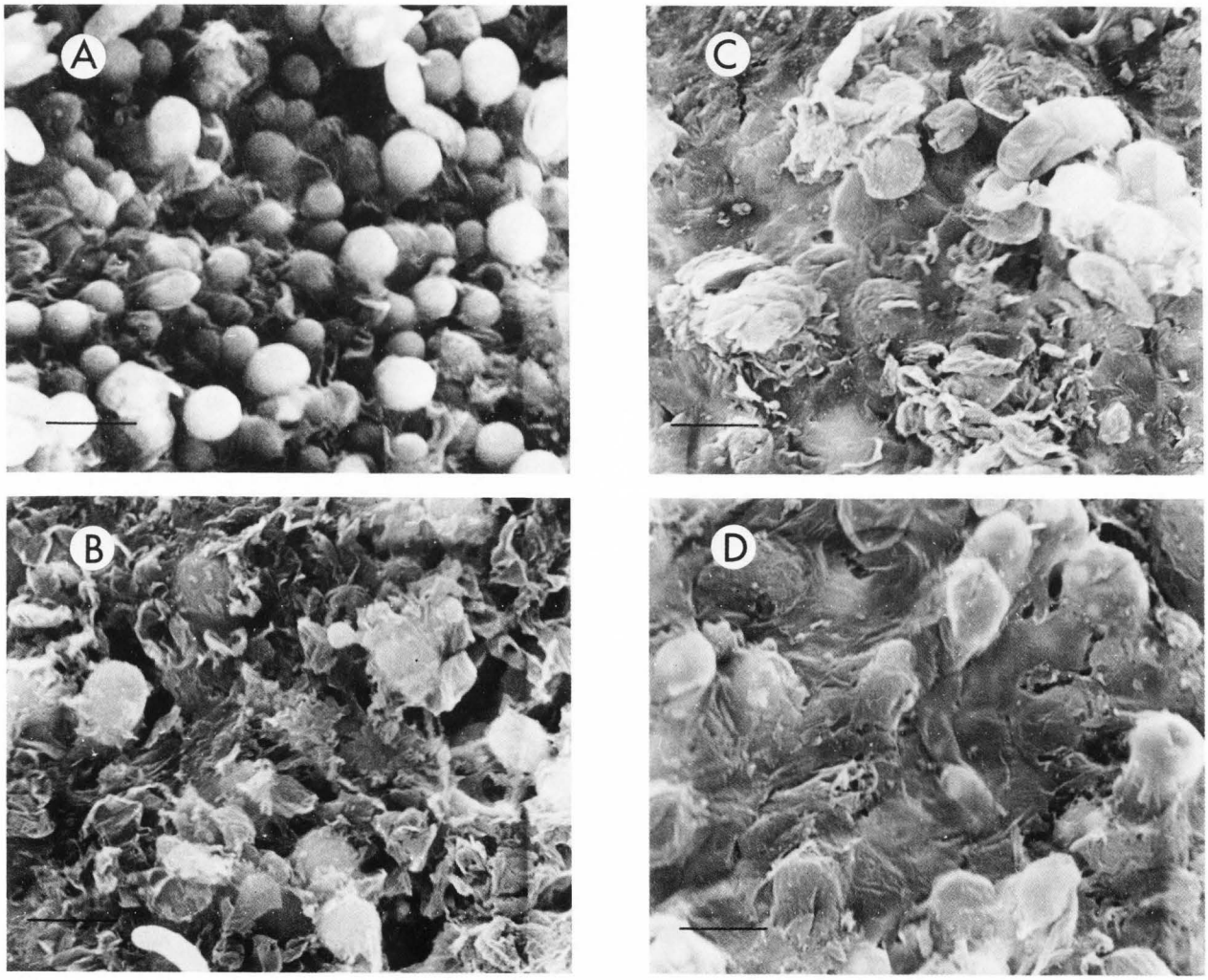

Fig. 4. SEM micrographs of the fresh control (A), stored control (B) and irradiated by 2.5 kGy in (C) or by 5.0 kGy in (D) samples of P.ostreatus. Bars equal 4 µm.

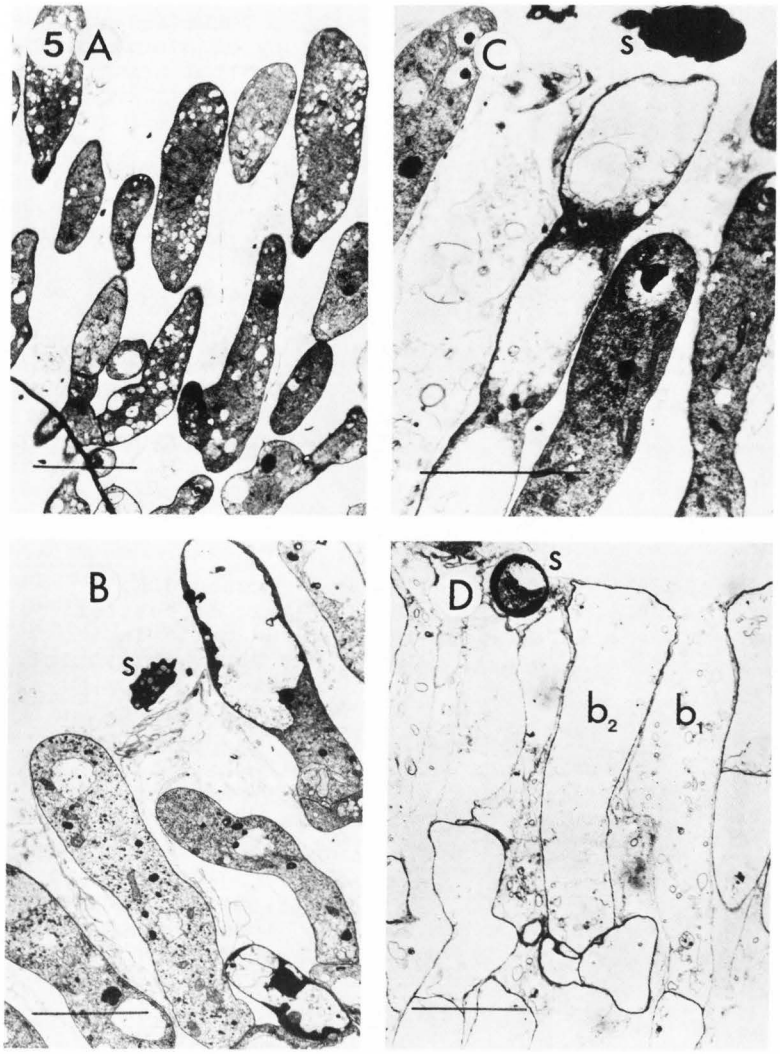

Fig. 5. TEM micrographs of the hymenium of P.ostreatus. s=spore. Bars=4 µm. A and B: fresh samples, C: stored sample, D: irradiated (2.5 kGy) then stored sample. Basidia necrotized before (b_1) or after (b_2) irradiation.

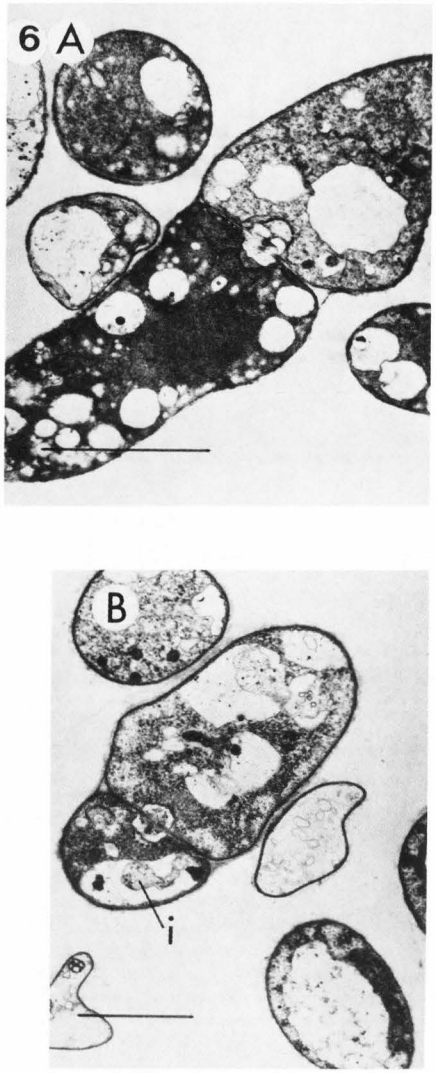

Fig. 6. TEM micrographs of the hymenophoral cells of P.ostreatus. Bars=2 µm. A: fresh sample, B: irradiated then stored sample, i=cytoplasmic intrusion.

apparently normal, mature spores were found in the sections, which may have formed before irradiation.

In the hymenophoral cells no significant changes were observed at the end of storage, so Fig. 3 A represents the ultrastructural features present in both fresh and stored controls. After irradiation (Fig. 3 B) many empty or even disintegrated cells occur in the subhymenium and trama. Also the plasma-containing cells show alterations; a relatively coarse cytoplasmic granulation as well as more frequent and larger dense bodies are present in the vacuoles.

P.ostreatus

SEM: In samples of fresh mushrooms basidia of different size are relatively close to each other (Fig. 4 A). In the stored control the surface is coated, the coat sparsely being broken through by basidia (Fig. 4 B). In the irradiated samples the basidia bulge out on the surface but do not seem to break through the coat. Basidia are less frequent than those of the control, their distribution is uneven, their shape sometimes being irregular (Figs. 4 C and D).

TEM: Hymenial cells of fresh P.ostreatus seem to be sparser than those of A.bisporus (Figs. 5 A and B). This is due to the presence of many necrotized and faint cell remnants among the living cells. The latter are all of the same cell type (basidia) as no idioblasts (e.g. cystidia) were found

among them. The fine structure of basidia, however, changed from sample to sample if they were taken from different freshly harvested carpophores. In one case, cells had moderately dense, finely granulated cytoplasm and numerous small vacuoles (Fig. 5 A). In another case, a more translucent cell content (possibly mictoplasm, see Angeli-Papa and Eyme, 1978) could be seen, with fewer vacuoles. In such sections there were also highly vacuolized basidia (Fig. 5 B). The reason for these differences may be that in P.ostreatus the age and developmental stage of fruiting bodies cannot be determined on a morphological basis. Therefore the carpophores used for sampling could be different in this respect.

As compared to the young samples of the fresh material, basidia in the stored material frequently had large vacuoles, sometimes with spores in their vicinity (Fig. 5 C). The spores seemed to be electron dense and flat in section, with a wavy outline (Figs. 5 B and C).

The effect of irradiation on cell structure was always pronounced (Fig.5 D). The hymenium consisted almost exclusively of empty cells, among which those necrotized after irradiation could be discerned on the basis of their denser wall from those necrotized earlier. The few plasma containing cells had a coarse granulation. Between some cells we observed unusual lateral fusion. The very few spores differed from those of the control.

The hymenophoral cells, although being mostly vacuolata did contain some cytoplasm and were less damaged than cells of the hymenium (Fig. 6). However, there were signs of destruction even in these cells, including coarse cytoplasmic granulation and intrusions into the vacuoles. These latter formations are regarded as the beginning of autophagy. Induced autophagy upon ionizing irradiation (X-rays or gamma rays) has been reported in other non-dividing cells or cell cultures (for references see Hamberg et al, 1976).

Conclusions

We have found in both species that ionizing radiation inhibits spore production by causing an abnormal development or necrosis of basidia rather than by the conservation of their juvenile stage.

In P.ostreatus the hymenium is more sensitive to irradiation than in A.bisporus. The hymenophoral cells in both species are less sensitive than the hymenium.

As the cellular responses of the gills cannot be generalized to other parts of the cap and to the stipe, we intend to investigate these parts of the carpophore after irradiation.

On the basis of these results, we regard electron microscopy as a suitable method to detect mushrooms that have received irradiation treatment.

Acknowledgements

We wish to thank Mrs. A. Gyurek, Mrs. J. Kirchner, Mrs. P. Petrovits, Miss S. Sipos and Mrs. Zs. Vörös for their valuable technical help.

References

Angeli-Papa, J. Eyme J. (1978) Ultrastructural changes during development of Agaricus bisporus and Agaricus sylvicola. In: Chang ST and Hayes WA (eds.) The biology and cultivation of edible mushrooms. Academic Press, 53-81.

Dieleman-van Zaayen A, Igesz O. (1969) Intracellular appearance of mushroom virus. Virology, 39, 147-152.

Hamberg H, Brunk UT, Ericsson JLE, Jung B. (1976) Cytoplasmic effects of X-irradiation on cultured cells in nondividing stage. Acta Path., Microbiol. Scand., Sect, A., 84, 201-214.

Kovács E, Vas K. (1970) Ionizáló sugárzások alkalmazása friss csiperkegomba eltarthatóságának növelésére. (Application of ionizing radiations to extend the storage life of fresh mushrooms). Atomtech. Tájék., 13, 319-320.

Kovács E, Vas K. (1974a) Effect of ionizing radiations on some organoleptic characteristics of edible mushrooms. Acta Alimentaria, 3, 11-17.

Kovács E, Vas K. (1974b) Effect of ionizing radiation on postharvest mushrooms (Agaricus bisporus) with special reference to the rates of respiration and ethylene production. Acta Alimentaria, 3, 19-25.

Kovács E, Vas K, Farkas J. (1968) A termesztett csiperkegomba eltarthatóságának növelése ionizáló sugárzással (Extension of the storage life of cultivated mushrooms by ionizing radiation). Atomtech. Tájék., 7, 349-354.

Kovács E, Vörös Zs, Farkas J. (1981) Dynamics of cap opening in Agaricus bisporus and changes in spore numbers vs. cap opening and radiation treatment. Acta Alimentaria, 10, 379-388.

Staden OL. (1964) Irradiated mushrooms taste better. Euroatom Bull. No. 3. ref: Fd Technol., 23, 114.

Staden OL. (1965) Radiation preservation of fresh mushrooms. Mushr. Sci., 6, 457-461.

Stoller BB. (1968) Anwendung von Gamma-Strahlung in der Champignonkultur. (Application of gamma irradiation in mushrooms cultivation). Der Champignon, 8, (78) 12-13, 16, 19.

Wahid M, Kovács E. (1980) Shelf life extension of mushrooms (Agaricus bisporus) by gamma irradiation. Acta Alimentaria, 9, 357-366.

Discussion with Reviewers

D.A. Wood: Have the ultrastructural changes observed been correlated with any biochemical changes in the gill tissue?
Authors: According to our unpublished investigations the cytokinin level seems to decrease in the gills after gamma-irradiation.

D.A. Wood: Does storage temperature have any effect on the ultrastructural changes observed?
Authors: We have not investigated the temperature dependence.

T.Cayle: Is irradiation the only cause of the observed differences? I doubt it.
Authors: To our best knowledge irradiation was the only difference between the treated and the stored control groups.

E.A.Davis: Has irradiation been used by others in the early stages of mushroom growth to accelerate and shorten the growth time?
Authors: We do not know about such experiments but on the analogy of stimulation of plants we can imagine an accelerated growth of mycelia irradiated with low doses.

FOOD MICROSTRUCTURE, Vol. 4 (1985), pp. 357-364
SEM Inc., AMF O'Hare (Chicago), IL 60666-0507 U.S.A.

0730-5419/85$1.00+.05

ULTRASTRUCTURAL UTILIZATION OF PLANTS BY HERBIVORES

L.H. Harbers

Animal Sciences & Industry
Kansas State University
Call Hall, Manhattan, Kansas 66506

Abstract

Study of the patterns of ruminal digestion of forages enhances the nutritional knowledge of how specific plant tissues are digested and adds its own dimension by characterizing the specific cells and the complex interactions of ruminal microflora with those tissues. A common pattern of digestibility exists for mono- and dicotyledon leaves: mesophyll and phloem are degraded readily, and sclerenchyma slowly, whereas cuticle and the remaining vascular tissues are rarely utilized. Digestion of stems is limited to parenchymal tissues in monocotyledons and to cortex and parenchyma in dicotyledons. Epidermal silica and cuticle are undigestible and restrict microbial entrance. Calcium oxalate crystals in legumes are utilized poorly by animals, suggesting the need for further attention to structure in feedstuff analyses. Future studies by animal scientists on plant utilization and by agronomists in genetics should include structural considerations along with the well recognized experimental procedures.

Initial paper received February 04 1985
Manuscript received September 11 1985
Direct inquiries to L.H. Harbers
Telephone number: 913 532 5654

Key Words: Forage digestion, ruminant digestion, digestibility, plant anatomy, scanning electron microscopy.

Introduction

Over the past century, animal nutritionists have relied almost exclusively on chemical analyses in their quest for improved feedstuff utilization and animal performance. Samples of forages, for example, are dried, ground through a 1-mm screen, and subjected to various physical, chemical, and biochemical analyses. While such tests have provided valuable data on total nutrient content, little information relative to nutrient location and specific tissue utilization has been obtained.

Attempts to use light microscopy to evaluate the digestive sequences and specific plant-tissue utilization have been impeded by lack of depth of field and resolution. The advent of the scanning electron microscope (SEM) greatly enhanced such studies because of the three dimensional perspective and the great depth of field at high magnifications. Research with the SEM on digestion of grasses, legumes, and silages is the subject of this review. Digested samples shown in photomicrographs were obtained using the nylon bag technique (14).

Grasses

Domestic ruminants generally graze on and consume hays from cool-season (C_3) or temperate and warm-season or tropical (C_4) grasses. The structural anatomy of leaves of these grasses differs (6,19); generally C_3 grasses are better utilized than C_4 species because of a greater percentage of mesophyllous tissues. Morphometric studies show that C_3 grasses characteristically contain a higher percentage of mesophyllous tissues (52–64%) compared with C_4 species (27–52%) (6). Leaf blades of tropical grasses average 22% less of the highly digestible tissues and 25% more of the tissues typically less digestible than do C_3 grasses (6). Starch, a readily digestible carbohydrate, is present in the mesophyll of C_3 species, but in C_4 species it is localized within bundle sheath cells surrounding vascular bundles. In all monocotyledon leaves studied, mesophyll and phloem are degraded readily, while lignified tissues such as sclerenchyma and xylem usually are not degraded (6,20). Cuticle is ruptured following prolonged digestion but is not degraded (15,22).

The C_3 grasses studied, including *Bromus inermis* Leyss. (bromegrass), *Festuca arundinacea* Schreb. (fescue), *Poa pratensis* L. (Kentucky bluegrass), and *Dactylis glomerata* L. (orchardgrass), show digestive patterns similar to those for C_4 plants or

to each other (Fig. 1). Mesophyll and phloem are degraded rapidly (within 24 h fermentation) followed by slow digestion of bundle sheath cells and sclerenchyma (2,6,13,22). Ruptured adaxial cuticle and intact abaxial cuticle remain after 72 h (22). Tissues from bromegrass appear to be degraded more rapidly than those from fescue; however, the extent of digestion is similar if the grass fragments remain in the rumen for 48 h (22). Recent studies with various C_4, C_3, and C_3/C_4 intermediates of *Panicum* species show that readily digestible mesophyllous tissues in leaves are degraded primarily by a diverse population of nonadhering bacteria, whereas parenchyma bundle sheaths, sclerenchyma, and epidermis require adhering encapsulated cocci and irregularly-shaped bacteria (9,11). Complex interrelationships exist between fiber-digesting bacteria and forage-plant cell walls during digestion and that relationship is probably related to variation in cell wall nutrient availability (1). Stems from grass species vary in parenchymal lignification and, thus, digestion, suggesting the possibility for genetically produced plants with no or little parenchymal lignification (5). One species, *Panicum antidotale* (C_4), shows no parenchymal lignification; the tissue is digested within 24 h.

Warm-season grasses studied by SEM initially involved *Cynodon* (bermudagrasses) and *Andropogon* (bluestems), but now include *Panicum* (13), *Digitaria pentzii* Stent. (10), *Bothriochloa,* and *Eragrostis* (4). These grasses contain much less of the readily available tissues (especially mesophyll), which partially accounts for their lower digestibilities compared with cool-season grasses (6). Mesophyllous tissues appear to be more compact and may have differential quantities and qualities of cell wall material (27). A typical example (Fig. 2) of a digested leaf shows the tissue remnants. Generally, lignified supportive cells (xylem, inner bundle sheath) are not degraded and stain positively with acid phloroglucinol, suggesting coniferaldehyde lignin. Slowly degradable cells such as sclerenchyma and outer bundle sheath are positive for chlorine-sulfite stain, probably because of syringyl groups (8,9). Horses also are able to digest the readily degradable tissues that ruminants digest but are unable to utilize these chlorine-sulfite-positive-cells that ruminants degrade slowly (24).

Starch is localized in bundle sheath cells of C_4 grasses (19). Hydrolysis of these granules cannot occur until bundle sheath walls have been ruptured (3,7). Transmission electron microscopy studies reveal a thin, suberin layer in outer tangential and radial walls of bundle sheath cells of immature and mature leaves of indiangrass (*Sorghastrum nutans* (L.) Nash) and big bluestem (*Andropogon gerardi* Vitman), which resist degradation. Mature leaf blades subjected to 120 h incubation show only 25 to 50% of bundle sheath cells degraded. Rupture of the bundle sheath is dependent upon bundle size and stage of development (27). Bacterial entry may be less restrictive where the cell walls are contiguous to vascular tissues (no suberin layer). Masticated and exposed edges of vascular bundles may provide channels for bacterial distribution, at least in smaller bundles.

Silages

Storing freshly harvested plant material by ensiling in air-tight structures permit bacterial fermentation (mainly lactate formation) prior to utilization by ruminants. Leaf and stem tissues from corn (*Zea mays* L.) and sorghum (*Sorghum bicolor* (L.) Moench.) treated by this process have been studied by SEM (26).

Bacterial attachment is more prevalent on adaxial compared with abaxial surfaces of leaf tissues of both forages removed from silos. In corn silage, hydrolytic activity occurs in starch granules of corn silage deposited along vascular protrusions of adaxial leaf surfaces during the ensiling procedure. These cuticular areas appear to be vulnerable to bacterial degradation (Fig. 3). Sorghum leaf surfaces are planar, thus starch granules do not accumulate during ensiling. Sorghum seeds are smaller than those of corn and generally escape fracture during harvesting. Internal leaf tissues remain intact, although numerous bacterial accumulation can be observed. Stem tissues remain intact. Corn stem parenchyma contains partially digested starch granules from ruptured corn kernels; sorghum stem parenchyma appears free of starch granules from seed as were the ensiled sorghum leaves.

Digestion of leaf tissues by rumen microorganisms shows that mesophyllous tissues are destroyed within 24 h in both corn and sorghum (Figs. 4,5). Sorghum epidermis is thicker and more resistant to rupture than that of corn. Unreported research suggests that there may be differences between sorghum lines in the rate of leaf degradation by rumen microflora (Akin DE, personal communication).

Examination of ensiled stem tissues shows that rumen microorganisms preferentially digest thin parenchymal cells (Figs. 6,7). Corn parenchyma is degraded within 48 h; however, sorghum stem parenchyma is degraded more slowly. Recent research in our laboratory suggests variation in digestion of stems between sorghum lines. Studies are currently underway to verify these findings and elucidate the reasons for resistance in some sorghum varieties.

Other structural inhibitors to digestion

Lignin, in combination with thick-walled cellular structures, forms major barriers to digestion of some internal tissues by microorganisms. The external leaf structures, silica and cuticle, provide a formidable barrier to microbial entrance, leaving only exposed edges and cuticle crushed from mastication as entrance sites (30).

Silica is deposited by a passive nonmetabolic mechanism (32) in grass epidermal cells (19), where it prevents microbial entrance (15). Grass cuticle is so resistant to microbial digestion that rumen fermentation has been used to isolate intact cuticle (31).

Typical X-ray dispersions of silica in adaxial and abaxial tissues of C_3 (fescue) and C_4 (bluestem) grasses are shown in Figs. 8 to 10. Silica in adaxial leaf surfaces of fescue (Fig. 8) is limited to cells contiguous to underlying vascular bundles, whereas abaxial cuticle contains silica in every cell (Fig. 9). Both surfaces show the characteristic fescutoid phytoliths. The nonsilicified cells of the adaxial cuticle are ruptured during fermentation (Fig. 1), probably by physical rupture, and so may aid in increased rate of passage of nonutilizable tissues by rapid particle reduction. Silica is present in each cell of adaxial and abaxial epidermis of bluestem (Fig. 10); dumbbell-shaped panicoid phytoliths are present in parallel rows on both surfaces. Cuticular resistance in C_4 plants is such that only a few epidermal cells are ruptured after underlying mesophyllous tissues are degraded (15).

Plants (fescue and bluestems) grown with and without silica (25) show that young grasses (30 days postemergence) with silica have cuticular barriers to digestion similar to those of naturally

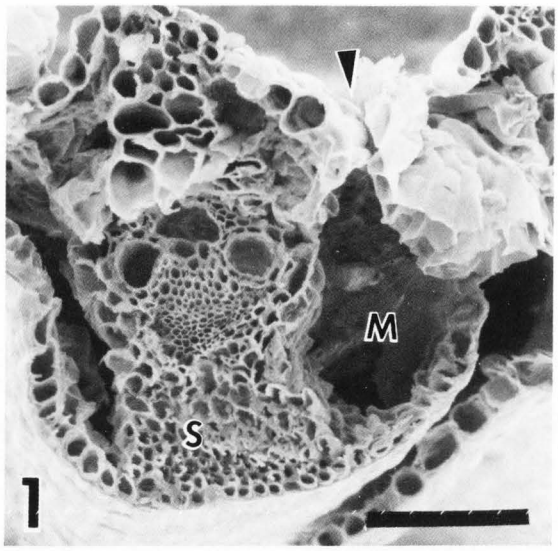

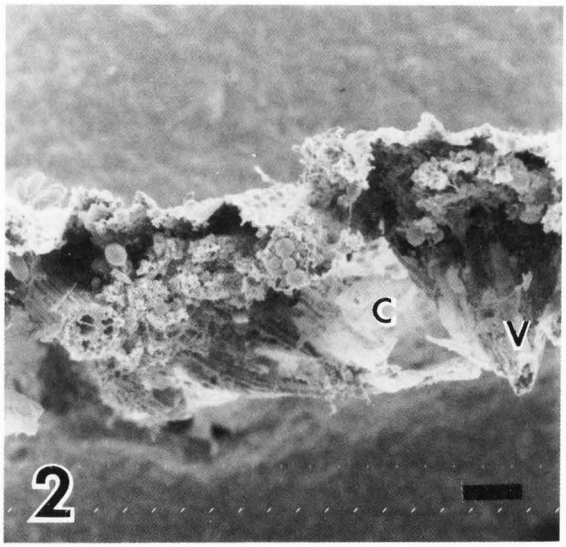

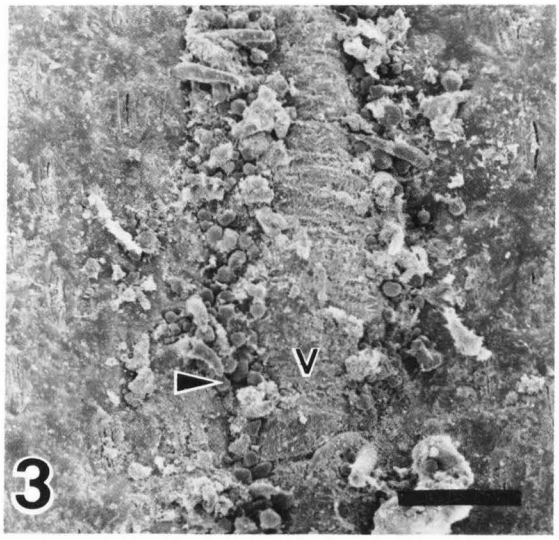

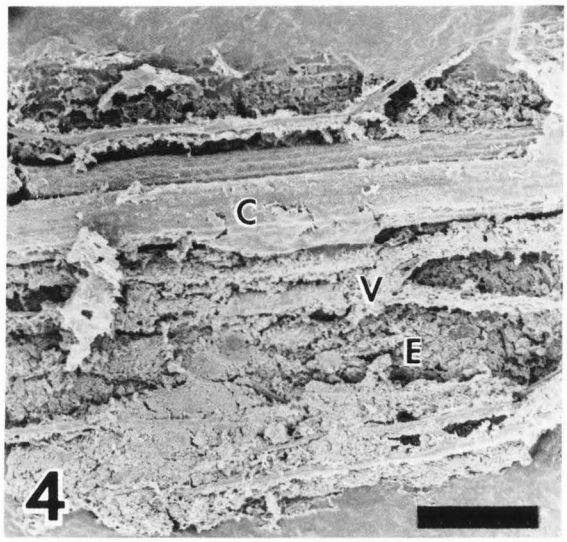

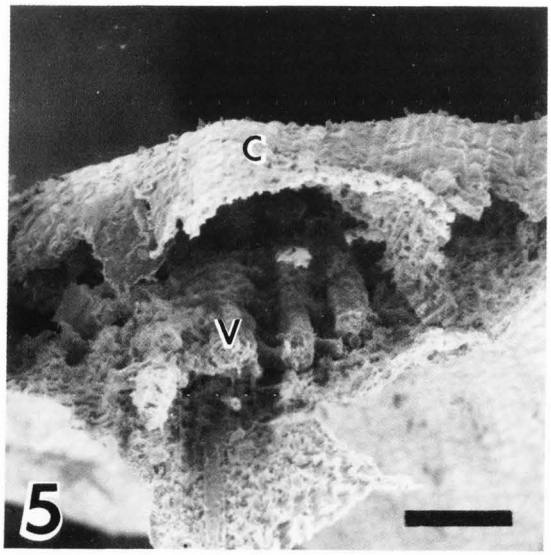

Fig. 1. Cross-section of fescue (C_3) leaf blade digested 24 h by rumen microorganisms showing degraded mesophyll (M), ruptured cuticle (arrow), and intact sclerenchyma (S). Bar = 10 μm.

Fig. 2. Cross-section of 24 h digested bluestem (C_4) leaf blade with intact cuticle (C) and vascular tissue (V). Bar = 100 μm.

Fig. 3. Adaxial surface of ensiled corn leaf with starch grain (arrow) deposit near protrusion over vascular tissue (V). Bar = 100 μm.

Fig. 4. Adaxial view of ensiled corn leaf blade after 72 h ruminal digestion showing remnants of adaxial cuticle (C), vascular tissue (V), and epidermal cells (E) attached to abaxial cuticle. Bar = 300 μm.

Fig. 5. Section of sorghum leaf blade digested 12 h showing vascular bundles (V) and cuticle (C) intact. Bar = 100 μm.

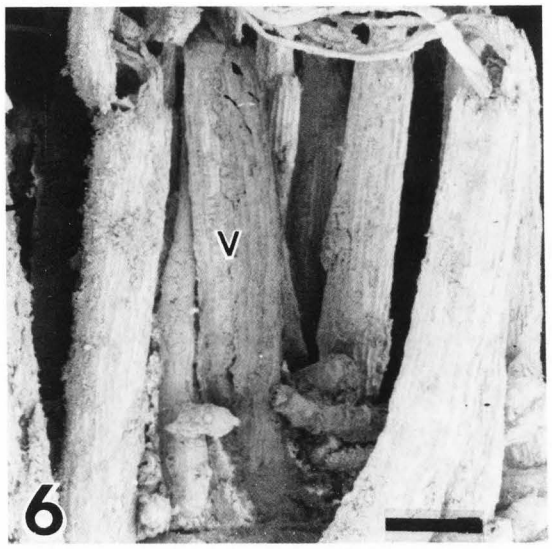

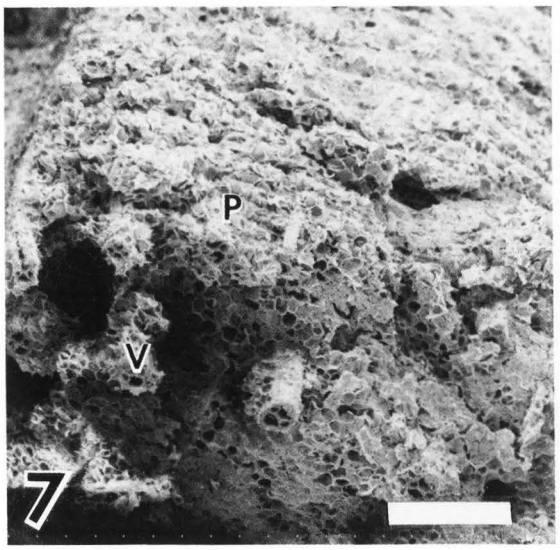

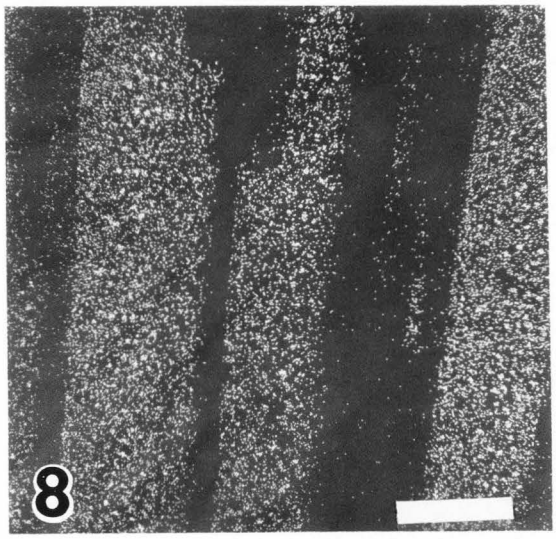

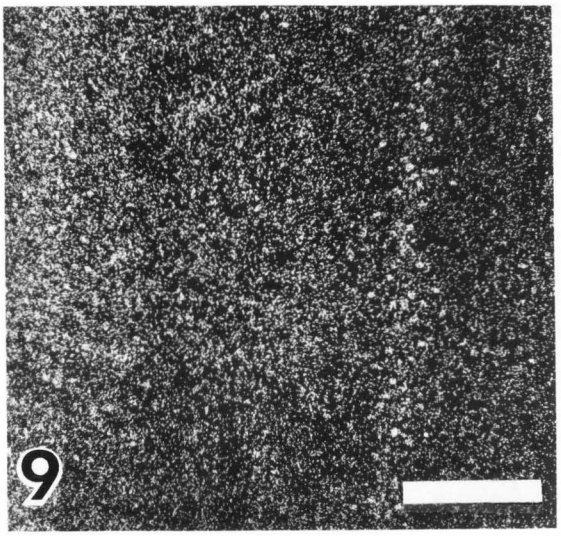

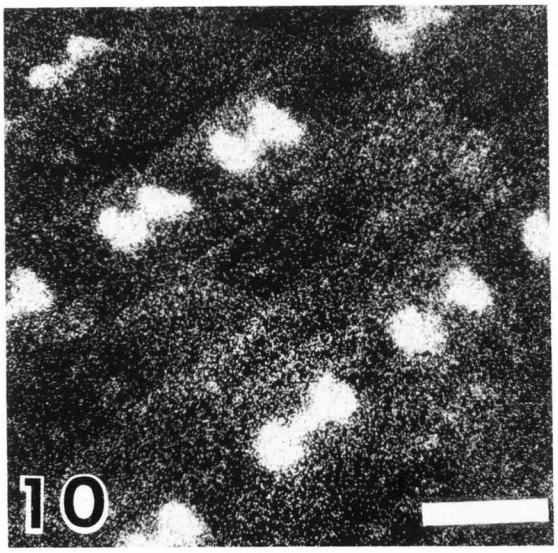

Fig. 6. Columns of vascular bundles (V) minus parenchyma after 48 h ruminal digestion of ensiled corn stem. Bar = 500 μm.

Fig. 7. Exposed vascular tissue (V) and parenchyma (P) remaining on sorghum stem digested 48 h. Bar = 400 μm.

Fig. 8. X-ray dispersion of silica on adaxial surface of fescue leaf. Bar = 400 μm.

Fig. 9. X-ray dispersion of silica on abaxial surface of fescue leaf. Bar = 300 μm.

Fig. 10. X-ray dispersion of silica and panicoid phytoliths on surface of bluestem leaf blade. Bar = 30 μm.

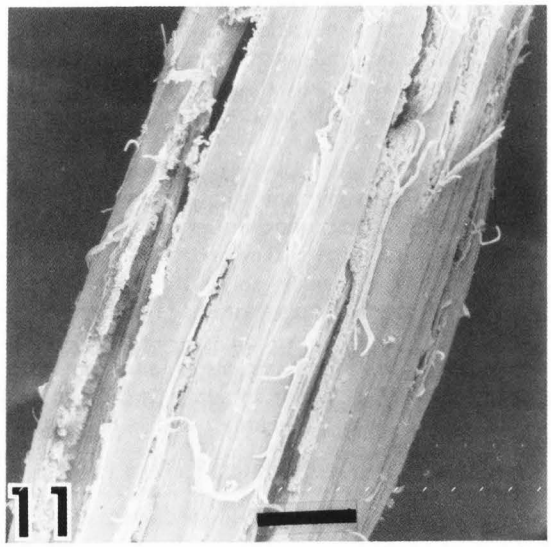

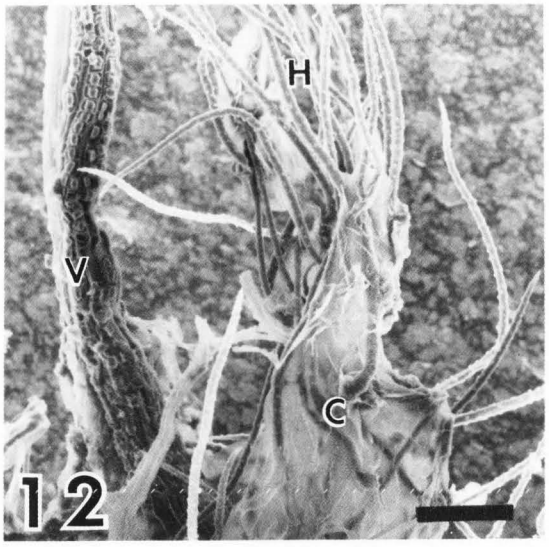

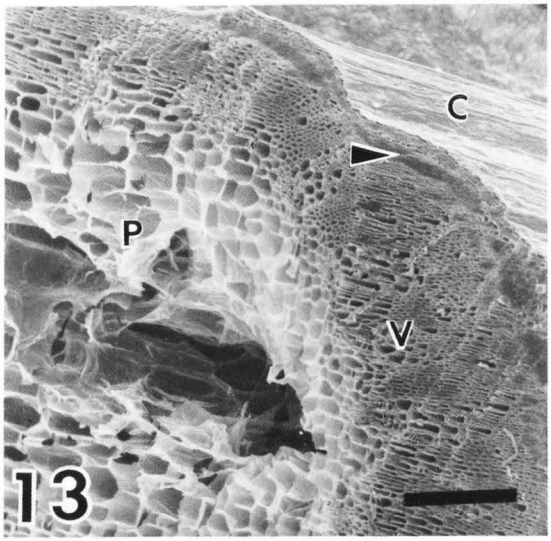

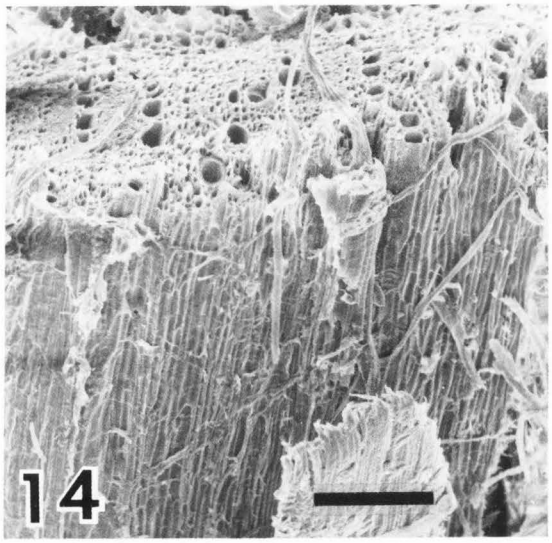

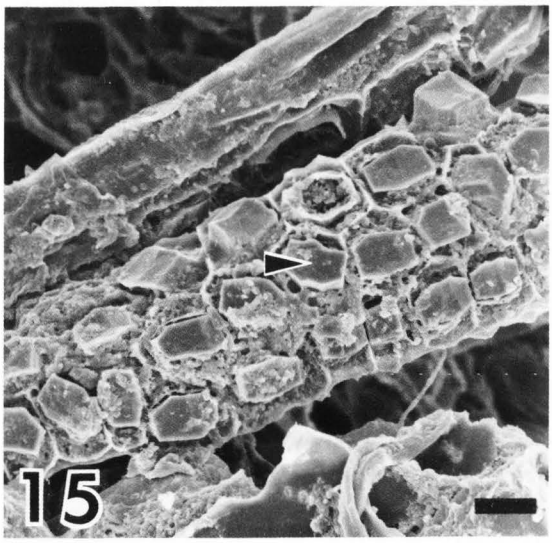

Fig. 11. Abaxial surface of young fescue leaf blade grown without silica showing cuticular rupture following 12 h digestion. Bar = 500 μm.

Fig. 12. Digested alfalfa leaflet (24 h) with vascular tissue (V), cuticle (C), and abaxial macrohair (H) as only remnants. Bar = 100 μm.

Fig. 13. Cross-section of alfalfa stem showing cuticle (C), cortex (arrow), vascular tissue (V), and parenchyma (P). Bar = 300 μm.

Fig. 14. Digested alfalfa stem (48 h) showing remnants of vascular tissue. Bar = 300 μm.

Fig. 15. Calcium oxalate crystals (arrow) on vascular bundle remnants of digested alfalfa (24 h). Bar = 10 μm.

grown plants. When silica is absent, massive rupture of the cuticular layers is possible (Fig. 11), suggesting that silica is a major deterrent to microbial entrance in young plants. In older plants (60 days postemergence), the absence of silica has no influence on microbial penetration; other structures and components in the cuticle and epidermis resist rupture (25).

Siliceous deposits are found also in leaves of corn and sorghum. Sorghum leaf cuticle is resistant to microbial and physical rupture following ensiling and rumen fermentation (Fig. 5), but adaxial corn leaf cuticle is not as resistant (Fig. 4), suggesting that cuticular components other than silica differ among these forages (26).

Legumes

The dicotyledons have received less attention than monocotyledons because leaves of most of the former are readily digestible; their quality as feed is dependent upon the amount of highly lignified stem. The high digestibility of alfalfa does not agree with the supposition that lignin decreases digestibility, since legumes such as alfalfa generally contain more lignin than do most grasses. The idea was proposed more than 30 years ago that the location of lignin may have more effect on utilization than its percentage (17,29).

Studies on the rumen fermentation patterns of fresh, intact legume leaves show that microorganisms rapidly enter through stomata, penetrate intercellular spaces, separate plant cells, and penetrate the cell walls by general disorganization (16). SEM studies (14) on alfalfa hay leaves show that ruminal fermentation results in random sloughing of adaxial cuticle with rapid digestion of mesophyll. By 24 h the remaining leaf tissues consist of vascular bundles and abaxial cuticle with its macrohairs intact (Fig. 12). The indigestible abaxial tissues are also a feature of monocotyledons; however, legumes do not contain silica in epidermal tissues.

The classic dicotyledon structures (epidermis, cortex, and vascular tissues) are distinguished easily in stem cross-section (Fig. 13). Ruminal fermentation results in sloughing of the cuticle and hydrolysis of the dense cortex to sieve cells of the vascular tissue and simultaneous degradation of part of the pith parenchyma (Fig. 14). No additional digestion has been observed in either rumen fermentations or fecal remnants.

Studies with leaf and steam tissues of clovers (12) indicate that reduced digestibility with maturity is due to reduced degradation of stem interfascicular parenchyma. Differences in digestibility between arrowleaf clover (*Trifolium vesiculosum* Savi) and crimson clover (*T. incarnatum* L.) could not be explained by anatomical differences (12).

The SEM has been an especially useful tool in elucidating a nutritional problem associated with the feeding of alfalfa hay. Our dairy group reported approximately a twofold discrepancy in the requirement of calcium for milk production from that recommended by the National Research Council (NRC) when alfalfa-sorghum grain-soybean meal rations were fed (34). The NRC calcium requirement was derived from studies involving rations providing calcium from inorganic sources. The true digestibility (a combination of chemical and radio-calcium balance studies) of alfalfa calcium was found to average only two-thirds that of inorganic sources (21), but the work was done with steers.

Leguminous plants have 1 to 2% calcium. Thus, when NRC recommended allowances for total calcium are followed, rations with alfalfa as the only source of roughage require additional phosphorous, but not calcium. Lactating dairy cows fed alfalfa as the sole roughage source did not reduce milk production appreciably but were removed early from the herd compared to calcium-supplemented animals because of apparent skeletal problems (33).

Using a combination of secondary imagery and x-ray dispersion with the SEM in combination with Raman microprobe analysis (36), we were able to show that crystals surrounding vascular bundles in alfalfa were calcium oxalate (Fig. 15), a condition reported much earlier in clovers (18,28). These crystals remained in their sclerenchymatous sheaths in the rumen and were found as loose crystals in fecal remnants (36). Fecal residues from domestic and zoo ruminants, nonruminant herbivores, and birds fed alfalfa hay or dehydrated pellets showed crystals still intact or loose (23). Further studies on extractability in acid (35) and oxalate digestion (37), as well as chick growth studies (38) confirmed poor utilization of oxalate calcium in alfalfa.

Conclusions

Microbial digestion of plant tissues follows a remarkably similar hydrolytic pattern: nonlignified tissues are degraded readily by cellulase enzymes, cells containing syringyl-type lignin are degraded slowly by two general types of attached bacteria, and structural tissues containing coniferaldehyde-type lignin resist digestion. Cuticle acts as a barrier to bacterial entrance in most monocotyledons, and suberin surrounding C_4 bundle-sheath cells delays entrance into these starch-containing tissues. The relatively high concentration of calcium in dicotyledons (such as alfalfa) is not as available as generally believed because of insoluble calcium oxalate crystals attached to leaf vascular bundles.

References

1. Akin DE. (1980). Evaluation by electron microscopy and anaerobic culture of types of rumen bacteria associated with digestion of forage cell walls. Appl. Environ. Microbiol. **39**, 242–252.

2. Akin DE, Amos HE. (1979). Mode of attack on orchardgrass leaf blades by rumen protozoa. Appl. Environ. Microbiol. **37**, 332–338.

3. Akin DE, Amos HE, Barton FE, Burdick D. (1973). Rumen microbial degradation of grass tissue revealed by scanning electron microscopy. Agron. J. **65**, 825–828.

4. Akin DE, Barton II, FE, Coleman SW. (1983). Structural factors affecting leaf degradation of Old World bluestem and weeping love grass. J. Anim. Sci. **56**, 1434–1446.

5. Akin DE, Brown RH, Rigsby LL. (1984). Digestion of stem tissues in *Panicum* species. Crop Sci. **24**, 769–773.

6. Akin DE, Burdick D. (1975). Percentage of tissue types in tropical and temperate grass leaf blades and degradation of tissues by rumen microorganisms. Crop Sci. **15**, 661–668.

7. Akin DE, Burdick D. (1977). Rumen microbial degradation of starch-containing bundle sheath cells in warm-season grasses. Crop Sci. **117**, 529–533.

8. Akin DE, Burdick D. (1981). Relationships of different histochemical types of lignified cell walls to forage digestibility. Crop Sci. **21**, 577–581.

9. Akin DE, Burdick D, Michaels GE. (1974). Rumen bacterial interrelationships with plant tissue during degradation revealed by transmission electron microscopy. Appl. Microbiol. **27**, 1149–1156.

10. Akin DE, Hogan JP. (1983). Sulfur fertilization and rumen microbial degradation of cell walls in *Digitaria pentzii* Stent. Crop Sci. **23**, 851–858.

11. Akin DE, Rigsby LL, Brown RH. (1984). Ultrastructure of cell wall degradation in *Panicum* species differing in digestibility. Crop Sci. **24**, 156–163.

12. Akin DE, Robinson EL. (1982). Structure of leaves and stems of arrowhead and crimson clovers as related to in vitro digestibility. Crop Sci. **22**, 24–29.

13. Akin DE, Wilson JR, Windham WR. (1983). Site and rate of tissue digestion in leaves of C_3, C_4, and C_3/C_4 intermediate *Panicum* species. Crop Sci. **23**, 147–155.

14. Brazle FK, Harbers LH. (1977). Digestion of alfalfa hay observed by scanning electron microscopy. J. Anim. Sci. **46**, 506–512.

15. Brazle FK, Harbers LH, Owensby CE. (1979). Structural inhibitors of big and little bluestem digestion observed by scanning electron microscopy. J. Anim. Sci. **48**, 1457–1463.

16. Cheng KJ, Fay JP, Howarth RE, Costerton JW. (1980). Sequence of events in the digestion of fresh legume leaves by rumen bacteria. Appl. Environ. Microbiol. **40**, 613–625.

17. Drapala WJ, Raymond LC, Crampton EW. (1947). The effects of maturity of the plant and its lignification and subsequent digestibility by animals as indicated by methods of plant histology. Sci. Agr. **27**, 36–41.

18. Erith AG. (1924). White Clover. Duckworth and Co., London, pp. 33, 47.

19. Esau K. (1965). Plant Anatomy. (2nd Ed.). Wiley, New York, pp. 29–30.

20. Hanna WW, Monson WG, Burton GW. (1973). Histological examination of fresh forage leaves after in vitro digestion. Crop Sci. **13**, 98–102.

21. Hansard SL, Crowder HM, Lyke WA. (1957). The biological availability of calcium in feeds for cattle. J. Anim. Sci. **16**, 437–443.

22. Harbers LH, Brazle FK, Raiten DJ, Owensby CE. (1980). Microbial degradation of smooth brome and tall fescue observed by scanning electron microscopy. J. Anim. Sci. **51**, 439–446.

23. Harbers LH, Callahan SL, Ward GM. (1980). Release of calcium oxalate crystals from alfalfa in the digestive tracts of domestic and zoo animals. J. Zoo Anim. Med. **117**, 52–56.

24. Harbers LH, McNally LK, Smith WH. (1981). Digestibility of three grass hays by the horse and scanning electron microscopy of undigested leaf remnants. J. Anim. Sci. **53**, 1671–1677.

25. Harbers LH, Raiten DJ, Paulsen GM. (1981). The role of plant epidermal silica as a structural inhibitor of rumen microbial digestion in steers. Nutr. Rpt. Intl. **24**, 1057–1066.

26. Harbers LH, Thouvenelle ML. (1980). Digestion of corn and sorghum silage observed by scanning electron microscopy. J. Anim. Sci. **50**, 514–526.

27. Hastert AA, Owensby CE, Harbers LH. (1983). Rumen microbial degradation of indiangrass and big bluestem leaf blades. J. Anim. Sci. **57**, 1626–1636.

28. Percival J. (1902). The occurrence of calcium-oxalate crystals in seedlings of alsike (*Trifolium hybridum* Linn.). Linn. J. Bot. **35**, 396–399.

29. Pigden WJ. (1953). The relation of lignin, cellulose, protein, starch and ether extract to the curing of range grasses. Can. J. Agr. Sci. **33**, 364–378.

30. Pond KR, Ellis WC, Akin DE. (1984). Ingestive mastication and fragmentation of forages. J. Anim. Sci. **58**, 1567–1574.

31. Powell JB, Monson WG, Chatterton NJ (1974). Isolation of cuticle and vascular bundles of leaves by mastication in rumen fluid. Stain Technol. **49**, 29–33.

32. Sangster AG. (1977). Characteristics of silica deposition in *Digitaria sanguinalis* (L.) Scop. (Crabgrass). Ann. Bot. **41**, 341–350.

33. Ward GM, Call EP. (1978). Long-term calcium-phosphorus studies in confined dairy cows. Proc. 11th Ann. Meet. Am. Assoc. Bovine Practitioners, 32–42. Available from AABP, c/o Harold E. Amstutz, Box 2139, W. Lafayette, IN 47906.

34. Ward GM, Dobson RC, Dunham JR. (1972). Influences of calcium and phosphorus intakes, vitamin D supplement and lactation on calcium and phosphorus balances. J. Dairy Sci. **55**, 768–776.

35. Ward GM, Harbers LH. (1982). Effect of pH on extractability of calcium and oxalate from alfalfa leaflets. J. Dairy Sci. **65**, 154–160.

36. Ward GM, Harbers LH, Blaha JJ. (1979). Calcium-containing crystals in alfalfa: Their fate in cattle. J. Dairy Sci. **62**, 715–722.

37. Ward GM, Harbers LH, Kahrs AJ. (1982). Oxalate passage and apparent digestibility of alfalfa rations fed to lambs and cockerels. Nutr. Rpt. Intl. **26**, 1123–1127.

38. Ward GM, Harbers LH, Kahrs AJ, Dayton A. (1984). Availability of calcium from alfalfa for chicks. Poult. Sci. **63**, 82–88.

Discussion with Reviewers

D.E. Akin: Could x-ray analysis of minerals and elements be used in re-defining NRC guidelines for animal feeding?

Author: X-ray analysis for minerals in biological specimens is generally limited to qualitative types of experiments. The methodology is extremely useful in defining insoluble minerals such as the studies with calcium oxalate and silica. Future studies localizing partially available mineral complexes such as phytin phosphate and other suspected mineral complexes resulting in water insoluble molecules could best be studied by microscopic techniques but would have to be confirmed by quantitative animal performance for re-defining NRC guidelines.

D.E. Akin: You referred to the fact that absence of silica did not affect the resistance of cuticles in older plants, and that other compounds are possible factors. Do you think that various waxes, lipids, or suberin-like compounds may differentially influence cuticle breakdown in various plants?

Author: Our investigations with corn and sorghum leaves as well as grasses grown with and without silica lead us to believe there are differences in cuticular composition. Literature on the chemical composition of leaves would certainly suggest differences.

D.E. Akin: What do you feel will be the most important thrust for electron microscopy in future exploration of plant-microbe interactions?

Author: Specifically for the ruminant animal, additional research is needed to identify plant species and varieties containing readily digestible tissues and coordinating such findings with animal production information. Further studies are needed to identify and characterize bacteria and fungi that attack slowly degradable tissues. Such information would be of immediate benefit to animal scientists and agronomists and in future decisions by genetic engineers as to appropriate changes in both plants and bacteria to achieve optimal plant digestion by ruminants.

Acknowledgements

Figures 2 and 11: Courtesy of Nutrition Reports International. Figures 3, 5, 7, 12, 13 and 14: Courtesy of the Journal of Animal Science.

SCANNING ELECTRON MICROSCOPY **Phone: 312-529-6677**
AMF O'Hare, IL 60666-0507, USA

MAJOR SUBJECT INDEX
OF FOOD RELATED PAPERS PUBLISHED BY SEM INC. FROM 1979 TO 1985

This index includes title, first author and first page number for:

(i) all papers from volumes 1 to 4 (years 1982-1985; page number and year given for each paper) of semi-annual journal **Food Microstructure** (subscription rate: $50 per year for U.S. delivery; $55 per year elsewhere); and

ii) Food related papers from 1979, 1980 & 1981 volumes of the Journal **Scanning Electron Microscopy** (page number, year, and part given in the index below). The SEM/1979 to 1981 papers were also published in the compilation, **Studies of Food Microstructure** (ISBN: 0-931288-22-3; Price $49.00 for U.S. delivery and $52.00 for outside delivery).

Reprints (or photo copies) of papers are available at $5.00 each.

Please contact SEM Inc. for further detail of its publications and programs.

PLANT FOODS

Seed Structure and Composition of Potential **New Crops;**
D.W. Irving (43/85

Application of Electron Spin Resonance Techniques to Model **Starch** Systems;
L.E. Pearce (83/85

Small Angle X-Ray Scattering by Hydrated **Wheat Starch** Granules;
M. Yang (107/85

Seed Microstructure: Review of Water Imbibition in **Legumes**;
B.G. Swanson (115/85

The Microstructure of **Wheat**: Its Development and Conversion into **Bread**;
D.B. Bechtel (125/85

The Application of Light and Scanning Electron Microscopy During **Flour** Milling and **Wheat** Processing;
R. Moss (135/85

REVIEW: Ultrastructural Studies on the Cultivation Processes and Growth and Development of the Cultivated **Mushroom** *Agaricus bisporus*;
D.A. Wood (143/85

Comparison of the Microstructure of Firm and Stem-end Softened **Cucumber Pickles** Preserved by Brine Fermentation;
W.M. Walter (165/85

Ultrastructural Study of **Yam Tuber** as Related to Postharvest Hardness;
L. Sealy (173/85

Microstructural Changes in Maturing Seeds of the Common **Bean**;
J.S. Hughes (183/85

Changes in Typical Organelles in Developing Cotyledons of **Soybean**;
K. Saio (191/85

Rheological and Ultrastructural Studies of **Wheat** Kernel Behaviour Under Compression as a Function of Water Content;
A. Al Saleh (199/85

Structure of Coarse and Fine Fractions of **Corn** Samples Ground on the Stenvert Hardness Tester;
Y. Pomeranz (213/85

Effect of Ionizing Irradiation and Storage on **Mushroom** Ultrastructure;
A Keresztes (349/85

TUTORIAL: Ultrastructural **Utilization of Plants** by Herbivores;
L.H. Harbers (357/85

X-Ray Microanalysis of Hollow Heart **Potatoes**;
W.P. Mohr (41/84

Determination of Element Concentration in Fresh and Processed **Vegetables** by Quantitative X-Ray Microanalysis;
M. Grote (49/84

Electron Microscopic Investigations of the Cell Structure in Fresh and Processed **Vegetables (Carrots and Green Bean Pods)**;
M. Grote (55/84

Microstructural Changes in **Winged Bean and Soybean** During Fermentation into Miso;
K. Saio (65/84

The Effects of Microwave Energy and Convection Heating on **Wheat Starch** Granule Transformations;
N.K. Goebel (73/84

Preliminary Evaluation of Lectins as Fluorescent Probes of **Seed** Structure and Composition;
S. Shea Miller (133/84

Morphological Development in **Sorghum** Grain;
C.W. Glennie (141/84

Mineral Migration in the **Wheat** Kernel During Mill Conditioning;
A. Al Saleh (149/84

Light and Scanning Electron Microscopy of **Wheat- and Rye-Bread** Crumb. Interpretation of Specimens Prepared by Various Methods;
Y. Pomeranz (159/84

Ultrastructure of **Quinoa Fruit**. . . ;
E. Varriano-Marston (165/84

Ultrastructural Aspects of **Spun Pea and Fababean Proteins**;
D.J. Gallant (175/84

Effect of Environment on the Physical Structure of the **Peanut**;
C.T. Young (185/84

Ultrastructural Studies of Raw and Processed Tissue of the Major Cultivated **Mushroom,** *Agaricus bisporus;*
E.M. Jasinski (191/84

REVIEW: Ultrastructure Studies of **Pasta**;
P. Resmini (1/83

Endosperm Degradation of **Barley Kernels** that Synthesize α-Amylase in the Absence of Embryos and Exogenous Gibberellic Acid;
A.W. MacGregor (13/83

REVIEW: Field Spectroscopy in the **Food Production** Chain;
E.J. Brach (67/83

Structure of Fresh and Desiccated **Coconut**;
J.F. Heathcock (81/83

Infection of **Oriental Mustard** by Nematospora: A Fluorescence and Scanning Electron Microscope Study;
R.A. Holley (143/83

Evaluation of Selected Properties of **Chlorinated Wheat Flours** in a Lean **Cake** Formulation;
J. Grider (153/83

The Effects of Commercial Processing on the Structure and Microchemical Organization of **Rapeseed**;
S.H. Yiu (165/83

Microstructure of Winged Beans;
K. Saio (175/83

β-Glucans in the Caryopsis of **Sorghum**;
C.F. Earp (183/83

REVIEW: Food Microstructure: An Integrative Approach;
E.A. Davis (1/82

Correlation of Microscopic Structure of **Corn Starch** Granules with Rheological Properties of Cooked Pastes;
D.D. Christianson (13/82

Protein Bodies in Dormant, Imbibed and Germinated **Sunflower** Cotyledons;
R.D. Allen (63/82

REVIEW: Grain Structure and End-Use Properties;
Y. Pomeranz (107/82

Scanning Electron Microscopy of the Pericarp and Testa of Several **Sorghum** Varieties;
C.F. Earp (125/82

The Microscopic Structure and Chemistry of **Rapeseed** and its Products;
S.H. Yiu (135/82

Light Microscopy Preparation Techniques for **Starch** and Lipid Containing **Snack Foods**;
F.O. Flint (145/82

REVIEW: Fluorescence Microscopy of **Cereals**;
R.G. Fulcher (167/82

Freeze-Etch of Emulsified **Cake Batters** During Baking;
J.D. Cloke (177/82

Morphological and Textural Comparisons of **Soybean Mozzarella Cheese Analogs** Prepared with Different Hydrocolloids;
C.S. Yang (223/82

REVIEW: The Use of Microscopy to Explain the **Behaviour of Foodstuffs**;
D.F. Lewis (391/81/III

Soybean Seed-Coat Structural Features: Pits, Deposits and Cracks;
W.J. Wolf (531/81/III

An SEM Study of the Effects of Avian Digestion on the **Seed Coats** of Three Common Angiosperms;
L.B. Smith (545/81/III

REVIEW: Microstructure of Traditional **Japanese Soybean Foods**;
K. Saio (553/81/III

Effects of Exogenous Enzymes on **Oilseed Protein Bodies**;
R.D. Allen (561/81/III

Tannin Development and Location in **Bird-Resistant Sorghum** Grain;
P. Morrall (571/81/III

TUTORIAL: Light Microscopy of Plant Constituents in **Animal Feeds**;
J.G. Vaughan (577/81/III

Scanning Electron Microscopy of **Fluor-Water Doughs** Treated with Oxidizing and Reducing Agents;
L.G. Evans (583/81/III

The Microstructure of **Orange Juice**;
G.G. Jewell (593/81/III

TUTORIAL: Structural Studies of **Carrots** by SEM;
E.A. Davis (601/80/III

The Relationship Between **Wheat** Microstructure and **Flourmilling**;
R. Moss (613/80/III

REVIEW: Scanning Electron Microscopy of **Soybeans** and **Soybean Protein** Products;
W.J. Wolf (621/80/III

REVIEW: Some Examples of Scanning Electron Microscopy in **Food Science**;
R.J. Carroll (253/79/III

REVIEW: Preparation of **Food Science** Samples for SEM;
J.F. Chabot (279/79/III

REVIEW: Application of Scanning Electron Microscopy for the Development of **Materials for Food**;
C.-H. Lee (465/79/III

MILK & DAIRY PRODUCTS

REVIEW: The Size Distribution of **Bovine Casein** Micelles;
C. Holt (1/85

Characterisation of **Milk Proteins** in **Confectionery** Products;
J.F. Heathcock (17/85

Development of Microstructure in a **Cream Cheese** Based on **Queso Blanco Cheese**;
M. Kaláb (89/85

A Fluorescence Microscopic Study of **Cheese**;
S.H. Yiu (99/85

Structure Formation in **Acid Milk Gels**;
I. Heertje (267/85

Rheological and Scanning Electron Microscopic Examination of **Skim Milk Gels** Obtained by Fermenting with Ropy and Non-Ropy Strains of Lactic Acid Bacteria;
S.M. Schellhaass (279/85

Observations on the Air-Serum Interface of **Milk Foams**;
B.E. Brooker (289/85

REVIEW: Effects of Emulsifying Agents on the Microstructure and Other Characteristics of **Process Cheese**;
M. Carić (297/85

Properties of Calcium Caseinates with Disparate Performance in **Imitation Cheese**;
K. Fleming (313/85

Ultrastructural and Biochemical Investigations of Mature **Human Milk**;
R.J. Carrol (323/85

REVIEW: Particle Structure in **Spray-Dried Whole Milk** and in **Instant Skim Milk Powder** as Related to Lactose Crystallization;
Z. Saito (333/85

REVIEW: Microstructure of Set-Style **Yoghurt** Manufactured from Cow's Milk Fortified by Various Methods;
A.Y. Tamime (83/84

Transportation of Fragile Food Specimens such as **Milk Gels** Destined for Electron Microscopy;
P. Allan-Wojtas (93/84

Artefacts in Conventional Scanning Electron Microscopy of Some **Milk Products**;
M. Kaláb (95/84

A Simple Procedure for the Preparation of Stirred **Yoghurt** for Scanning Electron Microscopy;
P. Allan-Wojtas (197/84

Composition and Microstructure of **Soft Brine Cheese** Made From **Instant Whole Milk Powder**;
M.M. Omar (43/83

REVIEW: Development of Microstructure in Set-Style **Nonfat Yoghurt**;
M. Kaláb (51/83

Stranded Structure Development in Thermally Produced **Whey Protein Concentrate Gel**;
T. Beveridge (161/83

REVIEW: Structure and Properties of the Particulate Constituents of **Human Milk**;
M. Rüegg (25/82

Detection of **Buttermilk Solids** in **Meat Binders** by Electron Microscopy;
M. Kaláb (49/82

REVIEW: Ultrastructural Studies of **Milk Digestion** in the Suckling Rat;
P.B. Berendsen (83/82

REVIEW: Electron Microscopy of **Milk and Milk Products**: Problems and Possibilities;
D.G. Schmidt (151/82

REVIEW: Aspects of Sample Preparation for Freeze-Fracture/Freeze-Etch Studies of **Proteins and Lipids** in Food Systems;
W. Buchheim (189/82

Morphological and Textural Comparisons of **Soybean Mozzarella Cheese** Analogs Prepared with Different Hydrocolloids;
C.S. Yang (223/82

Electron Microscopic Localization of Solvent-Extractable Fat in Agglomerated Spray-Dried **Whole Milk Powder** Particles;
W. Buchheim (233/82

REVIEW: Electron Microscopy of Milk Products: A Review of Techniques;
M. Kaláb (453/81/III

Electron Microscopy and Sensory Evaluation of **Commercial Cream Cheese**;
M. Kaláb (473/81/III

Morphological and Textural Characterization of Soybean Mozzarella Cheese Analogs;
M.V. Taranto (483/81/III

A Comparison of the Microstructure of **Dried Milk Products** by Freeze-Fracturing Powder Suspensions in Non-Aqueous Media;
W. Buchheim (493/81/III

Effect of Acidulants and Temperature on Microstructure, Firmness and Susceptibility to Syneresis of **Skim Milk Gels**;
V.R. Harwalkar (503/81/III

Microstructure and Rheology of **Process Cheese**;
A.A. Ryan (635/80/III

Possibilities of an Electron-Microscopic Detection of **Buttermilk** Made from **Sweet Cream in Adulterated Skim Milk**;
M. Kaláb (645/80/III

A Scanning Electron Microscopical Investigation of the **Whipping of Cream**;
D.G. Schmidt (653/80/III

SEM Investigation of the Effect of **Lactose Crystallization** on the Storage Properties of **Spray Dried Whey**;
M. Saltmarch (659/80/III

REVIEW: Scanning Electron Microscopy of **Dairy Products**;
M. Kaláb (261/79/III

Morphological, Ultrastructural and Rheological Characterization of **Cheddar and Mozzarella Cheese**;
M.V. Taranto (273/79/III

MEAT

Scanning Electron Microscopic Study of **Rockfish** Preserved at Either Ambient Temperature or by Isothermal Freeze-Fixation;
L.E. Lampila (11/85

The Combined Effects of the Calcium Activated Factor and Cathepsin D on **Skeletal Muscle**;
E.A. Elgasim (55/85

REVIEW: Microstructure of **Meat Emulsions** in Relation to Fat Stabilization; C.M. Lee (63/85

Early Research on the Fibrous Microstructure of **Meat**;
H.J. Swatland (73/85

REVIEW: An Analysis of Microstructural Factors which Influence the Use of **Muscle** as Food;
R.G. Cassens (1/84

Studies on the Microdistribution of Aerobic Enzymes and Myoglobin in **Pork**;
H.J. Swatland (9/84

REVIEW: The Role of Gap Filaments in **Muscle** and in **Meat**;
R.H. Locker (17/84

REVIEW: Processing Effects on **Meat Product** Microstructure;
G.R. Schmidt (33/84

The Effect of **Salt** and Pyrophosphate on the Structure of **Meat**;
C.A. Voyle (113/84

TUTORIAL: Some Factors Influencing Ante-Mortem Changes in **Muscle**;
S.C. Seideman (127/84

An Alternative to Critical Point Drying for Preparing **Meat Emulsions** for Scanning Electron Microscopy;
E.J. Basgall (23/83

REVIEW: Image Analysis of Morphological Changes in **Wiener Batters** During Chopping and Cooking;
A.G. Kempton (27/83

Effect of Prerigor Pressurization on Bovine Lysosomal Enzyme Activity;
E.A. Elgasim (91/83

REVIEW: A Review of the **Muscle** Cell Cytoskeleton and its Possible Relation to **Meat** Texture and Sarcolemma Emptying;
D.W. Stanley (99/83

Myofibrillar Characteristics of **Porcine Stress Syndrome**;
P.K. Basrur (111/83

Sensory and Instrumental Texture Properties of **Flaked and Formed Beef**;
A.V. Cardello (119/83

Morphometry of **Meat** by Scanning Light Microscopy;
H.J. Swatland (135/83

REVIEW: Food Microstructure: An Integrative Approach;
E.A. Davis (1/82

Detection of **Buttermilk Solids** in **Meat Binders** by Electron Microscopy;
M. Kaláb (49/82

Effect of High Hydrostatic Pressure on **Meat** Microstructure;
E.A. Elgasim (75/82

Freeze-Induced Fibre Formation in Protein Extracts from Residues of Mechanically Separated **Poultry**;
R.A. Lawrence (91/82

Instrumental and Sensory Analysis of the Action of Catheptic Enzymes on Flaked and Formed **Beef**;
S.H. Cohen (99/82

REVIEW: The Use of Microscopy to Explain the Behaviour of **Foodstuffs**;
D.F. Lewis (391/81/III

TUTORIAL: Scanning Electron Microscopy in **Meat Science**;
C.A. Voyle (405/81/III

TUTORIAL: Preparation of **Muscle** Samples for Electron Microscopy;
H.D. Geissinger (415/81/III

Microscopical Observations on Electrically Stimulated **Bovine Muscles**;
C.A. Voyle (427/81/III

Scanning and Transmission Electron Microscopy of Normal and PSE **Porcine Muscle**;
J.D. Cloke (435/81/III

Meat Emulsions—Fine Structure Relationships and Stability;
R.J. Carroll (447/81/III

The Effect of Catheptic Enzymes on Chilled **Bovine Muscle**;
S.H. Cohen (595/80/III

REVIEW: Some Examples of Scanning Electron Microscopy in **Food Science**;
R.J. Carroll (253/79/III

REVIEW: Preparation of **Food Science** Samples for SEM;
J.F. Chabot (279/79/III

Identification of Fat and Protein Components in **Meat Emulsions** Using SEM and Light Microscopy;
F.K. Ray (473/79/III

FAT & EMULSION

REVIEW: The Light Microscopy of **Triglyceride Digestion**;
J.S. Patton (29/85

REVIEW: Microstructure of **Meat Emulsions** in Relation to Fat Stabilization;
C.M. Lee (63/85

Relation Between Microstructure, Destabilization Phenomena and Rheological Properties of **Whippable Emulsions**;
W. Buchheim (221/85

Thermal Analysis Microscopy for the Study of Phase Changes in **Fats**;
J.M. deMan (233/85

Combining Microscopy and Physical Techniques in the Study of **Cocoa Butter** Polymorphs and **Vegetable Fat Blends**;
J.D. Hicklin (241/85

REVIEW: Crystal Morphology of **Cocoa Butter**;
D.M. Manning (249/85

An Alternative to Critical Point Drying for Preparing **Meat Emulsions** for Scanning Electron Microscopy;
E.J. Basgall (23/83

REVIEW: Image Analysis of Morphological Changes in **Wiener Batters** During Chopping and Cooking;
A.G. Kempton (27/83

REVIEW: Some Effects of **Lipids** on the Structure of Foods;
K. Larsson (55/82

Light Microscopy Preparation Techniques for **Starch and Lipid Containing Snack Foods**;
F.O. Flint (145/82

REVIEW: Aspects of Sample Preparation for Freeze-Fracture/Freeze-Etch Studies of **Proteins and Lipids** in Food Systems;
W. Buchheim (189/82

REVIEW: Microscopy in the Study of **Fats and Emulsions**;
J.M. deMan (209/82

Electron Microscopic Localization of Solvent-Extractable **Fat** in Agglomerated **Spray-Dried Whole Milk** Powder Particles;
W. Buchheim (233/82

REVIEW: The Use of Microscopy to Explain the Behaviour of **Foodstuffs**;
D.F. Lewis (391/81/III

Meat Emulsions—Fine Structure Relationships and Stability;
R.J. Carroll (447/81/III

Microstructure of **Mayonnaise and Salad Dressing**;
M.A. Tung (523/81/III

Microstructure and Rheology of **Process Cheese**;
A.A. Rayan (635/80/III

Identification of **Fat** and **Protein** Components in **Meat Emulsions** Using SEM and Light Microscopy;
F.K. Ray (473/79/III

OTHER FOODS

Characterisation of **Milk** Proteins in **Confectionary** Products;
J.F. Heathcock (17/85

Microstructure of Spray-Dried and Freeze-Dried **Microalgal Powders**;
L.P. Lin (341/85

Stranded Structure Development in Thermally Produced **Whey Protein Concentrate Gel**;
T. Beveridge (161/83

REVIEW: The Use of Microscopy to Explain the Behaviour of **Foodstuffs;**
D.F. Lewis (391/81/III

Effect of Acidulatns and Temperature on Microstructure, Firmness and Susceptibility to Syneresis of **Skim Milk Gels**;
V.R. Harwalkar (503/81/III

Structures of Various Types of **Gels** as Revealed by Scanning Electron Microscopy;
V.E. Colombo (515/81/III

Microstructure of **Mayonnaise and Salad Dressing**;
M.A. Tung (523/81/III

Identification of **Foreign Matter in Foods**;
J.T. Stasny (599/81/III

SEM Investigation of the Effect of **Lactose** Crystallization on the Storage Properties of **Spray Dried Whey**;
M. Saltmarch (659/80/III

SCANNING ELECTRON MICROSCOPY, Inc.

FOOD MICROSTRUCTURE 1986

For more information contact:
Dr. Om Johari
Director, SEM Meetings
P.O. Box 66507
AMF O'Hare, IL 60666 U.S.A.
Phone: (312) 529-6677

FOOD MICROSTRUCTURE will be the subject of a program scheduled during **May 4–May 9, 1986** at the Clarion Hotel in New Orleans, Louisiana. Four special programs – on Meat Foods, Plant Foods, Dairy Foods and Fats, as well as several tutorials related to microscopy of foods are being planned.

All types of foods, including *vegetables, grains, sea foods, meat, dairy products and others* will be covered. Papers on the *fundamental aspects of food microstructure such as the molecular and colloidal forces which determine it, and the practical relationship between food microstructure and processing, ingredient changes, shelf life, consumer acceptability,* and other food-related areas are invited. *Techniques may include transmission electron microscopy, scanning electron microscopy, light microscopy, x-ray microanalysis or related microscopy/microanalytical methods.*

The organizers of the "Meat Microstructure" program are: **Prof. R.G. Cassens**, University of Wisconsin, Madison, WI; **Dr. S.H. Cohen**, U.S. Army Natick R&D Labs., Natick, MA; and **Dr. C.A. Voyle**, Food Research Institute, Bristol, U.K. The organizers of the "Microstructure of Foods from Plant Origin" program are: **Dr. W.J. Wolf**, U.S.D.A., Peoria, IL; **Dr. D.J. Gallant**, INRA, France; **Dr. K. Saio**, National Food Research Institute, Ibaraki, Japan, and **Dr. D.B. Bechtel**, U.S.D.A., Manhattan, KS. The organizers of the "Microstructure of Dairy Foods" program are: **Dr. M. Kaláb**, Agriculture Canada, Ottawa, and **Prof. Z. Saito**, Hokkaido University, Japan. The organizers of the "Microstructure of Fat" program are: **Prof. J.M. deMan**, University of Guelph, Ontario, Canada; **Prof. P.S. Dimick,** Penn. State University, Univ. Park, PA; and **Dr. N. Krog**, Grindsted Products, Brabrand, Denmark. The tutorials are being organized by **Prof. E.A. Davis**, University of Minnesota, St. Paul, MN.

Papers offered for this program will be published in the semi-annual Journal, **"FOOD MICROSTRUCTURE"**. The editors of this Journal are **Dr. S.H. Cohen**, U.S. Army R&D, Science and Advanced Technology Laboratory, Natick, Mass. (Telephone 617-651-4578); **Prof. E.A. Davis**, Food Science Department, University of Minnesota, St. Paul (Telephone 612-373-1158); **Dr. D.N. Holcomb**, Kraft R&D, Glenview, IL (Telephone 312-998-3724); **Dr. M. Kaláb**, Food Research Institute, Agriculture Canada, Ottawa (Telephone 613-995-3700 Ext. 272), and **Dr. W.J. Wolf**, USDA No. Reg. Res. Ctr., Peoria, IL (Telephone 309-685-4011, x350).

The Food Microstructure program in New Orleans will be held in conjunction with the **SCANNING ELECTRON MICROSCOPY/1986** meetings from **May 4 to 9, 1986. Registrants at the Food Microstructure program will be able to attend all of the activities of the SEM meeting at no additional charge.** Of particular interest should be: several tutorials, and programs on *Analytical Electron Microscopy (including STEM), Microprobe Surface Analytical Techniques, Particulate Characterization, Plants, and many areas of physical, biological and biomedical application.* A **comprehensive equipment exhibition** will take place during the meetings also. Complete details of SEM meetings are available on request.

The **registration fee** for this program is **$40.00**, if paid before Feb. 28, 1986, and **$55.00** after that. For subscription to the journal include an additional $50.00 (for U.S. delivery) or $55.00 (for elsewhere).

A Call for Papers, Registration Form, details of travel support and Hotel information are available on request. For more information on this program and the Journal, "Food Microstructure" contact Dr. Om Johari or one of the editors.

SEM PUBLICATIONS

(i) International Journal "Scanning Electron Microscopy"† (ISSN: 0586-5581)

SEM publishes the quarterly international journal "Scanning Electron Microscopy". Each issue (four issues in a year) is hardbound and contains over 40 papers and 400 pages covering all aspects of techniques, instrumentation, theory and applications of SEM and **related** techniques. Each paper is published after a thorough peer review and contains the unique features "Discussion with Reviewers" which provides added insight about the paper. The micrograph reproduction quality is superb.

Complete sets of Tables of Contents are separately available at $1.00 **per issue ($4.00 per year).**

Prices for SEM/1980, 1981, 1982, 1983, 1984, 1985 or 1986 each:

	U.S. Delivery	Elsewhere
☐ Complete Set (Parts 1-4)	$109.00	$119.00
☐ any 2 different parts	$ 84.00	$ 87.50
☐ any 1 part, also for 1979	$ 52.00	$ 55.00
SEM/1978 & 1979 (2 parts in 1978, 3 parts in 1979):		
☐ 1979(I+II) (Part III out of print)	$ 65.00	$ 71.50
☐ 1978/I (physical)	$ 37.00	$ 41.00
☐ 1978/II (biological)	$ 40.50	$ 44.50
☐ 1978/2 part set	$ 67.50	$ 74.00

(ii) International Journal Food Microstructure† (ISSN: 0730-5419)

Started in 1982 this semi-annual journal contains papers on all aspects of microstructure and microanalysis of foods, feeds, and their ingredients. There are 18 papers each in the two issues of Volume 4 (1985) covering meat, dairy products, plant foods, fats, etc. The subscription price **per year** is $50.00 (U.S. delivery) and $55.00 (elsewhere by surface mail) or $70.00 (outside U.S. by air mail). A major subject index of all food-related papers published by SEM is available on request.

(iii) Proceedings of "Pfefferkorn Conferences" Series (hardbound):

Started in 1982, this series is devoted to an in-depth coverage of basic topics related to electron microscopy.

1st – 1982: Electron Beam Interactions with Solids for Microscopy, Microanalysis and Microlithography
Edited by David F. Kyser, Dale E. Newbury, Heinz Niedrig, Ryuichi Shimizu (ISBN: 0-931288-30-4)
31 papers (372 pages) *$51.00 (U.S. delivery) and $54.00 (elsewhere).*

***2nd – 1983: The Science of Biological Specimen Preparation for Microscopy and Microanalysis**
Edited by Jean Paul Revel, Tudor Barnard, Geoffrey H. Haggis (ISBN: 0-931288-32-0)
28 papers (246 pages) *Price $40.00 (U.S. delivery) and $43.00 (elsewhere).*

3rd – 1984: Electron Optical Systems for Microscopy, Microanalysis, and Microlithography
Edited by John J. Hren, Friedrich A. Lenz, Eric Munro, Peter B. Sewell (ISBN: 0-931288-34-7)
27 papers (272 pages) *Price $44.00 (U.S. delivery) and $47.00 (elsewhere).*

(iv) Special Publications Derived from SEM Volumes:

1. The Integument: Scanning Electron Microscopy in Skin Biology—A soft cover book with 31 papers from SEM/1978 to 1985 (294 pages). *Price $34.00 (U.S. delivery), $37.00 (elsewhere).*

***2. Preparation of Biological Specimens for Scanning Electron Microscopy**—A soft cover book with 22 papers from SEM/ 1978 to 1984 (352 pages). *Price $32.00 (U.S. delivery), $35.00 (elsewhere).*

***3. SEM of Cells in Culture** — Soft cover book with 30 papers from SEM/1978 to 1983 (320 pages). *Price $29.00 (U.S. delivery), $32.00 (elsewhere).*

***4. Basic Methods in Biological X-ray Microanalysis** — A soft cover book with 20 papers from SEM/1979 to 1982 (284 pages). *Price $22.00 (U.S. delivery), $25.00 (elsewhere).*

***5. Ultrastructural Effects of Radiation on Tissues & Cells** — A soft cover book with 17 papers from SEM/1981 and 1982. *Price $18.00 (U.S. delivery), $20.50 (elsewhere).*

***6. Cell Surface Labeling** — A soft cover booklet with 10 papers from SEM/1979. *Price $10.00.*

7. Clinical Applications of the SEM — A soft cover booklet with 3 papers from SEM/1980. *Price $5.00.*

8. Brain Ventricular Surfaces — A soft cover booklet with 18 papers from SEM/1978. *Price $10.00.*

9. Studies of Food Microstructure — A hardbound book with 36 papers from SEM/1979, 1980 and 1981. *Price $49.00 (U.S. delivery), $52.00 (elsewhere).*

---

†Reprints (or copies) of papers from SEM publications are available at $5.00 each.

***Special price for six books marked with an asterisk $99.00 for U.S. delivery and $109.00 (elsewhere).**

STARCH CONVERSION TECHNOLOGY (Food Science and Technology Series, Volume 14). Edited by G.M.A. van Beynwy and J.A. Roels. 1985. Marcel Dekker (New York). 376 pages. $65.00.

Starch Conversion Technology is a volume of ten chapters describing recent developments in the conversion of starch from corn, wheat, potato and tapioca. Presently, only a small percentage of these starches are further processed but the products of conversion are gaining more and more importance. The book includes discussions of political and economic considerations as well as technological aspects of starch conversion.

Chapter 1 provides a brief overview of the application of starch and starch-derived products. The versatility of starch-based chemicals is readily apparent from the comprehensive table of products obtained from starch conversion.

Chapter 2 is a very readable summary of the sources, composition and structure of starch. The large amount of material concisely presented makes this chapter an excellent reference to anyone interested in the properties of starch.

Chapter 3 gives a thorough description of corn wet-milling and the production of corn syrups and dry starch. Such a chapter is appropriate but the extensive detail provided makes this chapter of interest primarily to those involved in plant design and construction.

Chapter 4 gives a brief introduction to chemical modification of starches. Readers should accept the information with caution because of the several errors found (e.g., source of the formulae are incorrectly drawn).

Chapter 5 on the enzymic degradation of starch emphasizes the production of syrups. However, the completeness with which the enzymes are described makes this chapter of value to anyone involved in basic biochemical or structural studies of starch.

Chapter 6 describes current technology and economics of fuel alcohol production from starch. The chapter adequately cautions that the overall economics are presently unfavorable. Interest in this chapter may be limited to those directly involved in fuel production.

Chapter 7 gives an up-to-date account of the conversion of glucose to fructose. This chapter would serve as an excellent reference on glucose isonierase and on enzyme immobilization technology.

Chapter 8 covers many aspects of fermentation. It is well-referenced and includes a discussion of future trends.

Chapter 9 describes a wide range of reactions using glucose as a starting material. Conversion to several important chemical commodities is covered in great detail. This chapter should appeal particularly to organic chemists in food science and medicine.

Chapter 10 summarizes the market for starch-based products with an emphasis on corn sweetners. Market estimates are given for several products. The information should be of interest to those involved in starch conversion and to those in industries purchasing the products of this technology.

This is a comprehensive book. The basics of starch chemistry, biochemistry and enzymology are well-presented. Sufficient basic information is given so that each chapter is readable as an independent unit. The practical application of many basic aspects of starch is easily understood. There is a lot of historical background which contributes to the completeness with which each subject is discussed. Economic and political aspects of the technology, important considerations for industrial application, are well-covered. This volume should be useful to anyone working on the structure and function of starch. It is a good reference book and could also be considered as a supplemental textbook for a course on sugars and starches.

Susan Gaud
Chyi Chen

VERARBEITUNG VON NAHRUNGSMITTELN OHNE QUALITATSEIN-BUSSE - WUNSCHTRAUM ODER WIRKLICHKEIT? (Handling of Food without Change of Quality - Dream or Reality?) Bibliotheca Nutrietio et Dieta Series, Vol. No. 34. Proceedings of the 3rd Symposium held by the International Foundation for the Promotion of Nutrition Research and Nutrition Education, in Bad Soden (Germany), November 1983. Edited by J.C. Somogyi. 1985. S. Karger, Basel. 109 + viii pages. $58.75. ISBN 3-8055-3926-6.

This booklet covers eight papers presented at this symposium. The authors review the literature data about losses of nutritional value (Somogyi, Paulus) and their sources and consequences. Two papers (Varela, Meier-Ploeger) are dealing with differences in home and industrial cooking with special emphasis on frying and possible effects on foods; cooking, freezing and reheating; microwave warming; minimizing environmental pollutants (like Hg, Pb, and pesticides). For practical reasons, Meier-Ploeger pointed out that consumer acceptance is restricted by only sensoric evaluation of foods.

The paper by Bender investigates changes in micronutrients due to industrial processing and concludes that vitamin deficiencies are caused more by malnutrition and dietary faults than by losses of nutritive value during processing. He couldn't reveal statistical differences in micronutrient losses for both home and industrial cooking procedures, since the micronutrients display high grade of variability.

The paper by Mauron comprises of valuable information on Influence of Processing on Protein Quality. The author reviews Protein-Protein-Interactions (formation of Isopeptides, Lysinoalanine formation, Racemization), Protein-Carbohydrate-Interactions (Millard reaction - early, advanced and final), Protein oxidized Lipid Interactions, and Pyrolysis Reactions under this category, and shows that not only the nutritive value of foods diminishes during processing, but also toxic or growth depressing and mutagenic substances may occur. In general, this must be regarded as unavoidable and not only detrimental. Processing provides a full range of organoleptic properties. Attention should be given to baby food and infant formula because infants don't have a wide variety of foodstuffs to supplement possible losses.

In the last two papers, Billek and Seher summarize the knowledge of possible effects of the fat refining process on the nutritive value (minimizing of heavy metals and pesticides, no evidence for any unwanted effects), fat oxidation by deep-frying and the bioavailability of hydrated fats, investigated in long time feeding experiments.

F. Kley

REVIEWING PROCEDURE
AND
DISCUSSION WITH REVIEWERS

Each paper in this volume contains a Discussion with Reviewers. This discussion follows the text and should be read with the paper. Each paper submitted to SEM, Inc. for publication is reviewed by at least three, up to an average of five, reviewers. The reviewers are asked to separate their comments from their questions. The comments are useful in determining the acceptability of the papers as submitted. Although the comments require no written response, in several cases, the authors have included responses to comments, or to questions phrased from, or based on, comments (either as a result of editorial suggestions or on the author's own initiative). Based on these comments approximately 15% of the submitted papers were not accepted for publication; while almost all of the others were asked to make changes involving from minor to major revisions.

The questions, for the most part, originate as a result of statements included in our cover letter accompanying each paper sent to the reviewers. The reviewers are asked to suppose they are attendees at a conference where this paper, as written, is being presented, and then ask relevant questions which would occur to them resulting from the presentation. From the questions so asked, some are not included with the published paper because the authors attended to them by text revisions. In some cases, editorial and/or space considerations may exclude inclusion of all questions asked by reviewers. The authors are asked to prepare their Discussion with Reviewers section in a camera-ready format. In some instances the authors edit the questions and/or combine several similar questions from different reviewers to provide one answer. While all efforts are made to check that the questions in the printed version faithfully follow the views of the specific reviewer, the editors apologize, if in some instances, the actual meaning and/or emphasis may have been changed by the author.

The cover letter to the reviewers states:

"1. Your name will be conveyed to the author with your review UNLESS YOU ASK US NOT TO.

2. The questions published in the Journal will be identified as originating from you UNLESS YOU ADVISE OTHERWISE..."

In all cases sincere efforts are made to respect the reviewer's wishes to remain anonymous; however, in nearly 95% of the cases, the reviewers have given permission to be identified; so their names are conveyed to the authors and are included with the questions printed with each paper. An overall list of reviewers is provided in the opening pages of each SEM part. We apologize for any error/omissions which may occur.

Finally, readers are urged to be cautious regarding the weight they attach to the authors' replies, since the answers to the questions represent the authors' unchallenged views--except for minor editorial changes--the authors generally have the last word. Also, please consider that the questions were, in most cases, relevant to the originally submitted paper, and they may not have the same significance for the revised paper published in this volume.

If you disagree with the results, conclusions or approaches in a paper, please send your comments, as a Letter to Editor, typed in a column format (each column is 4-1/8 inches wide and 11-1/2 inches long; i.e., 10.5 by 29.3 cm.). Your comments along with author's response will be published in a subsequent issue.

The editors gratefully thank the authors and reviewers (see p. i & ix) for their contributions, invite your comments on ways to improve this procedure and seek qualified volunteers to assist with reviewing papers in the future.

ERRATA: Despite the best efforts of authors, reviewers and editors, errors may remain. Please help by pointing out errors that you notice. Please provide enough information to locate each error (volume, page, column, line, etc.) and indicate suitable correction.

The Editors
Food Microstructure

REVIEWERS LIST

The help of the following reviewers for papers in this issue of **FOOD MICROSTRUCTURE** is gratefully acknowledged.

Akin, D.E.	USDA Russell Agri.Res.Ct., Athens, GA
Allan-Wojtas, P.	Agriculture Canada, Ottawa, Ont., Canada
Arnott, H.J.	University of Texas, Arlington, TX
Bechtel, D.B.	US Grain Market.Res. Lab., Manhattan, KS
Bragg, L.H.	Iowa State University, Ames, IA
Brooker, B.E.	Food Research Institute, Reading,Berk, U.K.
Buchheim, W.	Bundes. Milchforschung, Kiel, West Germany
Buma, T.J.	Carbohydrate Res.Inst.TNO, Groningen, Netherlands
Carpenter, D.E.	Kraft Research & Dev.Lab., Glenview, IL
Cayle, T.	Kraft Research & Dev.Lab., Glenview, IL
Chen, W.S.	Kraft Research & Dev.Lab., Glenview, IL
Davis, E.A.	University of Minnesota, Saint Paul, MN
deMan, J.M.	University of Guelph, Guelph, Ont., Canada
Dimick, P.S.	Pennsylvania State Univ., Univ. Park, PA
Dylewski, D.P.	Kraft Research & Dev.Lab., Glenview, IL
Eger-Hummel, G.	Inst.Pharmazent.Tech.Uni., Marburg-Lahn, West Germany
Emmons, D.B.	Agriculture Canada, Ottawa, Ont., Canada
Ernstrom, C.A.	Utah State University, Logan, UT
Fulcher, R.G.	Agriculture Canada, Ottawa, Ont., Canada
Gallant, D.J.	I.N.R.A.--L.T.A.A., Nantes Cedex, France
Hampson, J.W.	USDA-Eastern Reg.Res.Ctr., Philadelphia, PA
Hanna, W.W.	USDA-Agr.Res.,So.Atlantic, Tifton, GA
Heertje, I.	Unilever Research Lab., Vlaardingen, Netherlands
Holcomb, D.N.	Kraft Research & Dev.Lab., Glenview, IL
Holley, R.A.	Agriculture Canada, Ottawa, Ont., Canada
Holt, C.	Hannah Research Institute, Ayr,Scotland, U.K.
Jewell, G.G.	Cadbury Schweppes plc., Reading, U.K.
Kalab, M.	Agriculture Canada, Ottawa, Ont., Canada
Krog, N.	Grindsted Products A/S, Brabrand, Denmark
Larsson, K.	University of Lund, Lund, Sweden
Manning, D.M.	M & M Mars, Elizabethtwn, PA
Marshall, R.T.	University of Missouri, Columbia, MO
Modler, H.W.	Agriculture Canada, Ottawa, Ont., Canada
Morr, C.V.	Clemson University, Clemson, SC
Moss, R.	Bread Res.Inst.Australia, North Ryde, Australia
Nelson, M.L.	Washington State Univ., Pullman, WA
Patton, J.S.	Genentech Inc., S.San Fran., CA
Pomeranz, Y.	USDA Grain Marketing Res., Manhattan, KS
Resmini, P.	Inst. Industrie Agrarie, Milano, Italy
Ruegg, M.W.	Fed. Dairy Res. Institute, Liebefeld, Switzerland
Saio, K.	National Food Res. Inst., Tsukuba, Japan
Sasevich, F.J.	Kraft Research & Dev.Lab., Glenview, IL
Schmidt, D.G.	Netherland Inst.Dairy Res, Ede, Netherlands
Strandholm, J.J.	Kraft Research & Dev.Lab., Glenview, IL
Swaisgood, H.E.	No. Carolina State Univ., Raleigh, NC
Tamime, A.Y.	West Scotland Agr.College, Ayr,Scotland, U.K.
Taranto, M.V.	Frito-Lay Inc. Res.& Dev., Irving, TX
Varriano-Marston, E.	Hercules Research Center, Wilmington, DE
Vedamuthu, E.R.	Microlite Technics, Sarasota, FL
Walstra, P.	Agriculture Univ., Wageningen, Netherlands
Wiley, B.	Army Natick R & D Center, Natick, MA
Wolf, W.J.	USDA North. Reg. Res.Lab., Peoria, IL
Wood, D.A.	Glasshouse Crop.Res.Inst., Littlehamptn, U.K.
Zobel, H.F.	Corn Products Tech. Ctr., Argo, IL

CALL FOR REVIEWERS

The contribution of reviewers to the quality of this publication and our meetings is tremendous. We find suitable reviewers from the suggestions we receive from the authors, our advisors, and from past contacts. We will welcome your suggesting your name or other names (along with full mailing addresses) as reviewers.

SUBJECT INDEX

A - Band in Muscle 11, 73
Acid Milk Gels 267
Agaricus bisporus 143, 349
anaranthus 43
autoradiography 143, 173
beans 115, 183
beta casein 267
biosalts 29
bloom, fat 249
bread 125, 135
brine 165
bubble ghosts 289
calcium activated factor 55
calcium caseinate 313
calcium phosphate 267
calcium soaps 29
Canola oil 233
caramel 17
casein 89, 99, 267, 289, 313, 323
casein micelle 1, 267, 323
casein networks 99
cathepsin 55
cellulolytic 165
cereal 135
cheese 89, 99, 297, 313
cheese, Blue 99
cheese, Brie 99
cheese, Camembert 99
cheese, Cheddar 99
cheese, crystals 99
cheese, imitation 313
cheese, Latin American White 89
cheese, Mozzarella 99
cheese, process 99, 297
chocolate 17, 241
Chorella 341
chromatography 1
chymosin 1
citrates 297
cocoa butter 241, 249
colipase 29
comminution 63
confectionery products 17
corn 213
cotyledon 183, 191
cowpeas 115
cream cheese 89
crystallization 233, 241, 333
cucumber pickles 165
cytochemistry 173
cytoskeleton 73
differential scannning calorimetry 233, 241, 249
digestion 29, 357
Dioscorea dumetorum 173
dough 125
energy dispersive X-Ray microanalysis 297
elasticity, modulus of 199
electron spin resonance 83
electrophoreses 55, 323
electrophoreses SDS-PAGE 55, 323
emulsifying agents 297
emulsions 63, 221
endoplasmic reticulum 125, 135
endosperm 125, 135, 199
exopolymer 279
fat 17, 29, 89, 99, 221, 233, 241, 249, 323
fat bloom 249
fat digestion 29
fat dispersion 63
fat hardness 63
fat stabilization 63
fat, globules 89, 99, 323
fat, phase changes 233, 241
fat, whipping 221
fatty acid composition 43
fish 11
flour 135
fluorescence microscopy 99
foams 289
forage 357
freeze fixation 11, 221, 267
freeze-fracture 17, 125, 221, 241, 267, 341
fudge 17
gamma irradiation 349
gelation of milk 267, 279
gluten 135
Golgi apparatus 125
hardshell 115
Heinz fluid 333
herbivores 357
histochemistry 43, 165
hydrodynamic radius 1
hydrogenated vegetable fat 241
hyphae 165
I-band in muscle 11, 73
ice 11
ice crystals 11
image analysis 63, 199
imitation cream 221
Instron 199
interfacial film 63, 289
irradiation 349
lactation 323
lactic acid bacteria 279
lactose 333
lamella 165
legumes 115
light scattering 1
lipase 29
lipids 233
liquid crystals 29
low temperature SEM 17
meat 55, 63, 73
meat, emulsions 63
melting salts 297
mesquite 43
microalgal powders 341
milk 17, 89, 267, 279, 323
milk, coagulation 89
milk, crumb 17
milk, curd 89
milk, foams 289
milk, gels 267, 279
milk, human 323
milk, powder 17, 333
milk, protein 17
milling 125, 135
muscle 11
muscle, skeletal 55
muscle, structure 11
mushroom 143, 349
myofibrillar proteins 55, 73
NMR, pulsed 221
noodles 135
nuclear magnetic resonance 221
Olneya 43
pancreatic lipase 29
paraffin 165
parenchyma cells 173, 183
particles 333, 341
pectinolytic 165
phase microscope 55
Phaseolus vulgaris 115, 183
phosphates 297
photon spectroscopy 1
pickles 165
plasma asher 333
Pleurotus 349
polarized light microscopy 233, 249
polymorphism 233, 241
Prosopis 43
protein 55, 63, 267
protein, bodies 125, 183, 191
protein, matrix 63
protein, myofibrillar 55, 73
Queso Blanco 89
radiation 349
rheology 63, 199, 221, 279
ripening 55, 349
ruminant 357
sarcomere 11, 63
Schultz-Zimm distribution 1
seafood 11
seeds 43, 115, 183, 191
seeds, anatomy 43
seeds, coat 115, 183
seeds, composition 43
seeds, structure 43, 115, 183
size distribution 1, 29, 63, 323
skeletal muscle 55
small angle X-ray scattering 107
sodium dodecyl sulfate gel 55
solid fat content 221
soybeans 115, 191

spectroscopy 1
Spirulina 341
staining 17, 43, 99, 323
starch 83, 107, 115, 125, 135
starch, retrogradation 99
starch, wheat 99
Stenvert hardness tester 213
sugar 17
sugar crystals 17
surfactants 221
tempering 249
thermal microscopy 233
toppings 221
triglyceride 29, 233, 241, 249
ultracentrifugation 1
vascular system 183
viscosity 221, 279
vitreosity 199
water absorption 313
water activity 279
water content 199
water imbibition 115
wheat 107, 125, 135, 199
wheat flour 135
wheat grain 199
wheat kernel 199
wheat starch granules 107
whey proteins 267
whippable emulsions 221
X-ray diffraction 221, 241, 333
x-ray scattering 107
yam 173
yoghurt 279
Z - line in muscle 11, 55, 73
zeta potential 267

AUTHOR INDEX

Al Saleh, A. 199
Anglemier, A.F. 55
Atkey, P.T. 143
Barfod, N.M. 221
Basch, J.J. 323
Bechtel, D.B. 125
Becker, R. 43
Borgstrom, B. 29
Bouchet, B. 173
Brillouet, J.M. 173
Brooker, B.E. 289
Buchheim, W. 221
Carey, M.C. 29
Caric, M. 297
Carroll, R.J. 323
Craig, G.D. 143
Czuchajowska, Z. 213
Davis, E.A. 83, 107
deMan, J.M. 233
Dimick, P.S. 249
Elgasim, E.A. 55
Elkhalifa, E.A. 55
Farrell, Jr., H.M. 323
Fleming, H.P. 165
Fleming, K. 313
Gallant, D.J. 173, 199
Gantar, M. 297
Gordon, J. 83, 107
Grider, J. 107
Gull, K. 143
Hamosh, M. 29
Harbers, L.H. 357
Heathcock, J.F. 17, 241
Heertje, I. 267
Hicklin, J.D. 241
Holt, C. 1
Hughes, J.S. 115, 183
Irving, D.W. 43
Jenness, R. 313
Jewell, G.G. 241
Kalab, M. 89, 297
Kennick, W.H. 55
Keresztes, A. 349
Kondo, K. 191
Koohmaraie, M. 55
Kovacs, E. 349
Kovacs, J. 349
Krog, N. 221
Lampila, L.E. 11
Lee, C.M. 63
Lin, L.P. 341
Lindstrom, M. 29
Manning, D.M. 249
Miller, W.G. 83
Modler, H.W. 89
Mohr, V. 11
Morris, H.A. 279, 313
Moss, R. 135
Mostafa, A.N. 233
Newsam, R.J. 143
Patton, J.S. 29
Pearce, L.E. 83
Phillips, J.G. 323
Pomeranz, Y. 213
Rasmussen, H.P. 115
Reid, D.S. 11
Renaudin, S. 173
Saio, K. 191
Saito, Z. 333
Schellhaass, S.M. 279
Schmidt, R. 313
Sealy, L. 173
Smith, A.K. 233
Smits, P. 267
Sugimoto, T. 191
Swanson, B.G. 115, 183
Swatland, H.J. 73
Trigiano, R.N. 165
Vetter, R.D. 29
Visser, J. 267
Walter, Jr., W.M. 165
Wood, D.A. 143
Yang, M. 107
Yiu, S.H. 99

FOOD MICROSTRUCTURE
INSTRUCTIONS TO AUTHORS

Papers for publication in the international journal Food Microstructure are invited. Papers can cover all types of foods, including vegetables, grains, sea foods, meat, dairy products and others. Topics of interest are: Fundamental aspects of food microstructure such as the molecular and colloidal forces which determine it, and the practical relationship between food microstructure and processing, ingredient changes, shelf life, consumer acceptability, and other food-related areas. Techniques used may include transmission and scanning electron microscopy, light microscopy, x-ray microanalysis, or other related microscopy/microanalytical methods.

Papers for Food Microstructure (FM) may be offered at any time. Papers can be for publication only, or intended for oral presentation at the Annual Food Microstructure meeting in early spring. The latter papers are due two months prior to the start of the meeting; only papers acceptable for publication are allowed oral presentation. Oral presentation of a paper at some other meeting or publication as unreviewed abstract (e.g., in proceedings, etc.) does not preclude consideration of a paper by FM.

The letter accompanying the paper should contain names and complete addresses of at least **four persons competent to review the paper**. Suggested reviewers: **a.** must neither be from author's current or recent affiliations, nor coworkers; **b.** should preferably be active researchers in the field (e.g., whose work is being extensively referred to); and **c.** need not be personally known or contacted by the authors. The editors **will select** the most suitable reviewers irrespective of their location. Each paper will be intensely reviewed by at least three reviewers.

The **initial paper (hereafter referred to as "paper")** should conform to **these Instructions.** However, to be published after reviewing, **the final manuscript (hereafter referred to as "manuscript") should be either a. submitted on the model sheets conforming to the Manuscript Preparation Guidelines (mailed along with the reviewers' comments), or b. sent to SEM Inc. for preparation at a nominal cost (per details mailed with reviews).** In addition to all the text, the **manuscript** may have to contain the author's publishable responses to questions raised by the paper's reviewers (see the Discussion with Reviewers in papers published in FM).

The following types of contributions can be offered. A length limit is not imposed on papers. Short, but complete, papers are welcome.

RESEARCH PAPER: Presents new unpublished findings.

REVIEW PAPER: Includes an extended literature review and complete bibliography, **emphasizes author's new unpublished findings** and in an extended discussion puts the topic in proper perspective.

TUTORIAL PAPER: Contains an **organized comprehensive review** of **ALL** relevant published material as for a teaching lecture.

TECHNICAL TIP: Paper should have no more than 1000 words.

LETTER TO THE EDITOR: Commenting on paper already published in FM.

The author should indicate the type of paper and carefully adhere to the applicable definition, since the reviewers and editors judge the paper accordingly.

INSTRUCTIONS FOR SUBMISSION OF PAPERS

Type paper in **double-spaced** format on standard size paper.

The paper should include title page, abstract, all headings and text. On the **title page** include: **a.** a **short title** which accurately represents the contents of the paper; **b.** an **informative running head** consisting of no more than 50 characters; **c. names and affiliations** of all authors, **name and complete work and home addresses and phone numbers of the person to contact; d. 10 key words/phrases** suitable for subject index; and **e. for review papers, indicate page numbers containing new material** (e.g., "new material will be found on pages __.").

An **Abstract** (of 100-250 words) is required for all papers. The Abstract should be concise and include the purpose of the paper, major results obtained and conclusions. Phrases such as "will be described," "is discussed," "are presented" etc. should be avoided.

The **Introduction** of the paper **must** contain a clear, concise statement of the purpose of the paper and the relationship of this paper to what is already in the literature. As applicable, a **Materials and Methods** section with **complete specimen preparation** information must be included (even if already published elsewhere), so that the work can be duplicated by others.

Equations should be numbered consecutively, using arabic numerals. Each **symbol and abbreviation** should be defined when first used. **SI units must be used;** other metric units or U.S. customary units (English), if used, must be given in parentheses.

REFERENCES

Include all references relevant to paper which are either readily available published works or papers in press. Work in progress, manuscripts submitted or in preparation, unpublished findings, personal communications etc. must be excluded from the reference list but may be acknowledged in the text (in parentheses).

The reference list at the end of the paper must be organized in alphabetical order by the first authors' names. Names of all authors (last names and initials only, with a comma between names and no other punctuation), full titles of papers, appropriate bibliographic information (with standard abbreviations for journals, and editors and publishers for books and proceedings), and inclusive pagination must be included. Availability information must be included for all non-journal references.

When referencing **SEM Inc. publications**, use the following formats only:

SEM Journal: Frederik PM, Busing WM, Persson A. (1984). Surface defects on thin cryosections. Scanning Electron Microsc. 1984; I:433-443.

Food Microstructure: Elgasim EA, Kennick WH. (1982). Effect of high hydrostatic pressure on meat microstructure. Food Microstruc. 1, 75-82.

In the **text, cite references** in one of the following two styles:

a. Cowley (1967) or (Cowley, 1967) or Crewe and Wall (1970). If there are three or more authors, use the form Venables et al. (1978). If more than one paper is published in the same year by the same author (or group of authors) use the form (Rose, 1974a), etc.

b. As long as there is consistency, either superscript[1] or full-size numerals in brackets [1] can be used. In this case, the numbering must be in sequence in the reference list, but the references will generally not appear in sequence in the text.

ILLUSTRATIONS AND TABLES

Number each figure and table with **an arabic numeral and refer to them in sequence in the text.** Several illustrations within a figure must be designated a, b, c, etc. Each table must have a title. ***Each figure must have a caption*** – either on its own page or all captions should be placed together on separate pages. **Very important: Use arrows or letters to identify features referred to, and so indicate in the caption.** Illustrate text with the fewest photographs possible. Indicate magnification on photos by a line of, e.g., 1μm, 10μm, 100μm, or 1 mm length; identify either on the photo or in the caption. Use nm, μm, or mm, not μ, u or -X.

Quality of Illustrations. *Photos should be clear, clean, unscreened* (screened photos are not acceptable), *black and white glossy prints.* **Color photographs** can be published by prior arrangement between author and the managing editor, whereby the author will be asked to pay the additional cost.

Size. For the *manuscript*, illustrations and tables should preferably be 10.5 cm wide. The maximum permissible length for photographs will be 9 cm (3.5"); line drawings and tables may be longer than 9 cm but not wider than 10.5 cm. All letters and symbols on illustrations and tables must be larger than 2.0 mm. **THE ILLUSTRATIONS, TABLES AND LETTERING INCLUDED WITH THE PAPER MUST CONFORM TO THESE SIZES.** *Permission for larger illustrations and/or tables must be requested when the paper is submitted.*

SUBMISSIONS AND COMMUNICATIONS

Submit 4 copies of the paper. Each of the 4 copies must include its own set of illustrations and clear glossy prints of all photographs. (Retain the best set of prints for your manuscript, since illustrations sent with paper may not be returned.) Papers containing photocopies (Xerox, etc.) of photographs will not be processed for reviewing; manuscripts containing photocopies of tables and illustrations are not accepted. All illustrations must be organized in sequence (must not be mounted on cardboards) and placed in separate envelopes. Place each copy of the paper *(together with its envelope of illustrations) in a separate, unsealed, ready-to-mail envelope,* so that the paper can be sent directly to its reviewers.

For **submission** of papers and **inquiries** contact: one of the editors or **Dr. Om Johari**, Managing Editor, **(phone 312-529-6677)**, P.O. Box 66507, AMF O'Hare, IL 60666 USA. (**Street address,** if needed, is: 1034 Alabama Dr., Elk Grove Village, IL 60007, USA).

OTHER IMPORTANT ITEMS

Reprints. 15 complimentary tear sheets are provided. Information for ordering additional reprints is sent with the proofs.

Copyright. Food Microstructure is a copyrighted publication. Letters granting permission to use other copyrighted material must accompany the **manuscript.**

Continued from outside back cover

EFFECTS OF EMULSIFYING AGENTS ON THE MICROSTRUCTURE AND OTHER CHARACTERISTICS OF PROCESS CHEESE – A REVIEW
M. Carić, M. Gantar, M. Kaláb (Review Paper) 297

PROPERTIES OF CALCIUM CASEINATES WITH DISPARATE PERFORMANCE IN IMITATION CHEESE
K. Fleming, R. Jenness, H.A. Morris, R. Schmidt 313

ULTRASTRUCTURAL AND BIOCHEMICAL INVESTIGATIONS OF MATURE HUMAN MILK
R.J. Carroll, J.J. Basch, J.G. Phillips, H.M. Farrell, Jr. 323

PARTICLE STRUCTURE IN SPRAY-DRIED WHOLE MILK AND IN INSTANT SKIM MILK POWDER AS RELATED TO LACTOSE CRYSTALLIZATION
Z. Saito (Review Paper) 333

MICROSTRUCTURE OF SPRAY-DRIED AND FREEZE-DRIED MICROALGAL POWDERS
L.P. Lin 341

EFFECT OF IONIZING IRRADIATION AND STORAGE ON MUSHROOM ULTRASTRUCTURE. I. THE GILLS OF *AGARICUS BISPORUS* (LGE.) IMBACH AND *PLEUROTUS OSTREATUS* (JACQ. EX FR.) KUMMER
A. Keresztes, J. Kovács, E. Kovács 349

ULTRASTRUCTURAL UTILIZATION OF PLANTS BY HERBIVORES
L.H. Harbers (Tutorial Paper) 357

Major Subject Index of Food Microstructure and Related Papers Published by SEM Inc. from 1979–1985 i

Announcement of Food Microstructure/1986 Meeting v

SEM Publications vi

Book Reviews vii

Discussion with Reviewers viii

Reviewers List ix

Subject Index x

Author Index xi

Instructions to Authors xii

Copyright © 1985 Scanning Electron Microscopy, Inc., except for contributions in the public domain.
All rights reserved.

See Statement on the inside front cover.

Permission is granted to quote from this volume in scientific works with the customary acknowledgement of the source. To print a table, figure, micrograph or other excerpt requires, in addition, the consent of one of the original authors and notification to SEM, Inc. Republication or systematic or multiple reproduction of any material in this volume (including the abstracts) is permitted only after obtaining written approval from SEM, Inc., and in addition, SEM, Inc. requires that permission also be obtained from one of the original authors.

Every effort has been made to trace the ownership of all copyrighted material in this volume and to obtain permission for its use.

FOOD MICROSTRUCTURE

An International Journal on the Microstructure and Microanalysis of Foods, Feeds and their Ingredients

VOL. 4, NO. 2 (1985)

TABLE OF CONTENTS

MICROSTRUCTURAL CHANGES IN MATURING SEEDS OF THE COMMON BEAN (*Phaseolus vulgaris* L.)
J.S. Hughes, B.G. Swanson 183

CHANGES IN TYPICAL ORGANELLES IN DEVELOPING COTYLEDONS OF SOYBEAN
K. Saio, K. Kondo, T. Sugimoto 191

RHEOLOGICAL AND ULTRASTRUCTURAL STUDIES OF WHEAT KERNEL BEHAVIOUR UNDER COMPRESSION AS A FUNCTION OF WATER CONTENT
A. Al Saleh, D.J. Gallant 199

STRUCTURE OF COARSE AND FINE FRACTIONS OF CORN SAMPLES GROUND ON THE STENVERT HARDNESS TESTER
Y. Pomeranz, Z. Czuchajowska 213

RELATION BETWEEN MICROSTRUCTURE, DESTABILIZATION PHENOMENA AND RHEOLOGICAL PROPERTIES OF WHIPPABLE EMULSIONS
W. Buchheim, N.M. Barfod, N. Krog 221

THERMAL ANALYSIS MICROSCOPY FOR THE STUDY OF PHASE CHANGES IN FATS
J.M. deMan, A.N. Mostafa, A.K. Smith 233

COMBINING MICROSCOPY AND PHYSICAL TECHNIQUES IN THE STUDY OF COCOA BUTTER POLYMORPHS AND VEGETABLE FAT BLENDS
J.D. Hicklin, G.G. Jewell, J.F. Heathcock 241

CRYSTAL MORPHOLOGY OF COCOA BUTTER
D.M. Manning, P.S. Dimick (Review Paper) 249

STRUCTURE FORMATION IN ACID MILK GELS
I. Heertje, J. Visser, P. Smits 267

RHEOLOGICAL AND SCANNING ELECTRON MICROSCOPIC EXAMINATION OF SKIM MILK GELS OBTAINED BY FERMENTING WITH ROPY AND NON-ROPY STRAINS OF LACTIC BACTERIA
S.M. Schellhaass, H.A. Morris 279

OBSERVATIONS ON THE AIR-SERUM INTERFACE OF MILK FOAMS
B.E. Brooker 289

Continued on inside back cover